

NAT'L INST. OF STAND & TECH



A11106 262757

NBSIR 83-2742 (R)

Photonuclear Data - Abstract Sheets 1955 - 1982 Volume XII (Lanthanum - Lutetium)

Reference

NBS

PUBLICATIONS

U.S. DEPARTMENT OF COMMERCE
National Bureau of Standards
National Measurement Laboratory
Center for Radiation Research
Washington, DC 20234



U.S. DEPARTMENT OF COMMERCE

QC BUREAU OF STANDARDS

100

.U56

83-2742

1955-1982

VOL. XII

NBSIR 83-2742

PHOTONUCLEAR DATA - ABSTRACT SHEETS
1955 - 1982
VOLUME XII (LANTHANUM - LUTETIUM)

6
100
U\$6
83-2742
1955-1982
Vol. XII

E. G. Fuller, Henry Gerstenberg

U.S. DEPARTMENT OF COMMERCE
National Bureau of Standards
National Measurement Laboratory
Center for Radiation Research
Washington, DC 20234

U.S. DEPARTMENT OF COMMERCE, Malcolm Baldrige, *Secretary*
NATIONAL BUREAU OF STANDARDS, Ernest Ambler, *Director*

TABLE OF CONTENTS

Table of Contents	i
Introduction	1
Lanthanum (A=139)	3
Cerium (Natural)	45
Cerium (A=138)	75
Cerium (A=140)	79
Cerium (A=141)	97
Cerium (A=142)	101
Praseodymium (A=141)	107
Neodymium (Natural)	165
Neodymium (A=142)	179
Neodymium (A=143)	199
Neodymium (A=144)	203
Neodymium (A=145)	211
Neodymium (A=146)	217
Neodymium (A=148)	225
Neodymium (A=150)	233
Samarium (Natural)	245
Samarium (A=144)	255
Samarium (A=148)	271
Samarium (A=149)	281
Samarium (A=150)	285
Samarium (A=152)	293
Samarium (A=154)	313
Europium (Natural)	331
Europium (A=151)	335
Europium (A=153)	341

Gadolinium (Natural)	351
Gadolinium (A=152)	357
Gadolinium (A=154)	363
Gadolinium (A=155)	369
Gadolinium (A=156)	375
Gadolinium (A=157)	385
Gadolinium (A=158)	389
Gadolinium (A=160)	393
Terbium (A=159)	399
Dysprosium (Natural)	431
Dysprosium (A=162)	437
Dysprosium (A=163)	441
Holmium (A=165)	445
Holmium (A=166)	497
Erbium (Natural)	501
Erbium (A=166)	513
Erbium (A=167)	525
Erbium (A=168)	529
Erbium (A=170)	537
Thulium (A=169)	543
Ytterbium (Natural)	555
Ytterbium (A=173)	561
Ytterbium (A=174)	565
Ytterbium (A=176)	573
Lutetium (Natural)	577
Lutetium (A=175)	581
Lutetium (A=176)	591
Definitions of Abbreviations and Symbols	594

Photonuclear Data-Abstract Sheets
1955-1982

I. Introduction

As used in connection with this collection of data-abstract sheets, the term photonuclear data is taken to mean any data leading to information on the electromagnetic matrix element between the ground state and excited states of a given nuclide. The most common types of reactions included in this compilation are: (e,e') , (γ,γ) , (γ,γ') , (γ,n) , (γ,p) , etc. as well as ground-state particle capture reactions, e.g. (α,γ_0) . Two reactions which fit the matrix element criterion are not included in the compilation because of their rather special nature. These are heavy particle Coulomb excitation and the thermal neutron capture reaction (n,γ_0) . While the energy region of particular interest extends from 0 to 150 MeV, papers are indexed which report measurements in the region from 150 MeV to 4 GeV. Most of the experiments listed are concerned with the excitation energy range from 8 to 30 MeV, the region of the photonuclear giant resonance.

The hierarchical grouping of the photonuclear data-abstract sheets within the file is by: 1. Target Element, 2. Target Isotope, and 3. by the Bibliographic Reference Code assigned to the paper from which the data on the sheet were abstracted. In this file, colored pages are used to mark the beginning and end of the sheets for each chemical element. A brief historical sketch of the element is given on the divider sheet marking the start of each section; the information for this sketch was derived from references such as the Encyclopaedia Britannica. In those cases where the sheets for a given element make up a major part of a volume, colored pages are also used to delineate sections pertaining to the individual isotopes of the element. Each of the sections of the file, as delineated by two colored divider sheets, represents a 27 year history of the study of electromagnetic interactions in either a specific nuclide or a specific element.

The data-abstract sheets are filed under the element and/or isotope in which the ground-state electromagnetic transition takes place. For example, the abstract sheet for a total neutron yield measurement for a naturally occurring copper sample would appear in the elemental section of the copper file. On the other hand, a measurement of the ^{62}Cu 9.73 minute positron activity produced in the same sample by photons with energies below the three-neutron separation energy for ^{65}Cu (28.68 MeV) would be filed with the sheets for ^{63}Cu . Similarly a measurement of the ground-state neutron capture cross section in ^{12}C would be filed under ^{13}C while the corresponding ground-state alpha-particle capture cross section would be filed under ^{16}O .

At the end of this volume there is a master list of the abbreviations that have been used in the index section of the abstract sheets. The listings are those used in the final published index, Photonuclear Data Index, 1973-1981, NBSIR 82-2543, issued in August 1982 by the U. S. Department of Commerce, National Bureau of Standards, Washington, DC 20234. In some cases two notations are entered for the same quantity. The second entry is the abbreviation that was used in one or more of the earlier published editions of the index.

LANTHANUM

Z=57

Lanthanum is not a "true" earth. The rare earths are inner transition elements characterized by elections successively filling the incomplete 4f orbital shell. Geochemically, lanthanum is found in nature in close association with all the other rare earth elements. It was first separated by C. G. Mosander in 1839; he called it after the Greek word *lanthanein* meaning "to be concealed".

Beta-cron					REF. NO.		
REACTION	RESULT	EXCITATION ENERGY	SOURCE		DETECTOR		ANGLE
			TYPE	RANGE	TYPE	RANGE	
G, N	RLY	THR	C	THR	BF ₃ -I		4PI

See 58 Ka 1 for cross sections

TABLE I
 MEASURED PHOTONUETRON THRESHOLDS

THRESHOLD

Reaction	Measured Q value, Mev.	Other Q values, Mev.	Method	Reference
La ¹³⁷ (γ, n)La ¹³⁸	8.81 ± 0.05	8.50 = 0.20 8.73 = 0.20 9.07 ± 0.19 { Q ⁻ value	Threshold Mass data Mass data	Sher <i>et al.</i> (1951) Johnson and Nier (1957) Duckworth (unpublished) Glover and Walt (1957)

METHOD Betatron; ion chamber

REF. NO.	
58 Fu 1	NVB

REACTION	RESULT	EXCITATION ENERGY	SOURCE		DETECTOR		ANGLE
			TYPE	RANGE	TYPE	RANGE	
G, XN	ABY	7-40	C	7-40	BF ₃ -I		4PI

TABLE I. Target properties and results.

Element	Form used	Weight grams	$\sigma^*(\gamma, n)^*$ barns	$\frac{S_e dE}{NZ/A}$ Mev-b	"T" Mev
Sn	Sn	4.81	0.30	0.064	5.0
I	I	8.55	0.36	0.085	6.0
La	La	10.43	0.34	0.063	5.2
Ce	Ce	4.99	0.45	0.080	4.5
Sm	Sm ₂ O ₃	2.90	0.26	0.073	8.6
Tb	Tb ₂ O ₃	3.04	0.39	0.087	8.7
Ho	Ho ₂ O ₃	1.87	0.41	0.079	7.5
Er	Er ₂ O ₃	5.41	0.50	0.100	8.3
Yb	Yb ₂ O ₃	5.57	0.50	0.090	7.0
Ta	Ta	8.41	0.49	0.077	6.0
Au	Au	3.16	0.68	0.085	4.2
Pb	Pb	8.05	0.75	0.081	3.8

* $\sigma^*(\gamma, n)$ is the maximum value and "T" the full width at $\sigma^*(\gamma, n)/2$ of the neutron production cross section corrected for multiple neutron emission. Data were not fitted with resonance lines to determine these values.

^b Integrated neutron production cross sections corrected for multiple neutrons above $(\gamma, 2n)$ threshold.

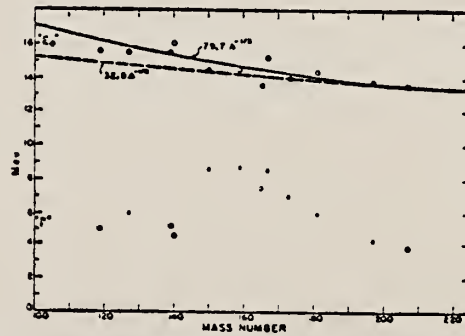


FIG. 6. Mean energy and width of giant resonances. "E₀" and "T" are the mean energy for photon absorption and the full width at half maximum of the giant resonance obtained from dashed histograms as in Fig. 5. No attempt was made to fit data with resonance curves to obtain these parameters.

La	139	57
REF. NO.	58 Ka 1	NVB

METHOD Betatron; neutron cross section; BF_3 counters; ion chamber monitor

REACTION	RESULT	EXCITATION ENERGY	SOURCE		DETECTOR		ANGLE
			TYPE	RANGE	TYPE	RANGE	
G, XN	ABX	9-22	C	9-22	$\text{BF}_3\text{-I}$		4PI

Таблица 2
Пороги испускания фотонейтронов

Изотоп	B_n , Мэс	B_m , Мэс	Изотоп	B_n , Мэс	B_m , Мэс
V ⁸¹	11.16	20.5	L ¹³⁹	8.81	16.1
Mn ⁵⁵	10.14	19.2	Pr ¹⁴¹	9.46	17.6
Co ⁶⁰	10.44	18.6	Tb ¹³⁹	8.16	14.8
As ⁷⁵	10.24	18.1	Ho ¹⁶⁵	8.10	14.6
Y ⁸⁸	11.82	20.7	Tm ¹⁶⁹	8.00	14.7
Nb ⁹³	8.86	17.1	Lu ¹⁷³	7.77	14.2
Rh ¹⁰³	9.45	16.8	Ta ¹⁸¹	7.66	13.8
J ¹²⁷	9.14	16.2	Au ¹⁹⁷	7.6	13.3
Cs ¹³³	9.11	16.5	Bi ²⁰⁹	7.4	14.5

THRESHOLDS

не приведены, поскольку они превышают 22 Мэс во всех случаях, кроме золота, для которого $B_{22} = 21$ Мэс. Свойства сечений $\sigma_C(\gamma)$ сведены в табл. 3.

Таблица 1

Изотоп	E_{\max} , Мэс	$\sigma_n(E_\gamma)$, барн	E , Мэс	σ^m , Мэс·барн	$\frac{\sigma}{\sigma_n}(E_{\gamma}) \cdot 10^4$, нейтрон/100 р·мэс
V ⁸¹	18.4	0.062	5.2	0.33	1.62
Mn ⁵⁵	20.2	0.060	7.0	0.39	2.01
Co ⁶⁰	18.3	0.068	6.3	0.44	2.30
As ⁷⁵	16.6	0.090	9.5	0.74	4.25
Y ⁸⁸	17.1	0.172	5.2	0.93	5.33
Nb ⁹³	18.0	0.156	7.5	1.17	6.80
Rh ¹⁰³	17.5	0.160	9.4	1.40	8.28
J ¹²⁷	15.2	0.273	6.8	1.76	11.9
Cs ¹³³	16.5	0.238	7.7	1.59	10.7
La ¹³⁹	15.5	0.325	3.8	1.55	11.2
Pr ¹⁴¹	15.0	0.320	4.9	1.93	13.1
Tb ¹³⁹	15.6	0.274	9.8	2.49	18.1
Ho ¹⁶⁵	13.5	0.305	8.9	2.52	18.7
Tm ¹⁶⁹	16.4	0.250	8.4	1.91	14.9
Lu ¹⁷³	16.0	0.225	8.4	1.90	23.0
Ta ¹⁸¹	14.5	0.350	8.5	3.15	22.0
Au ¹⁹⁷	13.8	0.475	4.7	3.04	22.6
Bi ²⁰⁹	13.2	0.455	5.9	2.89	23.2

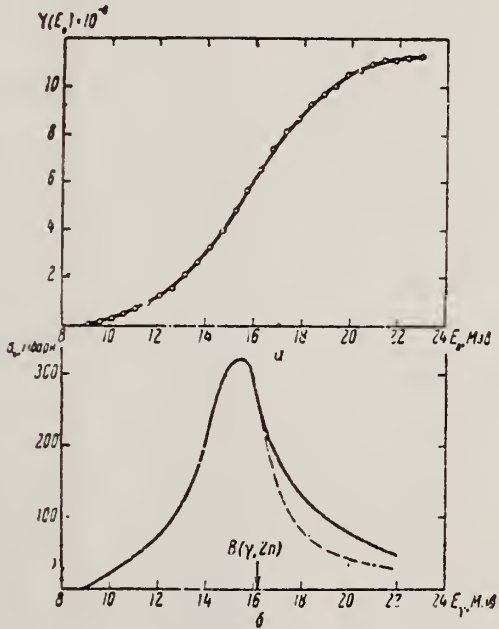


Рис. 10.
a — Выход фотонейтронов для La; b — $\frac{\sigma}{\sigma_n}(E_\gamma)$ для La

Method 18 MeV electron synchrotron; neutron counters, 25 r Victoreen monitor

Ref. No.
58 Sp 1

Reaction	E or ΔE	E_0	Γ	$\int \sigma dE$	$J\pi$	Notes
La(γ , n)	Bremss. 8-18					

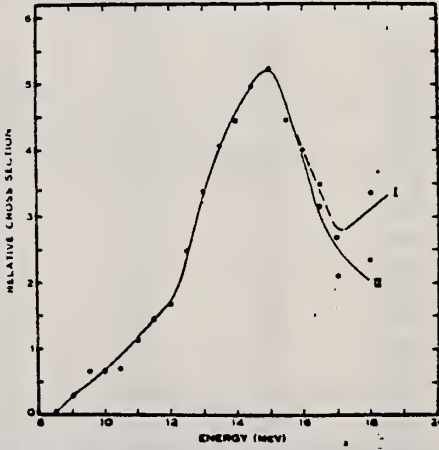


Fig. 6.—Cross section for nuclear absorption of γ -rays in lanthanum. Curve I is the cross section calculated from the neutron yield curve. Curve II is corrected for the effects of neutron multiplicity.

METHOD

Betatron; neutron threshold; ion chamber

REF. NO.

60 Ge 3

NVB

REACTION	RESULT	EXCITATION ENERGY	SOURCE		DETECTOR		ANGLE
			TYPE	RANGE	TYPE	RANGE	
G, N	NOX	THR	C THR		BF3-I		4 PI

THRESHOLD

TABLE I. Summary and comparison of neutron separation energies inferred from present threshold measurements with values predicted from mass data and reaction energetics. All energies are expressed in the center-of-mass system in Mev.

Reaction	No. runs	Present results	Other results	Method	Reference
$\text{La}^{140}(\gamma, n)\text{La}^{141}$	4	8.775 ± 0.025	8.73 ± 0.19 8.81 ± 0.05	mass data threshold	P

W. H. Johnson, Jr., and A. O. Nier, Phys. Rev. 105, 1014 (1957).

METHOD betatron; fast neutron yield; angular distribution; Al and Si threshold detectors; ion chamber

REF. NO.
61 Ba 2 NVB

REACTION	RESULT	EXCITATION ENERGY	SOURCE		DETECTOR		ANGLE
			TYPE	RANGE	TYPE	RANGE *	
G, XN	ABY	THR-22	C	22	THR-I	3-+	DST
G, XN	ABY	THR-22	C	22	THR-I	5-+	DST

In Tables 2 and 4:

* "3-+" is the detector range of Aluminum and "5-+" of Silicon.

$\bar{\sigma}$ = average cross section of detector weighted with neutron spectrum

Φ = neutrons/100 roentgen/mole

$$W(\theta) = \frac{1}{n=1} \overline{\sigma}_o [1 + A_n P_n (\cos \theta)]$$

TABLE II
Normalized yields for aluminum detectors

Element	Al(γ, γ) reaction					Al(π, p) reactions					
	30°	90°	150°	a_0	30°	60°	90°	a_0	a_1	a_2	$(\bar{\sigma}\Phi)^o \times 10^o$
Bismuth	398 473	567 ± 130 423 ± 130	620 641	541 ± 85 484 ± 85	3632	5139 ± 290	3168	4306 ± 185	0.06 ± 0.06	-0.35 ± 0.1	17.76
Lead	426	312 ± 120	725	420 ± 77	3123	5754 ± 260	3154	4591 ± 168	-0.004 ± 0.05	-0.51 ± 0.07	18.68
Tantalum	373	367 ± 190	688	441 ± 122	2757	3024 ± 425	2088	2757 ± 275	0.14 ± 0.14	-0.19 ± 0.17	11.23
Lanthanum	208	222 ± 110	330	243 ± 70	2139	3371 ± 250	1891	2768 ± 160	0.05 ± 0.07	-0.43 ± 0.10	11.27
Arsenic	77	100 ± 50	108	97 ± 32	788	937 ± 115	764	865 ± 74	0.02 ± 0.11	-0.16 ± 0.14	3.52
Copper	13	65 ± 30	70	55 ± 20	710	748 ± 70	569	700 ± 45	0.11 ± 0.08	-0.14 ± 0.11	2.85

*($\bar{\sigma}\Phi$) = 4.07×10^{-4} millibarn-neutron.

TABLE IV

I Element	II a_0	III a_1	IV a_2	V $(\bar{\sigma}\Phi) \times 10^{10}$	VI $\Phi_{max}(22 \text{ Mev}) \times 10^9$	VII Φ_{loss}/Φ_{max}
Vanadium	245 (1 ± 0.06)	0.01 ± 0.08	-0.00 ± 0.10	6.05	0.21	0.12
Chromium	164 (1 ± 0.03)	0.04 ± 0.04	-0.05 ± 0.05	4.05	0.17	0.10
Manganese	308 (1 ± 0.02)	0.07 ± 0.03	-0.09 ± 0.04	7.61	0.25	0.12
Iron	200 (1 ± 0.03)	0.05 ± 0.04	-0.17 ± 0.05	4.94	0.18	0.11
Cobalt	390 (1 ± 0.02)	0.08 ± 0.03	-0.22 ± 0.04	9.63	0.26	0.15
Nickel	145 (1 ± 0.05)	0.07 ± 0.07	-0.23 ± 0.09	3.58	0.12	0.12
Copper	347 (1 ± 0.02)	0.05 ± 0.03	-0.29 ± 0.04	8.57	0.30	0.12
Arsenic	482 (1 ± 0.03)	0.11 ± 0.04	-0.24 ± 0.05	11.91	0.33	0.15
Rubidium	638 (1 ± 0.05)	0.13 ± 0.06	-0.14 ± 0.08	15.76		
Strontium	409 (1 ± 0.05)	0.10 ± 0.06	-0.17 ± 0.08	10.10		
Yttrium	290 (1 ± 0.10)	0.08 ± 0.12	-0.12 ± 0.15	7.16		
Silver	590 (1 ± 0.04)	0.10 ± 0.06	-0.22 ± 0.08	14.57	0.87	0.07
Cadmium	905 (1 ± 0.02)	0.02 ± 0.02	-0.26 ± 0.03	22.35		
Iodine	1133 (1 ± 0.03)	0.04 ± 0.04	-0.29 ± 0.05	27.99	1.42	0.08
Barium	1048 (1 ± 0.04)	0.10 ± 0.06	-0.38 ± 0.08	25.89		
Lanthanum	1595 (1 ± 0.02)	0.02 ± 0.03	-0.42 ± 0.04	39.40	1.04	0.15
Cerium	1316 (1 ± 0.05)	0.05 ± 0.06	-0.39 ± 0.08	32.50		
Dysprosium	1652 (1 ± 0.08)	0.04 ± 0.10	-0.34 ± 0.13	40.80		
Tantalum	1558 (1 ± 0.02)	0.04 ± 0.03	-0.23 ± 0.04	38.48	2.50	0.06
Tungsten	1365 (1 ± 0.02)	-0.07 ± 0.03	-0.24 ± 0.04	33.71		
Mercury	1345 (1 ± 0.03)	0.04 ± 0.03	-0.31 ± 0.04	33.22		
Lead	2274 (1 ± 0.01)	0.02 ± 0.02	-0.42 ± 0.03	56.17	2.72	0.08
Bismuth	2162 (1 ± 0.02)	0.06 ± 0.03	-0.45 ± 0.04	53.40	3.36	0.06
Thorium	3031 (1 ± 0.04)	0.06 ± 0.05	-0.32 ± 0.07	74.87		
Uranium	4630 (1 ± 0.02)	0.05 ± 0.03	-0.17 ± 0.04	114.36		

*($\bar{\sigma}\Phi$) = 2.47×10^9 es millibarn-neutron. Errors are standard errors due to counting statistics only.

J. Miller, C. Schuhl, C. Tzara
 J. Phys. Radium 22, 529 (1961)

ELEM. SYM.	A	Z
La	139	57

METHOD

REF. NO.

Positron annihilation; neutron cross section; BF_3 counter; ion chamber

61 Mi 1

NVB

REACTION	RESULT	EXCITATION ENERGY	SOURCE		DETECTOR		ANGLE
			TYPE	RANGE	TYPE	RANGE	
G.XN	ABX	10-22	D	10-22	BF_3 -I		4PI

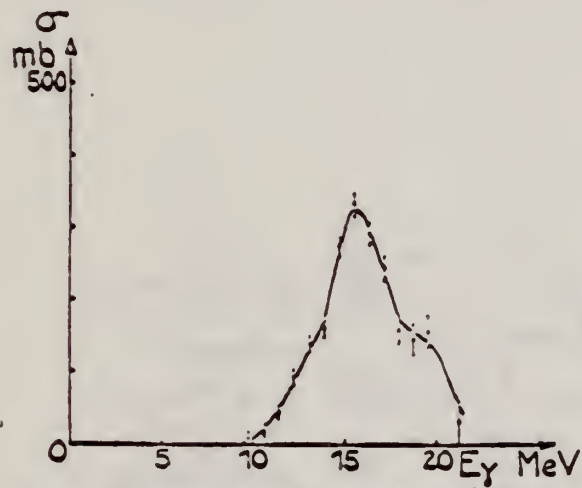


FIG. 6a. — Lanthane, $\sigma(\gamma, \alpha) + 2\sigma(\gamma, 2n) + \sigma(\gamma, np) + \dots$

Elcm. Sym.	A	Z
La	139	57

Method 22 MeV betatron; $\text{Si}^{28}(\text{n}, \text{p})\text{Al}^{28}$ threshold detector.

Ref. No.
 61 Ta 1 JHH

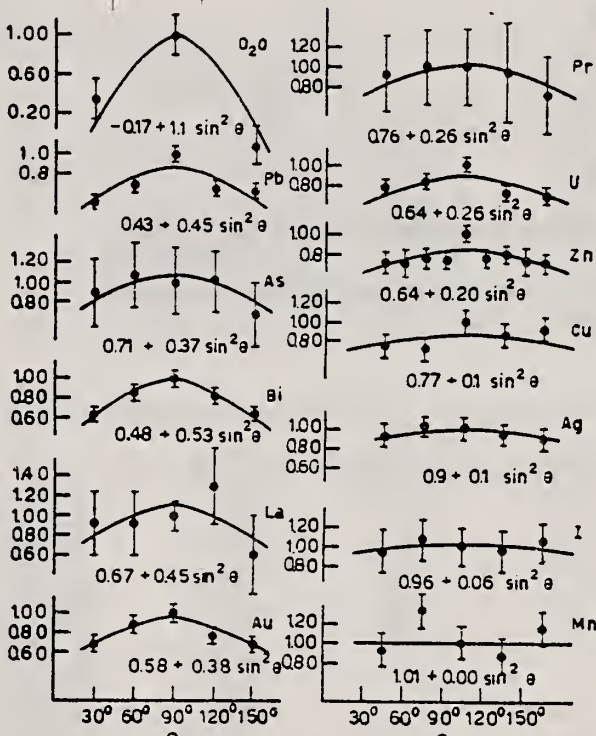
Reaction	E or ΔE	E_0	Γ	$\int \sigma dE$	$J\pi$	Notes
(γ, n)	Bremss.	22				$E_n > 6 \text{ MeV.}$ $W(\theta_n) = A + B \sin^2 \theta$ where $B/A = 0.67 \pm 0.48$ 

Fig. 4. Angular distributions of fast photoneutrons as observed with the $\text{Si}^{28}(\text{n}, \text{p})\text{Al}^{28}$ detector.
 Data normalized at 90° in each case.

Figure 4: Angular distributions of fast photoneutrons as observed with the $\text{Si}^{28}(\text{n}, \text{p})\text{Al}^{28}$ detector. Data normalized at 90° in each case.

Elem. Sym.	A	Z
La	139	57

Method 55 MeV betatron; synchrotron; $\text{Si}^{28}(\text{n}, \text{p})\text{Al}^{28}$ activity; $\text{Cu}^{63}(\gamma, \text{n})\text{Cu}^{62}$ monitor.

Ref. No.
 62 Re 1 EGF

Reaction	E or ΔE	E_0	Γ	$\int \sigma dE$	$J\pi$	Notes
(γ, n)	Bremss. 55					<p>Figure 10: Dotted curve is of form $a_0 + a_1 \cos\theta + a_2 \cos^2\theta + a_3 \cos^3\theta - a_4 \cos^4\theta$; solid curve is of form $a_0 + a_1 \cos\theta + a_2 \cos^2\theta$; errors on points are statistical error in counting only.</p> <p>Fig. 10. Angular distribution of fast neutrons from lanthanum. See fig. 3</p>

TABLE 2
 Parameters of the fit (1) for the expressions $a_0 + a_1 \cos\theta + a_2 \cos^2\theta - a_3 \cos^3\theta + a_4 \cos^4\theta$ and $1 - t_1 P_1 - t_2 P_2 - t_3 P_3$

Tl	Ts	Pr	Ad	V	Hb	La
-1.00 ± 0.02	1.00 ± 0.02	1.00 ± 0.02	1.00 ± 0.02	1.00 ± 0.02	1.00 ± 0.02	1.00 ± 0.02
0.13 ± 0.01	0.18 ± 0.04	0.17 ± 0.04	0.14 ± 0.04	0.17 ± 0.06	0.12 ± 0.03	0.14 ± 0.03
0.47 ± 0.06	0.40 ± 0.08	0.41 ± 0.09	0.21 ± 0.07	0.15 ± 0.11	0.13 ± 0.06	0.49 ± 0.06
-0.18 ± 0.04	-0.21 ± 0.05	-0.20 ± 0.05	0.15 ± 0.04	0.18 ± 0.06	0.14 ± 0.04	0.16 ± 0.03
-0.17 ± 0.04	-0.31 ± 0.06	-0.32 ± 0.07	0.15 ± 0.05	0.11 ± 0.08	0.26 ± 0.05	0.30 ± 0.04
-0.53 ± 0.06	-0.60 ± 0.08	-0.50 ± 0.04	0.70 ± 0.07	0.82 ± 0.11	0.56 ± 0.06	0.61 ± 0.06
0.47 ± 0.06	0.40 ± 0.08	0.41 ± 0.09	0.21 ± 0.07	0.15 ± 0.11	0.34 ± 0.06	0.39 ± 0.06
-0.15 ± 0.01	-0.18 ± 0.04	-0.17 ± 0.04	0.14 ± 0.03	0.17 ± 0.06	0.12 ± 0.03	0.14 ± 0.03

normalized so that $t_1 = 1$

TABLE 4
 Parameters of the fit (3) for the expressions $a_0 - a_1 \cos\theta - a_2 \cos^2\theta - a_3 \cos^3\theta$, $1 - t_1 P_1 - t_2 P_2 - t_3 P_3$

Tl	Ts	Pr	Ad	V	Hb	La
-1.01 ± 0.02	1.00 ± 0.02	1.01 ± 0.03	0.98 ± 0.02	1.00 ± 0.03	1.00 ± 0.02	1.01 ± 0.02
0.19 ± 0.05	0.17 ± 0.07	0.21 ± 0.07	0.07 ± 0.06	0.16 ± 0.09	0.12 ± 0.03	0.17 ± 0.03
-0.58 ± 0.11	-0.37 ± 0.15	-0.30 ± 0.16	0.05 ± 0.12	0.13 ± 0.20	0.33 ± 0.12	0.47 ± 0.11
-0.17 ± 0.15	-0.05 ± 0.24	-0.17 ± 0.25	0.31 ± 0.19	0.05 ± 0.32	0.03 ± 0.19	-0.17 ± 0.17
-0.11 ± 0.15	-0.23 ± 0.18	-0.13 ± 0.20	0.27 ± 0.13	0.20 ± 0.22	0.15 ± 0.14	0.09 ± 0.13
-0.15 ± 0.09	-0.28 ± 0.11	-0.30 ± 0.12	0.03 ± 0.08	0.09 ± 0.14	0.24 ± 0.09	0.37 ± 0.09
-0.08 ± 0.09	-0.02 ± 0.11	-0.08 ± 0.12	0.13 ± 0.08	0.02 ± 0.13	0.01 ± 0.08	-0.08 ± 0.08

normalized so that $t_1 = 1$

ELEM. SYM.	A	Z
La	139	57

METHOD

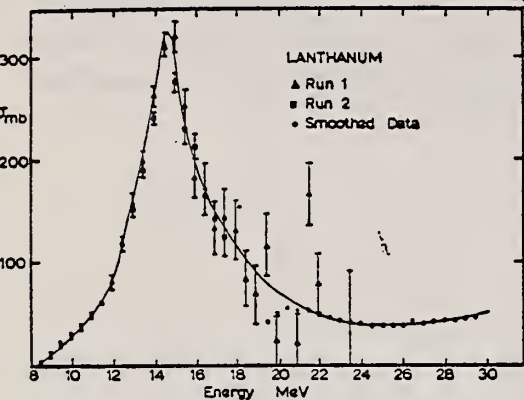
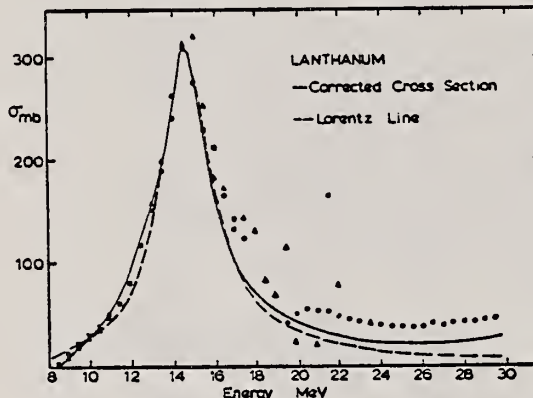
Synchrotron, NBS chamber

REF. NO.

64 Ri 1

NVB

REACTION	RESULT	EXCITATION ENERGY	SOURCE	DETECTOR	ANGLE
			TYPE	RANGE	
G,XN	ABX	8-30	C	8-30	BF ₃ -I
					LPI

FIG. 1. Lanthanum (γ, n) cross section uncorrected for neutron multiplicity.FIG. 3. Lanthanum (γ, n) cross section with neutron multiplicity correction (solid line); Lorentz line fitting to data points (dashed line).TABLE I. Experimentally determined parameters for the neutron photoproduction cross sections σ_m , maximum value of cross sections; E_m , energy at which maximum occurs; DSR, classical dipole-sum rule limit; Γ_0 twice the energy from half-maximum on low-energy side of curve to E_m ; Γ_{Lor} width used to fit the Lorentz curve

	σ_m mb	E_m MeV	$\int_{T_{\text{low}}}^{\infty} \sigma dE$ MeV-b	DSR MeV-b	Γ_0 MeV	Γ_{Lor} MeV
Uncorrected for multiplicity						
La	315 ± 15	14.8 ± 0.4	1.76	2.02		
Pr	305 ± 10	14.8 ± 0.4	1.74	2.06		
Corrected for ($\gamma, 2n$)						
La	304	14.5	1.36	2.02	3.2 ± 0.2	3.3
Pr	305	14.8	1.47	2.06	4.0 ± 0.2	3.3

METHOD

REF. NO.

Nuclear Resonance Scattering using N,G reactions.

66 Be 3

JDM

REACTION	RESULT	EXCITATION ENERGY	SOURCE		DETECTOR		ANGLE
			TYPE	RANGE	TYPE	RANGE	
G,G	RLX	5 - 10	D	5 - 10	NAI-D	5 - 10	135

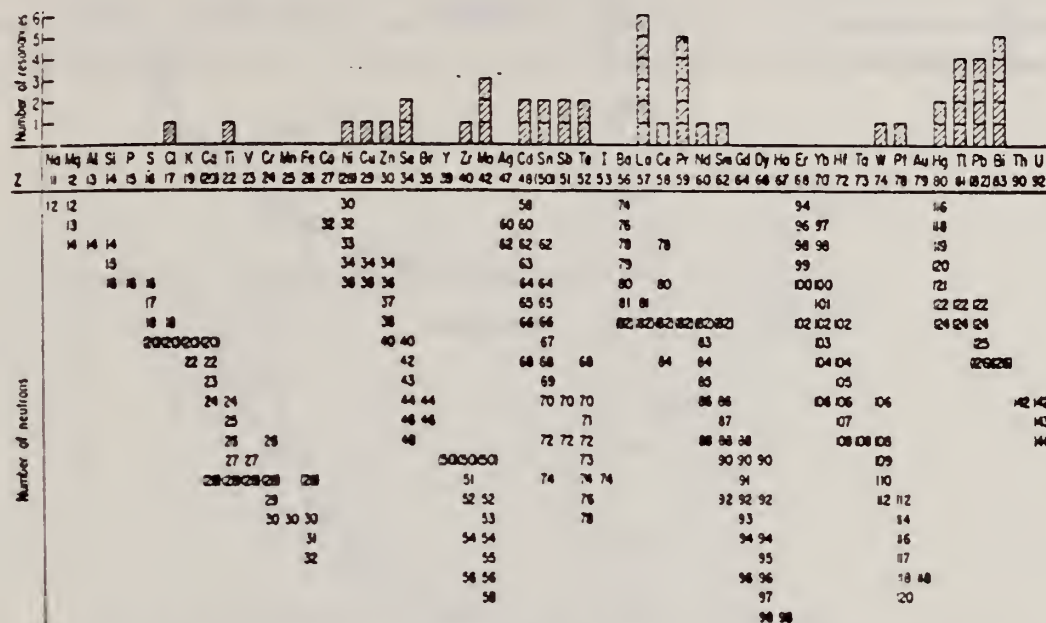


FIG. 3. Histogram of distribution of observed resonances among the different targets. The atomic number is given directly beneath the chemical symbol followed by the neutron numbers of the naturally occurring isotopes. Magic numbers are shown in brackets.

TABLE III. List of effective cross sections.

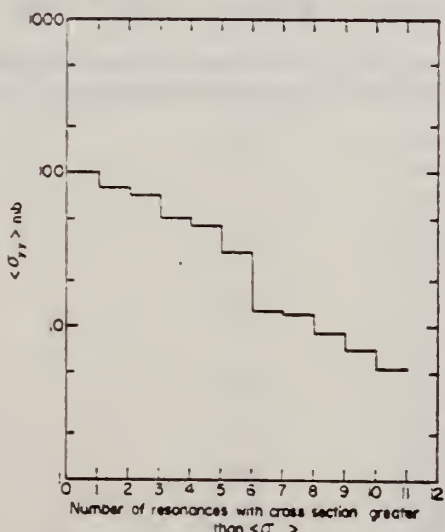


FIG. 5. Integral distribution of the effective cross sections for the 11 resonances in the mono-isotopic elements lanthanum and praseodymium.

Scatterer	Energy (MeV)	Gamma source	δ (mb)	Scatterer	Energy (MeV)	Gamma source	δ (mb)
Sm ¹⁴⁴	8.997	Ni	100	Sn	7.01	Cu	110
Pr ¹⁴¹	8.881	Cr	9	Nd	6.867	Co	30
La	8.532	Ni	6	Pr ¹⁴¹	6.867	Co	3
Te	8.532	Ni	3*	Te	6.7	Ni	..
Cu	8.499	Cr	24	La	6.54	Ag	12
Zr	8.496	Se	3050	Ci	6.174	Co	110
Zn	8.119	Ni	13	Mo	6.44	Hg	25*
Se	7.817	Ni	50	La	6.413	Ti	72
Se	7.76	K	90	Mo	6.413	Ti	10
Sb	7.67	V	...*	Tl	6.413	Ti	25
Cd	7.64	Fe	40*	W	6.3	Ti	..*
Ni	7.64	Fe	7*	Sb	6.31	Hg	6*
Pr ¹⁴¹	7.64	Fe	12*	Ti	6.31	Hg	2*
Tl	7.64	Fe	370*	Sn	6.27	Ag	75
La	7.634	Cu	7	Ph ²⁰⁸	6.15	Gd	...*
Mo	7.634	Cu	11	Te	5.8	Ni	..
Bi ¹⁷³	7.634	Cu	4	La	6.12	Cl	35
Te	7.523	Ni	66*	Pr ¹⁴¹	6.12	Cl	110
Bi ¹⁷³	7.416	Se	100	Pt	5.99	Hg	40*
Bi ¹⁷³	7.300	As	80*	Tl	5.99	Hg	5*
Pb ²⁰⁸	7.285	Fe	4100	Pb ²⁰⁸	5.9	Sr	...*
Cl	7.285	Fe	34	Ca	5.646	Co	17
Pr ¹⁴¹	7.185	Se	80	Bi ¹⁷³	5.646	Co	55
Tl	7.16	Cu	120	Pb ²⁰⁸	5.53	Ag	70
La	7.15	Mn	50	Hg	5.44	Hg	75*
Bi ¹⁷³	7.149	Tl	2000	Hg	4.903	Co	385

* High-energy component of a complex spectrum.

* A broad scattered spectrum with no observable peak structure.

* There are actually two lines of energies 7.647 and 7.633 MeV having equal intensities in the iron capture gamma spectrum. The cross section has therefore been corrected, although there is no possibility at present of deciding which line is responsible for each resonance.

* Is probably an independent level in the complex spectrum of Ni γ rays on Te.

* Rough estimate.

* May be inelastic component from 7.528 level in Te.

* The relative line intensities in this case are due to Grosber and co-workers.

* No line is known for the source at this energy.

* Difficult to resolve among the many source lines present at this energy.

ELEM. SYM.	A	Z
La	139	57

METHOD

REF. NO.

67 Hu 1

EGF

REACTION	RESULT	EXCITATION ENERGY	SOURCE	DETECTOR		ANGLE
			TYPE	RANGE	TYPE	
G,N	ABX	9-11	D	9-11	BF ₃ -I	4PI

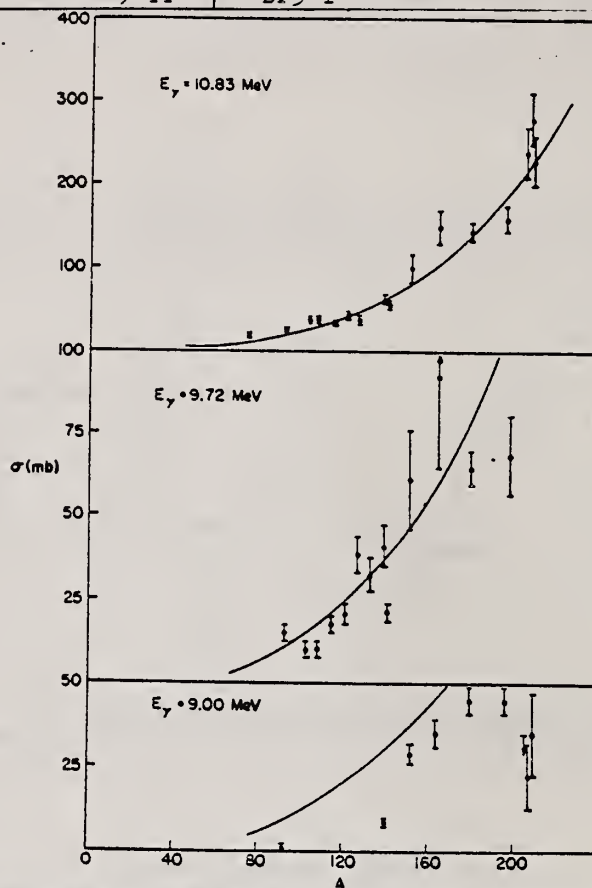


TABLE I
Photoneutron cross sections (mb)

Fig. 1. Cross section (in mb) versus mass number of the target for gamma-ray energies of 9.00, 9.72 and 10.83 MeV. The solid lines are plots of eq. (1) in the text.

Target	7.72 MeV	9.00 MeV	9.72 MeV	10.83 MeV
⁶⁰ Co				9.0 ± 0.8
⁷⁵ As				20.4 ± 1.7
⁹³ Nb			0.53 ± 0.10	25.8 ± 2.1
¹⁰³ Rh			14.6 ± 2.2	38.8 ± 3.1
¹⁰⁷ Ag			10.6 ± 1.7	
¹⁰⁹ Ag			10.0 ± 1.5	
¹¹⁵ In			17.1 ± 2.6	37.6 ± 2.9
¹²¹ Sb			20.7 ± 3.1	33.3 ± 2.7
¹²³ Sb			38.7 ± 5.8	42.5 ± 3.6
¹²⁷ I			31.7 ± 4.8	
¹³³ Cs			40.8 ± 6.5	38.8 ± 3.1
¹³⁸ La		8.61 ± 0.86	21.5 ± 3.2	52.5 ± 3.8
¹⁴¹ Pt			61.3 ± 14.7	63.0 ± 5.0
¹⁵¹ Eu		28.9 ± 3.2	61.3 ± 14.7	58.3 ± 4.1
¹⁶³ Eu			102 ± 18	
¹⁶⁶ Ho		35.6 ± 4.3	92.2 ± 27.6	150 ± 20
¹⁸¹ Ta	4.14 ± 0.36	45.4 ± 3.7	65.0 ± 5.5	146 ± 12
¹⁹⁷ Au		44.5 ± 3.6	68.4 ± 13.5	160 ± 15
²⁰⁸ Pb		<34.3		238 ± 29
²⁰⁹ Pb		22.6 ± 11.3		280 ± 31
²⁰⁹ Bi		36.1 ± 12.0		226 ± 27

U.S. DEPARTMENT OF COMMERCE
NATIONAL BUREAU OF STANDARDS

METHOD

REF. NO.
68 Be 5

egf

REACTION	RESULT	EXCITATION ENERGY	SOURCE		DETECTOR		ANGLE
			TYPE	RANGE	TYPE	RANGE	
G, N 98	ABX	THR-30	D	7-30	MOD-I		4PI
G, 2N 99	ABX	THR-30					
G, 3N 100+	ABX	THR-30					

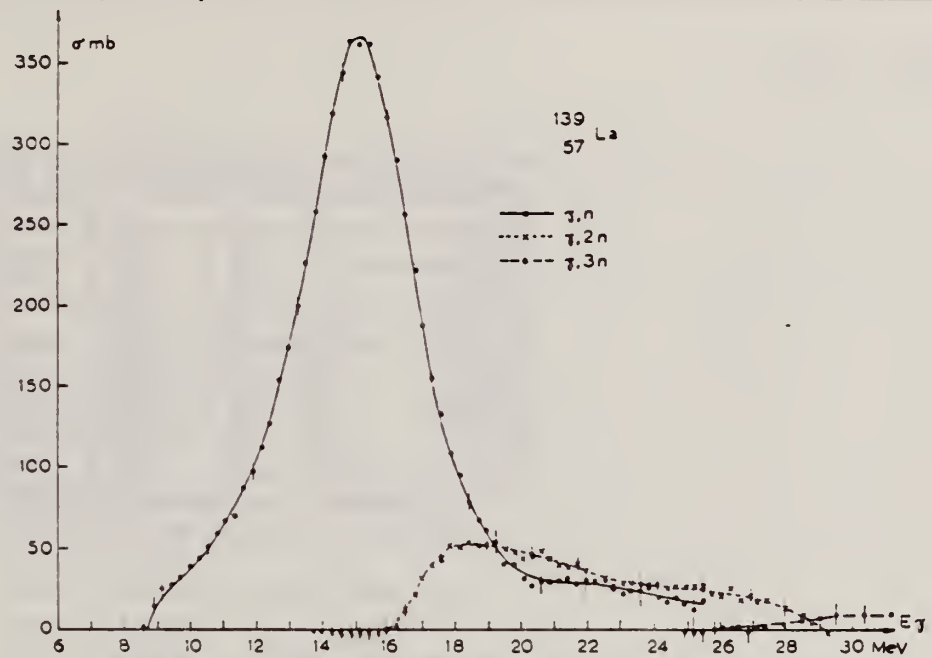


Fig. 9. Partial photonuclear cross sections $\sigma(\gamma, n)$, $\sigma(\gamma, 2n)$ and $\sigma(\gamma, 3n)$ of ^{139}La .

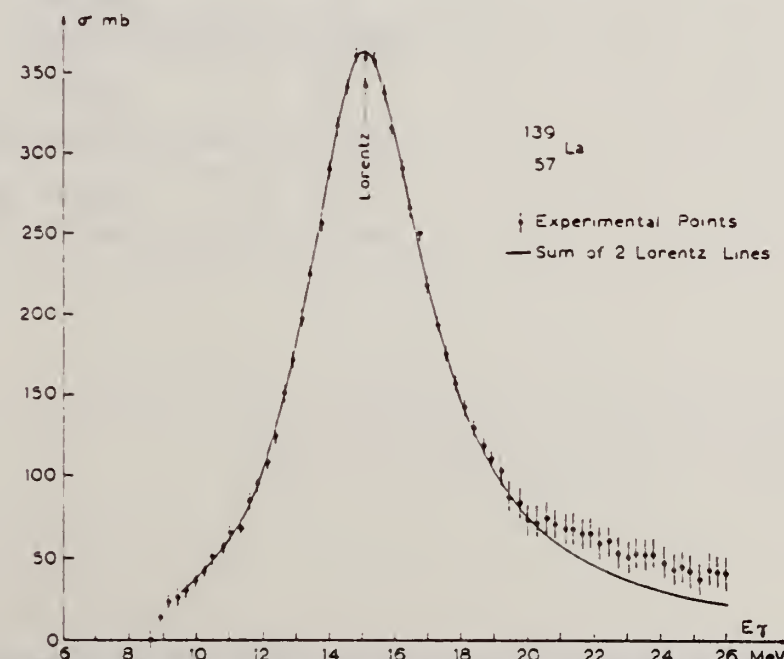


Fig. 10. Total cross section data showing a one Lorentz line fit for a ^{139}La target.

J. W. Jury, J. S. Hewitt, and K. G. McNeill
Can. J. Phys. 46, 1823 (1968)

ELEM. SYM.	A	Z
La	139	57

METHOD

REF. NO.

68 Ju 1

EGF

REACTION	RESULT	EXCITATION ENERGY	SOURCE		DETECTOR		ANGLE
			TYPE	RANGE	TYPE	RANGE	
G,N	NOX	THR-27	C	27	THR	5-	DST

$$W(\theta) = a_0 + a_1 P_1 + a_2 P_2$$

TABLE I

Target element	Z	Energy	a_0^*	a_1/a_0	a_2/a_0
Vanadium	23	32	640 ± 50	0.11 ± 0.10	-0.09 ± 0.11
Chromium	24	22	365 ± 39	0.02 ± 0.08	0.00 ± 0.10
Manganese	25	22	450 ± 33	0.07 ± 0.05	-0.11 ± 0.06
Bromine	35	27	874 ± 54	0.05 ± 0.06	-0.15 ± 0.08
Molybdenum	42	22	610 ± 60	0.09 ± 0.05	-0.35 ± 0.06
Ruthenium	44	27	1100 ± 25	0.12 ± 0.02	-0.29 ± 0.03
Rhodium	45	27	1270 ± 47	0.06 ± 0.03	-0.14 ± 0.03
Palladium	46	27	1350 ± 29	0.26 ± 0.02	-0.12 ± 0.02
Antimony	51	27	2140 ± 62	0.04 ± 0.08	-0.25 ± 0.11
Lanthanum	57	27	1940 ± 70	0.12 ± 0.10	-0.52 ± 0.14
Praseodymium	59	30	1800 ± 58	0.20 ± 0.08	-0.40 ± 0.09
Platinum	78	27	2600 ± 52	0.17 ± 0.02	-0.15 ± 0.03
Lead	82	22	2274 ± 59	0.08 ± 0.08	-0.46 ± 0.09

*The yield per mole per 100 r was normalized to a yield of 2274 for the lead sample at the same energy.

METHOD

REF. NO.

69 Be 7

hmg

REACTION	RESULT	EXCITATION ENERGY	SOURCE		DETECTOR		ANGLE
			TYPE	RANGE	TYPE	RANGE	
G,G	LFT	6.0	D	6.0	D		DST
		(6.413)		(6.413)			(90,135)

Self-Absorption.

6.413 MEV

Results of determination of the resonance-level parameters

Source-scatterer	E_γ , MeV	$\langle \sigma_{pp} \rangle$, mb	Γ_{γ_0} , eV	D, keV	Reference
Pb + Zn ⁶⁴	7.38	33±4.5	0.58±0.12	53.70±0.13	This work
Ti + Mo ⁹⁶	6.413	11.2 ±1.4	0.11±0.02	8.68±1.57	"
Ti + La ¹³⁹	6.413	16.04±2.10	0.28±0.05	8.03±1.42	"
Ti + Bi ²⁰⁹	7.15	1200±230	0.32±0.07	1.84±0.40	"
	6.996	1560	-	-	[1]
	7.15	2600±800	0.42±0.14	-	[5]
Ti + Cu ⁶⁵	6.07	423±108	0.34±0.08	99.1±17.4	This work
	6.07	440±130	0.36±0.07		[5]
Ti + Cu ⁶³	6.07	215±71	0.18±0.04	67.14±12.70	This work
	6.07	200±50	0.16±0.03	-	[6]
Cr + Cu ⁶³	3.50	22±7	0.25±0.08	130±40	This work
	8.499	35	75	-	[1]
	9.50	19±6	0.28±0.09	-	[6]
Cr + Cu ⁶⁵	8.50	36±9	0.47±0.10	21.35±4.54	This work
	8.499	80	10.5	-	[1]
	8.50	42±13	0.94±0.20	-	[6]
Ca + Sr ¹¹⁷	7.01	1150±240	0.15±0.04	0.44±0.12	This work
	7.01	1000	-	-	[1]
	7.01	1200±400	0.3±0.3	-	[5]
Hg + Mo ⁹⁶	6.44	201±27	0.12±0.04	0.23±3.07	This work

K. Shoda, M. Sugawara, T. Saito & H. Miyase
 PICNS-69 Proceedings of the Conference on Nuclear Isospin.
 Asilomar-Pacific Grove, California 1969 (Academic Press,
 New York & London 1969) p.137.

ELEM. SYM. A

La 139 57

METHOD

REF. NO.

69 Sh 8 egf

REACTION	RESULT	EXCITATION ENERGY	SOURCE		DETECTOR		ANGLE
			TYPE	RANGE	TYPE	RANGE	
E.P	SPC	11-22	D	30	MAG-D		UKN

UKN=UNKNOWN

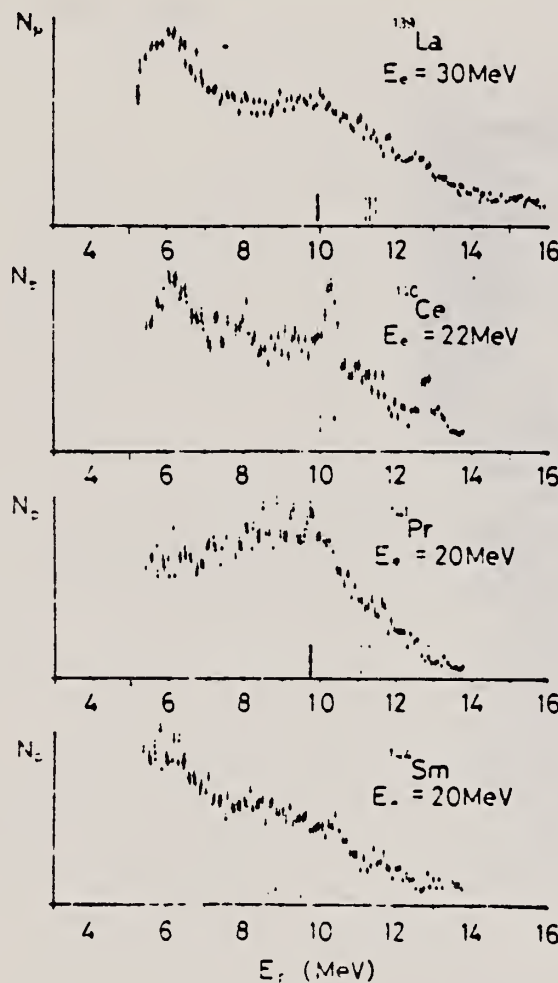


Fig. 1. Energy distributions of photoprottons. Vertical broken lines and solid lines indicate the position of p_0 corresponding to the ground IAS and electric dipole IAS (2).

ELEM.	SYM.	A	Z
La		139	57

METHOD

REF. NO.

70 Mo 2

hmg

REACTION	RESULT	EXCITATION ENERGY	SOURCE		DETECTOR		ANGLE
			TYPE	RANGE	TYPE	RANGE	
G, G	ABX	6	D	6	SCD-D		DST
		(6.018)		(6.018)			
		..					

6 = 6.018, LFT

TABLE III. Summary of the results of spins, parities, and total widths of resonance levels excited by γ rays obtained from neutron capture in iron. Parities in parentheses are uncertain.

Isotope	Energy (MeV)	$\delta = E_r - E_s $ (eV)	J^{π}_s	J^{π}_r	Transition	Γ_0/Γ_γ (=3%)	Γ_γ (10^{-3} eV)
^{59}Cr	8.888	18 ± 1	0 ⁺	1	...	0.90	750 ± 200
^{62}Ni	7.646	14 ± 1	0 ⁺	1 ⁻	$E1$	0.64	480 ± 50
^{74}Ge	6.013	4.5 ± 0.5	0 ⁺	1 ⁻	$E1$	0.19	120 ± 15
^{75}As	7.646	7.4 ± 0.3	3/2 ⁻	1/2 ⁽⁺⁾	...	0.11	360 ± 100
^{109}Ag	7.632	9 ± 1	1/2 ⁻	3/2	...	0.7	2 ± 1
^{112}Cd	7.632	4.8 ± 0.4	0 ⁺	1 ⁻	$E1$	0.55	86 ± 15
^{129}La	6.013	8.2 ± 0.6	7/2 ⁺	7/2 ⁺	$E1$	0.50	51^{+14}_{-10}
^{141}Pr	7.632	$11.4^{+0.1}_{-0.3}$	5/2 ⁺	5/2 ⁺	$M1$	0.46	72^{+14}_{-10}
^{205}Tl	7.646	9.3 ± 0.3	1/2 ⁺	1/2 ⁽⁻⁾	...	0.58	980 ± 90
^{208}Pb	7.279	7.1 ± 0.3	0 ⁺	1 ⁻	$M1$	1.00	780 ± 60

TABLE IV. Effective elastic scattering cross section $\langle\sigma_r\rangle = \sigma_0 (\Gamma_0/\Gamma_\gamma) \Psi(x_0, t_0)$, where δ , J , Γ_0 , Γ_γ were taken from Table III. The temperature of the scatterer was 300°K, while that of the iron γ source was 640°K.

Target	Resonance energy (MeV)	$\langle\sigma_r\rangle$ (mb)
^{59}Cr	8.888	905
^{62}Ni	7.646	569
^{74}Ge	6.013	61
^{75}As	7.646	4.4
^{109}Ag	7.632	3.5
^{112}Cd	7.632	193
^{129}La	6.013	39
^{141}Pr	7.632	20
^{205}Tl	7.646	574
^{208}Pb	7.279	5560

METHOD

REF. NO.

[Page 1 of 2]

70 Mo 3

hmg

REACTION	RESULT	EXCITATION ENERGY	SOURCE		DETECTOR		ANGLE
			TYPE	RANGE	TYPE	RANGE	
G,G	LFT	6	D	6	NAI-D	0-8	DST
		(6.018, 6.418)		(6.018, 6.418)			

J-PI; 6.018, 6.418

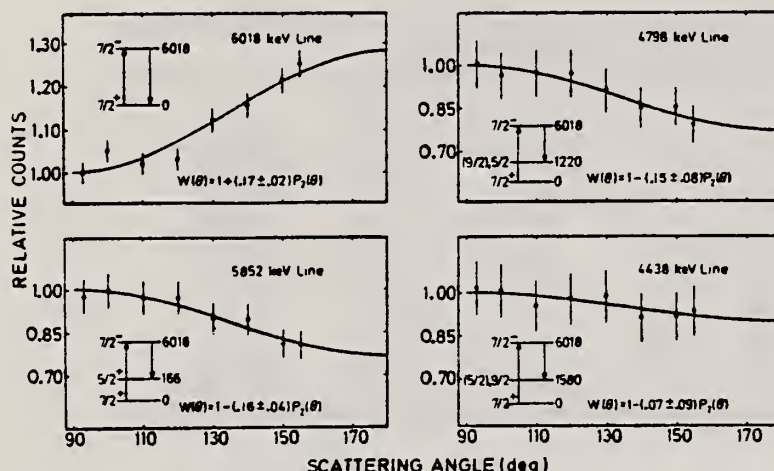


FIG. 4. Angular distribution of some intense γ lines scattered by ^{138}La using a γ source obtained from the $\text{Fe}(\text{n},\gamma)$ reaction; a 20-cc Ge(Li) detector was used. The solid lines have the form $W(\theta) = 1 + AP_2(\cos\theta)$ and are least-squares fits to the experimental distributions. In each case the corresponding γ - γ cascade is indicated.

The values of the parameters which best fitted all experiments were

$$\begin{aligned} \text{6018 keV: } & \Gamma_\gamma = 0.051^{+0.014}_{-0.006} \text{ eV}, \quad \Gamma_0/\Gamma_\gamma = 0.5, \\ & \langle \sigma_\nu \rangle = 39 \text{ mb}, \quad \delta = 8.2 \pm 0.6 \text{ eV}; \\ \text{6418 keV: } & \Gamma_\gamma = 0.081^{+0.018}_{-0.007} \text{ eV}, \quad \Gamma_0/\Gamma_\gamma = 0.78, \\ & \langle \sigma_\nu \rangle = 142 \text{ mb}, \quad \delta = 9.5 \pm 0.5 \text{ eV}. \end{aligned}$$

The values of $\langle \sigma_\nu \rangle$ are at a γ -source temperature of 380°C and a target temperature of 25°C.

[over]

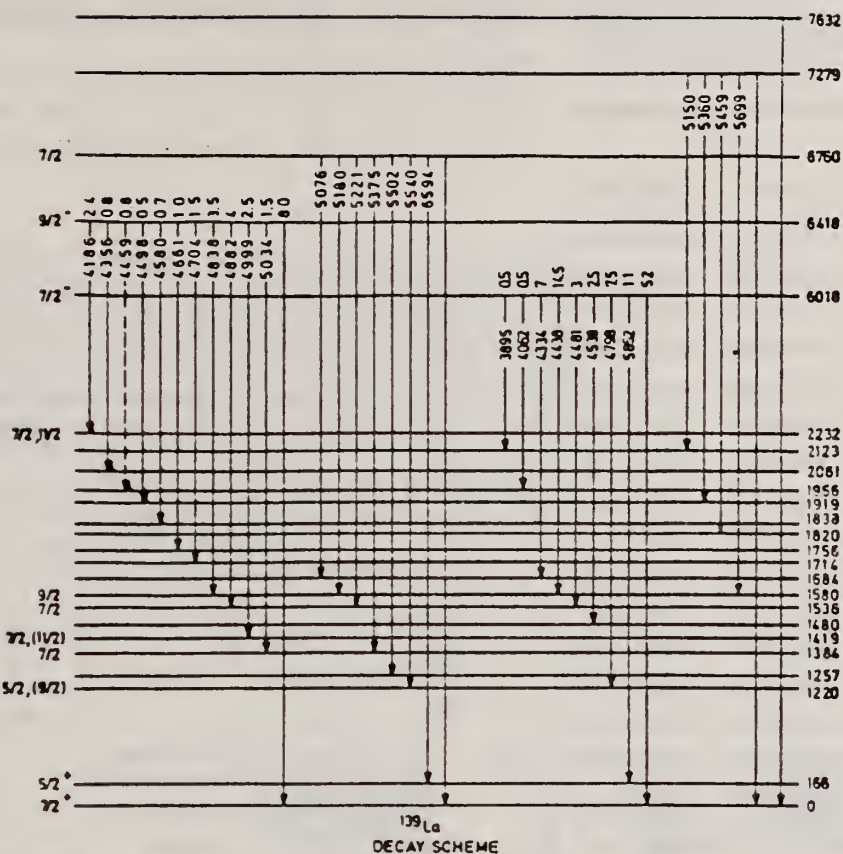


FIG. 3. Decay scheme of five resonance levels of ^{139}La showing branching ratios for only two strongly excited resonances where most of the inelastically scattered lines are believed to have been detected. Spin and parities for some levels assigned in the present work, are given. Parentheses and broken lines indicate uncertainties.

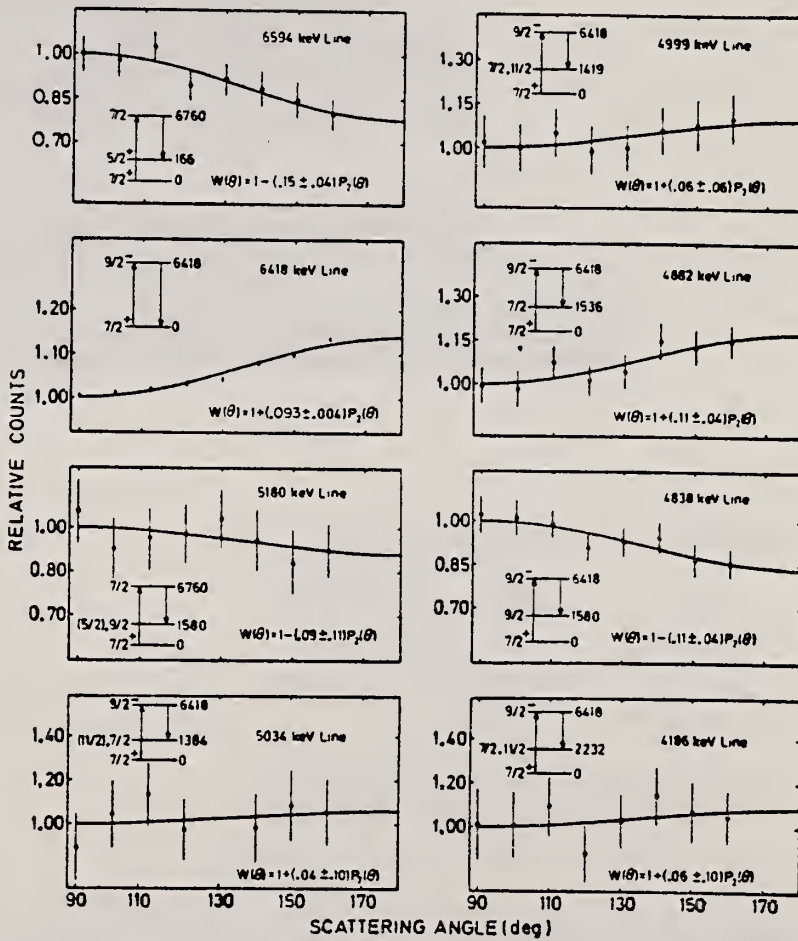
[Page 2 of 2]

TABLE V. Most probable spins and parities of levels in ^{139}La as found in the present work. Also listed are the corresponding γ -line energies, the experimental angular-distribution coefficients A , and the $M2/E1$ mixing amplitudes x . The values of x are given for more than one possible spin value. The 1580-keV level was populated by more than one resonance. Parentheses indicate uncertainties.

Level energy (keV)	Spin and parity	γ -line energy (keV)	$A + \Delta A$	x ($M2/E1$) ^a
6760	$\frac{1}{2}^-$	6594	-0.15 ± 0.04	-0.013 ± 0.056
6418	$\frac{3}{2}^-$	6418	0.093 ± 0.004	-0.001 ± 0.004
6018	$\frac{7}{2}^-$	6018	0.17 ± 0.02	-0.01 ± 0.03
166	$\frac{5}{2}^+$	5852	-0.16 ± 0.04	-0.02 ± 0.06
1220	$\frac{5}{2}^+$	4798	-0.15 ± 0.08	-0.03 ± 0.08
1220	$(\frac{3}{2})$	4798	-0.15 ± 0.08	0.15 ± 0.10
1384	$\frac{7}{2}^+$	5034	0.04 ± 0.10	0.10 ± 0.18
1419	$\frac{7}{2}^+$	4999	0.06 ± 0.06	0.06 ± 0.12
1419	$(\frac{11}{2})$	4999	0.06 ± 0.06	0.02 ± 0.14
1536	$\frac{7}{2}^+$	4882	0.11 ± 0.04	-0.03 ± 0.08
1580	$\frac{9}{2}^-$	4838	-0.11 ± 0.04	-0.09 ± 0.29
1580	$\frac{9}{2}^-$	4438	-0.07 ± 0.09	0.005 ± 0.115
1580	$\frac{7}{2}^+$	5180	-0.09 ± 0.11	0.03 ± 0.18
1580	$(\frac{5}{2})$	5180	-0.09 ± 0.11	0.07 ± 0.14
2232	$\frac{7}{2}^+$	4186	0.06 ± 0.10	0.07 ± 0.18
2232	$(\frac{11}{2})$	4186	0.06 ± 0.10	0.01 ± 0.23

^aHere it was tacitly assumed that all transitions are predominantly $E1$.

FIG. 5. Angular distributions of some intense γ lines scattered by ^{139}La using a γ source obtained from the Ti-(n,γ) reaction. See caption to Fig. 4.



METHOD

REF. NO.

70 Sz 1

egf

REACTION	RESULT	EXCITATION ENERGY	SOURCE		DETECTOR		ANGLE
			TYPE	RANGE	TYPE	RANGE	
G,G	LFT	6-9	D	6-9	SCD-D	4-9	DST

6 LEVELS

Abstract: Nuclear resonant scattering of photons from several (n,γ) reactions was used to study bound nuclear levels in the 6-9 MeV region in ^{139}La . The results obtained in the de-excitation of six resonant levels at energies 6115, 6418, 6760, 7637, 8527 and 8582 keV are presented. From the angular distribution of the elastically scattered photons, a spin of $\frac{3}{2}$ was deduced for the 6115 and 6418 keV levels. On the basis of the angular distribution of the inelastically scattered photons the following spin assignments were made for four of the low-lying levels: 1219($\frac{1}{2}$), 1421($\frac{3}{2}$ or $\frac{5}{2}$), 1687($\frac{5}{2}$) and 1770($\frac{7}{2}$). Hitherto unknown levels were found at 1894 and 2159 keV. Total radiation widths were measured and found to be 79 ± 17 meV for the 6115 keV resonant level, 45 ± 9 meV for the 6418 keV level and > 60 meV for the 6760 keV level.

NUCLEAR REACTIONS $^{139}\text{La}(\gamma, \gamma')$, $E = 6115, 6418, 6760, 7637, 8527$ and 8582 keV; measured E_γ, E' , $\sigma(E', \theta)$. ^{139}La deduced levels, J , total and partial radiation widths. Natural target, Ge(Li) detector.

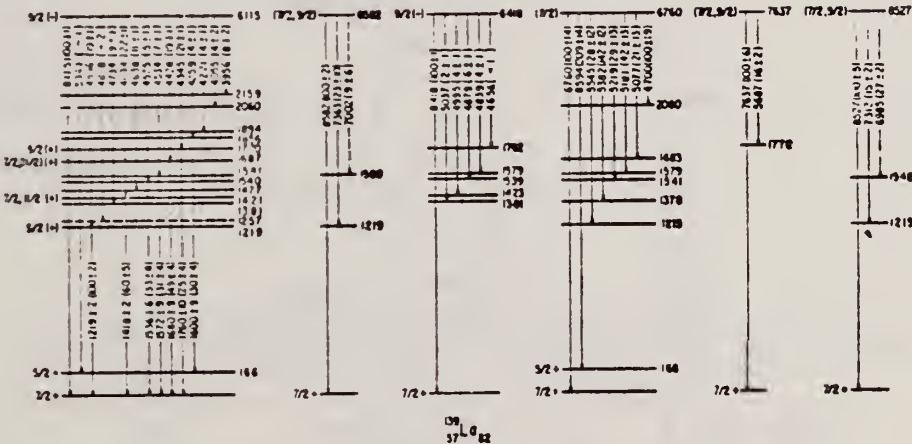


Fig. 3. Decay scheme for the observed resonant levels of ^{139}La .

H. Beil, R. Bergere, P. Carlos, A. Lepretre, A. Veyssiere and
A. Parlag
Nucl. Phys. A172, 426 (1971)

ELEM. SYM.	A	Z
La	139	57

METHOD

REF. NO.

71 Be 4

egf

REACTION	RESULT	EXCITATION ENERGY	SOURCE		DETECTOR		ANGLE
			TYPE	RANGE	TYPE	RANGE	
G,SN	368+	ABX	8-18	D	8-18	MOD-I	4PI
							366+

TABLE I
Lorentz line parameters corresponding to fits of total γ -photoneutron cross sections presented in fig. 1

	^{56}Ba	^{139}La	^{58}Ce	$^{141}_{59}\text{Pr}$	^{60}Nd	$^{141}_{59}\text{Pr}^*$
σ_1 (mb)	356 ± 15	340 ± 15	360 ± 15	350 ± 15	315 ± 15	320 ± 20
E_1 (MeV)	15.3 ± 0.1	15.2 ± 0.1	15.0 ± 0.10	15.1 ± 0.1	14.9 ± 0.1	15.16 ± 0.08
Γ_1 (MeV)	4.70 ± 0.15	4.45 ± 0.05	4.35 ± 0.05	4.26 ± 0.05	4.90 ± 0.05	4.49 ± 0.05
$\frac{1}{2}\pi\sigma_1\Gamma_1$ (MeV · b)	2.6 ± 0.15	2.35 ± 0.13	2.42 ± 0.15	2.35 ± 0.13	2.43 ± 0.13	2.42 ± 0.17
$\frac{1}{2}\pi\sigma_1\Gamma_1$ $0.06NZA^{-1}$	1.30 ± 0.08	1.16 ± 0.08	1.19 ± 0.08	1.14 ± 0.08	1.15 ± 0.08	

*) Lorentz line parameters given in ref. ¹⁰) for ^{141}Pr .

¹⁰ R. L. Bramblett, J.T. Caldwell, B.L. Berman, R.R. Harvey and S.C. Fultz, Phys. Rev. 148, 1198 (1966).

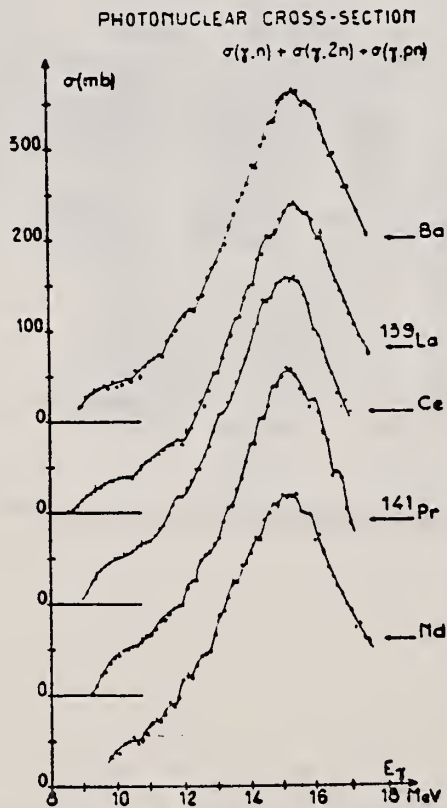


Fig. 1. Total photoneutron cross sections for Ba, ^{139}La , Ce, ^{141}Pr and Nd as a function of incident photon energy E .

METHOD

REF. NO.

71 Me 1

egf

REACTION	RESULT	EXCITATION ENERGY	SOURCE		DETECTOR		ANGLE
			TYPE	RANGE	TYPE	RANGE	
G,F	ABY	THR-900	C	300-900	FRG-I		4PI

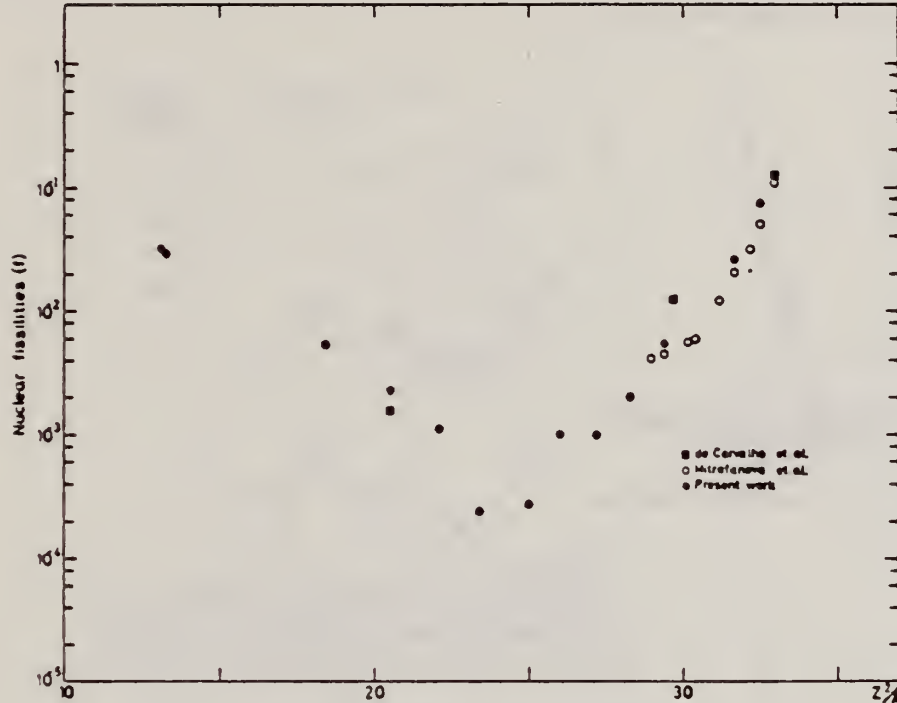


Fig. 2. Nuclear fissionabilities as a function of Z^2/A .

TABLE I
The constant fission cross sections above the threshold

Element	σ_f (cm ²)	Element	σ_f (cm ²)
Pb	$(5.0 \pm 0.2) \times 10^{-27}$	La	$(1.1 \pm 0.1) \times 10^{-29}$
Au	$(1.7 \pm 0.1) \times 10^{-27}$	Sn	$(4.3 \pm 1.1) \times 10^{-29}$
Ta	$(3.3 \pm 0.2) \times 10^{-28}$	Ag	$(8.4 \pm 2.0) \times 10^{-29}$
Yb	$(1.2 \pm 0.2) \times 10^{-28}$	Mo	$(1.7 \pm 0.4) \times 10^{-28}$
Ho	$(5.5 \pm 0.3) \times 10^{-29}$	Cu	$(6.6 \pm 1.2) \times 10^{-28}$
Gd	$(5.3 \pm 0.8) \times 10^{-29}$	Ni	$(5.8 \pm 0.1) \times 10^{-28}$
Nd	$(1.3 \pm 0.2) \times 10^{-29}$		

[over]

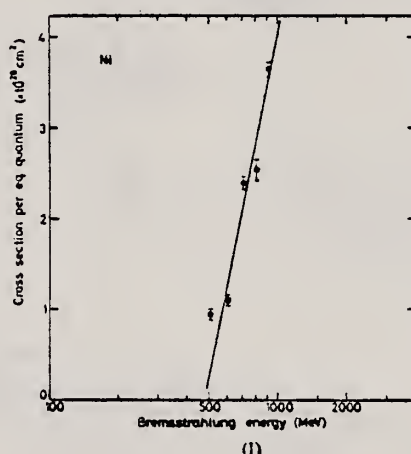
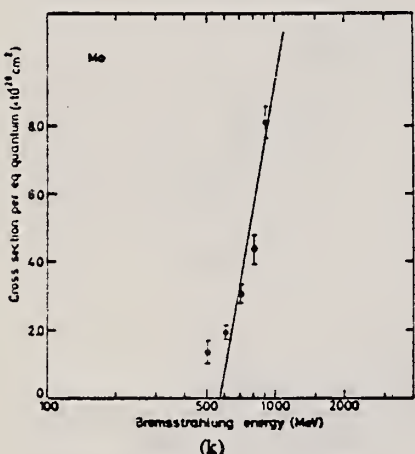
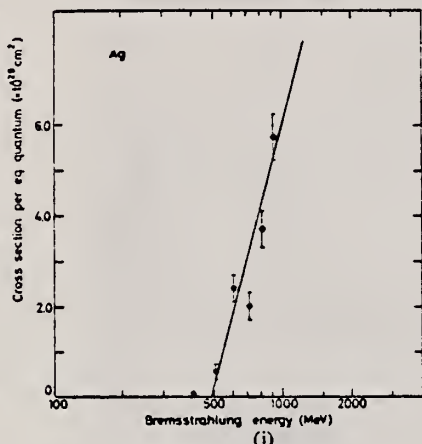
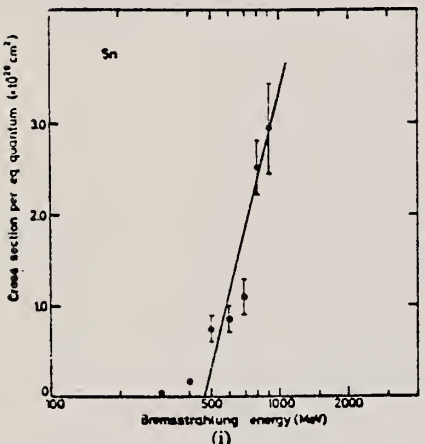
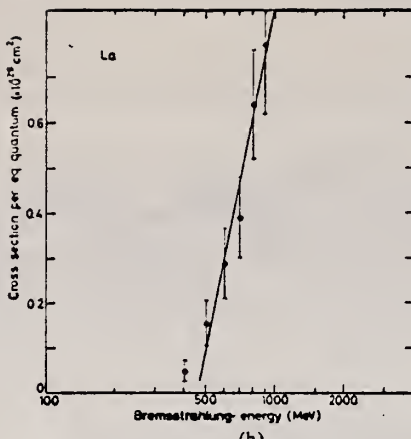
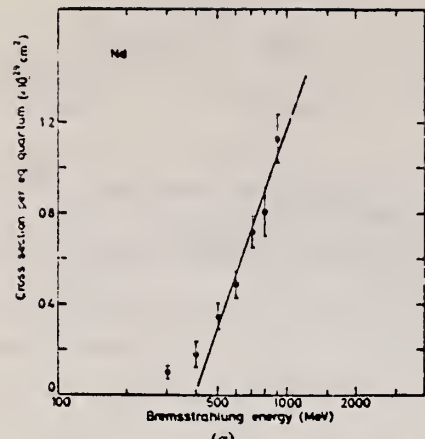


Fig. 1. Cross sections per equivalent quantum $\sigma_q(E)$ as a function of $\log E$.

ELEM. SYM.	A	Z
La	139	57

METHOD

REF. NO.

71 Pi 1

egf

REACTION	RESULT	EXCITATION ENERGY	SOURCE		DETECTOR		ANGLE
			TYPE	RANGE	TYPE	RANGE	
E, E/	SPC	4-18		50,65	MAG-D		DST

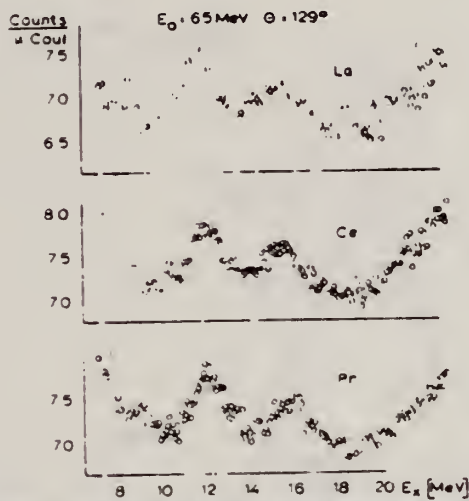


Fig. 2. Spectra of electrons scattered inelastically from La, Ce and Pr targets at the same primary energy and the same laboratory scattering angle. No background has been subtracted. Note the suppressed zeros of the ordinate scales.

METHOD

REF. NO.

72 De 3

egf

REACTION	RESULT	EXCITATION ENERGY	SOURCE		DETECTOR		ANGLE
			TYPE	RANGE	TYPE	RANGE	
G, xn	ABX	9-24	C	8-24	BF ₃ -I		4PI

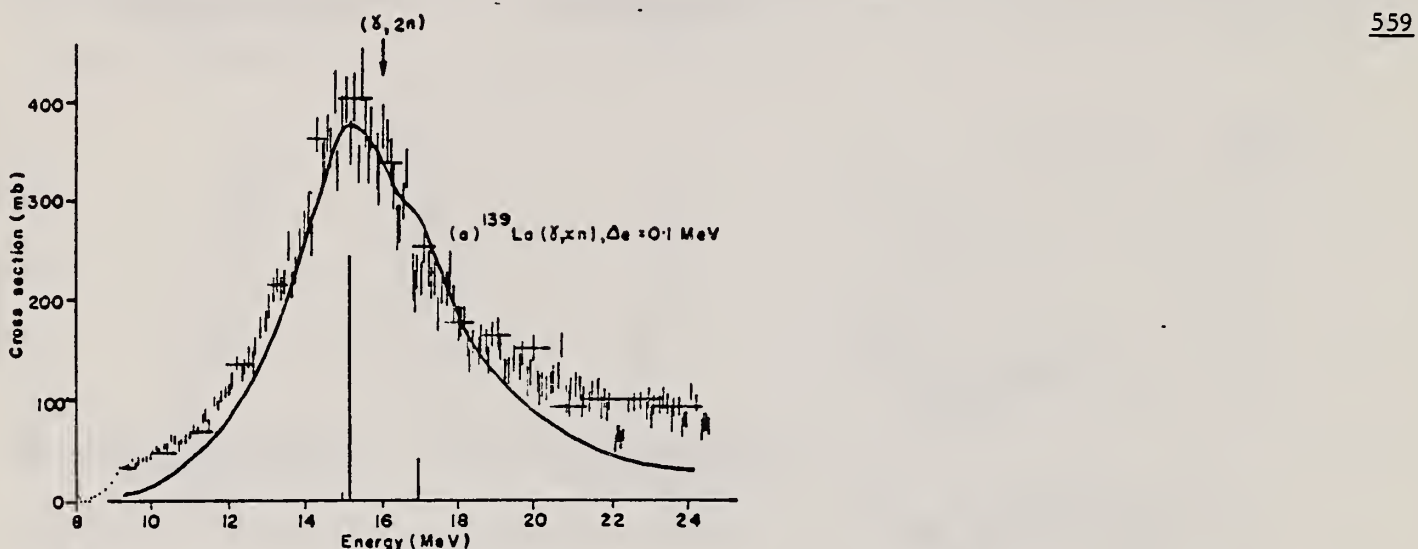


TABLE I
The integrated $^{139}\text{La}(\gamma, \text{xn})$ and $^{141}\text{Pr}(\gamma, \text{xn})$ cross sections and their minus-first and minus-second moments, compared with the appropriate sum rules

Nucleus	Ref.	σ_0 (mb · MeV)	$0.06 NZA^{-1}$	σ_{-1} (mb)	$0.16 A^3$	σ_{-2} (mb · MeV $^{-1}$)	$0.00225 A^4$
^{139}La	present work	2.51 ± 0.5	2.02	158 ± 30	115	10.4 ± 2	8.4
	ref. ²⁰⁾	2.20 ± 0.3		141 ± 12		9.4 ± 0.7	
^{141}Pr	present work	1.84 ± 0.3	2.06	121 ± 20	117	8.1 ± 1.3	8.6
	ref. ¹⁹⁾	1.83 ± 0.16					

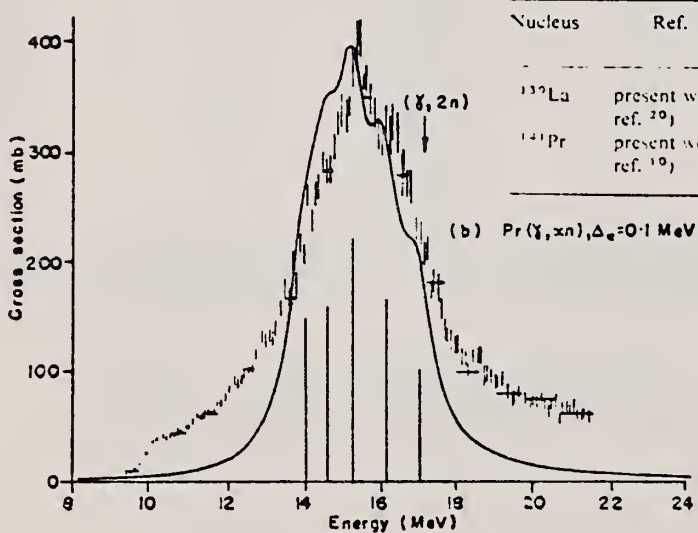


Fig. 1. (a) The $^{139}\text{La}(\gamma, \text{xn})$ cross section, obtained by VBPL unfolding from yield data measured in 0.1 MeV steps. Also shown is the DCM dipole spectrum for ^{142}Nd , and a fit to it of Lorentz line shapes with widths 4.0 MeV (solid line). (b) The $^{141}\text{Pr}(\gamma, \text{xn})$ cross section, obtained by VBPL unfolding from yield data measured in 0.1 MeV steps. Also shown is the DCM dipole spectrum for ^{146}Nd , and a fit to it of Lorentz line shapes with widths 1.0 MeV (solid line).

ELEM. SYM.	A	Z
La	139	57

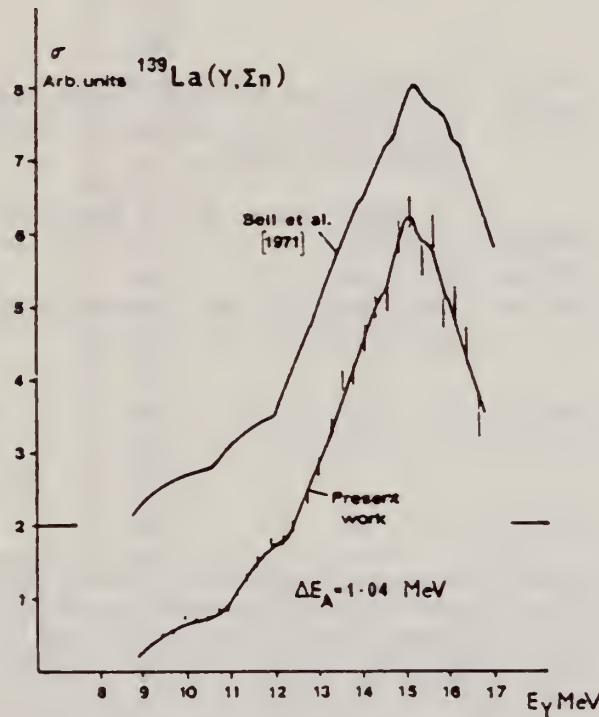
METHOD

REF. NO.

72 Th 2

egf

REACTION	RESULT	EXCITATION ENERGY	SOURCE		DETECTOR		ANGLE
			TYPE	RANGE	TYPE	RANGE	
G,XN	RLX	9-17	C	8-16	BF3-I		4PI

Fig. 7. Cross section for $^{139}\text{La}(\gamma, \Sigma n)$.

ELEM. SYM.	A	Z
La	139	57

METHOD

REF. NO.

73 Ba 20

egf

REACTION	RESULT	EXCITATION ENERGY	SOURCE		DETECTOR		ANGLE
			TYPE	RANGE	TYPE	RANGE	
G,N	NOX	THR- 27	C	10- 27	BF3-I		4PI

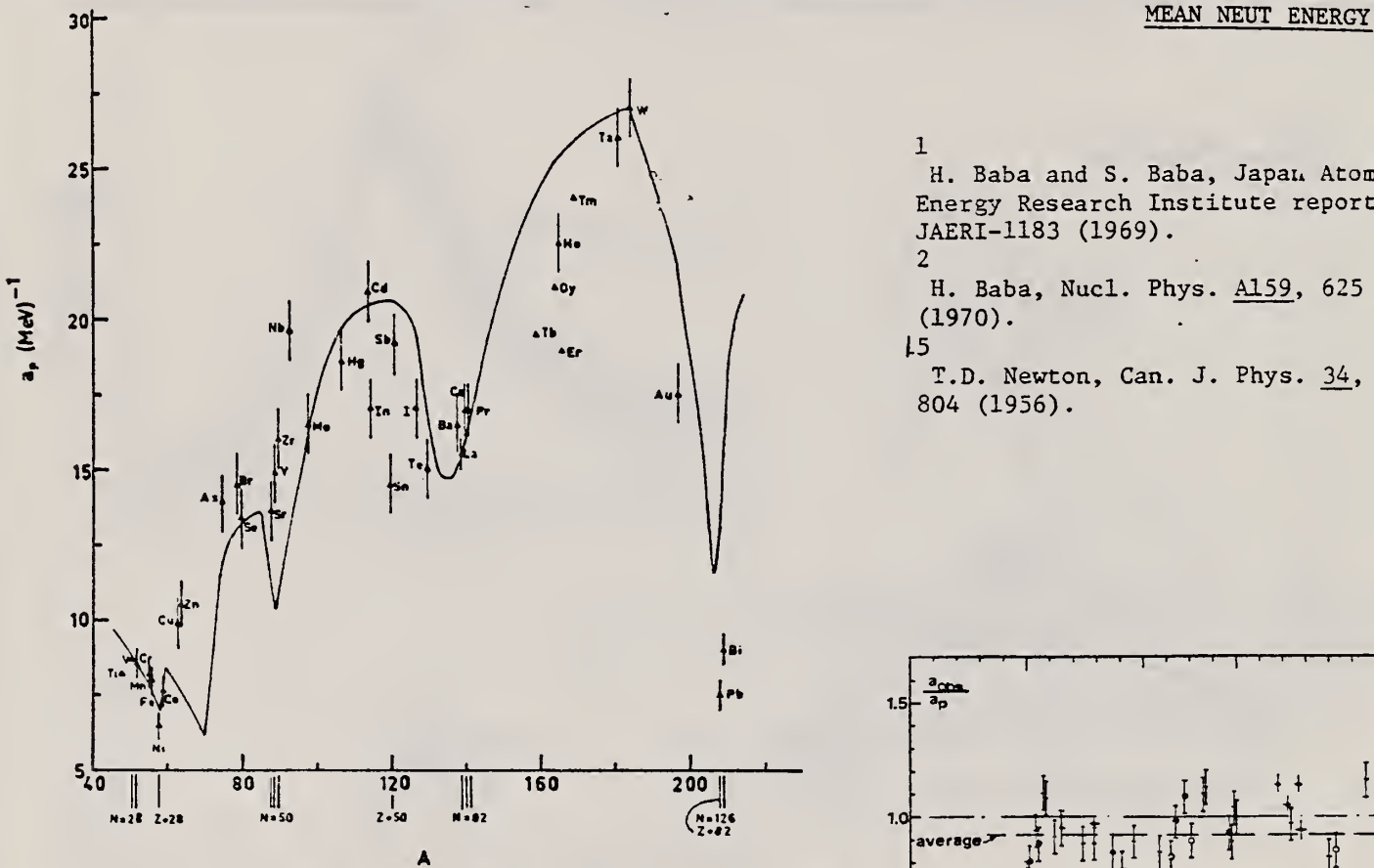


Fig. 12. Experimental values of the level density parameter a_p (Fermi gas formula plus pairing correction) versus atomic number A . The continuous curve is a least-squares fit to the data of a theoretical calculation from Newton ¹⁵.

- 1 H. Baba and S. Baba, Japan Atomic Energy Research Institute report JAERI-1183 (1969).
 2 H. Baba, Nucl. Phys. A159, 625 (1970).
 15 T.D. Newton, Can. J. Phys. 34, 804 (1956).

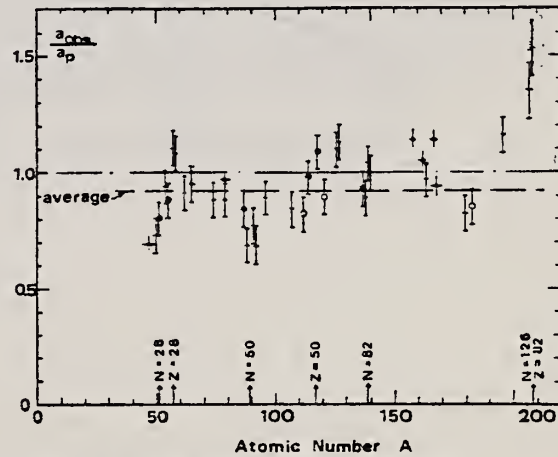


Fig. 15. Ratio a_{00}/a_p versus atomic number A . Here a_{00} is the level density parameter taken from the neutron resonance work of refs. ¹⁻², and a_p is the level density parameter derived from the present (γ, n) work. Filled circles represent points where nuclei in the neutron resonance and in the (γ, n) experiment were the same. Open circles represent points where the respective nuclei were approximately matched. Triangles represent points which are based on measurement of neutron mean energies at two bremsstrahlung energies only.

(over)

TABLE 3 (continued)

Target	<i>N</i> (residual nucleus) ^{a)}	Goodness of fit ^{b)}		$\hat{E}_0(24)$ (MeV) ^{c)}	<i>T</i> (MeV) ^{d)}	a_p (MeV ⁻¹) ^{e)}	a_{obs} (MeV ⁻¹) ^{f)}	a_{obs}/a_p	
		no p.c.	with p.c.						
Ba	75	1%	F	1.16	$16.5 - ^{136}\text{Ba}$	$15.39 - ^{136}\text{Ba}$	0.93		
	77	2%							
	78	7%							
	79	8%							
	80	11%							
	81	71%							
La	80	100%	F	F	1.25	0.72	$15.5 - ^{138}\text{La}$	$13.76 - ^{139}\text{La}$	0.89
Ce	81	89%	F	G	1.24	0.70	$17.0 - ^{139}\text{Ce}$	$17.8 - ^{141}\text{Ce}$	1.04
	83	11%							
Pr	81	100%	G	G	1.17	0.65	$17.0 - ^{140}\text{Pr}$	$17.05 - ^{142}\text{Pr}$	1.00
Tb ^{g)}	93	100%			1.15		$19.3 - ^{158}\text{Tb}$	$21.85 - ^{160}\text{Tb}$	1.14
Dy ^{g)}	93	2%			1.06		$20.9 - ^{161.5}\text{Dy}$	$21.9 - ^{162}\text{Dy}$	1.05
	94	19%							
	95	25%							
	96	25%							
	97	28%							
Ho	97	100%	P	G	1.06	0.56	$21.4 - ^{164}\text{Ho}$	$20.66 - ^{166}\text{Ho}$	0.97
Er ^{h)}	95	2%			1.11		$19.2 - ^{166}\text{Er}$	$21.9 - ^{166}\text{Er}$	1.14
	97	33%							
	98	23%							
	99	27%							
	101	15%							
Tm ^{g)}	99	100%			1.03		$24.0 - ^{168}\text{Tm}$	$22.58 - ^{170}\text{Tm}$	0.94
Ta	107	100%		G	1.00	0.49	$26.0 - ^{180}\text{Ta}$	$21.2 - ^{181}\text{Ta}$	0.82
W	107	26%	G	F	0.98	0.50	$27.0 - ^{183}\text{W}$	$23.0 - ^{183}\text{W}$	0.85
	108	14%							
	109	31%							
	111	28%							
Au	117	100%		G	1.19		$17.5 - ^{196}\text{Au}$	$20.24 - ^{198}\text{Au}$	1.16
Pb	123	24%		V.P.	1.87	1.20	$7.5 - ^{206}\text{Pb}$	$10.1 - ^{207}\text{Pb}$	1.35
(Z = 82)	124	23%							
	125	52%							
Bi	125	100%		F	1.65	1.03	$9.0 - ^{208}\text{Bi}$	$13.8 - ^{210}\text{Bi}$	1.53

^{a)} Neutron numbers and abundances of respective residual nuclei in (γ , n) experiments.^{b)} These give an assessment of the goodness of fit of a calculated \hat{E}_0 versus E_0 curve to the observed data, using the Fermi gas level density formula both without and with pairing corrections.^{c)} Bremsstrahlung photoneutron mean energies \hat{E}_0 for peak bremsstrahlung energy $E_0 = 24$ MeV.^{d)} Nuclear temperature from fit with constant-temperature formula.^{e)} Level density parameter a_p derived from the present (γ , n) experiment, using a Fermi gas formula plus pairing correction, and corresponding residual nucleus (the atomic weight shown is the weighted average of atomic weights of the respective isotopes present).^{f)} As column 7, but using data on n-resonance absorption from refs. ^{1, 2}.^{g)} Measurements of $\hat{E}_0(E_0)$ for these nuclei were made only for $E_0 = 21, 23$ and 24 MeV.

METHOD

REF. NO.

73 Bu 14

hmg

REACTION	RESULT	EXCITATION ENERGY	SOURCE		DETECTOR		ANGLE
			TYPE	RANGE	TYPE	RANGE	
E,E/	SPC	2- 20	C	50,65	MAG-D		DST

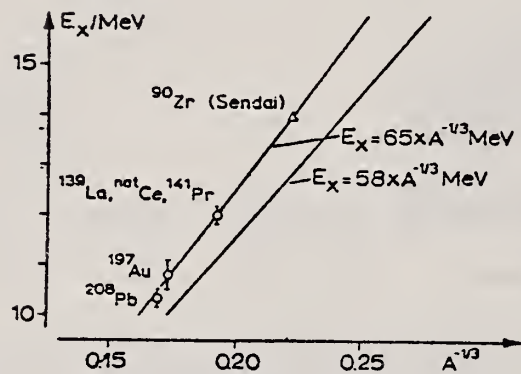


Fig. 2

part should depend on A through $E_x = 58 A^{-1/3}$ MeV. The data of Fig. 2 are consistent with $E_x = 65 A^{-1/3}$ MeV suggesting to identify the observed resonances with this type of E2 excitation.

The E2 resonance which is clearly visible at 10.8 ± 0.2 MeV exhausts more than 50 % of the sum rule. Fig. 2 shows the excitation energy of this resonance as a function of $A^{-1/3}$ for the nuclei measured at Darmstadt and the Sendai result for ⁹⁰Zr [5]. Bohr and Mottelson [9] predicted a collective E2 resonance whose isoscalar

$A^{-1/3}$ MeV. The data of Fig. 2 are

consistent with $E_x = 65 A^{-1/3}$ MeV suggesting to identify the observed reso-

nances with this type of E2 excitation.

ELEM. SYM.	A	Z
La	139	57
REF. NO.	73 Pi 3	egf

METHOD

REACTION	RESULT	EXCITATION ENERGY	SOURCE		DETECTOR		ANGLE
			TYPE	RANGE	TYPE	RANGE	
E,E/	ABX	7- 21	D	50	MAG-D		165

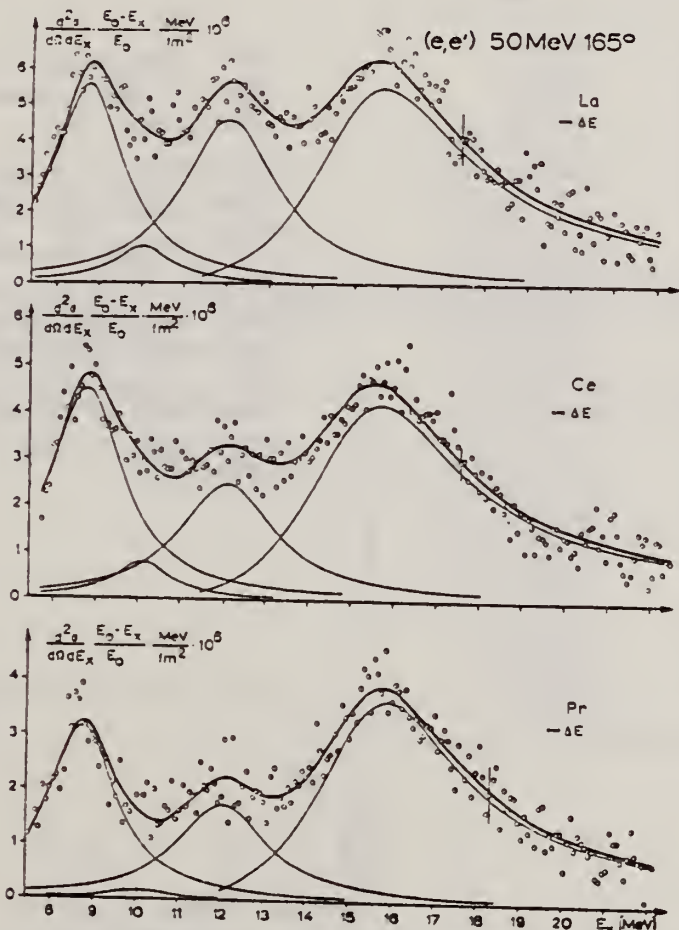


Fig. 7. Spektren von unelastisch an La, Ce und Pr gestreuten Elektronen, sonst wie Fig. 5, s. Text

ELEM. SYM.	A	Z
La	139	57

METHOD	REF. NO.	egf
	76 Em 2	
REACTION	RESULT	EXCITATION ENERGY
G, F	ABY	THR-999
		C 999
		TRK-I
		4PI

TABLE I

Measured values of σ_q at $E = 1000$ MeV and deduced values of σ_k assumed constant from E_0 to 1000 MeV999 = 1 GEV

Element	Z^2/A	σ_q (mb)	E_0 (MeV)	σ_k (mb)
Bi	32.96	12.3 ± 0.6	200	7.6 ± 0.6
Pb	32.45	5.4 ± 0.4	220	3.6 ± 0.3
Tl	32.10	4.1 ± 0.3	230	2.8 ± 0.3
Au	31.68	2.0 ± 0.15	240	1.4 ± 0.2
Pt	31.18	1.1 ± 0.08	255	$(8 \pm 0.7) \times 10^{-1}$
Re	30.21	$(3.7 \pm 0.3) \times 10^{-1}$	280	$(2.9 \pm 0.3) \times 10^{-1}$
W	29.78	$(3.5 \pm 0.3) \times 10^{-1}$	290	$(2.8 \pm 0.3) \times 10^{-1}$
Ta	29.45	$(3.3 \pm 0.3) \times 10^{-1}$	300	$(2.7 \pm 0.3) \times 10^{-1}$
Hf	29.04	$(1.7 \pm 0.2) \times 10^{-1}$	310	$(1.4 \pm 0.2) \times 10^{-1}$
Yb	28.31	$(1.3 \pm 0.1) \times 10^{-1}$	330	$(1.2 \pm 0.1) \times 10^{-1}$
Tm	28.18	$(7.5 \pm 0.8) \times 10^{-2}$	335	$(6.8 \pm 0.8) \times 10^{-2}$
Ho	27.21	$(3.6 \pm 0.4) \times 10^{-2}$	355	$(3.5 \pm 0.4) \times 10^{-2}$
Dy	26.80	$(2.6 \pm 0.3) \times 10^{-2}$	360	$(2.5 \pm 0.3) \times 10^{-2}$
Tb	26.58	$(2.5 \pm 0.3) \times 10^{-2}$	370	$(2.5 \pm 0.3) \times 10^{-2}$
Gd	26.04	$(1.6 \pm 0.2) \times 10^{-2}$	380	$(1.7 \pm 0.2) \times 10^{-2}$
Sm	25.56	$(1.3 \pm 0.2) \times 10^{-2}$	390	$(1.4 \pm 0.2) \times 10^{-2}$
Nd	24.96	$(9.2 \pm 0.9) \times 10^{-3}$	405	$(1 \pm 0.1) \times 10^{-2}$
Ce	24.00	$(8 \pm 0.9) \times 10^{-3}$	420	$(9 \pm 1) \times 10^{-3}$
La	23.39	$(8.4 \pm 0.9) \times 10^{-3}$	430	$(1 \pm 0.1) \times 10^{-3}$
Sb	21.36	$(1.2 \pm 0.2) \times 10^{-2}$	460	$(1.5 \pm 0.3) \times 10^{-2}$
Te	21.19	$(8.8 \pm 1) \times 10^{-3}$	465	$(1.2 \pm 0.2) \times 10^{-2}$
Sn	21.06	$(1.3 \pm 0.2) \times 10^{-2}$	465	$(1.7 \pm 0.3) \times 10^{-2}$
Cd	20.49	$(1.7 \pm 0.3) \times 10^{-2}$	470	$(2.2 \pm 0.4) \times 10^{-2}$
Ag	20.47	$(2 \pm 0.3) \times 10^{-2}$	470	$(2.6 \pm 0.4) \times 10^{-2}$
Zn	13.76	$(2 \pm 0.4) \times 10^{-1}$	515	$(3 \pm 0.6) \times 10^{-1}$
Cu	13.44	$(2.4 \pm 0.5) \times 10^{-1}$	515	$(3.6 \pm 0.8) \times 10^{-1}$
Ni	13.35	$(2.4 \pm 0.5) \times 10^{-1}$	510	$(3.6 \pm 0.8) \times 10^{-1}$
Fe	12.10	$(3 \pm 0.6) \times 10^{-1}$	510	$(4.4 \pm 0.9) \times 10^{-1}$

⁴A.V. Mitrofanova et al.
 Sov. J. Nucl. Phys. 6,
 512 (1968).

⁷T. Methasiri et al., Nucl.
 Phys. A167, 97 (1971).

¹²J.R. Nix et al., Nucl. Phys.
81, 61 (1966).

²⁰N.A. Perifilov et al., JETP
 (Sov. Phys.) 14, 623 (1962);
 Proc. Symp. on the physics &
 chemistry of fission, Salzburg
 1965, vol. 2 (IAEA) Vienna,
 1965, p.283.

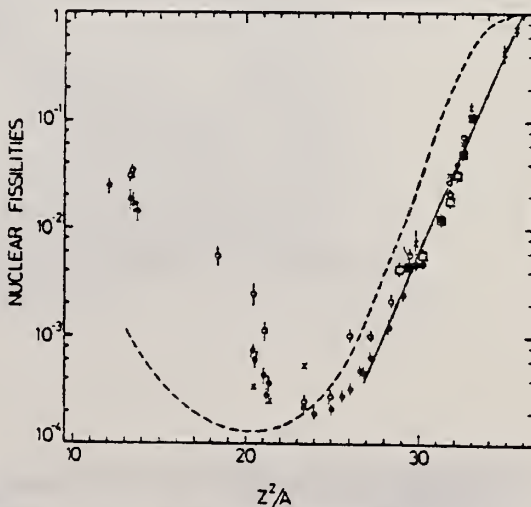


Fig. 2. Nuclear fissilities as a function of Z^2/A . Experimental points: solid circles represent our data; open squares, the data from ref. ⁴; open circles, the data from ref. ⁷; and crosses, the data from (p,f) experiments²⁰. The straight line is the best fit calculated from our data for $Z^2/A > 26$. The dashed curve is the curve VI calculated by Nix and Sassi¹².

REACTION	RESULT	EXCITATION ENERGY	SOURCE		DETECTOR		ANGLE
			TYPE	RANGE	TYPE	RANGE	
G, NA24	ABY	THR-999	C	400-999	ACT-I		4PI

999=1 GEV

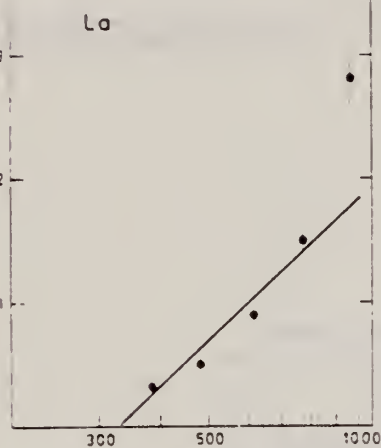


Fig. 1b Bremsstrahlung energy (MeV)

Fig. 1a-j. The measured yield as a function of bremsstrahlung end point energy. The error bars give the statistical errors in the numbers of γ -rays detected. The solid lines are fitted to the yield points with the least-squares method. The yield from Cu (Fig. 1a) is measured in [1] and has been recalculated using the monitor curve of [5]

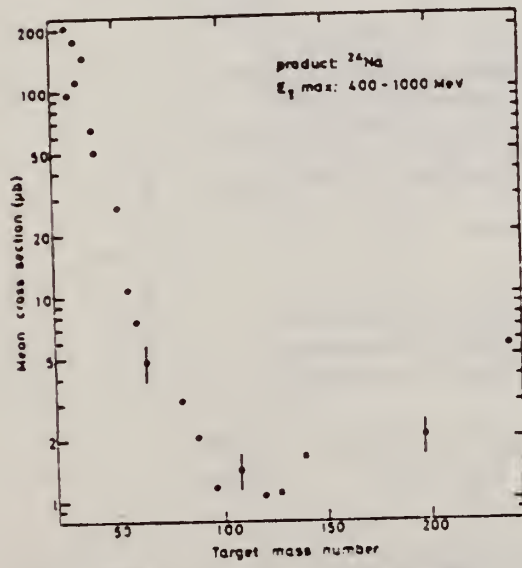


Fig. 2. The mean cross section in the energy range 400 to 1000 MeV calculated from the yields of Figure 1 in this work and of Figures 1 to 6. The errors given by bars in some points

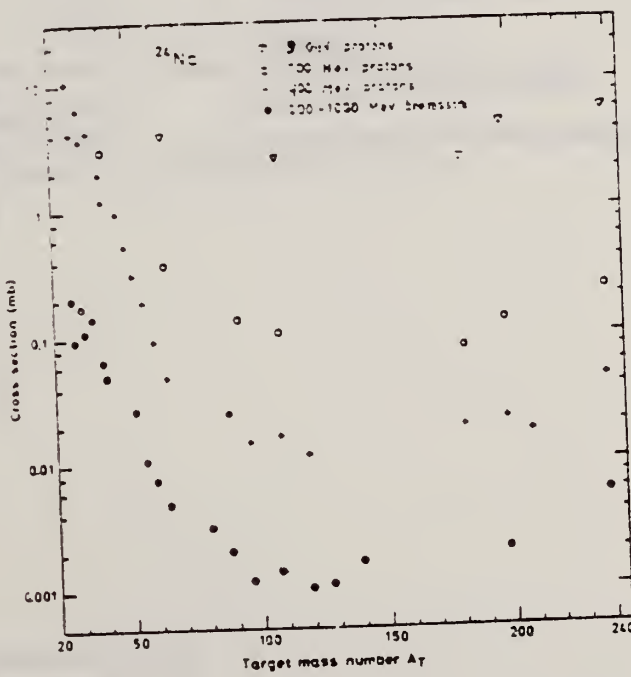


Fig. 4. Mean cross sections of the present work and of [1] (●) compared with the cross sections in proton irradiations: + 400 MeV from [4], ○ 700 MeV from [16] and an extrapolated value from [17]. ▽ 3 GeV from [18]

ELEM. SYM.	A	Z
La	139	57

METHOD	REF. NO.	
	77 Ja 4	egf

Abstract: A variable-energy γ -source is obtained by nuclear resonance scattering of neutron-capture γ -rays through various scattering angles. An energy resolution of less than 10^{-6} is obtained. Pb and Cd targets were employed to scatter the 7.279 and 7.632 MeV photons, respectively, of the neutron capture γ -rays of Fe. Variation of the angle of the resonantly scattered photons between 60° - 150° permits an energy scan of ≈ 370 eV (for Pb) and ≈ 760 eV (for Cd) in any absorber. Thus nuclear energy levels in ^{139}La , Ce, Cd and ^{209}Bi absorbers were photoexcited and the corresponding values of $g\Gamma_0$ were extracted from the measured absorption curve.

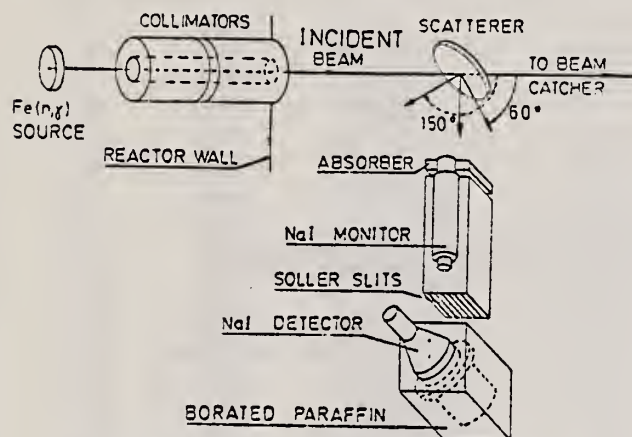


Fig. 1. Schematic diagram of the experimental arrangement.

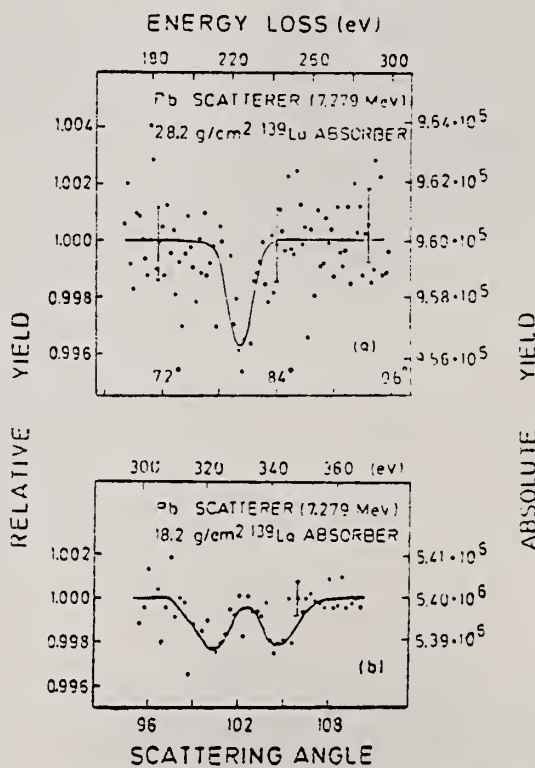


Fig. 3. (a) Portion of the normalized absorption spectrum obtained using a 28.2 g/cm^2 thick La absorber.
(b) Another portion of the spectrum obtained with a 18.2 g/cm^2 thick absorber using higher statistics of $\approx 5 \times 10^6$ counts/channel.

TABLE 2
Summary of experimental data and measured values of $g\Gamma_0$ obtained using the γ -monochromator

Isotope	Thickness (g/cm ²)	Angle of dip (deg)	ΔE *) (eV)	Effect (%)	$g\Gamma_0$ (meV)
¹¹² Cd *)	35	128.0	505	3.5	150 \pm 20
¹³⁹ La	23.2	80.0	225	0.40	8.0 \pm 2.0
¹³⁹ La	18.2	100.5	322	0.27	7.1 \pm 1.9
¹³⁹ La	18.2	104.8	345	0.22	5.5 \pm 1.8
¹⁴⁰ Ce *)	26.5	90.0	273	1.3	25 \pm 3
²⁰⁹ Pb	31.5	73.5	196	2.0	43 \pm 8
²⁰⁹ Pb*	31.5	68.8	404	1.8	92 \pm 12

The asterisk denotes a level at 7.632 MeV photoexcited by a Cd scatterer. All other levels are at 7.279 MeV and were photoexcited by a Pb scatterer.

*) The absorbing isotope was arbitrarily assumed to be ¹¹²Cd.

**) The absorbing isotope was arbitrarily assumed to be ¹⁴⁰Ce.

*) Here ΔE is the energy difference between the incident γ -line and the resonance level (assuming no recoil correction in the absorbing nucleus).

METHOD	REF. NO.	
	78 Ue 1	rs

TABLE I
Strength of the resonance in the (γ, p_0) and (γ, p) reactions on ^{139}La and ^{141}Pr , and the ratio of proton group 1 and proton group 2 emitted through the $f_{7/2}$ IAR

	$\int \sigma_{(\gamma, p_0)} dE$ ($\mu\text{b} \cdot \text{MeV}$)	$\int \sigma_{(\gamma, p)} dE$ ($\mu\text{b} \cdot \text{MeV}$)	Proton group 1 (%)	Proton group 2 (%)
^{141}Pr	44 ± 9	240 ± 30	40 ± 10	60 ± 10
^{139}La	< 5	260 ± 30	5 ± 5	95 ± 5

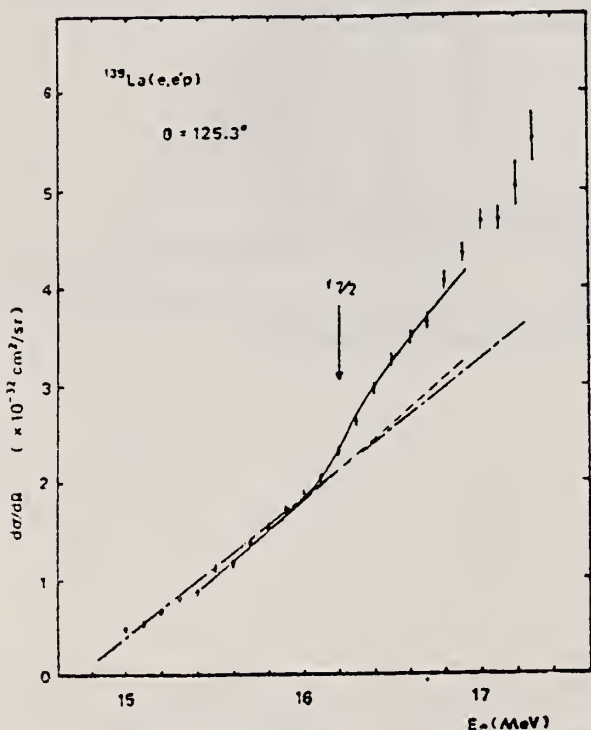


Fig. 2. The differential cross section of the $^{139}\text{La}(e, e'p)$ reaction for $\theta = 125.3^\circ$. The solid line shows the result of a least-square fitting with eq. (4). The dashed line shows the T_e part. The dash-dot line is used in order to define the position of the sudden increase as shown in fig. 6.

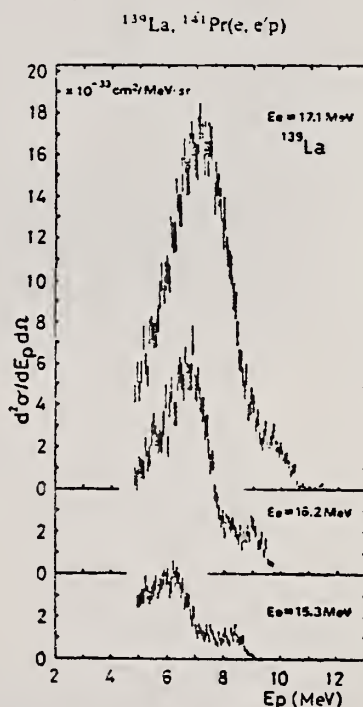


Fig. 5. The proton spectra of the $^{139}\text{La}(e, e'p)$ reactions for $\theta = 125.3^\circ$.

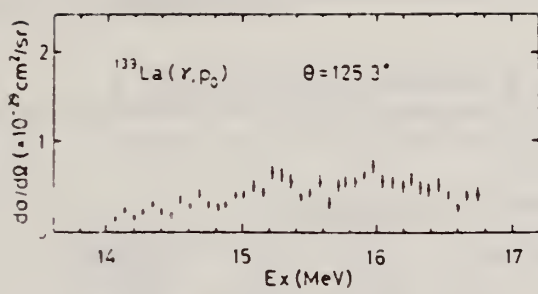


Fig. 7. The $^{133}\text{La}(\gamma, p)$ cross section

ELEM. SYM.	A	Z
La	139	57
REF. NO.		
80 Ue 1		hg

METHOD

REACTION	RESULT	EXCITATION ENERGY	SOURCE		DETECTOR		ANGLE
			TYPE	RANGE	TYPE	RANGE	
E,P	ABX	11-25	D	15-25	MAG-D		125

Abstract: The cross sections and the proton energy distributions of the (e, p) reactions on ^{139}La and ^{141}Pr have been measured around the T_2 GDR. The energies of the T_2 GDR have been given as $E_R = 21.0$ MeV in ^{139}La and $E_R = 20.4$ MeV in ^{141}Pr . The decay protons of the T_2 GDR have been studied. The proton groups which leave the residual nucleus in the neutron particle-hole states have been clearly seen in the same energy regions as the decay protons emitted through the low-lying IAR.

VIRT PHOTON ANALYSIS

E NUCLEAR REACTIONS ^{139}La , $^{141}\text{Pr}(e, p)$, $E = 15\text{--}25$ MeV; measured $\sigma(E_e)$, $\sigma(E_p)$; deduced $\sigma(\gamma, p)$ vs. E_p . Natural target.

TABLE I
Results of the energy-weighted integrated cross-section calculations

Element	E_e^* (MeV)	E_R^* (MeV)	$E_R^* - E_e^*$ (MeV)		$\sigma_{-1}^*(\text{mb})$ exp.	$\sigma_{-1}^*(\text{mb})$ theor.	$\sigma_{-1}^*/\sigma_{-1}^*(\%)$	
			exp.	theor.			exp.	theor.
^{139}La	15.2 ± 0.1 ^{b)}	21.0 ± 0.2	5.8 ± 0.3	5.83 ^{c)}	136 ^{b)}	1.01 ± 0.07	0.74	2.3 ^{c)}
^{141}Pr	15.1 ± 0.1 ^{b)}	20.4 ± 0.2	5.3 ± 0.3	5.32 ^{c)}	125 ^{b)}	1.27 ± 0.24	1.0	3.0 ^{c)}

^{a)} The notation shows $\sigma_{-1}^* = \int (\sigma_e/E)dE$, $\sigma_{-1}^* = \int (\sigma_p/E)dE$.

^{b)} Ref. ¹⁰). Integrals were carried out up to 25.0 MeV by present authors.

^{c)} Calculated by using eqs. (1) and (2) in the text Refs. ^{3,4}).

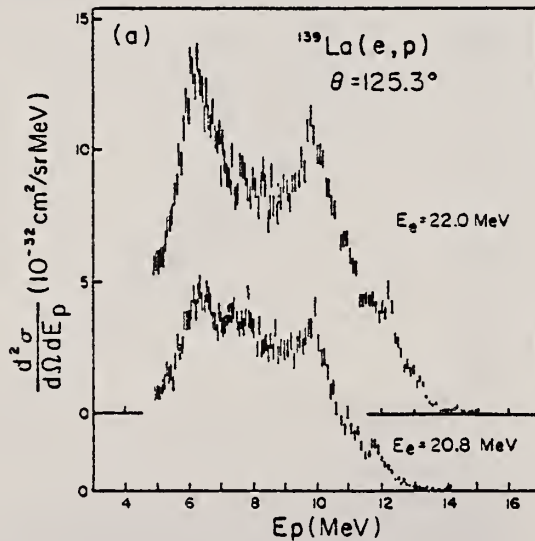


Fig. 1. The proton spectra of the (e, p) reaction at $\theta = 125.3^\circ$ laboratory. (a) ^{139}La . Bombarding energies are $E_e = 22.0$ MeV and $E_e = 20.8$ MeV, respectively. (b) ^{141}Pr . Bombarding energies are $E_e = 21.4$ MeV and $E_e = 20.2$ MeV, respectively.

OVER

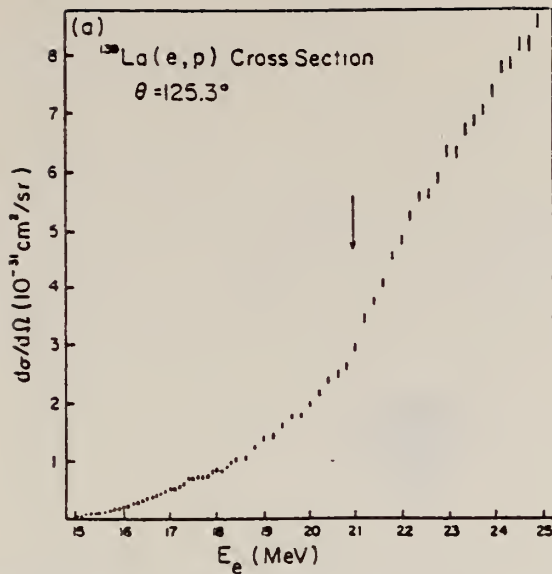


Fig. 2. The differential cross sections of the (e, p) reaction at $\theta = 125.3^\circ$ lab. The arrows show the positions of inflection caused by T_c , GDR. (a) ^{139}La . (b) ^{141}Pr .

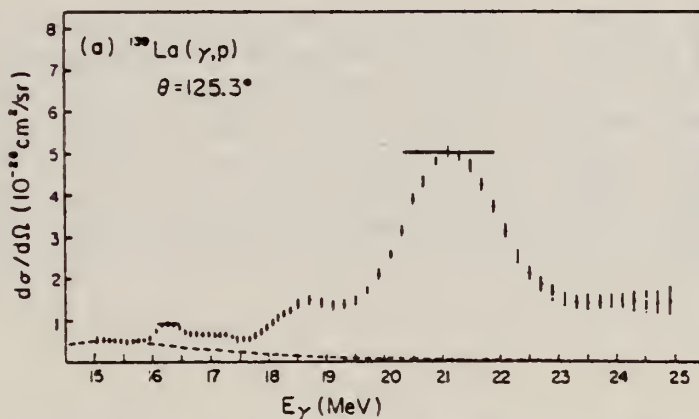


Fig. 3. The (γ , p) differential cross sections calculated from the present (e, p) differential cross section by the least structure method [ref. 1)]. The broken lines indicate assumed contribution of the T_c GDR to the (γ , p) cross section. (a) ^{139}La . (b) ^{141}Pr .

CERIUM

Z=58

Cerium was discovered in 1803 by J. Berzelius and W. Hisinger working together as well as by M. Klaproth working separately. An interesting alloy of cerium is misch metal which contains 50% cerium, 25% lanthanum, and various other rare earths as well as iron. It is this material, used in lighter flints, that produces the shower of sparks. It is also used in making tracer bullets that ignite from the friction of the air and display the bullet's trajectory.

ELEM. SYM.	A	Z
Ce		58

THOO
 Betatron; ion chamber

REF. NO.
 58 Fu 1 NVB

REACTION	RESULT	EXCITATION ENERGY	SOURCE		DETECTOR		ANGLE
			TYPE	RANGE	TYPE	RANGE	
G, XN	ABY	7-40	C	7-40	BF ₃ -I		4PI

TABLE I Target properties and results.

Element	Form used	Weight grams	$\sigma^*(\gamma, n)$ barns	$\frac{S \cdot dE}{NZ/A}$ Mev-b	" Γ " Mev
Sn	Sn	4.81	0.30	0.064	5.0
I	I	8.55	0.36	0.035	6.0
La	La	10.43	0.34	0.063	5.2
Ce	Ce	4.99	0.45	0.080	4.5
Sm	Sm ₂ O ₃	2.90	0.26	0.073	8.6
Tb	Tb ₂ O ₃	3.04	0.39	0.087	8.7
Ho	Ho ₂ O ₃	1.87	0.41	0.079	7.5
Er	Er ₂ O ₃	5.41	0.50	0.100	8.5
Yb	Yb ₂ O ₃	3.57	0.50	0.090	7.0
Ta	Ta	8.41	0.49	0.077	6.0
Au	Au	3.16	0.68	0.085	4.2
Pb	Pb	8.05	0.75	0.081	3.8

^a $\sigma^*(\gamma, n)$ is the maximum value and " Γ " the full width at $\sigma^*(\gamma, n)/2$ of the neutron production cross section corrected for multiple neutron emission. Data were not fitted with resonance lines to determine these values.

^b Integrated neutron production cross sections corrected for multiple neutrons above ($\gamma, 2n$) threshold.

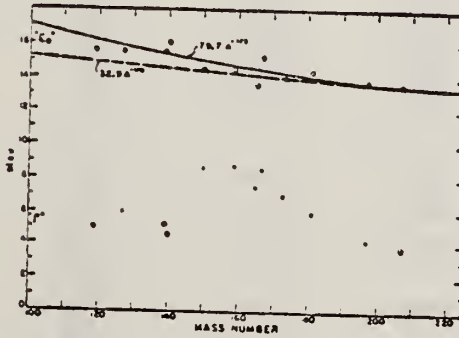


FIG. 6. Mean energy and width of giant resonances. " E_0 " and " Γ " are the mean energy for photon absorption and the full width at half maximum of the giant resonance obtained from dashed histograms as in Fig. 5. No attempt was made to fit data with resonance curves to obtain these parameters.

REF.

F. I. Havlicek
Nuovo Cimento 13, 969-73 (1959)

ELEM. SYM.	A	Z
Ce		58

METHOD

REF. NO.

Betatron

59 Ha 2

NVB

REACTION	RESULT	EXCITATION ENERGY	SOURCE		DETECTOR		ANGLE
			TYPE	RANGE	TYPE	RANGE	
G,A	SPC	THR - 30	C	30	EMU-D	2 - 5	DST

CHEM. SYM.	A	Z
Ce		
	58	

METHOD Betatron; fast neutron yield angular distribution; Si threshold detector; ion chamber

REF. NO.

61 Ba 2

NVB

REACTION	RESULT	EXCITATION ENERGY	SOURCE		DETECTOR		ANGLE
			TYPE	RANGE	TYPE	RANGE	
G, XN	ABY	THR-22	C	22	THR-I	5+	DST

In Table 4:

$\bar{\sigma}$ = average cross section of detector weighted with neutron spectrum

μ = neutrons/10C roentgen/mole

$$\bar{\sigma} = \frac{1}{\mu} \sum_{n=1}^{\infty} [1 + A_n P_n (\cos \theta)]$$

TABLE IV

I Element	II a_0	III a_1	IV a_2	V $(\bar{\sigma}\Phi) \times 10^{40}$	VI $\Phi_{\text{total}} (22 \text{ Mev}) \times 10^3$	VII $\Phi_{\text{total}} / \Phi_{\text{beam}}$
Vanadium	245 (1 ± 0.06)	0.01 ± 0.08	-0.00 ± 0.10	6.05	0.21	0.12
Chromium	164 (1 ± 0.03)	0.04 ± 0.04	-0.05 ± 0.05	4.05	0.17	0.10
Manganese	308 (1 ± 0.02)	0.07 ± 0.03	-0.09 ± 0.04	7.61	0.25	0.12
Iron	200 (1 ± 0.03)	0.05 ± 0.04	-0.17 ± 0.05	4.94	0.18	0.11
Cobalt	390 (1 ± 0.02)	0.08 ± 0.03	-0.22 ± 0.04	9.63	0.26	0.15
Nickel	145 (1 ± 0.05)	0.07 ± 0.07	-0.23 ± 0.09	3.58	0.13	0.12
Copper	347 (1 ± 0.02)	0.05 ± 0.03	-0.20 ± 0.04	8.57	0.30	0.12
Arsenic	482 (1 ± 0.03)	0.11 ± 0.04	-0.24 ± 0.05	11.91	0.33	0.15
Rubidium	638 (1 ± 0.05)	0.13 ± 0.06	-0.14 ± 0.08	15.76		
Strontium	409 (1 ± 0.03)	0.10 ± 0.06	-0.17 ± 0.08	10.10		
Yttrium	290 (1 ± 0.10)	0.08 ± 0.12	-0.12 ± 0.15	7.16		
Silver	590 (1 ± 0.04)	0.10 ± 0.06	-0.22 ± 0.08	14.57	0.87	0.07
Cadmium	905 (1 ± 0.02)	0.02 ± 0.02	-0.26 ± 0.03	22.35		
Iodine	1133 (1 ± 0.03)	0.04 ± 0.04	-0.29 ± 0.05	27.99	1.42	0.08
Barium	1048 (1 ± 0.04)	0.10 ± 0.06	-0.38 ± 0.08	25.80		
Lanthanum	1595 (1 ± 0.02)	0.02 ± 0.03	-0.42 ± 0.04	30.40	1.04	0.15
Cerium	1316 (1 ± 0.05)	0.05 ± 0.06	-0.39 ± 0.08	32.50		
Dysprosium	1652 (1 ± 0.05)	0.04 ± 0.10	-0.34 ± 0.13	40.80		
Tantalum	1558 (1 ± 0.02)	0.04 ± 0.03	-0.22 ± 0.04	38.48	2.50	0.06
Tungsten	1365 (1 ± 0.02)	-0.07 ± 0.03	-0.24 ± 0.04	33.71		
Mercury	1345 (1 ± 0.02)	0.04 ± 0.03	-0.31 ± 0.04	33.22		
Lead	2274 (1 ± 0.01)	0.02 ± 0.02	-0.42 ± 0.03	50.17	2.72	0.08
Bismuth	2162 (1 ± 0.02)	0.05 ± 0.03	-0.45 ± 0.04	53.40	3.34	0.06
Thorium	3031 (1 ± 0.04)	0.00 ± 0.05	-0.32 ± 0.07	74.87		
Uranium	4630 (1 ± 0.02)	0.05 ± 0.03	-0.17 ± 0.04	114.33		

$\Phi(\Phi) = 2.47 \times 10^4 \text{ es}$ millibars-neutron. Errors are standard errors due to counting statistics only.

REF. J. Miller, C. Schuhl, C. Tzara
J. Phys. Radium 22, 529 (1961)

ELEM. SYM.	A	Z
Ce		58

METHOD

Positron annihilation; neutron cross section; BF_3 counter;
ion chamber

REF. NO.	NVB
61 Mi 1	

REACTION	RESULT	EXCITATION ENERGY	SOURCE		DETECTOR		ANGLE
			TYPE	RANGE	TYPE	RANGE	
G,XN	ABX	8-21	D	8-21	$\text{BF}_3\text{-I}$		4PI

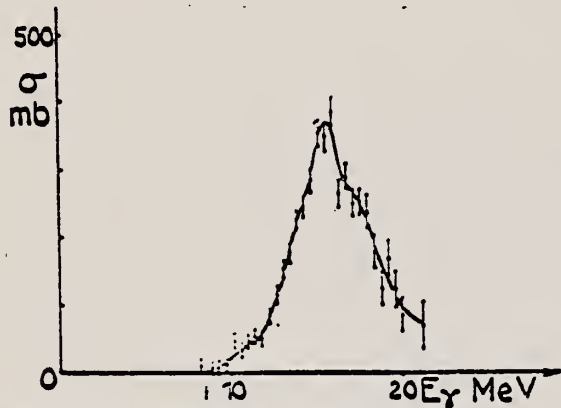


FIG. 4b. — Cerium, $\sigma(\gamma, n) + 2\sigma(\gamma, 2n) + \sigma(\gamma, np) + \dots$

Elem. Sym.	A	Z
Ce		58

Method	Ref. No.
Linac; monoenergetic photons by e^+ annihilation in flight; NaI monitor; γ BF ₃ detector	62 Mi 3

Reaction	E or ΔE	E_0	Γ	$\int \sigma dE$	$J\pi$	Notes
Ce (γ, xn)	10-21.2	15.6 ± 0.5		21.2 $\int = 1.88 \pm 0.03$ θ MeV-b		

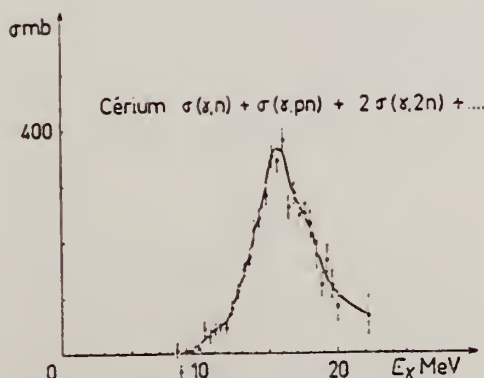


Fig. 8. Section efficace
 $\sigma = \sigma(\gamma, n) + \sigma(\gamma, np) + 2\sigma(\gamma, 2n) + \dots$ pour le céryum.

TABLEAU 5
 Résultats expérimentaux

Éléments	Fig. No.	E_0 (MeV)	σ_{stat} (MeV · b) ^a	σ_{stat} 0.06 N/Z/A	γ, n	γ, p	$\gamma, 2n$	Seuls γ, np
Cu	6	17 ± 0.5	0.45 ± 0.013	0.47 ± 0.013				
La	7	15.6 ± 0.5	1.91 ± 0.03	0.94 ± 0.013				
Ce {	9	15.6 ± 0.5	1.88 ± 0.03	0.92 ± 0.013	$9.05^{(1)}$	$8.50^{(1)}$	$14.1^{(1)}$	
140					$7.15^{(1)}$	$9.50^{(1)}$	$14.3^{(1)}$	
142								
Ta 181	9	13 ± 0.5	2.97 ± 0.05	1.13 ± 0.02	$7.55^{(1)}$		$13.84^{(1)}$	$13.47^{(1)}$
			16.3 ± 0.5					
Au 197	10	14.2 ± 0.5	3.00 ± 0.05	1.06 ± 0.02	$7.90^{(1)}$		$13.71^{(1)}$	$12.94^{(1)}$
206					$10.8^{(1)}$	$7.1^{(1)}$	$14.3^{(1)}$	$14.5^{(1)}$
Pb {	11	13.8 ± 0.5	4.10 ± 0.06	1.38 ± 0.02	$7.2^{(1)}$	$9.2^{(1)}$	$14.3^{(1)}$	$17.9^{(1)}$
207					$6.9^{(1)}$	$9.6^{(1)}$	$15.0^{(1)}$	$14.2^{(1)}$
208								
Bi 209	12	14.0 ± 0.5	3.73 ± 0.06	1.24 ± 0.02	$7.44^{(1)}$	$3.78^{(1)}$	$10.4^{(1)}$	

^a) L'intégrale $\int_0^\infty \sigma dE$ est prise jusqu'à x égal à 19.6 MeV pour Cu, à 21.2 MeV pour La et Ce et à 22 MeV pour Ta, Au, Pb et Bi. D'autre part, les erreurs indiquées sont les erreurs statistiques.

REF.

R.B. Begzhanov and A.A. Islamov

Zhur. Eksp. i Teoret. Fiz. 46, 1486-1488 (1964)Soviet Phys. JETP 19, 1005 (1964)

ELEM. SYM.

Ce

Z

58

METHOD

Radioactive source La ¹⁴⁰; resonance scattering cross section,
self-absorption

REF. NO.

64 Be 4

NVB

REACTION	RESULT	EXCITATION ENERGY	SOURCE		DETECTOR		ANGLE
			TYPE	RANGE	TYPE	RANGE	
G,G	LFT	2 (1.597)	D	2 (1.597)	NAI-D		120

$$\text{Average resonance scattering cross section} = (3.7 \pm 0.4) \times 10^{-26} \text{ cm}^2$$

$$\text{Lifetime of 1.597 MeV state} = (2.15 \pm 0.080) \times 10^{-13} \text{ sec.}$$

METHOD

REF. NO.

Nuclear Resonance Scattering using N,G reactions.

66 Be 3

JDM

REACTION	RESULT	EXCITATION ENERGY	SOURCE		DETECTOR		ANGLE
			TYPE	RANGE	TYPE	RANGE	
G,G	RLX	5 - 10	D	5 - 10	NAI-D	5 - 10	135

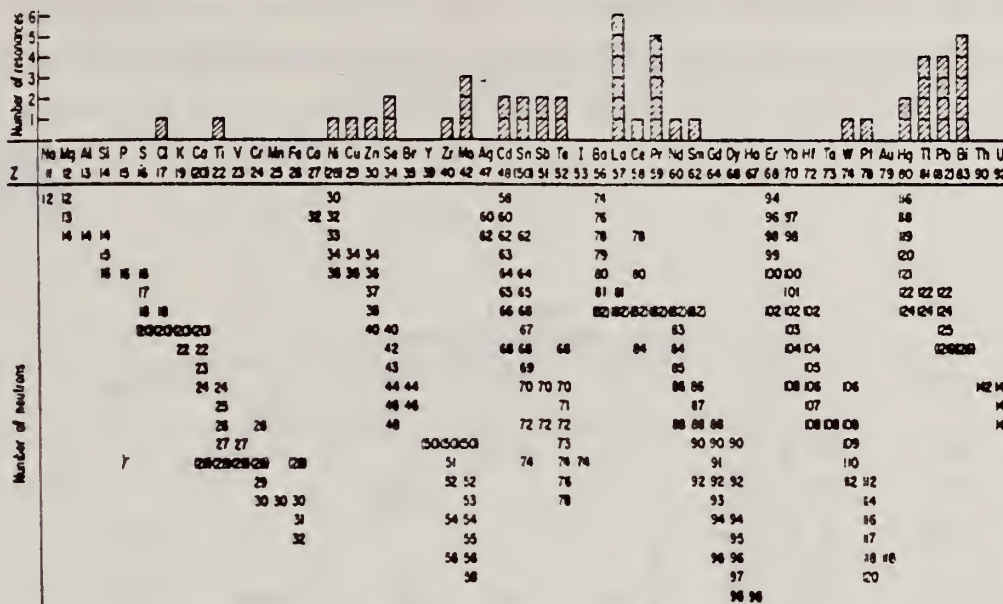


FIG. 3. Histogram of distribution of observed resonances among the different targets. The atomic number is given directly beneath the chemical symbol followed by the neutron numbers of the naturally occurring isotopes. Magic numbers are shown in brackets.

TABLE III. List of effective cross sections.

Scatterer	Energy (MeV)	Gamma source	δ (mb)	Scatterer	Energy (MeV)	Gamma source	δ (mb)
Sm ¹⁴⁴	8.997	Ni	100	Sn	7.01	Cu	11.0
Pr ¹⁴⁴	8.481	Cr	9	Nd	6.867	Co	30
La	8.532	Ni	6	Pr ¹⁴⁴	6.867	Co	3
Te	8.532	Ni	3*	Te	6.7	Ni	..
Cu	8.499	Cr	24	La	6.54	Ag	12
Zr	8.496	Se	3050	Cd	6.474	Co	110
Zn	8.119	Ni	13	Mo	6.44	Hg	254
Se	7.817	Ni	50	La	6.413	Tl	72
Se	7.76	K	90	Mo	6.413	Tl	10
Sb	7.67	V	..*	Tl	6.413	Tl	25
Cr	7.64	Fe	40*	W	~6.3	Ti	..*
Ni	7.64	Fe	7*	Sb	6.31	Hg	6*
Pr ¹⁴⁴	7.64	Fe	12*	Ti	6.31	Hg	2*
Tl	7.64	Fe	370*	Sn	6.27	Ag	75
La	7.614	Cu	7	Pb ²⁰⁸	6.15	Gd	..*
Mo	7.634	Cu	11	Te	5.8	Ni	..
Pr ¹⁴⁴	7.634	Cu	4	La	6.12	Cl	35
Te	7.528	Ni	664	Pr ¹⁴⁴	6.12	Cl	110
Bi ²⁰⁸	7.416	Se	100	Pt	5.99	Hg	40*
Bi ²⁰⁸	7.300	As	30*	Tl	5.99	Hg	5*
Pb ²⁰⁸	7.285	Fe	4100	Pb ²⁰⁸	5.9	Sr	..*
Cl	7.285	Fe	34	Ce	5.646	Co	17
Pr ¹⁴⁴	7.185	Se	80	Bi ²⁰⁸	5.646	Co	55
Tl	7.16	Cu	120	Pb ²⁰⁸	5.53	Ag	70
La	7.15	Mn	50	Hg	5.44	Hg	754
Bi ²⁰⁸	7.149	Tl	2000	Hg	4.903	Co	385

* High-energy component of a complex spectrum.

† A broad scattered spectrum with no observable peak structure.

‡ There are actually two lines of energies 7.647 and 7.633 MeV having equal intensities in the iron capture gamma spectrum. The cross section has therefore been corrected, although there is no possibility at present of deciding which line is responsible for each resonance.

§ Is probably an independent level in the complex spectrum of Ni 7 rays on Te.

** Rough estimate.

†† May be inelastic component from 7.528 level in Te.

†† The relative line intensities in this case are due to Groshev and co-workers.

‡ No line is known for the source at this energy.

† Difficult to resolve among the many source lines present at this energy.

METHOD

REF. NO.

69 Be 6

egf

REACTION	RESULT	EXCITATION ENERGY	SOURCE		DETECTOR		ANGLE
			TYPE	RANGE	TYPE	RANGE	
G, N	ABX	8-23	D	8-30	MOD-I		4PI
G, 2N	ABX	12-30	D	8-30	MOD-I		4PI
G, 3N	ABX	24-30	D	8-30	MOD-I		4PI

 x = fraction of total cross section resulting in a direct neutron n_d = fraction of neutrons emitted by direct effect at an energy where all the evaporation neutrons go to $(\gamma, 2n)$ cross section

$$n_d = x/(2-x)$$

603+(G,N)
604 (G,2N)
477+(G,3N)

TABLEAU 3
Moments quadrupolaires intrinsèques

Cible	% isotopes	a/b ex	β_2 ex	$\beta_2[B(E_2)]$	Q_0 ex (b)	Q'_0
$^{131}_{\Lambda}$ I	100 % ^{127}I	0.85	0.172		-2.3 ± 0.4	
$^{140}_{\Lambda}$ Ce	88.5 % ^{140}Ce 11.1 % ^{142}Ce			0.104 0.118		
$^{142}_{\Lambda}$ Sm	15 % ^{142}Sm 11.2 % ^{148}Sm 13.8 % ^{149}Sm 7.5 % ^{150}Sm 26.6 % ^{152}Sm 22.5 % ^{154}Sm	1.23	0.219	0.190 0.304 0.351	4.5 ± 0.4	0.158 3.53 5.93 6.58
$^{144}_{\Lambda}$ Er	33.4 % ^{166}Er 22.9 % ^{167}Er 27.1 % ^{168}Er 14.9 % ^{170}Er	1.314	0.288	0.341 0.339 0.329	6.96 ± 0.4	7.60 7.80 7.60 7.45
$^{144}_{\Lambda}$ Lu	97.4 % ^{175}Lu	1.282	0.262		6.95 ± 0.3	7.20

TABLEAU 5
Valeurs de la température nucléaire et du paramètre a de densité des niveaux

	x	n_d	Θ (MeV)	$E'_{\gamma} - E_n$ (MeV)	a (MeV $^{-1}$)	a' (MeV $^{-1}$)	a'' (MeV $^{-1}$)
I	0.05 ± 0.005	0.03 ± 0.03	1.30 ± 0.20	10	6 ± 2.5	10 ± 3	10 ± 2
^{140}Ce	0.21 ± 0.05	0.12 ± 0.03	1.05 ± 0.20	10	9 ± 3.5	7 ± 3	
^{142}Ce			0.8 ± 0.20	6	9 ± 4	8 ± 3	
Sm	0.18 ± 0.04	0.10 ± 0.03					
Er	0.20 ± 0.05	0.11 ± 0.03					(12 ± 4)
Lu	0.26 ± 0.06	0.15 ± 0.03	0.85 ± 0.1	9	12.5 ± 2.5	15 ± 3	

[over]

COMMERCE
STANDARDS

TABLEAU 4
Règles de somme

Noyer cible (éléments naturels)	σ_0 (MeV · b)	σ'_0 (McV · b)	0.06 $\frac{NZ}{A}$	$\frac{\sigma_0 A}{0.06 NZ}$	$\frac{\sigma'_0 A}{0.06 NZ}$	σ_{-1} (mb)	$\sigma_{-1} A^{-1}$	σ_{-2} (mb · McV $^{-1}$)	$\sigma_{-2} A^{-1}$
^{53}Sc	2.02 ± 0.14	2.30 ± 0.12	1.85	1.09 ± 0.07	1.24 ± 0.07	129 ± 0.10	0.20 ± 0.02	8.6 ± 0.6	2.7 ± 0.2
^{58}Ce	2.13 ± 0.15	2.53 ± 0.13	2.04	1.05 ± 0.07	1.24 ± 0.07	140 ± 0.12	0.19 ± 0.02	9.5 ± 0.6	2.5 ± 0.2
^{62}Sn	2.48 ± 0.17	2.92 ± 0.14	2.18	1.14 ± 0.07	1.34 ± 0.07	167 ± 0.14	0.21 ± 0.02	11.8 ± 0.8	2.75 ± 0.2
^{68}Er	2.70 ± 0.19	3.04 ± 0.16	2.42	1.12 ± 0.07	1.26 ± 0.07	186 ± 0.15	0.20 ± 0.02	13.6 ± 1	2.7 ± 0.2
^{71}Lu	2.65 ± 0.18	2.96 ± 0.16	2.53	1.05 ± 0.07	1.17 ± 0.07	182 ± 0.15	0.185 ± 0.02	12.9 ± 1	2.35 ± 0.2
valeur moyenne pour ces 5 corps				1.09 ± 0.07	1.25 ± 0.07		0.20 ± 0.02		2.6 ± 0.2

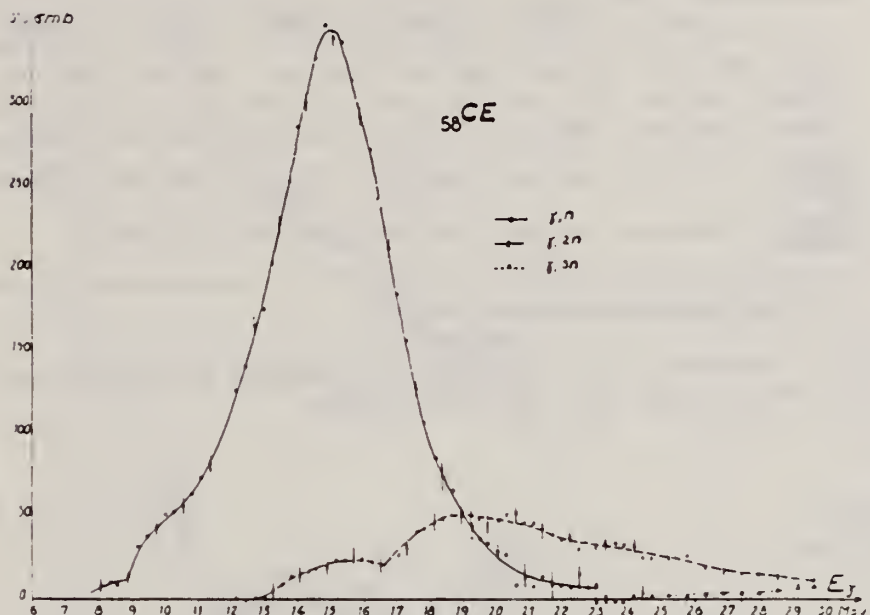
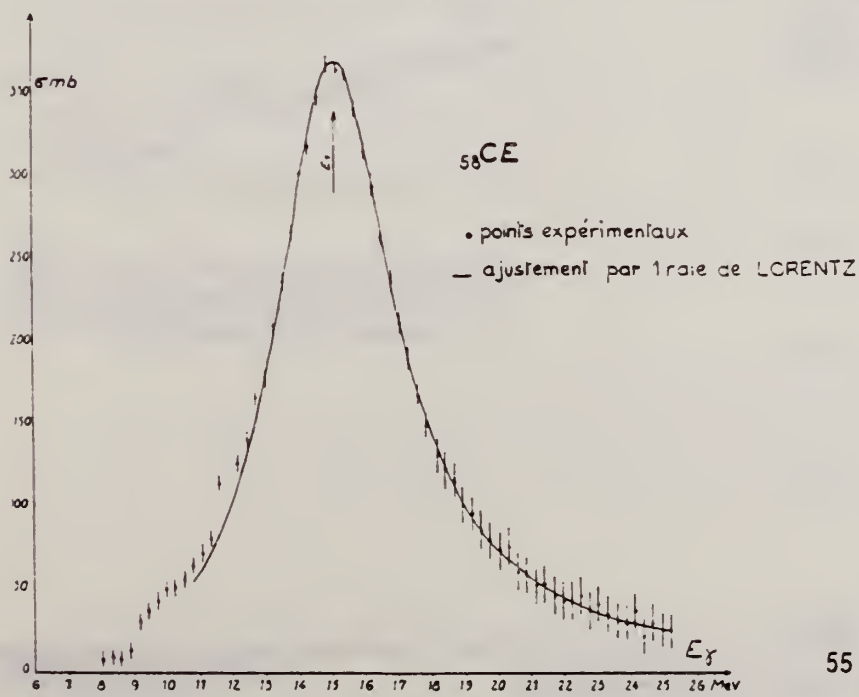


Fig. 3.



55

Fig. 4.

REF.

H. Beil, R. Bergere, P. Carlos, A. Lepretre, A. Veyssiere and
 A. Parlag
 Nucl. Phys. A172, 426 (1971)

ELEM. SYM.	A	Z
Ce		58

METHOD

REF. NO.
71 Be 4

egf

REACTION	RESULT	EXCITATION ENERGY	SOURCE		DETECTOR		ANGLE
			TYPE	RANGE	TYPE	RANGE	
G, SN	ABX	9-18	D	9-18	MOD-I		4PI
							363+

TABLE I
 Lorentz line parameters corresponding to fits of total photoneutron cross sections presented in fig. 1

	^{90}Ba	^{139}La	^{90}Ce	^{141}Pr	^{140}Nd	$^{141}\text{Pr}^a)$
σ_1 (mb)	356 \pm 15	340 \pm 15	360 \pm 15	350 \pm 15	315 \pm 15	320 \pm 20
E_1 (MeV)	15.3 \pm 0.1	15.2 \pm 0.1	15.0 \pm 0.10	15.1 \pm 0.1	14.9 \pm 0.1	15.16 \pm 0.08
Γ_1 (MeV)	4.70 \pm 0.15	4.45 \pm 0.05	4.35 \pm 0.05	4.26 \pm 0.05	4.90 \pm 0.05	4.49 \pm 0.05
$\frac{1}{2}\pi\sigma_1\Gamma_1$ (MeV · b)	2.6 \pm 0.15	2.35 \pm 0.13	2.42 \pm 0.15	2.35 \pm 0.13	2.43 \pm 0.13	2.42 \pm 0.17
$\frac{1}{2}\pi\sigma_1\Gamma_1$ $0.06NZA^{-1}$	1.30 \pm 0.08	1.16 \pm 0.08	1.19 \pm 0.08	1.14 \pm 0.08	1.15 \pm 0.08	

^{a)} Lorentz line parameters given in ref. ¹⁰) for ^{141}Pr .

¹⁰ R. L. Bramblett, J. T. Caldwell, B. L. Berman, R. R. Harvey and S. C. Fultz, Phys. Rev. 148, 1198 (1966).

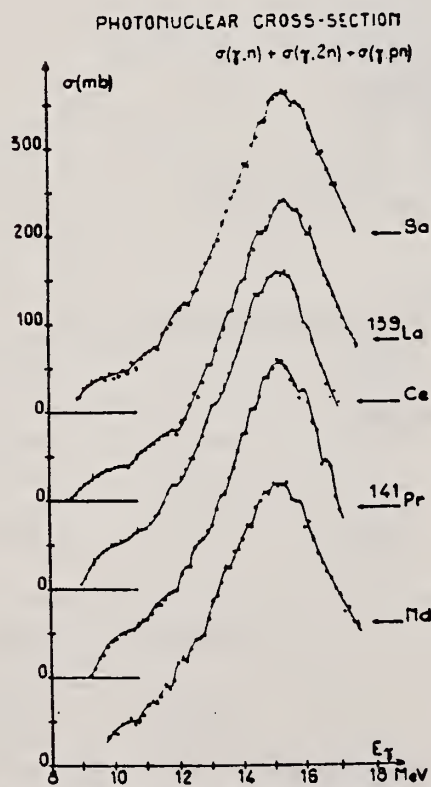


Fig. I. Total photoneutron cross sections for Ba, ^{139}La , Ce, ^{141}Pr and Nd as a function of incident photon energy E .

ELEM. SYM.	A	Z
Ce		58

METHOD

REF. NO.

71 Pi 1

egf

REACTION	RESULT	EXCITATION ENERGY	SOURCE		DETECTOR		ANGLE
			TYPE	RANGE	TYPE	RANGE	
E, E/	SPC	4 - 18		50, 65	MAG-D		DST

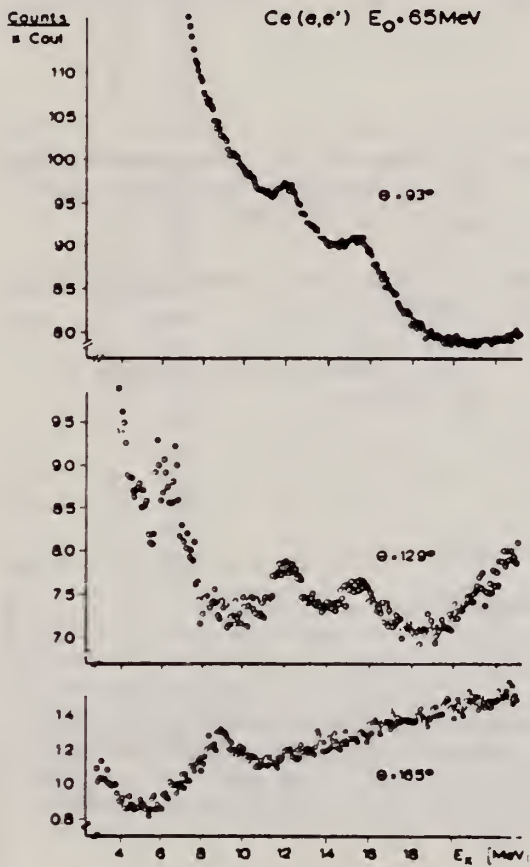


Fig. 1. Spectra of electrons scattered inelastically from cerium; parameters as indicated. No background has been subtracted. Note the suppressed zeros and the different scales of the ordinates.

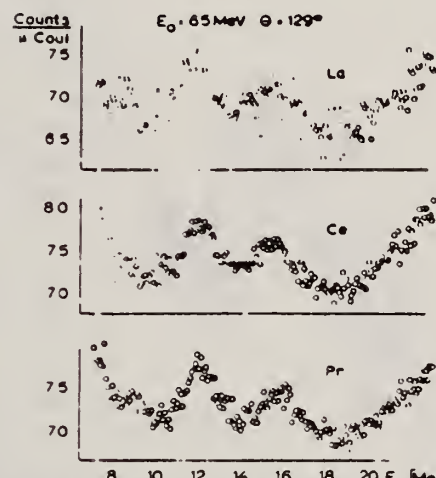
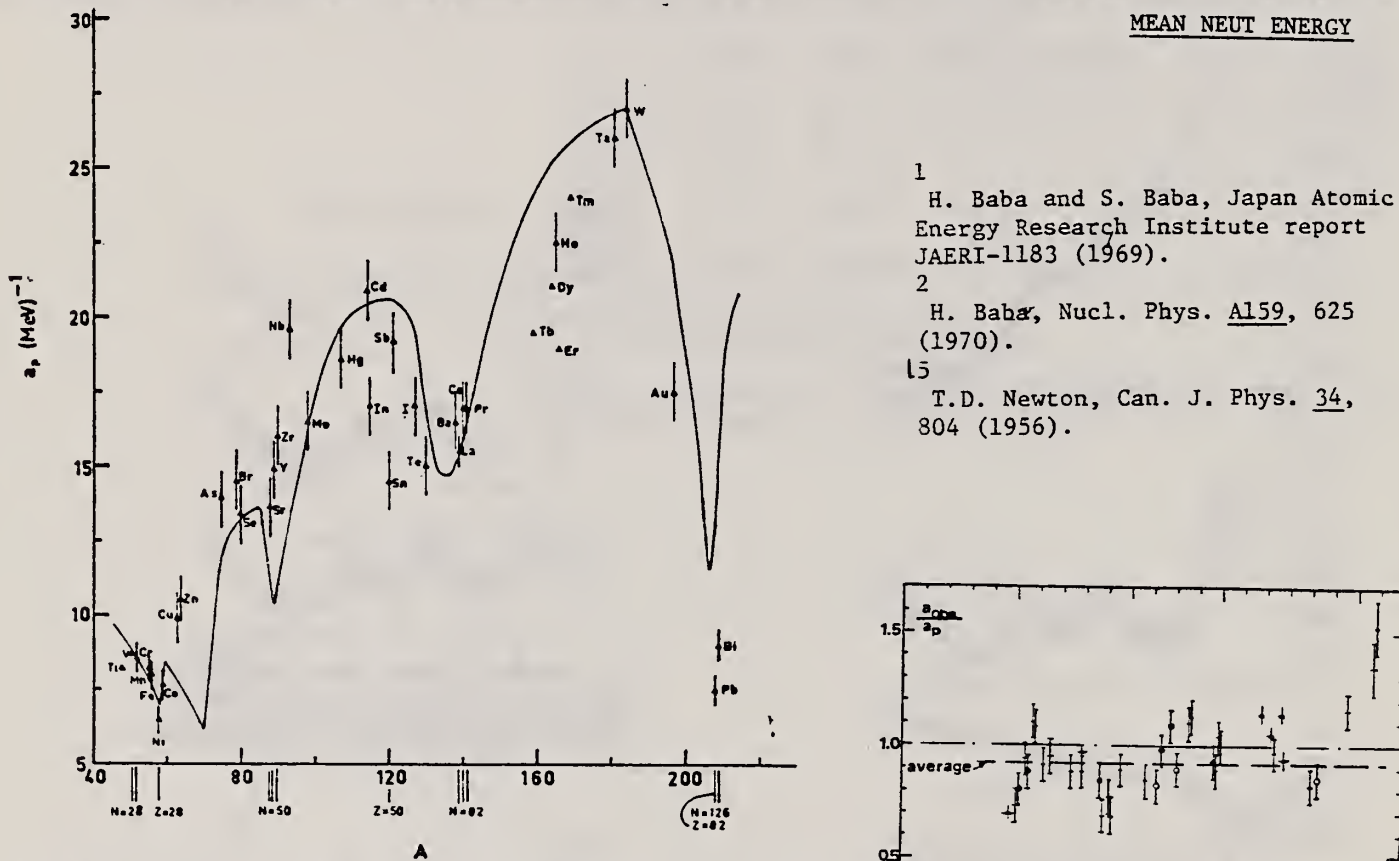


Fig. 2. Spectra of electrons scattered inelastically from La, Ce and Pr targets at the same primary energy and the same laboratory scattering angle. No background has been subtracted. Note the suppressed zeros of the ordinate scales.

ELEM. SYM.	A	Z
Ce		58

METHOD			REF. NO.	
			73 Ba 20	egf
REACTION	RESULT	EXCITATION ENERGY	SOURCE	DETECTOR
G,N	NOX	THR- 27	C 10- 27	BF3-T
				APT



- 1 H. Baba and S. Baba, Japan Atomic Energy Research Institute report JAERI-1183 (1969).
 2 H. Baba, Nucl. Phys. A159, 625 (1970).
 15 T.D. Newton, Can. J. Phys. 34, 804 (1956).

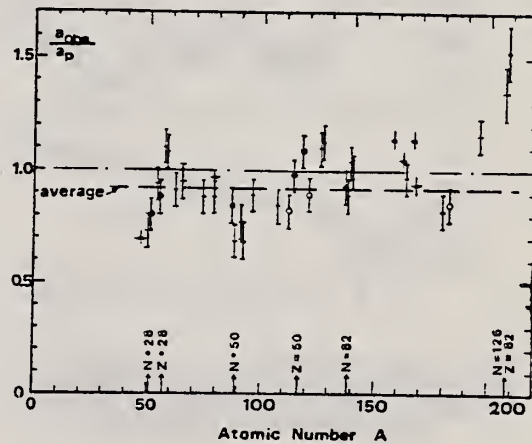


Fig. 15. Ratio a_{obs}/a_p versus atomic number A . Here a_{obs} is the level density parameter taken from the neutron resonance work of refs. ^{1,2}, and a_p is the level density parameter derived from the present (γ, n) work. Filled circles represent points where nuclei in the neutron resonance and in the (γ, n) experiment were the same. Open circles represent points where the respective nuclei were approximately matched. Triangles represent points which are based on measurement of neutron mean energies at two bremsstrahlung energies only.

TABLE 3 (continued)

Target	<i>N</i> (residual nucleus) ^{a)}	Goodness of fit ^{b)}		$\bar{E}_n(24)$ (MeV) ^{c)}	<i>T</i> (MeV) ^{d)}	a_p (MeV ⁻¹) ^{e)}	a_{obs}/a_p		
		no with p.c.	p.c.						
Ba	75	1%	F	1.16	16.5- ¹³⁶ Ba	15.39- ¹³⁶ Ba	0.93		
	77	2%							
	78	7%							
	79	8%							
	80	11%							
	81	71%							
La	80	100%	F	F	1.25	0.72	15.5- ¹³⁸ La	13.76- ¹³⁹ La	0.89
Ce	81	89%	F	G	1.24	0.70	17.0- ¹³⁹ Ce	17.8- ¹⁴¹ Ce	1.04
	83	11%							
Pr	81	100%	G	G	1.17	0.65	17.0- ¹⁴⁰ Pr	17.05- ¹⁴² Pr	1.00
Tb ^{f)}	93	100%			1.15		19.3- ¹⁵⁸ Tb	21.85- ¹⁶⁰ Tb	1.14
Dy ^{f)}	93	2%			1.06		20.9- ^{161.5} Dy	21.9- ¹⁶² Dy	1.05
	94	19%							
	95	25%							
	96	25%							
	97	28%							
Ho	97	100%	P	G	1.06	0.56	21.4- ¹⁶⁴ Ho	20.66- ¹⁶⁶ Ho	0.97
Er ^{f)}	95	2%			1.11		19.2- ¹⁶⁶ Er	21.9- ¹⁶⁶ Er	1.14
	97	33%							
	98	23%							
	99	27%							
	101	15%							
Tm ^{f)}	99	100%			1.03		24.0- ¹⁶⁸ Tm	22.58- ¹⁷⁰ Tm	0.94
Ta	107	100%		G	1.00	0.49	26.0- ¹⁸⁰ Ta	21.2- ¹⁸¹ Ta	0.82
W	107	26%	G	F	0.98	0.50	27.0- ¹⁸³ W	23.0- ¹⁸³ W	0.85
	108	14%							
	109	31%							
	111	28%							
Au	117	100%		G	1.19		17.5- ¹⁹⁶ Au	20.24- ¹⁹⁸ Au	1.16
Pb	123	24%	V.P.	1.87	1.20		7.5- ²⁰⁶ Pb	10.1- ²⁰⁷ Pb	1.35
(Z = 82)	124	23%							
	125	52%							
Bi	125	100%	F	1.65	1.03		9.0- ²⁰⁸ Bi	13.8- ²¹⁰ Bi	1.53

^{a)} Neutron numbers and abundances of respective residual nuclei in (γ , n) experiments.^{b)} These give an assessment of the goodness of fit of a calculated \bar{E}_n versus E_0 curve to the observed data, using the Fermi gas level density formula both without and with pairing corrections.^{c)} Bremsstrahlung photoneutron mean energies \bar{E}_n for peak bremsstrahlung energy $E_0 = 24$ MeV.^{d)} Nuclear temperature from fit with constant-temperature formula.^{e)} Level density parameter a_p derived from the present (γ , n) experiment, using a Fermi gas formula plus pairing correction, and corresponding residual nucleus (the atomic weight shown is the weighted average of atomic weights of the respective isotopes present).^{f)} As column 7, but using data on n-resonance absorption from refs. ¹⁻².^{g)} Measurements of $\bar{E}_n(E_0)$ for these nuclei were made only for $E_0 = 21, 23$ and 24 MeV.

ELEM. SYM.	A	z
Ge		58
REF. NO.		
73 Bu 14	hang	

METHOD	REF. NO.	
	73 Bu 14	hang

REACTION	RESULT	EXCITATION ENERGY	SOURCE		DETECTOR		ANGLE
			TYPE	RANGE	TYPE	RANGE	
E, E/	SPC	2- 20	C	50, 65	MAG-D		DST

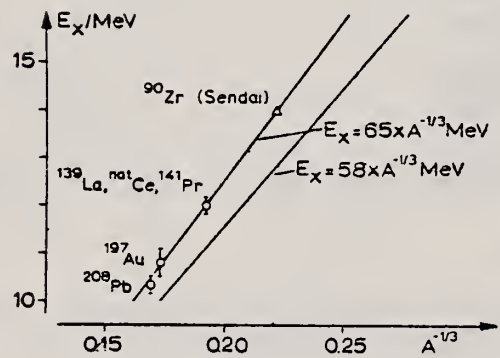


Fig. 2

part should depend on A through $E_x = 58 A^{-1/3}$ MeV. The data of Fig. 2 are consistent with $E_x = 65 A^{-1/3}$ MeV suggesting to identify the observed resonances with this type of E2 excitation.

The E2 resonance which is clearly visible at 10.8 ± 0.2 MeV exhausts more than 50 % of the sum rule. Fig. 2 shows the excitation energy of this resonance as a function of $A^{-1/3}$ for the nuclei measured at Darmstadt and the Sendai result for ^{90}Zr [5]. Bohr and Mottelson [9] predicted a collective E2 resonance whose isoscalar

ELEM. SYM.	A	Z
Ce		58
REF. NO.		
73 Pl 3		egf

METHOD				REF. NO.	
REACTION	RESULT	EXCITATION ENERGY	SOURCE	DETECTOR	ANGLE
E, E/	ABX	7 - 21	D TYPE 50, 65	MAG-D	DST

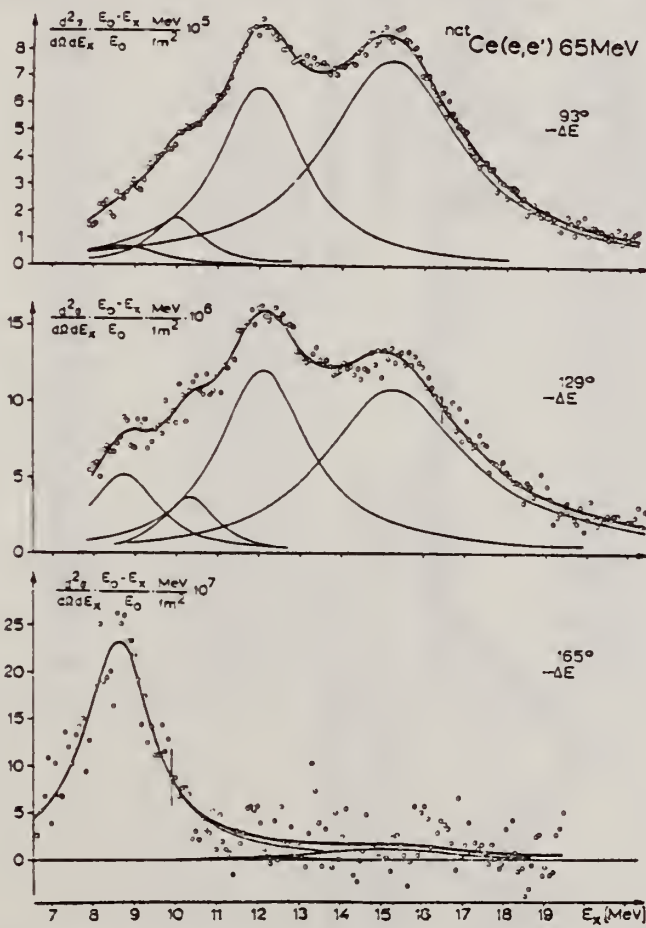


Fig. 5. Wie Fig. 2, aber nach Abzug des angepaßten Untergrundes. Die Zerlegung des Spektrums in die Einzelresonanzen (nach Gl.(2)) ist eingezeichnet, ΔE ist die Halbwertsbreite der elastischen Linie

(over)

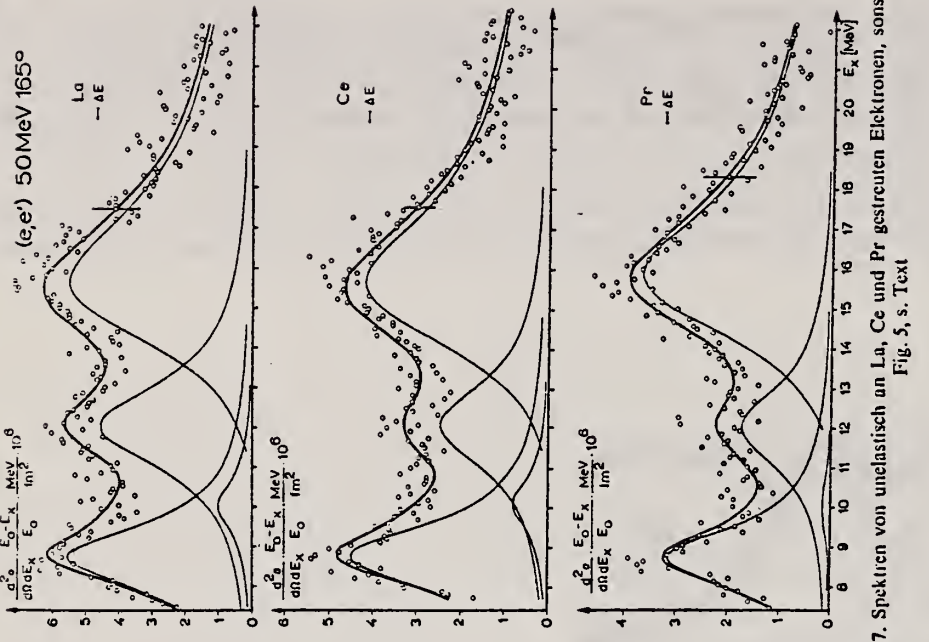


Fig. 7. Spektren von unelastisch an La, Ce und Pr gestreuten Elektronen, sonst wie Fig. 5, s. Text

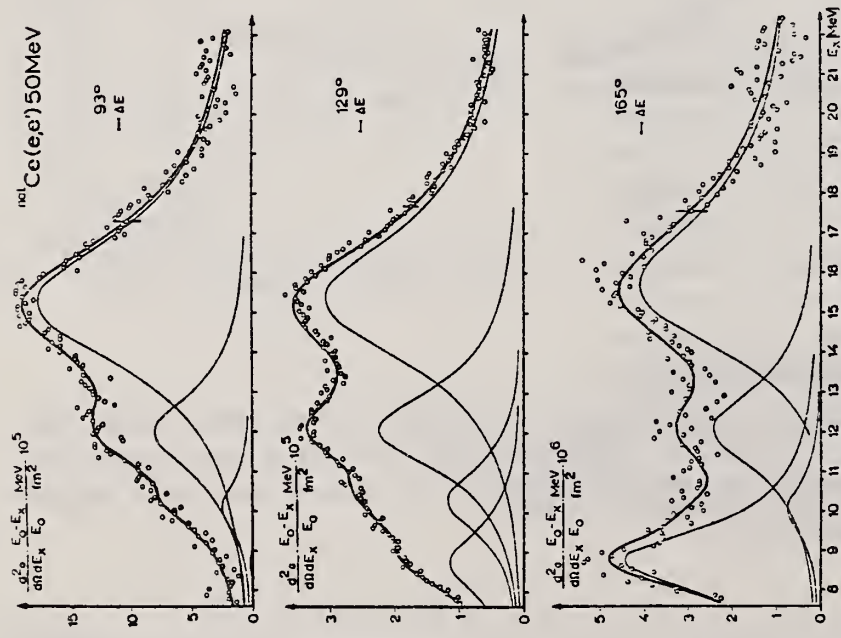


Fig. 6. Wie Fig. 5, aber für eine andere Primärenergie

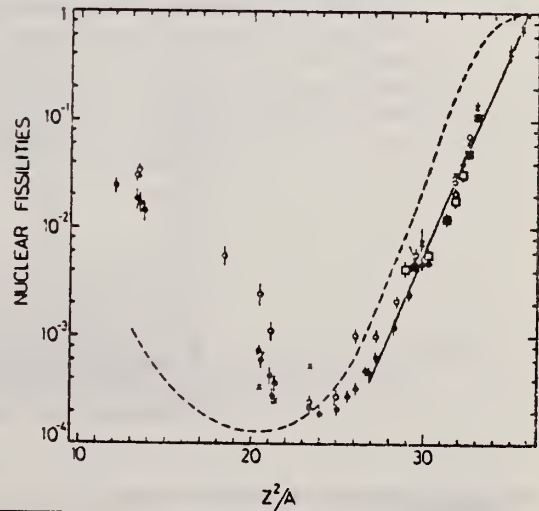
	ELEM. SYM.	A	Z
	Ce		58
METHOD	REF. NO.	76 Em 2	egf

REACTION	RESULT	EXCITATION ENERGY	SOURCE		DETECTOR		ANGLE
			TYPE	RANGE	TYPE	RANGE	
G, F	ABY	THR-999	C	999	TRK-I		4PI
		-					

TABLE I
Measured values of σ_q at $E = 1000$ MeV and deduced values of σ_t assumed constant from E_0 to 1000 MeV999 = 1 GEV

Element	Z^2/A	σ_q (mb)	E_0 (MeV)	σ_t (mb)
Bi	32.96	12.3 ± 0.6	200	7.6 ± 0.6
Pb	32.45	5.4 ± 0.4	220	3.6 ± 0.3
Tl	32.10	4.1 ± 0.3	230	2.8 ± 0.3
Au	31.68	2.0 ± 0.15	240	1.4 ± 0.2
Pt	31.18	1.1 ± 0.08	255	$(8 \pm 0.7) \times 10^{-1}$
Re	30.21	$(3.7 \pm 0.3) \times 10^{-1}$	280	$(2.9 \pm 0.3) \times 10^{-1}$
W	29.78	$(3.5 \pm 0.3) \times 10^{-1}$	290	$(2.8 \pm 0.3) \times 10^{-1}$
Ta	29.45	$(3.3 \pm 0.3) \times 10^{-1}$	300	$(2.7 \pm 0.3) \times 10^{-1}$
Hf	29.04	$(1.7 \pm 0.2) \times 10^{-1}$	310	$(1.4 \pm 0.2) \times 10^{-1}$
Yb	28.31	$(1.3 \pm 0.1) \times 10^{-1}$	330	$(1.2 \pm 0.1) \times 10^{-1}$
Tm	28.18	$(7.5 \pm 0.8) \times 10^{-2}$	335	$(6.8 \pm 0.8) \times 10^{-2}$
Ho	27.21	$(3.6 \pm 0.4) \times 10^{-2}$	355	$(3.5 \pm 0.4) \times 10^{-2}$
Dy	26.80	$(2.6 \pm 0.3) \times 10^{-2}$	360	$(2.5 \pm 0.3) \times 10^{-2}$
Tb	26.58	$(2.5 \pm 0.3) \times 10^{-2}$	370	$(2.5 \pm 0.3) \times 10^{-2}$
Gd	26.04	$(1.6 \pm 0.2) \times 10^{-2}$	380	$(1.7 \pm 0.2) \times 10^{-2}$
Sm	25.56	$(1.3 \pm 0.2) \times 10^{-2}$	390	$(1.4 \pm 0.2) \times 10^{-2}$
Nd	24.96	$(9.2 \pm 0.9) \times 10^{-3}$	405	$(1 \pm 0.1) \times 10^{-2}$
Ce	24.00	$(8 \pm 0.9) \times 10^{-3}$	420	$(9 \pm 1) \times 10^{-3}$
La	23.39	$(8.4 \pm 0.9) \times 10^{-3}$	430	$(1 \pm 0.1) \times 10^{-3}$
Sb	21.36	$(1.2 \pm 0.2) \times 10^{-2}$	460	$(1.5 \pm 0.3) \times 10^{-2}$
Te	21.19	$(8.8 \pm 1) \times 10^{-3}$	465	$(1.2 \pm 0.2) \times 10^{-2}$
Sn	21.06	$(1.3 \pm 0.2) \times 10^{-2}$	465	$(1.7 \pm 0.3) \times 10^{-2}$
Cd	20.49	$(1.7 \pm 0.3) \times 10^{-2}$	470	$(2.2 \pm 0.4) \times 10^{-2}$
Ag	20.47	$(2 \pm 0.3) \times 10^{-2}$	470	$(2.6 \pm 0.4) \times 10^{-2}$
Zn	13.76	$(2 \pm 0.4) \times 10^{-1}$	515	$(3 \pm 0.6) \times 10^{-1}$
Cu	13.44	$(2.4 \pm 0.5) \times 10^{-1}$	515	$(3.6 \pm 0.8) \times 10^{-1}$
Ni	13.35	$(2.4 \pm 0.5) \times 10^{-1}$	510	$(3.6 \pm 0.8) \times 10^{-1}$
Fe	12.10	$(3 \pm 0.6) \times 10^{-1}$	510	$(4.4 \pm 0.9) \times 10^{-1}$

- ⁴ A.V. Mitrofanova et al., Sov. J. Nucl. Phys. 6, 512 (1968).
⁷ T. Methasiri et al., Nucl. Phys. A167, 97 (1971).
¹² J.R. Nix et al., Nucl. Phys. 81, 61 (1966).
²⁰ N.A. Perifilov et al., JETP (Sov. Phys.) 14, 623 (1962); Proc. Symp. on the physics & chemistry of fission, Salzburg 1965, vol. 2 (IAEA) Vienna, 1965, p. 283.

Fig. 2. Nuclear fissilities as a function of Z^2/A . Experimental points: solid circles represent our data; squares, the data from ref. ⁴; open circles, the data from ref. ⁷; and crosses, the data from (p,n) experiments²⁰). The straight line is the best fit calculated from our data for $Z^2/A > 26$. The dashed curve is the curve VI calculated by Nix and Sassi¹².

ELEM. SYM.	A	Z
Ce		58
REF. NO.		
77 Ja 4	egf	

METHOD

REACTION	RESULT	EXCITATION ENERGY	SOURCE	DETECTOR	ANGLE
			TYPE	RANGE	
G,MUT	LFT	7	D	7	NAI-D
		(7.29,7.632)		(7.29,7.632)	
		-			
		-			

Abstract: A variable-energy γ -source is obtained by nuclear resonance scattering of neutron-capture γ -rays through various scattering angles. An energy resolution of less than 10^{-6} is obtained. Pb and Cd targets were employed to scatter the 7.279 and 7.632 MeV photons, respectively, of the neutron capture γ -rays of Fe. Variation of the angle of the resonantly scattered photons between 60° - 150° permits an energy scan of ≈ 370 eV (for Pb) and ≈ 760 eV (for Cd) in any absorber. Thus nuclear energy levels in ^{139}La , Ce, Cd and ^{209}Bi absorbers were photoexcited and the corresponding values of $g\Gamma_0$ were extracted from the measured absorption curve.

7.28,7.63MeV,RES ABS

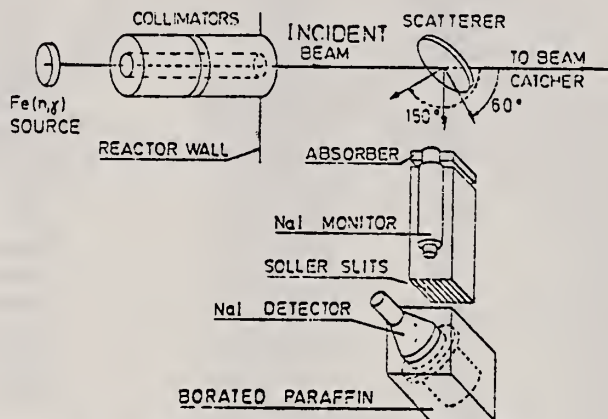


Fig. 1. Schematic diagram of the experimental arrangement.

TABLE 2
Summary of experimental data and measured values of $g\Gamma_0$ obtained using the γ -monochromator

Isotope	Thickness (g/cm^2)	Angle of dip (deg)	ΔE *) (eV)	Effect (%)	$g\Gamma_0$ (meV)
$^{112}\text{Cd}^*$	35	123.0	505	3.5	150 ± 20
^{139}La	28.2	80.0	225	0.40	8.0 ± 2.0
^{139}La	18.2	100.5	322	0.27	7.1 ± 1.9
^{139}La	18.2	104.8	345	0.22	5.5 ± 1.8
$^{140}\text{Ce}^b)$	26.5	90.0	273	1.3	25 ± 3
^{209}Bi	31.5	73.5	196	2.0	43 ± 8
$^{209}\text{Bi}^*$	31.5	68.8	404	1.8	92 ± 12

The asterisk denotes a level at 7.632 MeV photoexcited by a Cd scatterer. All other levels are at 7.279 MeV and were photoexcited by a Pb scatterer.

*) The absorbing isotope was arbitrarily assumed to be ^{112}Cd .

*) The absorbing isotope was arbitrarily assumed to be ^{140}Ce .

*) Here ΔE is the energy difference between the incident γ -line and the resonance level (assuming no recoil correction in the absorbing nucleus).

ELEM. SYM.	A	Z
Ce		58
REF. NO.		
78 Pi 2		rs

METHOD	REACTION	RESULT	EXCITATION ENERGY	SOURCE	DECTOR	ANGLE
				TYPE	RANGE	
	E, E/	FMF	5- 45	D	0* 1	MAG-D
						DST

(e, e') from the giant dipole resonance (GDR) in ^{140}Ce verifies the macroscopic model by Myers *et al.*, while ruling out the Steinwedel-Jensea model and, to a lesser extent, the Goldhaber-Teller model. This result leads to discrepancies between (α, α') and (e, e') concerning the existence of a giant-monopole (breathing-mode) state, particularly if one considers the independent verification of the Meyers *et al.* model by the experimental $A^{-0.23}$ energy dependence of the GDR.

*Q=0.3-0.7FM-1

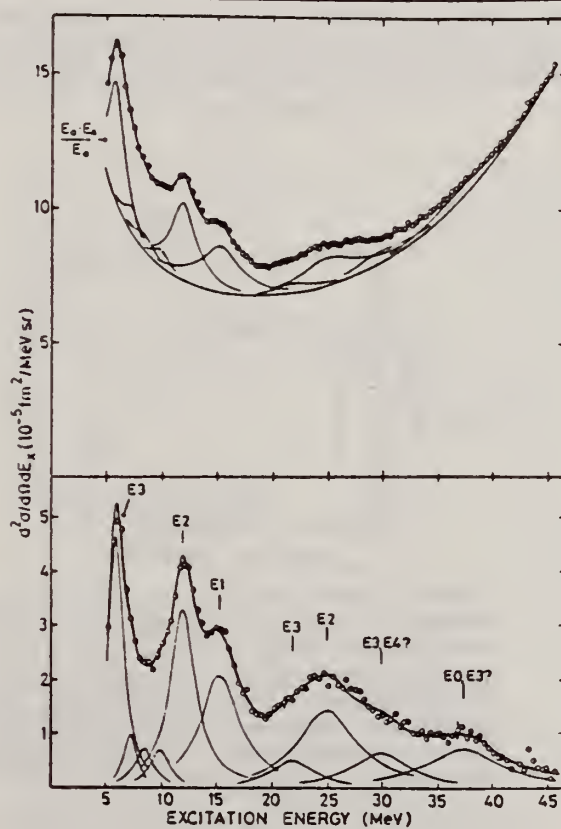


FIG. 1. Spectrum of 92.1-MeV electrons scattered inelastically from ^{140}Ce at 90°. The spectra with and without the background are shown together so that the difference between the two may be seen. The resonances which were used for fitting the spectrum and the background as described in the text are drawn. The "ghost peak" is subtracted from the lower graph. The spectrum was taken and fitted with 10 data points per MeV. For graphical purposes the number of points for the spectrum was reduced by a factor of 4. The fitting range was 4-46 MeV. The statistical error is shown on selected points. While the upper part has not been corrected for the constant dispersion of the magnetic spectrometer and thus shows the data points as measured, the subtracted spectrum has been corrected in order to show the cross sections of the resonances in their true relation. While lower states (ghost peak) and higher resonances (background sensitivity due to failure of the calculated radiation tail to account for the measured one above 20 MeV) have rather large uncertainties (up to 50%), the region between 10 and 20 MeV turned out to be very insensitive to the choice of the background function. Details of the principles of the analysis can be found in Ref. 9.

⁹R. Pitthan, F.R. Buskirk, E.B. Dally, J.O. Shannon, and W.H. Smith, Phys. Rev. C 16, 970 (1977).

Over

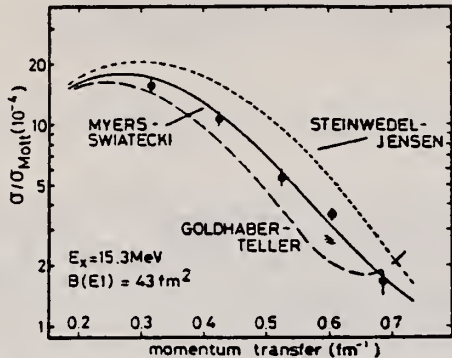


FIG. 2. Comparison between the experimental cross section divided by the Mott cross section [called form factor (squared) in the text] and DWBA calculations [S. T. Tuan *et al.*, Nucl. Instrum. Methods **60**, 70 (1968)] as a function of momentum transfer. Since the data were taken at four different energies (150 MeV, 93°; 65 MeV, 93°; 80 MeV, 90°; 92 MeV, 90° and 105°), form factors were constructed from separate calculations at the correct momentum transfer for each energy and connected by a smooth curve. Other methods presenting (e, e') data in this case are possible, but ours has the advantage of not manipulating the experimental points.

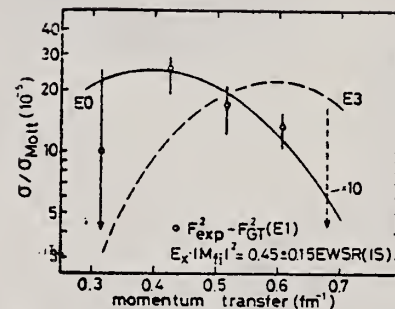


FIG. 3. The data points are identical to the difference between the cross section under the 15.3-MeV (E_1) resonance and a DWBA calculation based on the GT model and normalized to (γ, n) results (lowest curve in Fig. 2). Comparison with a monopole DWBA calculation shows that this difference is compatible with the presence of 45% of the E_0 EWSR. Reasons against such an interpretation are given in the text.

ELEM. SYM.	A	Z			
Ce		58			
METHOD	REF. NO.				
	79 Pi 4	hg			
REACTION	RESULT	EXCITATION ENERGY	SOURCE	DETECTOR	ANGLE
E,E/	ABX	6-38	D 50,92	MAG-D	DST

The cross section for electron scattering from natural cerium (39% ^{140}Ce) has been measured with electrons of 80 and 92 MeV at 90 and 105° between 4 and 48 MeV excitation energy. The nine resonances or resonance-like structures identified at $E_x = 6$ ($31 A^{-1/3}$), 7.4 ($38 A^{-1/3}$), 10 ($52 A^{-1/3}$), 12 ($62 A^{-1/3}$), 15.3 ($79 A^{-1/3}$), 22 ($114 A^{-1/3}$), 25 ($130 A^{-1/3}$), 31 ($160 A^{-1/3}$), and 37.5 ($195 A^{-1/3}$) MeV were classified on the basis of their momentum transfer dependence and discussed in the framework of the shell model. Since some of the arguments used are intricate we refer for quantitative particulars to the text. It is shown that the $E2$ sum rule strength not exhausted in the excitation range of this experiment may contribute up to 50% of the classical dipole sum rule to the photon cross section between 50 MeV and the pion threshold. The resonance at 10 MeV might be due to a separate oscillation of the excess neutrons against the rest of the nucleus.

[NUCLEAR REACTIONS $^{140}\text{Ce}(e, e')$, $E_0 = 50$ to 92 MeV. Measured $d^2\sigma/d\Omega dE_x$, bound and continuum states (giant resonances). Deduced multipolarity, reduced matrix element $B(E\bar{N})$, radiative width Γ_r , sum rule exhaustion of giant resonances, photon cross section to pion threshold, total width of continuum and clustered states.]

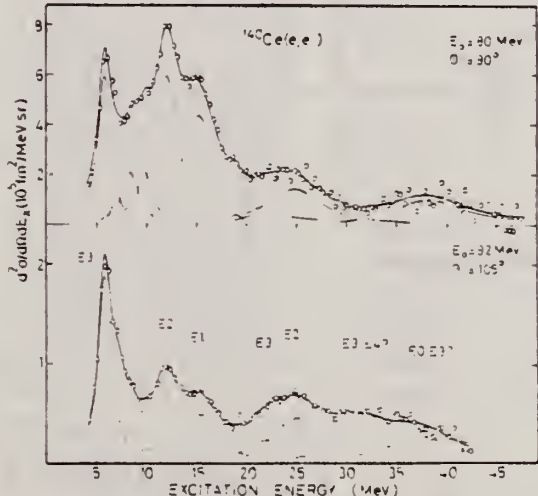


FIG. 3. Data of Fig. 2. after the fitted background (consisting of the radiation tail, the general room background, and experimental background) and the "ghost peak" as described in the text have been subtracted. These two spectra are shown together so that the shrinkage of smaller multipolarity transitions versus the growth of higher multipolarity transitions may be seen. The relative change in peak heights of the single resonances indicate very clearly the various multipoles contributing. Note, e.g., that the $E2$ cross sections fall off more than a factor of 6 between the 50 MeV and the 92 MeV spectra.

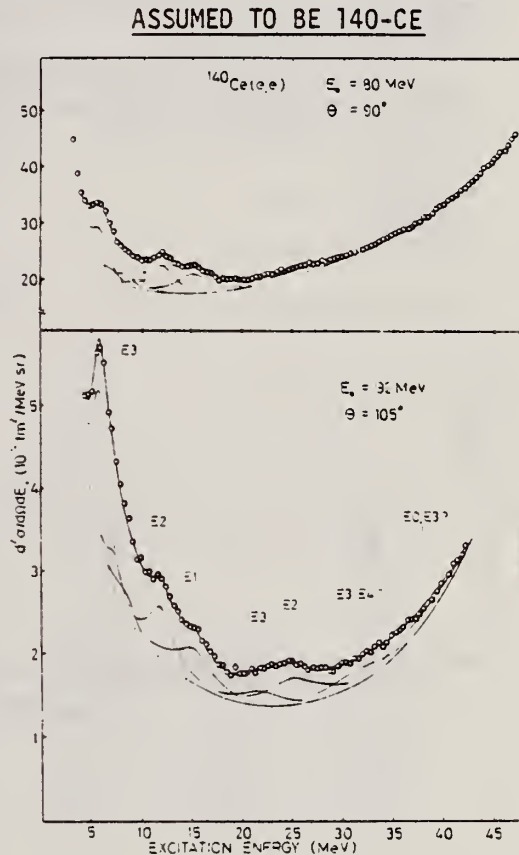


FIG. 2. Spectra of 80 and 92 MeV electrons scattered inelastically from ^{140}Ce . Resonances (or envelopes of discrete states) are indicated and discussed in more detail in the text. The bottom curved line in both parts is the fitted total background. Note that zero in the lower spectrum is not suppressed. The ghost peak has not been subtracted from the data, neither are the cross sections corrected for the constant dispersion of the magnetic spectrometer. The spectra were taken and fitted with 10 points per MeV, which were reduced for graphical purposes by a factor of 4. Resolution was 500 keV, approximately $\frac{1}{3}$ of the width of the smallest resonance found; the statistical error is shown on selected points in the lower spectrum; it was smaller than the circles in the upper one. The fitted range of the spectra shown was 4-48 MeV for the upper, and 4-42 MeV for the lower spectrum (see discussion in text in conjunction with the 37 MeV state).

(over)

TABLE X. Results in units of the reduced transition probabilities (B values), ground state radiation width (Γ_γ^0), and energy weighted sum rule exhaustion, for the major resonances found in this experiment. Some results for weaker states, and those inferred from differences between cross sections and DWBA calculation, are, together with the appropriate discussion, scattered in the text. The isospin assignments are not determined by this experiment, but were taken from comparison with other experiments and theory.

E_x (MeV)	$E_x A^{-1/3}$ (MeV)	Γ (MeV)	$E\lambda$	ΔT	B_{exp} ($\text{fm}^2 \lambda$) ^a	Γ_γ^0 (eV)	R ^b	Std. dev. ^c	Total error ^d
6.0 ± 0.2	31	1.7 ± 0.2	3	0	1.3×10^5	2.0×10^{-3}	19	± 3	± 6
10.0 ± 0.2	52	1.8 ± 0.2	2	0	430	7.6	9	± 2	± 4
			0	0	770		13	± 2	± 6
12.0 ± 0.2	62	2.8 ± 0.2	2	0	2.5×10^3	10.0	63 ^e	± 17	± 13
			2	0	2.0×10^3	8.7	50 ^f	± 5	± 10
15.3 ± 0.2	79	4.4 ± 0.2	1	1	41	5.1×10^4	122 ^g	± 12	± 20
			1	1	55	6.9×10^4	167 ^h	± 40	± 27
22 ± 1	114	5 ± 1	3	0	3.7×10^4	4.9	19	± 2	± 10
25 ± 1	130	6.5 ± 1	2	1	1.3×10^3	2.1×10^3	50 ⁱ	± 8	± 15
			2	1	2.1×10^3	3.3×10^3	77 ^h	± 25	± 23
34 - 38	175	7 - 10	3	0	1.2×10^5	6.8×10^2	75	± 10	± 15
	195		0	1	2.8×10^3		130	± 20	± 30

^aFor the monopole the measured quantity is $|M_{if}|^2$ (fm^4).

^b $R = E_x B(E\lambda) / \text{EWSR}(E\lambda, \Delta T) \times 100$.

^cThe error given (in units of R) is the standard deviation of the average sum rule exhaustion and is, therefore, more a measure for the fit to a certain model than a measure for the total uncertainty.

^dThe total error (in units of R) is based on the maximum and minimum values found for the areas under the curves during the many attempts to fit the spectra.

^e $c_{ii} = 1.0c$.

^f $c_{ii} = 0.95c$.

^gMS model with $\alpha = 0.76$.

^hGT model.

ⁱMS model with $\alpha = 1.0$.

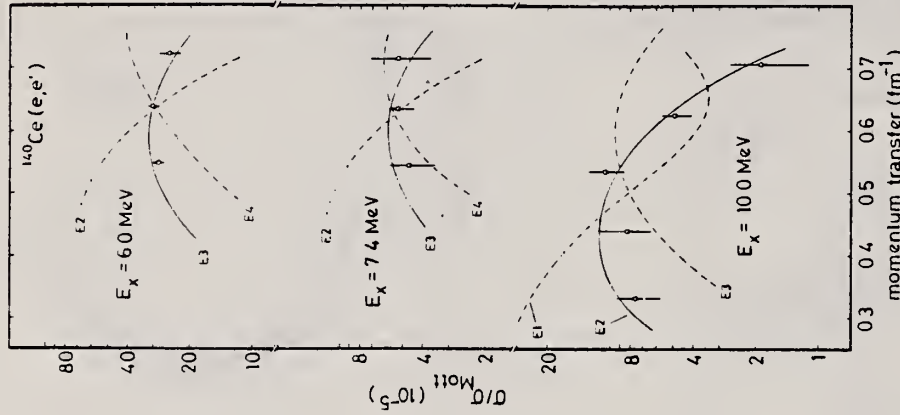


FIG. 12. Comparison of the DWBA and experimental form factors for the resonances found at 6.0, 7.4, and 10.0 MeV. The Goldhaber-Teller model for an $E3$ transition fits the experimental form factors of the resonance found at 6.0 MeV. The Goldhaber-Teller model for both an $E3$ and for an $E4$ transition fits the experimental form factors for the resonance found at 7.4 MeV. Both the Goldhaber-Teller and the Myers-Swiatecki $E2$ models were fit to the experimental form factors for the resonance found at 22 MeV (Table X). The Myers-Swiatecki model with a mixture ratio of 1.0 was found to fit the data better than the Goldhaber-Teller model as explained in the text. The assignment of an $E3$ transition can be clearly ruled out. The experimental form factor of the resonance found at 31 MeV fit the Goldhaber-Teller model for both $E3$ and $E4$ transitions. An upper value could only be estimated for the form factor obtained from the 80 MeV/90° experiment, based on the statistical error of the measurement. The assignment of an $E2$ transition can be ruled out. The assignment of the resonance around 37 MeV is the most difficult. Because of the intricate arguments, we refer to the text.

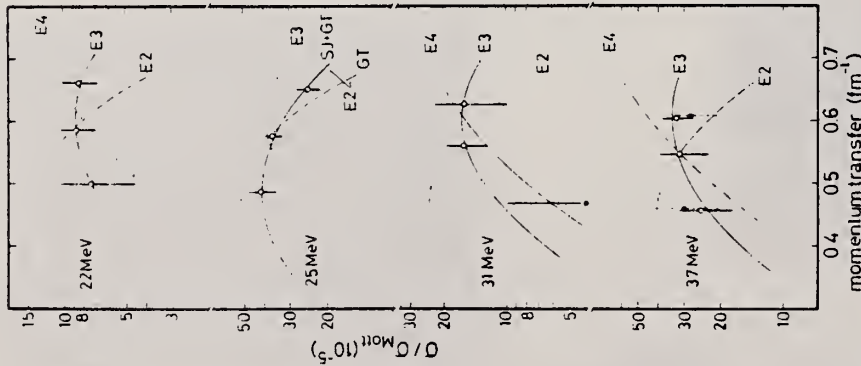


FIG. 10. Comparison of the DWBA and experimental form factors for the resonances found at 22, 25, 31, and 37 MeV. The Goldhaber-Teller model for an $E3$ transition fits the experimental form factors of the resonance found at 22 MeV. Both the Goldhaber-Teller and the Myers-Swiatecki $E2$ models were fit to the experimental form factors for the resonance found at 25 MeV (Table X). The Myers-Swiatecki model with a mixture ratio of 1.0 was found to fit the data better than the Goldhaber-Teller model as explained in the text. The assignment of an $E3$ transition can be clearly ruled out. The experimental form factor of the resonance found at 31 MeV fit the Goldhaber-Teller model for both $E3$ and $E4$ transitions. An upper value could only be estimated for the form factor obtained from the 80 MeV/90° experiment, based on the statistical error of the measurement. The assignment of an $E2$ transition can be ruled out. The assignment of the resonance around 37 MeV is the most difficult. Because of the intricate arguments, we refer to the text.

REF. A. Leprêtre, H. Beil, R. Bergère, P. Carlos, J. Fagot, A. De Miniac, A. Veyssiére Nucl. Phys. A367, 237 (1981)	ELEM. SYM.	A	Z
Ce			58

METHOD			REF. NO.	81 Le 1	egf
REACTION	RESULT	EXCITATION ENERGY	SOURCE	DETECTOR	ANGLE
G,SN	ABX	25-140	D 25-140	MOD-I	4PI
G,XN	ABX	25-140	D 25-140	MOD-I	4PI

(G,SN) NO G,IN IN G,SN
See 82LE3

Abstract: The total photonuclear absorption cross section for Sn, Ce, Ta, Pb and U has been studied from 25 to 140 MeV using a continuously variable monochromatic photon beam obtained from the annihilation in flight of monoenergetic positrons. The basic experimental results are a set of data giving sums of inclusive multiple photoneutron production cross sections of the form $\sigma^{(i)}(E_\gamma) = \sum_{i=1}^{\infty} \sigma(\gamma, in: E_\gamma)$ for neutron multiplicities ranging from $i = 1$ to 12. From these data the total photonuclear absorption cross section $\sigma(\text{tot}: E_\gamma)$ has been deduced. It is concluded that Levinger's modified quasideuteron model describes the total cross sections reasonably well. When these data are combined with lower energy data and integrated to 140 MeV they indicate the need for an enhancement factor K for the Thomas-Reiche-Kuhn sum rule of 0.76 ± 0.10 . No evidence was found that would indicate an A -dependence for the enhancement factor.

E PHOTONUCLEAR REACTIONS Sn, Ce, Ta, Pb, U(γ , xn), $E_\gamma = 25\text{-}140$ MeV; measured $a(E_\gamma)$ summed for $x = 1\text{-}12$; deduced $\sigma(E_\gamma, \text{total})$, integrated σ , interaction models. Monochromatic photons.

$$\sigma^{(i)}(E_\gamma) = \sum_{i=1}^{\infty} \sigma(\gamma, in: E_\gamma).$$

TABLE 3
Integrated cross sections

	Sn	Ce	Ta	Pb	U	U
$\sigma_0 = 0.06NZ/A$ (MeV · b)	1.74	2.04	2.61	2.97	3.40	3.40
$E_{\gamma 0}$ (MeV)	29.7	25	25	25	18	18.30
$M = \int_{E_{\gamma 0}}^{E_{\gamma 0}} \sigma_{GDR}(E_\gamma) dE_\gamma$ (MeV · b) (σ_0 unit)	2.0 ± 0.15^a	2.13 ± 0.15^b	2.90 ± 0.23^b	3.48 ± 0.23^b	2.98 ± 0.15^d	3.58^b
$N = \int_{E_{\gamma 0}}^{140 \text{ MeV}} \sigma^{(2)}(E_\gamma) dE_\gamma$ (MeV · b) (σ_0 unit)	0.96 ± 0.1	1.27 ± 0.1	1.73 ± 0.15	1.69 ± 0.15	2.59 ± 9.2	2.59 ± 0.2
$M + N$ (MeV · b) (σ_0 unit)	2.96 ± 0.2	3.40 ± 0.2	4.63 ± 0.3	5.17 ± 0.3	5.57 ± 0.3	6.17 ± 0.3
$(M + N) + \text{evaluation of the}$ $\int_{E_{\gamma 0}}^{140 \text{ MeV}} \sigma^{(1)} - \sigma^{(2)} dE_\gamma$, contribution $= (1 + K) (\sigma_0 \text{ unit})$	1.74 ± 0.15	1.71 ± 0.15	1.81 ± 0.15	1.78 ± 0.15	1.68 ± 0.15	1.85 ± 0.15
$\int_{E_{\gamma 0}}^{\infty} \sigma_L(E_\gamma) dE_\gamma$ (σ_0 unit)	1.28^a	1.24^b	1.30^b	1.35^b	1.18^d	1.43^b

^a) Ref. ²⁶). ^b) Ref. ²⁷). ^c) Ref. ⁵). ^d) Ref. ²⁸). ^e) Ref. ²⁹.

The symbols M and N are defined in the text. The last row gives the integrated cross sections for the Lorentz line fit, $\sigma_L(E_\gamma)$, to the GDR data, published in the above references.

(OVER)

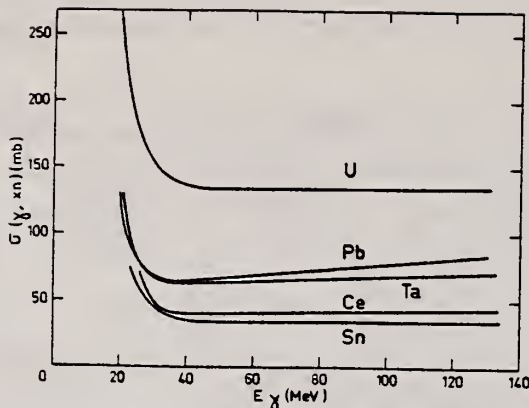


Fig. 11. The general behaviour of the "smoothed" average neutron yield cross sections $\sigma(\gamma, xn) = \sum_i i\sigma(\gamma, in : E_\gamma)$ for the Sn, Ce, Ta, Pb and U nuclei studied in the present paper (see text).

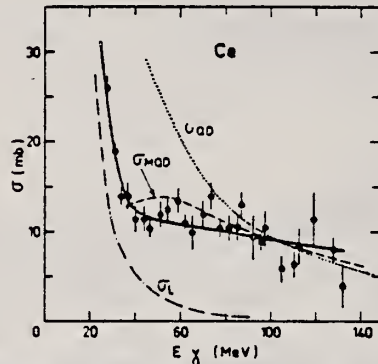


Fig. 15. Total photonuclear absorption cross sections $\sigma(\text{tot} : E_\gamma) \approx \sigma^{(2)}(E_\gamma)$ from the present paper, represented by the experimental points and the corresponding full lines, are shown for Pb, Sn, Ce, Ta and U. These experimental results for photon energies E_γ between 20 and 140 MeV are compared with: (a) Lorentz line fits to the GDR data of the appropriate nucleus represented by the dot-dash $\sigma_L(E_\gamma)$ plots. (b) Quasideuteron cross sections, $\sigma_{OD}(E_\gamma) = (4.6NZ/A)\sigma_D(E_\gamma)$ for the appropriate nuclei, represented by the dotted $\sigma_{OD}(E_\gamma)$ plots. Here $\sigma_D(E_\gamma)$ is the photodisintegration cross section of deuterium. (c) Modified quasideuteron cross sections, $\sigma_{MOD}(E_\gamma) = (8NZ/A)\sigma_D(E_\gamma) \exp(-D/E_\gamma)$ with $D = 60$ MeV, represented by the dashed $\sigma_{MOD}(E_\gamma)$ plots. Pertinent GDR data for Pb, Sn, Ce, Ta and U were taken from refs. ^{5,26-28}.

ELEM. SYM.	A	Z
Ce		58
METHOD	REF. NO.	
	81 Sc 6	egf

REACTION	RESULT	EXCITATION ENERGY	SOURCE	DETECTOR		ANGLE
			TYPE	RANGE	TYPE	
G,G	ABX	2-7	2-7	SCD-D		90

2.60-6.76 MEV

Elastic scattering by nuclei in the range of mass numbers between 64 and 238 has been studied with monochromatic photons in the energy range between 2 and 8 MeV. These photons were provided either by a Ti(n,γ) source installed in the tangential through channel of the Grenoble high flux reactor, or by ^{24}Na and ^{56}Co sources produced by deuteron bombardment of Al or Fe at the Göttingen cyclotron. The photoexcitation of 23 nuclear levels has been observed and the decay properties and groundstate widths of the majority of these levels have been determined. For the lead scattering target the coherent elastic differential cross section has been studied in detail. There is evidence that below the photo-neutron threshold the elastic scattering via virtual photoexcitation of the nucleus can be approximated by extrapolating the real part of the Giant Dipole Resonance amplitude along a Lorentzian curve. Coulomb corrections to Delbrück scattering seem to play a small role at 6.5 MeV.

Table 4. Properties of levels observed by photoexcitation. $(d\sigma/d\Omega)^{\text{RF}}$: experimental differential cross section per identified isotope or element for resonance scattering through $\Theta=90^\circ$; I^π : spin-parity of excited level; $W(\Theta)$: angular correlation function; $g=(2I_{ss}+1)(2I_g+1)$; Γ_0 : radiative groundstate transition width; Γ : total level width. Errors in the last digits are given in parentheses

Isotope	E_γ (MeV)	$(d\sigma/d\Omega)^{\text{RF}}$ (pb/sr)	I^π	Γ_0/Γ^*	$W(\Theta)g\Gamma_0^2/\Gamma$ (meV)	Γ_0^r (meV)	Γ_0^s (meV)
^{238}U	2.754	13 (4)	(1)	0.77	0.145	0.084	-
^{238}U	3.254	421 (5)	1^-	0.24	0.83	1.5	$0.52(15)^a$
^{209}Bi	6.555	$2.1 (4)\cdot 10^2$	-	-	0.74	0.74^b	-
^{209}Bi	7.168	$1.7 (3)\cdot 10^3$	$9/2^{++}$	1.00	710	786	-
^{203}Tl	6.418	$8.75(30)\cdot 10^3$	$1/2^+$	0.28	30	102	$820 (40)^a$
Tl	6.759	7 (3)	-	-	-	-	-
Hg	6.555	68 (17)	-	-	-	-	-
^{196}W	6.418	$5.2 (3)\cdot 10^2$	1^{+-}	0.32	1.75	2.4	-
^{184}W	6.555	$9.8 (10)\cdot 10^2$	(1)	0.22	3.44	2.9	-
^{184}W	6.759	46 (10)	(1)	0.58	0.17	0.13	-
^{181}Ta	3.010	174 (17)	-	0.72	0.42	0.59	-
^{181}Ta	6.418	62 (4)	-	0.73	0.2	0.27^c	-
^{181}Ta	6.759	4.8 (12)	-	-	0.018	0.018^b	-
^{105}Ho	6.418	10.3 (30)	-	-	0.035	0.035^b	-
^{105}Ho	6.759	5.6 (14)	-	-	0.021	0.021^b	-
Nd	2.754	2.6 (5)	-	-	-	-	-
Nd	3.254	14.0 (10)	-	-	-	-	-
Ce	6.759	13.4 (10)	-	-	-	-	-
^{121}Sb	3.452	$2.20 (5)\cdot 10^3$	-	0.60	2.9	4.9^b	-
^{100}Mo	6.418	$1.53 (4)\cdot 10^4$	1^{-4}	0.88	52	26	$25 (8)^a$
^{94}Mo	6.555	$4.4 (4)\cdot 10^3$	(1)	0.33	15	21	-
Mo	6.759	6.2 (15)	-	-	-	-	-
Mo	7.168	$8.2 (26)\cdot 10^2$	-	-	-	-	-

^a [11] ^b $W(\Theta)g\Gamma_0/\Gamma=1$ assumed ^c $W(\Theta)g=1$ assumed

^d [28] (a small correction has been applied to the data of [28])

^e Upper limits in case not all the transitions to lower levels were observed

^f Present work ^g Previous work

(OVER)

Table 1. Differential cross sections for elastic scattering ($d\sigma/d\Omega$)^{exp} of photons from ^{56}Co and ^{24}Na sources by different scattering targets, in units of $\mu\text{b}/\text{sr}$. Errors in the last digits are given in parentheses.

Θ deg	Scattering targets	2.599 ^a (MeV)	2.754 ^b (MeV)	3.010 ^a (MeV)	3.202 ^a (MeV)	3.254 ^a (MeV)	3.273 ^a (MeV)	3.452 ^a (MeV)
90	^{238}U	52.7(25)	57.5(25) ^c	56(16)	47(4)	456 (10) ^c	34(6)	39(14)
	^{209}Bi	33.1(30)	32 (2)	33(11)	32(4)	25.6(20)	29(6)	33(15)
	^{nat}Pb	31.5(23)	31.0(16)	35 (8)	27(3)	26.6(22)	25(4)	23 (8)
	^{nat}Tl	31.5(33)	-	27(12)	32(5)	24 (3)	22(7)	34(15)
	^{nat}Hg	30.0(27)	-	24(10)	28(5)	25.5(18)	26(8)	20 (8)
	^{nat}W	22.5(11)	-	17 (7)	19(3)	18.4(15)	18(5)	21 (6)
	^{181}Ta	20.0(15)	19.2 (6)	193(20) ^c	20(4)	17.3(21)	18(5)	21 (8)
	^{165}Ho	15.9(13)	-	17(10)	13(6)	15.6(20)	18(8)	-
	^{nat}Nd	11.4 (7)	14.2 (5) ^d	15 (7)	14(3)	24.2(12) ^d	13(3)	9 (6)
	^{nat}Ce	11.1 (9)	11.0 (5)	-	11(3)	9.5(13)	8(4)	-
	^{127}I	8.4(10)	8.6 (5)	-	9(2)	7 (1)	5(3)	-
	^{nat}Sb	8.0(11)	-	-	10(4)	6.8(19)	-	1.270(50) ^e
	^{nat}Sn	6.5 (7)	7.0 (5)	-	5(2)	7.6 (8)	6(3)	-
	^{nat}Cd	6.2 (5)	-	-	6(2)	6.6 (8)	7(3)	-
120	^{238}U	55.1(25)	64 (4) ^c	43(15)	55(5)	574 (10) ^c	48(5)	48(11)
	^{181}Ta	27.5(15)	25.0 (9)	227(20) ^c	22(5)	21 (2)	22(8)	-
	^{nat}Nd	17.9(30)	17.0 (9) ^d	-	-	29.8(47) ^d	-	-

^a ^{56}Co source in Fe lattice

^b ^{24}Na source in Al lattice (part of data have been published elsewhere)

^c Transitions to excited states observed in addition to the ground-state transition

^d Photoexcitation of nuclear level identified from the size of the differential cross section

Table 2. Elastic differential cross sections $d\sigma/d\Omega(\Theta=90^\circ)$ in $\mu\text{b}/\text{sr}$ measured with the $\text{Ti}(n,\gamma)$ source and compared with theoretical predictions. n : predicted number of levels in a $\Delta E=25\text{ eV}$ interval at 6.5 MeV. Errors in the last digits are given in parentheses

Scattering target	6.418 MeV		6.555 MeV		6.759 MeV		7.168 MeV		n
	exp.	th.	exp.	th.	exp.	th.	exp.	th.	
^{238}U	23 (12)	10.3	-	-	-	-	-	-	45
^{209}Bi	-	-	219(39) ^{b,c}	8.0	12 (4)	7.4	1.5(3) · 10 ⁵ ^{b,c}	5.7	0.1
^{nat}Pb	7.0(15)	8.6	-	-	6.5(11)	7.4	-	-	0.05
^{nat}Tl	2,586 (92) ^{a,c}	7.5	-	-	13 (3) ^b	6.0	-	-	0.4
^{nat}Hg	12 (3)	7.8	74(17) ^b	6.5	6.7(15)	6.4	-	-	3.4
^{nat}W	159 (10) ^{a,c}	6.6	306(33) ^{a,c}	6.3	20 (2) ^{a,c}	5.6	-	-	13
^{181}Ta	68 (4) ^{a,c}	6.3	-	-	10.1(12) ^{b,c}	5.3	-	-	28
^{165}Ho	15 (3) ^b	4.7	-	-	9.5(14) ^b	3.9	-	-	18
^{nat}Ce	4.1(21)	4.1	-	-	17 (1) ^{b,c}	3.6	-	-	0.04
^{nat}Sn	4.2(13)	3.0	-	-	2.5 (5)	2.7	-	-	1.9
^{nat}Mo	1,474 (44) ^{a,c}	2.5	407(39) ^{a,c}	2.5	8.5(15) ^{b,c}	2.3	817(258) ^{b,c}	2.0	0.5
^{nat}Zn	2.4 (8)	1.6	-	-	1.8 (5)	1.5	-	-	0.3

^a Transitions to excited states observed

^b Photoexcitation identified from size of differential cross section

^c Photoexcitation reported in [11]

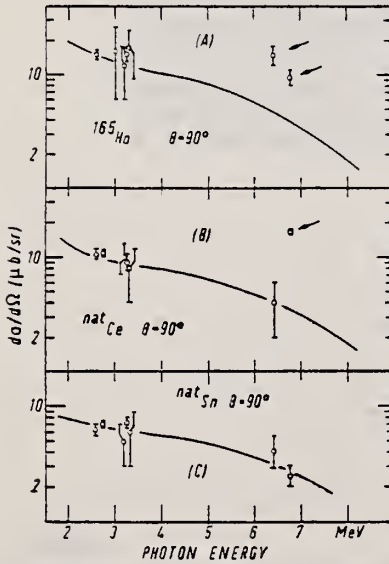


Fig. 11. Same as Fig. 9 but for (A) ^{165}Ho , (B) ^{nat}Ce and (C) ^{nat}Sn

REF. A. Leprétre, H. Beil, R. Bergère, P. Carlos, J. Fagot, A. Veyssiére
 I. Halpern
 Nucl. Phys. A390, 221 (1982)

ELEM. SYM.	A	z
Ce		58

METHOD	REF. NO.	EGF				
	82 Le 3					
REACTION	RESULT	EXCITATION ENERGY	SOURCE	DETECTOR	ANGLE	
G,XN	NOX	30-140	D	30-140	MOD-I	4PI

See also A. Lepretre et al. NP A390, 240 (1982)

MULT ANAL 81LE1

Abstract: From event-by-event records of observed photoneutron multiplicities for photons from 30 to 140 MeV on several heavy targets (Sn, Ce, Ta and Pb), it was possible to determine the mean number of photoneutrons, $\bar{\nu}$, for each photon energy and the widths W of the multiplicity distributions. The mean neutron numbers increase smoothly from about three to six over the photon energy span for all four targets. The widths go from about one to two neutrons in the same interval. When these measurements are combined with other photonuclear information, it is possible to extract the average numbers of fast neutrons and fast protons and the average number of evaporation neutrons emitted per photoabsorption.

E PHOTONUCLEAR REACTIONS Sn, Ce, Ta, Pb(γ , xn), $E = 25-140$ MeV; measured photoneutron mean numbers, width distributions; deduced fast evaporation neutron, fast proton average numbers. Monochromatic photons.

TABLE 2
 Photonucleon emission features for four targets at 70 MeV

	Sn	Ce	Ta	Pb
$\bar{\nu}$	4.3 ± 0.2	4 ± 0.2	4.5 ± 0.2	4.8 ± 0.2
$\bar{\nu}_f$	0.50 ± 0.11	0.59 ± 0.13	0.71 ± 0.16	0.66 ± 0.15
$\bar{\nu}_e$	0.24 ± 0.05	0.26 ± 0.05	0.27 ± 0.05	0.23 ± 0.04
$\bar{\nu}_s$	3.8 ± 0.3	3.4 ± 0.3	3.8 ± 0.3	4.1 ± 0.3
E_f (MeV)	23.4 ± 5	26.3 ± 6	28.7 ± 6	26.6 ± 6
E^* (MeV)	46.6 ± 6	43.7 ± 5	41.3 ± 5	43.4 ± 5

(See caption under table 1.)

Experimental data are taken from ref.¹⁾ and fig. 2 of this paper. ν stands for neutrons and π for protons; f stands for fast particles and s for evaporated particles. E^* is the residual excitation energy after all fast particles have escaped - carrying with them energy E_f . The coefficients α and β have to do with the ratio of fast neutrons to fast protons that are emitted. They are explained in the text. The uncertainties in this table are statistical only.

(OVER)

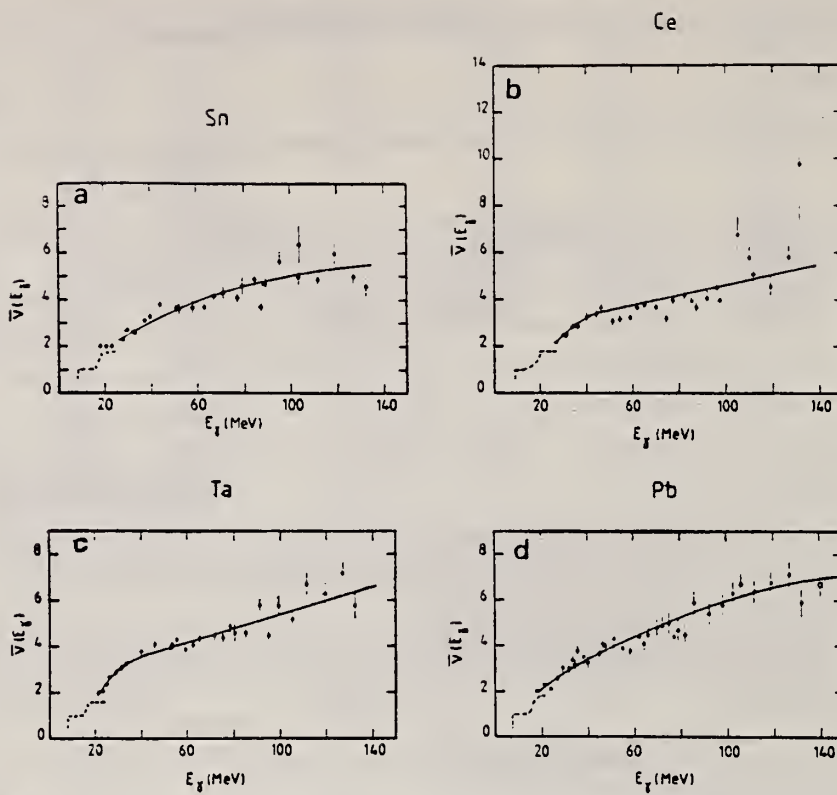


Fig. 2. Average experimental photoneutron multiplicities $\bar{\nu}(E_\gamma)$ plotted against photon energy E_γ for $25 \text{ MeV} \leq E_\gamma \leq 140 \text{ MeV}$. Data points were evaluated using results from ref. ¹⁾. The full line represents a smoothed average behaviour. The dashed line represents $\bar{\nu}(E_\gamma)$ values, measured in the giant dipole resonance (GDR) region, in previous Saclay experiments ²⁾. Fig. 2a: Sn; fig. 2b: Ce; fig. 2c: Ta; fig. 2d: Pb [where the \square point refers to the SIN ¹⁹⁾ measurement with stopped π^-].

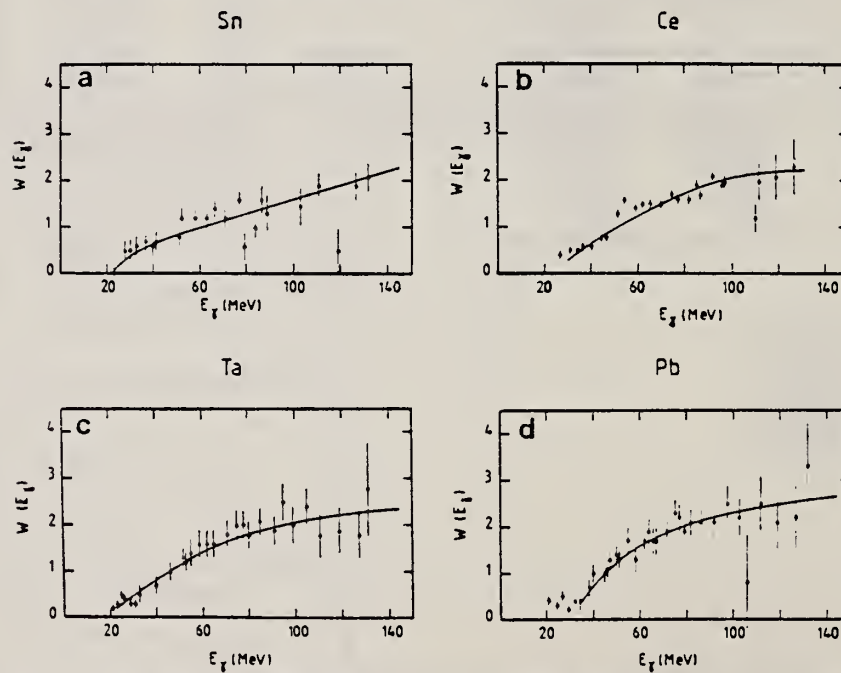


Fig. 3. Widths, $W(E_\gamma)$, of the experimental photoneutron multiplicity distributions as a function of the photon energy E_γ for $25 \text{ MeV} \leq E_\gamma \leq 140 \text{ MeV}$. Data points were evaluated using results from ref. ¹⁾. The full line represents a smoothed average behaviour. Fig. 3a: Sn; fig. 3b: Ce; fig. 3c: Ta; fig. 3d: Pb.

CE
A=138

CE
A=138

CE
A=138

REF.

P. E. Haustein and A. F. Voigt
J. inorg. nucl. Chem. 33, 289 (1971)

ELEM. SYM.	A	Z
Ce	138	58

METHOD

REF. NO.

71 Ha 2

egf

REACTION	RESULT	EXCITATION ENERGY	SOURCE		DETECTOR		ANGLE
			TYPE	RANGE	TYPE	RANGE	
G,N	RLY	10-70	C	70	ACT-I		4PI

Isomer ratio = (yield to low spin state)/(yield to high spin state)

ISOMER RATIOTable 2. Isomer ratio measurements for ^{96}Mo , ^{132}Ce , and ^{144}Nd

Reaction	Isomer ratio	J^π Target	J^π Ground state	J^π Isomer state	Threshold (MeV)	$41A^{-1/2}$ (MeV)
$^{96}\text{Mo}(\gamma, n)^{95}\text{Mo}$	1.92 ± 0.15	0°		$9/2^+$	13.13	16.60
$^{96}\text{Mo}(\gamma, 3n)^{94}\text{Mo}$	1.59 ± 0.16	0°		$1/2^-$	30.72	16.52
$^{132}\text{Ce}(\gamma, n)^{133}\text{Ce}$	3.1	0°		$3/2^+$	10.31	15.30
$^{132}\text{Ce}(\gamma, 3n)^{131}\text{Ce}$	1.10 ± 0.12	0°		$11/2^+$	26.34	15.26
$^{144}\text{Nd}(\gamma, n)^{145}\text{Nd}$	5.2 ± 0.3	0°		$3/2^+$	9.79	15.22
$^{144}\text{Nd}(\gamma, 3n)^{143}\text{Nd}$	1.80 ± 0.25	0°		$11/2^+$	23.67	15.17

C_E
A=140

C_E
A=140

C_E
A=140

Method	50 MeV electron synchrotron; activation; NaI					Ref. No.
						62 Ca 1

Reaction	E or ΔE	E_0	Γ	$\int \sigma dE$	$J\pi$	Notes
Ce ¹⁴⁰ (γ, n)	Bremss.					

50

TABLE I
 Isomeric ratios from (γ, n) reactions

Target nucleus	J_π	Residual nucleus						Isomer ratio $Y_i/(Y_i + Y_s)$	σ		
		Ground state		Metastable state		Intermediate state					
		Spin	Half-life	Spin	Half-life	Spin					
Co ⁵⁹	$\frac{5}{2}^-$	Co ⁵⁸	2+	71.3 d	5+	9.2 h		0.44 ± 0.02	3.2 ± 0.2		
Ge ⁷⁰	0+	Ge ⁷⁰	$\frac{1}{2}^-$	82 min	5+	49 s		0.48 ± 0.07	2.8 ± 0.5		
Br ⁸¹	$\frac{1}{2}^-$	Br ⁸⁰	1+	18 min	5-	4.4 h	2-	0.32 ± 0.02	6.5 ± 1.0		
Sr ⁸⁶	0+	Sr ⁸⁵	$\frac{1}{2}^+$	64 d	1-	70 min	$\frac{3}{2}^+$	0.36 ± 0.07	2.2 ± 0.4		
Zr ⁹⁰	0+	Zr ⁸⁹	$\frac{3}{2}^+$	79 h	1-	4.4 min		0.33 ± 0.10	2.8 ± 0.7		
Mo ⁹¹	0	Mo ⁹¹	$\frac{3}{2}^+$	15.7 min	1-	66 s		0.46 ± 0.04	6.4		
Ag ¹⁰⁷	$\frac{1}{2}^-$	Ag ¹⁰⁶	1+	24 min	6	8.3 d		0.04 ± 0.02	2.0 ± 0.3		
In ¹¹³	$\frac{1}{2}^+$	In ¹¹³	1+	14.5 min	4+	20.7 min	7-	0.8 ± 0.1	3.1 ± 0.7		
Cd ¹¹⁶	0+	Cd ¹¹⁶	$\frac{3}{2}^+$	53 h	1-	43 d		≤ 0.2	≤ 3		
Ce ¹⁴⁰	0+	Ce ¹³⁹	$\frac{3}{2}^+$	140 d	1-	55 s		0.08 ± 0.01	2.5 ± 0.2		
Hg ¹⁹²	0-	Hg ¹⁹¹	$\frac{1}{2}^-$	65 h	1+	24 h	1-	0.05 ± 0.01	3.4 ± 0.5		
				..			1-				

Ref. Previous work

Br ⁸¹ 10)	$\frac{1}{2}^-$	Br ⁸⁰	1+	18 min	5-	4.4 h	2-	0.33	6.5
Sc ⁸³ 11)	0+	Sc ⁸¹	$\frac{1}{2}^-$	18 min	5+	57 min		0.5	3.0
Zr ⁹⁰ 11)	0+	Zr ⁸⁹	$\frac{3}{2}^+$	79 h	1-	4.3 min		0.44 ± 0.06	4.5 ± 1
In ¹¹⁴ 12)	$\frac{1}{2}^+$	In ¹¹⁴	1+	72 s	5+	50 d	8	0.85	5.0

($T_{1/2} = 2.5$ s)

The yields Y_i and Y_s are for (γ, n) reactions ending in the isomeric- or ground-state. The yield Y_1 is for the higher-spin state.

References

- 1) J. R. Huizenga and R. Vandenbosch, Phys. Rev. 120 (1960) 1305
- 2) T. Ericson, Advances in Physics 9 (1960) 425
- 3) D. L. Allan, Nuclear Physics 24 (1961) 274
- 4) C. T. Hibdon, Phys. Rev. 114 (1959) 179
- 5) C. T. Hibdon, Phys. Rev. 122 (1961) 1233
- 6) T. Ericson, Nuclear Physics 11 (1959) 481
- 7) J. H. Carver, and G. A. Jones, Nuclear Physics 19 (1960) 184
- 8) A. C. Douglas and N. MacDonald, Nuclear Physics 13 (1959) 382
- 9) T. Ericson and V. M. Scrutinski, Nuclear Physics 8 (1958) 284
- 10) L. Katz, L. Pease and H. Moody, Can. J. Phys. 30 (1952) 476
- 11) L. Katz, R. G. Baker and R. Montalbetti, Can. J. Phys. 31 (1953) 250
- 12) E. Silva and J. Goldemberg, An Acad. Brasil Ciencia 28 (1956) 275
- 13) J. H. Carver and D. C. Peaslee, Phys. Rev. 120 (1960) 2155
- 14) J. M. Blatt and V. F. Weisskopf, Theoretical nuclear physics (John Wiley, New York, 1952)
- 15) S. H. Vegers, L. L. Marsden and R. L. Heath, U. S. Atomic Energy Commission Report IDO-16370 (1958)
- 16) Nuclear Data Sheets (National Research Council, Washington, 1960) sets 1-5 inclusive
- 17) R. Vandenbosch and J. R. Huizenga, Phys. Rev. 120 (1960) 1313
- 18) E. Weigold and R. N. Glover, Nuclear Physics 32 (1962) 106
- 19) K. J. Le Couteur and D. W. Lang, Nuclear Physics 13 (1958) 32
- 20) T. D. Newton, Can. J. Phys. 34 (1956) 804
- 21) D. W. Lang, Nuclear Physics 26 (1961) 434
- 22) M. E. Rose, Internal conversion coefficients (North Holland Publ. Co., Amsterdam, 1953)
- 23) J. Goldemberg and L. Katz, Phys. Rev. 90 (1953) 308

H. Fuchs, R. Kosiek, U. Meyer-Berkhout
Z. Physik 166, 590 (1962)

ELEM. SYM.	A	Z
Ce	140	58

METHOD

Betatron; neutron yield; radioactivity

REF. NO.	NVB
62 Fu 6	

REACTION	RESULT	EXCITATION ENERGY	SOURCE		DETECTOR		ANGLE
			TYPE	RANGE	TYPE	RANGE	
G,N	RLY	5 - 31	C	31	ACT - I		4PI

$$\frac{Y(Ce^{139 \text{ m+g}})}{Y(Cu^{62})} = 3.2 \pm 0.35, E_0 = 31 \text{ MeV}$$

Tabelle 2. Ausbeuteverhältnisse für die Reaktionen am Silber und Cer. E_0 ist die Maximalenergie der Bremsstrahlung, Y_1/Y_2 ist das Verhältnis der Ausbeute der in der ersten Spalte genannten Reaktion zu der Ausbeute der Reaktion in der zweiten Spalte

Reaktion 1	Reaktion 2	E_0 (MeV)	Y_1/Y_2
$Ag^{107}(\gamma, n) Ag^{106m}$	$Ag^{107}(\gamma, n) Ag^{106g}$	34	0.08 ± 0.015
$Ag^{107}(\gamma, n) Ag^{106m}$	$Ag^{107}(\gamma, n) Ag^{106g}$	18	0.06 ± 0.010
$Ag^{107}(\gamma, n) Ag^{106m+g}$	$Ag^{107}(\gamma, n) Ag^{106g}$	34	1.08 ± 0.015
$Ag^{107}(\gamma, 2n) Ag^{105}$	$Ag^{107}(\gamma, n) Ag^{106g}$	34	0.12 ± 0.06
$Ag^{107}(\gamma, 2n) Ag^{105}$	$Ag^{107}(\gamma, n) Ag^{106g}$	18	0.06 ± 0.03
$Ag^{108}(\gamma, n) Ag^{108}$	$Ag^{107}(\gamma, n) Ag^{106g}$	34	0.92 ± 0.14
$Ce^{140}(\gamma, n) Ce^{139m}$	$Ce^{140}(\gamma, n) Ce^{139g}$	31	0.193 ± 0.014
$Ce^{140}(\gamma, n) Ce^{139m}$	$Ce^{140}(\gamma, n) Ce^{139g}$	23,8	0.182 ± 0.018

ELEM. SYM.	A	Z
Ce	140	58

METHOD					REF. NO.		
REACTION	RESULT	EXCITATION ENERGY	SOURCE		DETECTOR		ANGLE
			TYPE	RANGE	TYPE	RANGE	
G,N	ABY	THR-20	C	20	ACT-I		4PI

ISOMERIC YIELDTABLE I. THE PARTICULARS OF THE (γ, n) REACTION PRODUCTS AND THE DATA OBTAINED WITH 20 MeV BREMSSTRAHLUNG

Nuclide		Half-life of product (sec)	Gamma-ray determined			Limit of detection (μg)	Yield ($\text{mol}^{-1} \cdot \text{R}^{-1}$)
Parent (Natural abundance, %)	Residual		Energy (MeV)	Branching ratio (%)	Photopeak activity ($\text{cpm}/\text{mg}^{\text{a}}$)		
²⁴ Mg(78.60)	²³ Mg	9.9	0.511	200	2.04×10^4	0.49	8.1×10^4
⁷⁶ Ge(7.67)	^{75m} Ge	48	0.139	100	6.37×10^4	1.6	1.1×10^4
⁷⁸ Sc(23.52)	^{77m} Sc	17	0.162	100	1.82×10^4	0.55	1.2×10^4
⁹² Mo(15.86)	^{91m} Mo	65	0.650	57	2.22×10^4	4.5	2.7×10^4
¹⁴⁰ Ce(88.48)	^{139m} Ce	58	0.745	100	1.06×10^4	0.95	1.3×10^4
¹⁴² Nd(27.13)	^{141m} Nd	64	0.760	100	3.19×10^4	3.1	1.4×10^4
¹⁵⁸ Tb(100)	^{157m} Tb	11	0.111	100	2.56×10^4	3.8	2.2×10^4

a) The value corrected at the end of one-minute irradiation with the dose rate of 10^7 R/min ; Counting geometry is 20% with a 3"dia. \times 3"NaI(Tl) detector.

ELEM. SYM.	A	Z
Ce	140	58

METHOD

REF. NO.

68 Sh 4

egf

REACTION	RESULT	EXCITATION ENERGY	SOURCE		DETECTOR		ANGLE
			TYPE	RANGE	TYPE	RANGE	
E,P	SPC	13-30	D	30	MAG-D	5-15	90

ANALOGUE STATES

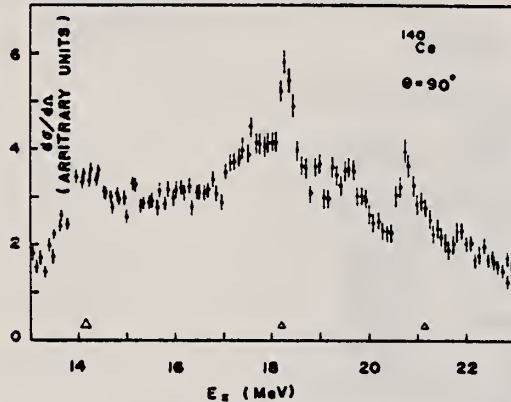


Fig. 2. Photopion cross section for ^{140}Ce calculated from the energy distribution of the $E_{\gamma} = 30.0$ MeV bombardment.

The scale was constructed under the assumption that observed protons correspond to ground-state transitions. The triangles show the energy resolution. The solid curve is the (γ, p_0) cross section calculated from the (p, γ_0) data.

K. Shoda, M. Sugawara, T. Saito & H. Miyase
 PICNS-69 Proceedings of the Conference on Nuclear Isospin.
 Asilomar-Pacific Grove, California 1969 (Academic Press,
 New York & London 1969) p.137.

ELEM. SYM.	A	Z
Ce	140	58

METHOD

REF. NO.	egf
69 Sh 8	

REACTION	RESULT	EXCITATION ENERGY	SOURCE		DETECTOR		ANGLE
			TYPE	RANGE	TYPE	RANGE	
E, P	SPC	13-22	D	20, 22	MAG-D		DST

Table 1. Angular distributions of strong proton groups from ^{140}Ce and ^{141}Pr .

Nucleus	E_p (MeV)	$w(\theta)$
^{140}Ce	10.3	$1+(0.4+0.1)P_1-(0.0+0.1)P_2$
	12.8	$1+(0.2+0.1)P_1-(0.4+0.2)P_2$
^{141}Pr	9.7	$1+(0.0+0.1)P_1+(0.1+0.2)P_2$

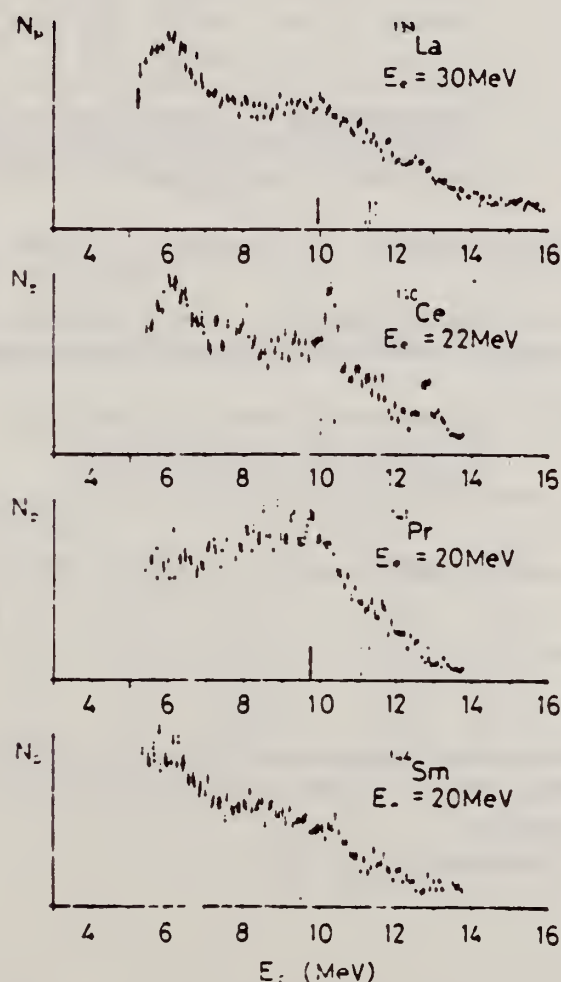


Fig. 1. Energy distributions of photoprottons. Vertical broken lines and solid lines indicate the position of p_0 corresponding to the ground IAS and electric dipole IAS (2).

(over)

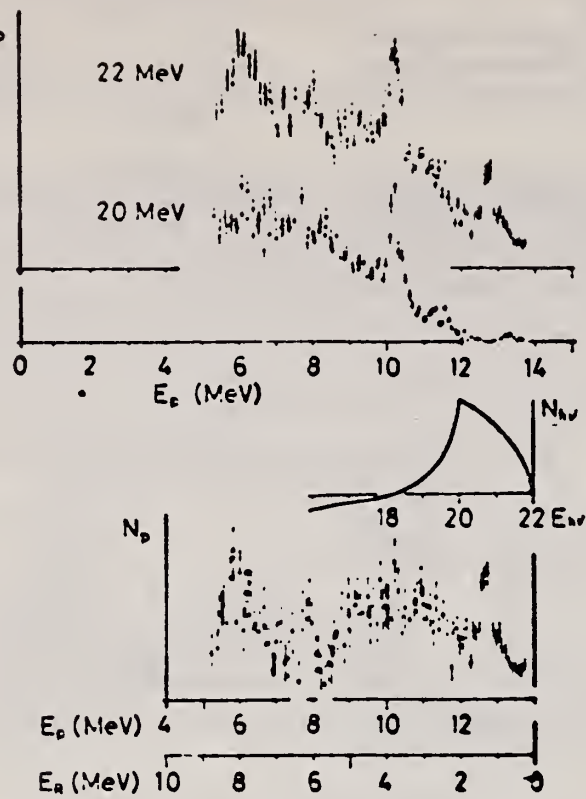


Fig. 2. Comparison of energy distributions on ^{140}Ce irradiated by 20.0 MeV and 22.0 MeV electron beam. The lowest spectrum is a difference of the two. Photon spectrum corresponding to this difference is also shown.

Table 2. The radiative widths of the main IAS. The results are compared with the single particle strength in W.u..

Nucleus	E_p (MeV)	E_x (MeV)	(a)	Γ_{p_0}/Γ	Γ_γ (eV)	$2(T+1)\Gamma_{\gamma_0}$ (W.u.)
^{140}Ce	10.3	18.3		1 (b)	50	0.1
	—	12.8	20.8	1 (c)	90	0.1
^{151}Pr	—	9.7	15.1	12/60(c)	40	0.2
^{152}Sm	10.6	16.6		1 (b)	20	0.05

(a) Ground state is assumed for the residual state.

(b) Assumption.

(c) P. VonBrentano et al. (2).

ELEM. SYM.	A	Z
Ce	140	58

METHOD

REF. NO.

70 Pi 1

egf

REACTION	RESULT	EXCITATION ENERGY	SOURCE		DETECTOR		ANGLE
			TYPE	RANGE	TYPE	RANGE	
E, E/	LFT	1-4	D	50, 60	MAG-D		141

6 LEVELS, J-PI

E _x /MeV	J ^π	Y _{Duke}	Y _{exp}	Γ _γ %/eV	Γ _γ %/Γ _W
1,60	2 ⁺	0,65	0,67 ± 0,05	6,7 · 10 ⁻³	18 ± 2
2,08	4 ⁺	2,20	2,27 ± 0,56	1,5 · 10 ⁻³	21 ± 4
2,46	3 ⁻	1,28	1,31 ± 0,11	6,2 · 10 ⁻³	26 ± 3
2,90	1 ⁺	0,29	—		
	2 ⁺	0,65	0,58 ± 0,19	9,5 · 10 ⁻³	1,3 ± 0,5
3,12	1 ⁺	0,29	—		
	2 ⁺	0,65	0,58 ± 0,13	26 · 10 ⁻³	2,6 ± 0,5
3,32	1 ⁺	0,29	—		
	2 ⁺	0,65	0,73 ± 0,28	19 · 10 ⁻³	1,3 ± 0,6

Tab. 1. Vorläufige Ergebnisse. Y ist das Verhältnis der bei 60 MeV und 50 MeV Primärenergie gemessenen differentiellen Wirkungsquerschnitte ($\Theta = 141^\circ$). Spins und Paritäten J^π nach Ref. ¹⁰. Γ_W : Weisskopf-Einheit (WE) nach WILKINSON ¹³.

¹⁰ H.W. Baer, J.J. Reidy u. M.L. Wiedenbeck, Nucl. Phys. A113, 33 (1968).

¹³ D.H. Wilkinson, in F. Ajzenberg-Selove, Nucl. Spectroscopy, New York und London 1960.

REF.

P. E. Haustein and A. F. Voigt
 J. inorg. nucl. Chem. 33, 289 (1971)

ELEM. SYM.	A	Z
Ce	140	58

METHOD

REF. NO.

71 Ha 2

egf

REACTION	RESULT	EXCITATION ENERGY	SOURCE		DETECTOR		ANGLE
			TYPE	RANGE	TYPE	RANGE	
G, 3N	RLY	26-70	C	70	ACT-I		4PI

Isomer ratio = (yield to low spin state)/(yield to high spin state)

ISOMER RATIOTable 2. Isomer ratio measurements for ⁹¹Mo, ¹³⁷Ce, and ¹⁴¹Nd

Reaction	Isomer ratio	I^π Target	I^π Ground state	I^π Isomer	Threshold (MeV)	$4IA^{-1/2}$ (MeV)
⁹¹ Mo(γ, n) ⁹¹ Mo	1.92 ± 0.15	0^+			13.13	16.60
⁹¹ Mo($\gamma, 3n$) ⁹¹ Mo	1.59 ± 0.16	0^+	$9/2^+$	$1/2^-$	30.72	16.52
¹³⁷ Ce(γ, n) ¹³⁷ Ce	3.1	0^+			10.31	15.30
¹⁴⁰ Ce($\gamma, 3n$) ¹³⁷ Ce	1.10 ± 0.12	0^+	$3/2^+$	$11/2^+$	26.34	15.26
¹⁴² Nd(γ, n) ¹⁴¹ Nd	5.2 ± 0.3	0^+			9.79	15.22
¹⁴⁴ Nd($\gamma, 3n$) ¹⁴¹ Nd	1.80 ± 0.25	0^+	$3/2^+$	$11/2^+$	23.67	15.17

METHOD

REF. NO.

71 Sh 3

hmrg

REACTION	RESULT	EXCITATION ENERGY	SOURCE		DETECTOR		ANGLE
			TYPE	RANGE	TYPE	RANGE	
E, P	ABX	15-22	D	23	MAG-D		90

The energy distributions of protons from the $(e, e'p)$ reaction on $N=82$ nuclei with even Z have been measured. The cross sections of the $(\gamma, p_0 + p_1)$ reaction have been estimated. Two prominent isobaric analogs have been found in each nucleus. The results were used for the systematic discussion of the odd-odd parent nuclei ^{138}Cs , ^{140}La , ^{142}Pr , and ^{144}Pm . The 1^- states are estimated at 600 and ~ 2500 keV for ^{138}Cs , 500 and 3000 keV for ^{140}La , 1100 and 3700 keV for ^{142}Pr , and 1400 and 4300 keV for ^{144}Pm . The parameters of these states are discussed in terms of a quasiproton and single-neutron model.

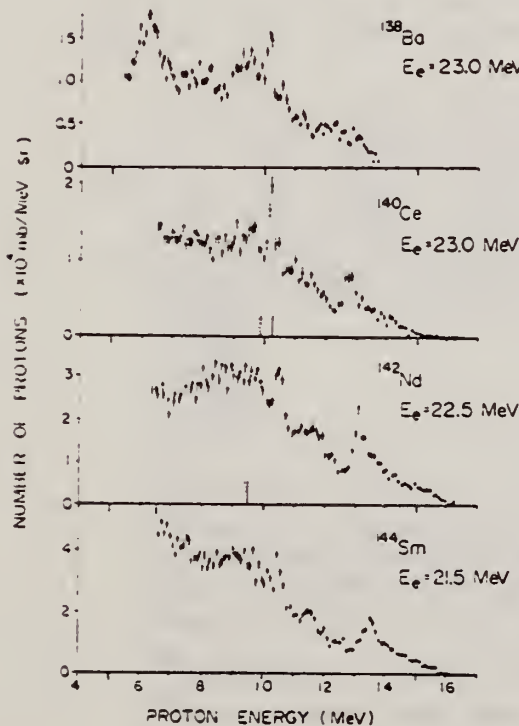


FIG. 1. Energy distributions of protons emitted from the $(e, e'p)$ reaction at $\theta = 90^\circ$.

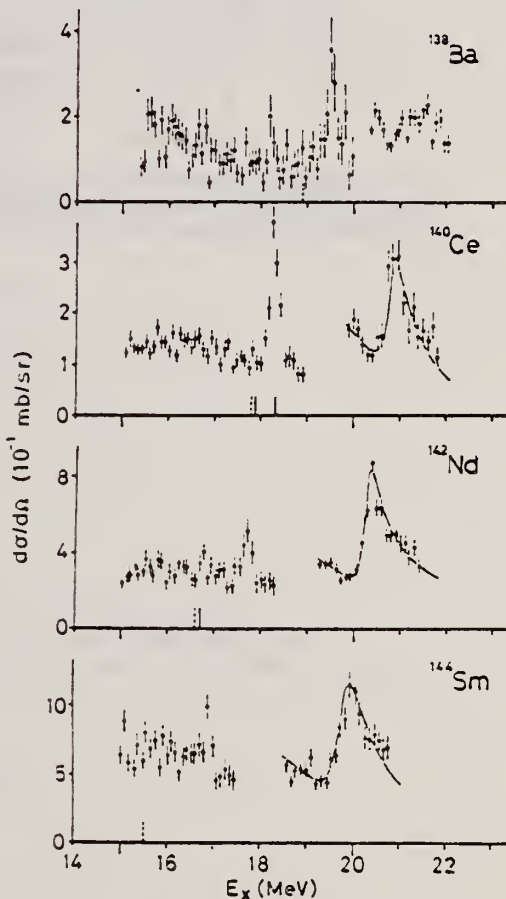


FIG. 2. The photopion cross sections for $p_0 - p_1$ at $\theta = 90^\circ$ in the vicinity of the isobaric analog resonances. The curves for the broad resonances were obtained from the fitting of the interference formula.

(over)

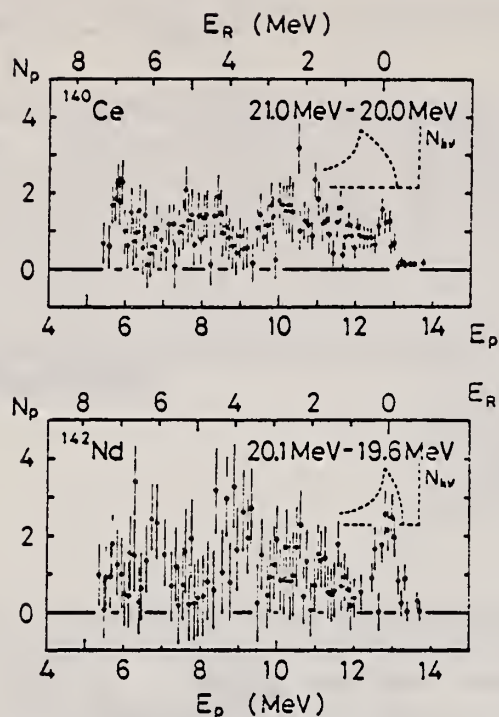


FIG. 5. The proton groups emitted through the isobaric analogs at 20.8 MeV in ^{140}Ce and at 20.3 MeV in ^{142}Nd . The energies of the residual states are also indicated by E_R .

ELEM. SYM.	A	Z
Ce	140	58

METHOD	REF. NO.				
	73 Pi 3	egf			
REACTION	RESULT	EXCITATION ENERGY	SOURCE	DETECTOR	ANGLE
E, E/	LFT	1- 3	D	50, 65	MAG-D
					DST

2+, 3-, 4+ LEVELS

Tabelle 2. Meßergebnisse der untersuchten Kernniveaus in Ce. Die B -Werte sind die $B(E\lambda, q=0, 0^+ \rightarrow \lambda^+)$, vgl. [1]. Weißkopfeinhheiten Γ_W für die Ergebnisse dieser Arbeit nach Wilkinson, D. H. (in: Nuclear Spectroscopy, ed. F. Ajzenberg-Selove, New York und London 1960) mit $R=1,2$ fm; die zitierten Werte anderer Autoren weichen davon bis zu 3% ab

Isotop	λ_1^+	E_x MeV	$B(E\lambda, 0)$ fm 2	Γ_γ^0 eV	Γ_γ^0/Γ_W	Andere Autoren Γ_γ^0/Γ_W	Theoret. Werte Γ_γ^0/Γ_W
¹⁴⁰ Ce	2 ₁ ⁺	1,60	$2,7 \cdot 10^3$	$4,6 \cdot 10^{-3}$	$12,5 \pm 2$	$16,0 \pm 2,5$ ^a $12,5 \pm 1,8$ ^b $8,3 \pm 0,8$ ^d	13,0 ^c
	3 ₁ ⁻	2,46	$2,0 \cdot 10^5$	$6,4 \cdot 10^{-6}$	24 ± 3	$93 \pm (30-45)$ ^e $6,0 \pm 0,6$ ^d	12,5 ^f
	4 ₁ ⁺	2,08	$5,9 \cdot 10^6$	$5,4 \cdot 10^{-11}$	20 ± 4	$5,5 \pm 0,6$ ^d	15,0 ^g
¹⁴² Ce	2 ₁ ⁺	0,64	$6,5 \cdot 10^3$	$1,1 \cdot 10^{-5}$	30 ± 15	$19,5 \pm 0,5$ ^b	35,0 ^f
	3 ₁ ⁻	1,65	$9,0 \cdot 10^3$	$1,8 \cdot 10^{-6}$	110 ± 40	135 ± 70 ^c	
	4 ₁ ⁺	1,22	$1,3 \cdot 10^7$	$9,7 \cdot 10^{-13}$	45 ± 25		

^a Ofer, S., Schwarzschild, A.: Phys. Rev. 116, 725 (1959).

^b Eccleshall, D., Yates, M. J. L., Simpson, J. J.: Nucl. Phys. 78, 481 (1966).

^c Ref. [21].

^d Ref. [24].

^e Ref. [27].

^f Ref. [29].

^g Ref. [28].

²¹ Hansen, O., Nathan, N.: Nucl. Phys. 42, 197 (1963).

²⁴ Baker, F. T., Tickle, R. S.: Phys. Lett. 32B, 47 (1970). Die Übergänge sind zitiert nach: Baer, H. W., Griffin, H. C., Gray, W. S.: Phys. Rev. C3, 1398 (1971), denn die Autoren selbst geben keine Zahlen an.

²⁷ Rho, M.: Nucl. Phys. 65, 497 (1965).

²⁸ Waroquier, M., Heyde, K.: Nucl. Phys. A164, 113 (1971).

²⁹ Mustafa, S. M.: Nucl. Phys. A185, 309 (1972).

ELEM.	SYM.	A	Z
Ce		140	58

METHOD					REF. NO.		
REACTION	RESULT	EXCITATION ENERGY	SOURCE		DETECTOR		ANGLE
			TYPE	RANGE	TYPE	RANGE	
G,G	LFT	5	D	4- 8	SCD-D		DST

5=5.66

TABLE 2

Measured angular distribution coefficients A_2 , the ratios $N_{||}/N_{\perp}$, the spins and parities of the ground and the resonance levels, J_0^{π} and J_r^{π} , and the character of the ground state transition

Scatterer	E_{γ} (keV)	A_2	$N_{ }/N_{\perp}$	J_0^{π}	J_r^{π}	Transition
⁵⁵ Mn	7491	0.01 ± 0.02	1.00 ± 0.02	$\frac{1}{2}^-$	$\frac{3}{2}^+$	
¹⁴⁰ Ce	5660	0.51 ± 0.02	1.14 ± 0.04	0^+	1^-	E1
¹⁴¹ Pr	6877	0.11 ± 0.02	0.95 ± 0.03	$\frac{1}{2}^+$	$\frac{3}{2}^+$	M1
¹⁴² Nd	6877	0.51 ± 0.03	1.10 ± 0.04	0^+	1^-	E1
²⁰² Hg	4922	0.51 ± 0.02	1.18 ± 0.03	0^+	1^-	E1
²⁰⁹ Bi	5603	0.06 ± 0.02	0.97 ± 0.02	$\frac{1}{2}^-$	$\frac{3}{2}^-$	M1

TABLE 4

Values of Γ , Γ_0 and the energy separation δ (between the incident γ -line and the resonance level) as obtained from the analysis of the various experiments

Scatterer	E_{γ} (keV)	Γ (meV)	Γ_0 (meV)	δ (eV)	D (eV)	K_{E1} (10^{-9} MeV $^{-3}$)	K_{M1} (10^{-9} MeV $^{-3}$)
⁵⁵ Mn	7491	450 ± 250	80 ± 40	17 ± 1			
¹⁴⁰ Ce *)	5660	13 ± 3	12 ± 2	4.7 ± 0.3	6800	0.33	
¹⁴¹ Pr *)	6877	85 ± 35	17 ± 9	6.7 ± 1.5	450		116
¹⁴² Nd *)	6877	340 ± 40	270 ± 20	12.4 ± 0.3	1200	26	
²⁰² Hg	4922	300 ± 50	260 ± 20	4.2 ± 0.5	19000	3.4	
²⁰⁹ Bi *)	5603	950 ± 200	950 ± 200	13 ± 1	34000		160

The radiative strengths K_{E1} and K_{M1} are also given. The level spacing D refers to the excitation energy of the resonance level E_{γ} .

*) These values are slightly different from those of ref. *) and were obtained from a renewed analysis of the experimental results.

8

A. Wolf, R. Moreh, A. Nof, O. Shahal, J. Tenenbaum,
Phys. Rev. C5, 2276 (1972).

REF.

R.M. Laszewski, R.J. Holt, and H.E. Jackson
 Phys. Rev. C13, 2257 (1976)

ELEM. SYM.	A	Z
Ce	140	58

METHOD	REF. NO.	hmg
	76 La 4	

THRESHOLD MEAS

The $^{140}\text{Ce}(\gamma, n)^{139}\text{Ce}$ reaction has been studied near threshold with high energy resolution. The angular distribution of photoneutrons was measured at 90° and 135° , and the $M1$ and $E1$ strength functions at an excitation of approximately 9.1 MeV were determined. The measured integrated $M1$ strength was found to be consistent with the existence of a giant $M1$ resonance centered at 8.7 MeV as suggested both by calculation and previous electron scattering data. The integrated $E1$ strength was also found to be consistent with what is known of the $E1$ strength function in the threshold region.

TABLE II. $M1$ and $E1$ ground-state transition strengths integrated over the 40-keV interval centered at 9.08 MeV. Statistical uncertainties are estimated to be of the order 1%. Possible systematic uncertainties of the order 10% are estimated as discussed in the text.

Transitions	$\sum \Gamma_\gamma(M(E)1)$	$B(\gamma, M(E)1)$	$\bar{k}_{M(E)1}$
$M1$	1.1 eV	$0.39 \left(\frac{e\hbar}{2mc} \right)^2$	37×10^{-3}
$E1$	1.7 eV	$6.6 \times 10^{-3} e^2 \text{ fm}^2$	2.2×10^{-3}

METHOD	REF. NO.	egf
	76 Le 2	

REACTION	RESULT	EXCITATION ENERGY	SOURCE		DETECTOR		ANGLE
			TYPE	RANGE	TYPE	RANGE	
G, N	ABX	8 - 26	D	8 - 26	MOD-I		4PI
G, 2N	ABX	16 - 26	D	8 - 26	MOD-I		4PI

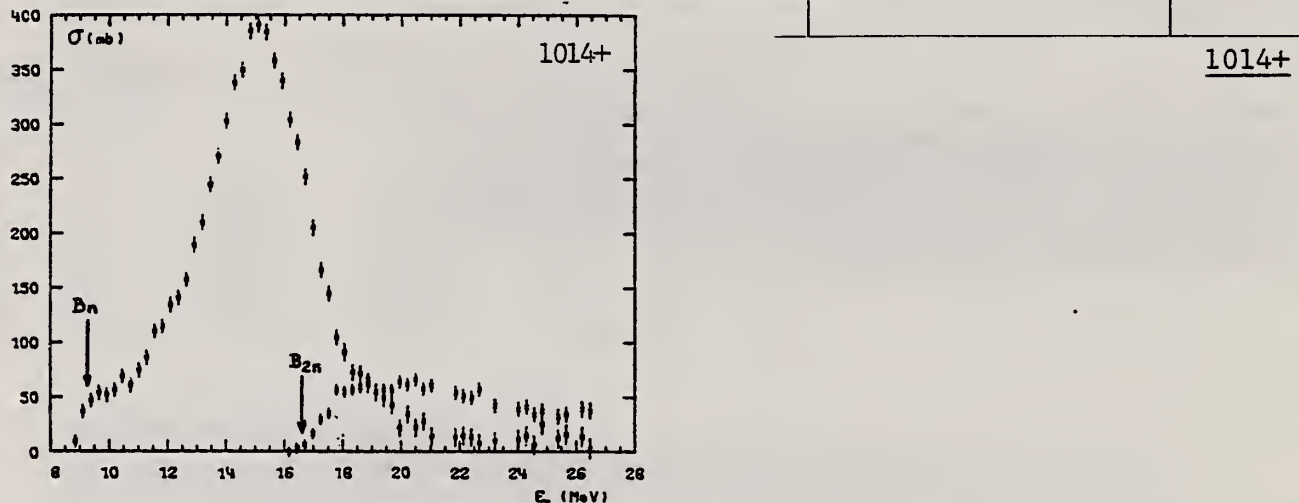


Fig. 5. Partial photoneutron cross sections $[\sigma(\gamma, n) + \sigma(\gamma, pn)]$ and $\sigma(\gamma, 2n)$ for ^{140}Ce . Arrows B_n and B_{2n} indicate theoretical threshold values for (γ, n) and $(\gamma, 2n)$ reactions respectively.

TABLE 3
Lorentz line parameters corresponding to best fits shown in figs. 9 and 10

Nucleus	^{124}Te	^{126}Te	^{128}Te	^{130}Te	^{140}Ce	^{142}Ce
σ_1 (mb)	281 ± 15	294 ± 15	304 ± 15	318 ± 16	384 ± 20	332 ± 17
Γ_1 (MeV)	5.5 ± 0.2	5.6 ± 0.2	5.4 ± 0.2	5.1 ± 0.2	4.4 ± 0.1	5.2 ± 0.2
E_1 (MeV)	15.2 ± 0.1	15.1 ± 0.1	15.1 ± 0.1	15.1 ± 0.1	15.0 ± 0.1	14.9 ± 0.1

TABLE 4
Integrated photoneutron cross sections and comparison with sum rules

Nucleus	^{124}Te	^{126}Te	^{128}Te	^{130}Te	^{140}Ce	^{142}Ce
E_M (MeV)	26.5	25.1	26.2	25.9	26.5	23.5
σ_0 (MeV · b)	2.04	2.04	2.11	2.19	2.40	2.21
$\frac{\sigma_0 A}{0.06 NZ}$	1.12	1.11	1.14	1.17	1.18	1.07
σ'_0 (MeV · b)	2.44	2.56	2.58	2.55	2.65	2.69
$\frac{\sigma'_0 A}{0.06 NZ}$	1.34	1.39	1.39	1.36	1.30	1.30
σ_{-1} (mb)	128	130	135	140	154	149
$\sigma_{-1} A^{-1}$ (mb)	0.21	0.20	0.21	0.21	0.21	0.20
σ_{-2} (mb · MeV ⁻¹)	8.4	8.6	9.1	9.4	10.3	10.6
$\sigma_{-2} A^{-1}$ ($\mu\text{b} \cdot \text{MeV}^{-1}$)	2.7	2.7	2.8	2.8	2.7	2.7

ELEM. SYM.	A	Z
Ce	140	58

METHOD

REF. NO.
 81 Me 2

hg

REACTION	RESULT	EXCITATION ENERGY	SOURCE		DETECTOR		ANGLE
			TYPE	RANGE	TYPE	RANGE	
E,E/	ABX	6-11	D	30-50	MAG-D		DST

A broad structure at $E_X \approx 9$ MeV in ^{140}Ce which hitherto had been interpreted as the M1 giant resonance is shown to consist of an accumulation of $J^\pi = 2^+$ states with a total strength of about $6 \times 10^3 \mu\text{K fm}^2$. There is no indication of an M1 giant resonance in the energy region $E_X \approx 7.5-10$ MeV, contrary to a recent theoretical prediction.

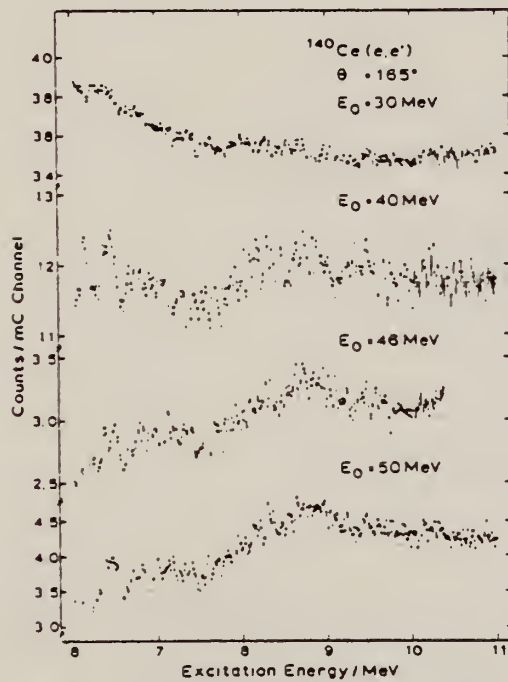


Fig. 1. Spectra of inelastically scattered electrons on ^{140}Ce without the background subtracted.

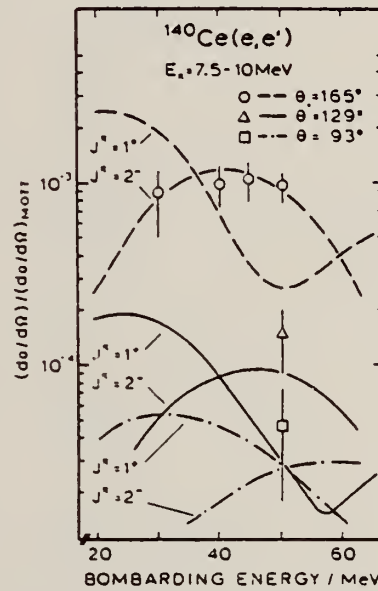


Fig. 2. Comparison of the experimental form factor for the broad structure between $E_X \approx 7.5-10$ MeV in fig. 1 (open symbols with error bars) and DWBA form factors in the frame of the RPA-MSI. The data definitely rule out an M1 form factor since its shape and relative magnitude between different angles disagrees with the data.

CE
A=141

CE
A=141

CE
A=141

ELEM. SYM.	A	Z
Ce	141	58

METHOD	REF. NO.	rs				
REACTION	RESULT	EXCITATION ENERGY	SOURCE	DETECTOR	ANGLE	
			TYPE	RANGE	TYPE	RANGE
N,G	ABX	11- 21	D	6- 16	NAI-D	90

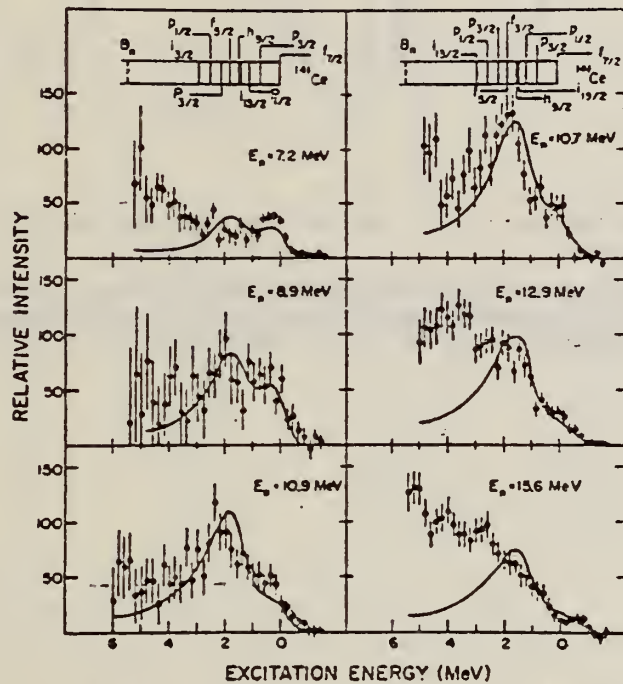


Fig. 2. Comparison of the measured spectra from neutron capture in cerium and those predicted from the DSD capture theory. The single-particle level scheme for ^{141}Ce is shown because ^{140}Ce is the dominant isotope (88.5%). The binding energies of single-particle levels in ^{143}Ce are about the same except for the $2f_{7/2}$ state (see text and table I). The observed and theoretical spectra were normalized to each other in the region corresponding to excitation energies below 2.6 MeV in ^{141}Ce . The interaction parameters chosen were $\epsilon_1 = 75$ MeV and $w_1 = 115$ MeV. (For further notation, see caption to fig. 1.)

over

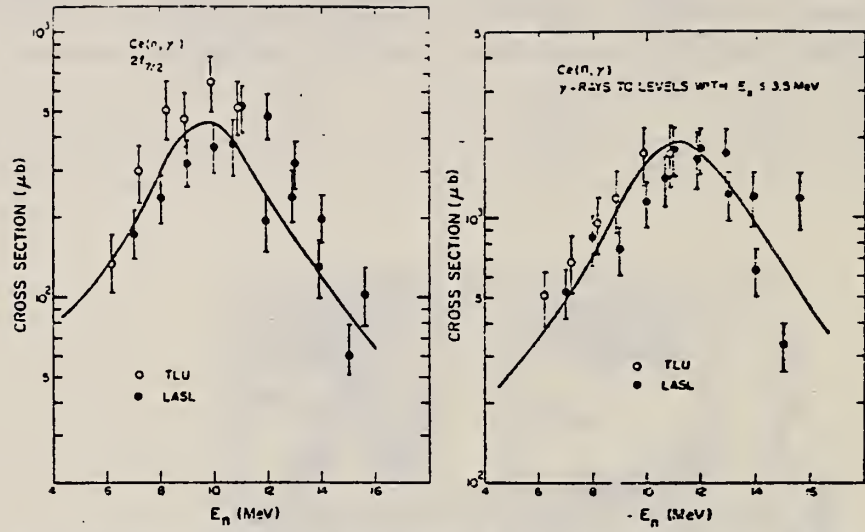


Fig. 4. Experimental (n, γ) cross sections for γ -ray transitions to the $2f_{7/2}$ states in ^{141}Ce ($E_g = 5.44$ MeV) and ^{143}Ce ($E_g = 5.15$ MeV), and the integrated cross section for γ -ray transitions to levels in the regions corresponding to excitation energies below 3.5 MeV in ^{141}Ce . (For further notation, see caption to fig. 3.)

CE

A=142

CE

A=142

CE

A=142

ELEM. SYM.	A	
Ce	142	58

METHOD

Betatron; neutron threshold; ion chamber

REF. NO.	60 Ge 3	NVB
----------	---------	-----

REACTION	RESULT	EXCITATION ENERGY	SOURCE	DETECTOR	ANGLE
			TYPE	RANGE	
G, N	NOX	THR	C THR	BF3-I	4 PI

THRESHOLD

TABLE I. Summary and comparison of neutron separation energies inferred from present threshold measurements with values predicted from mass data and reaction energies. All energies are expressed in the center-of-mass system in Mev.

Reaction	No. runs	Present results	Other results	Method	Reference
Ce ¹⁴² (γ, n)Ce ¹⁴¹	1	≤ 7.24 ± 0.07	6.97 ± 0.07	mass data	p

* W. H. Johnson, Jr., and A. O. Nier, Phys. Rev. 105, 1014 (1957).

TABLE II. Comparison of measured threshold energies with neutron binding energies predicted by mass data for transitions with $\Delta I \geq 7/2$. All energies in Mev.

Reaction	ΔI^a	Observed threshold	Mass data Q value	$E_{\text{u}} - Q$	Excited state energy
Cr ⁴⁸ (γ, n)Cr ⁴⁷	7/2	12.18 ± 0.14	12.053 ± 0.004 ^b	0.13 ± 0.14	...
Y ⁸⁹ (γ, n)Y ⁸⁸	7/2	11.59 ± 0.08	11.53 ± 0.40 ^c	0.06 ± 0.41	0.387 ^d
In ¹¹⁵ (γ, n)In ¹¹⁴	7/2	9.22 ± 0.03	9.35 ± 0.43 ^e	-0.13 ± 0.43	0.191 ^a
Ce ¹⁴² (γ, n)Ce ¹⁴¹	(7/2) ^f	7.24 ± 0.07	6.97 ± 0.07 ^f	0.27 ± 0.10	...
Nd ¹⁴⁴ (γ, n)Nd ¹⁴³	7/2	6.38 ± 0.16	5.97 ± 0.19 ^f	0.41 ± 0.25	0.690 ^a
Sm ¹⁴⁶ (γ, n)Sm ¹⁴⁵	7/2	6.45 ± 0.16	5.87 ± 0.28 ^f	0.58 ± 0.33	0.562 ^a
Er ¹⁶⁷ (γ, n)Er ¹⁶⁶	7/2	6.65 ± 0.08	6.45 ± 0.06 ^f	0.20 ± 0.10	0.081 ^a
Hf ¹⁷⁷ (γ, n)Hf ¹⁷⁶	7/2	6.69 ± 0.03	6.28 ± 0.06 ^f	0.64 ± 0.07	0.088 ^a
Hf ¹⁷⁹ (γ, n)Hf ¹⁷⁸	9/2	6.31 ± 0.07	6.17 ± 0.06 ^f	0.14 ± 0.09	0.093 ^a
Hf ¹⁸⁰ (γ, n)Hf ¹⁷⁹	9/2	7.85 ± 0.11	7.32 ± 0.06 ^f	0.53 ± 0.13	0.375 ^a

^a D. Strominger, J. M. Hollander, and G. T. Seaborg, Revs. Modern Phys. 30, 585 (1958).

^b C. F. Giese and J. L. Benson, Phys. Rev. 110, 712 (1958).

^c Henry E. Duckworth, *Mass Spectroscopy* (Cambridge University Press, New York, 1958), p. 177.

^d S. Dzhelepov and L. K. Peker, Atomic Energy of Canada Limited Report Tr. AECL-457 (unpublished).

^e The discrepancy in the case of Ce¹⁴² predicts a ground-state spin for Ce¹⁴¹ of 0, since the spin of Ce¹⁴² is known to be 7/2.

^f W. H. Johnson, Jr., and A. O. Nier, Phys. Rev. 105, 1014 (1957).

^g W. H. Johnson, Jr., and V. B. Bhanot, Phys. Rev. 107, 6 (1957).

REF.

Rainer Pithan
Z. Physik 260, 283 (1973)

ELEM. SYM.	A	Z
Ce	142	58

METHOD

REF. NO.	egf
73 P1 3	

REACTION	RESULT	EXCITATION ENERGY	SOURCE		DETECTOR		ANGLE
			TYPE	RANGE	TYPE	RANGE	
E, E/	LFT	0- 2	D	50, 65	MAG-D		DST

2+, 3-, 4+ LEVELS

Tabelle 2. Meßergebnisse der untersuchten Kernniveaus in Ce. Die B -Werte sind die $B(E1, q=0, 0^+ \rightarrow 1^+)$, vgl. [1]. Weisskopfeinheiten Γ_W für die Ergebnisse dieser Arbeit nach Wilkinson, D. H. (in: Nuclear Spectroscopy, ed. F. Ajzenberg-Selove, New York und London 1960) mit $R=1,2$ fm; die zitierten Werte anderer Autoren weichen davon bis zu 3% ab

Isotop	λ_n^x	E_x MeV	$B(E1, 0)$ fm 2	Γ_γ^0 eV	Γ_γ^0/Γ_W	Andere Autoren Γ_γ^0/Γ_W	Theoret. Werte Γ_γ^0/Γ_W
^{140}Ce	2_1^+	1,60	$2,7 \cdot 10^3$	$4,6 \cdot 10^{-3}$	$12,5 \pm 2$	$16,0 \pm 2,5^a$	$13,0^a$
						$12,5 \pm 1,8^b$	$12,5^f$
						$8,3 \pm 0,8^d$	$15,0^g$
	3_1^-	2,46	$2,0 \cdot 10^5$	$6,4 \cdot 10^{-6}$	24 ± 3	$93 \pm (30-45)^c$	$6,7^e$
						$6,0 \pm 0,6^d$	
	4_1^+	2,08	$5,9 \cdot 10^6$	$5,4 \cdot 10^{-11}$	20 ± 4	$5,5 \pm 0,6^d$	
^{142}Ce	2_1^+	0,64	$6,5 \cdot 10^3$	$1,1 \cdot 10^{-5}$	30 ± 15	$19,5 \pm 0,5^b$	$35,0^f$
	3_1^-	1,65	$9,0 \cdot 10^3$	$1,8 \cdot 10^{-6}$	110 ± 40	135 ± 70^c	
	4_1^+	1,22	$1,3 \cdot 10^7$	$9,7 \cdot 10^{-13}$	45 ± 25		

^a Ofer, S., Schwarzschild, A.: Phys. Rev. 116, 725 (1959).^b Eccleshall, D., Yates, M. J. L., Simpson, J. J.: Nucl. Phys. 78, 481 (1966).^c Ref. [21].^d Ref. [24].^e Ref. [27].^f Ref. [29].^g Ref. [28].²¹ Hansen, O., Nathan, N.: Nucl. Phys. 42, 197 (1963).²⁴ Baker, F. T., Tickle, R. S.: Phys. Lett. 32B, 47 (1970). Die Übergänge sind zitiert nach: Baer, H. W., Griffin, H. C., Gray, W. S.: Phys. Rev. C3, 1398 (1971), denn die Autoren selbst geben keine Zahlen an.²⁷ Rho, M.: Nucl. Phys. 93, 497 (1965).²⁸ Waroquier, M., Heyde, K.: Nucl. Phys. A164, 113 (1971).²⁹ Mustafa, S. M.: Nucl. Phys. A183, 309 (1972).

METHOD

REF. NO.

76 Le 2

egf

REACTION	RESULT	EXCITATION ENERGY	SOURCE		DETECTOR		ANGLE
			TYPE	RANGE	TYPE	RANGE	
G, N	ABX	8- 20	D	8- 26	MOD-I		4PI
G, 2N	ABX	12- 24	D	8- 26	MOD-I		4PI

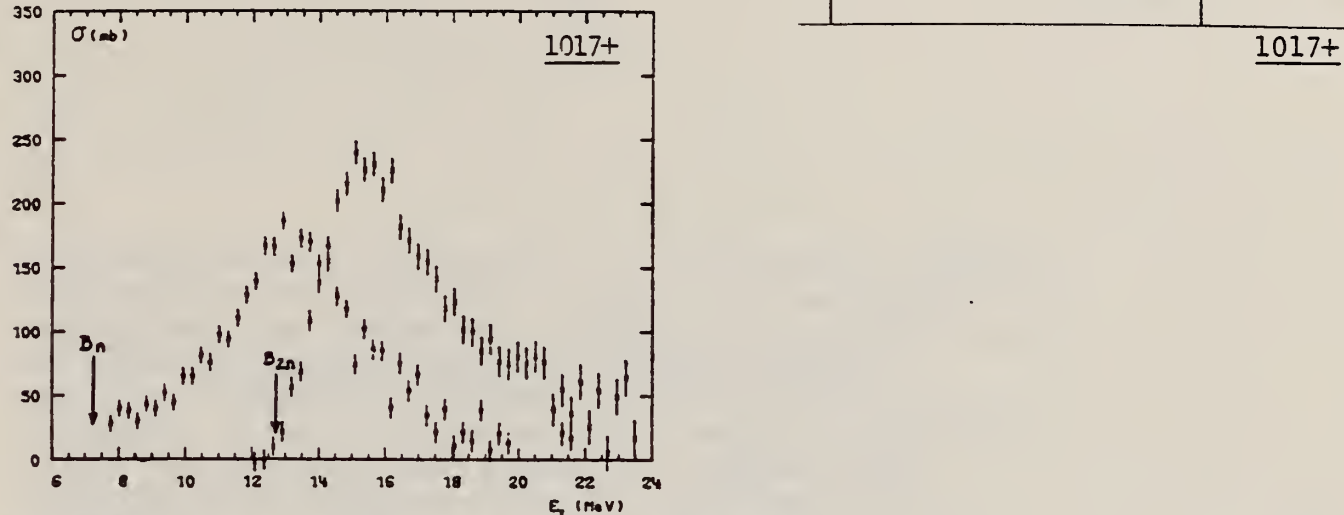


Fig. 6. Partial photoneutron cross sections $[\sigma(y, n) + \sigma(y, pn)]$ and $\sigma(y, 2n)$ for ^{142}Ce . Arrows B_n and B_{2n} indicate theoretical threshold values for (y, n) and $(y, 2n)$ reactions respectively. Data are not corrected for impurities.

TABLE 3

Lorentz line parameters corresponding to best fits shown in figs. 9 and 10

Nucleus	^{124}Te	^{126}Te	^{128}Te	^{130}Te	^{140}Ce	^{142}Ce
σ_0 (mb)	281 ± 15	294 ± 15	304 ± 15	318 ± 16	384 ± 20	332 ± 17
Γ_0 (MeV)	5.5 ± 0.2	5.6 ± 0.2	5.4 ± 0.2	5.1 ± 0.2	4.4 ± 0.1	5.2 ± 0.2
E_0 (MeV)	15.2 ± 0.1	15.1 ± 0.1	15.1 ± 0.1	15.1 ± 0.1	15.0 ± 0.1	14.9 ± 0.1

TABLE 4

Integrated photoneutron cross sections and comparison with sum rules

Nucleus	^{124}Te	^{126}Te	^{128}Te	^{130}Te	^{140}Ce	^{142}Ce
E_M (MeV)	26.5	25.1	26.2	25.9	26.5	23.5
σ_0 (MeV · b)	2.04	2.04	2.11	2.19	2.40	2.21
$\frac{\sigma_0 A}{0.06 NZ}$	1.12	1.11	1.14	1.17	1.18	1.07
σ'_0 (MeV · b)	2.44	2.56	2.58	2.55	2.65	2.69
$\frac{\sigma'_0 A}{0.06 NZ}$	1.34	1.39	1.39	1.36	1.30	1.30
σ_{-1} (mb)	128	130	135	140	154	149
$\sigma_{-1} A^{-1}$ (mb)	0.21	0.20	0.21	0.21	0.21	0.20
σ_{-2} (mb · MeV ⁻¹)	8.4	8.6	9.1	9.4	10.3	10.6
$\sigma_{-2} A^{-1}$ ($\mu\text{b} \cdot \text{MeV}^{-1}$)	2.7	2.7	2.8	2.8	2.7	2.7

PRASEODYMIUM
 $Z=59$

Praseodymium was discovered by C. A. von Welsbach in 1885 by separating from a green salt(didymium) the fractions of praseodymium and neodymium. The name is a shortened variant of the word praeseodidymum meaning green didymium.

Welsbach invented the automatic gas lighter based on a pyrophoric alloy of cerium and iron. He also invented the first lightbulb that used a metallic filament(osmium).

Welsbach is best remembered for his invention of the incandescent gas mantel — a truly great advance in the history of illumination.

PR
A=141

ELEM. SYM.	A	Z
Pr	141	59

METHOD
 Betatron

REF. NO.
 58 Ch 2 NVB

REACTION	RESULT	EXCITATION ENERGY	SOURCE		DETECTOR		ANGLE
			TYPE	RANGE	TYPE	RANGE	
G, N	RLY	THR	C	THR	BF ₃ -I		+PI

See 58 Ka 1 for cross sections

THRESHOLD

TABLE I
 MEASURED PHOTONEUTRON THRESHOLDS

Reaction	Measured Q value, Mev.	Other Q values, Mev.	Method	Reference
Pr ¹⁴⁴ (γ, n)Pr ¹⁴⁰	9.46 ± 0.05	9.40 ± 0.10	Threshold	Hanson <i>et al.</i> (1949)
		9.8 ± 0.3	Threshold	Ogle <i>et al.</i> (1950)
		9.30 ± 0.06	Mass data	Johnson and Nier (1957)

TABLE II
 COMPARISON OF THRESHOLDS FROM MASS DATA AND FROM PHOTONEUTRON REACTIONS

Reaction	Photoneutron threshold, Mev.	Mass data threshold, Mev.	Difference, Mev.
Na ²² (γ, n)Na ²¹	12.47 ± 0.05	12.417 ± 0.01	-0.05 ± 0.05
Al ²⁷ (γ, n)Al ²⁶	12.76 ± 0.06	13.03 ± 0.06	-0.07 ± 0.08
P ³¹ (γ, n)P ³⁰	12.48 ± 0.05	12.39 ± 0.04	-0.09 ± 0.06
Co ⁶⁰ (γ, n)Co ⁵⁹	10.44 ± 0.05	10.49 ± 0.01	+0.05 ± 0.05
Pr ¹⁴⁴ (γ, n)Pr ¹⁴⁰	9.46 ± 0.05	9.30 ± 0.06	-0.16 ± 0.08

METHOD Betatron; neutron cross section; BF_3 counters; ion chamber monitor

REF. NO.

58 Ka 1

NVB

REACTION	RESULT	EXCITATION ENERGY	SOURCE		DETECTOR		ANGLE
			TYPE	RANGE	TYPE	RANGE	
G, XN	ABX	10-22	C	10-22	BF ₃ -I		4PI

301

Таблица 2
 Пороги испускания фотонейтронов

Изотоп	B_{γ} , Мэс	$B_{\gamma\gamma}$, Мэс	Изотоп	B_{γ} , Мэс	$B_{\gamma\gamma}$, Мэс
V ⁵¹	11.16	20.5	L ¹³⁹	8.81	16.1
Mn ⁵⁵	10.14	19.2	Pr ¹⁴¹	9.46	17.6
Co ⁵⁹	10.44	18.6	Tb ¹⁵⁹	8.16	14.8
As ⁷⁵	10.24	18.1	Ho ¹⁶⁵	8.10	14.6
Y ⁸⁹	11.82	20.7	Tm ¹⁶⁹	8.00	14.7
Nb ⁹³	8.86	17.1	Lu ¹⁷⁵	7.77	14.2
Rh ¹⁰³	9.46	16.8	Ta ¹⁸¹	7.66	13.8
J ¹²⁷	9.14	16.2	Au ¹⁹⁷	7.96	13.3
Cs ¹³³	9.11	16.5	Bi ²⁰⁹	7.43	14.5

THRESHOLDS

не приведены, поскольку они превышают 22 Мэс во всех случаях, кроме золота, для которого $B_{\gamma\gamma}=21$ Мэс. Свойства сечений $\sigma_c(\gamma)$ сведены в табл. 3.

Таблица 1

Изотоп	E_{\max} , Мэс	$\sigma_n(E_\gamma)$, барн	Γ , Мэс	$\Sigma^{\gamma\gamma}$, Мэс·барн	$\Upsilon(22)$, 10^6 нейтрон/100 р-моль
V ⁵¹	18.4	0.062	5.2	0.33	1.62
Mn ⁵⁵	20.2	0.060	7.0	0.39	2.01
Co ⁵⁹	18.3	0.068	6.3	0.44	2.30
As ⁷⁵	16.4	0.090	9.5	0.74	4.25
Y ⁸⁹	17.1	0.172	5.2	0.93	5.33
Nb ⁹³	18.0	0.156	7.5	1.17	6.80
Rh ¹⁰³	17.5	0.160	9.4	1.40	8.28
J ¹²⁷	15.2	0.273	6.8	1.76	11.9
Cs ¹³³	16.5	0.238	7.7	1.59	10.7
La ¹³⁹	15.5	0.325	3.8	1.55	11.2
Pr ¹⁴¹	15.0	0.320	4.9	1.93	13.1
Tb ¹⁵⁹	15.6	0.274	9.8	2.49	18.1
Ho ¹⁶⁵	13.5	0.305	8.9	2.52	18.7
Tm ¹⁶⁹	16.4	0.250	8.4	1.91	14.9
Lu ¹⁷⁵	16.0	0.225	8.4	1.90	23.0
Ta ¹⁸¹	14.5	0.380	8.5	3.15	22.0
Au ¹⁹⁷	13.8	0.475	4.7	3.04	22.6
Bi ²⁰⁹	13.2	0.455	5.9	2.89	23.2

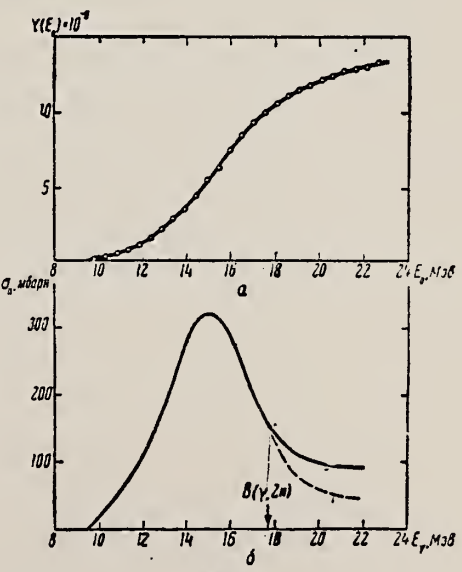


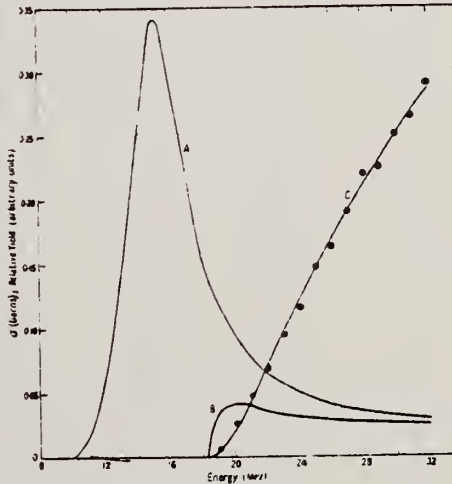
Рис. 11.
 — Выход фотонейтронов для Pr; б — $\sigma_n(E_\gamma)$
 и $\sigma_\gamma(\gamma)$ для Pr

Elem. Sym.	A	Z
Pr	141	59

Method 33 MeV electron synchrotron; neutron yield; radioactivity

Ref. No.
 59 Ca 2 EH

Reaction	E or ΔE	E_0	Γ	$\int \sigma dE$	$J\pi$	Notes	299+
$^{141}\text{Pr}(\gamma, n)$	Bremss.						
$^{141}\text{Pr}(\gamma, 2n)$	33 (300)		-	$\int_{31}^{31} = 2.6 \pm 0.4 \text{ MeV-b}$		$E_{th}(\gamma, 2n) = 18.3 \text{ MeV.}$	



Cross sections for the reactions: A, $^{141}\text{Pr}(\gamma, n)$; B, $^{141}\text{Pr}(\gamma, 2n)$; C, the activation curve for $^{141}\text{Pr}(\gamma, 2n)$.

Elem. Sym.	A	Z
Pr	141	59

Method 33 MeV synchrotron; radioactivity; NaI spectrometer; r chamber

Ref. No.
59 Ca 3 EH

Reaction	E or ΔE	E_0	Γ	$\int \sigma dE$	$J\pi$	Notes	<u>298</u>
$^{141}\text{Pr}(\gamma, n)$	Bremss. 10-32	15.3	4.3 MeV	$2.2 \pm 0.3 \text{ MeV-b}$			

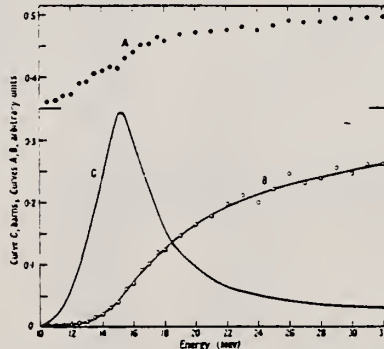


Figure 7. A, the ratio of activation curves ¹⁴¹Pr(y,n)/¹⁴¹Ta(y,n); B, activation curve for ¹⁴¹Pr(y,n); C, derived cross section: ¹⁴¹Pr(y,n).

Table 2

Activity	T_1 (min)	W_N (MeV)	K/β^+	$\frac{K\text{-capture}}{\text{Total capture}}$	W_K
¹⁴⁰ Pr	3.4	3.25	0.63	0.89	0.89
¹⁴¹ Nd	150	1.80	48	0.89	0.90
¹⁴² Sm	8.5	3.47	0.60	0.89	0.91

REF.

G. Di Caporiacco, M. Mandò, and F. Ferrero
 Nuovo Cimento 13, 522 (1959)

ELEM. SYM.	A	Z
Pr	141	59

METHOD

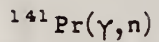
Betatron; ion chamber

REF. NO.

59 Di 1

NVB

REACTION	RESULT	EXCITATION ENERGY	SOURCE		DETECTOR		ANGLE
			TYPE	RANGE	TYPE	RANGE	
G, N	RLY	9-30	C	30	ACT-I		4PI



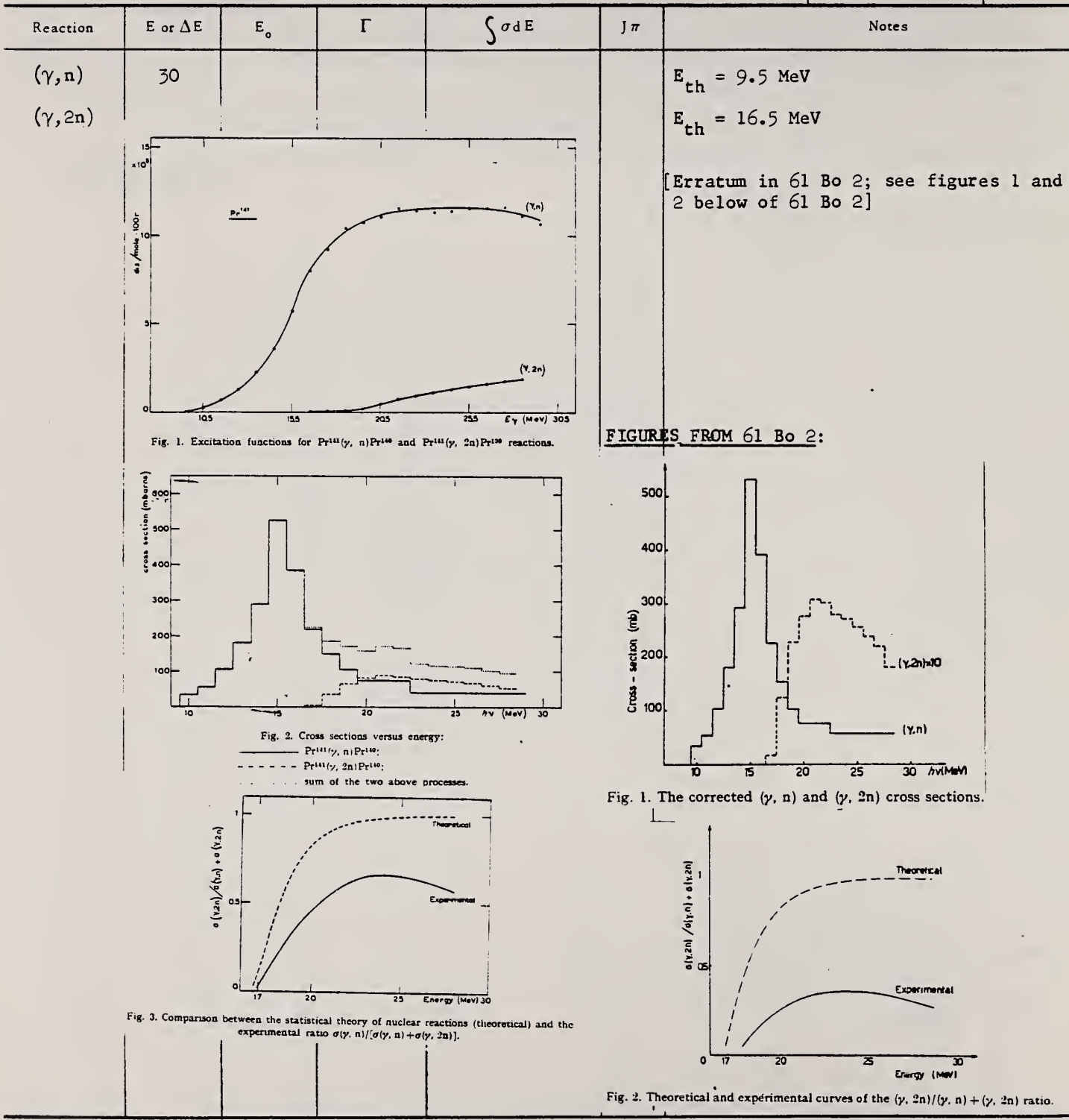
REL TO CU63 (G, N)

Yield ratio: $\frac{^{141}\text{Pr}(\gamma, n)}{^{63}\text{Cu}(\gamma, n)} = 3.79$

Elem. Sym.	A	Z
Pr	141	59

Method
31 MeV Betatron; radioactivity

Ref. No.
59 Fe 2 EH



ELEM. SYM.	A	Z
Pr	141	59

METHOD					REF. NO.	
Betatron; neutron threshold; ion chamber					60 Ge 3	NVB
REACTION	RESULT	EXCITATION ENERGY	SOURCE	DETECTOR		ANGLE
			TYPE	RANGE	TYPE	RANGE
G, N	NO X	THR	C	THR	ACT-I	4PI

THRESHOLD

TABLE I. Summary and comparison of neutron separation energies inferred from present threshold measurements with values predicted from mass data and reaction energies. All energies are expressed in the center-of-mass system in Mev.

Reaction	No. runs	Present results	Other results	Method	Reference
Pr ¹⁴¹ (γ,n)Pr ¹⁴⁰	4	9.361 ± 0.023	9.30 ± 0.06 9.46 ± 0.05	mass data threshold	p f

» W. H. Johnson, Jr., and A. O. Nier, Phys. Rev. 105, 1014 (1957).

Elem. Sym.	A	Z
Pr	141	59

Method	Ref. No.
18 MeV electron synchrotron; BF ₃ counters; ion chamber	60 Th 1

Reaction	E or ΔE	E_0	Γ	$\int \sigma dE$	$J\pi$	Notes	<u>302</u>
Pr ¹⁴¹ (γ , xn) 7-18	7-18	15.1				At $E_n = 15.1$ MeV, $\sigma_{\max} = 480$ mb.	

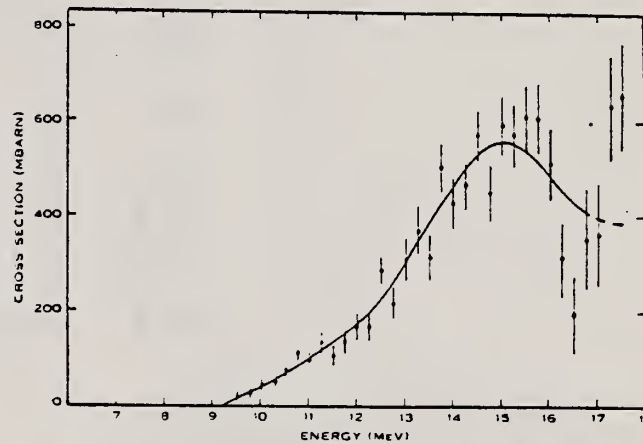


Fig. 5.—Total neutron production cross section for ¹⁴¹Pr. The points are obtained by analysis using the experimental points. The smooth curve is obtained by analysis of a smooth yield curve drawn through the experimental points.

TABLE I
 GIANT RESONANCE PARAMETERS FOR NON-DEFORMED NUCLEI

Nucleus...	¹³⁹ La	¹⁴¹ Pr	¹⁸⁷ Au
Reference ..	Spicer <i>et al.</i> (1958)	Present Paper	Fullor and Weiss (1958)
E (MeV)	14.9	15.1	13.5
$(\sigma)_{\max}$ (mbarn)	460	480	590
$2 \times \Gamma_{-1/2}$ (MeV)	4.2	4.4	4
$\Gamma_{G.R.}$ (MeV)	4.2	—	4.2

Method 100 MeV synchrotron; Activation

Ref. No.	JHH
61 Bo 1	

Reaction	E or ΔE	E_0	Γ	$\int \sigma dE$	$J\pi$	Notes
(γ, n) $(\gamma, 2n)$	10-29			$\left. \begin{array}{c} 3.0 \text{ MeV-mb} \\ 0 \end{array} \right $		<p>This paper is an erratum to results in Nuclear Phys. 10 423 (1959) [our file 59Fe2], incorporating a remeasured value of E.C./β^+ ratio in Pr^{139} = 4.8.</p> <p>This causes a correction factor to be applied to the old data:</p> $\sigma(\gamma, n) = 1.02 \sigma(\gamma, n) \quad [\text{new}] \quad [\text{old}]$ $\sigma(\gamma, 2n) = 0.35 \sigma(\gamma, 2n) \quad [\text{new}] \quad [\text{old}]$

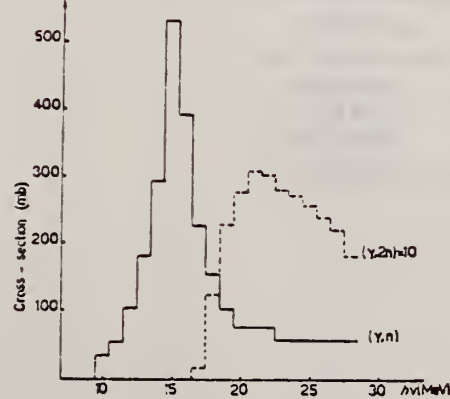
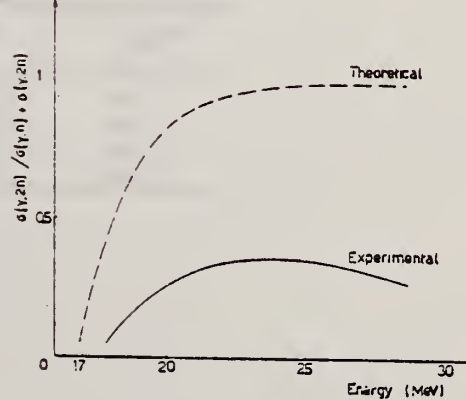


Fig. 1. The corrected (γ, n) and $(\gamma, 2n)$ cross sections. Fig. 2. Theoretical and experimental curves of the $(\gamma, 2n)/(\gamma, n) + (\gamma, 2n)$ ratio.



METHOD					REF. NO.		
REACTION	RESULT	EXCITATION ENERGY	SOURCE		DETECTOR		ANGLE
			TYPE	RANGE	TYPE	RANGE	
G, MU-T	ABX	11 - 20	C	11-20	ACT-I		

Used activity to measure total attenuation.

TABELA I

Reações	Material	Mín. vida (Mev)	Limiar (Mev)	Energia do Bóton		Energia Média (Mev)	
				P^{α} (Mev)	$P^{n\alpha}$ (Mev)	P^{α}	$P^{n\alpha}$
(a) Cu ⁶⁵ (γ , n) Cu ⁶⁵	Cobre	10,1	10,6	11,4	11,8	11,0	11,2
(b) Fe ⁵⁶ (γ , n) Fe ⁵⁶	Ferro	9,0	11,9	—	16,0	—	14,6
(c) O ¹⁶ (γ , n) O ¹⁶	Ácido borico	2,1	15,6	17,4	17,6	16,5	16,3
(d) C ¹² (γ , n) C ¹²	Policloro- tetileno	20,5	18,7	20,3	20,1	19,5	19,6

TABELA II — P^{α}

Energia em Mev	μ (cm cm ² /g)	σ (cm m barns)
11,0	$0,0237 \pm 0,0003$	1220 ± 15
16,5	$0,0235 \pm 0,0002$	1210 ± 10
19,5	$0,0250 \pm 0,0003$	1287 ± 15

TABELA III $P^{n\alpha}$

Energia em Mev	μ (cm cm ² /g)	σ (cm barns)
11,2	$0,0435 \pm 0,0009$	$10,19 \pm 0,21$
14,6	$0,0481 \pm 0,0008$	$11,26 \pm 0,19$
16,6	$0,0505 \pm 0,0008$	$11,83 \pm 0,19$
19,6	$0,0550 \pm 0,0005$	$13,00 \pm 0,12$

Ref. G.E. Coote, W.E. Turchinetz, I.F. Wright
 Nuclear Phys. 23, 468 (1961)

Elem. Sym.	A	Z
Pr	141	59

Method	Ref. No.
Li ⁷ (p, γ) source; activation; NaI	61 Co 2 JHH

Reaction	E or ΔE	E_0	Γ	$\int \sigma dE$	$J\pi$	Notes
(γ ,n)						$\sigma = 181 \pm 20 \text{ mb}$, relative to $59 \pm 6 \text{ mb}$ for Cu ⁶³ (γ ,n), measured for 440 keV (E_p) resonance radiation from Li ⁷ .

Ref. G. Moscati
 Nuclear Phys. 26, 321 (1961)

	Elem. Sym.	A	Z
Pr	141	59	

Method 33 MeV bremss. (Saclay Linac); activity measured NaI crystals; annihilation radiation.						Ref. No. 61 Mo 1	EGF
Reaction	E or ΔE	E_0	Γ	$\int \sigma dE$	$J\pi$	Notes	
Pr ¹⁴¹ (γ , 3n)	Bremss. 27-33			1 MeV-mb		E _{th} = 26.6±6 MeV [refer Johnson and Nier, Phys. Rev. <u>105</u> , 1014 (1957)] assumed linear.	

Ref. V.G. Shevchenko, B.A. Yur'ev
 - Zhur. Eksp. i Teoret. Fiz. 41, 1421 (1961)
 Soviet Phys. JETP 14, 1015 (1962)

Elem. Sym.	A	Z
Pr	141	59

Method

35 MeV betatron; emulsions

Ref. No.

61 Sh 2

JHH

Reaction	E or ΔE	E_0	Γ	$\int \sigma dE$	$J\pi$	Notes
(γ, p)	Bremss.: 22.5 { 33.5 {	* $6-7$ $9-10$ $6-7$ $9-10$	 			<p>$\sim 8 \times 10^4$ protons/mole-roentgen</p> <p>$\sim 1.3 \times 10^5$ protons/mole-roentgen</p> <p>Angular distributions fitted to: $a + b \sin^2\theta (1 + p \cos \theta)^2$ (see Table I parameters)</p> <p>Conclusion: $\sigma(\gamma, p)$ is mostly due to $E_\gamma \gtrsim 22$ MeV, and is mainly quadrupole.</p> <p>*Peaks in proton energy distribution at 6-7 and 9-10 MeV. (For Figures see page 2)</p>

Table I. Parameters of type (1) curves approximating the angular distributions of photoparticles from ^{141}Pr , and values of $\sigma_{E_2}/\sigma_{E_1+E_2}$ derived from the
 $\sigma_{E_2}/\sigma_{E_1} = p^2/5$

$E_{\gamma, \text{max}}, \text{MeV}$	Proton energy, Mev	a	b	p	$\sigma_{E_2}/\sigma_{E_1+E_2}, \%$
22.5	4.5-7.25	31	15.7	0.42	-3
	7.25-11.25	44	68	0.32	-2
	≥ 11.25	12	27.5	0.44	-4
33.5	4.5-7.25	71	23.4	1.4	-30
	7.25-11.25	153	57	2.2	-50
	≥ 11.25	50	71.4	1.8	-40

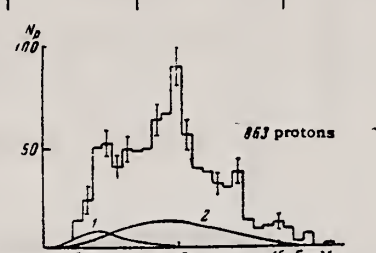
Method				Ref. No. 61 Sh 2 (PAGE 2)	JHH	
Reaction	E or ΔE	E_0	Γ	$\int \sigma dE$	$J\pi$	Notes
						

FIG. 2. Energy distribution of photoprottons from Pr^{141} produced by radiation having $E_{\gamma\max} = 22.5$ Mev. The continuous curve 1 is the computed spectrum of evaporation protons; curve 2 is the computed spectrum of direct-photo-effect protons.

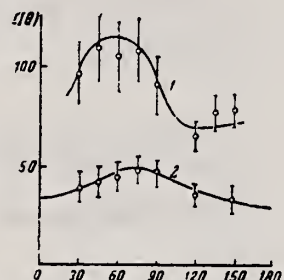


FIG. 4. Angular distribution of 4.5-7.25 Mev photoprottons (first group): 1 - for $E_{\gamma\max} = 33.5$ Mev; 2 - for $E_{\gamma\max} = 22.5$ Mev. The continuous approximating curves have the parameters given in Table I.

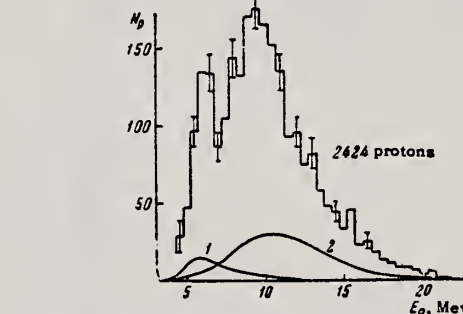


FIG. 3. Energy distribution of photoprottons from Pr^{141} produced by radiation having $E_{\gamma\max} = 33.5$ Mev. The notation is the same as in Fig. 2.

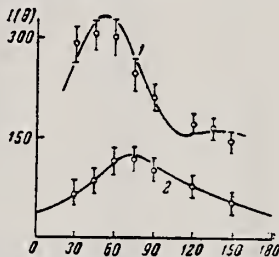


FIG. 5. Angular distribution of 7.25-11.25 Mev photoprottons (second group): 1 - for $E_{\gamma\max} = 33.5$ Mev; 2 - for $E_{\gamma\max} = 22.5$ Mev.

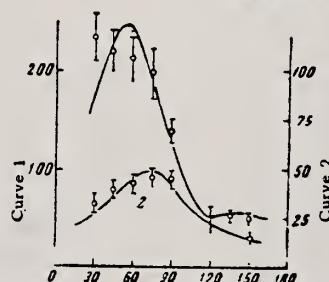


FIG. 6. Angular distribution of photoprottons of > 11.25 Mev (third group): 1 - for $E_{\gamma\max} = 33.5$ Mev; 2 - for $E_{\gamma\max} = 22.5$ Mev.

METHOD 22 MeV betatron; Si²⁸(n,p)Al²⁸ threshold detector.

Ref. No.	61 Ta 1	JHH
----------	---------	-----

Reaction	E or ΔE	E_0	Γ	$\int \sigma dE$	$J\pi$	Notes
(γ , n)	Bremss. 22					<p>$E_n > 6$ MeV.</p> <p>$W(\theta_n) = A + B \sin^2 \theta$ where $B/A = 0.34 \pm 0.16$</p>

Figure 4: Angular distributions of fast photoneutrons as observed with the Si²⁸(n,p)Al²⁸ detector. Data normalized at 90° in each case.

Elem. Sym.	A	Z
Pr	141	59

Method
(n,γ) reaction - NaI(Tl)Ref. No.
62Be2

86

Reaction	E or ΔE	E _o	Γ	∫ σ dE	J π	Notes
(γ,γ)	discrete energies in the range 5.44 - 8.997	6.12 7.64 8.881 8.997			σ _s (total) (mb) 230 4.0 1 0.4	γ source C1 Fe Cr Ni Detector at 135°.

Method Electrostatic generator, $H^2(p,\gamma)He^4$ reaction; activation of positron emitter; 2 NaI in coincidence.

Ref. No. 62 De 1	JHH
---------------------	-----

Reaction	E or ΔE	E_0	Γ	$\int \sigma dE$	$J\pi$	Notes
(γ, n)	20.48					$\sigma(\gamma, n) = 51.7 \pm 5.4 \text{ mb}$

Method 55 MeV betatron; synchrotron; $\text{Si}^{28}(\text{n},\text{p})\text{Al}^{28}$ activity; $\text{Cu}^{63}(\gamma,\text{n})\text{Cu}^{62}$
 monitor.

Ref. No.
 62 Re 1 EGF

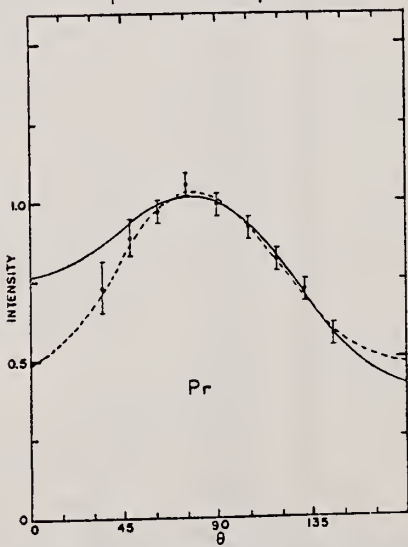
Reaction	E or ΔE	E_0	Γ	$\int \sigma dE$	$J \pi$	Notes
(γ, n)	Bremss. 55					<p><u>Figure 9:</u> Dotted curve is of form $a_0 + a_1 \cos \theta + a_2 \cos^2 \theta + a_3 \cos^2 \theta - a_4 \cos^2 \theta$; solid curve is of form $a_0 + a_1 \cos \theta + a_2 \cos^2 \theta$; errors on points are statistical errors in counting only.</p>  <p>Pr</p>

Fig. 9. Angular distribution of fast neutrons from praseodymium.
 See fig. 5.

TABLE 2
 Parameters of the fit (1) for the expressions $a_0 - a_1 \cos \theta + a_2 \cos^2 \theta$, $a + b \sin \theta - c \cos \theta$ and $A_0 - A_1 P_1 - A_2 P_2$

	Bi(1)	Bi(2)	Pr	Au	V	Hg	La
a_0	1.00 ± 0.02	1.00 ± 0.02	1.00 ± 0.02	1.00 ± 0.02	1.00 ± 0.03	1.00 ± 0.02	1.00 ± 0.01
a_1	0.15 ± 0.03	0.15 ± 0.04	0.17 ± 0.04	0.14 ± 0.03	0.17 ± 0.06	0.12 ± 0.03	0.14 ± 0.03
$-a_2$	0.47 ± 0.06	0.40 ± 0.08	0.41 ± 0.09	0.21 ± 0.07	0.15 ± 0.11	0.34 ± 0.08	0.39 ± 0.06
$-A_1^{(*)}$	0.18 ± 0.04	0.21 ± 0.05	0.20 ± 0.05	0.15 ± 0.04	0.18 ± 0.09	0.14 ± 0.04	0.16 ± 0.03
$-A_2^{(*)}$	0.37 ± 0.05	0.31 ± 0.06	0.32 ± 0.07	0.15 ± 0.05	0.11 ± 0.04	0.26 ± 0.05	0.30 ± 0.04
a	0.53 ± 0.06	0.60 ± 0.08	0.50 ± 0.09	0.70 ± 0.07	0.63 ± 0.11	0.66 ± 0.06	0.61 ± 0.06
b	0.47 ± 0.06	0.40 ± 0.08	0.41 ± 0.09	0.21 ± 0.07	0.15 ± 0.11	0.34 ± 0.06	0.39 ± 0.06
c	0.15 ± 0.03	0.18 ± 0.04	0.17 ± 0.04	0.14 ± 0.03	0.17 ± 0.08	0.12 ± 0.03	0.14 ± 0.03

* Renormalized so that $A_0 = 1$

TABLE 4
 Parameters of the fit (3) for the expressions $a_0 - a_1 \cos \theta + a_2 \cos^2 \theta - a_3 \cos^3 \theta$, $1 - A_1 P_1 - A_2 P_2 - A_3 P_3$

	Bi(1)	Bi(2)	Pr	Au	V	Hg	La
a_0	1.01 ± 0.02	1.00 ± 0.02	1.01 ± 0.03	0.98 ± 0.02	1.00 ± 0.03	1.00 ± 0.02	1.01 ± 0.02
a_1	0.19 ± 0.05	0.17 ± 0.07	0.21 ± 0.07	0.07 ± 0.06	0.16 ± 0.02	0.12 ± 0.05	0.17 ± 0.05
$-a_2$	0.56 ± 0.11	0.37 ± 0.15	0.50 ± 0.16	0.05 ± 0.12	0.13 ± 0.20	0.33 ± 0.12	0.47 ± 0.11
a_3	-0.17 ± 0.18	0.05 ± 0.24	-0.17 ± 0.25	0.31 ± 0.19	0.03 ± 0.32	0.03 ± 0.19	-0.17 ± 0.17
$-A_1^{(*)}$	0.11 ± 0.15	0.23 ± 0.18	0.13 ± 0.20	0.27 ± 0.13	0.20 ± 0.22	0.15 ± 0.14	0.09 ± 0.13
$-A_2^{(*)}$	0.45 ± 0.09	0.29 ± 0.11	0.39 ± 0.12	0.03 ± 0.08	0.03 ± 0.14	0.24 ± 0.09	0.37 ± 0.09
$-A_3^{(*)}$	-0.08 ± 0.09	0.02 ± 0.11	-0.08 ± 0.12	0.13 ± 0.08	0.02 ± 0.13	0.01 ± 0.08	-0.08 ± 0.08

* Renormalized so that $A_0 = 1$

Elem. Sym.	A	Z
Pr	141	59

Method
 35 MeV betatron; emulsions

Ref. No.
 62 Sh 4

JHH

Reaction	E or ΔE	E_0	Γ	$\int \sigma dE$	$J\pi$	Notes
$^{141}\text{Pr}(\gamma, p)$	Bremss.					Parameters a, b and p for
	22.5					$w(\theta_p) = a + b \sin^2 \theta_p (1 + p \cos \theta)^2$
	33.5					in Table I.

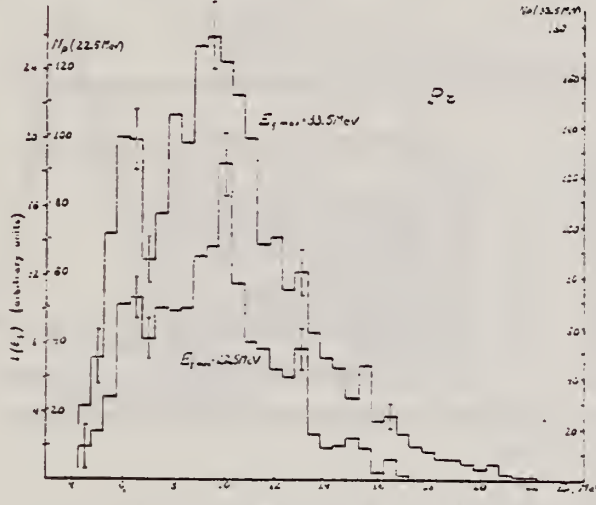


Fig. 3. Energy distributions of photoprotons from Pr^{141} .

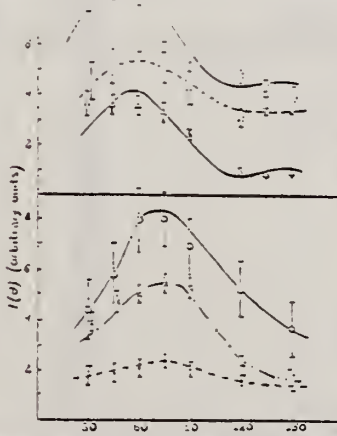


Fig. 8. Angular distributions of photoprotons from Pr^{141} . The experimental points for $E_{\max} = 22.5$ MeV are denoted by solid dots for $E_0 = 4.5-7.25$ MeV, by centred circles for $E_0 = 7.25-11.25$ MeV and by crosses for $E_0 > 11.25$ MeV. For the case of $E_{\max} = 33.5$ MeV solid squares denote $E_0 = 4.5-7.25$ MeV, centred squares $E_0 = 7.25-11.25$ MeV and centred triangles $E_0 > 11.25$ MeV.

Coefficients of expressions of type 1 in approximations and reactions and estimates of the contribution from the quadrupole						
Element	Z	E_{\max} (MeV)	E_0 (MeV)	a	b	p
Rh	45	22.5	3.25-9.25	1.0	0	0
		> 9.25	2.8	1.9	0.2	1
		33.5	3.25-9.25	12.2	0	0
Pr	59	> 9.25	4.5	3.7	1.2	≈ 20
		4.5-7.25	1.4	0.7	0.42	2
		7.25-11.25	2.9	4.4	0.62	2
		> 11.25	1.5	3.9	0.44	3
		4.5-7.25	3.2	1.2	1.0	≈ 13
W	74	7.25-11.25	4.2	1.55	2.2	≈ 50
		> 11.25	0.8	1.2	1.3	≈ 40
		6.25-8.75	0.8	0	0	0
		8.75-12.75	2.8	1.6	1.6	≈ 35
		> 12.75	2.2	0.5	2.6	≈ 55
Pt	78	6.25-8.75	1.2	0.95	1.44	+
		8.75-12.75	1.0	0.85	2.6	≈ 55
		> 12.75	0.53	0.5	3.4	≈ 70
		6.25-8.75	0.6	1.0	0.4	3
		8.75-11.75	2.5	1.0	1.2	≈ 20
Pb	82	> 11.75	1.4	0.56	2.6	≈ 55
		7.25-14.25	1.1	1.1	2.6	≈ 55
		> 14.25	0.5	0.5	3.1	≈ 70
		3.25-9.25	1.05	0.75	0.8	≈ 10
		> 9.25	0.75	1.75	2.2	≈ 50
Pb	82	3.25-10.25	1.9	1.2	1.2	≈ 20
		10.25-14.25	1.13	0.65	3.0	≈ 65
		> 14.25	1.5	1.0	3.3	≈ 70

TABLE 2
 Measured photoprotton yields and comparison with estimates by the models of evaporation and sequential nucleon knockout

Element	Sym	E_{\max} (MeV)	Y_{exp}	Y_{evap}	$Y_{\text{evap}}/Y_{\text{direct}}$
Rh	22.5	1.0 $\times 10^4$	≈ 3		≈ 3
	33.5	2.8 $\times 10^4$	≈ 9		≈ 4.5
Pr^{141}	22.5	6.7 $\times 10^4$	≈ 19		≈ 4.5
	33.5	1.0 $\times 10^5$	≈ 25		≈ 5
W	22.5	2.0 $\times 10^4$	$\approx 1.2 \times 10^4$		≈ 6
	33.5	0.8 $\times 10^4$	$\approx 3 \times 10^4$		≈ 11
Pt	22.5	2.1 $\times 10^4$	$\approx 5 \times 10^4$		≈ 5
	33.5	0.6 $\times 10^4$	$\approx 2 \times 10^4$		≈ 20
Pb	22.5	2.9 $\times 10^4$	$\approx 1.5 \times 10^5$		≈ 11
	33.5	0.2 $\times 10^5$	$\approx 5 \times 10^4$		≈ 55

a) The yield Y_{exp} is expressed in protons per mol per 10 e.v.

References

- M. E. Toms and W. E. Stephens, Phys. Rev. 93 (1954) 626
- M. M. Hoffman and A. G. W. Cameron, Phys. Rev. 92 (1953) 1154
- W. C. Barber and V. J. VanNuyse, Nuclear Physics 16 (1950) 351
- M. E. Toms and W. E. Stephens, Phys. Rev. 92 (1953) 362
- E. D. Makhotnovsky, JETP 33 (1960) 93
- R. B. Taylor, Nuclear Physics 19 (1960) 453
- A. G. W. Cameron, W. Harms and L. Katz, Phys. Rev. 83 (1951) 1264
- V. G. Neudachin, V. G. Shevchenko and N. P. Yudin, Report at the Second All-Union Conf. for Nuclear Reactions at Low and Medium Energies, Moscow, 1960
- E. D. Courant, Phys. Rev. 82 (1951) 703
- V. V. Balashov, V. G. Shevchenko and N. P. Yudin, JETP 41 (1961) 929

REF.
B. Arad (Huebschmann), G. Ben-David (Davis), I. Pelah,
Y. Schlesinger
Phys. Rev. 133, B684-700 (1964)

ELEM. SYM.	A	Z
Pr	141	59

METHOD

Reactor, (n,γ) reactions source

REF. NO.	
64 Ar 1	NVB

REACTION	RESULT	EXCITATION ENERGY	SOURCE		DETECTOR		ANGLE
			TYPE	RANGE	TYPE	RANGE	
G,G	ABX	6-9 (See Table II)	D	6-9	NAI-D		135

TABLE II. Capture gamma-ray sources and their properties.*

Source	Chemical composition	Mass kg	Principal γ rays (in MeV)
Al	Metal	1.640	7.73
Cl	polyvinyl Chloride	0.380	8.55, 7.78, 7.41, 6.96, 6.64, 6.12, 5.72
Co	CoO	0.230	7.49, 7.20, 6.98, 6.87, 6.68, 6.48, 5.97, 5.67
Cr	Metallic powder	0.480	9.72, 8.88, 8.49, 7.93, 7.09, 6.65, 5.60
Cu	Metal	1.860	7.91, 7.63, 7.29, 7.14, 7.00, 6.63
Fe	Metallic powder	0.440	9.30, 7.64, 7.28, 6.03
Hg	Hg ₂ (NO ₃) ₂ ·2H ₂ O	0.310	6.44, 6.31, 5.99, 5.67, 5.44
Mn	MnO ₂	0.240	7.26, 7.13, 7.04, 6.96, 6.79, 6.10, 5.76
Ni	Metal	0.900	9.00, 8.50, 8.10, 7.83, 7.58, 6.84, 6.64
Ti	TiO ₂	0.210	6.75, 6.56, 6.42
V	V ₂ O ₅	0.120	7.30, 7.16, 6.86, 6.51, 6.46, 5.87, 5.73
Y	Y ₂ O ₃	0.200	6.07, 5.63

* For more detailed information, additional lines, intensities, etc., see Ref. 6.

TABLE III. Effective cross sections.

γ source	Energy (MeV)	Element	Protons	Scatterer	Neutrons	$\langle\sigma_{\gamma\gamma}\rangle$ (mb)	Notes
Hg	5.44	Hg	80	116, 118, 119, 120, 121, 122, 124		128	
Cl	6.12	Pr ¹⁴¹	59	82		103	a
V	6.508	Sn	50	62, 64-70, 72		14	
Co	6.690	Pr ¹⁴¹	59	82		2.7	a
Co	6.867	Nd	60	82, 83, 84, 85, 86, 88		22	
Al	6.98	Pb ²⁰⁸	82	126		2900	b
Cl	6.98	Pb	82	124, 125, 126		346	a
Ti	6.996	Bi ²⁰⁸	83	126		1560	b
Cu	7.01	Sn	50	62, 64-70, 72		1000	b
Ti	7.149	Pb ²⁰⁸	82	126		1000	b
Co	7.201	Pb ²⁰⁸	82	126		25	
Mn	7.261	Pb ²⁰⁸	82	126		25	a
Fe	7.285	Pb ²⁰⁸	82	126		4100	a
V	7.305	Pb ²⁰⁸	82	126		12.5	
Hg	7.32	Pb	82	124, 125, 126		5500	c
Fe	7.639	Ni	23	30, 32, 34, 36		10.5	d
Fe	7.639	Pr ¹⁴¹	59	82		10	d
Cr	8.499	Cu	29	34, 36		24.4	
Cr	8.881	Pr ¹⁴¹	59	82		9.3	
Ni	8.997	Sm	62	82, 85-88, 90, 92		2.8	

* A large error could be introduced in the cross-section values because of large differences in line intensities quoted by Bartholomew and Higgs and by Groshev *et al.* (Ref. 6).

^b Because of the low counting rate, thick scatterers were used, which will introduce a systematic error in estimating $\langle\sigma_{\gamma\gamma}\rangle$ for resonances having a high nuclear cross section.

^c The cross section was evaluated assuming the gamma intensity to be 0.02 photons per 100 captured neutrons (see text).

^d Reference 6 gives the 7.639 line of iron capture gamma rays as a single line. However, a recent paper by Fiebig, Kand, and Segel [Phys. Rev. 125, 2031 (1962)] reports two different lines of equal intensities having energies of 7.647 and 7.633 MeV. The present experiment cannot resolve an energy difference of 14 keV; therefore, there is no possibility of deciding which line is responsible for the scattering.

ELEM. SYM.	A	Z
Pr	141	59

METHOD

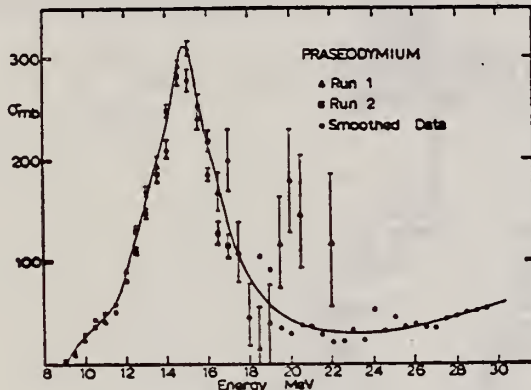
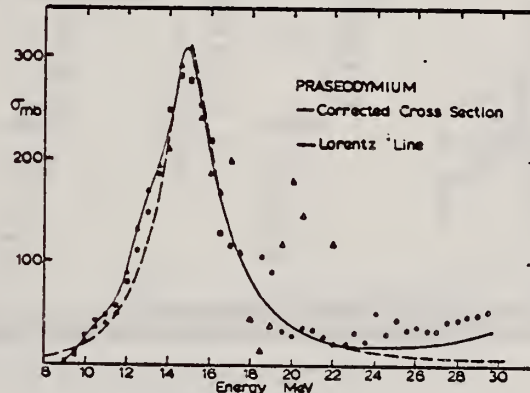
Synchrotron, NBS chamber

REF. NO.

64 Ri 1

NVB

REACTION	RESULT	EXCITATION ENERGY	SOURCE		DETECTOR		ANGLE
			TYPE	RANGE	TYPE	RANGE	
G, XN	ABX	9-30	C	9-30	BF ₃ -I		4PI

586FIG. 2. Praseodymium (γ, n) cross section uncorrected for neutron multiplicity.FIG. 4. Praseodymium (γ, n) cross section with neutron multiplicity correction (solid line); Lorentz line fitting to data points (dashed line).TABLE I. Experimentally determined parameters for the neutron photoproduction cross sections σ_m , maximum value of cross sections; E_m , energy at which maximum occurs; DSR, classical dipole-sum rule limit; Γ_0 twice the energy from half-maximum on low-energy side of curve to E_m ; Γ_{Lor} width used to fit the Lorentz curve

	σ_m mb	E_m MeV	$\int_{\text{Th}}^{\infty} \sigma dE$ MeV-b	DSR MeV-b	Γ_0 MeV	Γ_{Lor} MeV
Uncorrected for multiplicity						
La	315 ± 15	14.8 ± 0.4	1.76	2.02		
Pr	305 ± 10	14.8 ± 0.4	1.74	2.06		
Corrected for ($\gamma, 2n$)						
La	304	14.5	1.36	2.02	3.2 ± 0.2	3.3
Pr	305	14.8	1.47	2.06	4.0 ± 0.2	3.3

line in each figure is a result of a Lorentz curve fitting to the low-lying points on the low-energy side of the peak.

ELEM.	SYN.	A	Z
Pr		141	59

METHOD

REF. NO.	
66 Be 3	JDM

Nuclear Resonance Scattering using N,G reactions.

REACTION	RESULT	EXCITATION ENERGY	SOURCE		DETECTOR		ANGLE
			TYPE	RANGE	TYPE	RANGE	
G,G	RLX	5 - 10	D	5 - 10	NAI-D	5 - 10	135

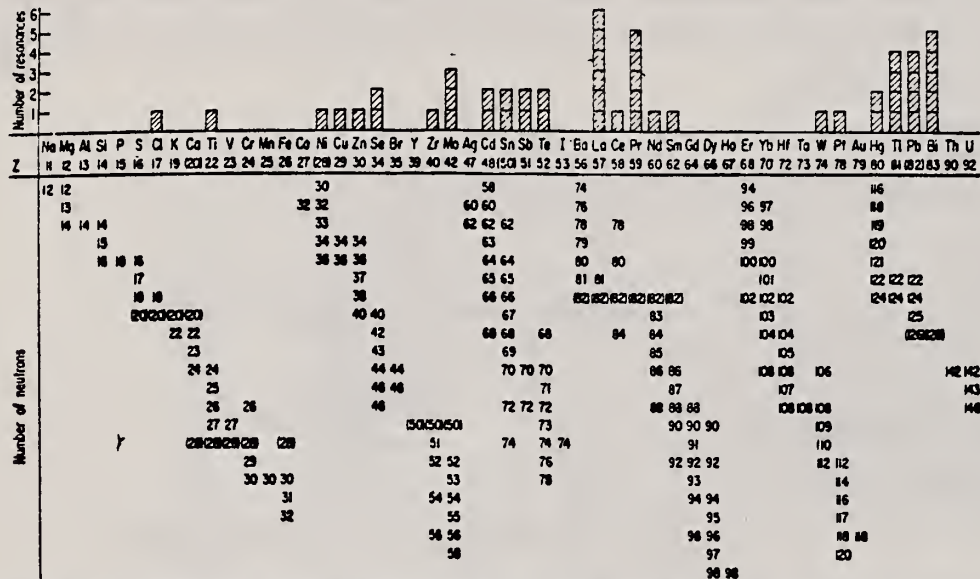


FIG. 3. Histogram of distribution of observed resonances among the different targets. The atomic number is given directly beneath the chemical symbol followed by the neutron numbers of the naturally occurring isotopes. Magic numbers are shown in brackets.

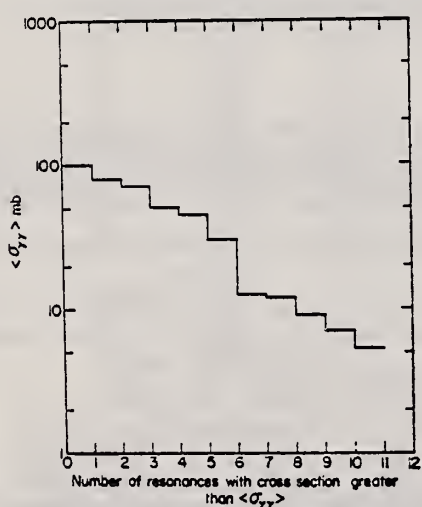


FIG. 5. Integral distribution of the effective cross sections for the 11 resonances in the mono-isotopic elements lanthanum and praseodymium.

TABLE III. List of effective cross sections.

Scatterer	Energy (MeV)	Gamma source	δ (mb)	Scatterer	Energy (MeV)	Gamma source	δ (mb)
Sm ¹⁴⁴	8.997	Ni	100	Sn	7.01	Cu	110
Pr ¹⁴¹	8.881	Cr	9	Nd	6.867	Co	30
La	8.532	Ni	6	Pr ¹⁴¹	6.867	Co	3
Te	8.532	Ni	3*	Te	6.7	Ni	...
Cu	8.499	Cr	24	La	6.54	Ag	12
Zr	8.496	Se	3050	Cd	6.474	Co	110
Zn	8.119	Ni	13	Mo	6.44	Hg	25*
Se	7.817	Ni	50	La	6.413	Ti	72
Se	7.76	K	90	Mo	6.413	Ti	10
Sb	7.67	V	...	Tl	6.413	Ti	25
Cd	7.64	Fe	40*	W	6.3	Ti	...
Ni	7.64	Fe	7*	Sb	6.31	Hg	6*
Pr ¹⁴¹	7.64	Fe	12*	Ti	6.31	Hg	2*
Tl	7.64	Fe	370*	Sn	6.27	Ag	75
La	7.634	Cu	7	Pb ²⁰⁸	6.15	Gd	...
Mo	7.634	Cu	11	Te	5.8	Ni	...
Bi ²⁰⁸	7.634	Cu	4	La	6.12	Cl	35
Te	7.528	Ni	664	Pr ¹⁴¹	6.12	Cl	110
Bi ²⁰⁸	7.416	Se	100	Pt	5.99	Hg	40*
Bi ²⁰⁸	7.300	As	80*	Tl	5.99	Hg	5*
Pb ²⁰⁸	7.285	Fe	4100	Pb ²⁰⁸	5.9	Sr	...
Cl	7.285	Fe	34	Ca	5.646	Co	17
Pr ¹⁴¹	7.185	Se	80	Bi ²⁰⁸	5.646	Co	55
Tl	7.16	Cu	120	Pb ²⁰⁸	5.53	Ag	70
La	7.15	Mn	50	Hg	5.44	Hg	75*
Bi ²⁰⁸	7.149	Ti	2000	Hg	4.903	Co	385

* High-energy component of a complex spectrum.

† A broad scattered spectrum with no observable peak structure.

‡ There are actually two lines of energies 7.647 and 7.633 MeV having equal intensities in the iron capture gamma spectrum. The cross section has therefore been corrected, although there is no possibility at present of deciding which line is responsible for each resonance.

§ Is probably an independent level in the complex spectrum of Ni γ rays on Te.

** Rough estimate.

† May be inelastic component from 7.528 level in Te.

¶ The relative line intensities in this case are due to Grobev and co-workers.

|| No line is known for the source at this energy.

|| Difficult to resolve among the many source lines present at this energy.

METHOD

REF. NO.

66 Br 1

JDM

REACTION	RESULT	EXCITATION ENERGY	SOURCE		DETECTOR		ANGLE
			TYPE	RANGE	TYPE	RANGE	
G, N	ABX	THR- 33	D	8- 33	BF3		4PI
G, 2N	ABX	THR- 30	D	8- 33	BF3		4PI
G, 3N	ABX	THR- 30	D	8- 33	BF3		4PI
	-	-					

$$\int_{\text{Thr}}^{30} \sigma dE = (2.3 \pm 0.2) \text{ MeV b}$$

(G, N) 304
(G, 2N) 305
(G, 3N) 306
(G, SN) 307

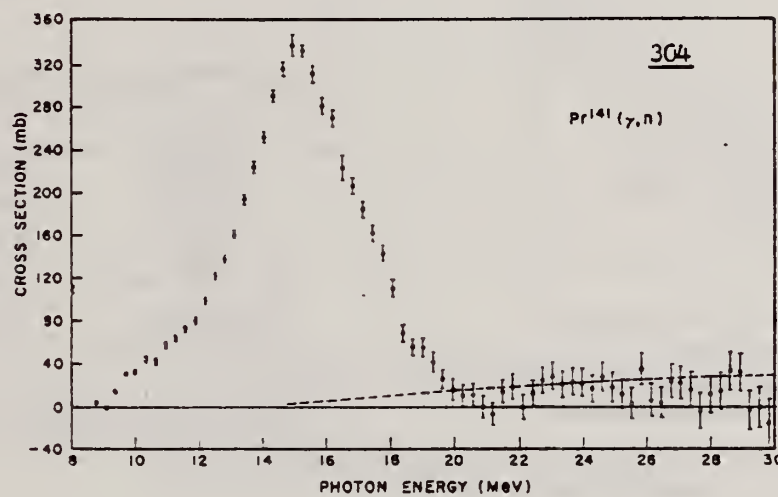


FIG. 1. The $\text{Pr}^{141}(\gamma, n)$ cross section obtained using annihilation photons and 4π neutron detector. A multiplicity-of-neutrons counting technique was used to separate the (γ, n) events from the $(\gamma, 2n)$ and $(\gamma, 3n)$ events. The error bars represent only statistical errors measured in standard deviations. The dashed line is an estimate of the systematic uncertainty due to normalization of position and electron runs.

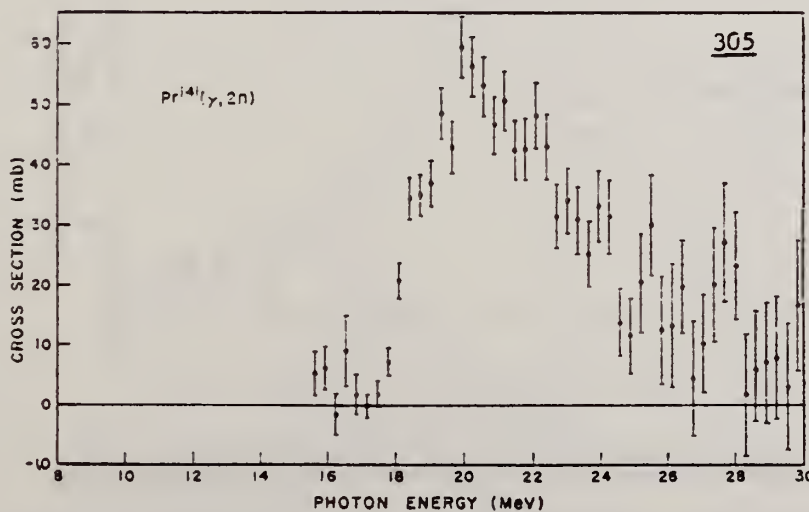


FIG. 2. The $\text{Pr}^{141}(\gamma, 2n)$ cross section.

(over)

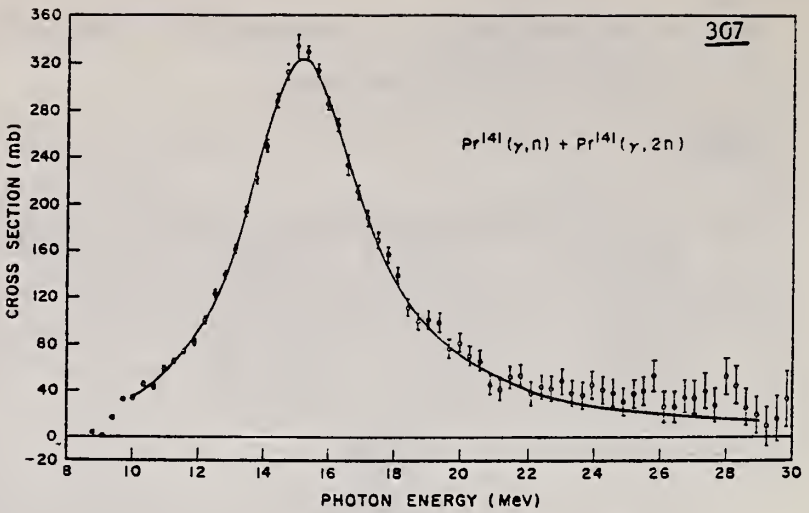


FIG. 4. The photon-absorption cross section of Pr^{141} . Charged particle emission has been neglected so the absorption cross section is the sum of the (γ, n) , $(\gamma, 2n)$ and $(\gamma, 3n)$ cross sections. A Lorentz-shaped curve has been least-squares adjusted to fit the data from 10 to 25 MeV.

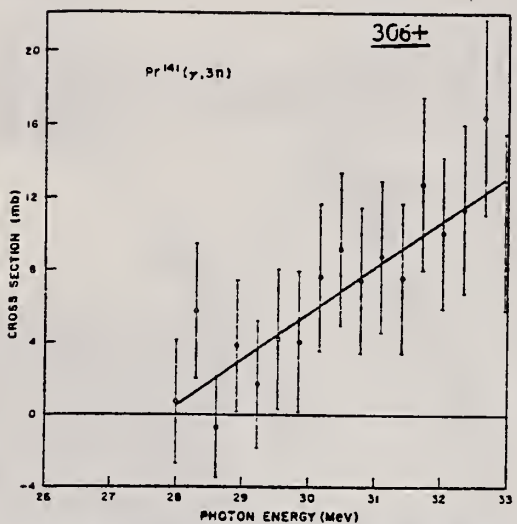


FIG. 3. The $\text{Pr}^{141}(\gamma, 3n)$ cross section. The straight line has been adjusted to fit the data by a least-squares procedure.

TABLE II. Giant resonance parameters of Pr^{141} and I^{127} .

Parameter	Pr^{141}	I^{127}
E_a (MeV)	15.16 ± 0.08	15.21 ± 0.08
E_b (MeV)	...	$1.04 E_a$
I_a (MeV)	4.49 ± 0.05	4.1 ± 0.2
I_b (MeV)	...	7.9 ± 1.5
σ_a (b)	0.32 ± 0.02	0.18 ± 0.02
σ_b (b)	...	0.05 ± 0.01
$\int_{\text{threshold}}^{\infty} \sigma dE$ (MeV b)	2.10 ± 0.15	1.79 ± 0.13
$\pi \sigma_0 I/2$ (MeV b)	2.27 ± 0.14	1.8 ± 0.2
$0.06 N Z / A$ (MeV b)	2.06	1.85
$\int_{\text{threshold}}^{\infty} \sigma dE + \text{wings}^*$ (MeV b)	2.42 ± 0.17	2.09 ± 0.14

* The wing corrections were obtained from the areas of the Lorentz curves which were adjusted to fit the giant resonance.

B.C. Cook, D.R. Hutchinson, R.C. Waring, J.N. Bradford,
 R.G. Johnson, and J.E. Griffin
 Phys. Rev. 143, B730 (1966)

ELEM. SYM.	A	Z
Pr	141	59

METHOD

70 MeV synchrotron

REF. NO.

66 Co 3

JDM

REACTION	RESULT	EXCITATION ENERGY	SOURCE		DETECTOR		ANGLE
			TYPE	RANGE	TYPE	RANGE	
G, N	ABX	THR = 65	C	THR = 70	ACT-I		4PI

30

$$\int \sigma dE = 1790 \pm 100 \text{ MeV mb}$$

0

85

$$\int \sigma dE = 440 \text{ MeV mb}$$

30

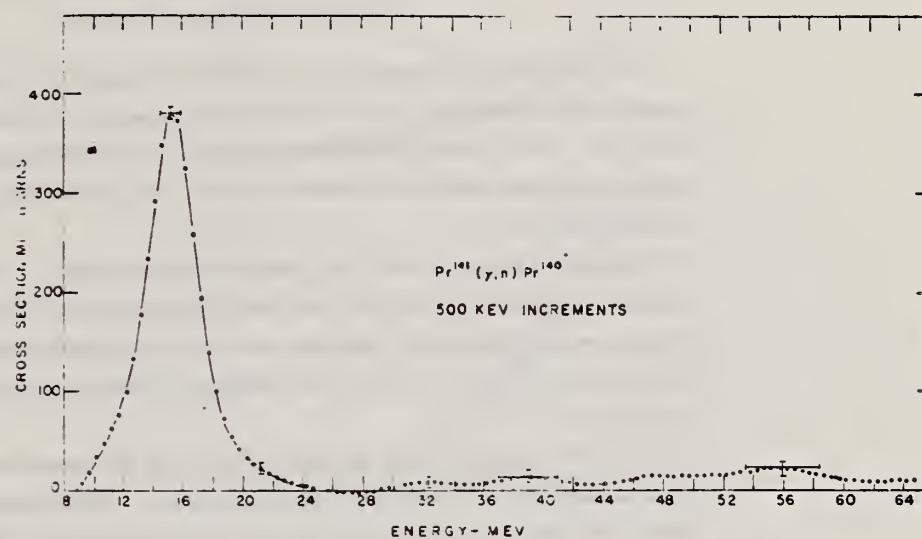


FIG. 1. Cross section for $\Pr^{141}(\gamma, n) \Pr^{140}$ from threshold energy to 65 MeV. The cross-section curve was calculated from yield data taken at 0.500-MeV increments. Horizontal error bars represent full width at half-maximum (FWHM) of experiment resolution and not uncertainty in energy.

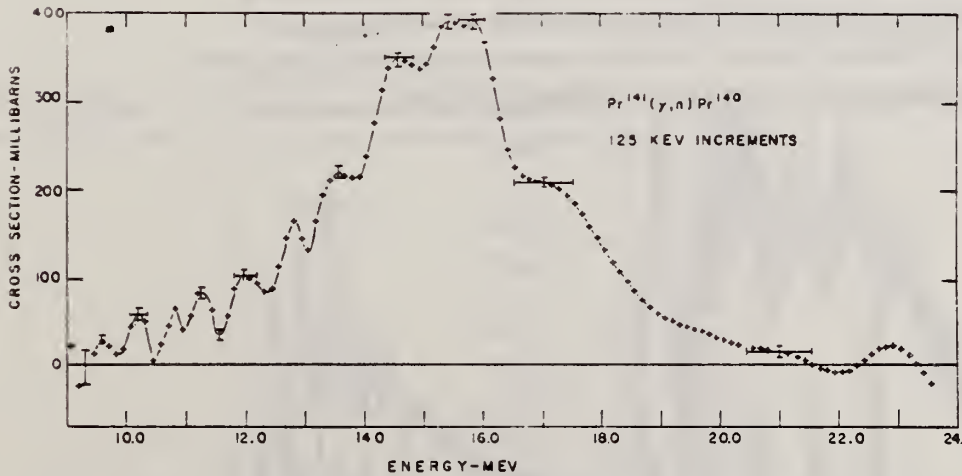


FIG. 2. Cross section for $\Pr^{141}(\gamma, n) \Pr^{140}$ from threshold energy to 24 MeV. The cross-section curve was calculated from yield data taken at 0.125-MeV increments. Horizontal error bars represent FWHM of experiment resolution and not uncertainty in energy.

REACTION	RESULT	EXCITATION ENERGY	SOURCE		DETECTOR		ANGLE
			TYPE	RANGE	TYPE	RANGE	
G,N	RLX	9-17	C	9-17	ACT-I		4PI

Experimental Measurements of Vibrational Splitting of the Giant Dipole Resonance*

P. H. Cannington, D. G. Owen, R.J.J. Stewart, E. G. Muirhead and B. M. Spicer

University of Melbourne, Australia

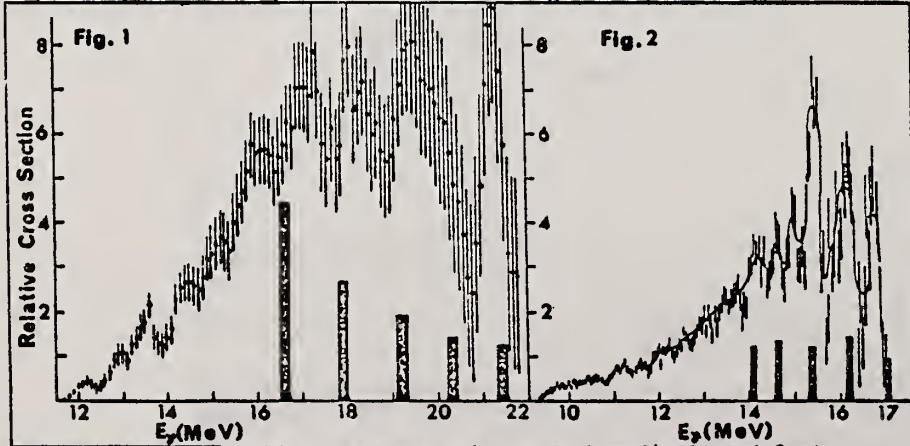
516

The yield curve for the reaction $Zn^{64}(\gamma, n)$ has been measured in 0.1 MeV steps from threshold to 23 MeV, and that for $Pr^{141}(\gamma, n)$ has been measured in 0.05 MeV steps from threshold to 17.5 MeV. In both cases, the positron activity of the residual nucleus was detected by counting annihilation radiation. The cross sections were obtained from the yield curve by the Leiss-Penfold method.

The cross section for the $Zn^{64}(\gamma, n)$ reaction is shown in Fig. 1. Also shown are the predictions of Greiner¹⁾, whose model considers the Goldhaber-Teller type dipole vibration, the low energy surface vibrations of spherical nuclei, and the coupling of these two vibrations. The predictions show only the energy, and integrated absorption cross section for the several transitions.

The $Pr^{141}(\gamma, n)$ cross section is shown in Fig. 2, and the calculations of Huber²⁾ are shown in blocked form; their detail is the same as above. In this case, the surface vibration phonon energy was not so easily fixed as in the case of even-A Zn^{64} . There were, in the case of Pr^{141} , two possible choices indicated by the low energy spectra of neighbouring nuclei. The more suitable one is indicated in Fig. 2.

In both cases, the amount of structure found experimentally exceeds that predicted by the dipole-surface vibration-interference model. However, by worsening the experimental resolution, the agreement can be readily improved. The surplus structure in both cross sections is presumably due to single particle effects which are neglected in the model.



*Supported in part by the U.S. Army Research Office and the Australian Research Grants Committee.

References: 1) W. Greiner, private communication (1968).

134

2) M. Huber, private communication (1966).

METHOD

Neutron capture gamma rays

REF. NO.

67 Hu 1

EGF

REACTION	RESULT	EXCITATION ENERGY	SOURCE	DETECTOR	ANGLE
			TYPE	RANGE	
G, N	ABX	10, 11	D	10, 11	BF ₃ -I
					4PI

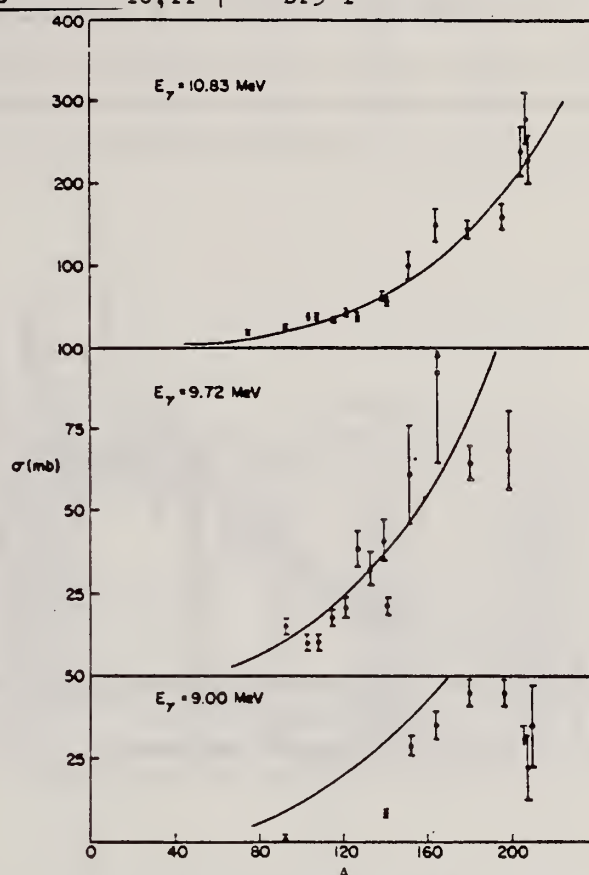


TABLE I
Photoneutron cross sections (mb)

Fig. 1. Cross section (in mb) versus mass number of the target for gamma-ray energies of 9.00, 9.72 and 10.83 MeV. The solid lines are plots of eq. (1) in the text.

Target	7.72 MeV	9.00 MeV	9.72 MeV	10.83 MeV
⁵⁹ Co				9.0 ± 0.8
⁷⁵ As				20.4 ± 1.7
⁹³ Nb		0.53 ± 0.10	14.6 ± 2.2	25.8 ± 2.1
¹⁰³ Rh			10.6 ± 1.7	38.8 ± 3.1
¹⁰⁷ Ag			10.0 ± 1.5	37.6 ± 2.9
¹⁰⁹ Ag			17.1 ± 2.6	33.3 ± 2.7
¹¹¹ In			20.7 ± 3.1	42.5 ± 3.6
¹²¹ Sb			38.7 ± 5.8	38.8 ± 3.1
¹²³ Sb			31.7 ± 4.8	52.5 ± 3.8
¹²⁷ I			8.61 ± 0.86	40.8 ± 6.5
¹³³ Cs			21.5 ± 3.2	63.0 ± 5.0
¹³⁹ La			28.9 ± 3.2	58.3 ± 4.1
¹⁴¹ Pr			61.3 ± 14.7	102 ± 18
¹⁴³ Eu			35.6 ± 4.3	92.2 ± 27.6
¹⁴⁵ Eu		4.14 ± 0.36	45.4 ± 3.7	150 ± 20
¹⁴⁷ Ta			44.5 ± 3.6	65.0 ± 5.5
¹⁵⁷ Au			<34.3	146 ± 12
²⁰⁹ Pb			22.6 ± 11.3	160 ± 15
²¹⁰ Pb			36.1 ± 12.0	238 ± 29
²¹⁰ Bi				280 ± 31
				226 ± 27

U.S. DEPARTMENT OF COMMERCE
NATIONAL BUREAU OF STANDARDS

REF. P. H. Cannington, R. J. J. Stewart, B. M. Spicer and M. G. Huber
 Nucl. Phys. A109, 385 (1968)

ELEM. SYM.	A	Z
Pr	141	59

METHOD

REF. NO.
 68 Ca 1 EGF

REACTION	RESULT	EXCITATION ENERGY	SOURCE		DETECTOR		ANGLE
			TYPE	RANGE	TYPE	RANGE	
G,N	ABX	9-17	C	9-17	ACT-I		APT

69

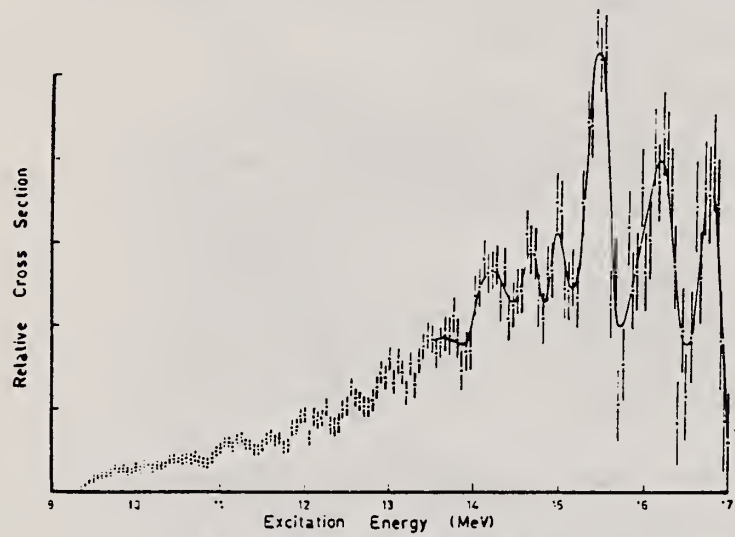


Fig. 1. The $^{141}\text{Pr}(\gamma, \text{n})^{140}\text{Pr}$ cross section.

REF.

J. W. Jury, J. S. Hewitt, and K. G. McNeill
 Can. J. Phys. 46, 1823 (1968)

ELEM. SYM.	A	Z
Pr	141	59

METHOD

REF. NO.

68 Ju 1

EGF

REACTION	RESULT	EXCITATION ENERGY	SOURCE		DETECTOR		ANGLE
			TYPE	RANGE	TYPE	RANGE	
G,N	NOX	THR-30	C	30	THR	5-	DST

$$W(\theta) = a_0 + a_1 P_1 + a_2 P_2$$

TABLE I

Target element	Z	Energy	a_0^*	a_1/a_0	a_2/a_0
Vanadium	23	32	640 ± 50	0.11 ± 0.10	-0.09 ± 0.11
Chromium	24	22	365 ± 39	0.02 ± 0.08	0.60 ± 0.10
Manganese	25	22	450 ± 33	0.07 ± 0.05	-0.11 ± 0.06
Bromine	35	27	874 ± 54	0.05 ± 0.06	-0.15 ± 0.08
Molybdenum	42	22	610 ± 60	0.09 ± 0.05	-0.35 ± 0.06
Ruthenium	44	27	1100 ± 25	0.12 ± 0.02	-0.29 ± 0.03
Rhodium	45	27	1270 ± 47	0.06 ± 0.03	-0.14 ± 0.03
Palladium	46	27	1350 ± 29	0.26 ± 0.02	-0.12 ± 0.02
Antimony	51	27	2140 ± 62	0.04 ± 0.08	-0.25 ± 0.11
Lanthanum	57	27	1940 ± 70	0.12 ± 0.10	-0.52 ± 0.14
Praseodymium	59	30	1800 ± 58	0.20 ± 0.08	-0.40 ± 0.09
Platinum	78	27	2600 ± 52	0.17 ± 0.02	-0.15 ± 0.03
Lead	82	22	2274 ± 59	0.08 ± 0.08	-0.46 ± 0.09

*The yield per mole per 100 r was normalized to a yield of 2274 for the lead sample at the same energy.

ELEM. SYM.	A	Z
Pr	141	59

METHOD	REF. NO.			EGF			
REACTION	RESULT	EXCITATION ENERGY	SOURCE	DETECTOR	ANGLE		
			TYPE	RANGE	TYPE	RANGE	
G,G	NOX	7	D	7	NAI-D	5-8	90

Compton polarimeter.

Table 1

Properties of levels populated by resonance scattering of iron capture γ rays; J_0 and J denote the spins of the ground and resonance levels, respectively.

Scattering isotope	J_0	Resonance level (MeV)	Resonance spin	$N(90, 90)/N(90, 0)$	Transition character
				exp.	calc.
^{208}Pb	0^+	7.279	1	1.18 ± 0.03	1.18
^{112}Cd	0^+	7.632	1	0.87 ± 0.04	0.855
^{141}Pr	$\frac{5}{2}^+$	7.632	$\frac{1}{2}$	1.03 ± 0.02	1.03
^{62}Ni	0^+	7.646	1	0.88 ± 0.04	0.855
^{203}Tl	$\frac{1}{2}^+$	7.646	$\frac{1}{2}$	1.00 ± 0.01	1.00
					-

REF.

H. Ejiri, P. Richard, S. Ferguson, R. Heffner and D. Perry
 Nucl. Phys. A128, 388 (1969)

ELEM. SYM.	A	Z
Pr	141	59

METHOD

REF. NO.	egf
69 Ej 1	

REACTION	RESULT	EXCITATION ENERGY	SOURCE		DETECTOR		ANGLE
			TYPE	RANGE	TYPE	RANGE	
P,G	ABX	15	D	9-11	SCI-D	6-15	DST

$$Y(90^\circ)/Y(125^\circ) = 1.18$$

$$15=14.95 \text{ MeV}$$

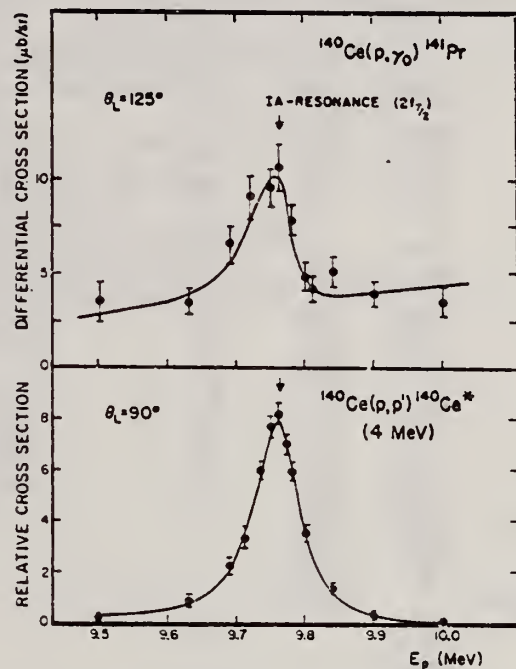


Fig. 4. Excitation function of the ${}^{140}\text{Ce}(\text{p}, \gamma){}^{141}\text{Pr}$ reaction through the $2f_{7/2}$ IA-resonance for the two-quanta escape peak of the ground state transition (upper part) and that of the ${}^{140}\text{Ce}(\text{p}, \text{p}'){}^{140}\text{Ce}^*$ reaction leaving the 4^- particle-hole state at 4 MeV (lower part). Solid lines are calculated ones. For the fit to the (p, p') excitation function, a slight interference effect $\sqrt{\Gamma_p}(E - E)$ is also used.

METHOD		REF. NO.	
		69 Mi 1	egf
G,G	SPC	6-8	DST

BRANCHING RATIOS

TABLE I
Experimental results

Target (source)	Isotope		Levels excited (MeV)		Level spin		Partial branching ratio ^{b)} this work	Branching ratio ^{a)}	
	literature ^{c)}	this work	literature ^{c)}	this work	literature ^{c)}	this work		literature ^{a)}	this work
Cd(Fe)	112 ^{b)}	112	7.629 ^{d)}	7.629	1 ^{b)}	1	0.48±0.06 ^{b)}	< 0.574±0.011	< 0.574±0.011
	112	0	0	0	0				
	112	0.62	0.62	2					
	112	1.22	1.22	0(1)	0				
	112	1.86	1.86	0(1)	0				
Sn(Cu)	117 ^{m)}	118	7.01 ^{d)}	7.01	1 ^{a)}	1	1.000	< 0.122±0.086	< 0.092±0.009
	118	0	0	0					
	118	1.23	1.23	2					
Pr(Cl)	141	6.12 ^{d)}	6.12				0.247±0.038	< 0.213±0.011	< 0.213±0.011
	141	0	0						
	141	0.145	0.145						
	141	1.451 ^{f)}	1.46						
Pr(Fe)	141	7.629 ^{d)}	7.629				0.173±0.045(0.13±0.04)*	< 0.802±0.042	< 0.198±0.030
	141	0	0						
	141	0.145	0.145						
	141	1.13	1.13						
	141	1.451 ^{f)}	1.46						
Cd(Co)	141	2.235 ^{f)}	2.25				(0.33±0.1)*	0.08 ^{f)}	< 0.600±0.032
	?	6.990 ^{a)}	6.990						
	110	6.490 ^{d)}	6.490		1				
	110	0.658	0.658	2					
Pb(Fe)	110	1.78	1.79				(0.2±0.1)*	0.075 ^{f)}	< 0.296±0.030
	doubly even		6.278		(1)				
	208 ^{s)}	7.277 ^{s)}		1 ^{a)}					
Bi(Ti)	209	7.149 ^{d)}							
Zr(Se)	doubly even		8.496		1 ^{a)}				

^{a)} Unless otherwise noted, data are from Nuclear Data Sheets, National Academy of Sciences - National Research Council, 2101 Constitution Avenue, Washington 25, D.C.; or from C. M. Lederer, J. A. Hollander and I. Perlman, Table of Isotopes, Sixth Edition (John Wiley and Sons, Inc., New York, 1967). Energy values are from refs. ¹²⁻¹³.

^{b)} Ref. ³). ^{c)} Ref. ¹⁰). ^{d)} Ref. ⁵). ^{e)} Ref. ⁹). ^{f)} Ref. ²⁰). ^{s)} Γ (resonance level → excited level)/ Γ (resonance level → ground level).

^{c)} Γ (resonance level → excited level)/ Γ (total width). ^{m)} Ref. ²). * Ratios taken only at 150°.

[over]

References

- 1) M. Giannini, P. Oliva, D. Prosperi and S. Sciuti, Nucl. Phys. 65 (1965) 344
- 2) M. Giannini, P. Oliva, D. Prosperi and G. Toumbev, Nucl. Phys. A101 (1967) 145
- 3) K. Min, Phys. Rev. 152 (1966) 1062
- 4) G. P. Estes and K. Min, Phys. Rev. 154 (1967) 1104
- 5) S. Ramchandran and J. A. McIntyre, Phys. Rev. 179 (1969) 1153
- 6) Y. Schlesinger, B. Arad and G. Ben-David, Israel Atomic Energy Commission Report IA-1128 (1966) and later reports
- 7) J. A. McIntyre and V. E. Michalk, Bull. Am. Phys. Soc. 12 (1967) 1205
- 8) R. Moreh and A. Nof, Bull. Am. Phys. Soc. 13 (1968) 1451
- 9) R. Moreh and A. Nof, report of the Nuclear Research Centre - Negev, Beer Sheva, Israel; Use of the (γ, γ') reaction for studying ^{141}Pr levels
- 10) G. Ben-David, B. Arad, T. Balderman and Y. Schlesinger, Phys. Rev. 146 (1966) 852
- 11) N. V. DeCastro Faria and R. J. A. Levesque, Nucl. Instr. 46 (1967) 325
- 12) L. V. Groshev, V. N. Lutsenko, A. M. Demidov and V. I. Felcov, Atlas of gamma spectra from radiative capture of thermal neutrons, translated from Russian by J. S. Sykes (Pergamon Press, 1959)
- 13) G. A. Bartholomew, A. Doveika, K. M. Eastwood, S. Monaro, L. V. Groshev, A. M. Demidov, V. I. Pelekhan and L. L. Sokolovskii, Nucl. Data A3 (1967) 367
- 14) C. M. Lederer, J. A. Hollander and L. Perlman, Table of isotopes, Sixth ed. (J. Wiley, New York, 1967)
- 15) Nuclear Data Sheets, National Academy of Sciences - National Research Council, 2101 Constitution Avenue, Washington 25, D.C.
- 16) H. Ferentz and N. Rosenzweig, Argonne Nat. Lab. Rep. ANL-5324
- 17) R. Moreh and M. Friedman, Phys. Lett. 26B (1968) 579
- 18) D. B. Beery, W. H. Kelly and W. C. McHarris, Phys. Rev. 171 (1968) 1283
- 19) H. W. Bear and J. Bardwick, Bull. Am. Phys. Soc. 13 (1968) 1430;
B. H. Wildenthal, R. L. Auble, E. Newman and J. A. Nolen, Bull. Am. Phys. Soc. 13 (1968) 1430
- 20) C. S. Young and D. T. Donahue, Phys. Rev. 132 (1963) 1724

REF.

K. Shoda, M. Sugawara, T. Saito & H. Miyase
 PICNS-69 Proceedings of the Conference on Nuclear Isospin.
 Asilomar-Pacific Grove, California 1969 (Academic Press,
 New York & London 1969) p.137.

ELEM. SYM.	A	Z
Pr	141	59

METHOD

REF. NO.
69 Sh 8

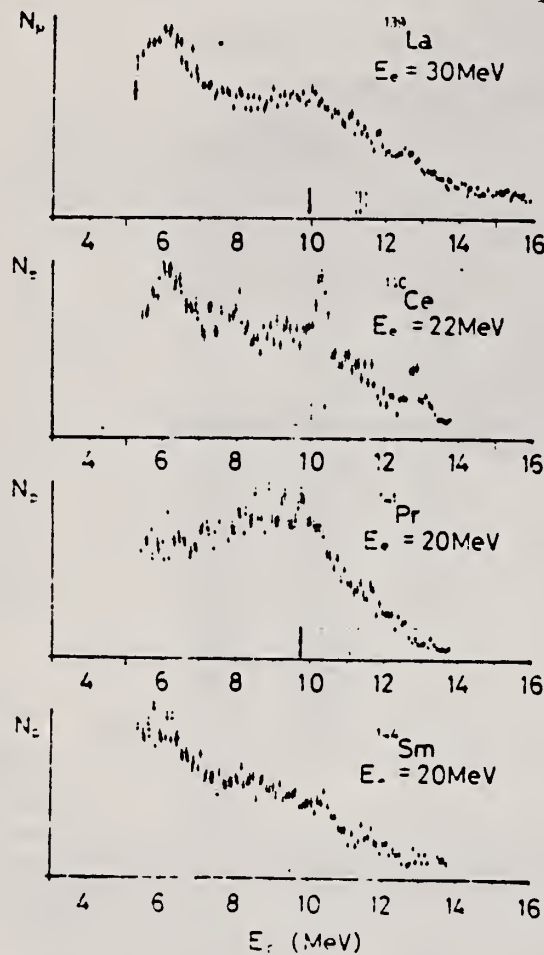


Fig. 1. Energy distributions of photoprotons. Vertical broken lines and solid lines indicate the position of p_0 corresponding to the ground IAS and electric dipole IAS (2).

Table 1. Angular distributions of strong proton groups from ^{140}Ce and ^{141}Pr .

Nucleus	E_p (MeV)	$W(\theta)$
^{140}Ce	10.3	$1+(0.4+0.1)P_1-(0.0+0.1)P_2$
	12.8	$1+(0.2+0.1)P_1-(0.4+0.2)P_2$
^{141}Pr	9.7	$1+(0.0+0.1)P_1+(0.1+0.2)P_2$

Table 2. The radiative widths of the main IAS. The results are compared with the single particle strength in W.u..

Nucleus	E_p (MeV)	E_x (a)	Γ_{p_0}/Γ	Γ_γ (eV)	$2(T+1)\Gamma_{\gamma_0}$ (W.u.)
^{140}Ce	10.3	18.3	1 (b)	50	0.1
	12.8	20.8	1 (b)	90	0.1
^{141}Pr	9.7	15.1	12/60(c)	40	0.2
^{144}Sm	10.6	16.6	1 (b)	20	0.05

(a) Ground state is assumed for the residual state.

(b) Assumption.

(c) P. Von Brentano et al. (2).

ELEM. SYM.	A	Z
Pr	141	59

METHOD

REF. NO.

70 Mc 1

egf

REACTION	RESULT	EXCITATION ENERGY	SOURCE		DETECTOR		ANGLE
			TYPE	RANGE	TYPE	RANGE	
G,XN	SPC	11-28	C	28	TOF-D	2-8	98
		-					
		-					
		-					

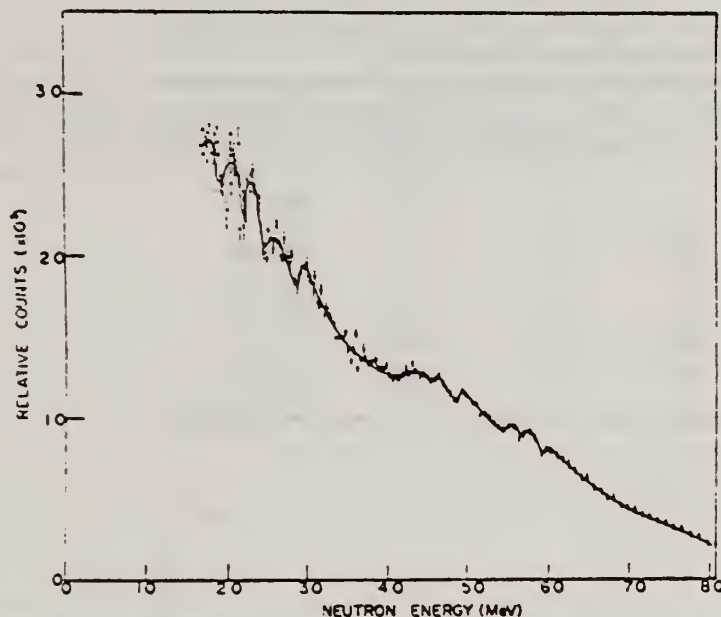


FIG. 1. The photoneutron spectrum obtained by the irradiation of praseodymium by bremsstrahlung of maximum energy 27.5 MeV, the flight path direction being at 98° to the bremsstrahlung beam. The line is merely to guide the eye.

TABLE I
 Correlation between peaks in the cross section and the neutron spectrum for the reaction $^{141}\text{Pr}(\gamma, n)^{140}\text{Pr}$

Neutron energy E_n (MeV)	Excitation energy $E_n + E_{threshold}$ (9.3 MeV)	Peaks in $\sigma(\gamma, n)$ Cannington <i>et al.</i> (1968) (MeV) [†]
2.2	11.5	11.6?
2.4	11.7	
2.7	12.0	12.0
3.0	12.3	12.2?
		12.6?
3.9	13.2	13.1
4.4	13.7	13.7
4.7	14.0	
5.0	14.3	14.2?
5.5	14.8	14.7
5.75	15.05	15.0

[†]The error on the experimentally determined neutron energy is in all cases between 70 and 100 keV.

[‡]The question marks indicate doubts expressed in the text of Cannington *et al.*

METHOD

REF. NO.

70 Mo 2

hmg

REACTION	RESULT	EXCITATION ENERGY	SOURCE		DETECTOR		ANGLE
			TYPE	RANGE	TYPE	RANGE	
G,G	ABX	8 (7.632)	D	8 (7.632)	SCD-D		DST

8 = 7.632, LFT

TABLE III. Summary of the results of spins, parities, and total widths of resonance levels excited by γ rays obtained from neutron capture in iron. Parities in parentheses are uncertain.

Isotope	Energy (MeV)	$\delta = E_r - E_s $ (eV)	J^{π}_0	J^{π}_r	Transition	Γ_0/Γ_γ ($\pm 8\%$)	Γ_γ (10^{-3} eV)
⁵⁰ Cr	8.888	18 ± 1	0 ⁺	1	...	0.90	750 ± 200
⁶² Ni	7.646	14 ± 1	0 ⁺	1 ⁻	E1	0.64	480 ± 50
⁷⁴ Ge	6.018	4.5 ± 0.5	0 ⁺	1 ⁻	E1	0.19	120 ± 15
⁷⁵ As	7.646	7.4 ± 0.3	3/2 ⁻	1/2 ⁽⁺⁾	...	0.11	360 ± 100
¹⁰⁹ Ag	7.632	9 ± 1	1/2 ⁻	3/2	...	0.7	2 ± 1
¹¹² Cd	7.632	4.8 ± 0.4	0 ⁺	1 ⁻	E1	0.55	86 ± 15
¹³⁹ La	6.018	8.2 ± 0.6	7/2 ⁺	7/2 ⁻	E1	0.50	51^{+14}_{-14}
¹⁴¹ Pr	7.632	$11.4^{+0.3}_{-0.9}$	5/2 ⁺	5/2 ⁺	M1	0.46	72^{+14}_{-14}
²⁰⁵ Tl	7.646	9.3 ± 0.3	1/2 ⁺	1/2 ⁽⁻⁾	...	0.58	980 ± 90
²⁰⁸ Pb	7.279	7.1 ± 0.3	0 ⁺	1 ⁺	M1	1.00	780 ± 60

TABLE IV. Effective elastic scattering cross section $\langle\sigma_r\rangle = \sigma_0^m (\Gamma_0/\Gamma_\gamma) \Psi(x_0, t_0)$, where δ , J , Γ_0 , Γ_γ were taken from Table III. The temperature of the scatterer was 300°K, while that of the iron γ source was 640°K.

Target	Resonance energy (MeV)	$\langle\sigma_r\rangle$ (mb)
⁵⁰ Cr	8.888	905
⁶² Ni	7.646	569
⁷⁴ Ge	6.018	61
⁷⁵ As	7.646	4.4
¹⁰⁹ Ag	7.632	3.5
¹¹² Cd	7.632	198
¹³⁹ La	6.018	39
¹⁴¹ Pr	7.632	20
²⁰⁵ Tl	7.646	574
²⁰⁸ Pb	7.279	5560

ELEM. SYM.	A	z
Pr	141	59
REF. NO.	70 Su 1	hmg

METHOD

REACTION	RESULT	EXCITATION ENERGY	SOURCE		DETECTOR		ANGLE
			TYPE	RANGE	TYPE	RANGE	
G ₃ N	ABX	9-24	D	9-24	ACT-I		4PI

211

The ¹⁴¹Pr(γ , n) cross section was measured from threshold to 24 MeV with a photon beam produced by the in-flight annihilation of positrons. The photon beam resolution was determined to be 1.26 (full width at half maximum) by elastically scattering the γ rays from the 15.1-MeV level in ¹²C. The (γ , n) cross section was found to have a maximum value of ~348 mb and an integrated value up to 24 MeV of 1.72 ± 0.16 MeV b. Within the statistics and the photon resolution of the measurement, the results indicate that there is no structure in the cross section, with the possible exception of a weak bump at approximately 17.5 MeV. The results are compared with previous measurements and with theory; the latter comparison indicates that the widths of states in the dynamic collective theory should be considerably broader than those which have been typically used.

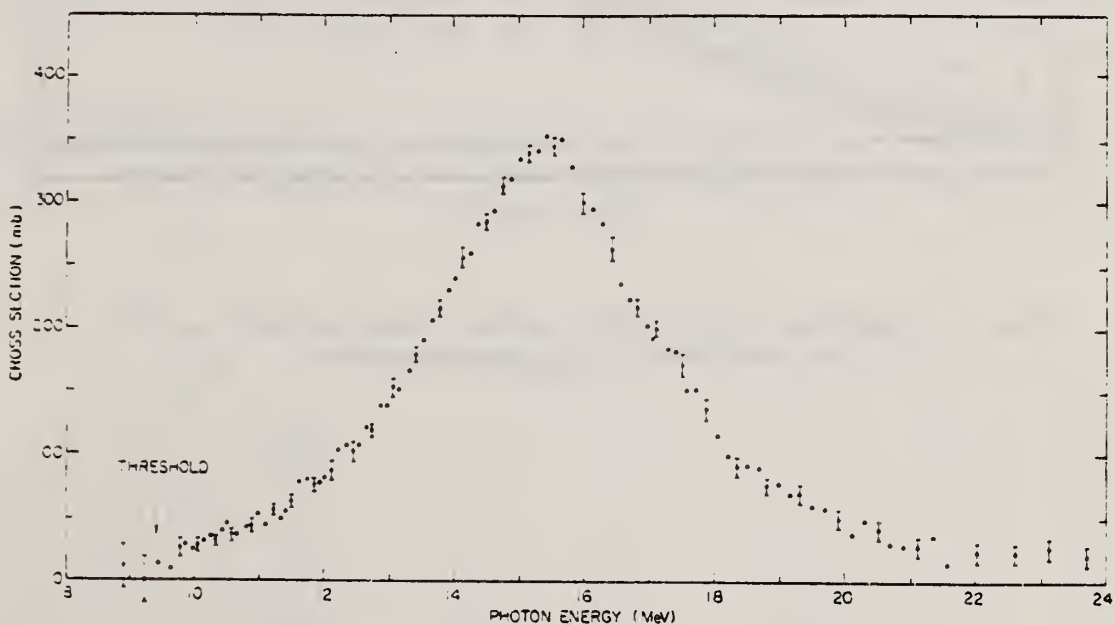


FIG. 4. ¹⁴¹Pr(γ , n) cross section.

REF.	J. Ahrens, H. Borchert, H.B. Eppler, H. Gimm, H. Gundrum, P. Riehn, G. Sita Ram, A. Zieger, and B. Ziegler Elba-71, Tagungsbericht Elektronen Beschleuniger Arbeits Gruppen (Sept. 1971) Justus Liebig-Universitat Giessen.	ELEM. SYM.	A	Z
METHOD		Pr	141	59

REF. NO.	71 Ah 1	hmg
----------	---------	-----

REACTION	RESULT	EXCITATION ENERGY	SOURCE		DETECTOR		ANGLE
			TYPE	RANGE	TYPE	RANGE	
G,MU-T	ABX	THR-150	C	10-150	MGC-D		4PI

519

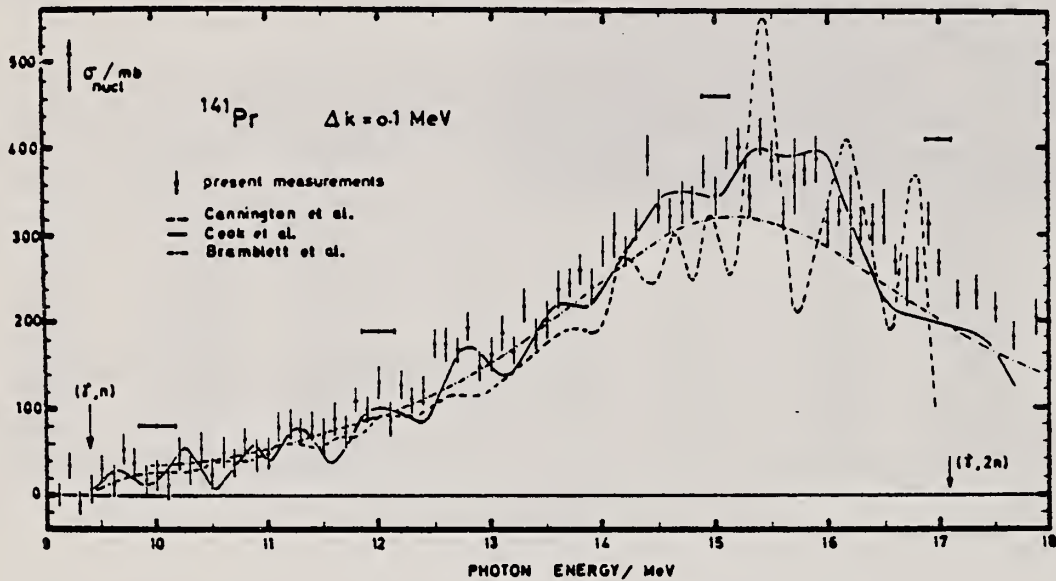


fig. 9: comparison of the total nuclear cross-section in ^{141}Pr with the results of (γ, n) -measurements

H. Beil, R. Bergere, P. Carlos, A. Lepretre, A. Veyssiere and
A. Parlag
Nucl. Phys. A172, 426 (1971)

EL EM. SYM.	A	Z
Pr	141	59

METHOD

REF. NO.

71 Be 4

egf

REACTION	RESULT	EXCITATION ENERGY	SOURCE		DETECTOR		ANGLE
			TYPE	RANGE	TYPE	RANGE	
G, N	ABX	9-17	D	9-17	MOD-T		4PI
							<u>390</u>

TABLE I
Lorentz line parameters corresponding to fits of total photoneutron cross sections presented in fig. 1

	^{90}Ba	^{139}La	^{90}Ce	^{141}Pr	^{60}Nd	$^{141}\text{Pr}^a$
σ_1 (mb)	356 ± 15	340 ± 15	360 ± 15	350 ± 15	315 ± 15	320 ± 20
E_1 (MeV)	15.3 ± 0.1	15.2 ± 0.1	15.0 ± 0.10	15.1 ± 0.1	14.9 ± 0.1	15.16 ± 0.08
Γ_1 (MeV)	4.70 ± 0.15	4.45 ± 0.05	4.35 ± 0.05	4.26 ± 0.05	4.90 ± 0.05	4.49 ± 0.05
$\frac{1}{2}\pi\sigma_1\Gamma_1$ (MeV · b)	2.6 ± 0.15	2.35 ± 0.13	2.42 ± 0.15	2.35 ± 0.13	2.43 ± 0.13	2.42 ± 0.17
$\frac{1}{2}\pi\sigma_1\Gamma_1$ $0.06NZA^{-1}$	1.30 ± 0.08	1.16 ± 0.08	1.19 ± 0.08	1.14 ± 0.08	1.15 ± 0.08	

^a) Lorentz line parameters given in ref. ¹⁰) for ^{141}Pr .

¹⁰ R. L. Bramblett, J. T. Caldwell, B. L. Berman, R. R. Harvey and S. C. Fultz, Phys. Rev. 148, 1198 (1966).

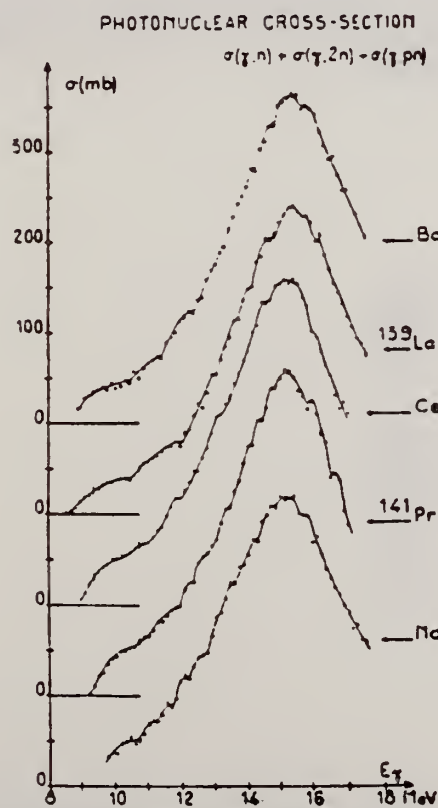


Fig. 1. Total photoneutron cross sections for Ba, ^{139}La , Ce, ^{141}Pr and Nd as a function of incident photon energy E_γ .

REF.

D. Pavel, G. Ben-David, Y. Schlesinger, H. Szichman
 Nucl. Phys. A160, 409 (1971)

ELEM. SYM.	A	Z
Pr	141	59

METHOD

REF. NO.

71 Pa 2

egf

REACTION	RESULT	EXCITATION ENERGY	SOURCE		DETECTOR		ANGLE
			TYPE	RANGE	TYPE	RANGE	
G,G	LFT	6-9	D	6-9	SCD-D	3-9	DST
		-					

5 LEVELS

TABLE 1
 Experimental A_{12} coefficients compared with theory assuming pure dipole transitions

Energy of transitions (keV)	Energy of final state (keV)	A_{12} coefficients for various assumed spin sequences					
		$\frac{1}{2} \rightarrow \frac{1}{2} \rightarrow \frac{1}{2}$ + 0.01000 °)	$\frac{1}{2} \rightarrow \frac{1}{2} \rightarrow \frac{1}{2}$ + 0.1828 °)	$\frac{1}{2} \rightarrow \frac{1}{2} \rightarrow \frac{1}{2}$ - 0.05713 °)	$\frac{1}{2} \rightarrow \frac{1}{2} \rightarrow \frac{1}{2}$ + 0.1071 °)	$\frac{1}{2} \rightarrow \frac{1}{2} \rightarrow \frac{1}{2}$ - 0.1428 °)	$\frac{1}{2} \rightarrow \frac{1}{2} \rightarrow \frac{1}{2}$ + 0.05001 °)
6115	0				+ 0.090 ± 0.037		
5970	145.4					- 0.161 ± 0.068	
4657	1457.9				+ 0.082 ± 0.078		+ 0.082 ± 0.078
7188	0	+ 0.225 ± 0.069					

*) Theoretical value ⁵).

M. Ferentz and N. Rosenzweig, Table of angular correlations coefficients, in Alpha-, beta- and gamma-ray spectroscopy, vol. 2, ed. K. Siegbahn, (North-Holland, Amsterdam, 1965) App.8.

TABLE 2
 Partial radiation reduced widths of the 6115 keV resonance level

Energy of transitions (keV)	Energy of final state (keV)	Branching ratio Γ_i/Γ	Reduced widths		Most likely character
			$k(E1)$ (eV·MeV ⁻⁴)	$k(M1) \times 10^3$	
6115	0	0.557 ± 0.010	27 ± 5	725 ± 139	E1
5970	145.4	0.264 ± 0.006	14 ± 3	370 ± 71	E1
4822	1292.8	0.013 ± 0.004	1.3 ± 0.4	35 ± 11	E1 or M1
4657	1457.9	0.087 ± 0.011	9.5 ± 2.6	256 ± 55	E1
4511	1603.7	0.013 ± 0.004	1.6 ± 0.5	42 ± 13	E1 or M1
4109	2006	0.011 ± 0.006	1.7 ± 0.8	47 ± 22	E1 or M1
3806	2309.3	0.014 ± 0.003	2.7 ± 0.7	76 ± 19	E1
3775	2340	0.015 ± 0.004	3.1 ± 0.9	83 ± 23	E1
3490	2625	0.025 ± 0.003	6.5 ± 1.0	174 ± 37	E1

[over]

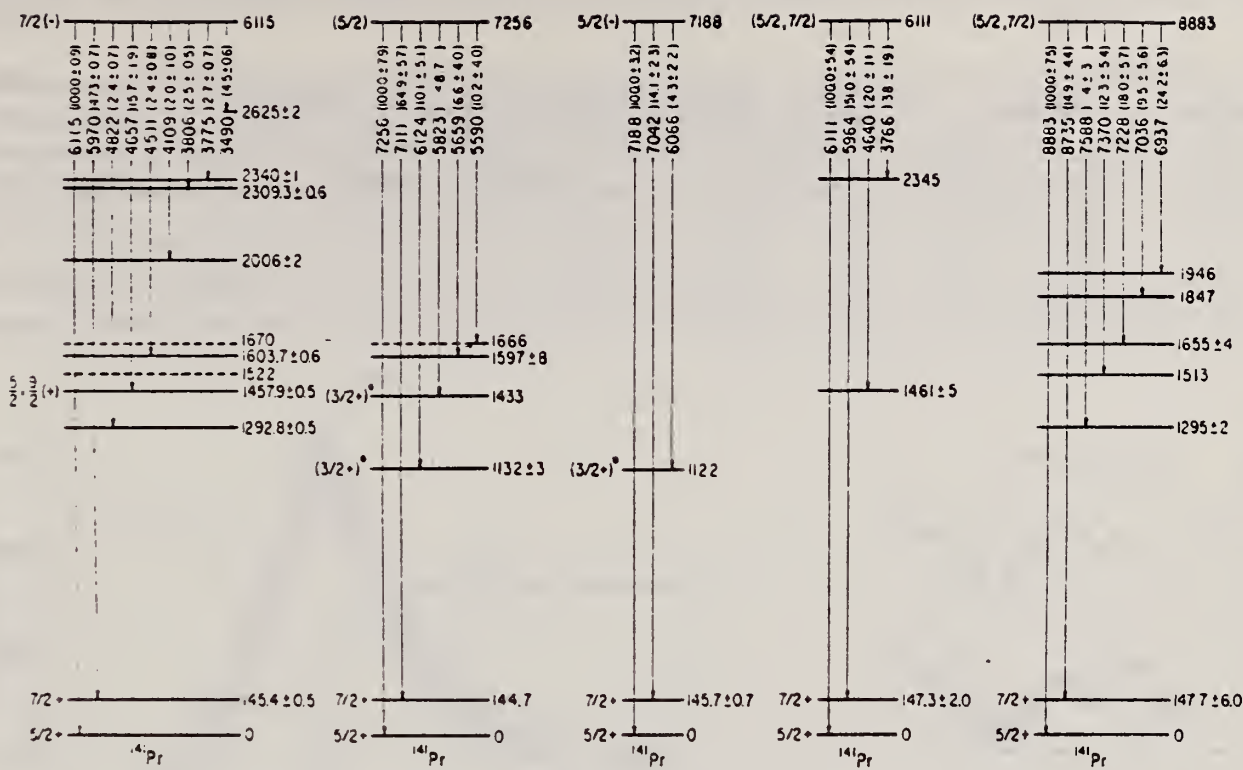


Fig. 2. Decay schemes of the observed resonant levels of ^{141}Pr . The uncertainties in the energy of the levels are estimated as ± 6 keV unless indicated explicitly.

R. Pitthan and Th. Walcher
Phys. Letters 36B, 563 (1971)

ELEM. SYM.	A	Z
Pr	141	59

METHOD

REF. NO.

71 Pi 1

egf

REACTION	RESULT	EXCITATION ENERGY	SOURCE		DETECTOR		ANGLE
			TYPE	RANGE	TYPE	RANGE	
E,E/	SPC	4-18		50.65	MAG-D		DST

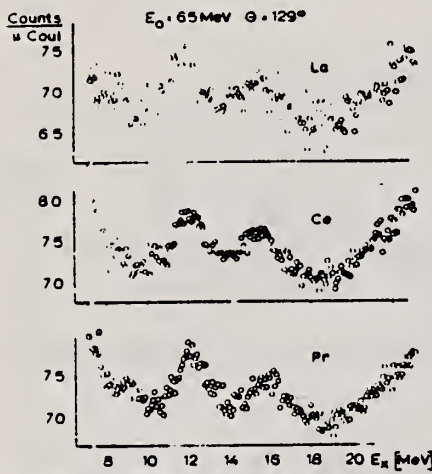


Fig. 2. Spectra of electrons scattered inelastically from La, Ce and Pr targets at the same primary energy and the same laboratory scattering angle. No background has been subtracted. Note the suppressed zeros of the ordinate scales.

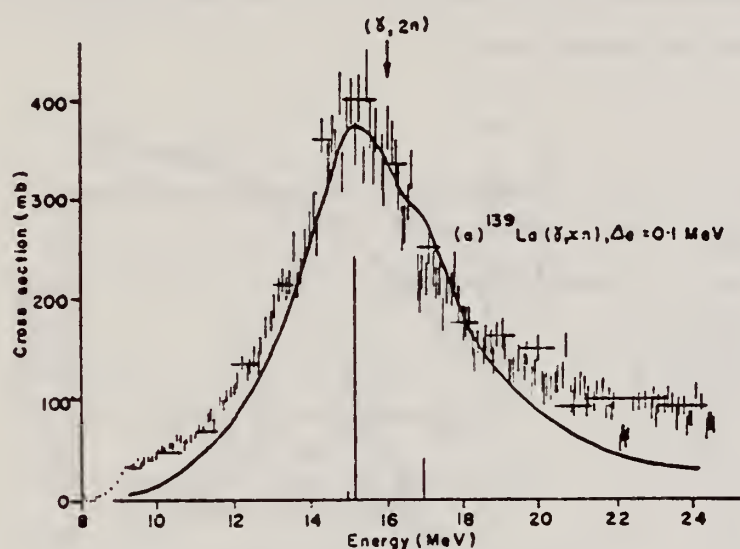
METHOD

REF. NO.

72 De 3

egf

REACTION	RESULT	EXCITATION ENERGY	SOURCE		DETECTOR		ANGLE
			TYPE	RANGE	TYPE	RANGE	
G,XN	ABX	9-22	C	9-22	BF3-I		4PI



560+

TABLE I
The integrated $^{139}\text{La}(\gamma, \text{xn})$ and $^{141}\text{Pr}(\gamma, \text{xn})$ cross sections and their minus-first and minus-second moments, compared with the appropriate sum rules

Nucleus	Ref.	σ_0 (b · MeV)	0.06 NZA^{-1}	σ_{-1} (mb)	$0.16 A^3$	σ_{-2} (mb · MeV $^{-1}$)	$0.00225 A^3$
^{139}La	present work	2.51 ± 0.5	2.02	158 ± 30	115	10.4 ± 2	8.4
	ref. ²⁰⁾	2.20 ± 0.3		141 ± 12		9.4 ± 0.7	
^{141}Pr	present work	1.84 ± 0.3	2.06	121 ± 20	117	8.1 ± 1.3	8.6
	ref. ¹⁰⁾	1.83 ± 0.16					

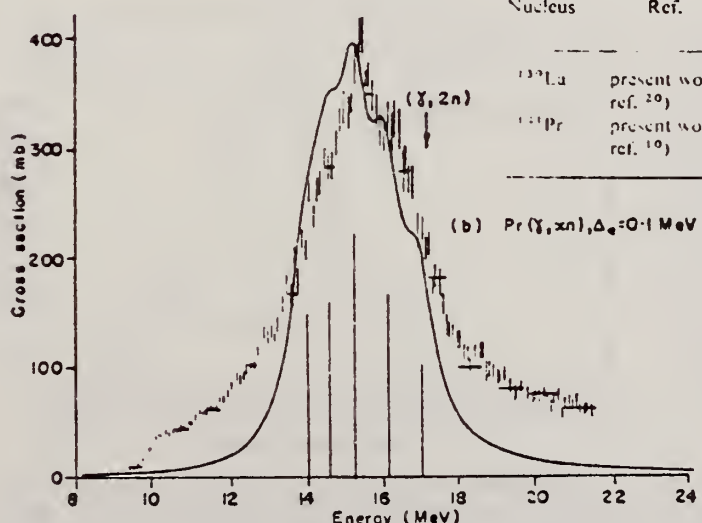


Fig. 1. (a) The $^{139}\text{La}(\gamma, \text{xn})$ cross section, obtained by VBPL unfolding from yield data measured in 0.1 MeV steps. Also shown is the DCM dipole spectrum for ^{147}Nd , and a fit to it of Lorentz line shapes with widths 4.0 MeV (solid line). (b) The $^{141}\text{Pr}(\gamma, \text{xn})$ cross section, obtained by VBPL unfolding from yield data measured in 0.1 MeV steps. Also shown is the DCM dipole spectrum for ^{146}Nd , and a fit to it of Lorentz line shapes with widths 1.0 MeV (solid line).

ELEM. SYM.	A	Z
Pr	141	59

METHOD	REF. NO.		
	72 Di 7		egf

REACTION	RESULT	EXCITATION ENERGY	SOURCE		DETECTOR		ANGLE
			TYPE	RANGE	TYPE	RANGE	
G,P	ABY	THR-300	C	106-300	ACT-I		4PI

One monitor unit = 0.735×10^7 ergs in beam.
Pr-140 yield is of the order of 10^6 reactions per monitor unit.

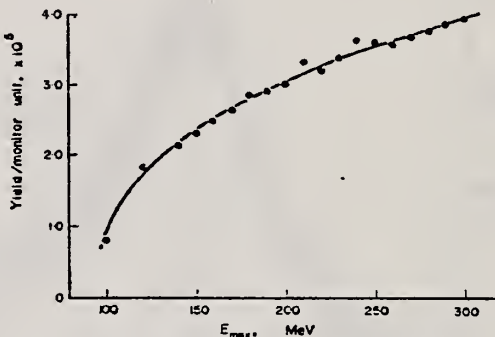


FIG. 2. Yield data from the production of ^{140}Nd in Pr_6O_{11} targets.

ELEM. SYM.	A	Z
Pr	141	59

METHOD

REF. NO.

72 Dr 2

egf

REACTION	RESULT	EXCITATION ENERGY	SOURCE		DETECTOR		ANGLE
			TYPE	RANGE	TYPE	RANGE	
G,N	ABX	9-20	C	9-20	ACT-I		4PI

447

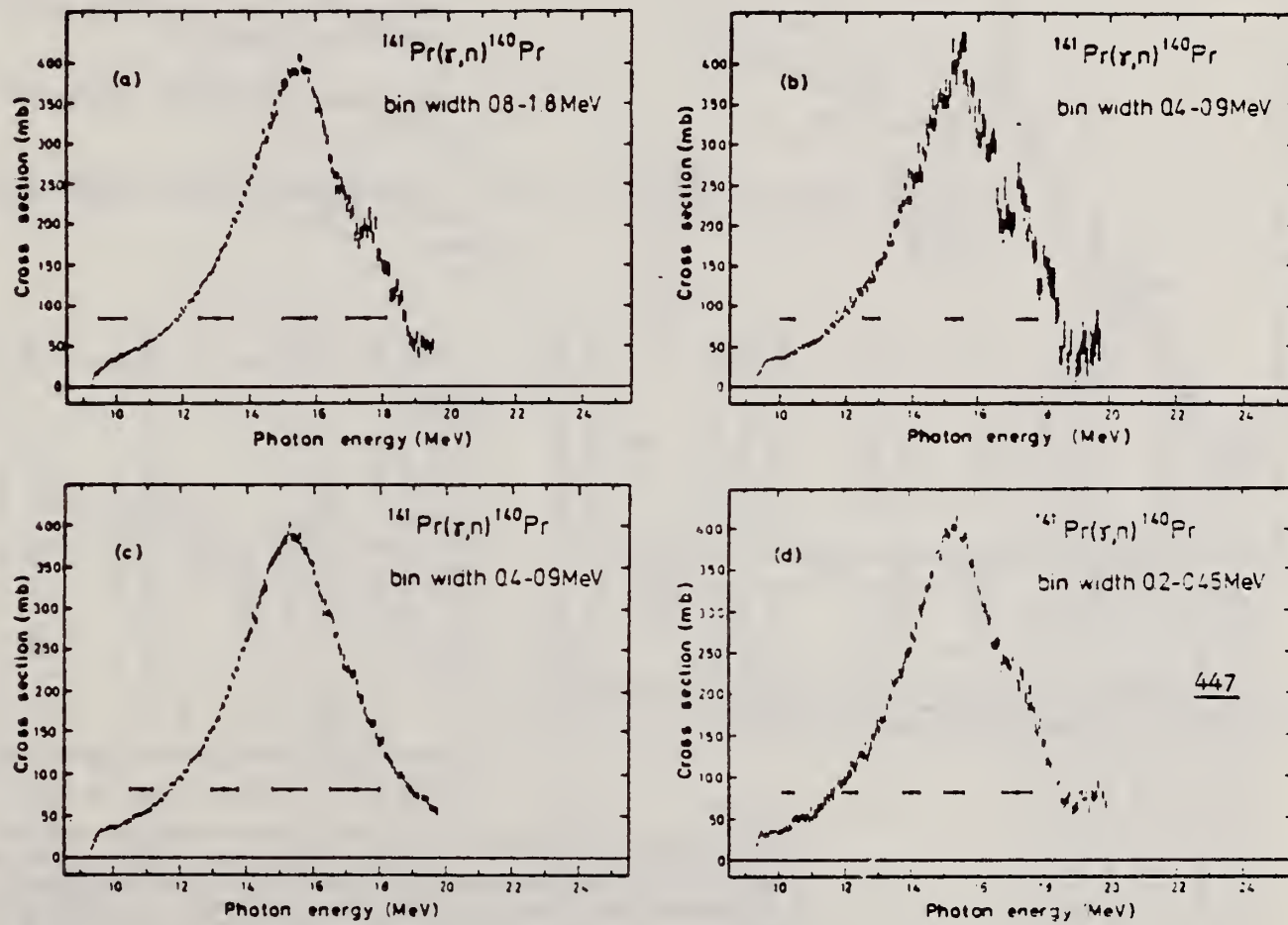


Fig. 3. Cross section for $^{141}\text{Pr}(\gamma, n)^{140}\text{Pr}$ from threshold energy to 19.5 MeV. (a) and (b) show the cross-section curve obtained with two different analysis bin widths using the LP method. The horizontal bars represent the bin width ΔE_0 increasing with the bremsstrahlung endpoint energy E_0 . (c) and (d) show the same cross section calculated with bin width from 0.4 to 0.9 MeV respectively 0.2 to 0.45 MeV using the CLS method. The horizontal bars represent the FWHM of experimental resolution and not the uncertainty in energy.

METHOD

REF. NO.

73 Ba 20

egf

REACTION	RESULT	EXCITATION ENERGY	SOURCE		DETECTOR		ANGLE
			TYPE	RANGE	TYPE	RANGE	
G,N	NOX	THR- 27	C	10- 27	BF3-I		4PI

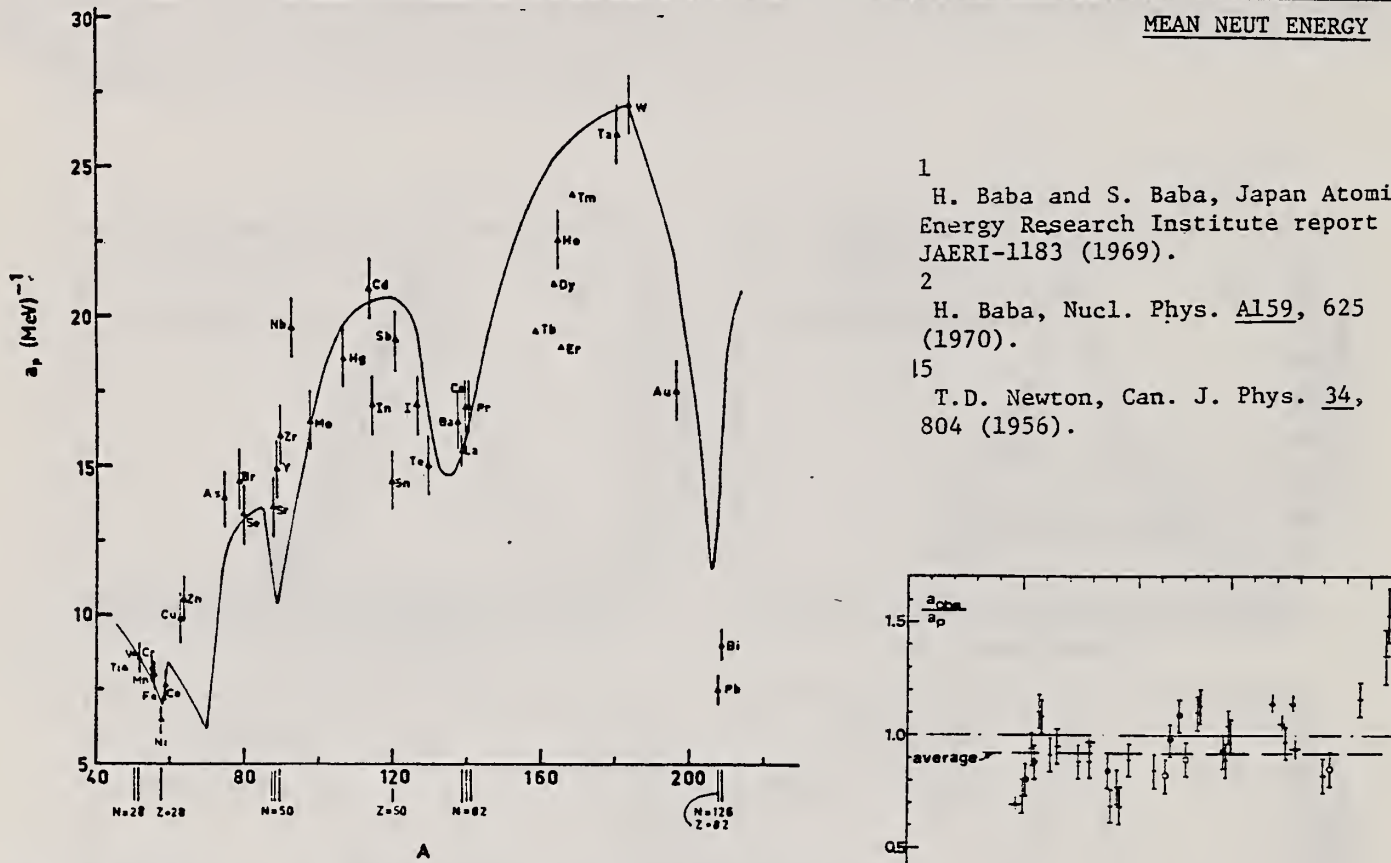


Fig. 12. Experimental values of the level density parameter a_p (Fermi gas formula plus pairing correction) versus atomic number A . The continuous curve is a least-squares fit to the data of a theoretical calculation from Newton ¹⁵.

- 1 H. Baba and S. Baba, Japan Atomic Energy Research Institute report JAERI-1183 (1969).
 2 H. Baba, Nucl. Phys. A159, 625 (1970).
 15 T.D. Newton, Can. J. Phys. 34, 804 (1956).

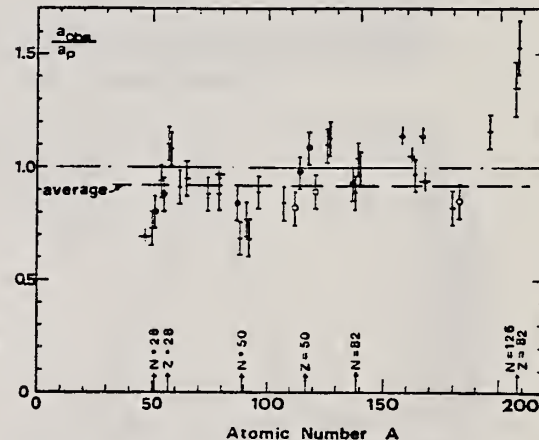


Fig. 15. Ratio a_{obe}/a_p versus atomic number A . Here a_{obe} is the level density parameter taken from the neutron resonance work of refs. ¹⁻², and a_p is the level density parameter derived from the present (γ, n) work. Filled circles represent points where nuclei in the neutron resonance and in the (γ, n) experiment were the same. Open circles represent points where the respective nuclei were approximately matched. Triangles represent points which are based on measurement of neutron mean energies at two bremsstrahlung energies only.

(over)

TABLE 3 (continued)

Target	<i>N</i>	Goodness of fit ^a)	$E_n^{(24)}$ (MeV) ^a)	T (MeV) ^a)	a_p (MeV ⁻¹) ^a)	a_{abs} (MeV ⁻¹) ^a)	a_{abs}/a_p	
Ba	75	1%	F	1.16	$16.5_{-1.0}^{+1.0}$ Ba	$15.39_{-1.0}^{+0.9}$ Ba	0.93	
	77	2%						
	78	7%						
	79	8%						
	80	11%						
	81	71%	F F	1.25	0.72	$15.5_{-1.0}^{+1.0}$ La	0.89	
La	80	100%	F G	1.24	0.70	$17.0_{-1.0}^{+1.0}$ Ce	1.04	
Ce	81	89%	F G	1.24	0.70			
	83	11%						
Pr	81	100%	G G	1.17	0.65	$17.0_{-1.0}^{+1.0}$ Pr	1.00	
Tb ^b)	93	100%	G G	1.15		$19.3_{-1.0}^{+1.0}$ Tb	1.14	
Dy ^b)	93	2%		1.06	$20.9_{-1.0}^{+1.0}$ Dy	$21.9_{-1.0}^{+1.0}$ Dy	1.05	
	94	19%						
	95	25%						
	96	25%						
	97	28%						
Ho	97	100%	P G	1.06	0.56	$21.4_{-1.0}^{+1.0}$ Ho	0.97	
Er ^b)	95	2%		1.11	$19.2_{-1.0}^{+1.0}$ Er	$21.9_{-1.0}^{+1.0}$ Er	1.14	
	97	33%						
	98	23%						
	99	27%						
	101	15%						
Tm ^b)	99	100%	G	1.03	$24.0_{-1.0}^{+1.0}$ Tm	$22.58_{-1.0}^{+1.0}$ Tm	0.94	
Ta	107	100%	G	1.00	0.49	$26.0_{-1.0}^{+1.0}$ Ta	$21.2_{-1.0}^{+1.0}$ Ta	0.82
	107	26%	G F	0.98	0.50	$27.0_{-1.0}^{+1.0}$ W	$23.0_{-1.0}^{+1.0}$ W	0.85
W	108	14%						
	109	31%						
	111	28%						
Au	117	100%	G	1.19	$17.5_{-1.0}^{+1.0}$ Au	$20.24_{-1.0}^{+1.0}$ Au	1.16	
Pb	123	24%	V.P.	1.87	1.20	$7.5_{-1.0}^{+1.0}$ Pb	1.35	
(Z = 82)	124	23%						
	125	52%						
Bi	125	100%	F	1.65	1.03	$9.0_{-1.0}^{+1.0}$ Bi	1.53	

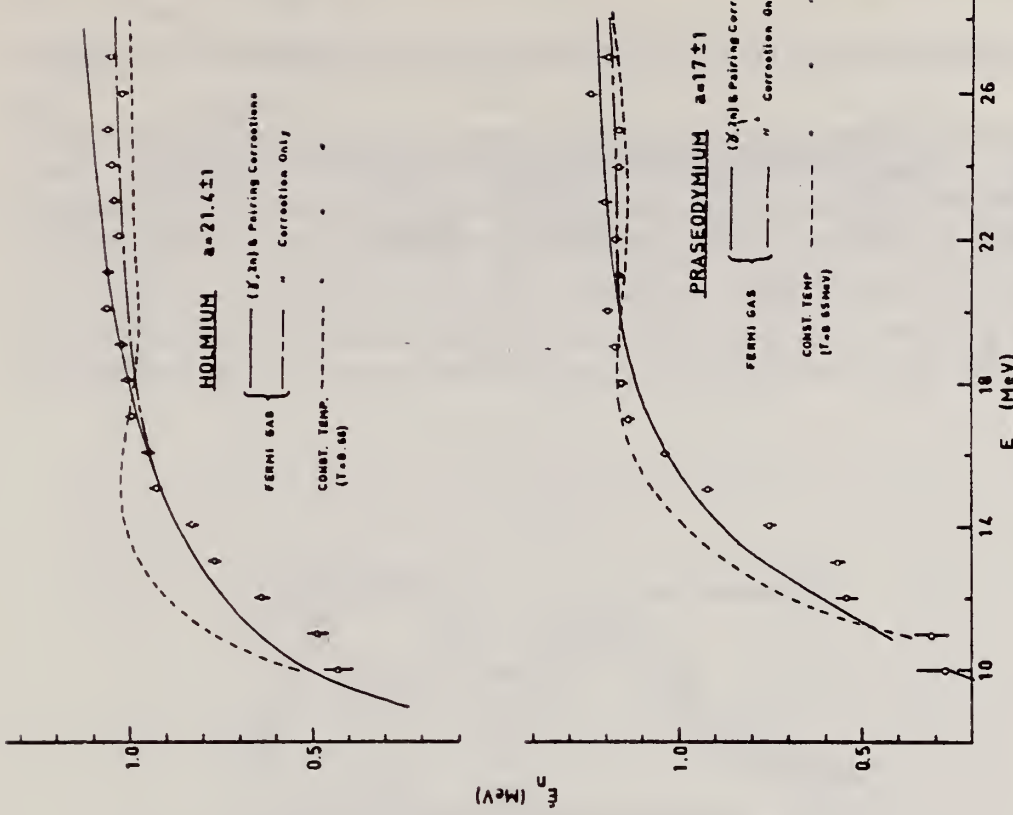
^a) Neutron numbers and abundances of respective residual nuclei in (γ , n) experiments.^b) These give an assessment of the goodness of fit of a calculated E_0 versus E_0 curve to the observed data, using the Fermi gas level density formula both without and with pairing corrections.^c) Bremsstrahlung photoneutron mean energies E_0 for peak bremsstrahlung energy $E_0 = 24$ MeV.^d) Nuclear temperature from fit with constant-temperature formula.^e) Level density parameter a_p derived from the present (γ , n) experiment, using a Fermi gas formula plus pairing correction, and corresponding residual nucleus (the atomic weight shown is the weighted average of atomic weights of the respective isotopes present).^f) As column 7, but using data on n-resonance absorption from refs. ^{1,2}.^g) Measurements of $E_0(E_0)$ for these nuclei were made only for $E_0 = 21, 23$ and 24 MeV.

Fig. 10. Same as fig. 5, for praseodymium and holmium.

REF. F.R. Buskirk, H.D. Graf, R. Pitthan, H. Theissen, O. Titze,
and Th. Walcher
PICNS-73, Vol.I, p.703 Asilomar

ELEM. SYM.	A	Z
Pr	141	59

METHOD	REF. NO.	
	73 Bu 14	hmg

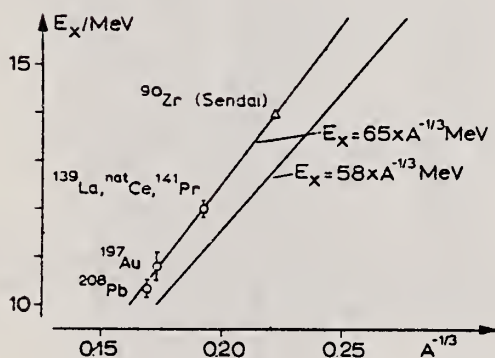


Fig. 2

part should depend on A through $E_x = 58 A^{-1/3}$ MeV. The data of Fig. 2 are consistent with $E_x = 65 A^{-1/3}$ MeV suggesting to identify the observed resonances with this type of E2 excitation.

The E2 resonance which is clearly visible at 10.8 ± 0.2 MeV exhausts more than 50 % of the sum rule. Fig. 2 shows the excitation energy of this resonance as a function of $A^{-1/3}$ for the nuclei measured at Darmstadt and the Sendai result for ${}^{90}\text{Zr}$ [5]. Bohr and Mottelson [9] predicted a collective E2 resonance whose isoscalar part

METHOD	REF. NO.	egf
	73 P1 3	

REACTION	RESULT	EXCITATION ENERGY	SOURCE		DETECTOR		ANGLE
			TYPE	RANGE	TYPE	RANGE	
E, E/	ABX	7 - 21	D	50	MAG-D		165

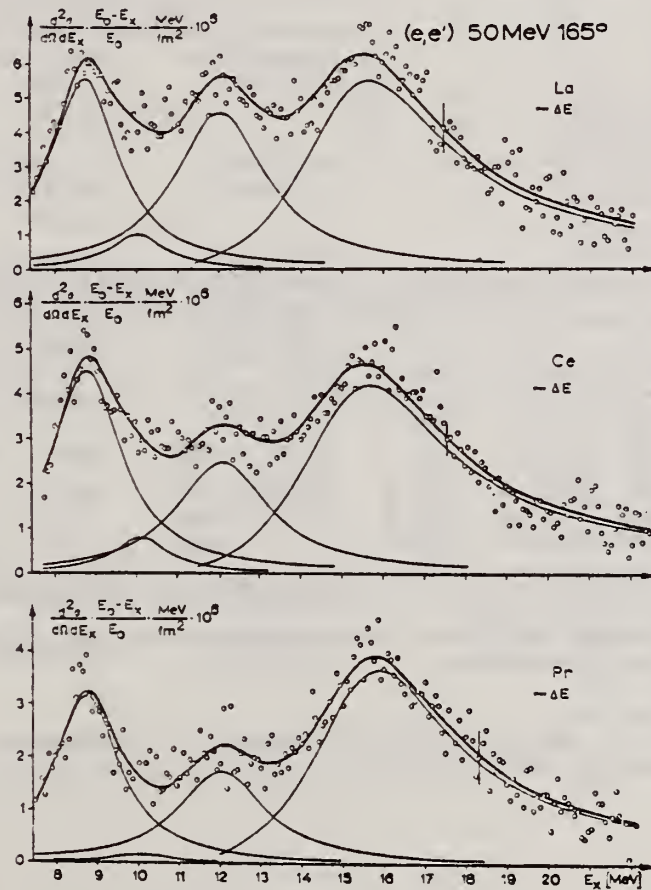


Fig. 7. Spektren von unelastisch an La, Ce und Pr gestreuten Elektronen, sonst wie Fig. 5, s. Text

METHOD

REF. NO.

74 Te 1

egf

REACTION	RESULT	EXCITATION ENERGY	SOURCE		DETECTOR		ANGLE
			TYPE	RANGE	TYPE	RANGE	
G,G	LFT	6	D	4- 8	SCD-D		DST

6=6.877

TABLE 2

Measured angular distribution coefficients A_2 , the ratios $N_{||}/N_{\perp}$, the spins and parities of the ground and the resonance levels, J_0'' and J_r'' , and the character of the ground state transition

Scatterer	E_{γ} (keV)	A_2	$N_{ }/N_{\perp}$	J_0''	J_r''	Transition
^{55}Mn	7491	0.01 ± 0.02	1.00 ± 0.02	$\frac{1}{2}^-$	$\frac{1}{2}$	
^{140}Ce	5660	0.51 ± 0.02	1.14 ± 0.04	0^+	1^-	E1
^{141}Pr	6877	0.11 ± 0.02	0.95 ± 0.03	$\frac{1}{2}^+$	$\frac{3}{2}^+$	M1
^{142}Nd	6877	0.51 ± 0.03	1.10 ± 0.04	0^+	1^-	E1
^{202}Hg	4922	0.51 ± 0.02	1.18 ± 0.03	0^+	1^-	E1
^{209}Bi	5603	0.06 ± 0.02	0.97 ± 0.02	$\frac{1}{2}^-$	$\frac{1}{2}^-$	M1

TABLE 4

Values of Γ , Γ_0 and the energy separation δ (between the incident γ -line and the resonance level) as obtained from the analysis of the various experiments

Scatterer	E_{γ} (keV)	Γ (meV)	Γ_0 (meV)	δ (eV)	D (eV)	K_{E1} (10^{-9} MeV $^{-3}$)	K_{M1} (10^{-9} MeV $^{-3}$)
^{55}Mn	7491	450 ± 250	80 ± 40	17 ± 1			
$^{140}\text{Ce}^*)$	5660	13 ± 3	12 ± 2	4.7 ± 0.3	6800	0.33	
$^{141}\text{Pr}^*)$	6877	85 ± 35	17 ± 9	6.7 ± 1.5	450		116
$^{142}\text{Nd}^*)$	6877	340 ± 40	270 ± 20	12.4 ± 0.3	1200	26	
^{202}Hg	4922	300 ± 50	260 ± 20	4.2 ± 0.5	19000	3.4	
$^{209}\text{Bi}^*)$	5603	950 ± 200	950 ± 200	13 ± 1	34000		160

The radiative strengths K_{E1} and K_{M1} are also given. The level spacing D refers to the excitation energy of the resonance level E_{γ} .

^{a)} These values are slightly different from those of ref. ^{a)} and were obtained from a renewed analysis of the experimental results.

⁸ A. Wolf, R. Moreh, A. Nof, O. Shahal, J. Tenenbaum, Phys. Rev. C6, 2276 (1972).

METHOD

REF. NO.

75 Ja 1

hmg

REACTION	RESULT	EXCITATION ENERGY	SOURCE		DETECTOR		ANGLE
			TYPE	RANGE	TYPE	RANGE	
G, G	ABX	11	D	11	SCD-D		150
		(11.387)		(11.387)			

RATIO RAMAN/ELASTIC

TABLE I. Differential cross sections measured for elastic and inelastic scattering of 11.39-MeV photons. States or states populated by inelastic scattering are indicated in parentheses beside the target. The errors given result from the statistical error in the measurement of the cross section relative to the calibration value, the 90° uranium elastic cross section.

θ (deg)	$d\sigma/d\omega$ (elastic) (mb/sr)	$d\sigma/d\omega$ (inelastic) (mb/sr)
^{238}U (2^+ , 45 keV)		
90	0.169 ± 0.011	0.173 ± 0.016
150	0.355 ± 0.041	0.236 ± 0.24
^{228}Th (2^+ , 45 keV)		
150	0.331 ± 0.035	0.210 ± 0.022
^{181}Ta ($\frac{5}{2}^+$, 136 keV) ($\frac{1}{2}^+$, 301 keV)		
90	0.073 ± 0.008	0.020 ± 0.004 0.009 ± 0.004
150	0.145 ± 0.015	0.017 ± 0.004 0.017 ± 0.004
^{165}Ho ($\frac{5}{2}^+$, 95 keV) ($\frac{1}{2}^+$, 210 keV)		
150	0.141 ± 0.014	0.022 ± 0.004 0.013 ± 0.004
^{158}Tb ($\frac{5}{2}^+$, 58 keV) ($\frac{1}{2}^+$, 138 keV)		
90	0.062 ± 0.006	0.024 ± 0.003 0.013 ± 0.003
150	0.134 ± 0.012	0.042 ± 0.004 0.019 ± 0.004
^{141}Pr		
150	0.030 ± 0.008	...

TABLE II. Comparison of calculated and observed values of the cross sections for elastic scattering and of the ratio of Raman to elastic scattering by various nuclei for 11.387-MeV photons at 90 and 150°. The parameters used in the calculations for column 5 are given in Table I. Column 4 describes results obtained by perturbing those parameter to meet the constraint of Eq. (3) (see text).

Target	Calc.	Exp.	$d\sigma(\theta)d\Omega$ (mb/sr)	
			$d\sigma_{\text{Raman}}(\theta)/d\sigma_{\text{elastic}}(\theta)$	
$\theta = 150^\circ$				
Pr	0.025	0.030 ± 0.008	0.0	0.0
Tb	0.094	0.134 ± 0.012	0.53	0.57
Ho	0.170	0.141 ± 0.014	0.28	0.28
Ta	0.160	0.145 ± 0.015	0.23	0.23
Tb	0.253	0.331 ± 0.035	0.59	0.63
U	0.289	0.355 ± 0.041	0.78	0.73
$\theta = 90^\circ$				
Tb	0.062	0.062 ± 0.006	0.76	0.82
Ta	0.109	0.074 ± 0.008	0.32	0.30
U	0.172	0.169 ± 0.008	1.29	1.15
1.03 ± 0.10				

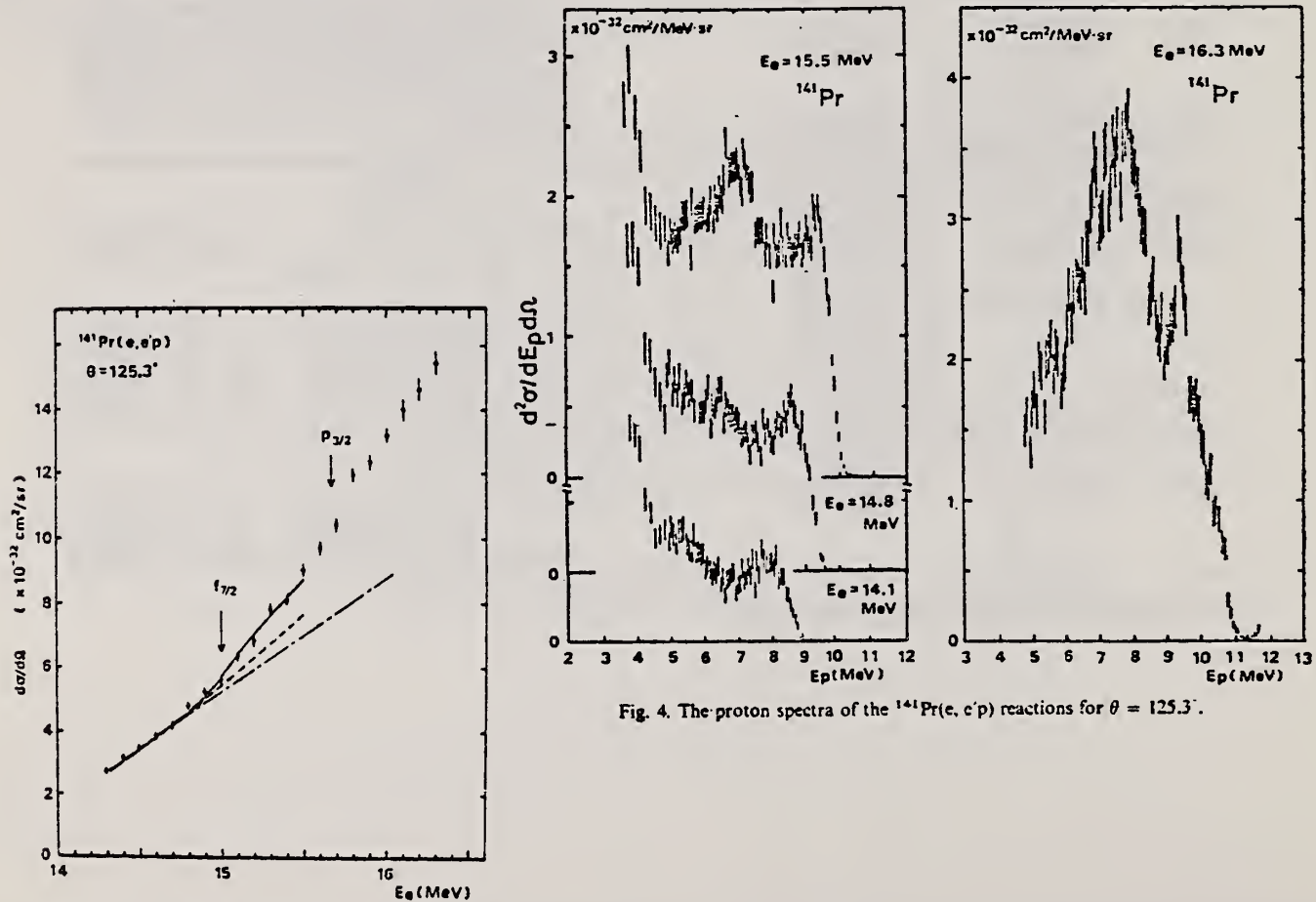
ELEM. SYM.	A	Z
Pr	141	59

METHOD	REF. NO.	rs				
	78 Ue 1					
REACTION	RESULT	EXCITATION ENERGY	SOURCE	DETECTOR	ANGLE	
E,P	ABX	12- 15	D	14- 17	MAG-D	125

TABLE I

Strength of the resonance in the (γ , p₀) and (γ , p) reactions on ¹³⁹La and ¹⁴¹Pr, and the ratio of proton group 1 and proton group 2 emitted through the f_{7/2} IAR

	$\int \sigma_{(\gamma, p_0)}^{IAS} dE$ ($\mu b \cdot MeV$)	$\int \sigma_{(\gamma, p)}^{IAS} dE$ ($\mu b \cdot MeV$)	Proton group 1 (%)	Proton group 2 (%)
¹⁴¹ Pr	44 ± 9	240 ± 30	40 ± 10	60 ± 10
¹³⁹ La	<5	260 ± 30	5 ± 5	95 ± 5

Fig. 4. The proton spectra of the ¹⁴¹Pr(e, e'p) reactions for $\theta = 125.3^\circ$.Fig. 3. The differential cross section of the ¹⁴¹Pr(e, e'p) reaction for $\theta = 125.3^\circ$ (see caption to fig. 2).

over

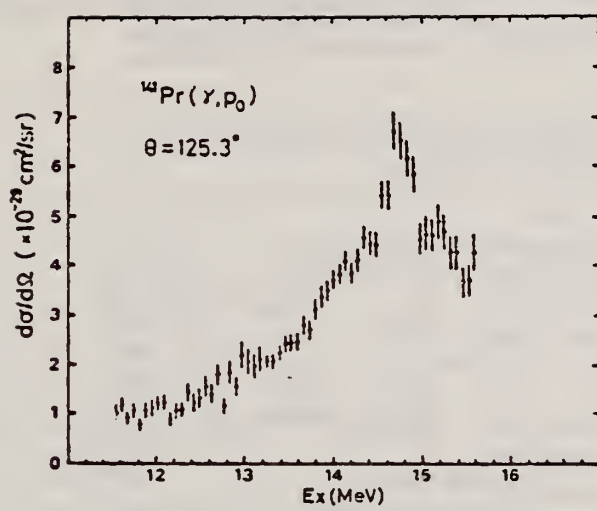


Fig. 8. The $^{141}\text{Pr}(\gamma, p_0)$ cross section.

ELEM. SYM.	A	Z
Pr	141	59

METHOD	REF. NO.					
	80 Ue 1	hg				
REACTION	RESULT	EXCITATION ENERGY				
TYPE	RANGE	TYPE	RANGE			
E, P	ABX	10-25	D	14-25	MAG-D	125
		-				
		-				
		-				

Abstract: The cross sections and the proton energy distributions of the (e, p) reactions on ^{139}La and ^{141}Pr have been measured around the T_2 GDR. The energies of the T_2 GDR have been given as $E_R = 21.0 \text{ MeV}$ in ^{139}La and $E_R = 20.4 \text{ MeV}$ in ^{141}Pr . The decay protons of the T_2 GDR have been studied. The proton groups which leave the residual nucleus in the neutron particle-hole states have been clearly seen in the same energy regions as the decay protons emitted through the low-lying IAR.

VIRT PHOTON ANALYSIS

E NUCLEAR REACTIONS $^{139}\text{La}, ^{141}\text{Pr}(e, p)$, $E = 15-25 \text{ MeV}$: measured $\sigma(E_e)$, $\sigma(E_p)$; deduced $\sigma(\gamma, p)$ vs. E_p . Natural target.

TABLE I
Results of the energy-weighted integrated cross-section calculations

Element	E_e^* (MeV)	E_p^* (MeV)	$E_p^2 - E_R^2$ (MeV)		$\sigma_{\leq 1}^{\leq 1} (\text{mb})$	$\sigma_{\geq 1}^{\geq 1} (\text{mb})$	$\sigma_{\geq 1}^{\leq 1}/\sigma_{\leq 1}^{\leq 1} (\%)$	
			exp.	theor.			exp.	theor.
^{139}La	15.2 ± 0.1^b	21.0 ± 0.2	5.8 ± 0.3	5.83^c	136^b	1.01 ± 0.07	0.74	2.3 ^c
^{141}Pr	15.1 ± 0.1^b	20.4 ± 0.2	5.3 ± 0.3	5.32^c	125^b	1.27 ± 0.24	1.0	3.0 ^c

^a) The notation shows $\sigma_{\leq 1}^{\leq 1} = \int (\sigma_{\leq 1}/E) dE$, $\sigma_{\geq 1}^{\geq 1} = \int (\sigma_{\geq 1}/E) dE$.

^b) Ref. ¹⁰). Integrals were carried out up to 25.0 MeV by present authors.

^c) Calculated by using eqs. (1) and (2) in the text. Refs. ^{3, 4}).

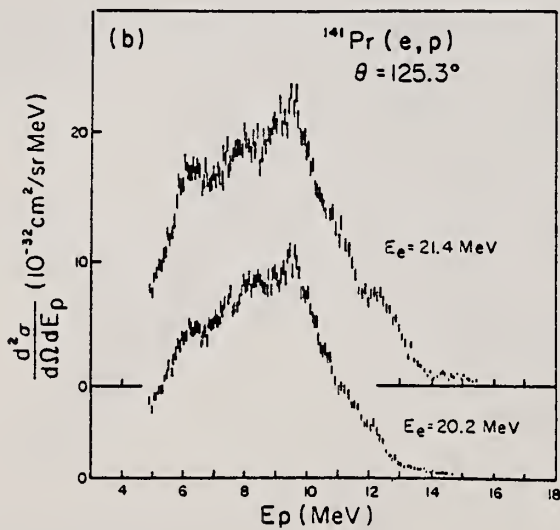


Fig. 1. The proton spectra of the (e, p) reaction at $\theta = 125.3^\circ$ laboratory. (a) ^{139}La . Bombarding energies are $E_e = 22.0 \text{ MeV}$ and $E_e = 20.8 \text{ MeV}$, respectively. (b) ^{141}Pr . Bombarding energies are $E_e = 21.4 \text{ MeV}$ and $E_e = 20.2 \text{ MeV}$, respectively.

OVER

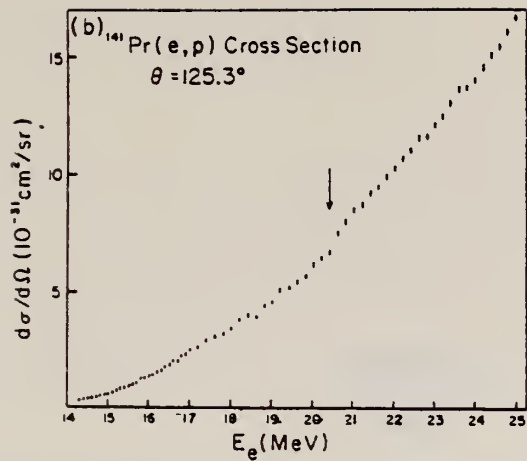


Fig. 2. The differential cross sections of the (e, p) reaction at $\theta = 125.3^\circ$ lab. The arrows show the positions of inflection caused by T_s , GDR. (a) ^{139}La . (b) ^{141}Pr .

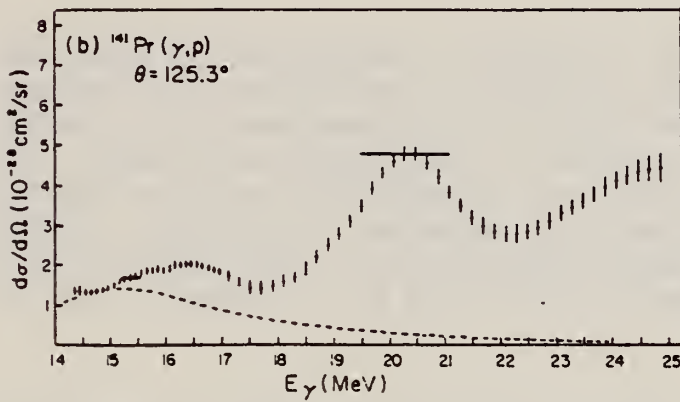


Fig. 3. The (γ , p) differential cross sections calculated from the present (e, p) differential cross sections by the least structure method [ref. 11)]. The broken lines indicate assumed contribution of the T_s GDR to the (γ , p) cross section. (a) ^{139}La . (b) ^{141}Pr .

Nd

NEODYMIUM

Z=60

Neodymium was discovered in 1885 by C. A. Welsbach when he separated didymium salts, a metal he thought was a simple element, into two chemically distinct fractions, neodymium (*neo*, "new") and prasesdymium. The crude oxide of neodymium is used for clearing the color, due to iron, in glass. A mixture of neodymium and prasedymium absorbs light in the region of the harmful sodium D lines and thus is used in welder's and glass blower's goggles.

Nd

Nd

REF.

F. I. Havlicek
 Nuovo Cimento 13, 969-73 (1959)

ELEM. SYM.	A	Z
Nd		60

METHOD					REF. NO.		
Betatron					59 Ha 2	NVB	
REACTION	RESULT	EXCITATION ENERGY	SOURCE		DETECTOR		ANGLE
			TYPE	RANGE	TYPE	RANGE	
G,A	SPC	THR - 30	C	30	EMU-D	2-5	DST

METHOD

Reactor, (n,γ) reactions source

REF. NO.	64 Ar 1	NVB
----------	---------	-----

REACTION	RESULT	EXCITATION ENERGY	SOURCE		DETECTOR		ANGLE
			TYPE	RANGE	TYPE	RANGE	
G,G	ABX	7 (6.867)	D	7 (6.867)	NAI-D		135

TABLE II. Capture gamma-ray sources and their properties.*

Source	Chemical composition	Mass kg	Principal γ rays (in MeV)
Al	Metal	1.640	7.73
Cl	Polyvinyl Chloride	0.380	8.55, 7.78, 7.41, 6.96, 6.64, 6.12, 5.72
Co	CoO	0.230	7.49, 7.20, 6.98, 6.87, 6.68, 6.48, 5.97, 5.67
Cr	Metallic powder	0.480	9.72, 8.88, 8.49, 7.93, 7.09, 6.63, 5.60
Cu	Metal	1.860	7.91, 7.63, 7.29, 7.14, 7.00, 6.63
Fe	Metallic powder	0.440	9.30, 7.64, 7.28, 6.03
Hg	Hg ₂ (NO ₃) ₂ · 2H ₂ O	0.310	6.44, 6.31, 5.99, 5.67, 5.44
Mn	MnO ₂	0.240	7.26, 7.15, 7.04, 6.96, 6.79, 6.10, 5.76
Ni	Metal	0.900	9.00, 8.50, 8.10, 7.83, 7.58, 6.84, 6.64
Ti	TiO ₂	0.210	6.73, 6.56, 6.42
V	V ₂ O ₅	0.120	7.30, 7.16, 6.86, 6.51, 6.46, 5.87, 5.73
Y	Y ₂ O ₃	0.200	6.07, 5.63

* For more detailed information, additional lines, intensities, etc., see Ref. 6.

TABLE III. Effective cross sections.

γ source	Energy (MeV)	Element	Protons	Scatterer	Neutrons	$\langle\sigma_{\gamma\gamma}\rangle$ (mb)	Notes
Hg	5.44	Hg	80	116, 118, 119, 120, 121, 122, 124		128	
Cl	6.12	Pr ¹⁴¹	59	82		103	a
V	6.508	Sn	50	62, 64-70, 72		14	
Co	6.690	Pr ¹⁴¹	59	82		2.7	a
Co	6.867	Nd	60	82, 83, 84, 85, 86, 88		22	
Al	6.98	Pb ²⁰⁸	82	126		2900	b
Cl	6.98	Pb	82	124, 125, 126		346	a
Ti	6.996	B ¹⁰	83	126		1560	b
Cu	7.01	Sn	50	62, 64-70, 72		1000	b
Ti	7.149	Pb ²⁰⁸	82	126		1000	b
Co	7.201	Pb ²⁰⁸	82	126		25	
Mn	7.261	Pb ²⁰⁸	82	126		25	a
Fe	7.285	Pb ²⁰⁸	82	126		4100	a
V	7.305	Pb ²⁰⁸	82	126		12.5	
Hg	7.32	Pb	82	124, 125, 126		5500	c
Fe	7.639	Ni	28	30, 32, 34, 36		10.5	d
Fe	7.639	Pr ¹⁴¹	59	82		10	d
Cr	8.499	Cu	29	34, 36		24.4	
Cr	8.881	Pr ¹⁴¹	59	82		9.3	
Ni	8.997	Sm	62	82, 85-88, 90, 92		2.8	

* A large error could be introduced in the cross-section values because of large differences in line intensities quoted by Bartholomew and Higgs and by Groshev *et al.* (Ref. 6).

Because of the low counting rate, thick scatterers were used, which will introduce a systematic error in estimating $\langle\sigma_{\gamma\gamma}\rangle$ for resonances having a high nuclear cross section.

* The cross section was evaluated assuming the gamma intensity to be 0.02 photons per 100 captured neutrons (see text).

^a Reference 6 gives the 7.639 line of iron capture gamma rays as a single line. However, a recent paper by Fiebig, Kaand, and Segel [Phys. Rev. 125, 2031 (1962)] reports two different lines of equal intensities having energies of 7.647 and 7.633 MeV. The present experiment cannot resolve an energy difference of 14 keV; therefore, there is no possibility of deciding which line is responsible for the scattering.

METHOD

REF. NO.

Nuclear Resonance Scattering using N,G reactions.

66 Be 3

JDM

REACTION	RESULT	EXCITATION ENERGY	SOURCE		DETECTOR		ANGLE
			TYPE	RANGE	TYPE	RANGE	
G,G	RLX	5 - 10	D	5 - 10	NAI-D	5 - 10	135

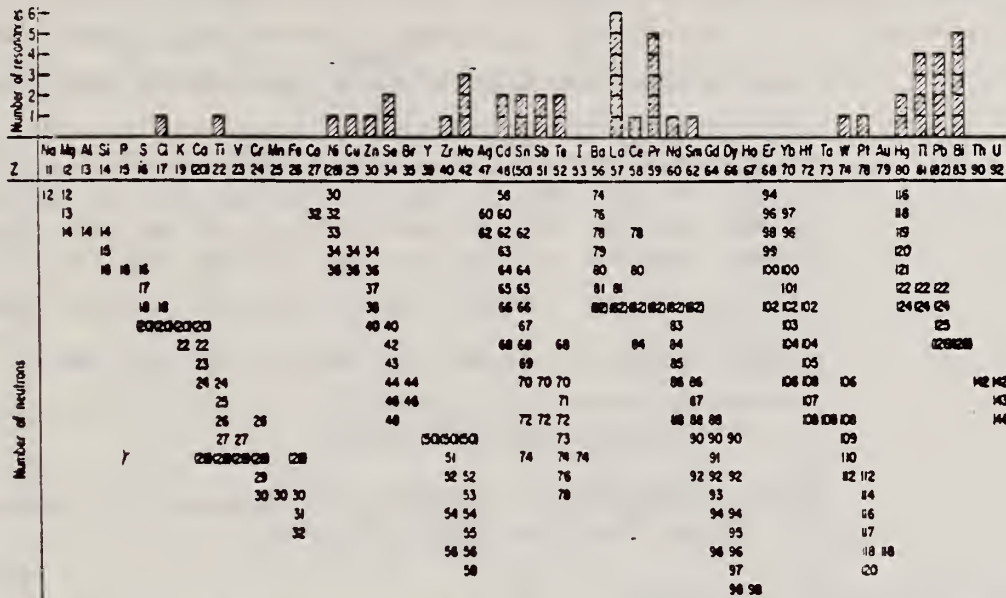


FIG. 3. Histogram of distribution of observed resonances among the different targets. The atomic number is given directly beneath the chemical symbol followed by the neutron numbers of the naturally occurring isotopes. Magic numbers are shown in brackets.

TABLE III. List of effective cross sections.

Scatterer	Energy (MeV)	Gamma source	δ (mb)	Scatterer	Energy (MeV)	Gamma source	δ (mb)
Sm ¹⁴⁴	8.997	Ni	100	Sn	7.01	Cu	110
Pr ¹⁴⁴	8.481	Cr	9	Nd	6.867	Co	30
La	8.532	Ni	6	Pr ¹⁴⁴	6.867	Co	3
Te	8.532	Ni	3 ^a	Te	5.7	Ni	...
Cu	8.499	Cr	24	La	6.54	Ag	12
Zr	8.496	Se	3050	Cd	6.474	Co	110
Zn	8.119	Ni	13	Mo	6.44	Hg	25 ^b
Se	7.817	Ni	50	La	6.413	Ti	72
Se	7.76	K	90	Mo	6.413	Ti	10
Sb	7.67	V	...	Tl	6.413	Ti	25
Cd	7.64	Fe	40 ^c	W	6.3	Ti	...
Ni	7.64	Fe	7 ^d	Sb	6.31	Hg	6 ^e
Pr ¹⁴⁴	7.64	Fe	12 ^f	Tl	6.31	Hg	...
Tl	7.64	Fe	370 ^g	Sn	6.27	Ag	75
La	7.634	Cu	7	Pb ²⁰⁸	6.15	Gd	...
Mo	7.634	Cu	11	Te	5.8	Ni	...
Bi ²⁰⁸	7.634	Cu	4	La	6.12	Cl	35
Te	7.528	Ni	66 ^d	Pr ¹⁴⁴	6.12	Cl	110
Bi ²⁰⁸	7.416	Se	100	Pt	5.99	Hg	40 ^g
Bi ²⁰⁸	7.300	As	80 ^d	Tl	5.99	Hg	5 ^e
Pb ²⁰⁸	7.283	Fe	4100	Pb ²⁰⁸	5.9	Sr	...
Cl	7.283	Fe	34	Ce	5.646	Co	17
Pr ¹⁴⁴	7.185	Se	80	Bi ²⁰⁸	5.646	Co	55
Tl	7.16	Cu	120	Pb ²⁰⁸	5.53	Ag	70
La	7.15	Mn	50	Hg	5.44	Hg	75 ^e
Bi ²⁰⁸	7.149	Tl	2000	Hg	4.903	Co	385

^a High-energy component of a complex spectrum.

^b A broad scattered spectrum with no observable peak structure.

^c There are actually two lines of energies 7.647 and 7.633 MeV having equal intensities in the iron capture gamma spectrum. The cross section has therefore been corrected, although there is no possibility at present of deciding which line is responsible for each resonance.

^d Is probably an independent level in the complex spectrum of Ni γ rays on Te.

^e Rough estimate.

^f May be inelastic component from 7.528 level in Te.

^g The relative line intensities in this case are due to Grobev and co-workers.

^h No line is known for the source at this energy.

ⁱ Difficult to resolve among the many source lines present at this energy.

H. Beil, R. Bergere, P. Carlos, A. Lepretre, A. Veyssiere and
A. Parlag
Nucl. Phys. A172, 426 (1971)

ELEM. SYM.	A	Z
Nd		60

METHOD			REF. NO.		
REACTION	RESULT	EXCITATION ENERGY	SOURCE	DETECTOR	ANGLE
G,SN	ABX	10-18	D	10-18	MOD-I
					4PI
					337+

TABLE I
Lorentz line parameters corresponding to fits of total photoneutron cross sections presented in fig. 1

	^{88}Ba	^{139}La	^{88}Ce	^{141}Pr	^{60}Nd	$^{141}\text{Pr}^a)$
σ_1 (mb)	356 \pm 15	340 \pm 15	360 \pm 15	350 \pm 15	315 \pm 15	320 \pm 20
E_1 (MeV)	15.3 \pm 0.1	15.2 \pm 0.1	15.0 \pm 0.10	15.1 \pm 0.1	14.9 \pm 0.1	15.16 \pm 0.08
Γ_1 (MeV)	4.70 \pm 0.15	4.45 \pm 0.05	4.35 \pm 0.05	4.26 \pm 0.05	4.90 \pm 0.05	4.49 \pm 0.05
$\frac{1}{2}\pi\sigma_1\Gamma_1$ (MeV · b)	2.6 \pm 0.15	2.35 \pm 0.13	2.42 \pm 0.15	2.35 \pm 0.13	2.43 \pm 0.13	2.42 \pm 0.17
$\frac{1}{2}\pi\sigma_1\Gamma_1$ $0.06NZA^{-1}$	1.30 \pm 0.08	1.16 \pm 0.08	1.19 \pm 0.08	1.14 \pm 0.08	1.15 \pm 0.08	

^{a)} Lorentz line parameters given in ref. ¹⁰) for ^{141}Pr .

¹⁰ R. L. Bramblett, J. T. Caldwell, B. L. Berman, R. R. Harvey and S. C. Fultz, Phys. Rev. 148, 1198 (1966).

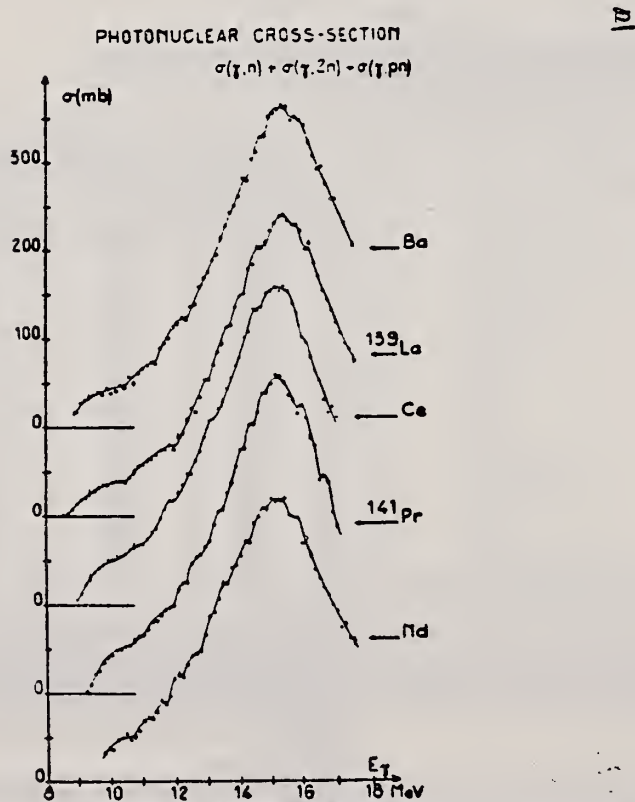


Fig. 1. Total photoneutron cross sections for Ba, ^{139}La , Ce, ^{141}Pr and Nd as a function of incident photon energy E_1 .

REF.

T. Methasiri and S. A. E. Johansson
 Nucl. Phys. A167, 97 (1971)

ELEM. SYM.	A	Z
Nd		60

METHOD

REF. NO.

71 Me 1

egf

REACTION	RESULT	EXCITATION ENERGY	SOURCE		DETECTOR		ANGLE
			TYPE	RANGE	TYPE	RANGE	
G, F	ABY	THR-900	C	300-900	FRG-I		4PI
	-	-					

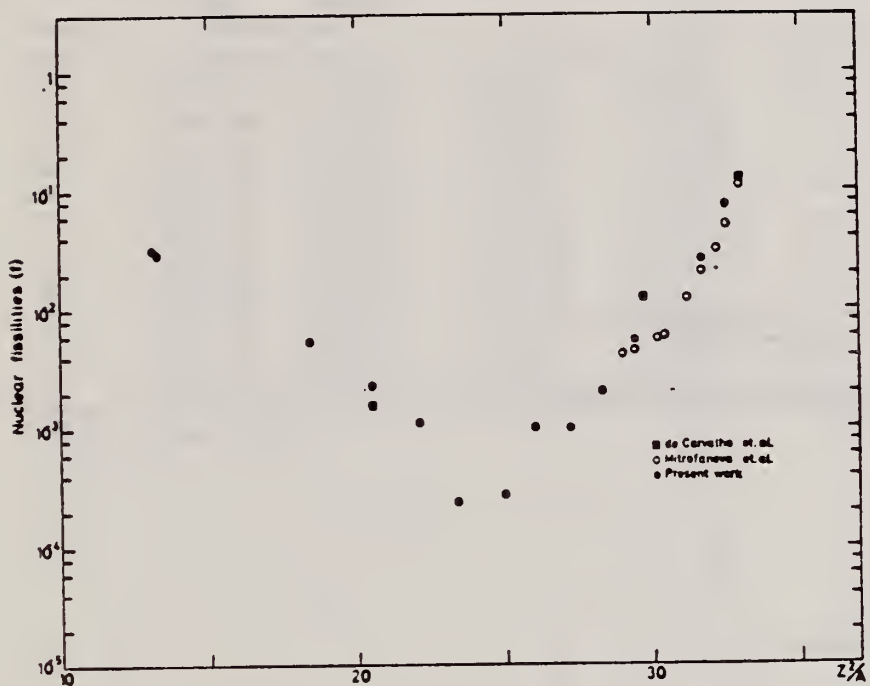
Fig. 2. Nuclear fissilities as a function of Z^2/A .

TABLE I
 The constant fission cross sections above the threshold

Element	σ_f (cm^2)	Element	σ_f (cm^2)
Pb	$(5.0 \pm 0.2) \times 10^{-27}$	La	$(1.1 \pm 0.1) \times 10^{-29}$
Au	$(1.7 \pm 0.1) \times 10^{-27}$	Sn	$(4.3 \pm 1.1) \times 10^{-29}$
Ta	$(3.3 \pm 0.2) \times 10^{-28}$	Ag	$(8.4 \pm 2.0) \times 10^{-29}$
Yb	$(1.2 \pm 0.2) \times 10^{-28}$	Mo	$(1.7 \pm 0.4) \times 10^{-28}$
Ho	$(5.5 \pm 0.3) \times 10^{-29}$	Cu	$(6.6 \pm 1.2) \times 10^{-28}$
Gd	$(5.3 \pm 0.8) \times 10^{-29}$	Ni	$(5.8 \pm 0.1) \times 10^{-28}$
Nd	$(1.3 \pm 0.2) \times 10^{-29}$		

[over]

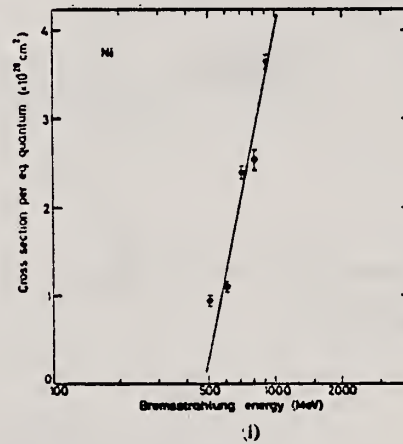
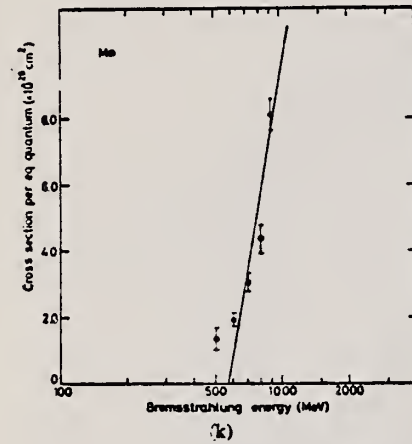
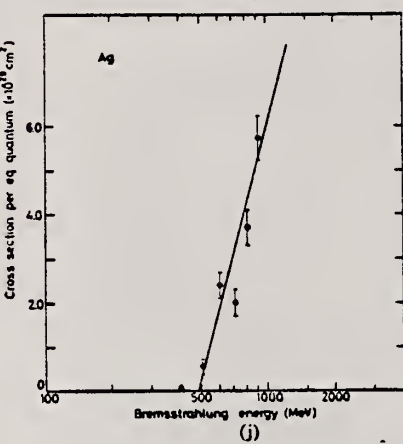
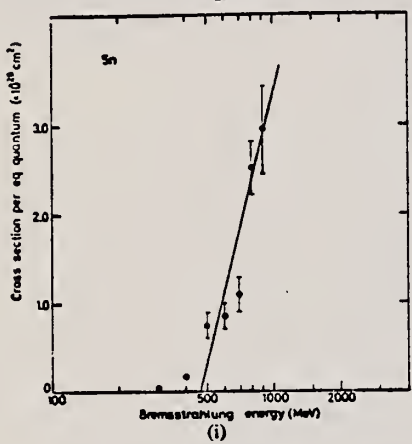
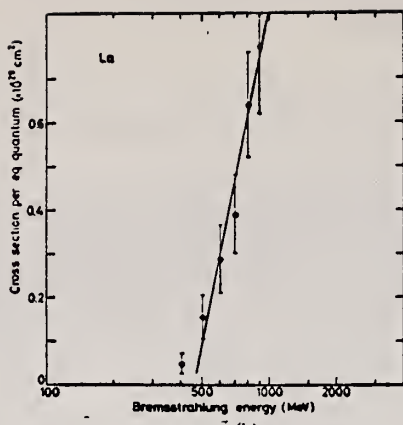
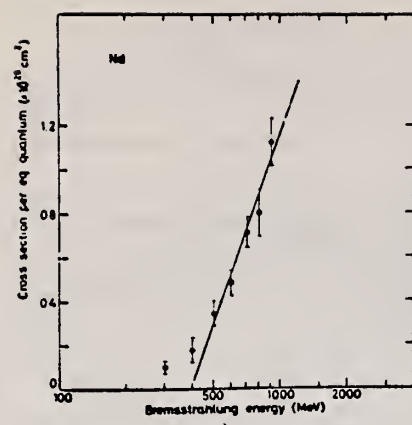


Fig. 1. Cross sections per equivalent quantum $\sigma_q(E)$ as a function of $\log E$.

REF.

E. Hayward, W. C. Barber, and J.J. McCarthy
 Phys. Rev. C10, 2652 (1974)

ELEM. SYM.	A	Z
Nd		60

METHOD

REF. NO.

74 Ha 4

hmg

REACTION	RESULT	EXCITATION ENERGY	SOURCE		DETECTOR		ANGLE
			TYPE	RANGE	TYPE	RANGE	
\$ G,G	ABX	15	D	15	NAI-D		90
		(15.1)		(15.1)			

POL PHOTONS

TABLE I. Results.

Target	$d\sigma^{\parallel}/d\Omega_F$ (Arbitrary units)	$d\sigma^{\perp}/d\Omega_F$ (Arbitrary units)	η_F	η	η (DCM)
Cd	0.042 ± 0.028	0.39 ± 0.05	0.11 ± 0.07	0.09 ± 0.07	-0.19
In ^a	0.026 ± 0.020	0.54 ± 0.04	0.05 ± 0.04	0.03 ± 0.04	0.19
Sn	0.084 ± 0.036	0.65 ± 0.06	0.13 ± 0.06	0.11 ± 0.06	0.07
Sb ^a	0.14 ± 0.030	0.77 ± 0.05	0.18 ± 0.05	0.16 ± 0.05	
Nd ^a	0.14 ± 0.07	1.03 ± 0.10	0.14 ± 0.07	0.12 ± 0.07	
Ta	0.24 ± 0.10	1.47 ± 0.14	0.16 ± 0.07	0.14 ± 0.07	0.20
W	0.52 ± 0.10	1.66 ± 0.12	0.31 ± 0.07	0.29 ± 0.07	0.20
Pt	0.23 ± 0.08	1.94 ± 0.13	0.12 ± 0.04	0.10 ± 0.04	0.08
Au	0.39 ± 0.11	2.08 ± 0.15	0.19 ± 0.06	0.17 ± 0.06	0.07
Hg ^a	0.33 ± 0.09	2.16 ± 0.15	0.15 ± 0.04	0.13 ± 0.04	0.03
Pb ^a	0.19 ± 0.14	2.42 ± 0.19	0.08 ± 0.06	0.06 ± 0.06	0
Bi	0.10 ± 0.15	2.65 ± 0.26	0.04 ± 0.06	0.02 ± 0.06	0
Th ^a	0.31 ± 0.12	2.26 ± 0.19	0.14 ± 0.05	0.12 ± 0.05	0.07
U ^a	0.21 ± 0.11	2.38 ± 0.19	0.09 ± 0.05	0.07 ± 0.05	0.08

^a Data not previously reported.

TABLE II. Comparison with Saclay data.

Target	$ A_0 ^2$ This experiment (Arbitrary units)	$ A_0 ^2$ Saclay (mb)	Ratio
Cd	0.337 ± 0.058	0.508	0.663 ± 0.114
In ^a	0.507 ± 0.046	0.591	0.859 ± 0.078
Sn	0.550 ± 0.072	0.822	0.669 ± 0.096
Sb ^a	0.590 ± 0.061	0.794	0.743 ± 0.077
Nd ^a	0.837 ± 0.100	1.170	0.715 ± 0.086
Ta	1.19 ± 0.18	1.98	0.633 ± 0.096
W	1.05 ± 0.17	2.05	0.512 ± 0.083
Pt	1.67 ± 0.16	2.70	0.619 ± 0.059
Au	1.62 ± 0.20	2.92	0.555 ± 0.068
Hg ^a	2.16 ± 0.20	3.29	0.540 ± 0.060
Pb ^a	2.20 ± 0.27	3.43	0.641 ± 0.078
Bi	2.53 ± 0.31	3.43	0.737 ± 0.090
Th ^a	1.89 ± 0.22	2.73	0.692 ± 0.080
U ^a	2.13 ± 0.22	2.83	0.754 ± 0.077
			0.656 ± 0.021

^a Data not previously reported.

ELEM. SYM.	A	Z
Nd		60
REF. NO.		
76 Em 2	egf	

METHOD

REACTION	RESULT	EXCITATION ENERGY	SOURCE		DETECTOR		ANGLE
			TYPE	RANGE	TYPE	RANGE	
G, F	ABY	THR-999	C	999	TRK-I		4PI

TABLE I

Measured values of σ_q at $E = 1000$ MeV and deduced values of σ_k assumed constant from E_0 to 1000 MeV999 = 1 GEV

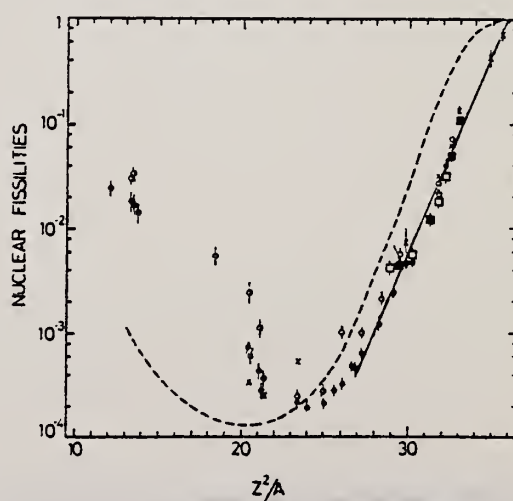
Element	Z^2/A	σ_q (mb)	E_0 (MeV)	σ_k (mb)
Bi	32.96	12.3 ± 0.6	300	7.6 ± 0.6
Pb	32.45	5.4 ± 0.4	220	3.6 ± 0.3
Tl	32.10	4.1 ± 0.3	230	2.8 ± 0.3
Au	31.68	2.0 ± 0.15	240	1.4 ± 0.2
Pt	31.18	1.1 ± 0.08	255	$(8 \pm 0.7) \times 10^{-1}$
Re	30.21	$(3.7 \pm 0.3) \times 10^{-1}$	280	$(2.9 \pm 0.3) \times 10^{-1}$
W	29.78	$(3.5 \pm 0.3) \times 10^{-1}$	290	$(2.8 \pm 0.3) \times 10^{-1}$
Ta	29.45	$(3.3 \pm 0.3) \times 10^{-1}$	300	$(2.7 \pm 0.3) \times 10^{-1}$
Hf	29.04	$(1.7 \pm 0.2) \times 10^{-1}$	310	$(1.4 \pm 0.2) \times 10^{-1}$
Yb	28.31	$(1.3 \pm 0.1) \times 10^{-1}$	330	$(1.2 \pm 0.1) \times 10^{-1}$
Tm	28.18	$(7.5 \pm 0.8) \times 10^{-2}$	335	$(6.8 \pm 0.8) \times 10^{-2}$
Ho	27.21	$(3.6 \pm 0.4) \times 10^{-2}$	355	$(3.5 \pm 0.4) \times 10^{-2}$
Dy	26.80	$(2.6 \pm 0.3) \times 10^{-2}$	360	$(2.5 \pm 0.3) \times 10^{-2}$
Tb	26.58	$(2.5 \pm 0.3) \times 10^{-2}$	370	$(2.5 \pm 0.3) \times 10^{-2}$
Gd	26.04	$(1.6 \pm 0.2) \times 10^{-2}$	380	$(1.7 \pm 0.2) \times 10^{-2}$
Sr	25.56	$(1.3 \pm 0.2) \times 10^{-2}$	390	$(1.4 \pm 0.2) \times 10^{-2}$
Nd	24.96	$(9.2 \pm 0.9) \times 10^{-3}$	405	$(1 \pm 0.1) \times 10^{-2}$
Ce	24.00	$(8 \pm 0.9) \times 10^{-3}$	420	$(9 \pm 1) \times 10^{-3}$
La	23.39	$(8.4 \pm 0.9) \times 10^{-3}$	430	$(1 \pm 0.1) \times 10^{-3}$
Sb	21.36	$(1.2 \pm 0.2) \times 10^{-2}$	460	$(1.5 \pm 0.3) \times 10^{-2}$
Tc	21.19	$(8.8 \pm 1) \times 10^{-3}$	465	$(1.2 \pm 0.2) \times 10^{-2}$
Sn	21.06	$(1.3 \pm 0.2) \times 10^{-2}$	465	$(1.7 \pm 0.3) \times 10^{-2}$
Cd	20.49	$(1.7 \pm 0.3) \times 10^{-2}$	470	$(2.2 \pm 0.4) \times 10^{-2}$
Ag	20.47	$(2 \pm 0.3) \times 10^{-2}$	470	$(2.6 \pm 0.4) \times 10^{-2}$
Zn	13.76	$(2 \pm 0.4) \times 10^{-1}$	515	$(3 \pm 0.6) \times 10^{-1}$
Cu	13.44	$(2.4 \pm 0.5) \times 10^{-1}$	515	$(3.6 \pm 0.8) \times 10^{-1}$
Ni	13.35	$(2.4 \pm 0.5) \times 10^{-1}$	510	$(3.6 \pm 0.8) \times 10^{-1}$
Fe	12.10	$(3 \pm 0.6) \times 10^{-1}$	510	$(4.4 \pm 0.9) \times 10^{-1}$

4 A.V. Mitrofanova et al.
Sov. J. Nucl. Phys. 6,
512 (1968).

7 T. Methasiri et al., Nucl.
Phys. A167, 97 (1971).

12 J.R. Nix et al., Nucl. Phys.
81, 61 (1966).

20 N.A. Perifilov et al., JETP
(Sov. Phys.) 14, 623 (1962);
Proc. Symp. on the physics &
chemistry of fission, Salzburg
1965, vol. 2 (IAEA) Vienna,
1965, p.283.



METHOD

REF. NO.	80 Mu 4	hg
----------	---------	----

REACTION	RESULT	EXCITATION ENERGY	SOURCE		DETECTOR		ANGLE
			TYPE	RANGE	TYPE	RANGE	
G,G	ABX	2-4	D	2-4	UKN-D		DST
		(2.754-3.254)	D	(2.5-3.5)			
		-					
		-					
		-					

LEV., 2.754, 3.205, 3.254

Elastic photon scattering investigated at energies of 2.5–3.5 MeV using radioactive sources has revealed a large probability for observing photoexcitation of nuclear levels. This finding removes inconsistencies in previously investigated properties of Delbrück scattering and provides a new access to nuclear resonance fluorescence.

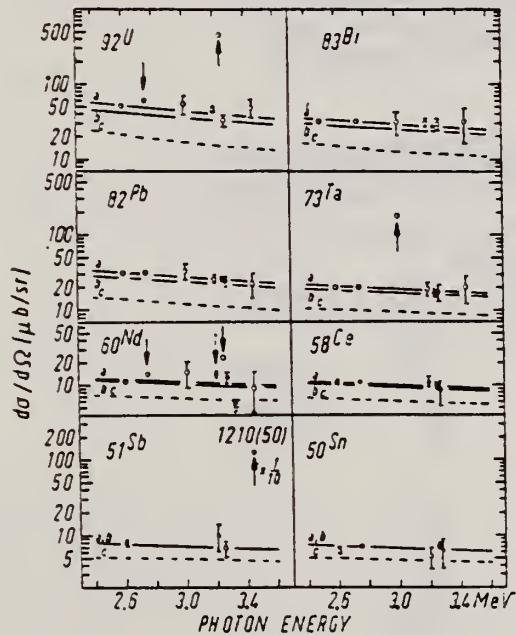


Fig. 1. Elastic differential cross sections versus photon energy. Unless error bars are given, the error intervals are at most equal to the diameter of the circles. Predicted differential cross sections: (a) including Coulomb corrections in addition to lowest-order D-, T-, R- and N-amplitudes, (b) including lowest-order D-, T-, R- and N-amplitudes, (c) including T-, R- and N-amplitudes.

Table 1
Levels observed via photoexcitation. ΔE : width of exciting photon line. D : predicted level spacing at 3 MeV. $I\pi$: spin-parity. $(d\sigma/d\Omega)_{\text{res}}$: elastic differential cross section for resonance fluorescence by the identified isotope or element measured for $\theta = 90^\circ$. Γ_0 : partial width of the level for γ -transition to the ground state. Γ : total level width. $g = (2I_{\text{ex}} + 1)/(2I_{\text{g}} + 1)$. $W(\theta)$: angular correlation function.

Isotope	Level (MeV)	ΔE (eV)	D (eV)	$I\pi$	$(d\sigma/d\Omega)_{\text{res}}$ (pb/sr)	$W(\theta)g\Gamma_0^2/\Gamma$ (meV)	Γ_0/Γ	Γ_0 (meV)
²³⁸ U	2.754	451	10^3	(1, 2) 1-	13 ± 4	0.145	$\lesssim 0.77$	$\gtrsim 0.084$ a)
	3.254	57	5×10^2	—	399 ± 5	0.79	0.24	1.5
¹⁸¹ Ta	3.010	81	5×10^2	—	165 ± 17	0.40	$\lesssim 0.72$	$\gtrsim 0.56$ b)
nat Nd	2.754	451	2×10^3	—	2.6 ± 0.5	—	—	—
	3.202	63	2×10^3	—	3.3 ± 1.5	—	—	—
	3.254	57	10^3	(3/2, 5/2)+	12.8 ± 1.0	—	—	—
¹²¹ Sb	3.452	35	10^3	2100 ± 50	2.8	0.60	4.7 b)	—

a) $I = 1$ assumed. b) $gW(\theta) = 1$ assumed.

ELEM. SYM.	A	z
Nd		
REF. NO.	81 Sc 6	egf

METHOD

REACTION	RESULT	EXCITATION ENERGY	SOURCE		DETECTOR		ANGLE
			TYPE	RANGE	TYPE	RANGE	
G,G	ABX	2,3		2,3	SCD-D		90

Elastic scattering by nuclei in the range of mass numbers between 64 and 238 has been studied with monochromatic photons in the energy range between 2 and 8 MeV. These photons were provided either by a $Ti(n,\gamma)$ source installed in the tangential through channel of the Grenoble high flux reactor, or by ^{24}Na and ^{56}Co sources produced by deuteron bombardment of Al or Fe at the Göttingen cyclotron. The photoexcitation of 23 nuclear levels has been observed and the decay properties and groundstate widths of the majority of these levels have been determined. For the lead scattering target the coherent elastic differential cross section has been studied in detail. There is evidence that below the photo-neutron threshold the elastic scattering via virtual photoexcitation of the nucleus can be approximated by extrapolating the real part of the Giant Dipole Resonance amplitude along a Lorentzian curve. Coulomb corrections to Delbrück scattering seem to play a small role at 6.5 MeV.

2.75, 3.25 MEV

Table 4. Properties of levels observed by photoexcitation. $(d\sigma/d\Omega)^{NRF}$: experimental differential cross section per identified isotope or element for resonance scattering through $\Theta=90^\circ$. I^* : spin-parity of excited level; $W(\Theta)$: angular correlation function: $g=(2I_{ee}+1)/(2I_g+1)$; Γ_0 : radiative groundstate transition width, Γ : total level width. Errors in the last digits are given in parentheses

Isotope	E , (MeV)	$(d\sigma/d\Omega)^{NRF}$ ($\mu b/sr$)	I^*	Γ_0/Γ^*	$W(\Theta)g\Gamma_0^2/\Gamma$ (meV)	Γ_0' (meV)	Γ_0'' (meV)
^{238}U	2.754	13 (4)	(1)	0.77	0.145	0.084	-
^{238}U	3.254	421 (5)	1-	0.24	0.83	1.5	0.52(15) ^a
^{209}Bi	6.555	2.1 (4) $\cdot 10^2$	-	-	0.74	0.74 ^b	-
^{209}Bi	7.168	1.7 (3) $\cdot 10^3$	9/2 ⁺ *	1.00	710	786	820 (40) ^a
^{203}Tl	6.418	$8.75(30) \cdot 10^3$	1/2 ⁺ *	0.28	30	102	82 (15) ^a
Tl	6.759	7 (3)	-	-	-	-	-
Hg	6.555	68 (17)	-	-	-	-	-
^{180}W	6.418	5.2 (3) $\cdot 10^2$	1--*	0.32	1.75	2.4	-
^{184}W	6.555	9.8 (10) $\cdot 10^2$	(1)	0.52	3.44	2.9	-
^{184}W	6.759	46 (10)	(1)	0.58	0.17	0.13	-
^{181}Ta	3.010	174 (17)	-	0.72	0.42	0.59	-
^{181}Ta	6.418	62 (4)	-	0.73	0.2	0.27 ^c	-
^{181}Ta	6.759	4.8 (12)	-	-	0.018	0.018 ^b	-
^{165}Ho	6.418	10.3 (30)	-	-	0.035	0.035 ^b	-
^{165}Ho	6.759	5.6 (14)	-	-	0.021	0.021 ^b	-
Nd	2.754	2.6 (5)	-	-	-	-	-
Nd	3.254	14.0 (10)	-	-	-	-	-
Ce	6.759	13.4 (10)	-	-	-	-	-
^{121}Sb	3.452	$2.20(5) \cdot 10^3$	-	0.60	2.9	4.9 ^b	-
^{100}Mo	6.418	$1.53(4) \cdot 10^4$	1--*	0.88	52	26	25 (8) ^a
^{94}Mo	6.555	$4.4(4) \cdot 10^3$	(1)	0.33	15	21	-
Mo	6.759	6.2 (15)	-	-	-	-	-
Mo	7.168	$8.2(26) \cdot 10^2$	-	-	-	-	-

^a [11] ^b $W(\Theta)g\Gamma_0/\Gamma=1$ assumed ^c $W(\Theta)g=1$ assumed

^d [28] (a small correction has been applied to the data of [28])

^e Upper limits in case not all the transitions to lower levels were observed

^f Present work ^g Previous work

(OVER)

Table 1. Differential cross sections for elastic scattering ($d\sigma/d\Omega$)^{exp} of photons from ^{59}Co and ^{24}Na sources by different scattering targets, in units of $\mu\text{b}/\text{sr}$. Errors in the last digits are given in parentheses.

Θ deg	Scattering targets	2.599 ^a (MeV)	2.754 ^b (MeV)	3.010 ^a (MeV)	3.202 ^a (MeV)	3.254 ^a (MeV)	3.273 ^a (MeV)	3.452 ^a (MeV)
90	^{238}U	52.7(25)	57.5(25) ^c	56(16)	47(4)	456 (10) ^c	34(6)	49(14)
	^{209}Bi	33.1(30)	32 (2)	33(11)	32(4)	25.6(20)	29(6)	33(15)
	^{nat}Pb	31.5(23)	31.0(16)	35 (8)	27(3)	26.6(22)	25(4)	23 (8)
	^{nat}Tl	31.5(33)	-	27(12)	32(5)	24 (3)	22(7)	34(15)
	^{nat}Hg	30.0(27)	-	24(10)	28(5)	25.5(18)	26(8)	20 (8)
	^{nat}W	22.5(11)	-	17 (7)	19(3)	18.4(15)	18(5)	21 (6)
	^{181}Ta	20.0(15)	19.2 (6)	193(20) ^c	20(4)	17.3(21)	18(5)	21 (8)
	^{165}Ho	15.9(13)	-	17(10)	13(6)	15.6(20)	18(8)	-
	^{nat}Nd	11.4 (7)	14.2 (5) ^d	15 (7)	14(3)	24.2(12) ^d	13(3)	9 (6)
	^{nat}Ce	11.1 (9)	11.0 (5)	-	11(3)	9.5(13)	8(4)	-
	^{127}I	8.4(10)	8.6 (5)	-	9(2)	7 (1)	5(3)	-
	^{nat}Sb	8.0(11)	-	-	10(4)	6.8(19)	-	1,270(50) ^c
	^{nat}Sn	6.5 (7)	7.0 (5)	-	5(2)	7.6 (8)	6(3)	-
	^{nat}Cd	6.2 (5)	-	-	6(2)	6.6 (8)	7(3)	-
120	^{238}U	55.1(25)	64 (4) ^c	43(15)	55(5)	574 (10) ^c	48(5)	48(11)
	^{181}Ta	27.5(15)	25.0 (9)	227(20) ^c	22(5)	21 (2)	22(8)	-
	^{nat}Nd	17.9(30)	17.0 (9) ^d	-	-	29.8(47) ^d	-	-

^a ^{59}Co source in Fe lattice ^b ^{24}Na source in Al lattice (part of data have been published elsewhere)

^c Transitions to excited states observed in addition to the ground-state transition

^d Photoexcitation of nuclear level identified from the size of the differential cross section

Method 33 MeV synchrotron; radioactivity; NaI spectrometer; r chamber

Ref. No.
59 Ca 3

EH

Reaction	E or ΔE	E_0	Γ	$\int \sigma dE$	$J\pi$	Notes
$^{142}\text{Nd}(\gamma, n)$	Bremss. 10-32	14.8	< 5.0 MeV	< 2.3 ± 0.3 MeV-b		

Figure 8. A, the ratio of activation curves $^{142}\text{Nd}(\gamma, n)/^{141}\text{Ta}(\gamma, n)$; B, activation curve for $^{142}\text{Nd}(\gamma, n)$; C, derived cross section: $^{142}\text{Nd}(\gamma, n)$.

Table 1

Isotope	% abundance	N	ϵ	B(n)	B(2n)	(γ, n) product nucleus	Principal γ -rays
^{143}Pr	100	32	~4	9.99	18.28	3.4 min	K x-ray, γ^+
^{142}Nd	27.13	32	0.04	10.47	19.3	2.5 hr	K x-ray, γ^-
^{144}Sm	3.16	32	—	10.2+	19.7+	8.5 min	K x-ray, γ^+
^{140}Nd	5.60	90	0.24	7.87	12.97	1.8 hr	2 groups: at 118 & 212 kev
^{145}Sm	22.53	92	0.32	8.2	14.77	47 hr	K x-ray, 102 kev
^{146}Gd	21.90	96	0.44	7.6+	12.70	18 hr	K x-ray, 362 kev
^{141}Ta	99.988	108	0.22	7.72	13.8+	8.15 hr	K x-ray

[†] Threshold determined from semi-empirical mass tables (Cameron 1957). The other thresholds are based on measured values (Johnson and Nier 1957, Wapatta 1955).

Table 2

Activity	T_1 (min)	W_0 (MeV)	K/β^+	$\frac{K\text{-capture}}{\text{Total capture}}$	W_K
^{143}Pr	3.4	3.25	0.63	0.89	0.89
^{142}Nd	150	1.80	48	0.89	0.90
^{144}Sm	8.5	3.47	0.60	0.89	0.91

FORM NBS-418
(8-1-63)
USCOMM-DC 18556-P63

U.S. DEPARTMENT OF COMMERCE
NATIONAL BUREAU OF STANDARDS

PHOTONUCLEAR DATA SHEET 178

Nb
 $A=142$

Nb
 $A=142$

Nb
 $A=142$

REF.

Y. Oka, T. Kato and A. Yamadera
 Bull. Chem. Soc. Japan 41, 1606 (1968)

ELEM. SYM.	A	Z
Nd	142	60

METHOD

REF. NO.

68 Ok 2

egf

REACTION	RESULT	EXCITATION ENERGY	SOURCE		DETECTOR		ANGLE
			TYPE	RANGE	TYPE	RANGE	
G,N	ABY	THR- 20	C	20	ACT-I		4PI

ISOMERIC YIELD

TABLE I. THE PARTICULARS OF THE (γ, n) REACTION PRODUCTS AND THE DATA OBTAINED WITH 20 MeV BREMSSTRAHLUNG

Nuclide		Half-life of product (sec)	Gamma-ray determined			Limit of detection (μg)	Yield ($\text{mol}^{-1} \cdot \text{R}^{-1}$)
Parent (Natural abundance, %)	Residual		Energy (MeV)	Branching ratio (%)	Photopeak activity ($\text{cpm}/\text{mg}^{\text{a}}$)		
$^{24}\text{Mg}(78.60)$	^{25}Mg	9.9	0.511	200	2.04×10^4	0.49	8.1×10^4
$^{78}\text{Ge}(7.67)$	^{75m}Ge	48	0.139	100	6.37×10^4	1.6	1.1×10^4
$^{78}\text{Se}(23.52)$	^{77m}Se	17	0.162	100	1.82×10^4	0.55	1.2×10^4
$^{92}\text{Mo}(15.86)$	^{91m}Mo	65	0.650	57	2.22×10^4	4.5	2.7×10^4
$^{140}\text{Ce}(88.48)$	^{139m}Ce	58	0.745	100	1.06×10^4	0.95	1.3×10^4
$^{142}\text{Nd}(27.13)$	^{141m}Nd	64	0.760	100	3.19×10^4	3.1	1.4×10^4
$^{159}\text{Tb}(100)$	^{158m}Tb	11	0.111	100	2.56×10^4	3.8	2.2×10^4

a) The value corrected at the end of one-minute irradiation with the dose rate of 10^7 R/min ; Counting geometry is 20% with a 3"dia. \times 3"NaI(Tl) detector.

P. Carlos, H. Beil, R. Bergere, A. Lepretre, A. Veyssiere
Nucl. Phys. A172, 437 (1971)

ELEM. SYM.	A	Z
Nd	142	60

METHOD

REF. NO.

71 Ca 1

egf

REACTION	RESULT	EXCITATION ENERGY	SOURCE		DETECTOR		ANGLE
			TYPE	RANGE	TYPE	RANGE	
G, N 391	ABX	10-20	D	8-20	MOD-I		4PI
G, 2N 393+	ABX	10-20	D	8-20	MOD-I		4PI

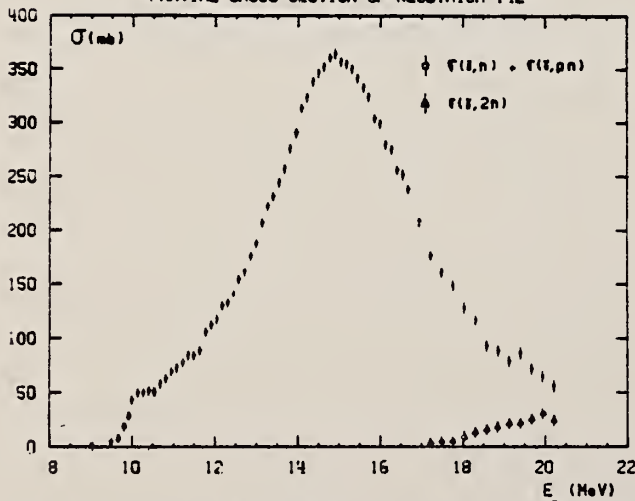
391+

TABLE 2
Parameters of the one- or two-Lorentz line fits to the σ_t curves for neodymium isotopes: parameters for Ce and Er extracted from earlier results ¹³⁾ are also shown

Ce	¹⁴² Nd	¹⁴³ Nd	¹⁴⁴ Nd	¹⁴⁵ Nd	¹⁴⁶ Nd	¹⁴⁸ Nd	¹⁵⁰ Nd	Er	
σ_1 (mb)	360 \pm 15	359 \pm 15	360 \pm 15	317 \pm 15	297 \pm 20	308 \pm 16	263 \pm 15	174 \pm 20	225 \pm 15
Γ_1 (MeV)	4.35 \pm 0.05	4.43 \pm 0.20	4.5 \pm 0.2	5.3 \pm 0.25	6.5 \pm 0.4	6 \pm 0.3	7.2 \pm 0.3	3.3 \pm 0.1	2.9 \pm 0.05
E_1 (MeV)	15.0 \pm 0.10	14.95 \pm 0.1	15 \pm 0.1	15.05 \pm 0.1	15 \pm 0.15	14.8 \pm 0.1	14.7 \pm 0.15	12.3 \pm 0.15	12.00 \pm 0.1
σ_2 (mb)							223 \pm 20	260 \pm 15	
Γ_2 (MeV)							5.2 \pm 0.15	5.0 \pm 0.05	
E_2 (MeV)							16 \pm 0.15	15.45 \pm 0.1	
$\frac{1}{2}\pi\sigma\Gamma$ MeV · b	2.5 \pm 0.2	2.54 \pm 0.2	2.6 \pm 0.2	3.0 \pm 0.3	2.9 \pm 0.2	3.0 \pm 0.2	2.7 \pm 0.3		
$\frac{1}{2}\pi\sigma\Gamma$ $0.06 NZA^{-1}$	1.20 \pm 0.10	1.22 \pm 0.10	1.25 \pm 0.10	1.4 \pm 0.15	1.35 \pm 0.10	1.4 \pm 0.1	1.27 \pm 0.15		

¹³⁾ R. Bergere, H. Beil, P. Carlos et A. Veyssiere, Nucl. Phys. A133, 417 (1969).

PARTIAL CROSS SECTION OF NEODYMIUM 142

Fig. 2. Partial photoneutron cross sections $\sigma(\gamma, n)$ and $\sigma(\gamma, 2n)$ of ¹⁴²Nd.

(over)

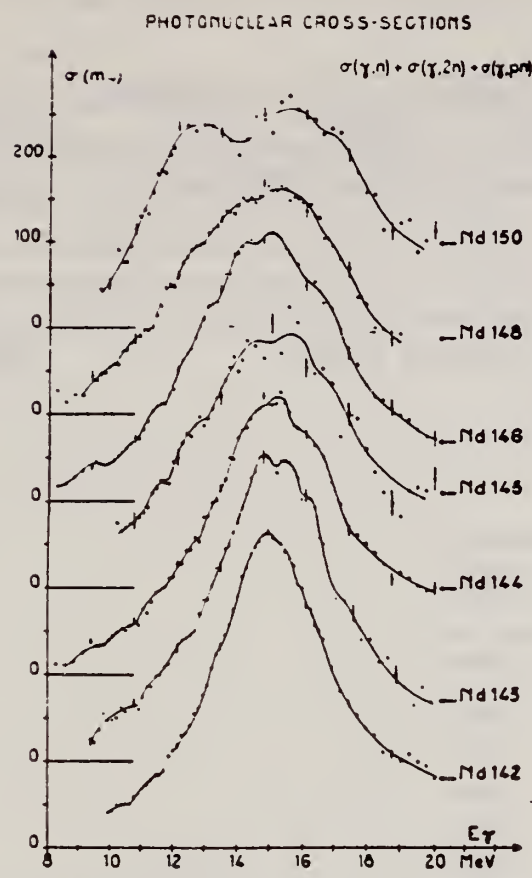


Fig. 9. Total photonuclear cross-section σ_T of neodymium isotopes. The full line drawn through the experimental points is merely meant to facilitate the identification of structure.

REF.

P. E. Haustein and A. F. Voigt
J. inorg. nucl. Chem. 33, 289 (1971)

ELEM. SYM.	A	Z
Nd	142	60

METHOD

REF. NO.	egf
71 Ha 2	

REACTION	RESULT	EXCITATION ENERGY	SOURCE		DETECTOR		ANGLE
			TYPE	RANGE	TYPE	RANGE	
G,N	RLY	10-70	C	70	ACT-I		4PI

Isomer ratio = (yield to low spin state)/(yield to high spin state)

ISOMER RATIOTable 2. Isomer ratio measurements for ^{96}Mo , ^{137}Ce , and ^{144}Nd

Reaction	Isomer ratio	J^π Target	J^π Ground state	J^π Isomer	Threshold (MeV)	$4 A^{-1/2} $ (MeV)
$^{96}\text{Mo}(\gamma, n)^{95}\text{Mo}$	1.92 ± 0.15	0^+			13.13	16.60
$^{96}\text{Mo}(\gamma, 3n)^{93}\text{Mo}$	1.59 ± 0.16	0^+	$9/2^+$	$1/2^-$	30.72	16.52
$^{137}\text{Ce}(\gamma, n)^{137}\text{Ce}$	3.1	0^+			10.31	15.30
$^{137}\text{Ce}(\gamma, 3n)^{137}\text{Ce}$	1.10 ± 0.12	0^+	$3/2^+$	$11/2^+$	26.34	15.26
$^{144}\text{Nd}(\gamma, n)^{143}\text{Nd}$	5.2 ± 0.3	0^+			9.79	15.22
$^{144}\text{Nd}(\gamma, 3n)^{141}\text{Nd}$	1.80 ± 0.25	0^+	$3/2^+$	$11/2^+$	23.67	15.17

REF.

D. W. Madsen, L. S. Cardman, J. R. Legg, C. K. Bockelman
 Nucl. Phys. A168, 97 (1971)

ELEM. SYM.	A	Z
Nd	142	60

METHOD

REF. NO.

71 Ma 1

egf

REACTION	RESULT	EXCITATION ENERGY	SOURCE		DETECTOR		ANGLE
			TYPE	RANGE	TYPE	RANGE	
E, E/	FMF	1, 2	D	60	MAG-D		DST
		-					

$$1=1.57, 2=2.09$$

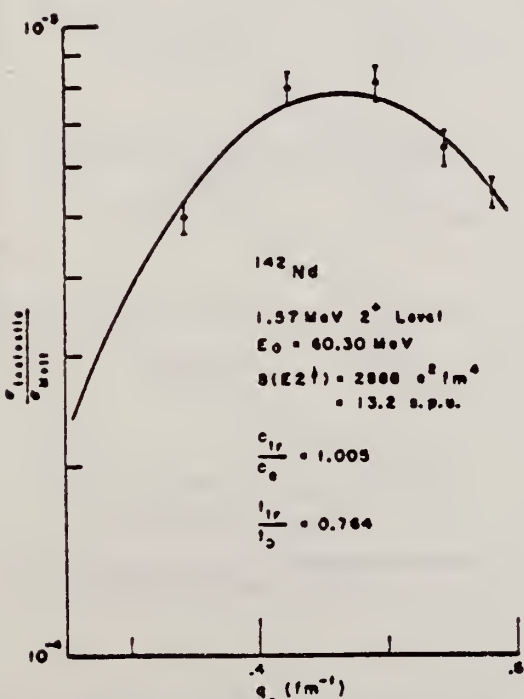


Fig. 14. Inelastic form factors for the 2^+ level at 1.57 MeV in ^{142}Nd as a function of inelastic momentum transfer. The experimental points are the findings of this experiment and the solid line is the best fit obtained with the parameters shown.

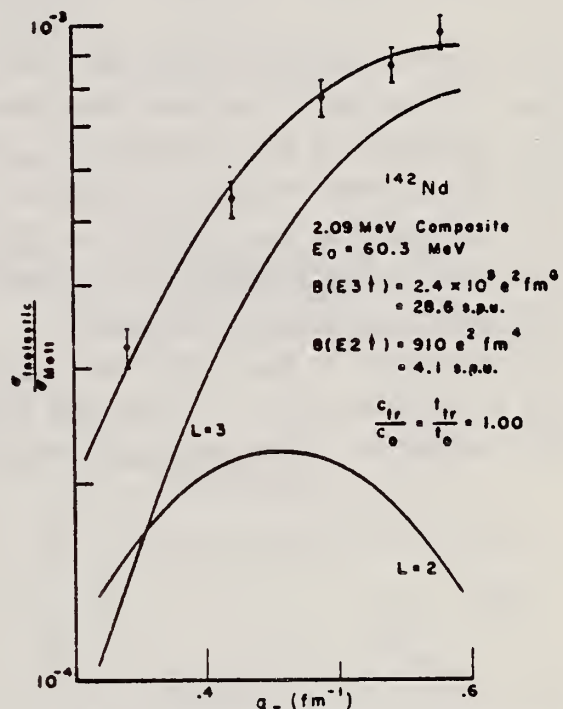


Fig. 15. Inelastic form factors for the excitation at approximately 2.09 MeV in ^{142}Nd . The experimental points are the findings of this experiment while the solid line through them represents the best fit obtained by an addition of the $L = 2$ and $L = 3$ curves shown. (L is the transition multipolarity.) The individual $B(E\mathcal{L}\uparrow)$ values are given in the figure. See text.

TABLE II

A comparison of this experiment's $B(E2)$ values with those of other experiments and theory

Nucleus	State (MeV)	This work	Pulsed beam	Heavy particle Coulomb excitation	Theory
2 ⁺ states					
¹⁴² Nd	1.57	13.1 ± 1.7		25.0 ± 7.3 ^{a)} 19.1 ± 2.3 ^{b)} 15.5 ± 7.8 ^{c)}	16.4 ^{d)} 16.3 ^{e)}
¹⁴² Nd	2.09	4.1 ± 1.1			
¹⁴⁶ Nd	0.45	30.9 ± 4.6		28.5 ± 0.4 ^{b)} 28.1 ± 6.6 ^{b)}	92.1 ^{f)}
¹⁵⁰ Nd	0.13	62.9 ± 10.5	113.9 ± 1.8 ^{f)} 116.8 ± 3.2 ^{f)} 112.4 ± 5.1 ^{b)}	112.7 ± 4.2 ^{f)}	
3 ⁻ state					
¹⁴² Nd	2.09	28.6 ± 5.0		52 ± 21 ^{b)}	

^{a)} Ref. ³⁹). ^{b)} Ref. ⁴⁰). ^{c)} Ref. ⁴¹). ^{d)} Ref. ³⁷). ^{e)} Ref. ⁴²). ^{f)} Ref. ⁴³).
^{g)} Ref. ⁴⁴). ^{h)} Ref. ⁴⁵). ⁱ⁾ Ref. ³⁸). ^{j)} Ref. ³⁹.

³³O. Hansen et al., Nucl. Phys. 42 (1963) 197.

³⁷L. S. Kisslinger et al., Rev. Mod. Phys. 35 (1963) 853.

³⁸J. Bjerregard et al., Nucl. Phys. 44 (1963) 280.

³⁹G. A. Burginyon, Thesis, Yale University (1967) unpub.

⁴⁰D. Eccleshall et al., Nucl. Phys. 78 (1966) 481.

⁴¹O. Nathan et al., Nucl. Phys. 21 (1960) 631.

⁴²M. Rho, Nucl. Phys. 65 (1965) 497.

⁴³J. D. Kurfess et al., Phys. Rev. 161 (1967) 1185.

⁴⁴F. W. Richter et al., Z. Phys. 213 (1968) 202.

⁴⁵M. Birk et al., Phys. Rev. 116 (1959) 730.

METHOD

REF. NO.

71 Sh 3

hmg

REACTION	RESULT	EXCITATION ENERGY	SOURCE		DETECTOR		ANGLE
			TYPE	RANGE	TYPE	RANGE	
E, P	ABX	15-22	D	23	MAG-D		90

ISOBARIC ANALOGS

The energy distributions of protons from the $(e, e' p)$ reaction on $N=82$ nuclei with even Z have been measured. The cross sections of the $(\gamma, p_0 + p_1)$ reaction have been estimated. Two prominent isobaric analogs have been found in each nucleus. The results were used for the systematic discussion of the odd-odd parent nuclei ^{132}Cs , ^{140}La , ^{142}Pr , and ^{144}Pm . The 1^- states are estimated at 600 and ~ 2500 keV for ^{138}Cs , 500 and 3000 keV for ^{145}La , 1100 and 3700 keV for ^{142}Pr , and 1400 and 4300 keV for ^{144}Pm . The parameters of these states are discussed in terms of a quasiproton and single-neutron model.

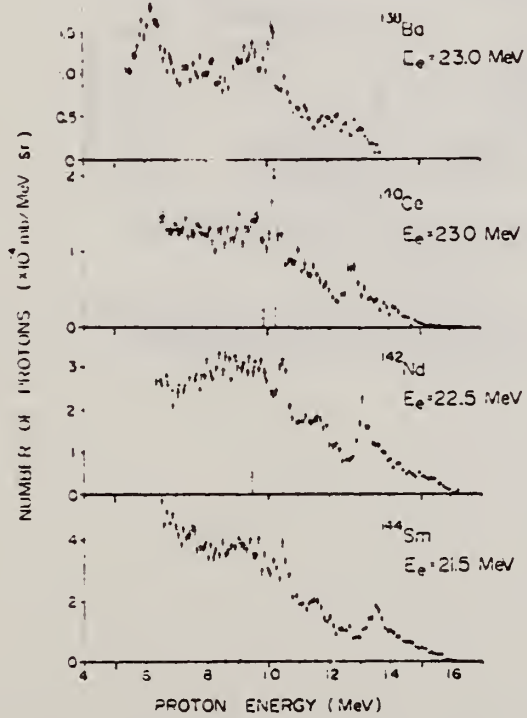


FIG. 1. Energy distributions of protons emitted from the $(e, e' p)$ reaction at $0 = 90^\circ$.

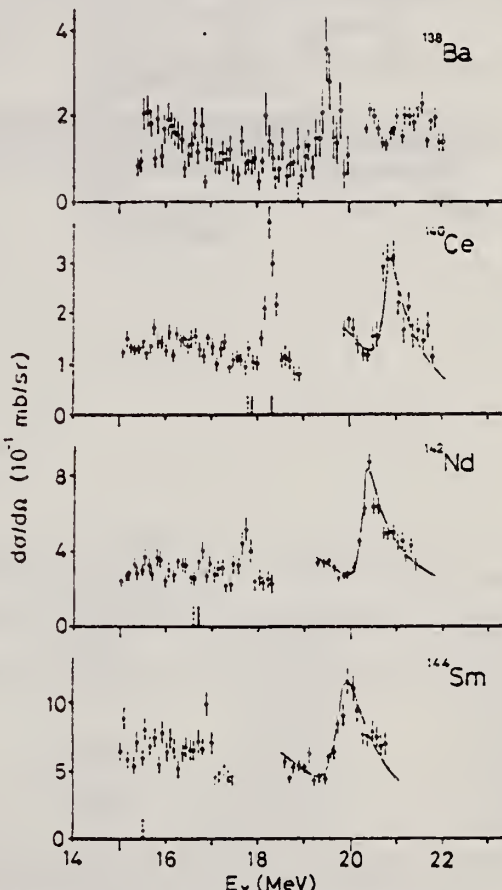


FIG. 2. The photoprotton cross sections for $p_0 + p_1$ at $0 = 90^\circ$ in the vicinity of the isobaric analog resonances. The curves for the broad resonances were obtained from the fitting of the interference formula.

(over)

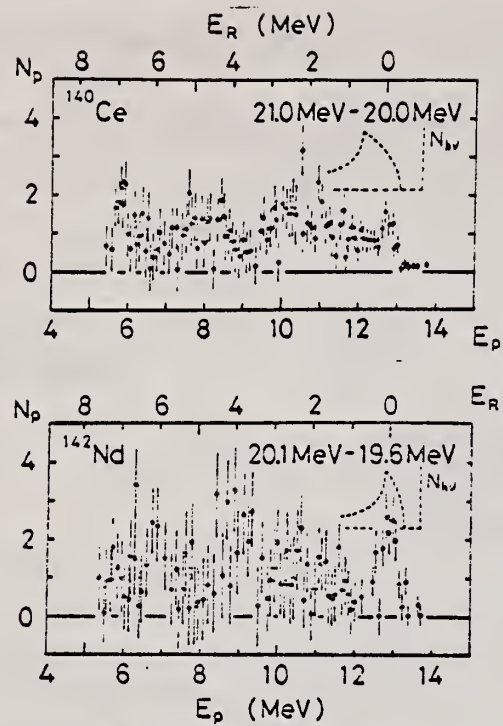


FIG. 5. The proton groups emitted through the isobaric analogs at 20.3 MeV in ^{140}Ce and at 20.3 MeV in ^{142}Nd . The energies of the residual states are also indicated by E_R .

REF.

M. Hasinoff, G.A. Fisher, P. Kurjan and S. S. Hanna
 Nucl. Phys. A195, 78 (1972)

ELEM. SYM.	A	Z
Nd	142	60

METHOD

REF. NO.

72 Ha 3

egf

REACTION	RESULT	EXCITATION ENERGY	SOURCE		DETECTOR		ANGLE
			TYPE	RANGE	TYPE	RANGE	
P ₁ G	ABX	14-24	D	6-17	NAI-D		DST

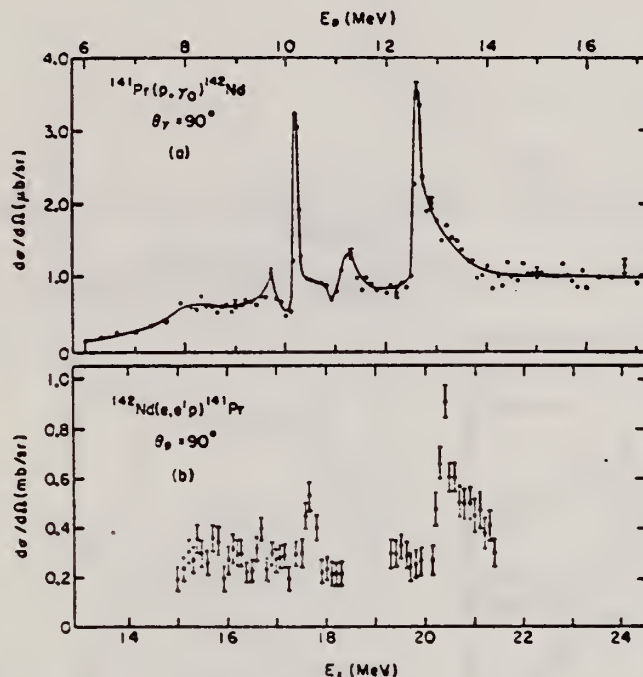


Fig. 3. (a) Differential yield curve of $^{141}\text{Pr}(p, \gamma_0)^{142}\text{Nd}$ at $\theta_\gamma = 90^\circ$. The line drawn is merely to guide the eye. (b) The $^{142}\text{Nd}(e, e' p_0 + p_1)^{141}\text{Pr}$ data of ref. ¹⁹.

15 K. Shoda et al., Phys. Rev. C4 (1971) 1842.

19 P. A. Moore et al., Phys. Rev. 180 (1969) 1213.

20 G. Clausnitzer et al., Nucl. Phys. A106 (1968) 99.

21 P. Von Brentano et al. Phys. Lett. 17 (1965) 124.

22 H. Ejiri et al. Nucl. Phys. A128 (1969) 388.

TABLE 2
 Resonance parameters obtained for three of the $1^-, T_+$ analogue resonances observed in $^{141}\text{Pr}(p, \gamma_0)^{142}\text{Nd}$

E_p (MeV)	E_t (MeV)	Γ (keV)	$\Gamma_{p_0} \Gamma_{\gamma_0}$ (keV ²)	$\phi_A - \phi_{GR}$ (deg.)
10.18	17.30	79 ± 4	1.1 ± 0.3 5.9 ± 1.9	-20 ± 10 -120 ± 15
11.20	18.30	220 ± 30	0.55 ± 0.28 35 ± 18	-25 ± 10 -120 ± 15
12.59	19.73	180 ± 20	6.5 ± 2.0 42 ± 13	-20 ± 10 -115 ± 15

For each resonance the first solution is given on the first line and the alternative solution on the second line.

The errors for $\Gamma_{p_0} \Gamma_{\gamma_0}$ include both the fitting errors and the estimated error in the determination of the absolute cross section ($\approx 30\%$).

(over)

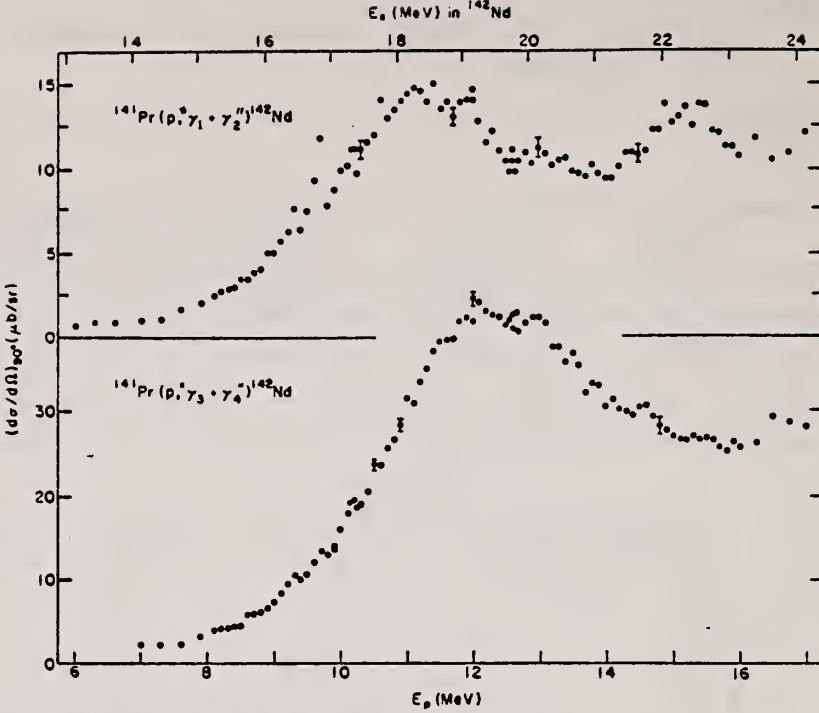


Fig. 4. Differential yield curves of $^{141}\text{Pr}(p, \gamma_1 + \gamma_2)^{142}\text{Nd}$ and $^{141}\text{Pr}(p, \gamma_3 + \gamma_4)^{142}\text{Nd}$ at $\theta_\gamma = 90^\circ$.

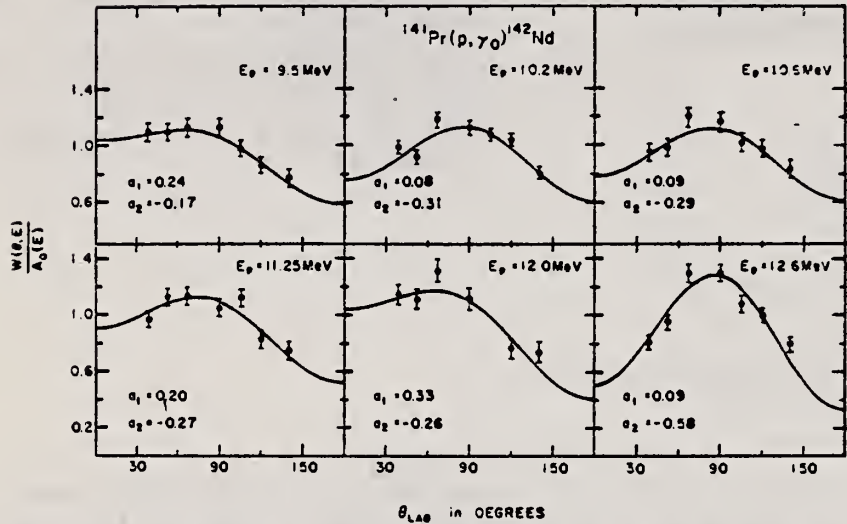


Fig. 5. Angular distributions in $^{141}\text{Pr}(p, \gamma_0)^{142}\text{Nd}$ measured on and off the three upper resonances. The on-resonance measurements are at $E_p = 10.2, 11.25$ and 12.6 MeV. The curves are fits obtained with the series $1 - a_1 P_1 - a_2 P_2$. The values of a_1 and a_2 are listed in each case.

TABLE 3
Comparison of radiative strengths for the two strong I^-, T_1 levels in ^{142}Nd

E_p (MeV)	$\Gamma_{\gamma_0} \Gamma_{p_0}/\Gamma^*$ (eV)	$\Gamma_{\gamma_0} (\Gamma_{p_0} + \Gamma_{p_1})/\Gamma^*$ (eV)	$\Gamma_{\gamma_0}^*$ (eV)	$\Gamma_{p_0}^*$ (eV)	$\Gamma_{p_1}^*$ (eV)	$\Gamma_{\gamma}^*/2(T_0+1)$ (eV)
10.18	13.8 ± 4.1 75 ± 25	6 ± 1	69 ± 22^a 375 ± 130^a	20 ± 3^a	13 ± 5 62 ± 26	680
12.59	37 ± 11 230 ± 71	58 ± 2 3300 ± 1000^a	530 ± 160^a	580 ± 20^a		1000

^a) Present work. The second line in each case corresponds to the alternative solution.

^b) Ref. 15).

^c) The E1 strength of the $2f_5/2 \rightarrow 2d_5$ transition in $^{140}\text{Ce}(p, \gamma_0)^{141}\text{Pr}$ [ref. 22].

^d) If $\Gamma_{p_0}/\Gamma \approx 0.2$ as obtained from refs. 19-21). An estimate for Γ_{p_1}/Γ of 0.5 Γ_{p_0}/Γ is used.

^e) If $(\Gamma_{p_0} + \Gamma_{p_1})/\Gamma \approx 0.10$ as given in ref. 15). An estimate for Γ_{p_1}/Γ of 0.5 Γ_{p_0}/Γ is used.

REF.

K. Shoda, M. Sugawara, T. Saito, H. Miyase, A. Suzuki, S. Oikawa,
and J. Uegaki
PICNS-72, 321 Sendai

ELEM. SYM.	A	Z
Nd	142	60

METHOD

REF. NO.

72 Sh 10

hvm

REACTION	RESULT	EXCITATION ENERGY	SOURCE		DETECTOR		ANGLE
			TYPE	RANGE	TYPE	RANGE	
G, P	ABX	15- 22	C	15- 22	MAG-D		UKN

I A STATES

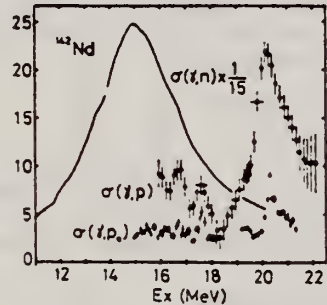
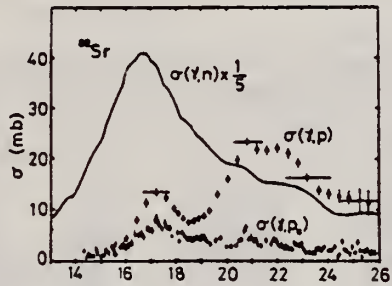
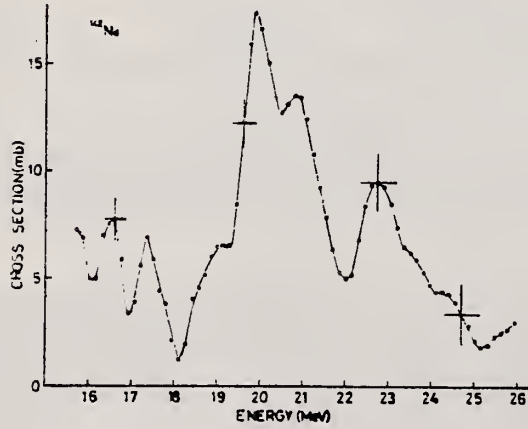
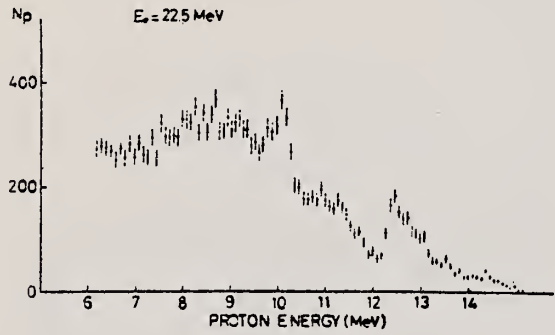


Fig. 11 The (γ, p) cross sections of ^{88}Sr and ^{142}Nd . The (γ, p_0) and (γ, n) cross sections are also shown.

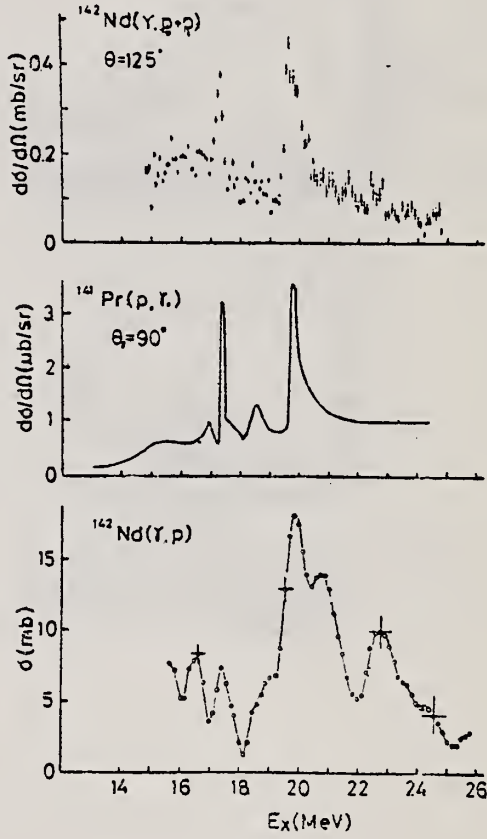
ELEM. SYM.	A	Z
Nd	142	60
REF. NO.		
73 Sa 7		hmg

METHOD

REACTION	RESULT	EXCITATION ENERGY	SOURCE		DETECTOR		ANGLE
			TYPE	RANGE	TYPE	RANGE	
γ, p	ABX	13- 26	C	15- 26	MAG-D		UKN
			-				



Total $\sigma(\gamma, p)$ from yield curve.



METHOD

REF. NO.

74 Te 1

egf

REACTION	RESULT	EXCITATION ENERGY	SOURCE		DETECTOR		ANGLE
			TYPE	RANGE	TYPE	RANGE	
G,G	LFT	6	D	4- 8	SCD-D		DST

 $\delta = 6.877$

TABLE 2

Measured angular distribution coefficients A_2 , the ratios $N_{||}/N_{\perp}$, the spins and parities of the ground and the resonance levels, J_0'' and J_r'' , and the character of the ground state transition

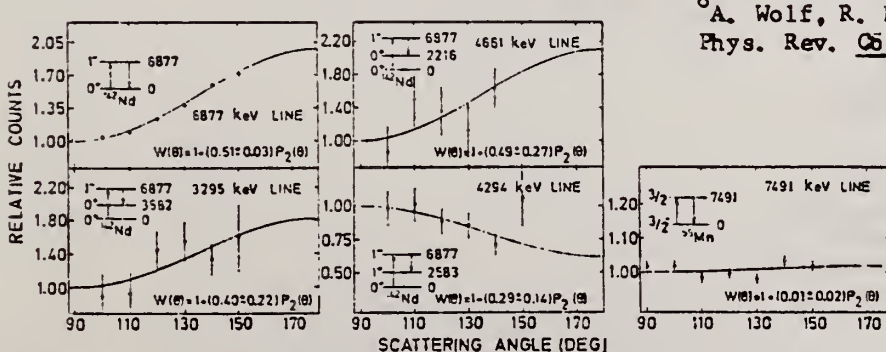
Scatterer	E_{γ} (keV)	A_2	$N_{ }/N_{\perp}$	J_0''	J_r''	Transition
⁵⁵ Mn	7491	0.01 ± 0.02	1.00 ± 0.02	$\frac{1}{2}^-$	$\frac{1}{2}^+$	
¹⁴⁰ Ce	5660	0.51 ± 0.02	1.14 ± 0.04	0^+	1^-	E1
¹⁴¹ Pr	6877	0.11 ± 0.02	0.95 ± 0.03	$\frac{1}{2}^+$	$\frac{1}{2}^+$	M1
¹⁴² Nd	6877	0.51 ± 0.03	1.10 ± 0.04	0^+	1^-	E1
²⁰² Hg	4922	0.51 ± 0.02	1.18 ± 0.03	0^+	1^-	E1
²⁰⁹ Bi	5603	0.06 ± 0.02	0.97 ± 0.02	$\frac{1}{2}^-$	$\frac{1}{2}^-$	M1

TABLE 4
 Values of Γ , Γ_0 and the energy separation δ (between the incident γ -line and the resonance level) as obtained from the analysis of the various experiments

Scatterer	E_{γ} (keV)	Γ (meV)	Γ_0 (meV)	δ (eV)	D (eV)	K_{E1} (10^{-9} MeV $^{-3}$)	K_{M1} (10^{-9} MeV $^{-3}$)
⁵⁵ Mn	7491	450 ± 250	80 ± 40	17 ± 1			
¹⁴⁰ Ce *)	5660	13 ± 3	12 ± 2	4.7 ± 0.3	6800	0.33	
¹⁴¹ Pr *)	6877	85 ± 35	17 ± 9	6.7 ± 1.5	450		116
¹⁴² Nd *)	6877	340 ± 40	270 ± 20	12.4 ± 0.3	1200	26	
²⁰² Hg	4922	300 ± 50	260 ± 20	4.2 ± 0.5	19000	3.4	
²⁰⁹ Bi *)	5603	950 ± 200	950 ± 200	13 ± 1	34000		160

The radiative strengths K_{E1} and K_{M1} are also given. The level spacing D refers to the excitation energy of the resonance level E_{γ} .

*) These values are slightly different from those of ref. *) and were obtained from a renewed analysis of the experimental results.



⁸A. Wolf, R. Moreh, A. Nof, O. Shahal, J. Tenenbaum, Phys. Rev. C6, 2276 (1972).

Fig. 5. Angular distributions of elastically scattered γ -lines from ⁵⁵Mn and ¹⁴²Nd. The distributions of three inelastic γ -lines from ¹⁴²Nd are also shown. The solid lines have the form $W(\theta) = 1 + A_2 P_2(\cos \theta)$ and are least squares fits to the experimental distribution. In each case the corresponding γ - γ cascade is indicated.

ELEM. SYM.	A	Z
Nd	142	60

METHOD	REF. NO.	
	75 Sc 2	egf

Inelastic electron scattering has been used to study the isoscalar E2 giant resonances in ^{142}Nd and ^{150}Nd , which were found at excitation energies of 12.0 and 11.2 MeV with total widths of 2.8 and 5.0 MeV, respectively. The energy shift and the larger width in ^{150}Nd indicate a splitting due to the deformation of ^{150}Nd .

E,E/SPECTRUM (E2)

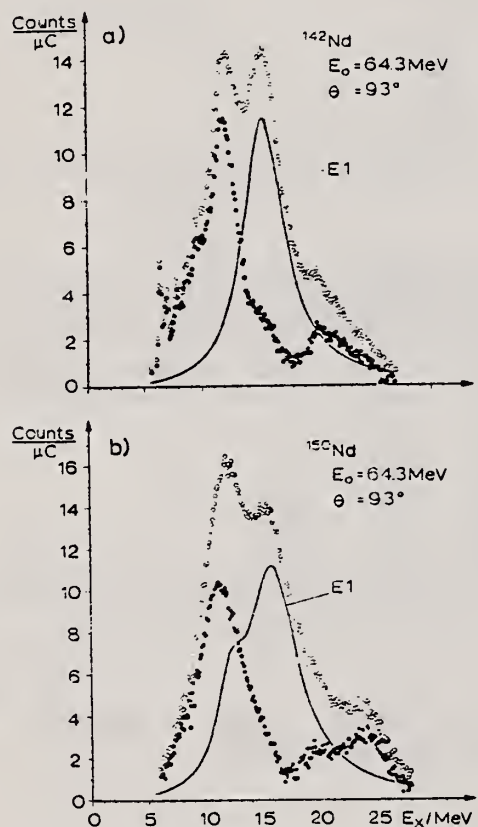


Fig. 1. Spectrum of inelastically scattered electrons after subtraction of radiation tail and background, a) ^{142}Nd , b) ^{150}Nd (open circles). Solid line: E1 cross section. Full circles: E1 cross section subtracted. The total number of counts/ μC in the region of the giant resonances is about 100.

REF.

H. Bartsch, K. Huber, U. Kneissl, H. Krieger
 Nucl. Phys. A256, 243 (1976)

ELEM. SYM.	A	Z
Nd	142	60

METHOD

REF. NO.

76 Ba 1

egf

REACTION	RESULT	EXCITATION ENERGY	SOURCE		DETECTOR		ANGLE
			TYPE	RANGE	TYPE	RANGE	
G, N	RLY	THR-UKN	C	UKN	SCD-D		4PI

ISOMER RATIO

TABLE I
 Experimental and theoretical results

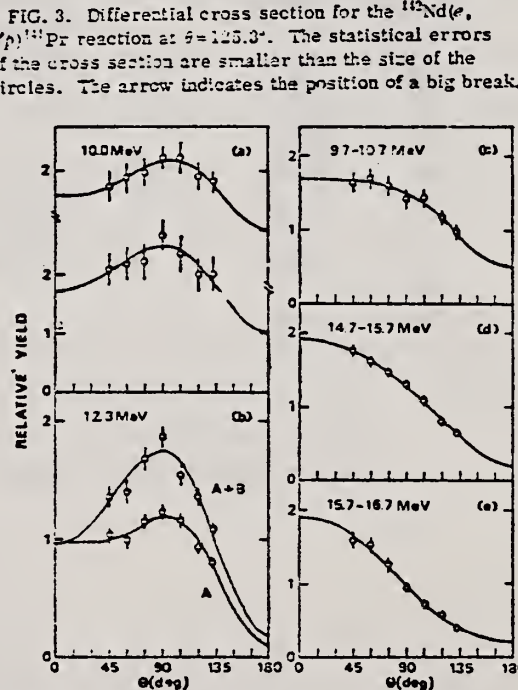
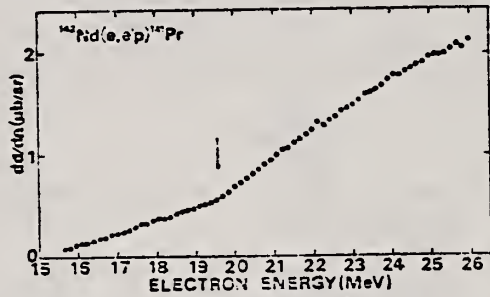
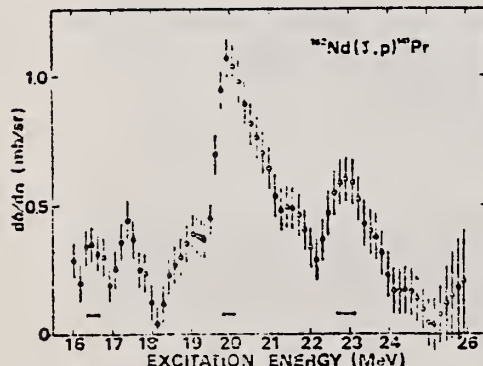
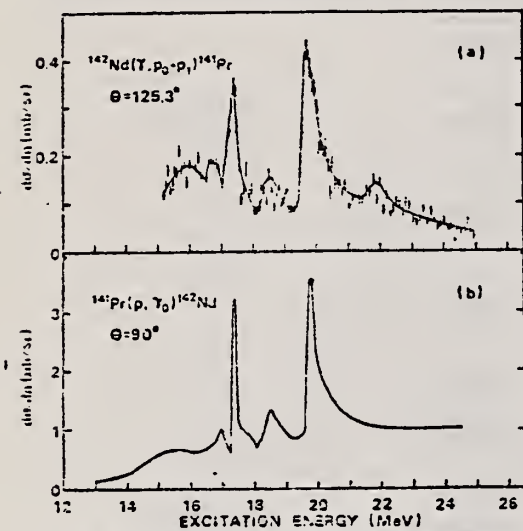
Process	Target-spin	E_{γ} (keV)	$T_{1/2}$	Spin high	Spin low	$R_{exp} = \frac{\sigma_{high}}{\sigma_{low}}$	SCOP (δ)
$^{181}\text{Ta}(\gamma, 3n)$	$\frac{7}{2}^+$	93	2.2 h 9.31 min 8.15 h	7^-	1^+	0.51 ± 0.09	3.6 ± 0.2
$^{142}\text{Nd}(\gamma, n)$	0^+	755 1100-1300, 145	63 s 2.5 h	$\frac{5}{2}^-$	$\frac{3}{2}^+$	0.055 ± 0.006 $0.19 \pm 0.01^a)$	2.20 ± 0.06
$^{92}\text{Mo}(\gamma, n)$	0^+	652.9 1208, 1508, 1581, 1637	66 s 15.49 min	$\frac{5}{2}^+$	$\frac{3}{2}^-$	1.03 ± 0.21 $0.85 \pm 0.07^b)$ $1.92 \pm 0.15^b)$	5.03 ± 0.75 4 ± 6
$^{90}\text{Mo}(\gamma, n)$	0^+	97.3 140.5	$16.8 \mu\text{s}$ 66.02 h	$\frac{5}{2}^+$	$\frac{3}{2}^+$	0.85 ± 0.24	1.72 ± 0.25
$^{100}\text{Pd}(\gamma, n)$	0^+	214.5 115	22 s 850 ns	$\frac{5}{2}^-$	$\frac{3}{2}^+$	0.5 ± 0.2	3.4 ± 0.5
$^{110}\text{Pd}(\gamma, n)$	0^+	188 113 87.7	4.7 min 390 ns 13.47 h	$\frac{5}{2}^-$	$\frac{3}{2}^+$	0.11 ± 0.02 0.41 ± 0.09 3.2 ± 0.7	3.14 ± 0.15 3.0 ± 0.25 3.3 ± 0.4
$^{89}\text{Y}(\gamma, n)$	$\frac{5}{2}^-$	231.7 442.3 392.5	14.2 ms 300 μs	8^+	1^+	0.056 ± 0.008	

^{a)} Ref. ¹⁴). ^{b)} Ref. ¹⁵).¹⁴ P.E. Haustein et al., J. Inorg. Nucl. Chem. 33, 289 (1971)¹⁵ J. H. Carver et al., Nucl. Phys. 37, 449 (1962)

ELEM. SYM.	A	Z
Nd	142	60
METHOD		REF. NO.
77 Sa 5		hmg

REACTION	RESULT	EXCITATION ENERGY	SOURCE	DETECTOR	ANGLE
			TYPE	RANGE	
E,P	ABX	15-26	D	15-26	MAG-D
					DST

The reaction $^{142}\text{Nd}(\text{e}, \text{e}'\text{p})^{141}\text{Pr}$ has been used to study the T_5 giant resonance in ^{142}Nd . Cross sections for the $^{142}\text{Nd}(\gamma, \text{p})^{141}\text{Pr}$ and $^{142}\text{Nd}(\gamma, \text{p}_0 + \text{p}_1)^{141}\text{Pr}$ reactions were measured for excitation energies from 15.9 to 26.0 MeV. These cross sections are compared with previous $^{141}\text{Pr}(\text{p}, \gamma_0)^{142}\text{Nd}$ data. The angular distributions for the larger resonances at 17.3, 19.7, and 22.9 MeV were measured. Analysis indicates that the 22.9-MeV state has about a 13% E2 component. The decay proton spectra from the 19.7- and 22.9-MeV resonances were analyzed with a schematic shell model and indicates that the core excitation process is dominant in these isobaric analog resonances. The measured (γ, p) cross section together with the (γ, n) cross section is found to be fairly consistent with the predictions of isospin splitting theory.



- ¹B. Gouliari and S. Fallieros, Can. J. Phys. 45, 3221 (1967); R. Ö. Akyüz and S. Fallieros, Phys. Rev. Lett. 27, 1016 (1971).
²K. Shoda, T. Saito, M. Sugawara, H. Miyase, S. Oikawa, and A. Suzuki, Phys. Rev. C 4, 1842 (1971).
³M. Hasinoff, G. A. Fisher, P. Kurjan, and S. S. Hanna, Nucl. Phys. A195, 78 (1972).
⁴P. Carlos, H. Bell, R. Berger, A. Lepretre, and A. Veyssiére, Nucl. Phys. A172, 437 (1971).
⁵M. Harchol, A. A. Jaffe, J. Zitron, and Ch. Drory, Nucl. Phys. A90, 473 (1967).

(over)

TABLE I. Excitation energies, integrated cross sections, radiative strengths, and branching ratios for the 1^+ states in ^{147}Nd .

$(\gamma, p)^a$	E_γ (MeV)	$\int \sigma^R(\gamma, p) dE^a$ (mb MeV)	Γ_γ^R (eV)	$\Gamma_\gamma^{\text{IAS}}$ (eV)	$\int \sigma^R(\gamma, p_0 + p_1) dE^a$ (mb MeV)	$\int \sigma^R(\gamma, p_0 + p_1) dE^c$ (mb MeV)	$\frac{\Gamma_{p_0} + \Gamma_{p_1}}{\Gamma}$
	$(\gamma, p_0 + p_1)^a$	$(p, n)^b$	$(p, n)^b$	$(p, n)^b$	$(p, n)^b$	$(p, n)^b$	$(p, n)^b$
16.5			3.2 ± 1.0	76 ± 23			
	16.86	16.9					
17.4	17.3	17.33	4.1 ± 1.2	110 ± 30	69 ± 22	0.80 ± 0.15	0.79 ± 0.14
18.0	18.5	18.43	3.8 ± 1.1	120 ± 40		0.34 ± 0.08	0.20 ± 0.07
19.0	19.6	19.71	22 ± 7	760 ± 230	530 ± 160	2.9 ± 0.4	0.09 ± 0.03
21.7	21.9		1.2 ± 0.6	49 ± 25		0.29 ± 0.09	0.13 ± 0.04
22.9			23 ± 7	1100 ± 300			0.24 ± 0.11

^aPresent data.^bReference 7.^cReference 19.^dReference 3. $\int \sigma^R(\gamma, p_0 + p_1) dE$ is corrected for the measured angular distribution.

TABLE II. Coefficients obtained from weighted least squares fits of the angular distributions for the ground-state transition to Legendre polynomials.

E_p (MeV)	E_s (MeV)	Present work			Hashimoto <i>et al.</i> (Ref. 7)	
		a_1	a_2	a_3	a_1	a_2
10.0	17.3	0.10 ± 0.15	-0.34 ± 0.13	0.07 ± 0.23	0.05	-0.31
10.0	17.3	0.03 ± 0.06	-0.32 ± 0.05	0.12 ± 0.10		
12.3 ^a	19.6	0.25 ± 0.09	-0.44 ± 0.08	0.20 ± 0.14	0.09	-0.58
12.3 ^b	19.6	0.19 ± 0.11	-0.57 ± 0.10	0.10 ± 0.18		
9.7 ≤ E_p ≤ 10.7	17.0 ≤ E_s ≤ 15.0	0.35 ± 0.09	-0.20 ± 0.09	0.05 ± 0.13		
14.7 ≤ E_p ≤ 15.7	22.0 ≤ E_s ≤ 23.0	0.63 ± 0.03	-0.13 ± 0.02	0.02 ± 0.04		
15.7 ≤ E_p ≤ 16.7	23.0 ≤ E_s ≤ 24.0	0.99 ± 0.07	0.06 ± 0.06	-0.04 ± 0.10		

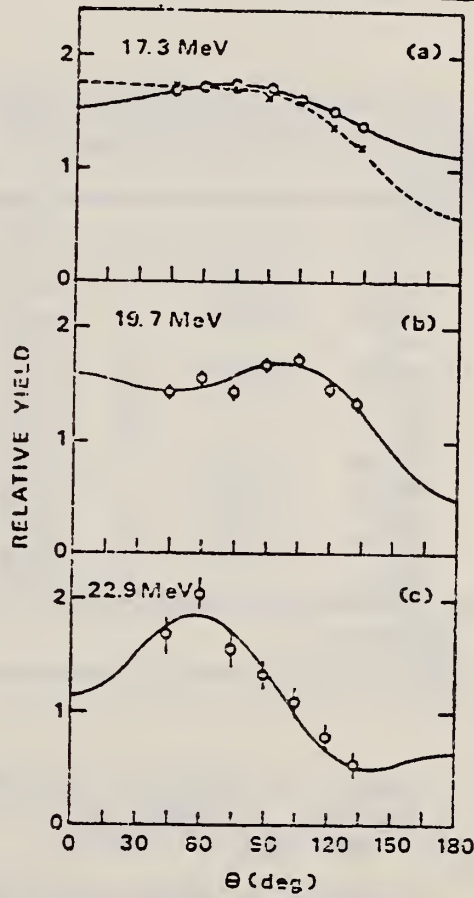
^a11.9 ≤ E_p ≤ 12.5.^b11.9 ≤ E_p ≤ 13.2.

TABLE III. Coefficients obtained from weighted least squares fits of the angular distributions for the 17.3-, 19.7-, and 22.9-MeV resonances.

E_R (MeV)		a_1	a_2	a_3
17.3	9.7 ≤ E_p ≤ 10.8	0.29 ± 0.05	-0.22 ± 0.03	0.10 ± 0.03
	4.7 ≤ E_p ≤ 10.8	0.13 ± 0.01	-0.16 ± 0.01	-0.01 ± 0.02
19.7		0.15 ± 0.11	-0.29 ± 0.10	0.22 ± 0.16
		0.62 ± 0.18	-0.27 ± 0.17	-0.42 ± 0.28

TABLE IV. Comparison of the experimental energy separation and relative strengths for $T_<$ and $T_>$ giant resonances with the theoretical predictions.

	$(\gamma, p)^a$	$(\gamma, n)^b$	Theory ^c
E_R (MeV)	19.7 ± 0.2 ^d	14.95 ± 0.1	
$\int \sigma dE$ (MeV mb)	21.1 ± 0.3 ^e		
	33 ± 10 ^f	1950 ± 150 ^f	
	59 ± 13 ^f	2050 ± 170 ^f	
σ_{p_0} (mb)	1.7 ± 0.3 ^f	130 ± 10 ^f	
	2.6 ± 0.8 ^f	135 ± 11 ^f	
$E_R - E_<$ (MeV)		4.8 ± 0.2 ^e	5.1
		6.2 ± 0.3 ^e	
$\sigma_{p_0}/(T_>)$		0.013 ± 0.004 ^f	0.035
$\sigma_{p_0}/(T_<)$		0.021 ± 0.007 ^f	

^aPresent work.^bReference 18.^cReference 2.^d E_R is evaluated by $\int_{17.0}^{22.9} \sigma(\gamma, p) dE / \int_{17.0}^{22.9} [\sigma(\gamma, p)/E] dE$.^e E_R is evaluated by $\int_{17.0}^{22.9} \sigma(\gamma, p) dE / \int_{17.0}^{22.9} [\sigma(\gamma, p)/E] dE$.^fIntegrated energy regions are 17.0–22.0 MeV and 9.3–22.0 MeV for (γ, p) and (γ, n) reactions, respectively.^gIntegrated energy regions are 17.0–26.0 MeV and 9.3–16.0 MeV for (γ, p) and (γ, n) reactions, respectively.FIG. 9. Angular distributions for (a) 17.3-, (b) 19.7-, and (c) 22.9-MeV resonances. In (a) crosses and circles show the angular distribution for the $p_0 + p_1$ groups while those for total protons, respectively, observed in bombardment of $E_\gamma = 19.0$ MeV. The solid curves show the Legendre polynomial fits.

ELEM. SYM.	A	Z
Nd	142	60

METHOD

REF. NO.
78 Me 8

REACTION	RESULT	EXCITATION ENERGY	SOURCE		DETECTOR		ANGLE
			TYPE	RANGE	TYPE	RANGE	
\$ G,G	LFT	1- 5	C	1- 5	SCD-D		DST

The resonant scattering of electron bremsstrahlung by an enriched sample of ^{142}Nd has been studied for photon energies of up to 5 MeV. It provides estimates of the radiative widths for 13 levels. Based on the relative yields at scattering angles of 96° and 126°, unambiguous spin assignments were made to 6 of these levels. Where feasible, the yield measurements were supplemented by self-absorption data and by linear polarization studies. For the strongest excitation, at 3.425 MeV, the resonance fluorescence experiments led to its identification as a 1^- state with a radiative width $\Gamma_0 = 370 \pm 45$ MeV. The corresponding $E1$ strength is comparable to the $E1$ strengths measured in other even-even $N = 82$ nuclei for the 1^- member of the quintuplet arising from the coupling of the lowest octupole vibration to the 2_1^+ level. The sum of the excitation energies of the 2_1^+ state and the 3_1^- state in ^{142}Nd is consistent with such an interpretation of the 3.425-MeV level.

POL SCD GAMMA

TABLE I. Spins and widths of ^{142}Nd levels, deduced from the yields of the reaction $^{142}\text{Nd}(\gamma, \gamma)$ at scattering angles of 96° and 126°. Standard deviations are listed throughout.

E_{level} (MeV)	$N(126^\circ)/N(96^\circ)$	Spin	Γ_0^2/Γ (meV)
1.576 (2)	0.45 ± 0.05	2	4.0 ± 0.3
2.385 (2)	0.52 ± 0.10	2	2.4 ± 0.4
2.583	...	1 ^a	0.6 ± 0.7
2.846 (2)	0.40 ± 0.06	2	11.5 ± 1.0
3.046 (2)	0.34 ± 0.36	(2)	1.4 ± 0.6
3.128	...	1,2 ^b	0.6 ± 0.9^c
3.358	...	1,2 ^b	0.1 ± 1.0^c
3.425 (2)	1.19 ± 0.07	1	330 ± 40
4.095 (2)	1.20 ± 0.11	1	110 ± 20
4.145 (2)	1.09 ± 0.13	1	85 ± 15
4.255 (4)	1.5 ± 0.8	1,2	20 ± 7^c
4.625 (3)	1.10 ± 0.24	(1)	100 ± 20
4.901 (3)	...	1,2	80 ± 30^c

^aSee Ref. 15.

^bAccording to Ref. 6.

^cA spin of 1 ($g=3$) was assumed in calculating this width.

6

S. Raman, J.L. Foster, Jr., O. Dietzschi,
D. Spalding, L. Bimbot, and B.H. Wildenthal,
Nucl. Phys. A201, 21 (1973)

15

J. Tenenbaum, R. Moreh, and A. Nof, Nucl.
Phys. A218, 95 (1974)

TABLE II. Self absorption by 11.87 g/cm^2 of Nd metal (natural composition), i.e., by $1.35 \times 10^{22} {^{142}\text{Nd}}$ nuclei/ cm^2 .

E_{level}	$N(\text{res. absorber})$ $N(\text{comparison abs.})$	Γ_0 (meV) ^a
3.425	0.52 ± 0.02	355 ± 30
4.095	0.82 ± 0.09	150 ± 100
4.145	0.87 ± 0.13	110 ± 130

^aAssuming $\Gamma_0/\Gamma = 1$.

TABLE III. ^{142}Nd : Results of the experiments using the Ge(Li) polarimeter.

E (MeV)	$100 \times \frac{N_u - N_d}{N_u + N_d}$	Multipole character	J_{exc}^{π}
3.425	$+1.9 \pm 1.6$	$E1$	1^-
4.095	-2.1 ± 4.2	$M1$ slightly favored	1^+
4.145	$+8.9 \pm 4.8$	$(E1)$	$1^{(-)}$

Nd
 $A=143$

Nd
 $A=143$

Nd
 $A=143$

ELEM. SYM.	A	Z
Nd	143	60

METHOD

REF. NO.

71 Ca 1

egf

REACTION	RESULT	EXCITATION ENERGY	SOURCE		DETECTOR		ANGLE
			TYPE	RANGE	TYPE	RANGE	
G, N 394	ABX	9-20	D	8-20	MOD-I		4PI
G, 2N 395+	ABX	9-20	D	8-20	MOD-I		4PI

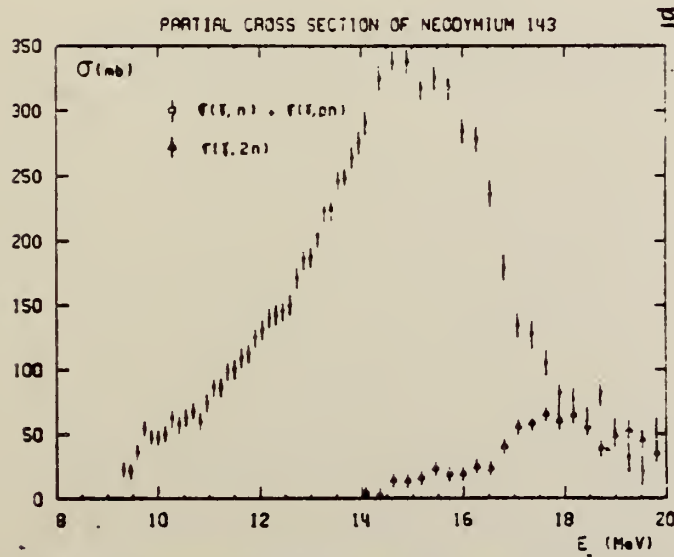
399+

TABLE 2

Parameters of the one- or two-Lorentz line fits to the σ_T curves for neodymium isotopes: parameters for Ce and Er extracted from earlier results¹³⁾ are also shown

Ce	^{142}Nd	^{143}Nd	^{144}Nd	^{145}Nd	^{146}Nd	^{148}Nd	^{150}Nd	Er
σ_1 (mb)	360 ± 15	359 ± 15	360 ± 15	317 ± 15	297 ± 20	308 ± 16	263 ± 15	174 ± 20
Γ_1 (MeV)	4.35 ± 0.05	4.43 ± 0.20	4.5 ± 0.2	5.3 ± 0.25	6.5 ± 0.4	6 ± 0.3	7.2 ± 0.3	3.3 ± 0.1
E_1 (MeV)	15.0 ± 0.10	14.95 ± 0.1	15 ± 0.1	15.05 ± 0.1	15 ± 0.15	14.8 ± 0.1	14.7 ± 0.15	12.3 ± 0.15
σ_2 (mb)							223 ± 20	260 ± 15
Γ_2 (MeV)							5.2 ± 0.15	5.0 ± 0.05
E_2 (MeV)							16 ± 0.15	15.45 ± 0.1
$\frac{1}{2} \pi \sigma \Gamma$ MeV · b		2.5 ± 0.2	2.54 ± 0.2	2.6 ± 0.2	3.0 ± 0.3	2.9 ± 0.2	3.0 ± 0.2	2.7 ± 0.3
$\frac{1}{2} \pi \sigma \Gamma$ 0.06 NZA^{-1}		1.20 ± 0.10	1.22 ± 0.10	1.25 ± 0.10	1.4 ± 0.15	1.35 ± 0.10	1.4 ± 0.1	1.27 ± 0.15

¹³⁾ R. Bergere, H. Beil, P. Carlos et A. Veyssiére, Nucl. Phys. A133, 417 (1969).

Fig. 3. Partial photoneutron cross sections $\sigma(\gamma, n)$ and $\sigma(\gamma, 2n)$ of ^{143}Nd .

(over)

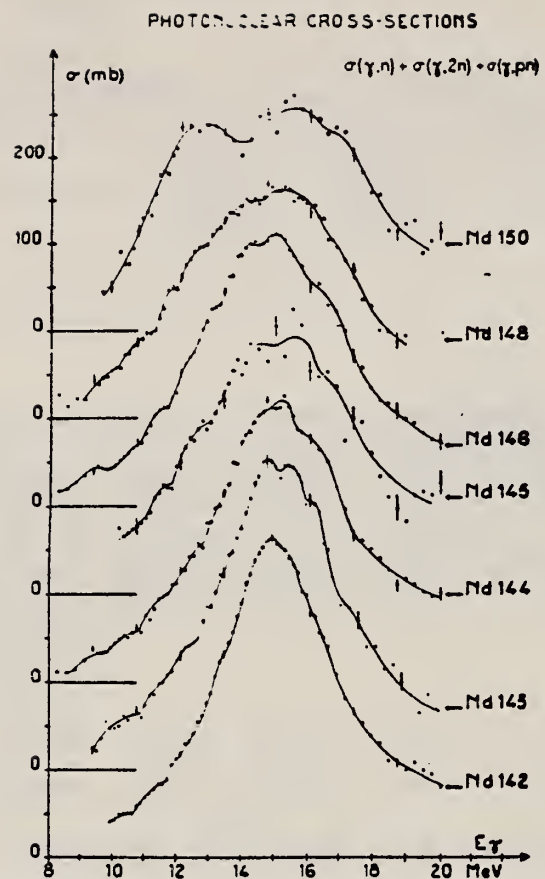


Fig. 9. Total photonuclear cross-section σ_T of neodymium isotopes. The full line drawn through the experimental points is merely meant to facilitate the identification of structure.

1D

A=144

1D

A=144

1D

A=144

METHOD

Radioactive source; photon scattering

REF. NO.

63 Bl 2

NVB

REACTION	RESULT	EXCITATION ENERGY	SOURCE		DETECTOR		ANGLE
			TYPE	RANGE	TYPE	RANGE	
G,G	ABX	2	D	2			
				(2.18)			

$$\sigma = (0.26 \pm 0.18) 10^{-27} \text{ cm}^2/\text{atom}$$

$$1.4 \times 10^{-14} \leq \tau \geq 3.4 \times 10^{-4} \text{ sec.}$$

METHOD radioactive source; photon scattering; NaI spectrometer					REF. NO.		
REACTION	RESULT	EXCITATION ENERGY	SOURCE		DETECTOR		ANGLE
			TYPE	RANGE	TYPE	RANGE	
G,G	LFT	2 (2.18)	D	2 (2.18)	NAI-D		90

$$\sigma = 1.93 \times 10^{-28} \text{ cm}^2$$

SEP ISOTPS, G-WDTH

$$\Gamma = 0.033 \text{ eV}$$

$$\text{Lifetime } \tau \geq (2.0 \pm 0.4) 10^{-14} \text{ sec.}$$

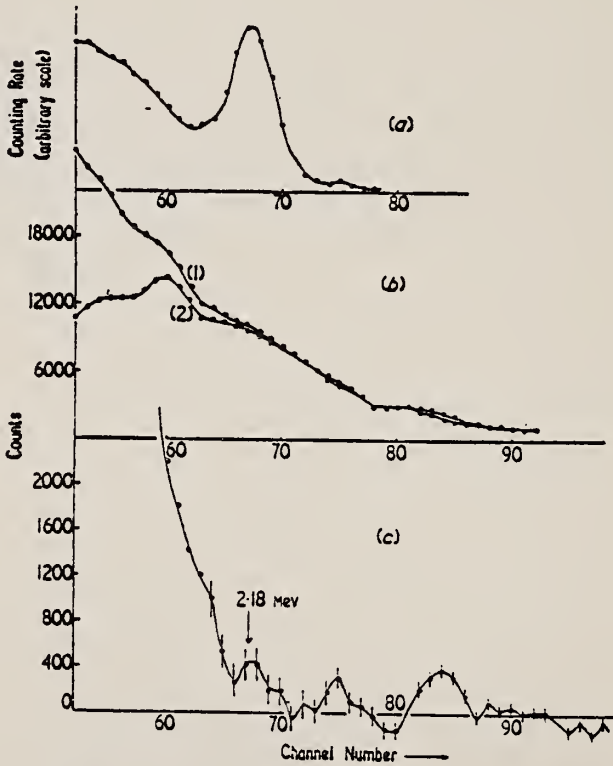


Figure 3. (a) Scintillation counter calibration; the 2.18 Mev γ ray as observed with the source in the position of the scatterer. (b) Actual pulse height distributions: (1) with source and scatterer present, (2) with only scatterer present (for 10 000 minute counting time). (c) Excess counts due to presence of ^{144}Nd source (for counting time of 10 000 minutes).

REF.

F. R. Metzger
 Phys. Rev. 187, 1700 (1969)

CLOCK. STM.	A	Z
Nd	144	60

METHOD

REF. NO.

69 Me 3

hmg

REACTION	RESULT	EXCITATION ENERGY	SOURCE		DETECTOR		ANGLE
			TYPE	RANGE	TYPE	RANGE	
G,G	LFT	2,2 (2.074, 2.186)	C	2,2 (2.174, 2.186)	SCD-D		DST (98,127)

B(EL), 2.074, 2.186

The resonant scattering of γ rays has been observed for the 2.186-MeV 1^- state in Nd¹⁴⁴. The electron bremsstrahlung from a Van de Graaf accelerator served as the exciting γ radiation. The scattered radiation was observed with a 40-cm³ Ge(Li) detector. If the value $\Gamma_0/\Gamma = 0.71$ is used for the branching ratio, the measured scattering yield corresponds to a partial width $\Gamma_0 = (3.1 \pm 0.4) \times 10^{-4}$ eV for the ground-state transition. The reduced $E1$ transition probability for the ground-state transition is intermediate between the $B(E1)$'s for the "spherical" nucleus Sm¹⁴⁴ and the deformed nucleus Sm¹⁴⁸. A level with spin 2 and with an excitation energy of 2.074 MeV has also been excited in Nd¹⁴⁴. From the observed scattering, $\Gamma_0^2/\Gamma = (1.2 \pm 0.3) \times 10^{-4}$ eV is obtained for this level.

REF.

P. Carlos, H. Beil, R. Bergere, A. Lepretre, A. Veyssiére
 Nucl. Phys. A172, 437 (1971)

ELEM. SYM.	A	Z
Nd	144	60

METHOD

REF. NO.

71 Ca 1

egf

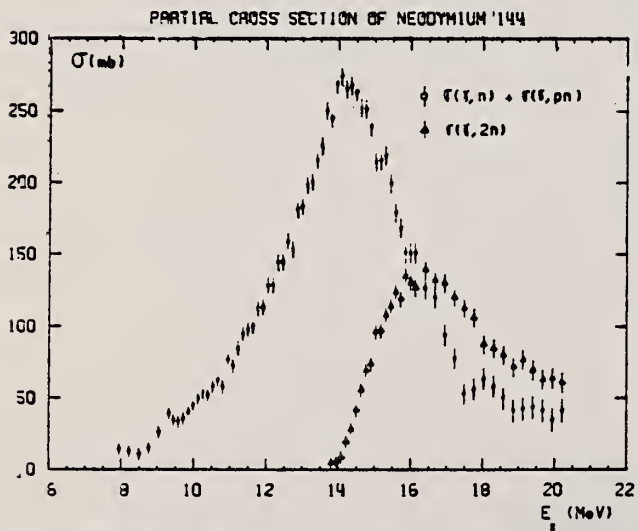
REACTION	RESULT	EXCITATION ENERGY	SOURCE		DETECTOR		ANGLE
			TYPE	RANGE	TYPE	RANGE	
G, N 397	ABX	8-20	D	8-20	MOD-I		4PI
G, 2N 398+	ABX	8-20	D	8-20	MOD-I		4PI
							397+

TABLE 2

Parameters of the one- or two-Lorentz line fits to the σ_T curves for neodymium isotopes: parameters for Ce and Er extracted from earlier results ¹³ are also shown

	Ce	¹⁴² Nd	¹⁴³ Nd	¹⁴⁴ Nd	¹⁴⁵ Nd	¹⁴⁶ Nd	¹⁴⁸ Nd	¹⁵⁰ Nd	Er
σ_1 (mb)	360 \pm 15	359 \pm 15	360 \pm 15	317 \pm 15	297 \pm 20	308 \pm 16	263 \pm 15	174 \pm 20	225 \pm 15
Γ_1 (MeV)	4.35 \pm 0.05	4.43 \pm 0.20	4.5 \pm 0.2	5.3 \pm 0.25	6.5 \pm 0.4	6 \pm 0.3	7.2 \pm 0.3	3.3 \pm 0.1	2.9 \pm 0.05
E_1 (MeV)	15.0 \pm 0.10	14.95 \pm 0.1	15 \pm 0.1	15.05 \pm 0.1	15 \pm 0.15	14.8 \pm 0.1	14.7 \pm 0.15	12.3 \pm 0.15	12.00 \pm 0.1
σ_2 (mb)								223 \pm 20	260 \pm 15
Γ_2 (MeV)								5.2 \pm 0.15	5.0 \pm 0.05
E_2 (MeV)								16 \pm 0.15	15.45 \pm 0.1
$\frac{1}{2}\pi\sigma\Gamma$ MeV · b		2.5 \pm 0.2	2.54 \pm 0.2	2.6 \pm 0.2	3.0 \pm 0.3	2.9 \pm 0.2	3.0 \pm 0.2	2.7 \pm 0.3	
$\frac{1}{2}\pi\sigma\Gamma$		1.20 \pm 0.10	1.22 \pm 0.10	1.25 \pm 0.10	1.4 \pm 0.15	1.35 \pm 0.10	1.4 \pm 0.1	1.27 \pm 0.15	
$0.06 NZA^{-1}$									

¹³ R. Bergere, H. Beil, P. Carlos et A. Veyssiére, Nucl. Phys. A133, 417 (1969).

Fig. 4. Partial photoneutron cross sections $\sigma(\gamma, n)$ and $\sigma(\gamma, 2n)$ of ¹⁴⁴Nd.

(over)

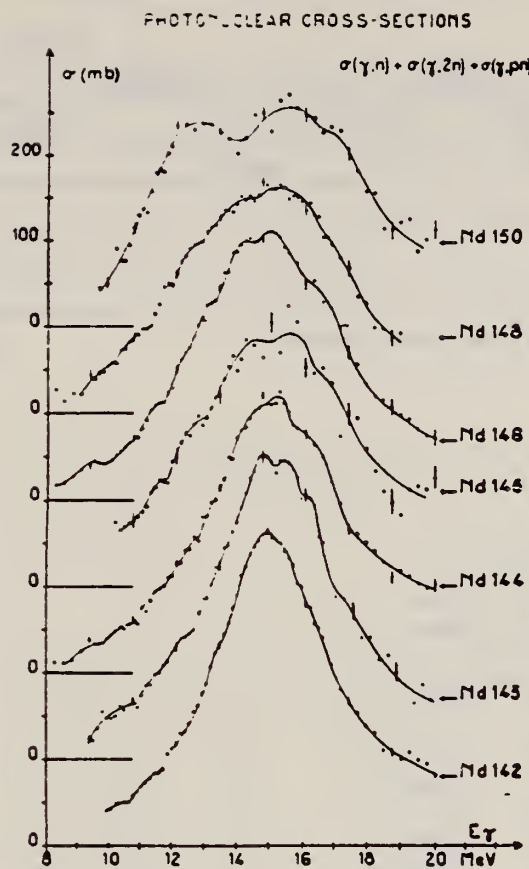


Fig. 9. Total photonuclear cross-section σ_T of neodymium isotopes. The full line drawn through the experimental points is merely meant to facilitate the identification of structure.

REF.

P. E. Haustein and A. F. Voigt
J. inorg. nucl. Chem. 33, 289 (1971)

ELEM. SYM.	A	Z
Nd	144	60

METHOD

REF. NO.
71 Ha 2

egf

REACTION	RESULT	EXCITATION ENERGY	SOURCE		DETECTOR		ANGLE
			TYPE	RANGE	TYPE	RANGE	
G, 3N	RLY	24-70	C	70	ACT-I		4PI

Isomer ratio = (yield to low spin state)/(yield to high spin state)

ISOMER RATIOTable 2. Isomer ratio measurements for ^{96}Mo , ^{137}Ce , and ^{144}Nd

Reaction	Isomer ratio	J^π Target	J^π Ground state	J^π Isomer	Threshold (MeV)	$41A^{-1/2}$ (MeV)
$^{96}\text{Mo}(\gamma, n)^{96}\text{Mo}$	1.92 ± 0.15	0^+		$9/2^+$	13.13	16.60
$^{96}\text{Mo}(\gamma, 3n)^{94}\text{Mo}$	1.59 ± 0.16	0^+		$1/2^-$	30.72	16.52
$^{137}\text{Ce}(\gamma, n)^{137}\text{Ce}$	3.1	0^+		$3/2^+$	10.31	15.30
$^{137}\text{Ce}(\gamma, 3n)^{137}\text{Ce}$	1.10 ± 0.12	0^+		$11/2^+$	26.34	15.26
$^{144}\text{Nd}(\gamma, n)^{144}\text{Nd}$	5.2 ± 0.3	0^+		$3/2^+$	9.79	15.22
$^{144}\text{Nd}(\gamma, 3n)^{141}\text{Nd}$	1.80 ± 0.25	0^+		$11/2^+$	23.67	15.17

Nd
 $A=145$

Nd
 $A=145$

Nd
 $A=145$

ELEM. ATM.		Nd	145	60
		REF. NO.	60 Ge 3	NVB

THRO

Betatron; neutron threshold; ion chamber

REACTION	RESULT	EXCITATION ENERGY	SOURCE	DETECTOR	ANGLE
			TYPE	RANGE	
G, N	NOX	THR	C THR	BF3-I	4 PI

THRESHOLD

TABLE I. Summary and comparison of neutron separation energies inferred from present threshold measurements with values predicted from mass data and reaction energies. All energies are expressed in the center-of-mass system in Mev.

Reaction	No. runs	Present results	Other results	Method	Reference
$\text{Nd}^{146}(\gamma, n)\text{Nd}^{144}$	1	$\leq 6.38 \pm 0.16$	5.97 ± 0.19	mass data	p W. H. Johnson, Jr., and A. O. Nier, Phys. Rev. 103, 1014 (1957).

TABLE II. Comparison of measured threshold energies with neutron binding energies predicted by mass data for transitions with $\Delta I \geq 7/2$. All energies in Mev.

Reaction	ΔI^a	Observed threshold	Mass data Q value	$E_{\alpha} - Q$	Excited state energy
$\text{Cr}^{49}(\gamma, n)\text{Cr}^{48}$	7/2	12.18 ± 0.14	12.053 ± 0.004^b	0.13 ± 0.14	...
$\text{Y}^{89}(\gamma, n)\text{Y}^{88}$	7/2	11.59 ± 0.08	11.53 ± 0.40^b	0.06 ± 0.41	0.387 ^c
$\text{In}^{113}(\gamma, n)\text{In}^{114}$	7/2	9.22 ± 0.03	9.35 ± 0.43^b	-0.13 ± 0.43	0.191 ^c
$\text{Ce}^{142}(\gamma, n)\text{Ce}^{141}$	(7/2) ^d	7.24 ± 0.07	6.97 ± 0.07^e	0.27 ± 0.10	...
$\text{Nd}^{146}(\gamma, n)\text{Nd}^{144}$	7/2	6.38 ± 0.16	5.97 ± 0.19^f	0.41 ± 0.25	0.690 ^c
$\text{Sm}^{149}(\gamma, n)\text{Sm}^{148}$	7/2	6.45 ± 0.16	5.87 ± 0.28^f	0.58 ± 0.33	0.562 ^c
$\text{Er}^{167}(\gamma, n)\text{Er}^{166}$	7/2	6.65 ± 0.08	6.45 ± 0.06^g	0.20 ± 0.10	0.081 ^c
$\text{Hf}^{177}(\gamma, n)\text{Hf}^{176}$	7/2	6.69 ± 0.03	6.28 ± 0.06^g	0.64 ± 0.07	0.088 ^c
$\text{Hf}^{179}(\gamma, n)\text{Hf}^{178}$	9/2	6.31 ± 0.07	6.17 ± 0.06^g	0.14 ± 0.09	0.093 ^c
$\text{Hf}^{180}(\gamma, n)\text{Hf}^{179}$	9/2	7.85 ± 0.11	7.32 ± 0.06^g	0.53 ± 0.13	0.375 ^c

^a D. Strominger, J. M. Hollander, and G. T. Seaborg, Revs. Modern Phys. 30, 585 (1958).^b C. F. Giese and J. L. Benson, Phys. Rev. 110, 712 (1958).^c Henry E. Duckworth, Mass Spectroscopy (Cambridge University Press, New York, 1958), p. 177.^d S. Dzlepov and L. K. Peker, Atomic Energy of Canada Limited Report Tr. AECL-457 (unpublished).^e The discrepancy in the case of Ce¹⁴² predicts a ground-state spin for Ce¹⁴¹ of 0, since the spin of Ce¹⁴¹ is known to be 7/2.^f W. H. Johnson, Jr., and A. O. Nier, Phys. Rev. 103, 1014 (1957).^g W. H. Johnson, Jr. and V. B. Bhanot, Phys. Rev. 107, 6 (1957).

P. Carlos, H. Beil, R. Bergere, A. Lepretre, A. Veyssiére
Nucl. Phys. A172, 437 (1971)

ELEM. SYM.	A	Z
Nd	145	60

METHOD

REF. NO.

71 Ca 1

egf

REACTION	RESULT	EXCITATION ENERGY	SOURCE		DETECTOR		ANGLE
			TYPE	RANGE	TYPE	RANGE	
G, N $\gamma + c$	ABX	10-20	D	8-20	MOD-I		4PI
G, 2N $\gamma + \alpha + p$	ABX	10-20	D	8-20	MOD-I		4PI

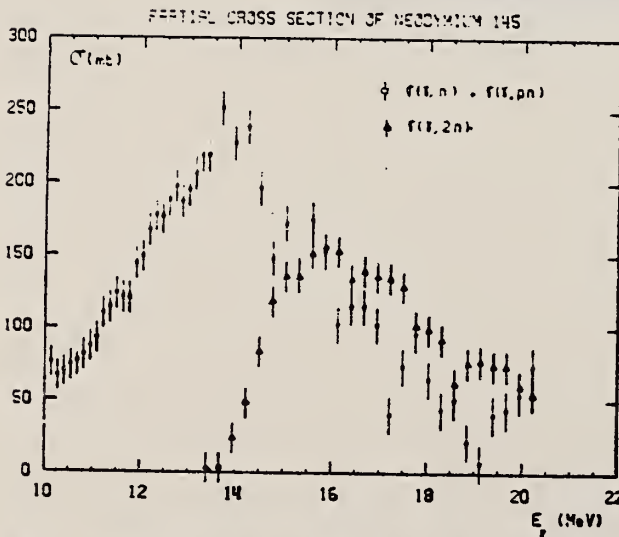
400+

TABLE 2

Parameters of the one- or two-Lorentz line fits to the σ_T curves for neodymium isotopes: parameters for Ce and Er extracted from earlier results¹³⁾ are also shown

Ce	^{142}Nd	^{143}Nd	^{144}Nd	^{145}Nd	^{146}Nd	^{148}Nd	^{150}Nd	Er
σ_1 (mb)	360 ± 15	359 ± 15	360 ± 15	317 ± 15	297 ± 20	308 ± 16	263 ± 15	174 ± 20
Γ_1 (MeV)	4.35 ± 0.05	4.43 ± 0.20	4.5 ± 0.2	5.3 ± 0.25	6.5 ± 0.4	6 ± 0.3	7.2 ± 0.3	3.3 ± 0.1
E_1 (MeV)	15.0 ± 0.10	14.95 ± 0.1	15 ± 0.1	15.05 ± 0.1	15 ± 0.15	14.8 ± 0.1	14.7 ± 0.15	12.3 ± 0.15
σ_2 (mb)							223 ± 20	260 ± 15
Γ_2 (MeV)							5.2 ± 0.15	5.0 ± 0.05
E_2 (MeV)							16 ± 0.15	15.45 ± 0.1
$\frac{1}{2} \pi \sigma \Gamma$ MeV · b		2.5 ± 0.2	2.54 ± 0.2	2.6 ± 0.2	3.0 ± 0.3	2.9 ± 0.2	3.0 ± 0.2	2.7 ± 0.3
$\frac{1}{2} \pi \sigma \Gamma$		1.20 ± 0.10	1.22 ± 0.10	1.25 ± 0.10	1.4 ± 0.15	1.35 ± 0.10	1.4 ± 0.1	1.27 ± 0.15
$0.06 NZA^{-1}$								

¹³⁾ R. Bergere, H. Beil, P. Carlos et A. Veyssiére, Nucl. Phys. A133, 417 (1969).

Fig. 5. Partial photoneutron cross sections $\sigma(\gamma, n)$ and $\sigma(\gamma, 2n)$ of ^{145}Nd .

(over)

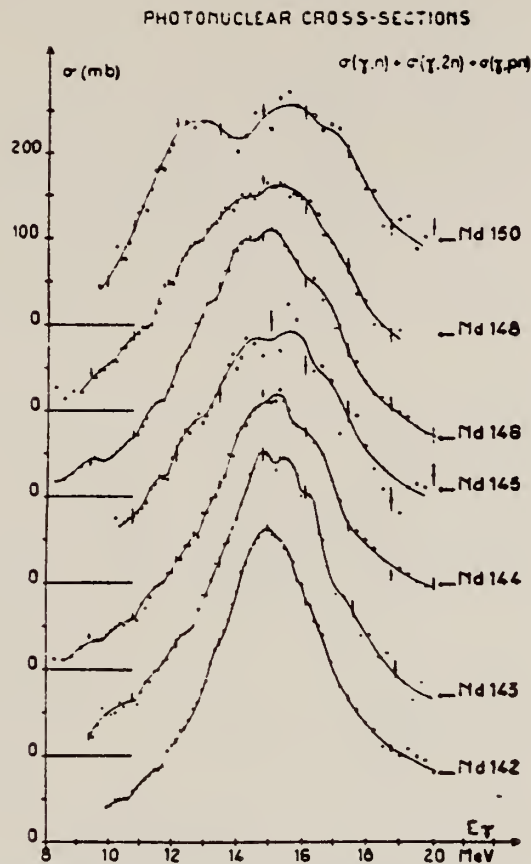


Fig. 9. Total photonuclear cross-section σ_T of neodymium isotopes. The full line drawn through the experimental points is merely meant to facilitate the identification of structure.

$\text{^{146}Nd}$
A=146

$\text{^{146}Nd}$
A=146

$\text{^{146}Nd}$
A=146

ELEM. SYM.	A	Z
Nd	146	60

METHOD

REF. NO.

71 Ca 1

egf

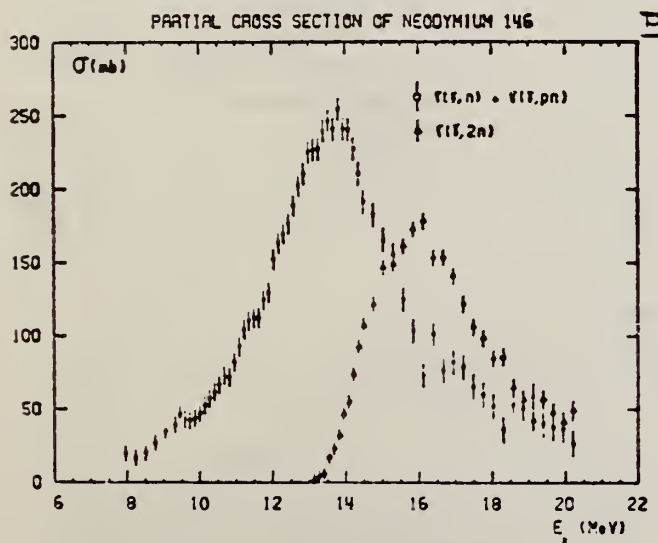
REACTION	RESULT	EXCITATION ENERGY	SOURCE		DETECTOR		ANGLE
			TYPE	RANGE	TYPE	RANGE	
G, N $\gamma\text{-}03$	ABX	8-20	D	8-20	MOD-I		4PI
G, 2N $\gamma\text{-}04+$	ABX	8-20	D	8-20	MOD-I		4PI
							403+

TABLE 2

Parameters of the one- or two-Lorentz line fits to the σ_t curves for neodymium isotopes: parameters for Ce and Er extracted from earlier results ¹³) are also shown

Ce	^{142}Nd	^{143}Nd	^{144}Nd	^{145}Nd	^{146}Nd	^{148}Nd	^{150}Nd	Er
σ_1 (mb)	360 ± 15	359 ± 15	360 ± 15	317 ± 15	297 ± 20	308 ± 16	263 ± 15	174 ± 20
Γ_1 (MeV)	4.35 ± 0.05	4.43 ± 0.20	4.5 ± 0.2	5.3 ± 0.25	6.5 ± 0.4	6 ± 0.3	7.2 ± 0.3	3.3 ± 0.1
E_1 (MeV)	15.0 ± 0.10	14.95 ± 0.1	15 ± 0.1	15.05 ± 0.1	15 ± 0.15	14.8 ± 0.1	14.7 ± 0.15	12.3 ± 0.15
σ_2 (mb)							223 ± 20	260 ± 15
Γ_2 (MeV)							5.2 ± 0.15	5.0 ± 0.05
E_2 (MeV)							16 ± 0.15	15.45 ± 0.1
$\frac{1}{2} \pi \sigma \Gamma$ MeV · b	2.5 ± 0.2	2.54 ± 0.2	2.6 ± 0.2	3.0 ± 0.3	2.9 ± 0.2	3.0 ± 0.2	2.7 ± 0.3	
$\frac{1}{2} \pi \sigma \Gamma$ 0.06 NZA^{-1}	1.20 ± 0.10	1.22 ± 0.10	1.25 ± 0.10	1.4 ± 0.15	1.35 ± 0.10	1.4 ± 0.1	1.27 ± 0.15	

¹³ R. Bergere, H. Beil, P. Carlos et A. Veyssiere, Nucl. Phys. A133, 417 (1969).

Fig. 6. Partial photoneutron cross sections $\sigma(\gamma, n)$ and $\sigma(\gamma, 2n)$ of ^{146}Nd .

(over)

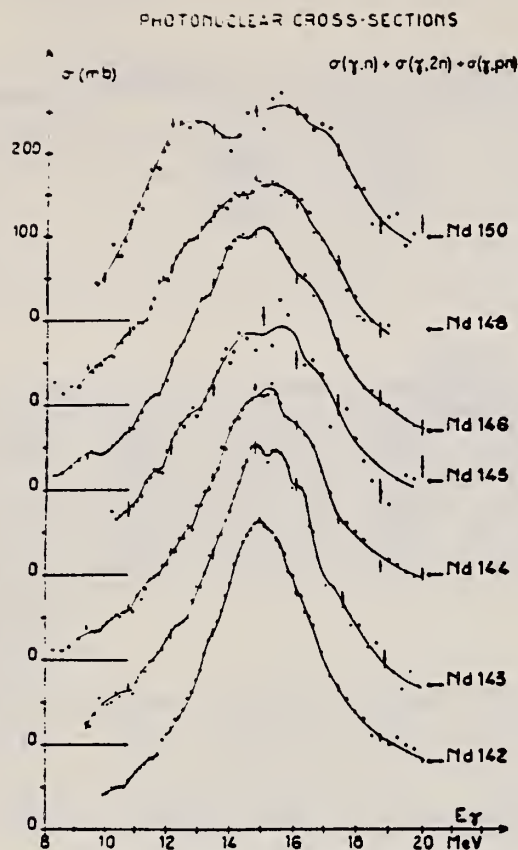


Fig. 9. Total photonuclear cross-section σ_T of neodymium isotopes. The full line drawn through the experimental points is merely meant to facilitate the identification of structure.

REF.

D. W. Madsen, L. S. Cardman, J. R. Legg, C. K. Bockelman
 Nucl. Phys. A168, 97 (1971)

ELEM. SYM.	A	Z
Nd	146	60
REF. NO.	71 Ma 1	egf

METHOD

REACTION	RESULT	EXCITATION ENERGY	SOURCE		DETECTOR		ANGLE
			TYPE	RANGE	TYPE	RANGE	
E, E/	FMF	0	D	41	MAG-D		DST

$$\theta = 0.45$$

TABLE II
 A comparison of this experiment's $B(E2\uparrow)$ values with those of other experiments and theory

Nucleus	State (MeV)	This work	Pulsed beam	Heavy particle Coulomb excitation	Theory
2 ⁺ states					
¹⁴² Nd	1.57	13.1 ± 1.7		25.0 ± 7.3 ^a) 19.1 ± 2.3 ^b) 15.5 ± 7.8 ^c)	16.4 ^d) 16.3 ^e)
¹⁴² Nd	2.09	4.1 ± 1.1			
¹⁴⁴ Nd	0.45	30.9 ± 4.6		28.5 ± 0.4 ^b) 28.1 ± 6.6 ^f)	92.1 ^g)
¹⁵⁰ Nd	0.13	62.9 ± 10.5	113.9 ± 1.8 ⁱ) 116.8 ± 3.2 ^j) 112.4 ± 5.1 ^k)	112.7 ± 4.2 ^l)	
3 ⁻ state					
¹⁴² Nd	2.09	28.6 ± 5.0		52 ± 21 ^l)	

^a) Ref. ³⁹). ^b) Ref. ⁴⁰). ^c) Ref. ⁴¹). ^d) Ref. ³⁷). ^e) Ref. ⁴²). ^f) Ref. ⁴³).

^g) Ref. ⁴⁴). ^h) Ref. ⁴⁵). ⁱ) Ref. ³⁸). ^j) Ref. ³²). ^k) Ref. ⁴⁶).

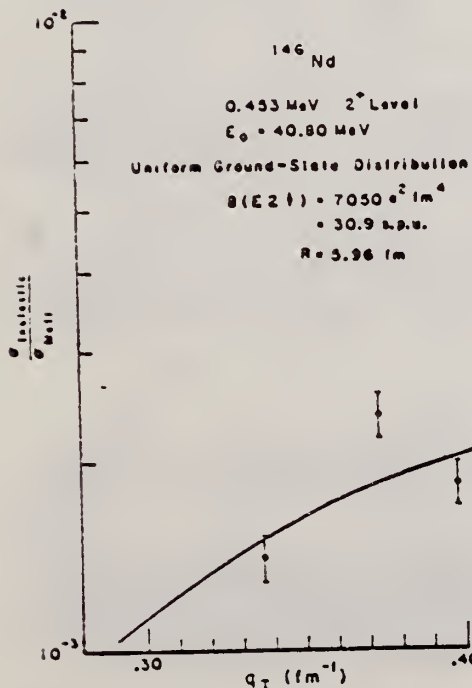


Fig. 16. Inelastic form factors for the 2⁺ level at 453 keV in ¹⁴⁶Nd as a function of inelastic momentum transfer. The experimental points are the findings of this experiment and the solid line is the best fit assuming a uniform ground state charge distribution with $R = 4.96$ fm and creating a pseudo delta function for $\rho_{\mu}^{(2)}$ in eq. (17).

METHOD								REF. NO.	
								71 Va 2	hmg
REACTION	RESULT	EXCITATION ENERGY		SOURCE		DETECTOR		ANGLE	
		TYPE	RANGE	TYPE	RANGE	TYPE	RANGE		
G,XN	ABX	7-24		C	7-24	BF3-I		4PI	
		(7.6-23.25)			(7.6-23.25)				

Table II. Parameters of giant dipole resonance

Isotope	σ_{ph} mb	E_{γ} MeV	Γ_{γ} MeV	Q_{abs} mb MeV ⁻¹	E_{γ} mb	E_{γ} MeV	Γ_{γ} MeV	Q_{abs} mb MeV ⁻¹	ϵ_{abs} mb/NrA	σ_{GDR} mb	σ_{GDR} mb	β_{eff}
Nd^{146}	332	13.8	4.1					2.12	1.10			
Sm^{148}	335	14.1	4.0					2.18	0.96			
Eu^{151}	147	12.0	3.0	0.693	259	15.0	3.2	1.29	1.09	0.90	1.87	1.25
Gd^{152}	161	11.9	2.4	0.612	250	15.0	3.5	1.39	1.01	0.89	2.27	1.26
Gd^{154}	180	11.9	2.6	0.739	243	15.2	3.6	1.37	2.11	0.94	1.86	1.27
Gd^{156}	165	11.7	2.6	0.682	249	14.9	3.8	1.49	2.16	0.94	2.25	1.28
Eu^{153}	285	14.0	4.5					2.02	0.92			
Eu^{155}	159	11.9	2.3	0.583	237	15.1	3.8	1.34	1.90	0.86	2.39	1.27

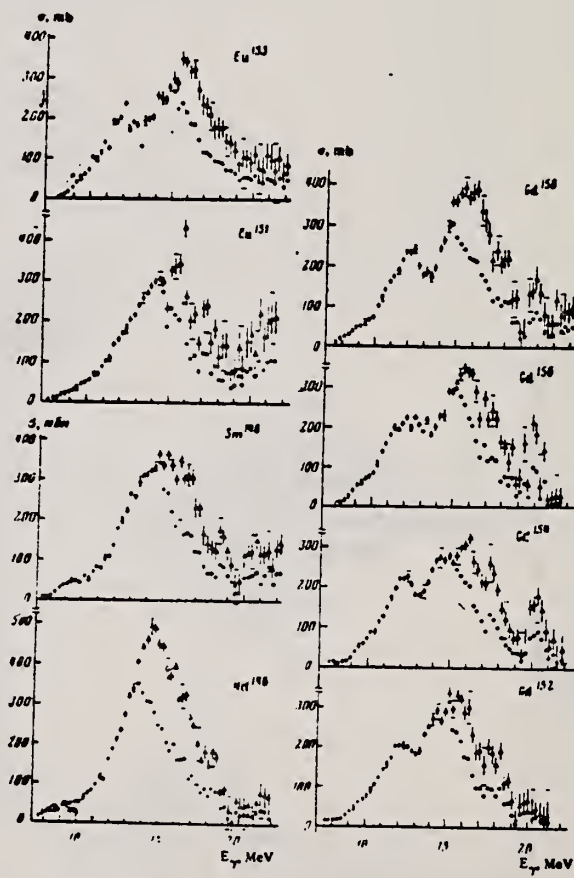


FIG. 1. Photoneutron cross sections and photoabsorption cross sections of Nd^{146} , Sm^{148} , Eu^{151} , Eu^{153} , Gd^{152} , Gd^{154} , Gd^{156} and Gd^{158} . Statistical and rms experimental errors are shown (the latter horizontal bars at 9.42 MeV, 10.42 MeV etc.). At photon energies above the (γ , 2n) threshold the photoabsorption cross section errors are not shown.

ELEM. SYM.	A	Z
Nd	146	60

METHOD

REF. NO.
77 Be 7

egf

REACTION	RESULT	EXCITATION ENERGY	SOURCE		DETECTOR		ANGLE
			TYPE	RANGE	TYPE	RANGE	
G,G	LFT	7	D	7	SCD-D		DST
		-					
		-					
		-					

7=7.163 MeV

TABLE 2

The γ -line energies E_γ of the scattered radiation from $^{144-146}\text{Nd}$ together with level energies E_x and angular distribution coefficients A

Isotope	E_γ (± 3 keV)	Intensity	A	E_x (± 3 keV)	J^π	E_x''
^{144}Nd	6709	13 ± 1	0.03 ± 0.04	454	2	453.8
	5475	3 ± 1		1688	0, 1, 2	1687
	5383	5 ± 1	0.03 ± 0.13	1778	2	1777.3
	4807	3 ± 1		2349	0, 1, 2	2350
	4701	3 ± 1		2460	0, 1, 2	2462
	4583	2 ± 1		2578	0, 1, 2	2575
	3891	1 ± 1		3280	0, 1, 2	3279
	7163	100	0.46 ± 0.09	7163	1 $^-$	
^{145}Nd	7096	< 1		67		67.0
	6107	< 3		1056		1052
	5569	2 ± 1		1594		1593.5
	5408	< 1		1755		1760
	7163	< 3		7163		
^{146}Nd	5820	< 1		695		696.49
	6515	< 1		6515		

The spins J^π are based either on the values of A or on the assumption that the resonance level is deexcited by dipole transitions.

¹) Only those levels of refs. ^{1, 9, 10} are listed which were also observed in the present work.

¹T.W. Burrows, Nucl. Data 14, no. 4 413 (1975)
⁹T.W. Burrows, Nucl. Data 12, 203 (1975)

¹⁰T.W. Burrows and R.L. Auble, Nucl. Data 16, 231 (1975)

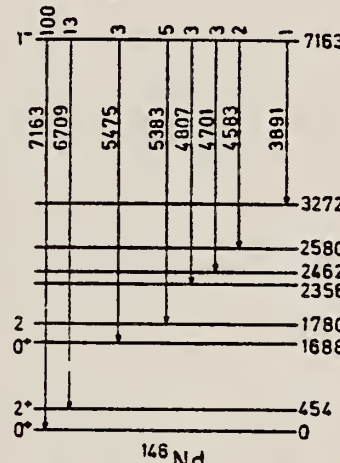


Fig. 3. Decay scheme of the 7163 keV level of ^{146}Nd showing level energies and relative intensities. The level spins are those obtained from the results of the present work (table 2).

TABLE 4

Values of Γ , Γ_0 , and the energy separation δ (between the incident γ -line and the resonance level)

Scatterer	E_γ (keV)	Γ (meV)	Γ_0 (meV)	δ (eV)
^{146}Nd	7163	125 ± 50	41 ± 13	13.7 ± 0.6
^{154}Sm	6465	105 ± 50	25 ± 13	3.6 ± 2.0

Nb

A=148

Nb

A=148

Nb

A=148

ELEM. SYM.	A	Z
Nd	148	60

METHOD

REF. NO.

69 Va 2

egf

REACTION	RESULT	EXCITATION ENERGY	SOURCE		DETECTOR		ANGLE
			TYPE	RANGE	TYPE	RANGE	
G,XN	ABX	8-23	C	8-23	BF ₃ -I		4PI

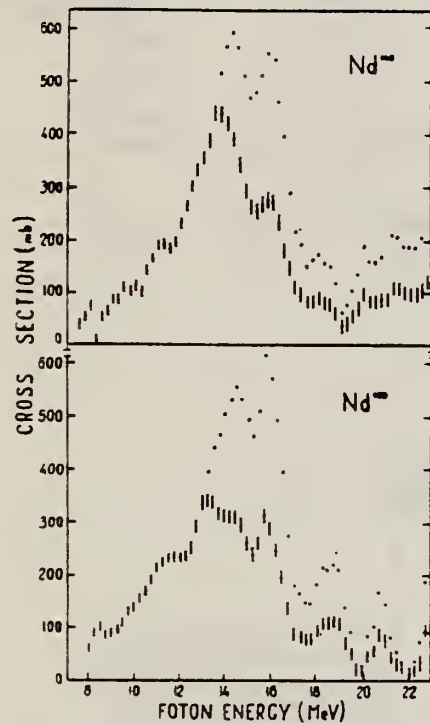
308

Fig. 2. The photoneutron cross section $\sigma(\gamma, n)$ and the photoabsorption cross sections σ_{tot} for ^{148}Nd and ^{150}Nd . The σ_{tot} are represented by dots. At the energies where σ_{tot} and $\sigma(\gamma, n)$ differ, the latter is represented by circles. Only statistical errors of σ_{tot} are plotted.

METHOD				REF. NO.	
REACTION	RESULT	EXCITATION ENERGY	SOURCE	DETECTOR	ANGLE
			TYPE RANGE	TYPE RANGE	
G,XN	ABX	8-22	C 8-22	BF3-I	4PI
			-		

SEE 69VA2 338

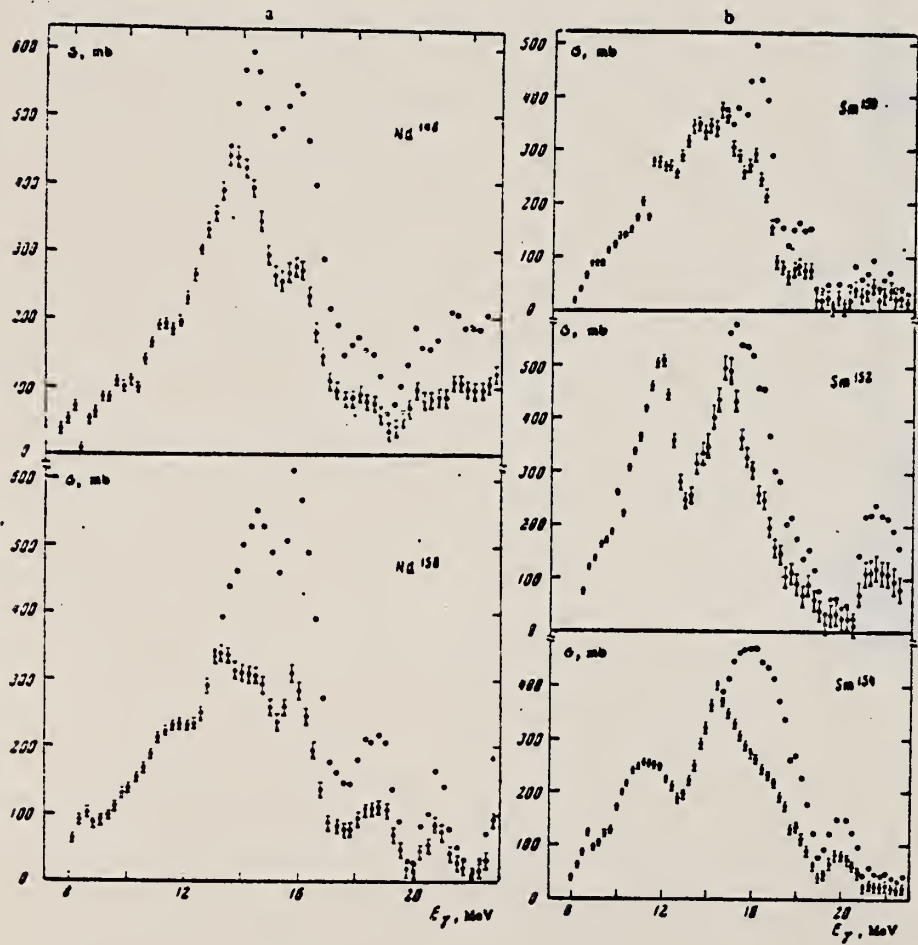


FIG. 2. Photoabsorption cross sections (black points) and photoneutron cross sections (light points): a — for Nd¹⁴⁸ and Nd¹⁵⁰ and b — for Sm¹⁵⁰, Sm¹⁵², and Sm¹⁵⁴. The indicated errors are statistical.

[over]

Table I. Giant resonance parameters of Nd^{148,150}
and Sm^{150,152,154}

Parameters	Nucleus				
	Nd ¹⁴⁸	Nd ¹⁵⁰	Sm ¹⁵⁰	Sm ¹⁵²	Sm ¹⁵⁴
σ_0 , mb		160.0		400.0	204.0
ω_0 , MeV		11.25		11.55	11.00
$\Delta\Gamma_0$, MeV		3.0		2.4	3.0
σ_0^{nd} , MeV-b	0.750		1.319	0.962	
ϵ_0 , mb	270.0		420.0	320.0	
$\Delta\omega_0$, MeV	14.50		14.65	15.25	
$\Delta\Gamma_0$, MeV	4.0		3.4	4.0	
σ_0^{nd} , MeV-b	1.695		2.242	2.01	
$\sigma_0^{\text{nd}}/\sigma_0^{\text{nd}}$	2.28		1.7	2.09	
σ^{nd} , MeV-b	2.406	2.213	2.213	3.079	2.478
$0.08 N/Z/A$	2.140	2.160	2.163	2.203	2.223
β_0	0.42		0.70	0.41	
β_0'	0.28		0.30	0.38	
ϵ_0 , mb	420	380			
$\Delta\omega_0$, MeV	13.65	13.6			
$\Delta\Gamma_0$, MeV	5.0	5.5			

REF.

P. Carlos, H. Beil, R. Bergere, A. Lepretre, A. Veyssiére
 Nucl. Phys. A172, 437 (1971)

ELEM. SYM.	A	Z
Nd	148	60

METHOD

REF. NO.

71 Ca 1

egf

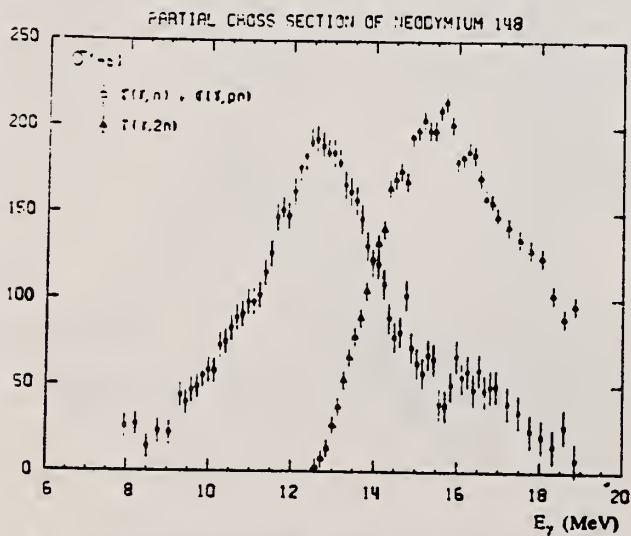
REACTION	RESULT	EXCITATION ENERGY	SOURCE		DETECTOR		ANGLE
			TYPE	RANGE	TYPE	RANGE	
G, N 406	ABX	8-20	D	8-20	MOD-I		4PI
G, 2N 407+	ABX	8-20	D	8-20	MOD-I		4PI
			.				
							406+

TABLE 2

Parameters of the one- or two-Lorentz line fits to the σ_T curves for neodymium isotopes: parameters for Ce and Er extracted from earlier results¹³ are also shown

Ce	^{142}Nd	^{143}Nd	^{144}Nd	^{145}Nd	^{146}Nd	^{148}Nd	^{150}Nd	Er
σ_1 (mb)	360 ± 15	359 ± 15	360 ± 15	317 ± 15	297 ± 20	308 ± 16	263 ± 15	174 ± 20
Γ_1 (MeV)	4.35 ± 0.05	4.43 ± 0.20	4.5 ± 0.2	5.3 ± 0.25	6.5 ± 0.4	6 ± 0.3	7.2 ± 0.3	3.3 ± 0.1
E_1 (MeV)	15.0 ± 0.10	14.95 ± 0.1	15 ± 0.1	15.05 ± 0.1	15 ± 0.15	14.8 ± 0.1	14.7 ± 0.15	12.3 ± 0.15
σ_2 (mb)							223 ± 20	260 ± 15
Γ_2 (MeV)							5.2 ± 0.15	5.0 ± 0.05
E_2 (MeV)							16 ± 0.15	15.45 ± 0.1
$\frac{1}{2}\pi\sigma\Gamma$ MeV · b		2.5 ± 0.2	2.54 ± 0.2	2.6 ± 0.2	3.0 ± 0.3	2.9 ± 0.2	3.0 ± 0.2	2.7 ± 0.3
$\frac{1}{2}\pi\sigma\Gamma$ 0.06 NZA^{-1}		1.20 ± 0.10	1.22 ± 0.10	1.25 ± 0.10	1.4 ± 0.15	1.35 ± 0.10	1.4 ± 0.1	1.27 ± 0.15

¹³ R. Bergere, H. Beil, P. Carlos et A. Veyssiére, Nucl. Phys. A133, 417 (1969).

Fig. 7. Partial photoneutron cross sections $\sigma(\gamma, n)$ and $\sigma(\gamma, 2n)$ of ^{148}Nd .

(over)

PHOTONUCLEAR CROSS-SECTIONS

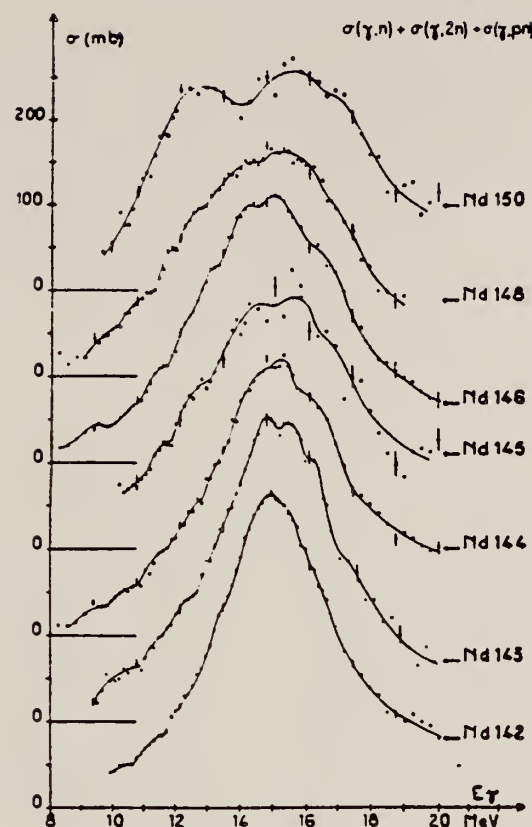


Fig. 9. Total photonuclear cross-section σ_T of neodymium isotopes. The full line drawn through the experimental points is merely meant to facilitate the identification of structure.

ND
A=150

ND
A=150

ND
A=150

Method 33 MeV Synchrotron; radioactivity; NaI spectrometer; ionization chamber

Ref. No.	59 Ca 3	EH
----------	---------	----

Reaction	E or ΔE	E_0	Γ	$\int \sigma dE$	$J\pi$	Notes
$Nd^{150}(\gamma, n)$	Bremss. $\sim 8-32$	13.2	5.7 MeV			

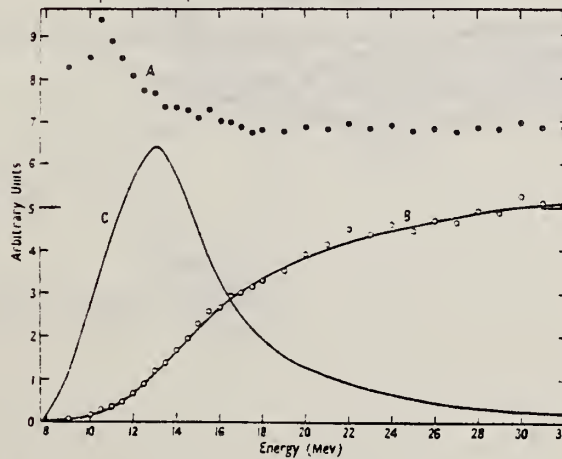


Figure 4. A, the ratio of activation curves $^{150}\text{Nd}(\gamma, n)/^{181}\text{Ta}(\gamma, n)$; B, activation curve for $^{150}\text{Nd}(\gamma, n)$; C, derived cross section: $^{150}\text{Nd}(\gamma, n)$.

ELEM. STM.	A	C
Nd	150	60

METHOD

REF. NO.	egf
69 Va 2	

REACTION	RESULT	EXCITATION ENERGY	SOURCE		DETECTOR		ANGLE
			TYPE	RANGE	TYPE	RANGE	
G,XN	ABX	8-23	C	8-23	BF3-I		4PI

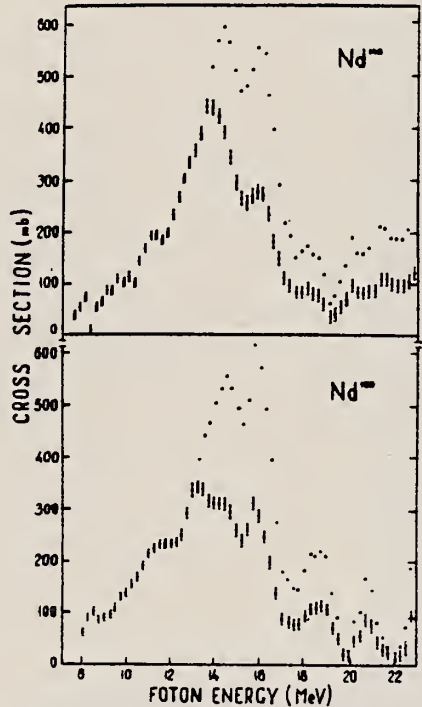
309+

Fig. 2. The photoneutron cross section $\sigma(\gamma, n)$ and the photoabsorption cross sections σ_{tot} for ^{148}Nd and ^{150}Nd . The σ_{tot} are represented by dots. At the energies where σ_{tot} and $\sigma(\gamma, n)$ differ, the latter is represented by circles. Only statistical errors of σ_{tot} are plotted.

ELEM.	SYM.	A	Z
Nd		150	60

METHOD

REF. NO.

69 Va 3

egf

REACTION	RESULT	EXCITATION ENERGY	SOURCE		DETECTOR		ANGLE
			TYPE	RANGE	TYPE	RANGE	
G,XN	ABX	8-22	C	8-22	BF3-I		4PI

239+ SEE 69VA2

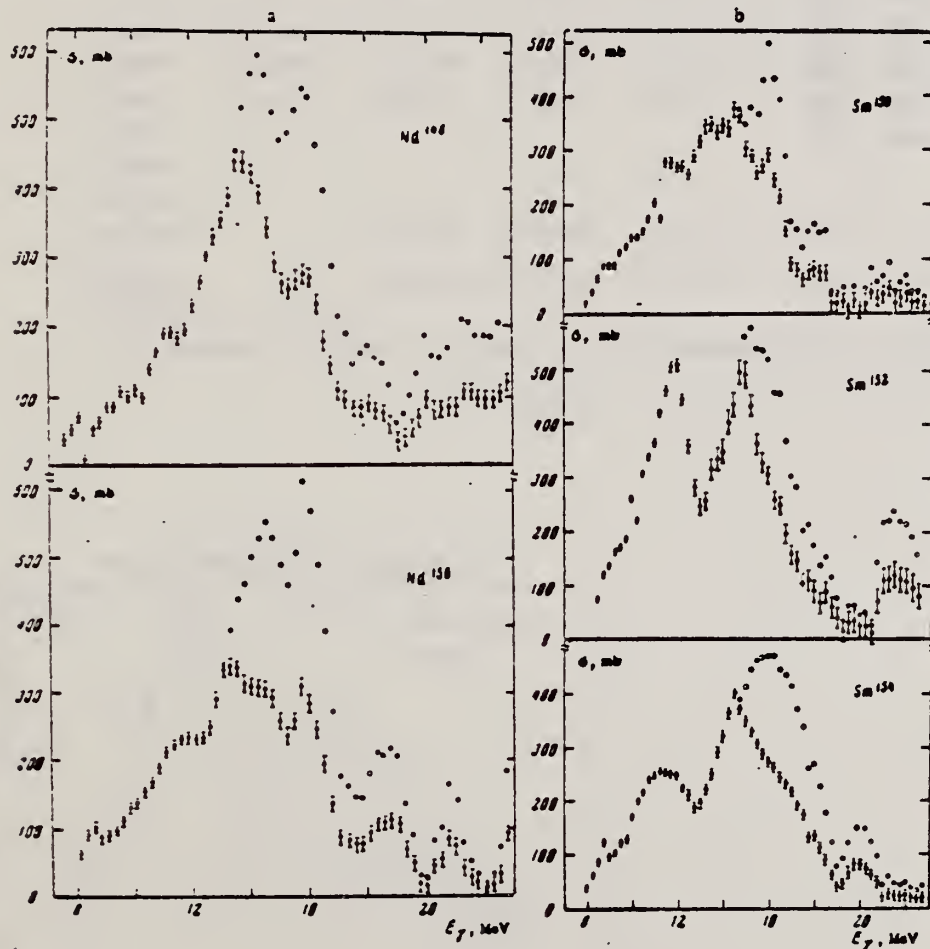


FIG. 2. Photoabsorption cross sections (black points) and photoneutron cross sections (light points): a — for Nd¹⁴⁴ and Nd¹⁵⁰ and b — for Sm¹⁵⁰, Sm¹⁵², and Sm¹⁵⁴. The indicated errors are statistical.

[over]

Table I. Giant resonance parameters of Nd^{148,150}
and Sm^{150,152,154}

Parameter	Nucleus				
	Nd ¹⁴⁸	Nd ¹⁵⁰	Sm ¹⁵⁰	Sm ¹⁵²	Sm ¹⁵⁴
σ_0 , mb		160.0		400.0	204.0
$\Delta\omega_0$, MeV		11.25		11.58	11.00
$\Delta\Gamma_0$, MeV		3.0		2.4	3.0
σ_0^{148} , MeV·mb		0.750		1.319	0.961
σ_0 , mb		270.0		420.0	220.0
$\Delta\omega_0$, MeV		14.50		14.65	15.25
$\Delta\Gamma_0$, MeV		4.0		3.4	4.0
σ_0^{150} , MeV·mb		1.695		2.242	2.01
$\sigma_0^{150}/\sigma_0^{148}$		2.28		1.7	2.09
σ_0^{150} , MeV·mb	2.406	2.213	2.213	3.079	2.478
$0.06 NZ/A$	2.160	2.160	2.162	2.203	2.222
ρ_0		0.32		0.20	0.41
β_0^G		0.28		0.30	0.35
σ_0 , mb	420		360		
$\Delta\omega_0$, MeV	13.65		13.6		
$\Delta\Gamma_0$, MeV	5.0		5.5		

REF.

P. Carlos, H. Beil, R. Bergere, A. Lepretre, A. Veyssiére
 Nucl. Phys. A172, 437 (1971)

ELEM. SYM.	A	Z
Nd	150	60

METHOD

REF. NO.

71 Ca 1

egf

REACTION	RESULT	EXCITATION ENERGY	SOURCE		DETECTOR		ANGLE
			TYPE	RANGE	TYPE	RANGE	
G, N 409	ABX	10-20	D	8-20	MOD-I		4PI
G, 2N 410 +	ABX	10-20	D	8-20	MOD-I		4PI

409+

TABLE 2

Parameters of the one- or two-Lorentz line fits to the σ_T curves for neodymium isotopes: parameters for Ce and Er extracted from earlier results ¹³⁾ are also shown

Ce	¹⁴² Nd	¹⁴³ Nd	¹⁴⁴ Nd	¹⁴⁵ Nd	¹⁴⁶ Nd	¹⁴⁸ Nd	¹⁵⁰ Nd	Er	
σ_1 (mb)	360 \pm 15	359 \pm 15	360 \pm 15	317 \pm 15	297 \pm 20	308 \pm 16	263 \pm 15	174 \pm 20	225 \pm 15
Γ_1 (MeV)	4.35 \pm 0.05	4.43 \pm 0.20	4.5 \pm 0.2	5.3 \pm 0.25	6.5 \pm 0.4	6 \pm 0.3	7.2 \pm 0.3	3.3 \pm 0.1	2.9 \pm 0.05
E_1 (MeV)	15.0 \pm 0.10	14.95 \pm 0.1	15 \pm 0.1	15.05 \pm 0.1	15 \pm 0.15	14.8 \pm 0.1	14.7 \pm 0.15	12.3 \pm 0.15	12.00 \pm 0.1
σ_2 (mb)								223 \pm 20	260 \pm 15
Γ_2 (MeV)								5.2 \pm 0.15	5.0 \pm 0.05
E_2 (MeV)								16 \pm 0.15	15.45 \pm 0.1
$\frac{1}{2}\pi\sigma\Gamma$ MeV · b		2.5 \pm 0.2	2.54 \pm 0.2	2.6 \pm 0.2	3.0 \pm 0.3	2.9 \pm 0.2	3.0 \pm 0.2	2.7 \pm 0.3	
$\frac{1}{2}\pi\sigma\Gamma$		1.20 \pm 0.10	1.22 \pm 0.10	1.25 \pm 0.10	1.4 \pm 0.15	1.35 \pm 0.10	1.4 \pm 0.1	1.27 \pm 0.15	
0.06 NZA^{-1}									

¹³⁾ R. Bergere, H. Beil, P. Carlos et A. Veyssiére, Nucl. Phys. A133, 417 (1969).

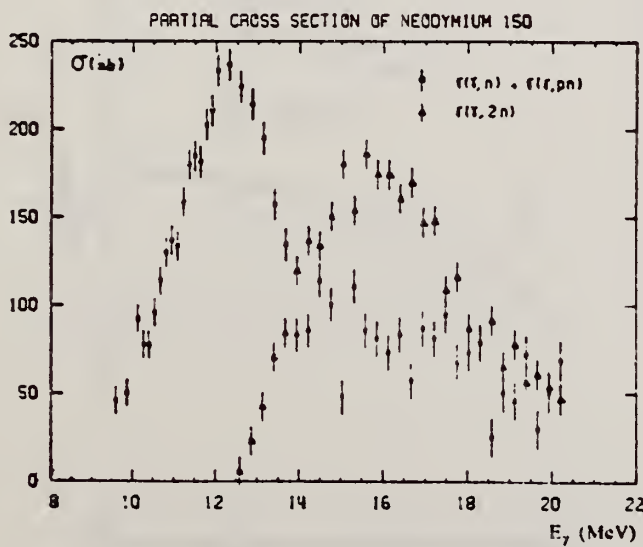


Fig. 8. Partial photoneutron cross sections $\sigma(\gamma; n)$ and $\sigma(\gamma; 2n)$ of ¹⁵⁰Nd.

(over)

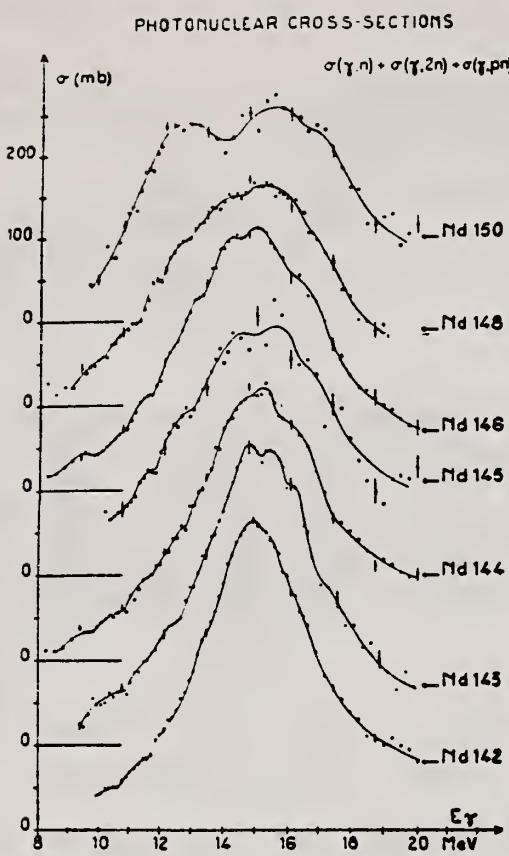


Fig. 9. Total photonuclear cross-section σ_T of neodymium isotopes. The full line drawn through the experimental points is merely meant to facilitate the identification of structure.

METHOD				REF. NO.	
REACTION	RESULT	EXCITATION ENERGY	SOURCE	DETECTOR	ANGLE
			TYPE RANGE	TYPE RANGE	
E,E/	FMF	0	D 60	MAG-D	DST

0 = 0.13

TABLE II
 A comparison of this experiment's $B(E2\uparrow)$ values with those of other experiments and theory

Nucleus	State (MeV)	This work	Pulsed beam	Heavy particle Coulomb excitation	Theory
2+ states					
^{142}Nd	1.57	13.1 ± 1.7		$25.0 \pm 7.3^a)$ $19.1 \pm 2.3^b)$ $15.5 \pm 7.8^c)$	$16.4^d)$ $16.3^e)$
^{142}Nd	2.09	4.1 ± 1.1			
^{144}Nd	0.45	30.9 ± 4.6		$28.5 \pm 0.4^b)$ $28.1 \pm 6.6^d)$	$92.1^d)$
^{150}Nd	0.13	62.9 ± 10.5	$113.9 \pm 1.8^f)$ $116.8 \pm 3.2^g)$ $112.4 \pm 5.1^h)$	$112.7 \pm 4.2^l)$	
3- state					
^{142}Nd	2.09	28.6 ± 5.0		$52 \pm 21^j)$	

^a) Ref. ³⁹). ^b) Ref. ⁴⁰). ^c) Ref. ⁴¹). ^d) Ref. ³⁷). ^e) Ref. ⁴²). ^f) Ref. ⁴³).

^g) Ref. ⁴⁴). ^h) Ref. ⁴⁵). ⁱ) Ref. ³⁸). ^j) Ref. ³³.

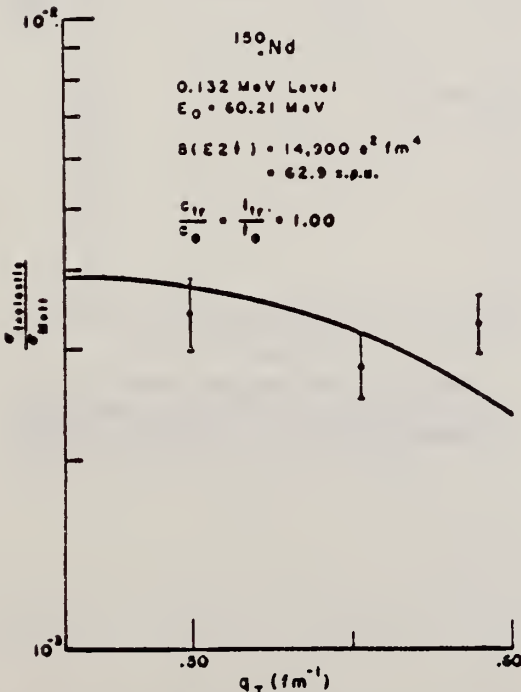


Fig. 17. Inelastic form factors for the 132 keV, 2+ level in ^{150}Nd as a function of inelastic momentum transfer. The experimental points are the results of this experiment while the solid line traces out the best fit provided by parameters shown.

ELEM. SYM.	A	z
Nd	150	60
REF. NO.	75 Sc 2	egf

METHOD

REACTION	RESULT	EXCITATION ENERGY	SOURCE	DETECTOR	ANGLE
			TYPE RANGE	TYPE RANGE	
E, E/	NOX	5- 28	D 50, 64	MAG-D	93
			-		

E.E/SPECTRUM (E2)

Inelastic electron scattering has been used to study the isoscalar E2 giant resonances in ^{142}Nd and ^{150}Nd , which were found at excitation energies of 12.0 and 11.2 MeV with total widths of 2.8 and 5.0 MeV, respectively. The energy shift and the larger width in ^{150}Nd indicate a splitting due to the deformation of ^{150}Nd .

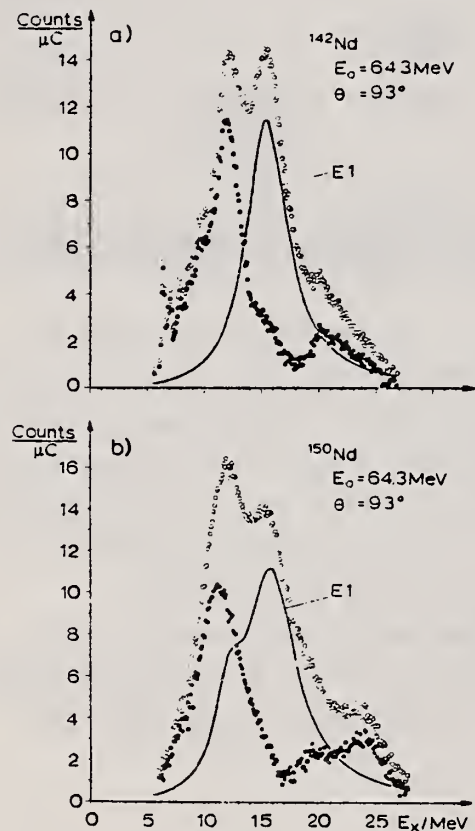


Fig. 1. Spectrum of inelastically scattered electrons after subtraction of radiation tail and background, a) ^{142}Nd , b) ^{150}Nd (open circles). Solid line: E1 cross section. Full circles: E1 cross section subtracted. The total number of counts/ μC in the region of the giant resonances is about 100.

ELEM. SYM.	A	Z
Nd	150	60

METHOD

REF. NO.
 78 Cr 1 hg

REACTION	RESULT	EXCITATION ENERGY	SOURCE		DETECTOR		ANGLE
			TYPE	RANGE	TYPE	RANGE	
E, E/	ABX	850*931	D	1*2	MAG-D		UKN

Recent electron scattering results on the 0.850 MeV level of ^{150}Nd , when analyzed in terms of the interacting boson model, are inconsistent with the interpretation of this level as a pure $J^\pi(K) = 2^+(0)$ state. Very recent ($n, n'\gamma$) work has shown this level to be a $1^-, 2^+$ doublet. Assuming this level to be the band-head of a "K" = 0⁻ octupole band, a simple model is used to predict electron scattering form factors for the 0.850 MeV state and a 3⁻ octupole level observed at 0.931 MeV. Comparison is made between these predicted form factors and recent electron scattering data.

*E KEV; Q .8-2. FM-1

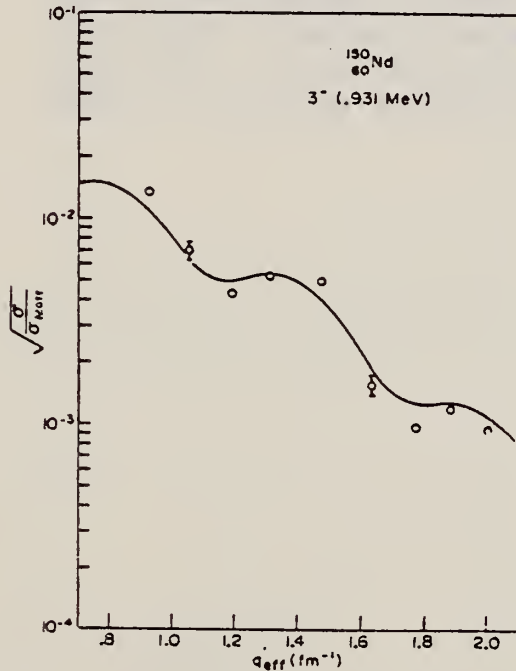


Fig. 2. Electron scattering form factor for the 3⁻ (0.931 MeV) state in ^{152}Nd . The curve represents a calculation in which the 3⁻ excitation is modeled as a small amplitude collective surface oscillation.

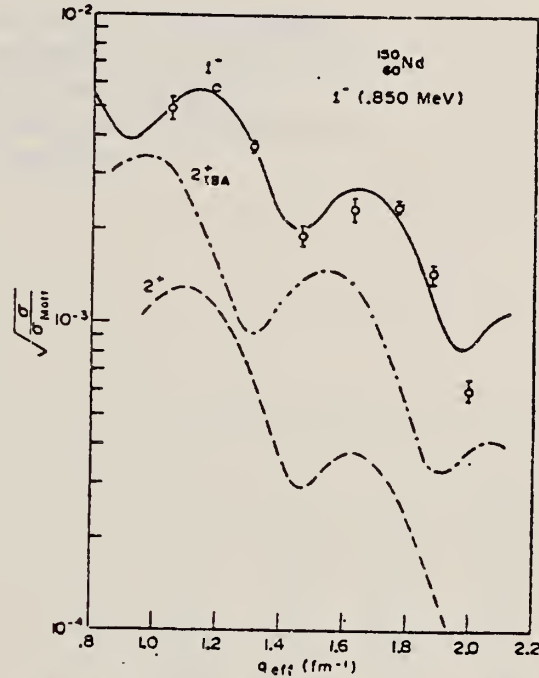


Fig. 3. Electron scattering form factor for the 0.850 MeV state in ^{150}Nd . The solid curve results from a calculation in which the state is represented as a $J^\pi(K) = 1^-(0)$ octupole surface oscillation belonging to the same band as the 3⁻ (0.931 MeV). The dashed curve is due to a calculation in which the state is represented as a $J^\pi(K) = 2^+(0)$ surface oscillation and the dot-dash curve represents the IBA 2⁺ prediction.

SAMARIUM
Z=62

Samarium's discovery is generally credited to Boisbaudran who in 1879 isolated "samaria" from "didymia", a mixture of rare earths from which cerium and lanthanum had been extracted. It was identified by its spectrum and named in honor of a Russian engineer, Col. M. Samarski.

SM

CLEM. SYM.	A	Z
Sm		62

METHOD
 Betatron; ion chamber

REF. NO.
 58 Fu 1 NVB

REACTION	RESULT	EXCITATION ENERGY	SOURCE		DETECTOR		ANGLE
			TYPE	RANGE	TYPE	RANGE	
G, XN	ABX	7-40	C	7-40	BF ₃ -I		4PI
							/

CF DANØS THEORY

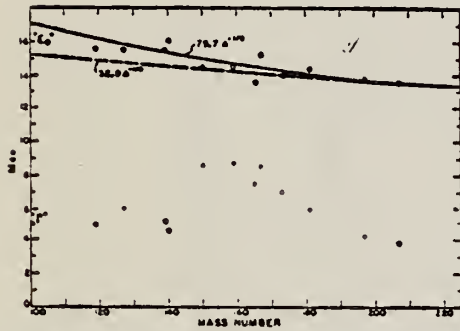


FIG. 6. Mean energy and width of giant resonances. "E₀" and "Γ" are the mean energy for photon absorption and the full width at half maximum of the giant resonance obtained from dashed histograms as in Fig. 5. No attempt was made to fit data with resonance curves to obtain these parameters.

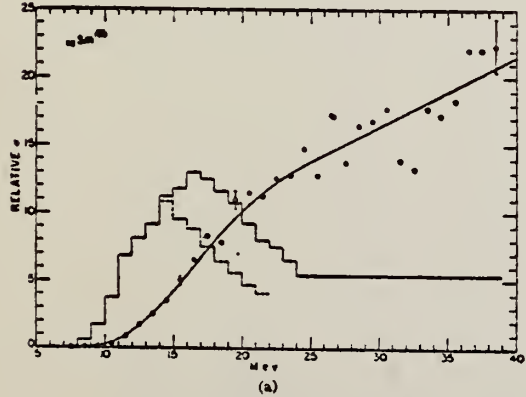


FIG. 5. Relative photoneutron production cross sections for tin, iodine, samarium, holmium, erbium, and lead. The points and smooth curves represent the integral neutron-production cross section defined by $\int_0^\infty \sigma_{Tn}(E) dE$, where $\sigma_{Tn}(E) = \sigma(\gamma, n) + 2\sigma(\gamma, 2n) + \sigma(\gamma, 3n) + \dots$. The scales are normalized to give approximately the same total neutron yield at 40 Mev. The errors indicated were obtained by propagating the statistical uncertainties, (\sqrt{n}) , in the original activation curve data through the integral cross section matrix. Solid histograms represent first differences of integral cross section curves. Dashed histograms show result of correcting for neutron multiplicity above the $(\gamma, 2n)$ threshold.

TABLE I. Target properties and results.

Element	Form used	Weight grams	$\sigma^*(\gamma, n)^*$ barns	$S_{ed} E^*$ NZ/A Mev-b	"Γ"** Mev
Sn	Sn	4.81	0.30	0.064	5.0
I	I	8.55	0.36	0.085	6.0
La	La	10.43	0.34	0.063	5.2
Ce	Ce	4.99	0.45	0.080	4.5
Sm	Sm ₂ O ₃	2.90	0.26	0.073	8.6
Tb	Tb ₂ O ₃	3.04	0.39	0.087	8.7
Ho	Ho ₂ O ₃	1.87	0.41	0.079	7.5
Er	Er ₂ O ₃	5.41	0.50	0.100	8.3
Yb	Yb ₂ O ₃	5.57	0.50	0.090	7.0
Ta	Ta	8.41	0.49	0.077	6.0
Au	Au	3.16	0.68	0.085	4.2
Pb	Pb	8.05	0.75	0.081	3.8

* $\sigma^*(\gamma, n)$ is the maximum value and "Γ" is the full width at $\sigma^*(\gamma, n)/2$ of the neutron production cross section corrected for multiple neutron emission. Data were not fitted with resonance lines to determine these values.

** Integrated neutron production cross sections corrected for multiple neutrons above $(\gamma, 2n)$ threshold.

REF.

F. I. Havlicek
 Nuovo Cimento 13, 969-73 (1959)

ELEM. SYM.	A	Z
Sm		62

METHOD

Betatron

REF. NO.

59 Ha 2

NVB

REACTION	RESULT	EXCITATION ENERGY	SOURCE		DETECTOR		ANGLE
			TYPE	RANGE	TYPE	RANGE	
G,A	SPC	THR - 30	C	30	EMU-D	1-5	DST

Ref.

B. Radha, A.Z. Mousa
Phys. Rev. 118, 701 (1960)

Elem. Sym.	A	Z
Sm		62

Method

Ref. 60 Re 1 JHH

γ 's from $\gamma^{19}(\rho, \pi\gamma)$ reaction; protons from Van de Graaff; Bal.

Reaction	E or ΔE	E_0	Γ	$\int \sigma dE$	$J\pi$	Notes
(γ, γ)	~ 7					$\langle \bar{\sigma} \rangle (E_p = 2.05 \text{ MeV}) = < 0.67 \text{ mb}$

Method (n,γ) reaction; NaI(Tl)						Ref. No.
						62 Be 2
Reaction	E or ΔE	E _o	Γ	∫ σ dE	J π	Notes
Sm(γ,γ)	5.44 - 8.997	8.997			σ_t 1 mb Detector at 135°.	γ source Ni

B. Arad (Huebschmann), G. Ben-David (Davis) I. Pelah,
 Y. Schlesinger
 Phys. Rev. 133, B684-700 (1964)

ELEM. SYM.	A	Z
Sm		62

METHOD

Reactor, (n,γ) reactions source

REF. NO.

64 Ar 1

NVB

REACTION	RESULT	EXCITATION ENERGY	SOURCE		DETECTOR		ANGLE
			TYPE	RANGE	TYPE	RANGE	
G,G	ABX	9	D	9	NAI-D		135
		(8.997)		(8.997)			

TABLE II. Capture gamma-ray sources and their properties.*

Source	Chemical composition	Mass kg	Principal γ rays (in MeV)
Al	Metal	1.640	7.73
Cl	polyvinyl Chloride	0.380	8.55, 7.78, 7.41, 6.96, 6.64, 6.12, 5.72
Co	CoO	0.230	7.49, 7.20, 6.98, 6.87, 6.68, 6.48, 5.97, 5.67
Cr	Metallic powder	0.480	9.72, 8.88, 8.49, 7.93, 7.09, 6.65, 5.60
Cu	Metal	1.860	7.91, 7.63, 7.29, 7.14, 7.00, 6.63
Fe	Metallic powder	0.440	9.30, 7.64, 7.28, 6.03
Hg	Hg ₂ (NO ₃) ₂ ·2H ₂ O	0.310	6.44, 6.31, 5.99, 5.67, 5.44
Mn	MnO ₂	0.240	7.26, 7.15, 7.04, 6.96, 6.79, 6.10, 5.76
Ni	Metal	0.900	9.00, 8.50, 8.10, 7.83, 7.58, 6.84, 6.64
Ti	TiO ₂	0.210	6.75, 6.56, 6.42
V	V ₂ O ₅	0.120	7.30, 7.16, 6.86, 6.51, 6.46, 5.87, 5.73
Y	Y ₂ O ₃	0.200	6.07, 5.63

* For more detailed information, additional lines, intensities, etc., see Ref. 6.

TABLE III. Effective cross sections.

γ source	Energy (MeV)	Element	Protons	Scatterer	Neutrons	$\langle\sigma_{\gamma\gamma}\rangle$ (mb)	Notes
Hg	5.44	Hg	80	116, 118, 119, 120, 121, 122, 124		128	
Cl	6.12	Pr ¹⁴¹	59	82		103	a
V	6.508	Sn	50	62, 64-70, 72		14	
Co	6.690	Pr ¹⁴¹	59	82		2.7	a
Co	6.867	Nd	60	82, 83, 84, 85, 86, 88		22	
Al	6.98	Pb ²⁰⁸	82	126		2900	b
Cl	6.98	Pb	82	124, 125, 126		346	a
Ti	6.996	Bi ²⁰⁸	83	126		1560	b
Cu	7.01	Sn	50	62, 64-70, 72		1000	b
Ti	7.149	Pb ²⁰⁸	82	126		1000	b
Co	7.201	Pb ²⁰⁸	53	126		25	
Mn	7.261	Pb ²⁰⁸	82	126		25	a
Fe	7.285	Pb ²⁰⁸	82	126		4100	a
V	7.305	Pb ²⁰⁸	82	126		12.5	
Hg	7.32	Pb	82	124, 125, 126		5500	c
Fe	7.639	Ni	28	30, 32, 34, 36		10.5	d
Fe	7.639	Pr ¹⁴¹	59	82		10	d
Cr	8.499	Cu	29	34, 36		24.4	
Cr	8.881	Pr ¹⁴¹	59	82		9.3	
Ni	8.997	Sm	62	82, 85-88, 90, 92		2.8	

* A large error could be introduced in the cross-section values because of large differences in line intensities quoted by Bartholomew and Higgs and by Groshev *et al.* (Ref. 6).b Because of the low counting rate, thick scatterers were used, which will introduce a systematic error in estimating $\langle\sigma_{\gamma\gamma}\rangle$ for resonances having a high nuclear cross section.

c The cross section was evaluated assuming the gamma intensity to be 0.02 photons per 100 captured neutrons (see text).

d Reference 6 gives the 7.639 line of iron capture gamma rays as a single line. However, a recent paper by Fiebig, Kano, and Segel [Phys. Rev. 125, 2031 (1962)] reports two different lines of equal intensities having energies of 7.647 and 7.633 MeV. The present experiment cannot resolve an energy difference of 14 keV, therefore, there is no possibility of deciding which line is responsible for the scattering.

ELEM. SYM.	A	Z
Sm		62

REF. NO.		
69 Be 6		egf

REACTION	RESULT	EXCITATION ENERGY	SOURCE		DETECTOR		ANGLE
			TYPE	RANGE	TYPE	RANGE	
G, N 478+	ABX	7-21	D	7-27	MOD-I		4PI
G, 2N 479	ABX	13-25	D	7-27	MOD-I		4PI
G, 3N 480	ABX	23-27	D	7-27	MOD-I		4PI

x = fraction of total cross section resulting in a direct neutron 478+

n_d = fraction of neutrons emitted by direct effect at an energy where all the evaporation neutrons go to $(\gamma, 2n)$ cross section

$$n_d = x/(2-x)$$

TABLEAU 3
Moments quadrupolaires intrinsèques

Cible	% isotopes	a/b ex	β_2 ex	$\beta_2[B(E_2)]$	Q_0 ex (b)	Q'
^{133}I	100 % ^{127}I	0.85	0.172		-2.3 ± 0.4	
^{148}Ce	88.5 % ^{140}Ce 11.1 % ^{142}Ce			0.104 0.118		
^{145}Sm	15 % ^{147}Sm 11.2 % ^{148}Sm 13.8 % ^{149}Sm 7.5 % ^{150}Sm 26.6 % ^{152}Sm 22.5 % ^{154}Sm	1.23	0.219	0.190 0.304 0.351	4.5 ± 0.4	0.158 3.53 5.93 6.58
^{168}Er	33.4 % ^{166}Er 22.9 % ^{167}Er 27.1 % ^{168}Er 14.9 % ^{170}Er	1.314	0.288	0.341 0.339 0.329	6.96 ± 0.4	7.60 7.80 7.60 7.45
^{171}Lu	97.4 % ^{173}Lu	1.282	0.262		6.95 ± 0.3	7.20

TABLEAU 5
Valeurs de la température nucléaire et du paramètre a de densité des niveaux

	x	n_d	Θ (MeV)	$E'_{\gamma} - E_n$ (MeV)	a (MeV $^{-1}$)	a' (MeV $^{-1}$)	a'' (MeV $^{-1}$)
I	0.05 ± 0.005	0.03 ± 0.03	1.30 ± 0.20	10	6 ± 2.5	10 ± 3	10 ± 2
^{140}Ce ^{142}Ce	0.21 ± 0.05	0.12 ± 0.03	1.05 ± 0.20 0.8 ± 0.20	10 6	9 ± 3.5 9 ± 4		7 ± 3 8 ± 3
Sm	0.18 ± 0.04	0.10 ± 0.03					
Er	0.20 ± 0.05	0.11 ± 0.03					(12 ± 4)
Lu	0.26 ± 0.06	0.15 ± 0.03	0.85 ± 0.1	9	12.5 ± 2.5		15 ± 3

[over]

TABLEAU 4
Règles de somme

Noyau cible (éléments naturels)	σ_0 (MeV · b)	σ'_0 (MeV · b)	$0.06 \frac{NZ}{A}$	$\frac{\sigma_0 A}{0.06 NZ}$	$\frac{\sigma'_0 A}{0.06 NZ}$	σ_{-1} (mb)	$\sigma_{-1} A^{-1}$	σ_{-2} (mb · MeV ⁻¹)	$\sigma_{-2} A^{-1}$
^{53}I	2.02 ± 0.14	2.30 ± 0.12	1.85	1.09 ± 0.07	1.24 ± 0.07	129 ± 0.10	0.20 ± 0.02	8.6 ± 0.6	2.7 ± 0.2
^{58}Cr	2.13 ± 0.15	2.53 ± 0.13	2.04	1.05 ± 0.07	1.24 ± 0.07	140 ± 0.12	0.19 ± 0.02	9.5 ± 0.6	2.5 ± 0.2
^{62}Sm	2.48 ± 0.17	2.92 ± 0.14	2.18	1.14 ± 0.07	1.34 ± 0.07	167 ± 0.14	0.21 ± 0.02	11.8 ± 0.8	2.75 ± 0.2
^{68}Er	2.70 ± 0.19	3.04 ± 0.16	2.42	1.12 ± 0.07	1.26 ± 0.07	186 ± 0.15	0.20 ± 0.02	13.6 ± 1	2.7 ± 0.2
^{71}Lu	2.65 ± 0.18	2.96 ± 0.16	2.53	1.05 ± 0.07	1.17 ± 0.07	182 ± 0.15	0.185 ± 0.02	12.9 ± 1	2.35 ± 0.2
valeur moyenne pour ces 5 corps				1.09 ± 0.07	1.25 ± 0.07		0.20 ± 0.02		2.6 ± 0.2

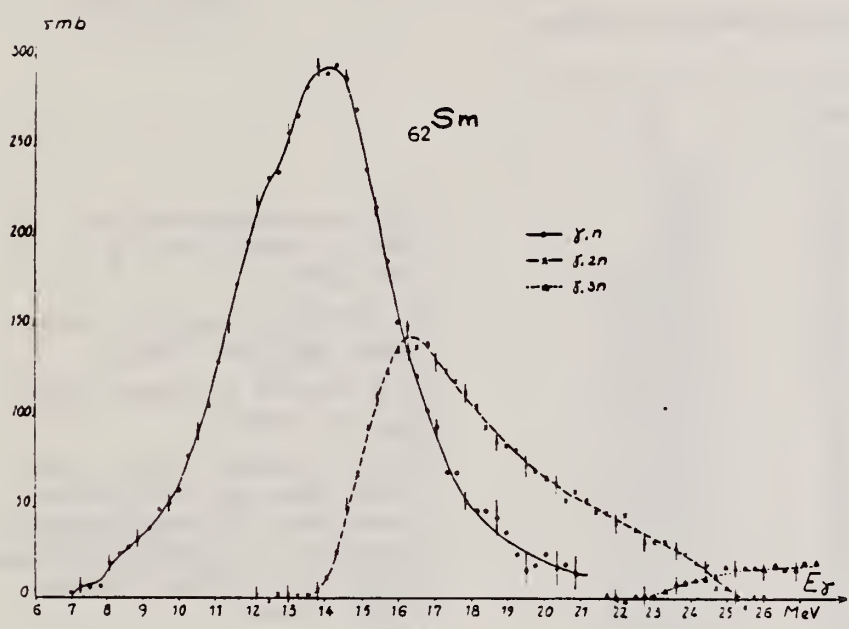


Fig. 5.

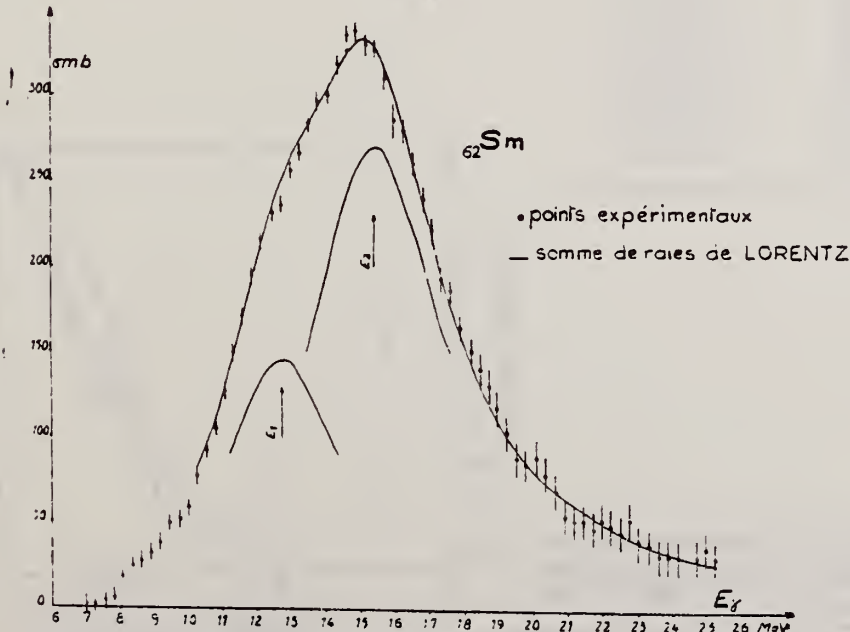


Fig. 6.

ELEM. SYM.	A	Z
Sm		62

METHOD

REF. NO.

76 Em 2

egf

REACTION	RESULT	EXCITATION ENERGY	SOURCE		DETECTOR		ANGLE
			TYPE	RANGE	TYPE	RANGE	
G, F	ABY	THR-999	C	999	TRK-I		4PI

TABLE I

Measured values of σ_q at $E = 1000$ MeV and deduced values of σ_k assumed constant from E_0 to 1000 MeV999 = 1 GEV

Element	Z^2/A	σ_q (mb)	E_0 (MeV)	σ_k (mb)
Bi	32.96	12.3 ± 0.6	200	7.6 ± 0.6
Pb	32.45	5.4 ± 0.4	220	3.6 ± 0.3
Tl	32.10	4.1 ± 0.3	230	2.8 ± 0.3
Au	31.68	2.0 ± 0.15	240	1.4 ± 0.2
Pt	31.18	1.1 ± 0.08	255	$(8 \pm 0.7) \times 10^{-1}$
Re	30.21	$(3.7 \pm 0.3) \times 10^{-1}$	280	$(2.9 \pm 0.3) \times 10^{-1}$
W	29.78	$(3.5 \pm 0.3) \times 10^{-1}$	290	$(2.8 \pm 0.3) \times 10^{-1}$
Ta	29.45	$(3.3 \pm 0.3) \times 10^{-1}$	300	$(2.7 \pm 0.3) \times 10^{-1}$
Hf	29.04	$(1.7 \pm 0.2) \times 10^{-1}$	310	$(1.4 \pm 0.2) \times 10^{-1}$
Yb	28.31	$(1.3 \pm 0.1) \times 10^{-1}$	330	$(1.2 \pm 0.1) \times 10^{-1}$
Tm	28.18	$(7.5 \pm 0.8) \times 10^{-2}$	335	$(6.8 \pm 0.8) \times 10^{-2}$
Ho	27.21	$(3.6 \pm 0.4) \times 10^{-2}$	355	$(3.5 \pm 0.4) \times 10^{-2}$
Dy	26.80	$(2.6 \pm 0.3) \times 10^{-2}$	360	$(2.5 \pm 0.3) \times 10^{-2}$
Tb	26.58	$(2.5 \pm 0.3) \times 10^{-2}$	370	$(2.5 \pm 0.3) \times 10^{-2}$
Gd	26.04	$(1.6 \pm 0.2) \times 10^{-2}$	380	$(1.7 \pm 0.2) \times 10^{-2}$
Sm	25.56	$(1.3 \pm 0.2) \times 10^{-2}$	390	$(1.4 \pm 0.2) \times 10^{-2}$
Nd	24.96	$(9.2 \pm 0.9) \times 10^{-3}$	405	$(1 \pm 0.1) \times 10^{-2}$
Ce	24.00	$(8 \pm 0.9) \times 10^{-3}$	420	$(9 \pm 1) \times 10^{-3}$
La	23.39	$(8.4 \pm 0.9) \times 10^{-3}$	430	$(1 \pm 0.1) \times 10^{-3}$
Sb	21.36	$(1.2 \pm 0.2) \times 10^{-2}$	460	$(1.5 \pm 0.3) \times 10^{-2}$
Te	21.19	$(8.8 \pm 1) \times 10^{-3}$	465	$(1.2 \pm 0.2) \times 10^{-2}$
Sn	21.06	$(1.3 \pm 0.2) \times 10^{-2}$	465	$(1.7 \pm 0.3) \times 10^{-2}$
Cd	20.49	$(1.7 \pm 0.3) \times 10^{-2}$	470	$(2.2 \pm 0.4) \times 10^{-2}$
Ag	20.47	$(2 \pm 0.3) \times 10^{-2}$	470	$(2.6 \pm 0.4) \times 10^{-2}$
Zn	13.76	$(2 \pm 0.4) \times 10^{-1}$	515	$(3 \pm 0.6) \times 10^{-1}$
Cu	13.44	$(2.4 \pm 0.5) \times 10^{-1}$	515	$(3.6 \pm 0.8) \times 10^{-1}$
Ni	13.35	$(2.4 \pm 0.5) \times 10^{-1}$	510	$(3.6 \pm 0.8) \times 10^{-1}$
Fe	12.10	$(3 \pm 0.6) \times 10^{-1}$	510	$(4.4 \pm 0.9) \times 10^{-1}$

⁴ A.V. Mitrofanova et al.
Sov. J. Nucl. Phys. 6,
512 (1968).

⁷ T. Methasiri et al., Nucl.
Phys. A167, 97 (1971).

¹² J.R. Nix et al., Nucl. Phys.
81, 61 (1966).

²⁰ N.A. Perifilov et al., JETP
(Sov. Phys.) 14, 623 (1962);
Proc. Symp. on the physics &
chemistry of fission, Salzburg
1965, vol. 2 (IAEA) Vienna,
1965, p. 283.

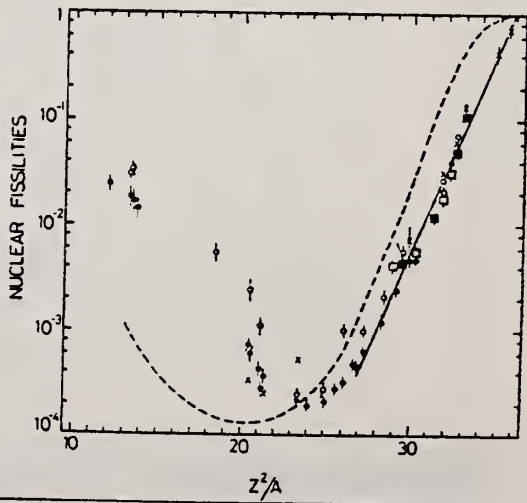


Fig. 2. Nuclear fission cross-sections as a function of Z^2/A . Experimental points: solid circles represent our data; squares, the data from ref. ⁴; open circles, the data from ref. ⁷; and crosses, the data from (p,f) experiments¹⁰). The straight line is the best fit calculated from our data for $Z^2/A > 26$. The dashed curve is the curve VI calculated by Nix and Sassi¹².

SM
A=144

SM
A=144

SM
A=144

ELEM. SYM.	A	Z
Sm	144	62

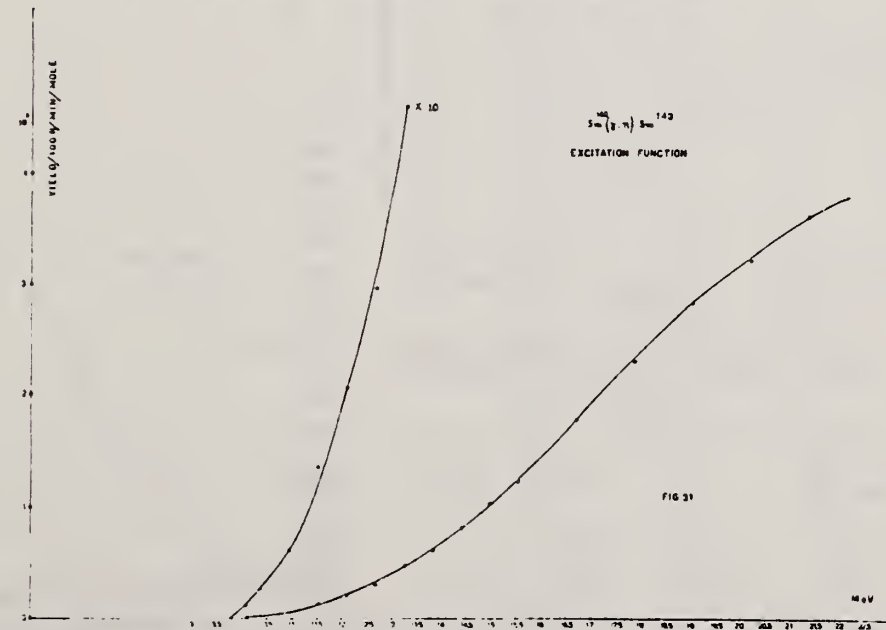
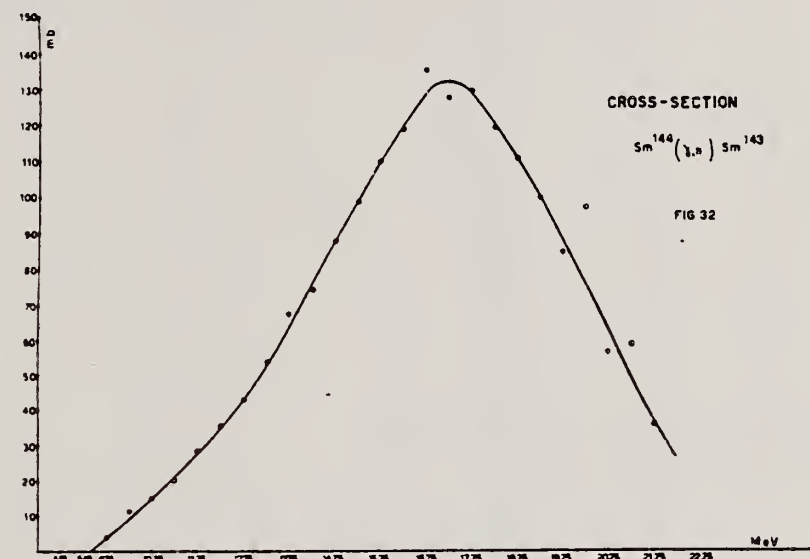
METHOD Betatron; neutron yield; radioactivity; r-chamber

REF. NO.

55 De 1

EGF

REACTION	RESULT	EXCITATION ENERGY	SOURCE		DETECTOR		ANGLE
			TYPE	RANGE	TYPE	RANGE	
G, N	ABX	9-23	C	9-23	ACT-I		4PI



Elem. Sym.	A	Z
Sm	144*	62

Method	Betatron; radioactivity					Ref. No.	
Reaction	E or ΔE	E_0	Γ	$\int \sigma dE$	$J\pi$	Notes	
$\text{Sm}^{144}(\gamma, n)$	22	17.25	6.8	$\int_{8.7}^{22} = 0.91 \text{ MeV-b}$		$E_{th} = 9.6 \text{ MeV}; \sigma = 135 \text{ mb.}$	* Some question as to isotope.

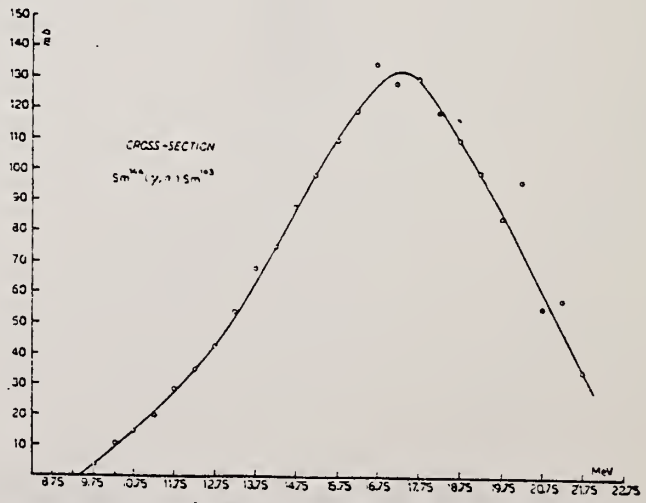


Fig. 3. - Cross section for the reaction $^{144}\text{Sm}(\gamma, n)^{143}\text{Sm}$.

Elem. Sym.	A	Z
Sm	144	62

Method 35 MeV Synchrotron; radioactivity; NaI spectrometer; r chamber

Ref. No.
59 Ca 3

EH

Reaction	E or ΔE	E_0	Γ	$\int \sigma dE$	$J\pi$	Notes
$^{144}\text{Sm}(\gamma, n)$	Bremss. 10-32	15.3	4.0 MeV	$2.5 \pm 0.4 \text{ MeV-b}$		

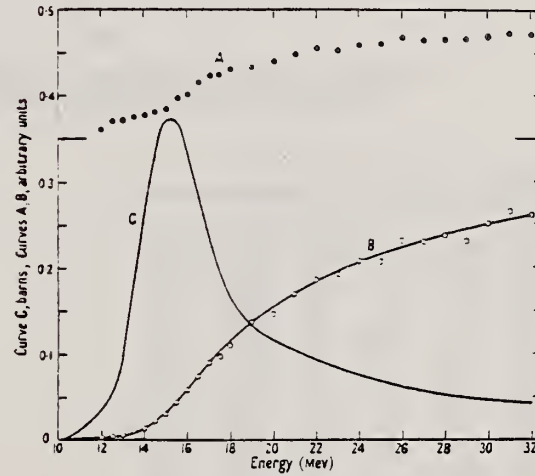


Figure 9. A, the ratio of activation curves $^{144}\text{Sm}(\gamma, n)/^{181}\text{Ta}(\gamma, n)$; B, activation curve for $^{144}\text{Sm}(\gamma, n)$; C, derived cross section: $^{144}\text{Sm}(\gamma, n)$.

Table 2

Activity	$T_{1/2}$ (min)	W_0 (MeV)	K/β^+	$\frac{K\text{-capture}}{\text{Total capture}}$	W_K
^{140}Pr	3.4	3.25	0.63	0.89	0.89
^{141}Nd	150	1.80	48	0.89	0.90
^{142}Sm	8.5	3.47	0.60	0.89	0.91

REF.

G. Di Caporiacco, M. Mandò, and F. Ferrero
 Nuovo Cimento 13, 522 (1959)

ELEM. SYM.	A	Z
Sm	144	62

METHOD

Betatron; ion chamber

REF. NO.

59 Di 1

NVB

REACTION	RESULT	EXCITATION ENERGY	SOURCE		DETECTOR		ANGLE
			TYPE	RANGE	TYPE	RANGE	
G, N	RLY	11-30	C	22,30	ACT-I		4PI

REL TO CU63 (G,N)

Yield ratios: $\frac{^{144}\text{Sm}(\gamma, n)}{^{141}\text{Pr}(\gamma, n)}$ = 1.088

$$\frac{^{141}\text{Pr}(\gamma, n)}{^{63}\text{Cu}(\gamma, n)} = 3.79$$

ELEM. SYM.	A	Z
Sm	144	62

METHOD

REF. NO.

Nuclear Resonance Scattering using N,G reactions.

66 Be 3

JDM

REACTION	RESULT	EXCITATION ENERGY	SOURCE		DETECTOR		ANGLE
			TYPE	RANGE	TYPE	RANGE	
G,G	RLX	5 - 10	D	5 - 10	NAI-D	5 - 10	135

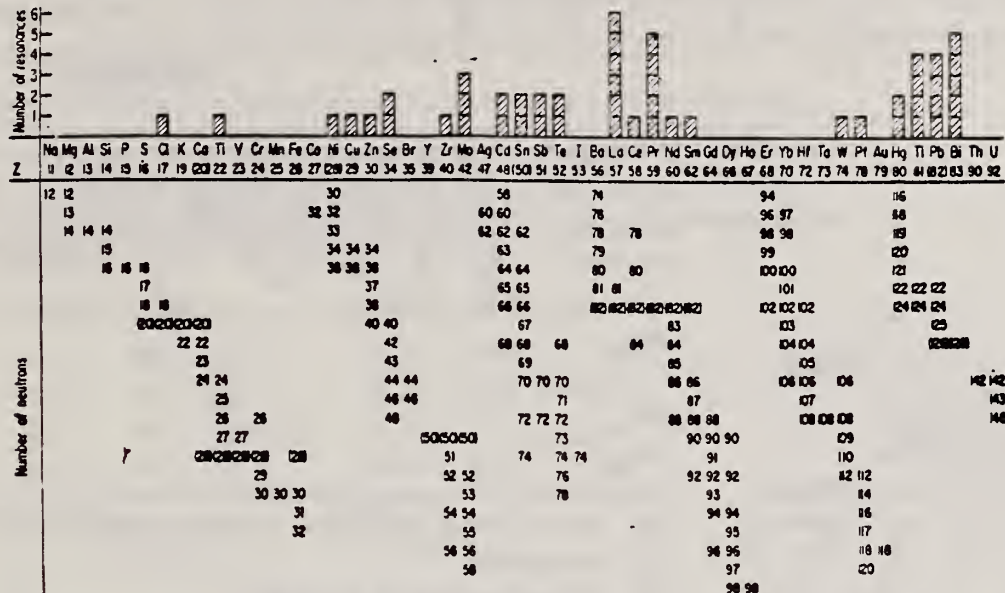


FIG. 3. Histogram of distribution of observed resonances among the different targets. The atomic number is given directly beneath the chemical symbol followed by the neutron numbers of the naturally occurring isotopes. Magic numbers are shown in brackets.

TABLE III. List of effective cross sections.

Scatterer	Energy (MeV)	Gamma source	δ (mb)	Scatterer	Energy (MeV)	Gamma source	δ (mb)
Sm ¹⁴⁴	8.997	Ni	100	Sn	7.01	Cu	110
Pr ¹⁴⁴	8.881	Cr	9	Nd	6.867	Co	30
La	8.532	Ni	6	Pr ¹⁴⁴	6.867	Co	3
Te	8.532	Ni	3*	Te	6.7	Ni	...
Cu	8.499	Cr	24	La	6.54	Ag	12
Zr	8.496	Se	3050	Cd	6.474	Co	110
Zn	8.119	Ni	13	Mo	6.44	Hg	110
Se	7.817	Ni	50	La	6.413	Tl	72
Se	7.76	K	90	Mo	6.413	Tl	10
Sb	7.67	V	...	Tl	6.413	Tl	25
Cd	7.64	Fe	40*	W	6.3	Tl	...
Ni	7.64	Fe	7*	Sb	6.31	Hg	6*
Pr ¹⁴⁴	7.64	Fe	12*	Tl	6.31	Hg	2*
Tl	7.64	Fe	370*	Sn	6.27	Ag	75
La	7.634	Cu	7	Pb ²⁰⁸	6.15	Gd	...
Mo	7.634	Cu	11	Te	5.8	Ni	...
Bi ²⁰⁸	7.634	Cu	4	La	6.12	Cl	35
Te	7.528	Ni	66*	Pr ¹⁴⁴	6.12	Cl	110
Bi ²⁰⁸	7.416	Se	100	Pt	5.99	Hg	5*
Bi ²⁰⁸	7.300	As	80*	Tl	5.99	Hg	2*
Pb ²⁰⁸	7.285	Fe	4100	Pb ²⁰⁸	5.9	Sr	...
Cl	7.285	Fe	34	Ge	5.646	Co	17
Pr ¹⁴⁴	7.185	Se	80	Pb ²⁰⁸	5.646	Co	55
Tl	7.16	Cu	120	Pb ²⁰⁸	5.53	Ag	70
La	7.15	Mn	50	Hg	5.44	Hg	75*
Bi ²⁰⁸	7.149	Ti	2000	Hg	4.903	Co	385

* High-energy component of a complex spectrum.

† A broad scattered spectrum with no observable peak structure.

‡ There are actually two lines of energies 7.647 and 7.633 MeV having equal intensities in the iron capture gamma spectrum. The cross section has therefore been corrected, although there is no possibility at present of deciding which line is responsible for each resonance.

§ It is probably an independent level in the complex spectrum of Ni γ rays on Te.

** Rough estimate.

† May be inelastic component from 7.528 level in Te.

‡ The relative line intensities in this case are due to Groshev and co-workers.

§ No line is known for the source at this energy.

¶ Difficult to resolve among the many source lines present at this energy.

REF.

K. Shoda, M. Sugawara, T. Saito & H. Miyase
 PICNS-69 Proceedings of the Conference on Nuclear Isospin.
 Asilomar-Pacific Grove, California 1969 (Academic Press,
 New York & London 1969) p.137.

ELEM. SYM.	A	Z
Sm	144	62

METHOD

REF. NO.
69 Sh 8

egf

REACTION	RESULT	EXCITATION ENERGY	SOURCE		DETECTOR		ANGLE
			TYPE	RANGE	TYPE	RANGE	
E, P	SPC	11-20	D	20	MAG-D		UKN

UKN=UNKNOWN

Table 2. The radiative widths of the main IAS.
 The results are compared with the single particle strength in W.u..

Nucleus	E_p (MeV)	E_x (a) (MeV)	Γ_{p_0}/Γ	Γ_γ (eV)	$2(T+1)\Gamma_\gamma$ (W.u.)
^{140}Ce	10.3	18.3	1 (b)	50	0.1
—	12.8	20.8	1 (b)	90	0.1
^{141}Pr	9.7	15.1	12/60(c)	40	0.2
^{144}Sm	10.6	16.6	1 (b)	20	0.05

(a) Ground state is assumed for the residual state.

(b) Assumption.

(c) P. VonBrentano et al. (2).

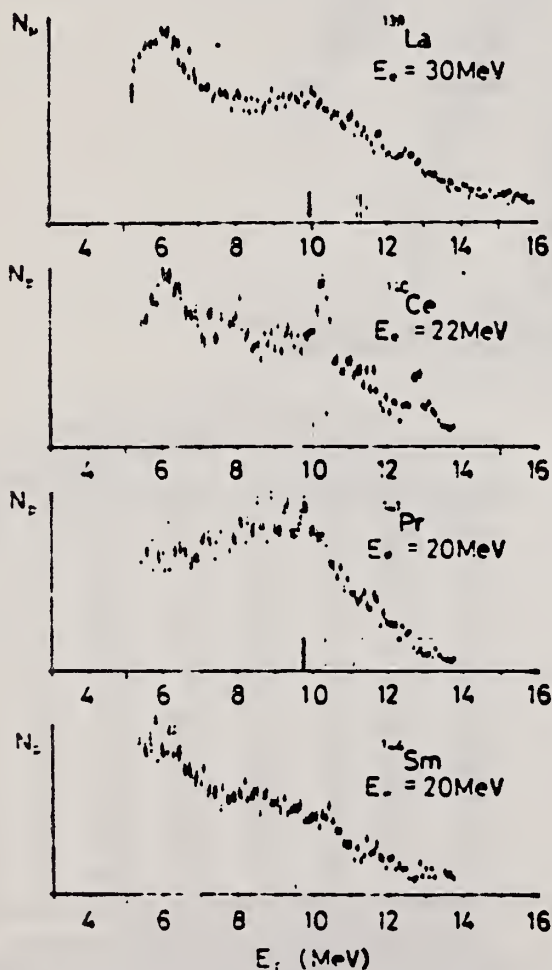


Fig. 1. Energy distributions of photoprottons. Vertical broken lines and solid lines indicate the position of p_0 corresponding to the ground IAS and electric dipole IAS (2).

METHOD

REF. NO.

71 Sh 3

hmg

REACTION	RESULT	EXCITATION ENERGY	SOURCE		DETECTOR		ANGLE
			TYPE	RANGE	TYPE	RANGE	
E, P	ABX	15-22	D	22	MAG-D		90

The energy distributions of protons from the $(e, e'p)$ reaction on $N=32$ nuclei with even Z have been measured. The cross sections of the $(\gamma, p_0 + p_1)$ reaction have been estimated. Two prominent isobaric analogs have been found in each nucleus. The results were used for the systematic discussion of the odd-odd parent nuclei ^{138}Cs , ^{140}La , ^{142}Pr , and ^{144}Pm . The 1^- states are estimated at 600 and ~ 2500 keV for ^{138}Cs , 500 and 3000 keV for ^{140}La , 1100 and 3700 keV for ^{142}Pr , and 1400 and 4300 keV for ^{144}Pm . The parameters of these states are discussed in terms of a quasiproton and single-neutron model.

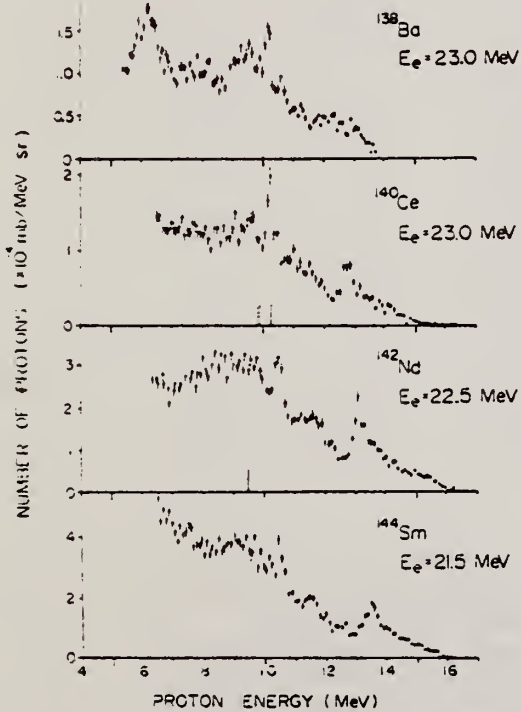


FIG. 1. Energy distributions of protons emitted from the $(e, e'p)$ reaction at $\theta = 90^\circ$.

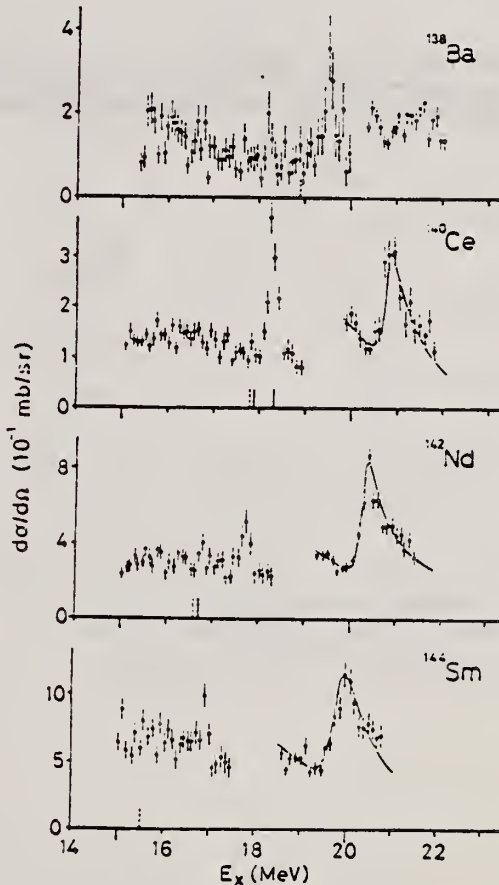


FIG. 2. The photoprotton cross sections for $p_0 + p_1$ at $\theta = 90^\circ$ in the vicinity of the isobaric analog resonances. The curves for the broad resonances were obtained from the fitting of the interference formula.

REF.

B. Arad, G. Ben-David, Y. Schlesinger, M. Hass
 Phys. Rev. C6, 670 (1972)

ELEM. SYM.	A	Z
Sm	144	62

METHOD

REF. NO.

72 Ar 1

hmg

REACTION	RESULT	EXCITATION ENERGY	SOURCE		DETECTOR		ANGLE
			TYPE	RANGE	TYPE	RANGE	
G,G	LFT	9	D	9	SCD-D		135

No new data; re-evaluation of old data
 gives the following:

$$\begin{aligned}\Gamma &= .27 \pm .08 \text{ eV} \\ \Gamma_{\text{o}} &= .063 \pm .013 \text{ eV} \\ D &= 110 \text{ eV}\end{aligned}$$

SEE 66BE3, 9 = 8.998

The 8.998-MeV resonance level excited by the (γ, γ') reaction, which was previously assigned to ^{136}Sm , is shown to belong to ^{144}Sm . The level scheme of ^{144}Sm is given and the re-evaluated level parameters of the 8.998-MeV resonance are presented.

REF.

R. Bergere, H. Beil, P. Carlos, A. Lepretre, A. Veyssiere
PICNS-73, Vol.I, p.525 Asilomar

ELEM. SYM.	A	Z
Sm	144	62

METHOD

REF. NO.

73 Be 10

hmg

REACTION	RESULT	EXCITATION ENERGY	SOURCE		DETECTOR		ANGLE
			TYPE	RANGE	TYPE	RANGE	
G, SN	ABX	10-21	D	10- 21	BF3-I		4PI
		-					
		-					
		-					
		-					

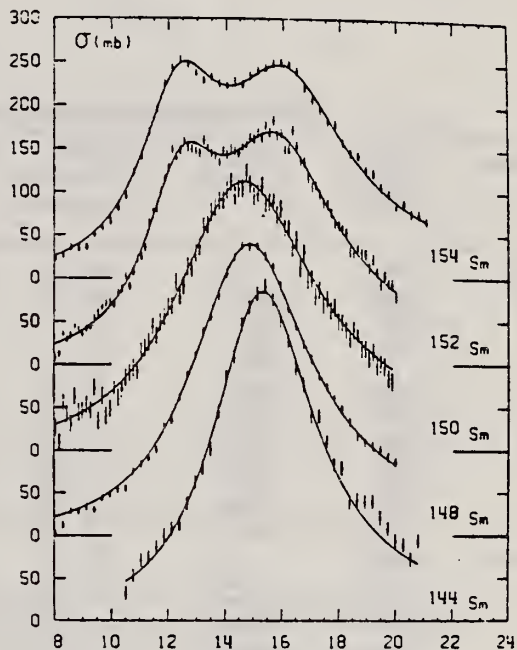


Fig. 19 Total photoneutron cross section $\sigma(\gamma, n) + \sigma(\gamma, 2n)$ of Sm isotopes. The solid lines show the best 1 Lorentz line fit (^{144}Sm , ^{148}Sm , ^{150}Sm) or 2 Lorentz lines fit (^{152}Sm and ^{154}Sm).

Table III

	E_1 (MeV)	Γ_1 (MeV)	σ_1 (mb)
^{144}Sm	15.30 ± 0.1	4.37 ± 0.15	384 ± 20
^{148}Sm	14.82 ± 0.1	5.10 ± 0.20	340 ± 12
^{150}Sm	14.60 ± 0.1	6.00 ± 0.20	312 ± 20

EL EM. SYM.	A	Z
Sm	144	62

METHOD

REF. NO.

73 Sz 2

egf

REACTION	RESULT	EXCITATION ENERGY	SOURCE		DETECTOR		ANGLE
			TYPE	RANGE	TYPE	RANGE	
G,G	LFT	9	D	9	SCD-D		DST

9 = 8.995Table 1. Reduced partial radiation widths of resonance levels in ⁶⁶Zn, ¹⁴⁴Sm and ¹²⁰Sn

Nucleus	Energy of transition (keV)	Energy of final state	Relative intensity Γ_j/Γ_0 (in percent)	Reduced widths ($eV \cdot meV^{-4} \times 10^3$)		Most likely characters	Derived spin and parity values $J\pi$
				K(E1)	K(M1)		
⁶⁶ Zn	7693	0	100 ± 1	6 ± 1	105 ± 21	E1	0+
	6654	1039.2	42 ± 1	4 ± 1	68 ± 14	E1	2+
	5819	1874	<2	<0.3	<5	E1 or M1	0, 1, 2
	5321	2372	<3	<0.6	<9	E1 or M1	0, 1, 2
	4930	2763	<2	<0.5	<8	E1 or M1	0, 1, 2
	4755	2938.1	24 ± 2	7 ± 2	106 ± 23	E1	0+
	4587	3105.8	8 ± 1	2.4 ± 0.6	39 ± 9	E1 or M1	0, 1, 2
	4480	3212.6	21 ± 2	7 ± 2	111 ± 25	E1	0+
	4452	3240.6	7 ± 2	2.3 ± 0.8	38 ± 13	E1 or M1	0, 1, 2
	4361	3331.7	13 ± 2	5 ± 1	75 ± 19	E1	0, 2+
	4263	3430.0	25 ± 3	9 ± 2	154 ± 36	E1	0, 2+
	4187	3506.3	8 ± 2	3 ± 1	52 ± 17	E1 or M1	0, 1, 2
¹⁴⁴ Sm	8995	0	100 ± 1	15 ± 3	412 ± 82	E1	0+
	7333	1662.0	33 ± 1	9 ± 2	251 ± 50	E1	2+
	6828	2167	3 ± 1	10 ± 4	28 ± 11	E1 or M1	0, 1, 2
	6568	2426.5	21 ± 1	8 ± 2	222 ± 44	E1	2+
	6514	2480.7	46 ± 1	18 ± 4	499 ± 100	E1	0+
	6191	2804.1	12 ± 1	6 ± 1	164 ± 33	E1	2+
¹²⁰ Sn	7693	0	100 ± 1.0	38 ± 11	932 ± 266	E1	0+
	6522	1171.4	7.3 ± 0.5	5 ± 1	112 ± 32	E1	2+
	5520	2172.9	1.4 ± 0.3	1.4 ± 0.4	35 ± 10	E1 or M1	0, 1, 2
	5337	2356.0	12.3 ± 0.8	14 ± 4	343 ± 98	E1	2+

METHOD

REF. NO.

74 Ca 5

egf

REACTION	RESULT	EXCITATION ENERGY	SOURCE		DETECTOR		ANGLE
			TYPE	RANGE	TYPE	RANGE	
G, N *	ABX	10- 21	D	10- 21	BF3-I		4PI
G, 2N **	ABX	18- 21	D	18- 21	BF3-I		4PI

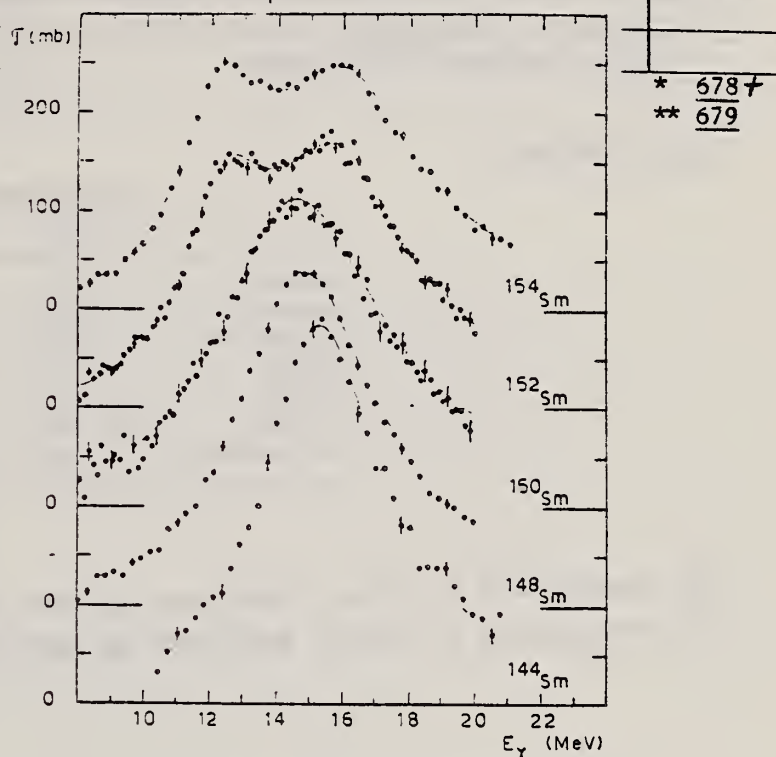


Fig. 7. Total photoneutron cross sections $\sigma_T(E)$ of the doubly even samarium isotopes. Best single Lorentz line fits are shown for ^{144}Sm , ^{148}Sm and ^{150}Sm . For ^{152}Sm and ^{154}Sm the best two Lorentz line fits are presented. Corresponding Lorentz line parameters are given in table 2.

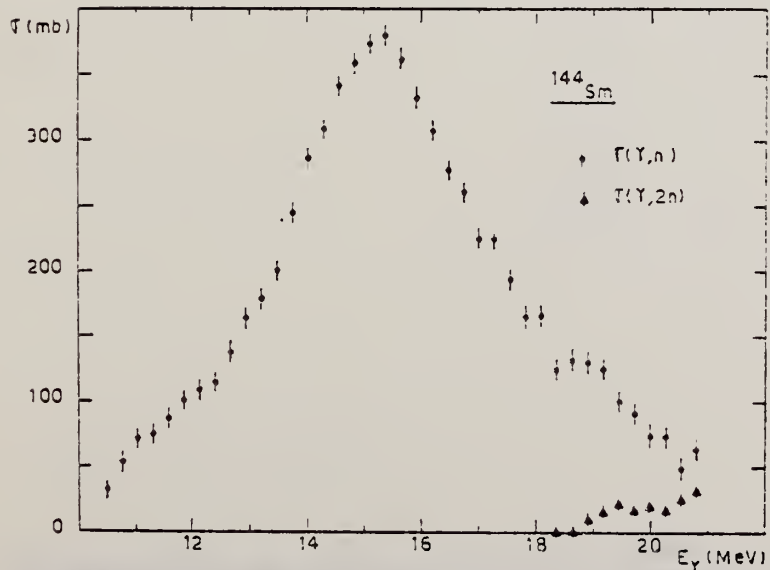


Fig. 2. Partial photoneutron cross sections $[\sigma(\gamma, n) + \sigma(\gamma, np)]$ and $\sigma(\gamma, 2n)$ of ^{144}Sm .

TABLE 2
Lorentz line parameters

	E_1 (MeV)	σ_1 (mb)	Γ_1 (MeV)	E_2 (MeV)	σ_2 (mb)	Γ_2 (MeV)
$^{144}\text{Sm}^*$	15.3 \pm 0.1	384 \pm 20	4.37 \pm 0.15			
$^{148}\text{Sm}^*$	14.8 \pm 0.1	339 \pm 12	5.1 \pm 0.2			
$^{148}\text{Sm}^{**}$	14.1	335	4			
$^{150}\text{Sm}^*$	14.6 \pm 0.1	312 \pm 20	6.0 \pm 0.2			
$^{150}\text{Sm}^{**}$	13.6	360	5.5			
$^{152}\text{Sm}^*$	12.45 \pm 0.10	183 \pm 10	3.2 \pm 0.15	15.85 \pm 0.10	226 \pm 10	5.1 \pm 0.2
$^{152}\text{Sm}^{**}$	11.55	400	2.4	14.65	420	3.4
$^{154}\text{Sm}^*$	12.35 \pm 0.10	192 \pm 10	3.35 \pm 0.15	16.1 \pm 0.1	204 \pm 10	5.25 \pm 0.2
$^{154}\text{Sm}^{**}$	11	204	3	15.25	320	4

* Corresponding to best fits shown in fig. 7.

** Values taken from Vassilijev ^{23, 24)} for comparison.

TABLE 3
Different integrated cross sections as defined in the text

	^{144}Sm	^{148}Sm	^{150}Sm	^{152}Sm	^{154}Sm
E_M (MeV)	21	20	20	20	21
σ_0 (MeV · b)	2 \pm 0.14	1.94 \pm 0.1	2 \pm 0.14	2.05 \pm 0.1	2.07 \pm 0.1
σ'_0 (MeV · b)	2.63	2.71	2.94	2.75	2.65
$\frac{\sigma'_0 A}{0.06 NZ}$	1.24	1.25	1.35	1.24	1.2
σ_{-1} (mb)	131 \pm 15	134 \pm 10	141 \pm 15	144 \pm 10	145 \pm 12
σ_{-2} (mb · MeV ⁻¹)	8.7 \pm 0.8	9.5 \pm 0.7	10.3 \pm 0.9	10.6 \pm 0.7	10.9 \pm 0.7

²³O. Vasilijev et al., Sov. J. Nucl. Phys. 10, 263 (1970)

²⁴O. Vasilijev et al., Sov. J. Nucl. Phys. 13, 463 (1971)

REF.

F. R. Metzger
Phys. Rev. C14, 543 (1976)

ELEM. SYM.	A	Z
Sm	144	62

METHOD

REF. NO.

76 Me 6

hmg

REACTION	RESULT	EXCITATION ENERGY	SOURCE		DETECTOR		ANGLE
			TYPE	RANGE	TYPE	RANGE	
\$ G,G	LFT	3	C	1- 4	SCD-D		DST
		(3.225)					
		-					
		-					

$$\frac{N_{\parallel} - N_{\perp}}{N_{\parallel} + N_{\perp}} = (+3.6 \pm 2.7)\%.$$

POLARIMETER EXPER

TABLE I. Properties of the low-lying 1^- levels in the stable even Sm isotopes.

Isotope	$E_{exc}(1^-)$	Γ_0 (meV)	$10^3 \times \frac{B(E1; 1^- \rightarrow 0^+)}{B(E1)_{sp}}$	N
^{144}Sm	3.225	220 ± 30	3.5 ± 0.5	82
^{146}Sm	1.465	3.1 ± 0.4	0.5 ± 0.1	86
^{150}Sm	1.166	5.4 ± 0.5	1.8 ± 0.2	88
^{152}Sm	0.963	7.3 ± 0.6	4.2 ± 0.4	90
^{154}Sm	0.921	7.4 ± 1.0	4.8 ± 0.7	92

REF.

F.R. Metzger
Phys. Rev. C 17, 939 (1978)

ELEM. SYM.	A	Z
Sm	144	62

METHOD

REF. NO.

78 Me 2

egf

REACTION	RESULT	EXCITATION ENERGY	SOURCE		DETECTOR		ANGLE
			TYPE	RANGE	TYPE	RANGE	
G,G	LFT	1- 5	C	5	SCD-D		DST

12 LEVELS SELF-ABS

Using electron bremsstrahlung with up to 5.2-MeV end-point energy, the resonant scattering of γ rays by an enriched sample of ^{144}Sm has been studied. Ground-state transitions were observed from a dozen levels, and the scattering yields, measured at 96° and 126° , were evaluated in terms of radiative widths and level spins. For the strongest excitations, these measurements were supplemented by self-absorption and linear-polarization studies. Some of the observed $E1$ transitions originate from 1^- states which, according to isobaric-analog-resonance studies, contain large neutron-particle-hole components. On the other hand, the 3.225- and 3.891-MeV levels, which exhibit the strongest $E1$ ground-state transitions, occur at energies which suggest that they arise from the coupling of the lowest octupole vibration to the 2_1^+ and 2_2^+ levels.

TABLE I. Spins and widths derived from the yields of the reaction $^{144}\text{Sm}(\gamma, \gamma)$ at scattering angles of 96° and 126° . Standard deviations are listed throughout.

$E_{\gamma, \text{rel}}$ (MeV)	$N(126^\circ)/N(96^\circ)$	Spin	Γ_γ^2/Γ (meV)
1.660(1)	0.42 ± 0.06	2	5.1 ± 1.2
2.423(1)	0.47 ± 0.08	2	14 ± 2
2.799(2)	0.58 ± 0.20	(2)	4.7 ± 0.9
3.225(1)	1.15 ± 0.09	1	220 ± 20
3.318(3)	0.8 ± 0.3	1,2	11 ± 3
3.891(2)	1.22 ± 0.17	1	210 ± 30
3.905(3)	2.0 ± 0.8	(1)	25 ± 8
3.966(2)	1.27 ± 0.17	1	70 ± 10
4.262(2)	1.20 ± 0.19	1	170 ± 30
5.015(5)	1.10 ± 0.40	(1)	140 ± 40
5.103(3)	0.9 ± 0.3	1,2	140 ± 40
5.151(3)	1.3 ± 0.3	(1)	290 ± 60

S_M
 $A=148$

S_M
 $A=148$

S_M
 $A=148$

REF.

F. R. Metzger
Phys. Rev. 137, B1415-20 (1965)

ELEM. SYM.	A	Z
Sm	148	62

METHOD

Radioactive source.

REF. NO.
65 Me 1

NVB

REACTION	RESULT	EXCITATION ENERGY	SOURCE		DETECTOR		ANGLE
			TYPE	RANGE	TYPE	RANGE	
G,G	LFT	1	D	1	NAI-D		DST
		(1.46)		(1.46)			

$$\tau = (1.4 - 0.3) \times 10^{-13} \text{ sec.} \quad + 0.6$$

TABLE II. Summary of the transition probabilities determined in this work, and comparison with the predictions of the single-particle model (Ref. 16).

Nucleus	E_{γ} (MeV)	Transi- tion	Transition probability (sec ⁻¹)	$B(E1)_d$ (10 ⁻²⁸ e ² cm ⁴)	$\frac{B(E1)_d}{B(E1)_m}$
Sm^{148}	1.46	$1^- \rightarrow 0^+$	$(4.3 \pm 1.2) \times 10^{13}$	0.9	5×10^{-4}
	0.91	$1^- \rightarrow 2^+$	$(2.7 \pm 0.8) \times 10^{13}$	2.3	12×10^{-4}
Sm^{148}	0.96	$1^- \rightarrow 0^+$	$(11 \pm 1) \times 10^{13}$	7.9	4×10^{-3}
	0.84	$1^- \rightarrow 2^+$	$(14 \pm 2) \times 10^{13}$	15.4	8×10^{-3}

METHOD

REF. NO.

71 Va 2

hmg

REACTION	RESULT	EXCITATION ENERGY	SOURCE		DETECTOR		ANGLE
			TYPE	RANGE	TYPE	RANGE	
G,XN	ABX	8-24	C	8-24	BF3-I		4PI
		(8.1-23.25)			(8.1-23.25)		

Table II. Parameters of giant dipole resonance

Isotope	σ_0 , mb	E_0 , MeV	Γ_0 , MeV	Q_{eff} , MeV	E_1 , MeV	Γ_1 , MeV	Q_{eff} , MeV	E_{γ} , MeV	Γ_{γ} , MeV	c_{rel}	c_{abs} , MeV	θ_{abs} , MeV	$\epsilon_{\gamma}^{(1)}$	β_{eff}
Nd ¹⁴⁴	332	13.8	4.1							2.12	1.00			
Sm ¹⁴⁸	335	14.1	4.0							2.08	0.96			
Gd ¹⁴²	147	12.0	3.0	0.693	259	15.0	3.2	1.29	1.99	0.90	1.87	1.25	0.28	
Gd ¹⁴⁴	161	11.9	2.6	0.612	250	15.0	3.5	1.39	2.01	0.89	2.27	1.26	0.39	
Gd ¹⁴⁶	180	11.9	2.6	0.738	243	15.2	3.6	1.37	2.11	0.94	1.86	1.27	0.31	
Gd ¹⁴⁸	165	11.7	2.6	0.662	249	14.9	3.8	1.49	2.16	0.94	2.25	1.28	0.32	
Eu ¹⁵²	285	14.0	4.5							2.02	0.92			
Eu ¹⁵⁴	159	11.9	2.3	0.562	237	15.1	3.6	1.34	1.90	0.86	2.39	1.27	0.31	

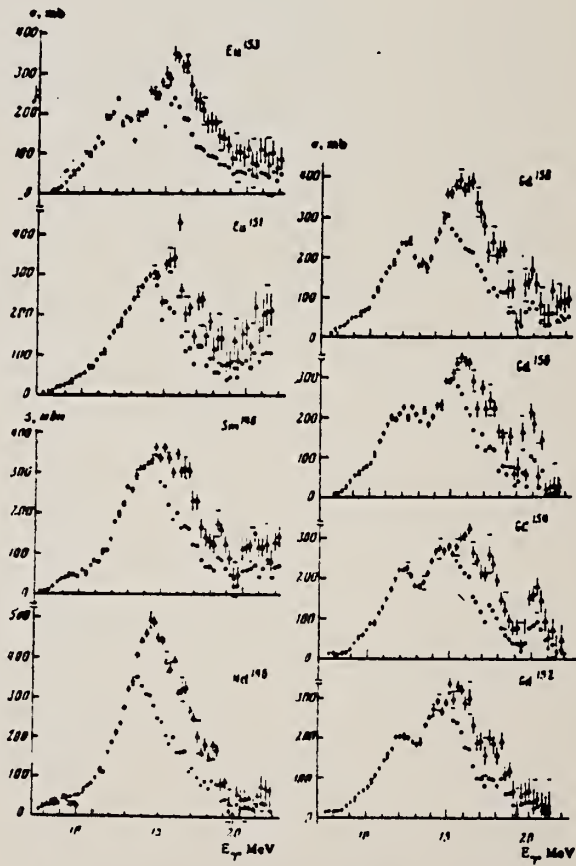


FIG. 1. Photoneutron cross sections and photoabsorption cross sections of Nd¹⁴⁴, Sm¹⁴⁸, Eu¹⁵², Eu¹⁵³, Gd¹⁵², Gd¹⁵⁴ and Gd¹⁵⁶. Statistical and rms experimental errors are shown (the latter horizontal bars at 9.42 MeV, 10.42 MeV etc.) At photon energies above the (γ , 2n) threshold the photoabsorption cross section errors are not shown.

REF. R. Berger, H. Beil, P. Carlos, A. Lepretre, A. Veyssiére
PICNS-73, Vol. I, p. 525 Asilomar

ELEM. SYM.	A	Z
Sm	148	62

METHOD	REF. NO.					
REACTION	RESULT	EXCITATION ENERGY	SOURCE	DETECTOR	ANGLE	
			TYPE	RANGE	TYPE	RANGE
G, SN	ABX	8- 20	D	8- 20	BF3-I	
					4PI	

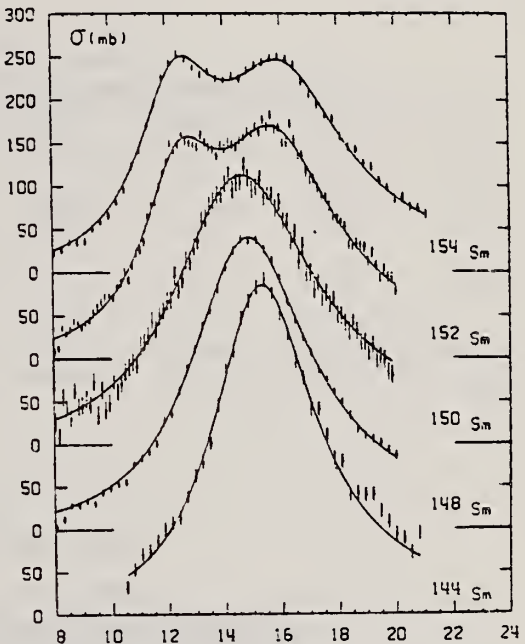


Fig. 19 Total photoneutron cross section $\sigma(\gamma, n) + \sigma(\gamma, 2n)$ of Sm isotopes. The solid lines show the best 1 Lorentz line fit (^{144}Sm , ^{148}Sm , ^{150}Sm) or 2 Lorentz lines fit (^{152}Sm and ^{154}Sm).

Table III

	E_1 (MeV)	Γ_1 (MeV)	σ_1 (mb)
^{144}Sm	15.30 ± 0.1	4.37 ± 0.15	384 ± 20
^{148}Sm	14.82 ± 0.1	5.10 ± 0.20	340 ± 12
^{150}Sm	14.60 ± 0.1	6.00 ± 0.20	312 ± 20

REF.

P. Carlos, H. Beil, R. Bergere, A. Lepretre, A. De Miniac,
and A. Veyssiére
Nucl. Phys. A225, 171 (1974)

ELEM. SYM.	A	Z
Sm	148	62

METHOD

REF. NO.

74 Ca 5

egf

REACTION	RESULT	EXCITATION ENERGY	SOURCE		DETECTOR		ANGLE
			TYPE	RANGE	TYPE	RANGE	
G, N *	ABX	8- 20	D	8- 20	BF3-I		4PI
G, 2N **	ABX	13- 20	D	13- 20	BF3-I		4PI

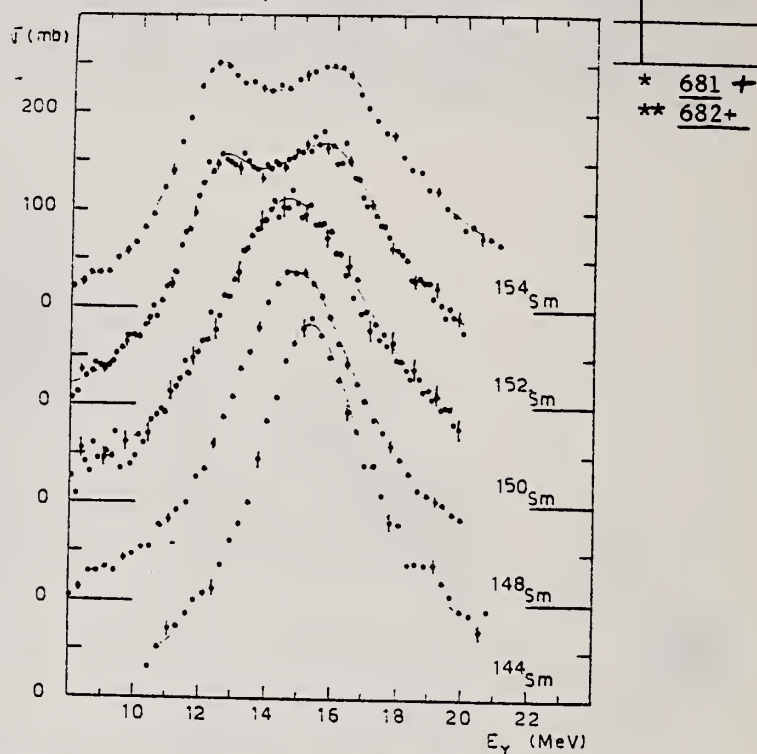


Fig. 7. Total photoneutron cross sections $\sigma_T(E)$ of the doubly even samarium isotopes. Best single Lorentz line fits are shown for ^{144}Sm , ^{148}Sm and ^{150}Sm . For ^{152}Sm and ^{154}Sm the best two Lorentz line fits are presented. Corresponding Lorentz line parameters are given in table 2.

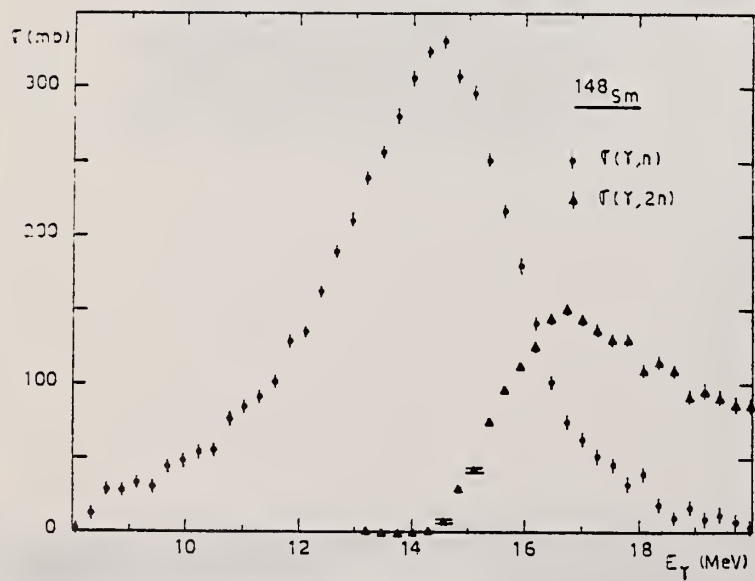


Fig. 3. Partial photoneutron cross sections $[\sigma(\gamma, n) + \sigma(\gamma, np)]$ and $\sigma(\gamma, 2n)$ of ^{148}Sm .

ET 276

(over)
U.S. DEPARTMENT OF COMMERCE
NATIONAL BUREAU OF STANDARDS

TABLE 2
Lorentz line parameters

	E_1 (MeV)	σ_1 (mb)	Γ_1 (MeV)	E_2 (MeV)	σ_2 (mb)	Γ_2 (MeV)
$^{144}\text{Sm}^*$	15.3 \pm 0.1	384 \pm 20	4.37 \pm 0.15			
$^{148}\text{Sm}^*$	14.8 \pm 0.1	339 \pm 12	5.1 \pm 0.2			
$^{148}\text{Sm}^{**}$	14.1	335	4			
$^{150}\text{Sm}^*$	14.6 \pm 0.1	312 \pm 20	6.0 \pm 0.2			
$^{150}\text{Sm}^{**}$	13.6	360	5.5			
$^{152}\text{Sm}^*$	12.45 \pm 0.10	183 \pm 10	3.2 \pm 0.15	15.85 \pm 0.10	226 \pm 10	5.1 \pm 0.1
$^{152}\text{Sm}^{**}$	11.55	400	2.4	14.65	420	4
$^{154}\text{Sm}^*$	12.35 \pm 0.10	192 \pm 10	3.35 \pm 0.15	16.1 \pm 0.1	204 \pm 10	5.25 \pm 0.1
$^{154}\text{Sm}^{**}$	11	204	3	15.25	320	4

* Corresponding to best fits shown in fig. 7.

** Values taken from Vassilijev ^{23,24}) for comparison.

TABLE 3
Different integrated cross sections as defined in the text

	^{144}Sm	^{148}Sm	^{150}Sm	^{152}Sm	^{154}Sm
E_M (MeV)	21	20	20	20	21
σ_0 (MeV · b)	2 \pm 0.14	1.94 \pm 0.1	2 \pm 0.14	2.05 \pm 0.1	2.07 \pm 0.1
σ'_0 (MeV · b)	2.63	2.71	2.94	2.75	2.69
$\frac{\sigma'_0 A}{0.06 NZ}$	1.24	1.25	1.35	1.24	1.2
σ_{-1} (mb)	131 \pm 15	134 \pm 10	141 \pm 15	144 \pm 10	145 \pm 10
σ_{-2} (mb · MeV ⁻¹)	8.7 \pm 0.8	9.5 \pm 0.7	10.3 \pm 0.9	10.6 \pm 0.7	10.6 \pm 0.7

²³O. Vasilijev et al., Sov.J.Nucl.Phys. 10, 263 (1970)

²⁴O. Vasilijev et al., Sov.J.Nucl.Phys. 13, 463 (1971)

REF.

F. R. Metzger
 Phys. Rev. C14, 543 (1976)

ELEM. SYM.	A	Z
Sm	148	62
METHOD	REF. NO.	
	76 Me 6	hmg

REACTION	RESULT	EXCITATION ENERGY	SOURCE		DETECTOR		ANGLE
			TYPE	RANGE	TYPE	RANGE	
G, G	LFT	2 (1.465)	C	1- 4	SCD-D		DST

$$\frac{N_{||} - N_{\perp}}{N_{||} + N_{\perp}} = (+3.6 \pm 2.7)\%$$

TABLE I. Properties of the low-lying 1^- levels in the stable even Sm isotopes.

Isotope	$E_{\text{exc}}(1^-)$	Γ_0 (meV)	$10^3 \times \frac{B(E1; 1^- \rightarrow 0^+)}{B(E1)_{\text{sp.}}}$	N
^{144}Sm	3.225	220 ± 30	3.5 ± 0.5	82
^{146}Sm	1.465	3.1 ± 0.4	0.5 ± 0.1	86
^{150}Sm	1.166	5.4 ± 0.5	1.8 ± 0.2	88
^{152}Sm	0.963	7.3 ± 0.6	4.2 ± 0.4	90
^{154}Sm	0.921	7.4 ± 1.0	4.8 ± 0.7	92

REF. B.S. Dolbilkin, S. Ohsawa, Y. Torizuka, T. Saito, Y. Mizuno,
 K. Saito
 Phys. Rev. C25, 2255 (1982)

ELEM. SYM.	A	z
Sm	148	62

METHOD	REF. NO.					
	82 Do 6	egf				
REACTION	RESULT	EXCITATION ENERGY	SOURCE	DETECTOR		ANGLE
		5-33	D	RANGE	TYPE	
E, E/			150-215		MAG-D	DST

The electron scattering cross sections from the enriched ^{148}Sm (96.5%) and ^{152}Sm (99.2%) isotopes have been measured between 5 and 33 MeV excitation energies for incident energies in the range of between 150 and 215 MeV and scattering angles of 30°, 35°, and 40°. The giant resonances at $E_x = 14.8 (784^{-1/3})$, $11.6 (614^{-1/3})$, $15.5 (824^{-1/3})$, and $24 (1294^{-1/3})$ MeV for ^{148}Sm were classified according to their momentum transfer dependence. The K splittings of the giant $E1 (T=1)$ and $E2 (T=0,1)$ resonances for deformed ^{152}Sm were observed in agreement with a vibrating potential model. The splittings between the $K=0^+$ and 2^+ components for the isoscalar and isovector quadrupole resonances are ~ 2 MeV and ~ 5 MeV, respectively. The fitted parameters classified as the giant monopole resonance are the same for spherical ^{148}Sm and for deformed ^{152}Sm . The difference between the isoscalar giant resonance parameters for resonance energies and width found from hadron scattering and those for electron scattering is discussed for the rare-earth region.

Q .38-.64 FM-1

[NUCLEAR REACTIONS $^{148,152}\text{Sm}(e,e')$, enriched targets, $E_0 = 150$ to 215 MeV, $\theta = 30^\circ, 35^\circ, 40^\circ$, $q = 0.38 - 0.64 \text{ fm}^{-1}$. Measured $d^2\sigma/d\Omega dE_x$ up to 33 MeV in excitation energy; deduced multipolarity, excitation energy, width, sum rule exhaustion of giant resonances.]

TABLE IV. Comparison between (e,e') results and theoretical results for the giant multipole resonance energy (MeV).

Type	Nucleus	Isoscalar			Isovector		
		Present work	Ref. 10	Theory Ref. 9	Ref. 24	Present work	Ref. 10
GMR	^{148}Sm	15.5 ± 0.3			15.1		
	^{152}Sm	15.7 ± 0.3		10.7 18.3	10.5 15.9		
GDR	^{148}Sm				14.8	14.8	
	^{152}Sm				12.45 15.85	12.3 16.3	12.0 15.0
GQR	^{148}Sm	11.6 ± 0.2	10.9	11.0	11.9	24.3 ± 0.4	26.4
		10.6 ± 0.2	9.9	11.0	10.5	21.0 ± 0.9	24.1
	^{152}Sm	11.4 ± 0.4	10.4	12.0	13.1	23.2 ± 1.0	25.2
		12.7 ± 0.4	11.8	13.0		26.0 ± 0.5	25.5

(OVER)

TABLE V. Parameters of the isoscalar GQR in the Sm isotopes.

Nucleus	E_x (MeV)	Γ (MeV)	EWSR (%)	Reaction	Reference
^{144}Sm	13.0 ± 0.3	3.9 ± 0.2	91 ± 25	(α, α')	25
^{144}Sm	12.4 ± 0.4	2.6 ± 0.4	85 ± 15	(α, α')	6
^{144}Sm	12.1 ± 0.2	2.4 ± 0.2	45 ± 15	(α, α')	8
^{144}Sm	12.5	3.4	60	(α, α')	26
^{144}Sm	11.9 ± 0.2	2.9 ± 0.2		(e, e')	27
^{144}Sm	12.5 ± 0.2	4.3 ± 0.2	104 ± 25	(α, α')	25
^{144}Sm	11.6 ± 0.2	3.1 ± 0.2	100 ± 10	(e, e')	Present work
^{150}Sm	11.8 ± 0.2	3.3 ± 0.2		(e, e')	27
	10.6 ± 0.2	2.4 ± 0.2	20 ± 5		
^{152}Sm	11.4 ± 0.4	2.7 ± 0.2	45 ± 9	(e, e')	Present work
	12.7 ± 0.4	3.0 ± 0.2	35 ± 7		
^{154}Sm	12.4 ± 0.3	4.7 ± 0.3	102 ± 25	(α, α')	25
^{154}Sm	12.2	4.5		(α, α')	7
^{154}Sm	11.8 ± 0.3	3.7 ± 0.3		(α, α')	8
^{154}Sm	10.9 ± 0.2	4.5 ± 0.2		(e, e')	27

TABLE VI. Comparison of the GMR parameters in the Sm isotopes obtained from various reactions.

Nucleus	E_x (MeV)	Γ (MeV)	EWSR (%)	Reaction	Reference
^{144}Sm	15.1 ± 0.5	2.9 ± 0.5	100 ± 50	(α, α')	6
^{144}Sm	14.6 ± 0.2	3.0 ± 0.3	140 ± 40	(α, α')	8
^{144}Sm	15.2	2.5		(α, α')	26
^{144}Sm	15.5 ± 0.5	2.5 ± 0.5	100 ± 25	(p, p')	31
^{144}Sm	14.7 ± 0.2	2.9 ± 0.2	67 ± 13	$(^3\text{He}, ^3\text{He}')$	32
^{144}Sm	14.8 ± 0.2	2.4 ± 0.15	20 ± 10	(e, e')	30
^{148}Sm	15.5 ± 0.3	3.0 ± 0.2	100 ± 10	(e, e')	Present work
^{150}Sm	15.1 ± 0.25	3.0 ± 0.25	60 ± 19	$(^3\text{He}, ^3\text{He}')$	32
^{152}Sm	14.8 ± 0.25	3.1 ± 0.25	54 ± 9	$(^3\text{He}, ^3\text{He}')$	32
^{152}Sm	15.7 ± 0.3	3.1 ± 0.4	100 ± 20	(e, e')	Present work
^{154}Sm	15.5 ± 0.5	2.5 ± 0.5	100 ± 25	(p, p')	31
^{154}Sm	14.9 ± 0.3	2.6 ± 0.4	55 ± 15	(α, α')	8

SM
A=149

SM
A=149

SM
A=149

METHOD

Betatron; neutron threshold; ion chamber

REF. NO.

60 Ge 3

NVB

REACTION	RESULT	EXCITATION ENERGY	SOURCE		DETECTOR		ANGLE
			TYPE	RANGE	TYPE	RANGE	
G, N	NOX	THR	C THR		BF3-I		4 PI

THRESHOLD

TABLE I. Summary and comparison of neutron separation energies inferred from present threshold measurements with values predicted from mass data and reaction energetics. All energies are expressed in the center-of-mass system in Mev.

Reaction	No. runs	Present results	Other results	Method	Reference
Sm ¹⁴⁰ (γ,n)Sm ¹⁴¹	1	6.45 ± 0.16(5.89)	5.87 ± 0.28	mass data	p

* W. H. Johnson, Jr., and A. O. Nier, Phys. Rev. 105, 1014 (1957).

TABLE II. Comparison of measured threshold energies with neutron binding energies predicted by mass data for transitions with $\Delta I \geq 7/2$. All energies in Mev.

Reaction	ΔI^a	Observed threshold	Mass data Q value	$E_{\text{th}} - Q$	Excited state energy
Cr ⁵² (γ,n)Cr ⁵¹	7/2	12.18 ± 0.14	12.053 ± 0.004 ^b	0.13 ± 0.14	...
V ⁵¹ (γ,n)V ⁵⁰	7/2	11.59 ± 0.08	11.53 ± 0.40 ^c	0.06 ± 0.41	0.387 ^d
In ¹¹³ (γ,n)In ¹¹⁴	7/2	9.22 ± 0.03	9.35 ± 0.43 ^e	-0.13 ± 0.43	0.191 ^e
Ce ¹⁴² (γ,n)Ce ¹⁴¹	(7/2) ^f	7.24 ± 0.07	6.97 ± 0.07 ^f	0.27 ± 0.10	...
Nd ¹⁴³ (γ,n)Nd ¹⁴⁴	7/2	6.38 ± 0.16	5.97 ± 0.19 ^f	0.41 ± 0.25	0.690 ^a
Sm ¹⁴⁰ (γ,n)Sm ¹⁴⁸	7/2	6.45 ± 0.16	5.87 ± 0.28 ^f	0.58 ± 0.33	0.562 ^a
Er ¹⁴¹ (γ,n)Er ¹⁴⁶	7/2	6.65 ± 0.08	6.45 ± 0.06 ^f	0.20 ± 0.10	0.081 ^a
Hf ¹⁷¹ (γ,n)Hf ¹⁷⁶	7/2	6.69 ± 0.03	6.28 ± 0.06 ^f	0.64 ± 0.07	0.088 ^a
Hf ¹⁷² (γ,n)Hf ¹⁷⁸	9/2	6.31 ± 0.07	6.17 ± 0.06 ^f	0.14 ± 0.09	0.093 ^a
Hf ¹⁷⁴ (γ,n)Hf ¹⁷⁹	9/2	7.85 ± 0.11	7.32 ± 0.06 ^f	0.53 ± 0.13	0.375 ^a

^a Strominger, J. M. Hollander, and G. T. Seaborg, Revs. Modern Phys. 30, 585 (1958).

^b F. Giese and J. L. Benson, Phys. Rev. 110, 712 (1958).

^c E. Duckworth, Mass Spectroscopy (Cambridge University Press, New York, 1958), p. 177.

^d Dzhelev and L. K. Peker, Atomic Energy of Canada Limited Report Tr. AECL-457 (unpublished).

^e Discrepancy in the case of Ce¹⁴¹ predicts a ground-state spin for Ce¹⁴¹ of 0, since the spin of Ce¹⁴¹ is known to be 7/2.

^f W. H. Johnson, Jr., and A. O. Nier, Phys. Rev. 105, 1014 (1957).

S_M
 $A=150$

S_M
 $A=150$

S_M
 $A=150$

METHOD

REF. NO.

69 Va 2

egf

REACTION	RESULT	EXCITATION ENERGY	SOURCE		DETECTOR		ANGLE
			TYPE	RANGE	TYPE	RANGE	
G,XN	ABX	8-23	C	8-23	BF3-I		4PI

310

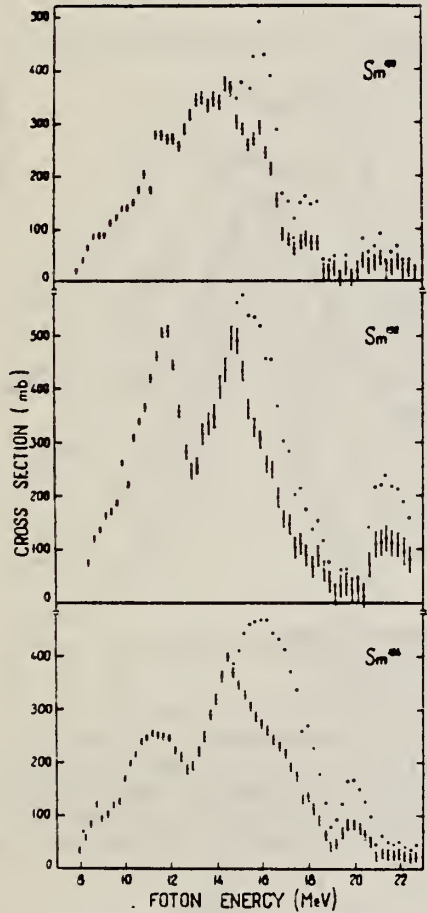


Fig. 3. The photoneutron and photoabsorption cross sections of ^{150}Sm , ^{152}Sm and ^{154}Sm . The symbols are the same as in fig. 2.

ELEM. SYM.	A	Z
Sm	150	62

METHOD	REF. NO.				
	73 Be 10	hmg			
REACTION	RESULT	EXCITATION ENERGY	SOURCE	DETECTOR	ANGLE
G,SN	ABX	8- 20	D	8- 20	
					4PI

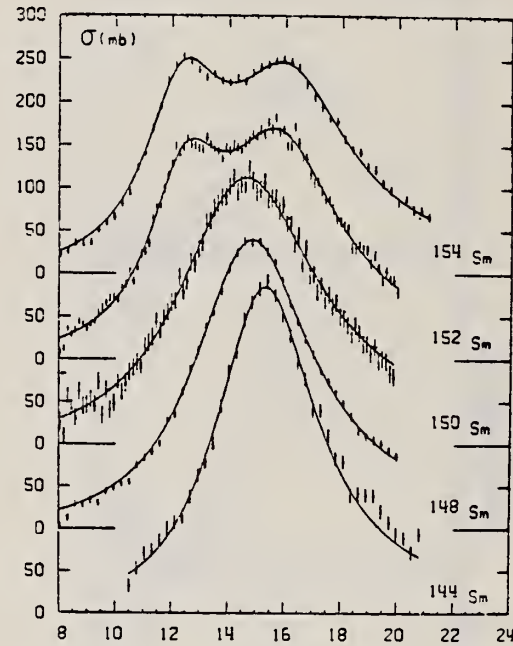


Fig. 19 Total photoneutron cross section $\sigma(\gamma, n) + \sigma(\gamma, 2n)$ of Sm isotopes. The solid lines show the best 1 Lorentz line fit (^{144}Sm , ^{148}Sm , ^{150}Sm) or 2 Lorentz lines fit (^{152}Sm and ^{154}Sm).

Table III

	E_1 (MeV)	Γ_1 (MeV)	σ_1 (mb)
^{144}Sm	15.30 ± 0.1	4.37 ± 0.15	384 ± 20
^{148}Sm	14.82 ± 0.1	5.10 ± 0.20	340 ± 12
^{150}Sm	14.60 ± 0.1	6.00 ± 0.20	312 ± 20

METHOD

REF. NO.

74 Ca 5

egf

REACTION	RESULT	EXCITATION ENERGY	SOURCE		DETECTOR		ANGLE
			TYPE	RANGE	TYPE	RANGE	
G,N *	ABX	8- 20	D	8- 20	BF3-I		4PI
G,2N **	ABX	13- 20	D	13- 20	BF3-I		4PI

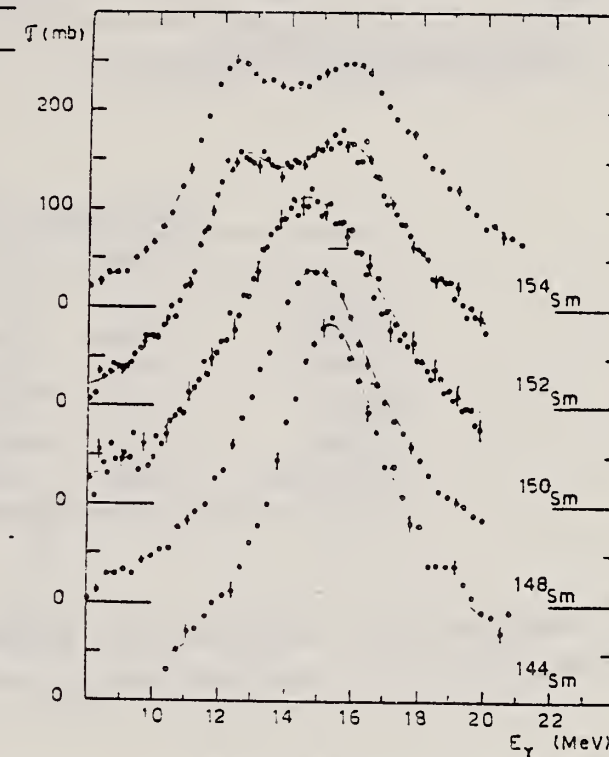


Fig. 7. Total photoneutron cross sections $\sigma_T(E)$ of the doubly even samarium isotopes. Best single Lorentz line fits are shown for ^{144}Sm , ^{148}Sm and ^{150}Sm . For ^{152}Sm and ^{154}Sm the best two Lorentz line fits are presented. Corresponding Lorentz line parameters are given in table 2.

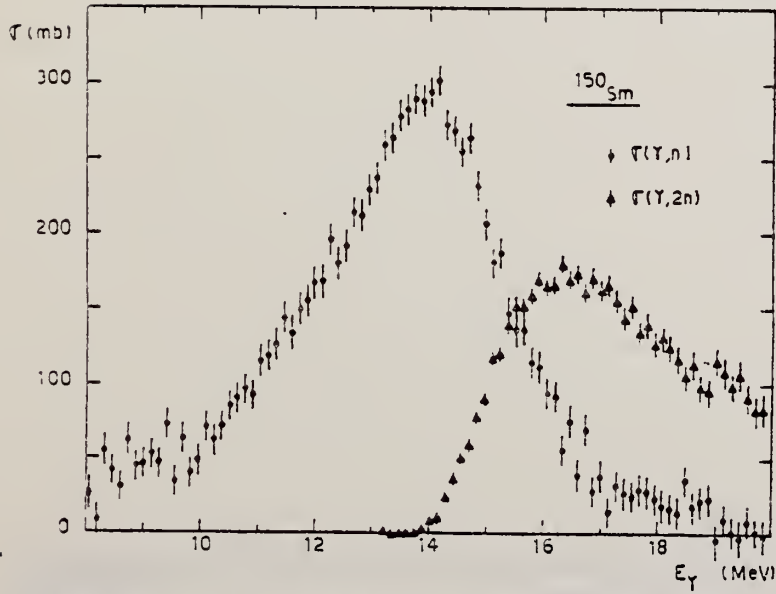


Fig. 4. Partial photoneutron cross sections $[\sigma(\gamma, n) + \sigma(\gamma, np)]$ and $\sigma(\gamma, 2n)$ of ^{150}Sm .

(over)

TABLE 2
Lorentz line parameters

E_1 (MeV)	σ_1 (mb)	Γ_1 (MeV)	E_2 (MeV)	σ_2 (mb)	Γ_2 (MeV)
$^{144}\text{Sm}^*$	15.3 ± 0.1	384 ± 20	4.37 ± 0.15		
$^{148}\text{Sm}^*$	14.8 ± 0.1	339 ± 12	5.1 ± 0.2		
$^{148}\text{Sm}^{**}$	14.1	335	4		
$^{150}\text{Sm}^*$	14.6 ± 0.1	312 ± 20	6.0 ± 0.2		
$^{150}\text{Sm}^{**}$	13.6	360	5.5		
$^{152}\text{Sm}^*$	12.45 ± 0.10	183 ± 10	3.2 ± 0.15	15.85 ± 0.10	226 ± 10
$^{152}\text{Sm}^{**}$	11.55	400	2.4	14.65	420
$^{154}\text{Sm}^*$	12.35 ± 0.10	192 ± 10	3.35 ± 0.15	16.1 ± 0.1	204 ± 10
$^{154}\text{Sm}^{**}$	11	204	3	15.25	320
					4

* Corresponding to best fits shown in fig. 7.

** Values taken from Vassilijev ^{23,24)} for comparison.

TABLE 3
Different integrated cross sections as defined in the text

	^{144}Sm	^{148}Sm	^{150}Sm	^{152}Sm	^{154}Sm
E_M (MeV)	21	20	20	20	21
σ_0 (MeV · b)	2 ± 0.14	1.94 ± 0.1	2 ± 0.14	2.05 ± 0.1	2.07 ± 0.1
σ'_0 (MeV · b)	2.63	2.71	2.94	2.75	2.65
$\frac{\sigma'_0 A}{0.06 NZ}$	1.24	1.25	1.35	1.24	1.21
σ_{-1} (mb)	131 ± 15	134 ± 10	141 ± 15	144 ± 10	145 ± 10
σ_{-2} (mb · MeV ⁻¹)	8.7 ± 0.8	9.5 ± 0.7	10.3 ± 0.9	10.6 ± 0.7	10.6 ± 0.7

²³O. Vasilijev et al., Sov.J.Nucl.Phys. 10, 263 (1970)

²⁴O. Vasilijev et al., Sov.J.Nucl.Phys. 13, 463 (1971)

REF.

F. R. Metzger
Phys. Rev. Cl4, 543 (1976)

ELEM. SYM.	A	Z
Sm	150	62

METHOD

REF. NO.
76 Me 6

REACTION	RESULT	EXCITATION ENERGY	SOURCE		DETECTOR		ANGLE
			TYPE	RANGE	TYPE	RANGE	
G,G	LFT	2	C	1- 4	SCD-D		DST
		(1.166)					
		-					

$$\frac{N - N}{N + N} = (+3.6 \pm 2.7)\%$$

TABLE I. Properties of the low-lying 1^- levels in the stable even Sm isotopes.

Isotope	$E_{exc}(1^-)$	Γ_0 (meV)	$10^3 \times \frac{B(E1; 1^- \rightarrow 0^+)}{B(E1)_{up.}}$	N
^{144}Sm	3.225	220 ± 30	3.5 ± 0.5	82
^{142}Sm	1.465	3.1 ± 0.4	0.5 ± 0.1	86
^{140}Sm	1.166	5.4 ± 0.5	1.8 ± 0.2	88
^{138}Sm	0.963	7.3 ± 0.6	4.2 ± 0.4	90
^{136}Sm	0.921	7.4 ± 1.0	4.8 ± 0.7	92

S_M

A=152

S_M

A=152

S_M

A=152

REF.	ELEM. SYM.	A	Z
F. R. Metzger Phys. Rev. 137, B1415-20 (1965)	Sm	152	62

METHOD				REF. NO.	
Radioactive source.				65 Me 1	
REACTION	RESULT	EXCITATION ENERGY	SOURCE	DETECTOR	ANGLE
			TYPE RANGE	TYPE RANGE	
G, G	LFT	1 (0.96)	D 1 (0.96)	NAI-D	105

$$\tau = (3.9 \pm 0.4) \times 10^{-14} \text{ sec.}$$

TABLE II. Summary of the transition probabilities determined in this work, and comparison with the predictions of the single-particle model (Ref. 16).

Nucleus	E_7 (MeV)	Transi- tion	Transition probability (sec $^{-1}$)	$B(E1)_d$ (10 $^{-20}$ e 2 cm 2)	$\frac{B(E1)_d}{B(E1)_p}$
Sm^{146}	1.46	$1^- \rightarrow 0^+$	$(4.3 \pm 1.2) \times 10^{18}$	0.9	5×10^{-6}
	0.91	$1^- \rightarrow 2^+$	$(2.7 \pm 0.8) \times 10^{18}$	2.3	12×10^{-6}
Sm^{145}	0.96	$1^- \rightarrow 0^+$	$(11 \pm 1) \times 10^{18}$	7.9	4×10^{-6}
	0.84	$1^- \rightarrow 2^+$	$(14 \pm 2) \times 10^{18}$	15.4	8×10^{-6}

REF. R. B. Begzhanov, A. A. Islamov, and S. V. Starodubtsev
 J. Nucl. Phys. (USSR) 5, 250 (1967)
 Sov. J. Nucl. Phys. 5, 176 (1967)

ELEM. SYM.	A	Z
Sm	152	62

METHOD

REF. NO.

67 Be 4

HMG

REACTION	RESULT	EXCITATION ENERGY	SOURCE		DETECTOR		ANGLE
			TYPE	RANGE	TYPE	RANGE	
G,G	LFT	1.0 (963 keV)	D	1.0	NAI-D		120

$$\tau = 5.15 \pm 0.50 \times 10^{-14} \text{ sec}$$

Table I

$E_{\text{exc.}}$ keV	Solid source		Liquid source		$N(E_p)_{\text{sol}}/N(E_p)_{\text{liq.}}$	$\Gamma_\gamma(963)^*$ 10^{-4} ev	$\tau, 10^{-14} \text{ sec}$
	$\bar{\sigma}, 10^{-28} \text{ cm}^2$	$N(E_p)_{\text{sol.}} \text{ ev}^{-1}$	$\bar{\sigma}, 10^{-28} \text{ cm}^2$	$N(E_p)_{\text{liq.}} \text{ ev}^{-1}$			
963	6.0 ± 0.2	0.0171	7.1 ± 0.4	0.0202	0.85 ± 0.02	3.8 ± 0.4	7.6 ± 0.8

* We used the values of $\bar{\sigma}_{\text{ne}}$ and the calculated value $N(E_p)_{\text{gas}} = 0.0149$.

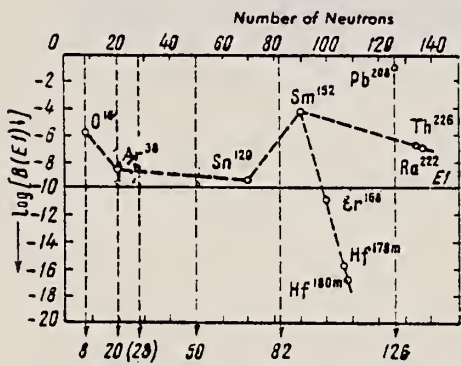


Fig. 2. Dependence of the logarithm of the reduced probability of the E1 transition on the number of neutrons for certain even-even nuclei.

ELEM. SYM.	A	Z
Sm	152	62

METHOD

REF. NO.

68 Ta 2

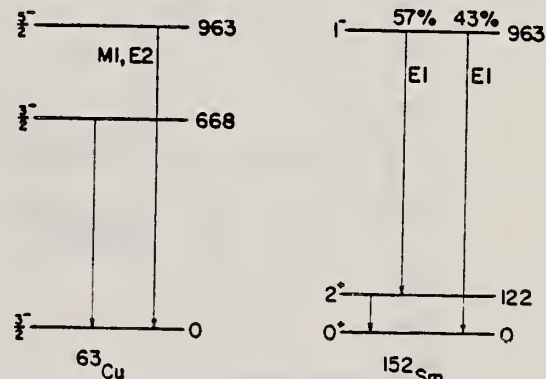
egf

REACTION	RESULT	EXCITATION ENERGY	SOURCE		DETECTOR		ANGLE
			TYPE	RANGE	TYPE	RANGE	
G,G	LFT	1	D	1	NAI-D	1	90
		(963 keV)		(963 keV)			

COMPTON SCTD SOURCETABLE I
Lifetime measurements.

Line	Mean life (10^{-14} sec)	Investigator
	963-keV level in ^{63}Cu	
1	91 ± 6	Avg. of ref. 18-20)
2	110 ± 16	This measurement
	963-keV level in ^{152}Sm	
3	4.3 ± 0.3	Avg. of ref. 23,24)
4	7.1 ± 2.1	This measurement
	Ratio $\tau(\text{Cu})/\tau(\text{Sm})$	
5	21 ± 2	From 1 and 3
6	16 ± 5	This measurement

- ¹⁸) J. B. Cumming, A. Schwarzschild, A. W. Sunyar and N. T. Porile, Phys. Rev. 120 (1960) 2128.
¹⁹) T. Rotherm, F. R. Metzger and C. P. Swann, Nucl. Physics 22 (1961) 505.
²⁰) M. A. Eswaran, H. E. Gove, A. E. Litherland and C. Broadbent, Phys. Letters 8 (1964) 52.
²¹) I. Marklund, Nucl. Physics 9 (1958) 83.
²²) I. Grodzins, Phys. Rev. 109 (1958) 1014.
²³) G. G. Shute and B. S. Sood, Proc. Roy. Soc. (London) A25 (1950) 52.
²⁴) F. R. Metzger, Phys. Rev. 137 (1965) B1415.

Fig. 11. Level schemes of ^{63}Cu and ^{152}Sm below 1000 keV. All energies are in keV.

O. V. Vasilijev, G. N. Zalesny, S. F. Semenko, V. A. Semenov
 Phys. Letters 30B, 97 (1969)

ELEM. SYM.	A	Z
Sm	152	62

METHOD

REF. NO.

69 Va 2

egf

REACTION	RESULT	EXCITATION ENERGY	SOURCE		DETECTOR		ANGLE
			TYPE	RANGE	TYPE	RANGE	
G,XN	ABX	8-23	C	8-23	BF3-I		4PI

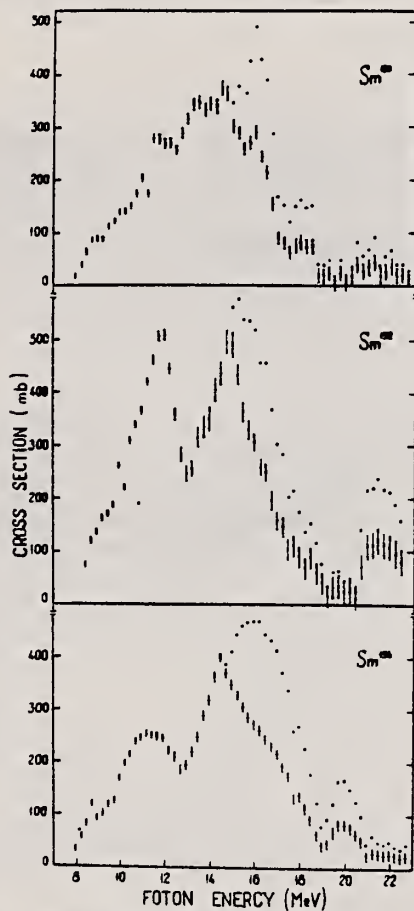
311

Fig. 3. The photoneutron and photoabsorption cross sections of ^{150}Sm , ^{152}Sm and ^{154}Sm . The symbols are the same as in fig. 2.

METHOD

REF. NO.

69 Va 3

egf

REACTION	RESULT	EXCITATION ENERGY	SOURCE		DETECTOR		ANGLE
			TYPE	RANGE	TYPE	RANGE	
G,XN	ABX	8-22	C	8-22	BF ₃ -I		4PI
		-					

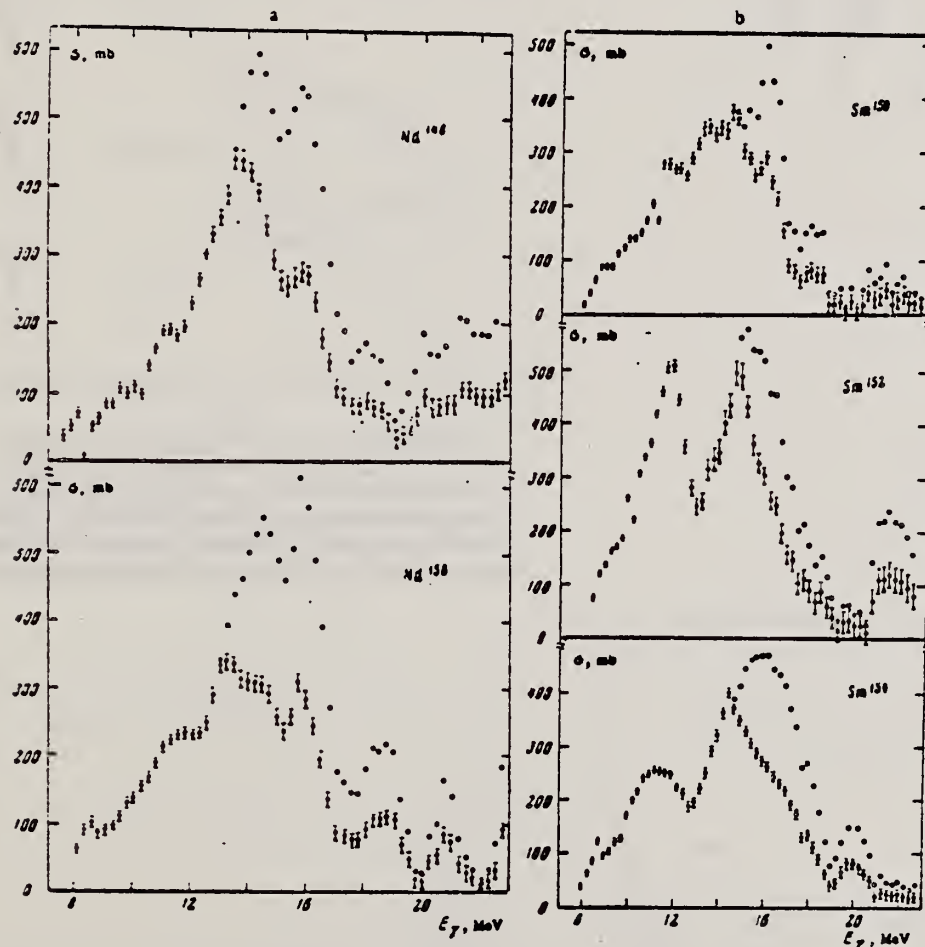
241+ SEE 69VA2

FIG. 2. Photoabsorption cross sections (black points) and photoneutron cross sections (light points): a — for Nd¹⁴⁴ and Nd¹⁵⁰ and b — for Sm¹⁵⁰, Sm¹⁵², and Sm¹⁵⁴. The indicated errors are statistical.

Table I. Giant resonance parameters of Nd^{148,150}
and Sm^{150,152,154}

Parameters	Nucleus				
	Nd ¹⁴⁸	Nd ¹⁵⁰	Sm ¹⁵⁰	Sm ¹⁵²	Sm ¹⁵⁴
σ_0 , mb		160.0		400.0	204.0
$\Delta\omega_0$, MeV		11.25		11.55	11.00
$\Delta\Gamma_0$, MeV		3.0		2.4	3.0
$\sigma_0^{(N)}$, MeV-b		0.750		1.319	0.962
σ_0 , mb		270.0		420.0	220.0
$\Delta\omega_0$, MeV		14.50		14.65	15.25
$\Delta\Gamma_0$, MeV		4.0		3.4	4.0
$\sigma_0^{(M)}$, MeV-b		1.695		2.242	2.01
$\sigma_0^{(A)}/\sigma_0^{(M)}$		2.28		1.7	2.00
$\sigma_0^{(M)}$, MeV-b	2.406	2.213	2.213	3.079	2.478
0.08 NZ/A	2.140	2.160	2.182	2.203	2.222
ρ_0		0.32		0.30	0.41
ρ_0^G		0.24		0.20	0.35
σ_0 , mb	420		280		
$\Delta\omega_0$, MeV	13.65		13.6		
$\Delta\Gamma_0$, MeV	3.0		5.5		

METHOD

REF. NO.

72 Be 3

hmg

REACTION	RESULT	EXCITATION ENERGY	SOURCE		DETECTOR		ANGLE
			TYPE	RANGE	TYPE	RANGE	
E,E/	FMF	0-1	D	50-105	MAG-D		DST

.122, .367 MEV LEVELS

Ground-state rotational band.

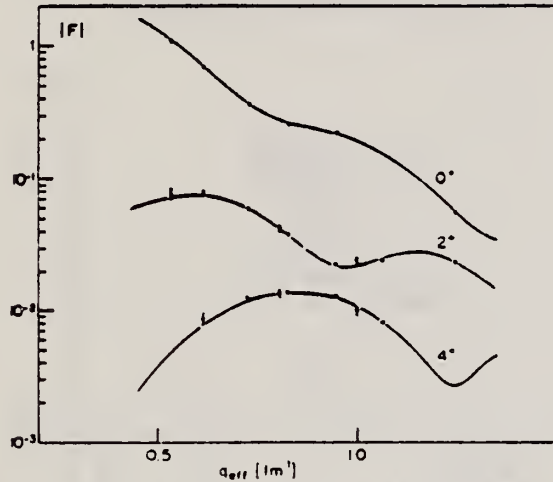
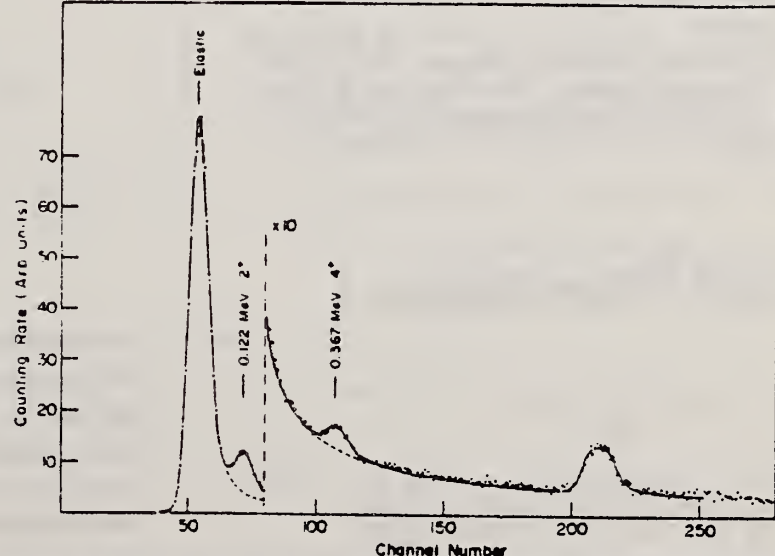


FIG. 2. Form factor F for the excitation of the ground-state rotational band; $F = (\sigma/\sigma_{\text{Wouth}})^{1/2}$. For $q_{\text{eff}} = 1.1 \text{ fm}^{-1}$ the average of two experimental points is plotted. Error bars shown represent standard deviations due to counting statistics. Where not shown, the standard deviations are smaller than the plotted points.



301

ELEM. SYM.	A	Z
Sm	152	62
REF. NO.	72 Be 13	hvm

METHOD	REF. NO.			
	72 Be 13			
REACTION	RESULT	EXCITATION ENERGY	SOURCE	DETECTOR
E, E/	FMF	0, 0	D 50-105	MAG-D

$\theta = 122^\circ, \phi = 367^\circ$ MEV

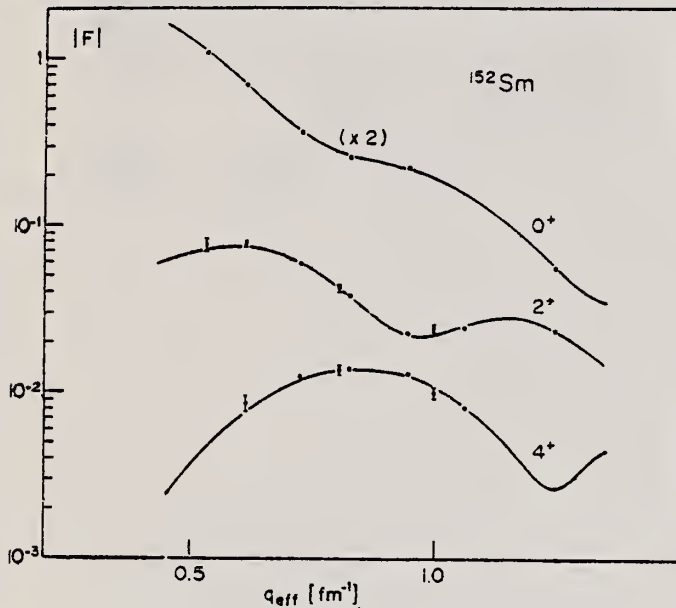


Fig. 2. Form factor F for the excitation of the ground state rotational band.

$F = \sqrt{\sigma/\sigma_{\text{mott}}}$. For $q_{\text{eff}} = 1.1 \text{ fm}^{-1}$ the average of two experimental points is plotted. Error bars shown represent standard deviations due to counting statistics. Where not shown, the standard deviations are smaller than the plotted points.

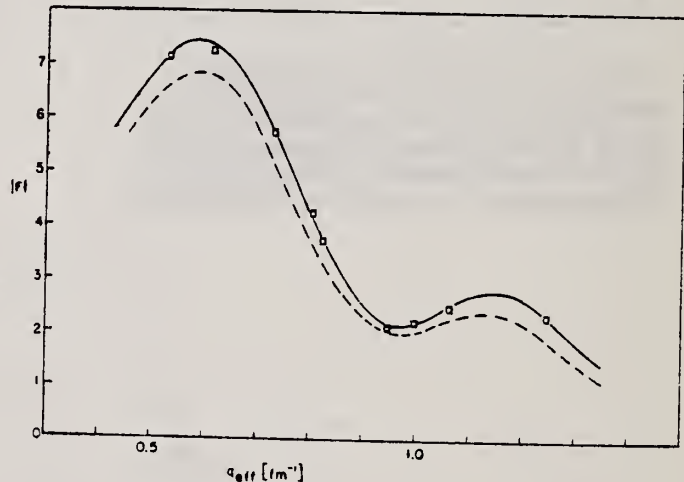


Fig. 3. Form factor for the $0-2^+$ transition, $F = \sqrt{\sigma/\sigma_{\text{mott}}}$. The solid curve assumes $\rho(r,\theta) = \bar{\rho}[1 + \exp \frac{r-R(\theta)}{t}]^{-1}$ and the skin thickness is constant. The dashed curve assumes $\rho(r,\theta) = \bar{\rho}[1 + \exp \frac{\alpha-\theta}{t}]^{-1}$ with $\alpha = r[1/(1 + \sum B_L Y_L)]$. In this last choice the skin thickness actually varies as the radius.

REF. Y. Torizuka, Y. Kojima, T. Saito, K. Itoh, A. Nakada,
 S. Mitsunobu, M. Nagao, K. Hosoyama, S. Fukuda
 PICNS-72, p.171 Sendai

ELEM. SYM.	A	Z
Sm	152	62

METHOD	REF. NO.	
	72 To 6	hvm
REACTION	RESULT	EXCITATION ENERGY
E,E/	SPC	0- 31
		D 150-250
		MAG-D
		35

Fig. 8. The K=0 and K=1 form factors in ^{152}Sm calculated by assuming a deformed Fermi type charge distribution.

LEVELS 11.5, 15.5

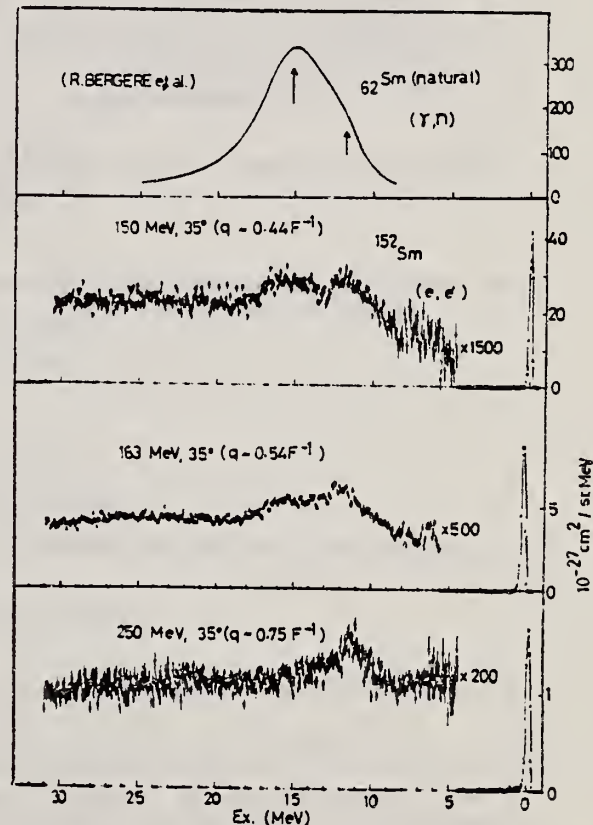
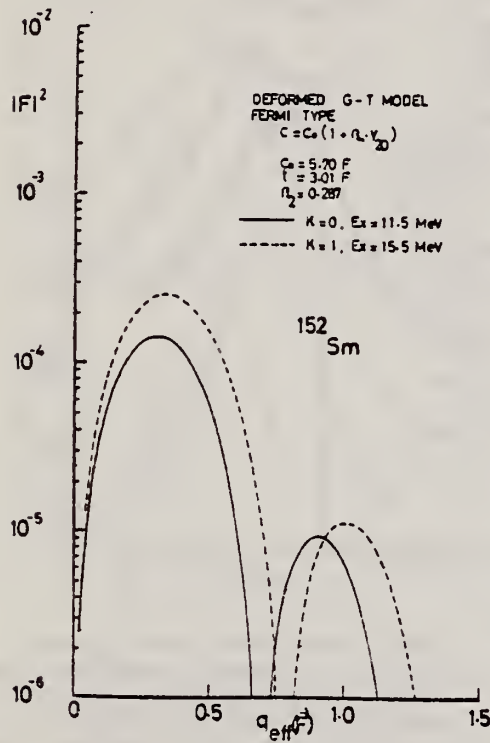


Fig. 7. The spectra of the deformed ^{152}Sm displayed as a function of the momentum transfer. The distinct peaks are seen at 11.5 and 15.5 MeV.

ELEM. SYM.	A	Z
Sm	152	62

METHOD	REF. NO.	hmg
	73 Be 10	

REACTION	RESULT	EXCITATION ENERGY	SOURCE		DETECTOR		ANGLE
			TYPE	RANGE	TYPE	RANGE	
G,SN	ABX	8- 20	D	8- 20	BF3-I		4PI
				-			

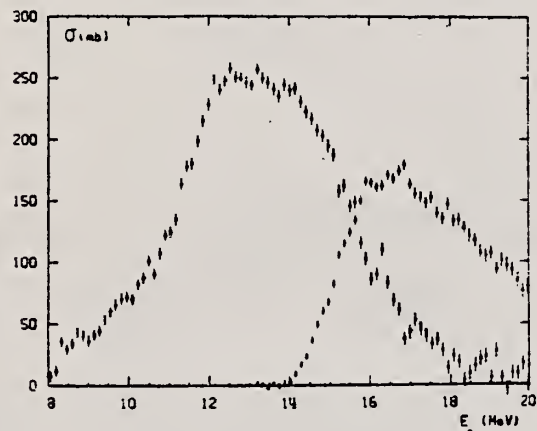


Fig. 18 Partial photoneutron cross-sections $\sigma(\gamma, n)$ and $\sigma(\gamma, 2n)$ of ^{152}Sm .

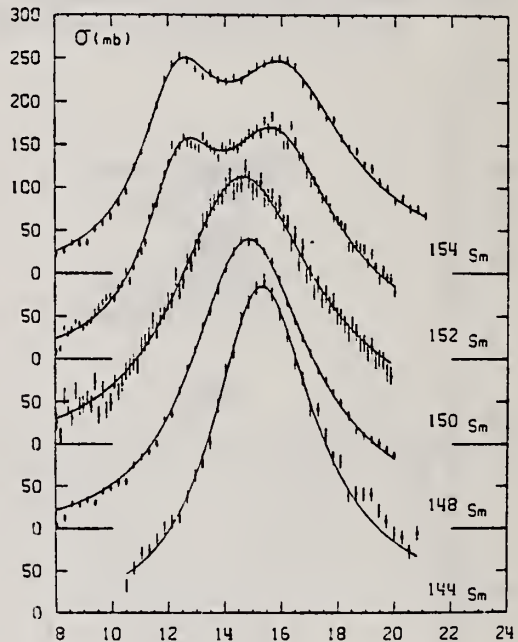


Fig. 19 Total photoneutron cross section $\sigma(\gamma, n) + \sigma(\gamma, 2n)$ of Sm isotopes. The solid lines show the best 1 Lorentz line fit (^{144}Sm , ^{148}Sm , ^{150}Sm) or 2 Lorentz lines fit (^{152}Sm and ^{154}Sm).

Table IV

	E_1 MeV	Γ_1 MeV	σ_1 mb	E_2 MeV	Γ_2 MeV	σ_2 mb
^{152}Sm	12.45 ± 0.1	3.20 ± 0.15	183 ± 10	15.85 ± 0.1	5.10 ± 0.20	226 ± 10
^{154}Sm	12.35 ± 0.1	3.37 ± 0.15	192 ± 10	16.10 ± 0.1	5.25 ± 0.20	204 ± 10

ELEM. SYM.	A	Z
Sm	152	62

METHOD	REF. NO.	
	73 Go 6	hmrg
REACTION	RESULT	EXCITATION ENERGY
G,XN	ABX	8- 20
		C
		8- 20
		BF3-I
ANGLE		
		4PI

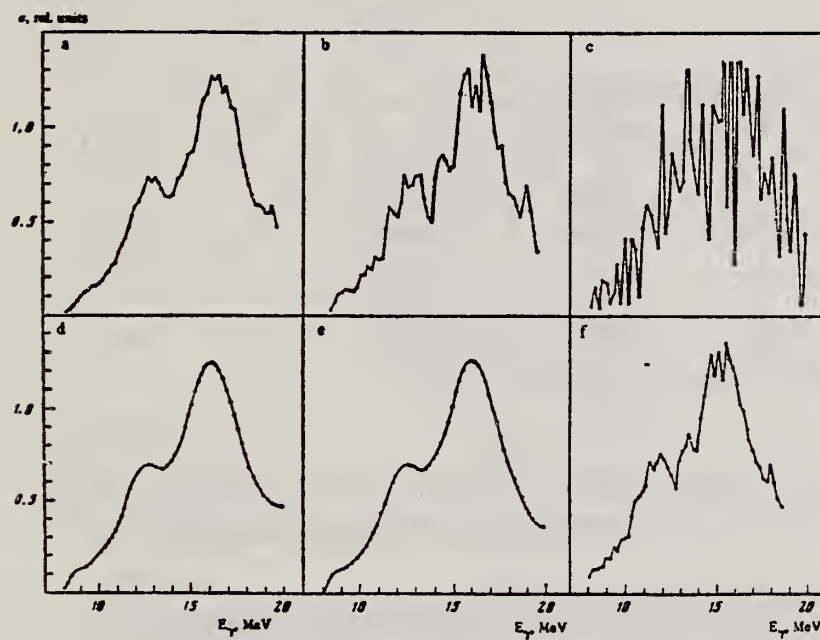


FIG. 1. Calculations of the cross section for Sm^{152} by different methods: a, b, c—the Penfold-Leiss method with 1-, 0.5-, and 0.2-MeV spacings; [16] d—the method of Tikhonov; [15] e—the method of Cook; [18] f—the cross section in c, smoothed as proposed in [17].

[15] A.N. Tikhonov, Dokl. Akad. Nauk SSSR 151, 501 (1963).

[16] A.S. Penfold and J.E. Leiss, Phys. Rev. 114, 1332 (1959).

[17] V.N. Orlin, Abstracts and Reports at the XXII Conference on Nuclear Spectroscopy and Structure, Kiev, 1972 (in Russian).

[18] B.C. Cook, Nucl. Instr. and Meth. 24, 256 (1963).

METHOD

REF. NO.

74 Ca 5

egf

REACTION	RESULT	EXCITATION ENERGY	SOURCE		DETECTOR		ANGLE
			TYPE	RANGE	TYPE	RANGE	
G,N *	ABX	8- 20	D	8- 20	BF3-I		4PI
G,ZN **	ABX	13- 20	D	13- 20	BF3-I		4PI

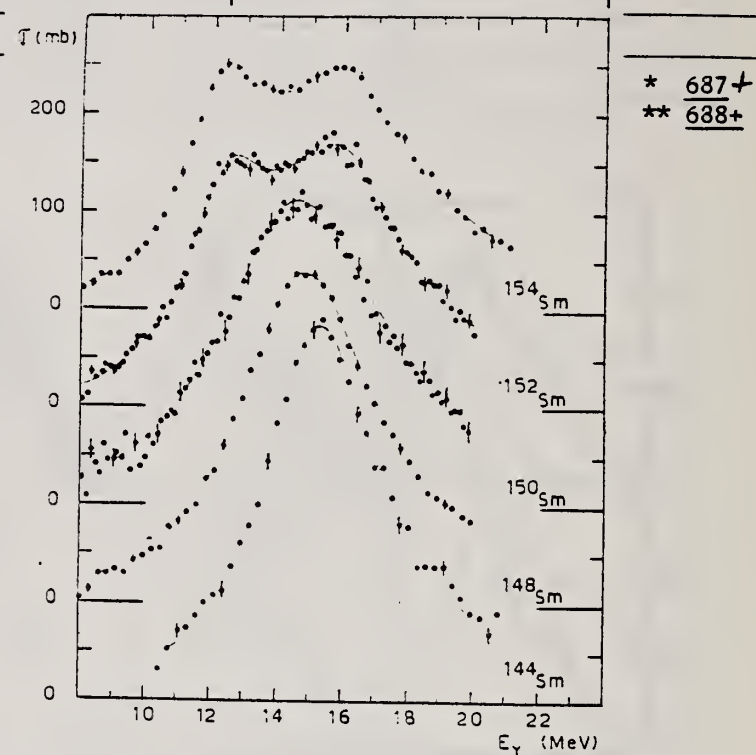


Fig. 7. Total photoneutron cross sections $\sigma_T(E)$ of the doubly even samarium isotopes. Best single Lorentz line fits are shown for ^{144}Sm , ^{148}Sm and ^{150}Sm . For ^{152}Sm and ^{154}Sm the best two Lorentz line fits are presented. Corresponding Lorentz line parameters are given in table 2.

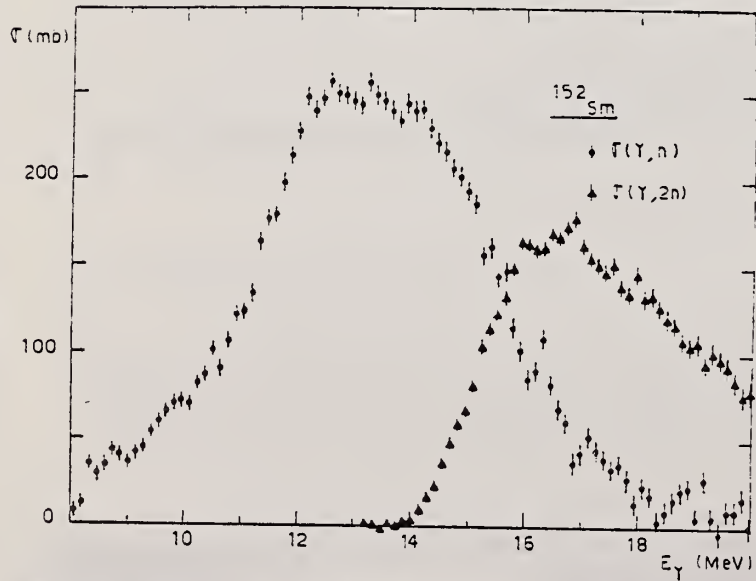


Fig. 5. Partial photoneutron cross sections $[\sigma(\gamma, n) + \sigma(\gamma, np)]$ and $\sigma(\gamma, 2n)$ of ^{152}Sm .

EET 306

(over)
U.S. DEPARTMENT OF COMMERCE
NATIONAL BUREAU OF STANDARDS

TABLE 2
Lorentz line parameters

	E_1 (MeV)	σ_1 (mb)	Γ_1 (MeV)	E_2 (MeV)	σ_2 (mb)	Γ_2 (MeV)
$^{144}\text{Sm}^*$	15.3 \pm 0.1	384 \pm 20	4.37 \pm 0.15			
$^{148}\text{Sm}^*$	14.8 \pm 0.1	339 \pm 12	5.1 \pm 0.2			
$^{148}\text{Sm}^{**}$	14.1	335	4			
$^{150}\text{Sm}^*$	14.6 \pm 0.1	312 \pm 20	6.0 \pm 0.2			
$^{150}\text{Sm}^{**}$	13.6	360	5.5			
$^{152}\text{Sm}^*$	12.45 \pm 0.10	183 \pm 10	3.2 \pm 0.15	15.85 \pm 0.10	226 \pm 10	5.1 \pm 0.1
$^{152}\text{Sm}^{**}$	11.55	400	2.4	14.65	420	3.4
$^{154}\text{Sm}^*$	12.35 \pm 0.10	192 \pm 10	3.35 \pm 0.15	16.1 \pm 0.1	204 \pm 10	5.23 \pm 0.12
$^{154}\text{Sm}^{**}$	11	204	3	15.25	320	4

* Corresponding to best fits shown in fig. 7.

** Values taken from Vasilijev ^{23,24)} for comparison.

TABLE 3
Different integrated cross sections as defined in the text

	^{144}Sm	^{148}Sm	^{150}Sm	^{152}Sm	^{154}Sm
E_M (MeV)	21	20	20	20	21
σ_0 (MeV · b)	2 \pm 0.14	1.94 \pm 0.1	2 \pm 0.14	2.05 \pm 0.1	2.07 \pm 0.1
σ'_0 (MeV · b)	2.63	2.71	2.94	2.75	2.65
$\frac{\sigma'_0 A}{0.06 NZ}$	1.24	1.25	1.35	1.24	1.2
σ_{-1} (mb)	131 \pm 15	134 \pm 10	141 \pm 15	144 \pm 10	145 \pm 13
σ_{-2} (mb · MeV ⁻¹)	8.7 \pm 0.8	9.5 \pm 0.7	10.3 \pm 0.9	10.6 \pm 0.7	10.6 \pm 0.7

²³O. Vasilijev et al., Sov.J.Nucl.Phys.10, 263 (1970)

²⁴O. Vasilijev et al., Sov.J.Nucl.Phys.13, 463 (1971)

REF.

T. Cooper, W. Bertozzi, J. Heisenberg, S. Kowalski,
 W. Turchinetz, C. Williamson, L. Cardman, S. Fivozinsky,
 J. Lightbody, Jr., and S. Penner
 Phys. Rev. C13, 1083 (1976)

ELEM. SYM.	A	Z
Sm	152	62

METHOD

REF. NO.
76 Co 3

hmg

REACTION	RESULT	EXCITATION ENERGY	SOURCE		DETECTOR		ANGLE
			TYPE	RANGE	TYPE	RANGE	
E,E/	FMF	1, 1	D	49-106	MAG-D		DST
				-			

LEVELS .3665, .1218

TABLE II. Cross sections from ^{152}Sm data.

Energy (MeV)	Angle (deg)	q_{eff} (fm $^{-1}$)	Elastic		$\frac{d\sigma}{d\Omega_{\text{exp}}}$ (mb)	$\frac{d\sigma}{d\Omega_{\text{best fit}}}$ (mb)	$\frac{d\sigma}{d\Omega_{\text{exp}}}$ (mb)	$\frac{d\sigma}{d\Omega_{\text{exp}}}$ (mb)
			2^+	4^+				
49.60	93.43	0.535	$0.400 \times 10 \pm 4\%$	0.398×10	$0.802 \times 10^{-1} \pm 15\%$...	
60.53	93.43	0.615	$0.111 \times 10 \pm 4\%$	0.109×10	$0.545 \times 10^{-1} \pm 10\%$	$0.680 \times 10^{-3} \pm 25\%$		
60.50	145.65	0.805	...	0.214×10^{-1}	$0.140 \times 10^{-2} \pm 10\%$	$0.961 \times 10^{-4} \pm 12\%$		
67.08	93.43	0.729	$0.190 \pm 4\%$	0.188	$0.197 \times 10^{-1} \pm 7\%$	$0.905 \times 10^{-3} \pm 6\%$		
80.38	145.65	0.998	...	0.524×10^{-2}	$0.195 \times 10^{-3} \pm 10\%$	$0.300 \times 10^{-3} \pm 15\%$		
89.75	93.14	0.827	$0.675 \times 10^{-1} \pm 4\%$	0.762×10^{-1}	$0.590 \times 10^{-2} \pm 7\%$	$0.786 \times 10^{-3} \pm 5\%$		
105.71	93.46	0.947	$0.378 \times 10^{-1} \pm 8\%$	0.377×10^{-1}	$0.130 \times 10^{-2} \pm 7\%$	$0.453 \times 10^{-3} \pm 5\%$		
104.95	110.79	1.062	...	0.106×10^{-1}	$0.809 \times 10^{-3} \pm 5\%$	$0.933 \times 10^{-4} \pm 7\%$		
105.68	146.01	1.216	$0.168 \times 10^{-3} \pm 4\%$	0.182×10^{-3}	$0.119 \times 10^{-3} \pm 5\%$	$\leq 0.38 \times 10^{-6}$		

TABLE VIII. Deformed Fermi best fit parameters.

	Units	^{152}Sm	^{154}Sm	^{222}Th	^{232}U
c_0	fm	5.8044	5.9387	6.7915	6.8054
t	fm	0.5814	0.5223	0.5713	0.6049
β_2		0.297 ± 0.003	0.311 ± 0.003	0.233 ± 0.002	0.261 ± 0.002
β_4		0.070 ± 0.003	0.087 ± 0.002	0.101 ± 0.003	0.097 ± 0.003
β_6		-0.0120	-0.180	0.0	0.0
$B(E2)$	$e^2 b^2$	3.38 ± 0.07	4.40 ± 0.09	$9.21 = 0.09$	11.70 ± 0.15
$B(E4)$	$e^2 b^4$	0.136 ± 0.013	0.221 ± 0.010	$1.16 = 0.05$	1.20 ± 0.06
rms radius	fm	5.0322	5.126	5.7723	5.842
ρ_2 Transition radius	fm	6.937	6.950	7.895	7.979
ρ_4 Transition radius	fm	7.757	7.704	8.540	8.748

REF. A. Nakada, N. Haik, J. Alster, J. B. Bellicard, S. Cochavi,
 B. Frois, M. Huet, P. Leconte, P. Ludeau, M. A. Moinester,
 Phan Xuan Ho, and S. Turck
 Phys. Rev. Lett. 38, 584 (1977)

ELEM. SYM.	A	Z
Sm	152	62
REF. NO.		
77 Na 2		hmg

METHOD

REACTION	RESULT	EXCITATION ENERGY	SOURCE	DETECTOR	ANGLE	
			TYPE	RANGE	TYPE	RANGE
E,E/	LFT	0- 1 (.122-.712)	D	252	MAG-D	-
						DST

Elastic and inelastic angular distributions were measured, including that for the 6^+ state at 0.712 MeV. Parameters of the charge distribution were determined, and compared with those obtained with low-energy electrons and with mass deformation parameters from α scattering. The data also compared to a Hartree-Fock calculation.

2+,4+,6+ STATES

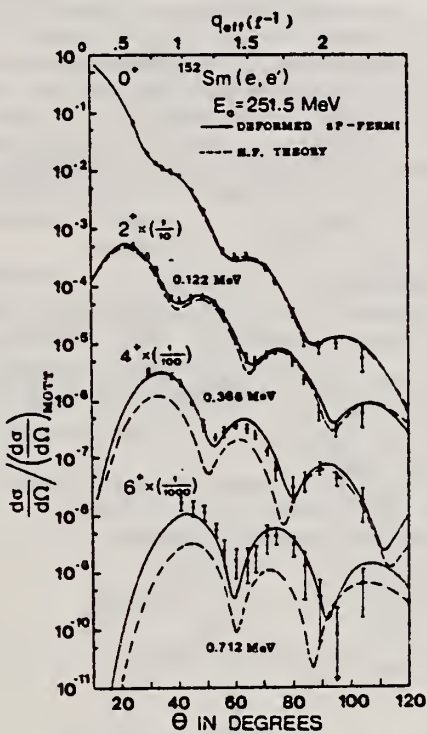


FIG. 1. Experimental values of $\sigma/\sigma_{\text{Mott}}$ for the ground-state rotational band of ^{152}Sm , as a function of angle and $q_{\text{eff}} = q(1 + \frac{1}{2}Z\alpha(r^2)^{-1/2}E^{-1})$. The solid lines are phenomenological fits (see text) and the dashed lines are the results of the use of HF wave functions.

Over

TABLE I. Charge and mass distribution parameters of Sm¹⁵².

Reaction	Reference	$\langle r^2 \rangle^{1/2}$	c_0	t	β_2	β_4	β_6	$B(E2)$ ($e^2 \cdot b^2$)	$B(E4)$ ($e^2 \cdot b^2$)	$B(E6)$ ($e^2 \cdot b^2$)
250 MeV (e, e')	Present work	5.0246	5.778	0.545	0.286	0.092	0.010	3.45	0.210	0.0114
			± 0.010	± 0.037	± 0.002	± 0.002	± 0.002	± 0.06	± 0.013	± 0.0007
Low energy (e, e')	2,4	5.0922	5.804	0.581	0.287	0.070	-0.012^a	3.38	0.136	
					± 0.003	± 0.003		± 0.07	± 0.013	
Coulomb exci- tation (α, α')	5				0.276	0.065		3.45	0.137	
50 MeV (α, α')	2,15				± 0.012	± 0.029		± 0.07	± 0.078	
HF calcu- lation	12	4.998			0.256	0.061	-0.006			
								2.99	0.089	0.0027

^aFixed.

²D.L. Hendrie, N.K. Glendenning, B.G. Harvey,
O.N. Jarvis, H.H. Duhm, J. Saudinos, and
J. Mahoney, Phys. Lett. 26B, 127 (1968)

⁴W. Bertozzi, T. Cooper, N. Ensslin, J. Heisenberg,
S. Kowalski, M. Mills, W. Turchinetz, C. Williamson,
S.P. Fivozinsky, J.W. Lightbody, Jr., and S. Penner,
Phys. Rev. Lett. 28, 1711 (1972); T. Cooper,
W. Bertozzi, J. Heisenberg, S. Kowalski, W. Turchinetz,
C. Williamson, L. Cardman, S. Fivozinsky, J.W. Lightbody,
Jr., and S. Penner, Phys. Rev. C 13, 1083 (1976).

⁵T.K. Saylor, J.X. Saladin, I.Y. Lee, and K.A. Erb,
Phys. Lett. 42B, 51 (1972); W. Bruckner, D. Husar,
D. Pelte, K. Traxel, M. Samuel, and U. Smilansky,
Nucl. Phys. A321, 159 (1974)

¹²D. Gogny, in Nuclear Self Consistent Fields,
edited by G. Ripka and M. Porneuf (North-
Holland, Amsterdam, 1976); J. Decharge,
M. Girod, and D. Gogny, Phys. Lett. 55B,
361 (1975)

¹⁵D.L. Hendrie, Phys. Lett. 31, 478 (1973)

REF. B.S. Dolbilkin, S. Ohsawa, Y. Torizuka, T. Saito, Y. Mizuno,
 K. Saito
 Phys. Rev. C25, 2255 (1982)

ELEM. SYM.	A	Z
Sm	152	62

METHOD	REF. NO.	egf
	82 Do 6	
REACTION	RESULT	EXCITATION ENERGY
E,E/		5-33
		D
		150-215
		MAG-D
		DST

Q .38-.64 FM-1

The electron scattering cross sections from the enriched ^{148}Sm (96.5%) and ^{152}Sm (99.2%) isotopes have been measured between 5 and 33 MeV excitation energies for incident energies in the range of between 150 and 215 MeV and scattering angles of 30°, 35°, and 40°. The giant resonances at $E_x = 14.8 (78A^{-1/3})$, 11.6 ($61A^{-1/3}$), 15.5 ($82A^{-1/3}$), and 24 ($129A^{-1/3}$) MeV for ^{148}Sm were classified according to their momentum transfer dependence. The K splittings of the giant $E1 (T=1)$ and $E2 (T=0,1)$ resonances for deformed ^{152}Sm were observed in agreement with a vibrating potential model. The splittings between the $K=0^+$ and 2^+ components for the isoscalar and isovector quadrupole resonances are ~ 2 MeV and ~ 5 MeV, respectively. The fitted parameters classified as the giant monopole resonance are the same for spherical ^{148}Sm and for deformed ^{152}Sm . The difference between the isoscalar giant resonance parameters for resonance energies and width found from hadron scattering and those for electron scattering is discussed for the rare-earth region.

NUCLEAR REACTIONS $^{148,152}\text{Sm}(e,e')$, enriched targets, $E_0 = 150$ to 215 MeV, $\theta = 30^\circ, 35^\circ, 40^\circ$, $q = 0.38 - 0.64 \text{ fm}^{-1}$. Measured $d^2\sigma/d\Omega dE_x$ up to 33 MeV in excitation energy; deduced multipolarity, excitation energy, width, sum rule exhaustion of giant resonances.

TABLE IV. Comparison between (e,e') results and theoretical results for the giant multipole resonance energy (MeV).

Type	Nucleus	Isoscalar		Isovector				
		Present work	Ref. 10	Theory Ref. 9	Ref. 24	Present work	Theory Ref. 10	Ref. 9
GMR	^{148}Sm	15.5 ± 0.3			15.1			
	^{152}Sm	15.7 ± 0.3		10.7	10.5			
GDR	^{148}Sm			18.3	15.9			
	^{152}Sm					14.8	14.8	
GQR	^{148}Sm					12.45	12.3	12.0
	^{152}Sm					15.85	16.3	15.0
	^{148}Sm	11.6 ± 0.2	10.9		11.9	24.3 ± 0.4	26.4	
	^{152}Sm	10.6 ± 0.2	9.9	11.0	10.5	21.0 ± 0.9	24.1	19.5
	^{148}Sm	11.4 ± 0.4	10.4	12.0		23.2 ± 1.0	25.2	22.5
	^{152}Sm	12.7 ± 0.4	11.8	13.0	13.1	26.0 ± 0.5	28.8	25.5

(OVER)

TABLE V. Parameters of the isoscalar GQR in the Sm isotopes.

Nucleus	E_x (MeV)	Γ (MeV)	EWSR (%)	Reaction	Reference
^{144}Sm	13.0 ± 0.3	3.9 ± 0.2	91 ± 25	(α, α')	25
^{144}Sm	12.4 ± 0.4	2.6 ± 0.4	85 ± 15	(α, α')	6
^{144}Sm	12.1 ± 0.2	2.4 ± 0.2	45 ± 15	(α, α')	8
^{144}Sm	12.5	3.4	60	(α, α')	26
^{144}Sm	11.9 ± 0.2	2.9 ± 0.2		(e, e')	27
^{148}Sm	12.5 ± 0.2	4.3 ± 0.2	104 ± 25	(α, α')	25
^{148}Sm	11.6 ± 0.2	3.1 ± 0.2	100 ± 10	(e, e')	Present work
^{150}Sm	11.8 ± 0.2	3.3 ± 0.2		(e, e')	27
	10.6 ± 0.2	2.4 ± 0.2	20 ± 5		
^{152}Sm	11.4 ± 0.4	2.7 ± 0.2	45 ± 9	(e, e')	Present work
	12.7 ± 0.4	3.0 ± 0.2	35 ± 7		
^{154}Sm	12.4 ± 0.3	4.7 ± 0.3	102 ± 25	(α, α')	25
^{154}Sm	12.2	4.5		(α, α')	7
^{154}Sm	11.8 ± 0.3	3.7 ± 0.3		(α, α')	8
^{154}Sm	10.9 ± 0.2	4.5 ± 0.2		(e, e')	27

TABLE VI. Comparison of the GMR parameters in the Sm isotopes obtained from various reactions.

Nucleus	E_x (MeV)	Γ (MeV)	EWSR (%)	Reaction	Reference
^{144}Sm	15.1 ± 0.5	2.9 ± 0.5	100 ± 50	(α, α')	6
^{144}Sm	14.6 ± 0.2	3.0 ± 0.3	140 ± 40	(α, α')	8
^{144}Sm	15.2	2.5		(α, α')	26
^{144}Sm	15.5 ± 0.5	2.5 ± 0.5	100 ± 25	(p, p')	31
^{144}Sm	14.7 ± 0.2	2.9 ± 0.2	67 ± 13	$(^3\text{He}, ^3\text{He}')$	32
^{144}Sm	14.8 ± 0.2	2.4 ± 0.15	20 ± 10	(e, e')	30
^{148}Sm	15.5 ± 0.3	3.0 ± 0.2	100 ± 10	(e, e')	Present work
^{150}Sm	15.1 ± 0.25	3.0 ± 0.25	60 ± 19	$(^3\text{He}, ^3\text{He}')$	32
^{152}Sm	14.8 ± 0.25	3.1 ± 0.25	54 ± 9	$(^3\text{He}, ^3\text{He}')$	32
^{152}Sm	15.7 ± 0.3	3.1 ± 0.4	100 ± 20	(e, e')	Present work
^{154}Sm	15.5 ± 0.5	2.5 ± 0.5	100 ± 25	(p, p')	31
^{154}Sm	14.9 ± 0.3	2.6 ± 0.4	55 ± 15	(α, α')	8

S_M
 $A=154$

S_M
 $A=154$

S_M
 $A=154$

Elem. Sym.	A	Z
Sm	154	62

Method 33 MeV Synchrotron; radioactivity; NaI spectrometer; ionization chamber

Ref. No.
 59 Ca 3

Reaction	E or ΔE	E_0	Γ	$\int \sigma dE$	$J\pi$	Notes
$^{154}\text{Sm}(\gamma, n)$	Bremss. ~ 8-32	13.6	6.5 MeV	2.4 ± 0.4 MeV-b		

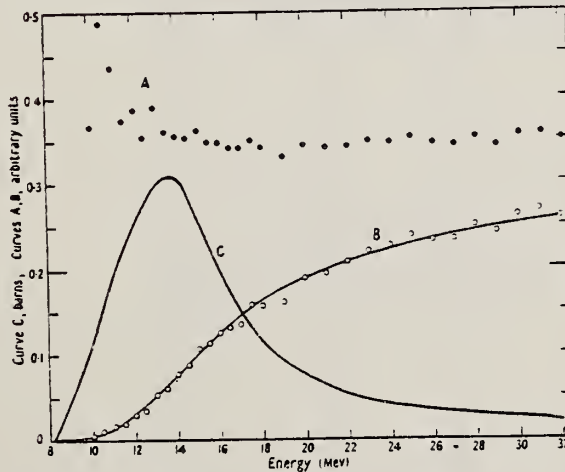


Figure 5. A, the ratio of activation curves $^{154}\text{Sm}(\gamma, n)/^{181}\text{Ta}(\gamma, n)$; B, activation curve for $^{154}\text{Sm}(\gamma, n)$; C, derived cross section: $^{154}\text{Sm}(\gamma, n)$.

Elem. Sym.	A	Z
Sm	154	62

Method						Ref. No.
Linac; radioactivity					62 Ko 3	JHH
Reaction	E or ΔE	E_0	Γ	$\int \sigma dE$	$J\pi$	Notes
$\text{Sm}^{154}(\gamma, p)$	Bremss. 20					Product nucleus, Pm^{153} , has $T_{1/2} = 5.5 \pm 0.2$ min., E_β end-pt. = 1.65 ± 0.05 MeV, E_γ 's = 0.125, 0.180 MeV. $\frac{\sigma_{\text{Sm}^{154}(\gamma, p)}}{\sigma_{\text{Sm}^{154}(\gamma, n)}} = 1/950$

METHOD

REF. NO.

69 Mo 1

hmg

REACTION	RESULT	EXCITATION ENERGY	SOURCE		DETECTOR		ANGLE
			TYPE	RANGE	TYPE	RANGE	
E, F	ABX	THR-999	D	60-999	TRK-I		DST
G, F	ABX	THR-999	C	60-999	TRK-I		DST

Tabular data given; angular distribution isotopes

999=1 GEV

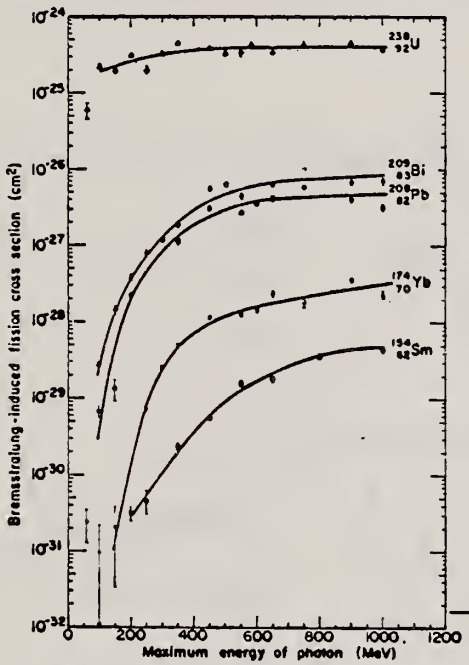


FIG. 4. Bremsstrahlung-induced fission cross section per equivalent quantum.

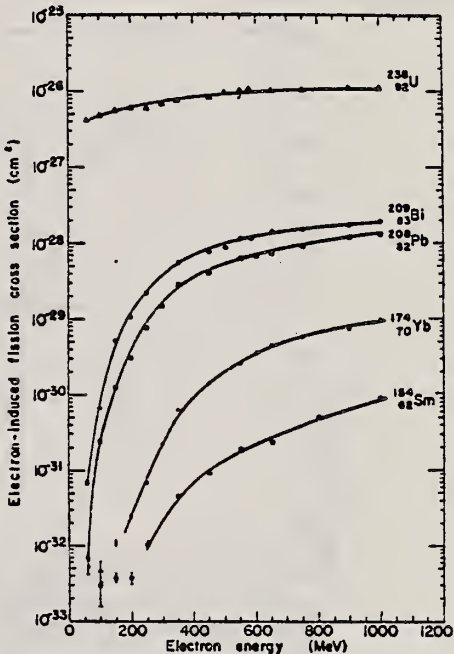


FIG. 2. Electron-induced fission cross-section data. Different symbols for the same isotope refer to different targets.

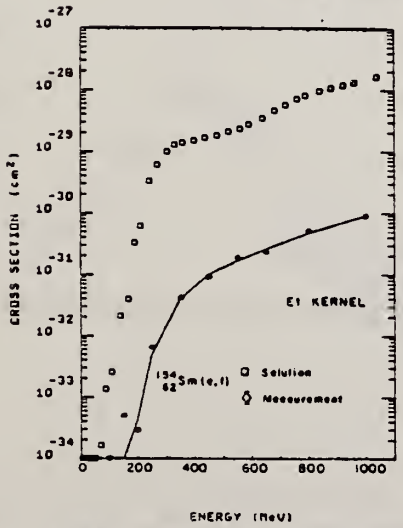


FIG. 10. Photofission cross section as a function of energy for ¹⁵⁴Sm (open squares) as obtained by unfolding the electron-induced fission cross-section data (diamonds) with the E1 kernel. The solid line is the fit to the electron-induced fission cross sections which is obtained by folding back the photofission cross section into the E1 kernel.

REF.

O. V. Vasilijev, G. N. Zalesny, S. F. Semenko, V. A. Semenov
 Phys. Letters 30B, 97 (1969)

ELEM. SYM.	A	Z
Sm	154	62
REF. NO.		
69 Va 2		egf

METHOD

REACTION	RESULT	EXCITATION ENERGY	SOURCE		DETECTOR		ANGLE
			TYPE	RANGE	TYPE	RANGE	
G,XN	ABX	8-23	C	8-23	BF3-I		4PI

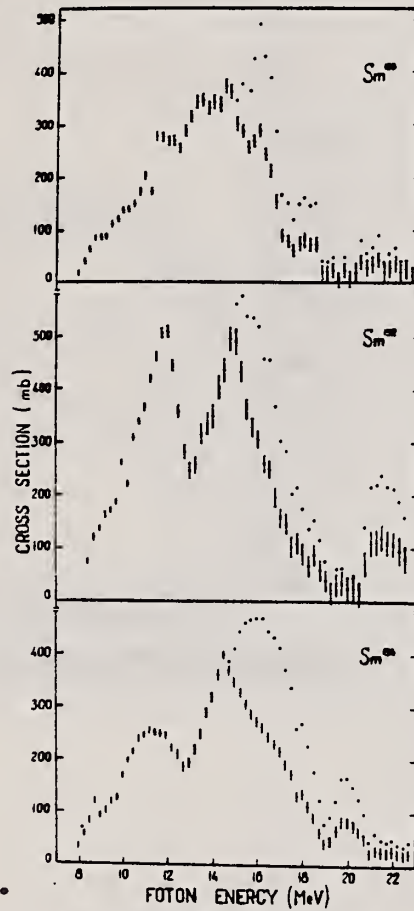
212

Fig. 3. The photoneutron and photoabsorption cross sections of ^{150}Sm , ^{152}Sm and ^{154}Sm . The symbols are the same as in fig. 2.

METHOD

REF. NO.

69 Va 3

egf

REACTION	RESULT	EXCITATION ENERGY	SOURCE		DETECTOR		ANGLE
			TYPE	RANGE	TYPE	RANGE	
G,XN	ABX	S-22	C	S-22	BF ₃ -I		4PI

242 SEE 69VA2

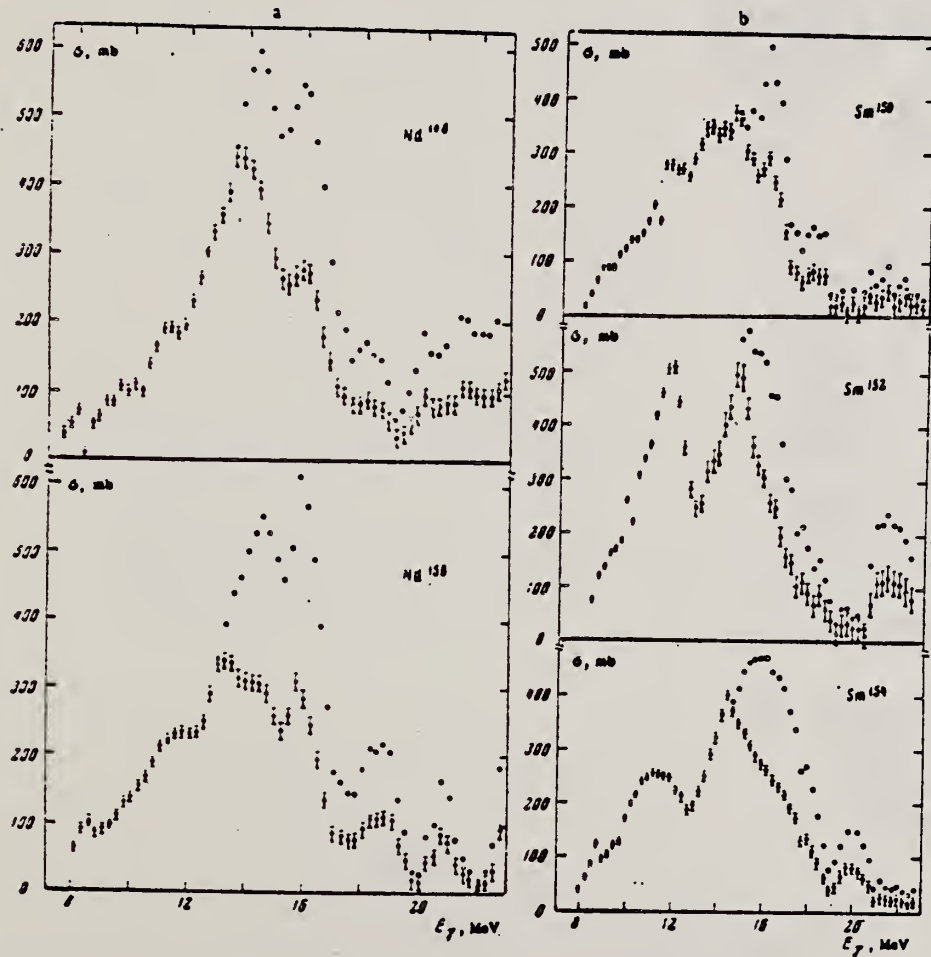


FIG. 2. Photoabsorption cross sections (black points) and photoneutron cross sections (light points): a — for Nd¹⁴⁴ and Nd¹⁵⁰ and b — for Sm¹⁵⁰, Sm¹⁵², and Sm¹⁵⁴. The indicated errors are statistical.

[over]

Table I. Giant resonance parameters of Nd^{148,150}
and Sm^{156,158,154}

Parameters	Nucleus				
	Nd- [*]	Nd ^{**}	Sm ¹⁵⁶	Sm ¹⁵⁸	Sm ¹⁵⁴
σ_0 , mb		160.0		400.0	204.0
$\Delta\omega_0$, MeV		11.25		11.55	11.00
$\Delta\Gamma_0$, MeV		3.0		2.4	3.0
$\sigma_0^{(inf)}$, MeV-b		0.750		1.319	0.962
τ_0 , mb		270.0		420.0	320.0
$\Delta\omega_0$, MeV		14.50		14.65	15.25
$\Delta\Gamma_0$, MeV		5.0		3.4	4.0
$\sigma_0^{(inf)}$, MeV-b		1.695		2.242	2.01
$\sigma_0^{(inf)}/\sigma_0^{(inf)}$		2.28		1.7	2.00
$\sigma^{(inf)}$, MeV-b	2.406	2.213	2.213	3.079	2.478
$0.06 NZ/A$	2.140	2.160	2.182	2.203	2.223
ρ_0		0.32		0.30	0.41
ρ_0'		0.28		0.30	0.35
σ_0 , mb	420		380		
$\Delta\omega_0$, MeV	13.63		13.6		
$\Delta\Gamma_0$, MeV	5.0		5.5		

ELEM. SYM.	A	Z
Sm	154	62

METHOD

REF. NO.

73 Be 10

hmg

REACTION	RESULT	EXCITATION ENERGY	SOURCE		DETECTOR		ANGLE
			TYPE	RANGE	TYPE	RANGE	
G, SN	ABX	8- 22	D	8- 22	BF3-I		4PI

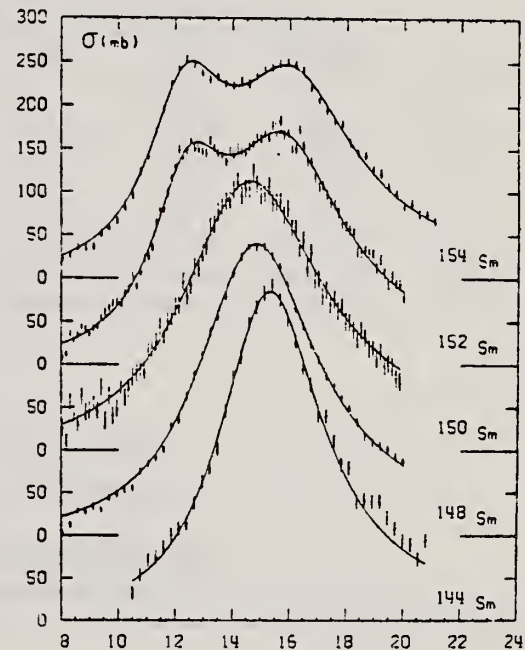


Fig. 19 Total photoneutron cross section $\sigma(\gamma, n) + \sigma(\gamma, 2n)$ of Sm isotopes. The solid lines show the best 1 Lorentz line fit (^{144}Sm , ^{148}Sm , ^{150}Sm) or 2 Lorentz lines fit (^{152}Sm and ^{154}Sm).

Table IV

	E_1 MeV	Γ_1 MeV	σ_1 mb	E_2 MeV	Γ_2 MeV	σ_2 mb
^{152}Sm	12.45 ± 0.1	3.20 ± 0.15	183 ± 10	15.85 ± 0.1	5.10 ± 0.20	226 ± 10
^{154}Sm	12.35 ± 0.1	3.37 ± 0.15	192 ± 10	16.10 ± 0.1	5.25 ± 0.20	204 ± 10

P. Carlos, H. Beil, R. Bergere, A. Lepretre, A. De Miniac,
and A. Veyssiére
Nucl. Phys. A225, 171 (1974)

ELEM. SYM.	A	Z
Sm	154	62

METHOD

REF. NO.

74 Ca 5

egf

REACTION	RESULT	EXCITATION ENERGY	SOURCE		DETECTOR		ANGLE
			TYPE	RANGE	TYPE	RANGE	
G, N *	ABX	8- 21	D	8- 21	BF3-I		4PI
G, 2N **	ABX	13- 21	D	13- 21	BF3-I		4PI

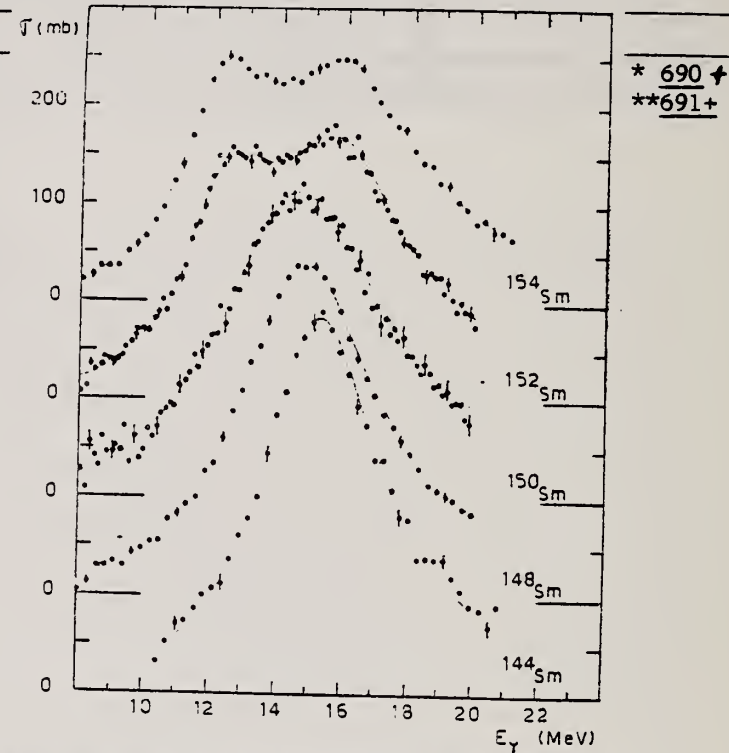


Fig. 7. Total photoneutron cross sections $\sigma_\tau(E)$ of the doubly even samarium isotopes. Best single Lorentz line fits are shown for ^{144}Sm , ^{148}Sm and ^{150}Sm . For ^{152}Sm and ^{154}Sm the best two Lorentz line fits are presented. Corresponding Lorentz line parameters are given in table 2.

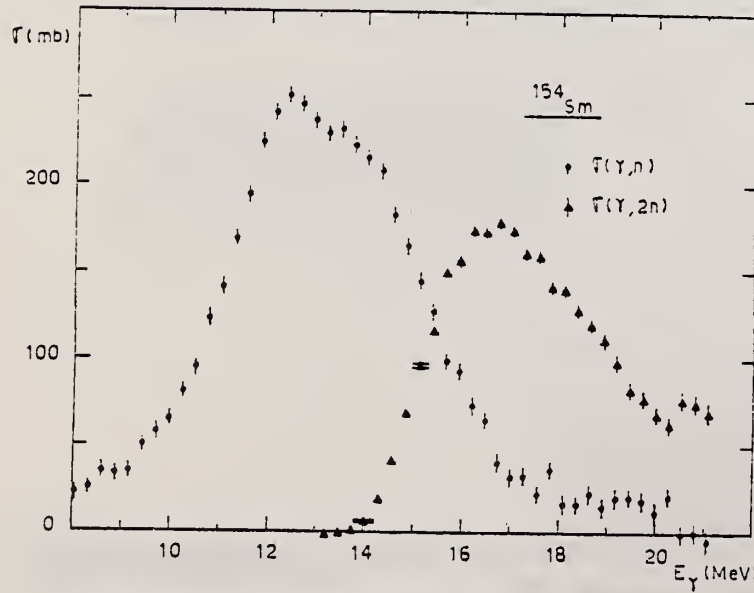


Fig. 6. Partial photoneutron cross sections $[\sigma(\gamma, n) + \sigma(\gamma, np)]$ and $\sigma(\gamma, 2n)$ of ^{154}Sm .

(over)

EET 322

U.S. DEPARTMENT OF COMMERCE
NATIONAL BUREAU OF STANDARDS

TABLE 2
Lorentz line parameters

	E_1 (MeV)	σ_1 (mb)	I'_1 (MeV)	E_2 (MeV)	σ_2 (mb)	I'_2 (MeV)
$^{144}\text{Sm}^*$	15.3 \pm 0.1	384 \pm 20	4.37 \pm 0.15			
$^{148}\text{Sm}^*$	14.8 \pm 0.1	339 \pm 12	5.1 \pm 0.2			
$^{148}\text{Sm}^{**}$	14.1	335	4			
$^{150}\text{Sm}^*$	14.6 \pm 0.1	312 \pm 20	6.0 \pm 0.2			
$^{150}\text{Sm}^{**}$	13.6	360	5.5			
$^{152}\text{Sm}^*$	12.45 \pm 0.10	183 \pm 10	3.2 \pm 0.15	15.85 \pm 0.10	226 \pm 10	5.1 \pm 0.2
$^{152}\text{Sm}^{**}$	11.55	400	2.4	14.65	420	7.4
$^{154}\text{Sm}^*$	12.35 \pm 0.10	192 \pm 10	3.35 \pm 0.15	16.1 \pm 0.1	204 \pm 10	5.25 \pm 0.2
$^{154}\text{Sm}^{**}$	11	204	3	15.25	320	4

* Corresponding to best fits shown in fig. 7.

** Values taken from Vassilijev ^{23, 24)} for comparison.

TABLE 3
Different integrated cross sections as defined in the text

	^{144}Sm	^{148}Sm	^{150}Sm	^{152}Sm	^{154}Sm
E_M (MeV)	21	20	20	20	21
σ_0 (MeV · b)	2 \pm 0.14	1.94 \pm 0.1	2 \pm 0.14	2.05 \pm 0.1	2.07 \pm 0.1
σ'_0 (MeV · b)	2.63	2.71	2.94	2.75	2.65
$\frac{\sigma'_0 A}{0.06 NZ}$	1.24	1.25	1.35	1.24	1.2
σ_{-1} (mb)	131 \pm 15	134 \pm 10	141 \pm 15	144 \pm 10	145 \pm 10
σ_{-2} (mb · MeV ⁻¹)	8.7 \pm 0.8	9.5 \pm 0.7	10.3 \pm 0.9	10.6 \pm 0.7	10.6 \pm 0.7

²³O. Vasilijev et al., Sov.J.Nucl.Phys. 10, 263 (1970)

²⁴O. Vasilijev et al., Sov.J.Nucl.Phys. 13, 463 (1971)

REF.

T. Cooper, W. Bertozzi, J. Heisenberg, S. Kowalski,
 W. Turchinetz, C. Williamson, L. Cardman, S. Fivozinsky,
 J. Lightbody, Jr., and S. Penner
 Phys. Rev. C13, 1083 (1976)

ELEM. SYM.	A	Z
Sm	154	62

METHOD

REF. NO.

76 Co 3

hmg

REACTION	RESULT	EXCITATION ENERGY	SOURCE		DETECTOR		ANGLE
			TYPE	RANGE	TYPE	RANGE	
E,E/	FMF	1, 1	D	44-106	MAG-D		DST

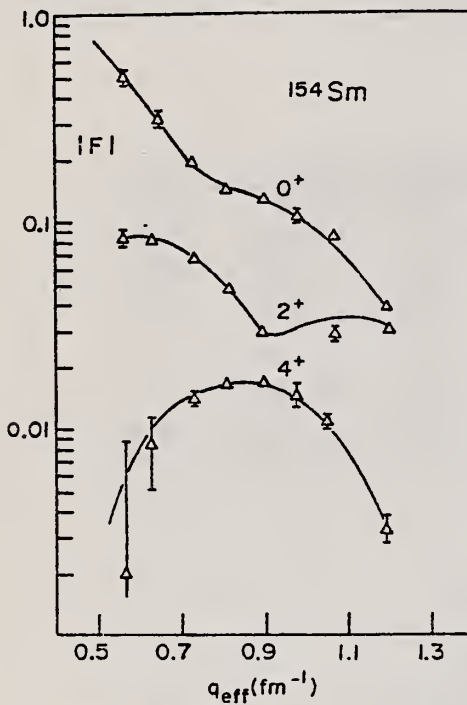


FIG. 1. Measured form factors for the elastic (0^+) and the inelastic 0.082-MeV (2^+) and 0.267-MeV (4^+) states in ^{154}Sm . The fitted curves are based on a best fit deformed Fermi charge distribution.

TABLE III. Cross sections from ^{154}Sm data.

Energy (MeV)	Angle (deg)	q_{eff} (fm $^{-1}$)	Elastic			
			$\frac{d\sigma}{d\Omega_{\text{exp}}}$ (mb)	$\frac{d\sigma}{d\Omega_{\text{bestfit}}}$ (mb)	$\frac{d\sigma}{d\Omega_{\text{exp}}}^{2^+}$ (mb)	$\frac{d\sigma}{d\Omega_{\text{exp}}}^{(2^+)}$ (mb)
44.82	110.22	0.566	0.195×10 $\pm 3\%$	0.193×10	0.520×10^{-1}	...
54.73	110.06	0.648	0.507 $\pm 5\%$	0.495	0.336×10^{-1}	$0.355 \times 10^{-3} \pm 35\%$
65.05	110.27	0.734	0.131 $\pm 3\%$	0.131	0.159×10^{-1}	$0.712 \times 10^{-3} \pm 6\%$
74.93	110.22	0.817	$0.545 \times 10^{-1} \pm 3\%$	0.580×10^{-1}	0.582×10^{-2}	$0.727 \times 10^{-3} \pm 5\%$
85.09	110.24	0.900	$0.358 \times 10^{-1} \pm 4\%$	0.347×10^{-1}	0.178×10^{-2}	$0.577 \times 10^{-3} \pm 4\%$
95.00	109.81	0.981	$0.195 \times 10^{-1} \pm 7\%$	0.200×10^{-1}	...	$0.351 \times 10^{-3} \pm 20\%$
100.33	144.97	1.195	$0.425 \times 10^{-3} \pm 5\%$	0.411×10^{-3}	0.257×10^{-3}	$0.348 \times 10^{-5} \pm 31\%$
105.24	110.02	1.068	$0.953 \times 10^{-2} \pm 5\%$	0.878×10^{-2}	0.130×10^{-2}	$0.139 \times 10^{-3} \pm 8\%$

TABLE VIII. Deformed Fermi best fit parameters.

	Units	^{152}Sm	^{154}Sm	^{232}Th	^{233}U
c_0	fm	5.8044	5.9387	6.7915	6.8054
t	fm	0.5814	0.5223	0.5713	0.6049
β_2		0.287 ± 0.003	0.311 ± 0.003	0.233 ± 0.002	0.261 ± 0.002
β_4		0.070 ± 0.003	0.087 ± 0.002	0.101 ± 0.003	0.037 ± 0.003
β_6		-0.0120	-0.180	0.0	0.0
$B(E2)$	$e^2 b^2$	3.28 ± 0.07	4.40 ± 0.09	9.21 ± 0.09	11.70 ± 0.15
$B(E4)$	$e^2 b^4$	0.136 ± 0.013	0.221 ± 0.010	1.16 ± 0.05	1.20 ± 0.06
rms radius	fm	5.0922	5.126	5.7723	5.842
ρ_2 Transition radius	fm	6.937	6.950	7.895	7.979
ρ_4 Transition radius	fm	7.757	7.704	8.540	8.748

REF.

F. R. Metzger
Phys. Rev. C14, 543 (1976)

ELEM. SYM.	A	Z
Sm	154	62

METHOD

REF. NO.

76 Me 6

hmg

REACTION	RESULT	EXCITATION ENERGY	SOURCE		DETECTOR		ANGLE
			TYPE	RANGE	TYPE	RANGE	
G, G	LFT	1	C	1- 4	SCD-D		DST
		(.921)					
		-					

$$\frac{N_{\parallel} - N_{\perp}}{N_{\parallel} + N_{\perp}} = (+3.6 \pm 2.7)\%$$

TABLE I. Properties of the low-lying 1^- levels in the stable even Sm isotopes.

Isotope	$E_{exc}(1^-)$	Γ_0 (meV)	$10^3 \times \frac{B(E1; 1^- \rightarrow 0^+)}{B(E1)_{sp.}}$	N
^{144}Sm	3.225	220 ± 30	3.5 ± 0.5	82
^{146}Sm	1.465	3.1 ± 0.4	0.5 ± 0.1	86
^{148}Sm	1.166	5.4 ± 0.5	1.8 ± 0.2	88
^{150}Sm	0.963	7.3 ± 0.6	4.2 ± 0.4	90
^{152}Sm	0.921	7.4 ± 1.0	4.8 ± 0.7	92

ELEM. SYM.	A	Z
Sm	154	62
REF. NO.		
77 Be 6		egf

METHOD

REACTION	RESULT	EXCITATION ENERGY	SOURCE		DETECTOR		ANGLE
			TYPE	RANGE	TYPE	RANGE	
G,G	LFT	6	D	6	SCD-D		DST
				-			

6=6.465 MeV

TABLE I

The γ -line energies E_γ of the scattered radiation from ^{154}Sm together with level energies E_n and angular distribution coefficients A .

$E_n (\pm 3 \text{ keV})$	Intensity	A	Present work		Refs. ^{2,3)} *)	
			$E_\gamma (\pm 3 \text{ keV})$	J^π	E_n	J^π
6383	67±1	0.105±0.011	82	2	82.05	2 ⁺
5544	8±2	-0.14 ± 0.005	921	1	921.7	1 ⁻
5366	45±1	0.45 ± 0.07	1099	0	1099.8	0 ⁺
5287	8±2	0.07 ± 0.06	1178	2	1177.6	2 ⁺
5263	7±1	0.40 ± 0.18	1202	(0)	1204	1 [±] , 0 ⁺
5025	5±3		1440	0, 1, 2	1440	2 ⁺
4709	4±3		1756	0, 1, 2	1755.8	2, 3
4543	10±2		1922	0, 1, 2	1923	2, 3, 4
4479	< 1		1986	0, 1, 2	1987	2, 3, 4
3979	10±2					
6465	100	0.54±0.07	6465	1 ⁻		

The spins J^π are obtained from the results of the present work and are based either on the values of A or on the assumption that the resonance level is deexcited by dipole transitions only.

*) Only those levels of refs. ^{2,3)} are listed which are also observed in the present work.

² J.M. D'Auria, D. Ostrom and S.C. Guirathi,
Nucl. Phys. A178, 172 (1971)

³ S.A. Elbakr et al., Nucl. Phys. A211, 493
(1973)

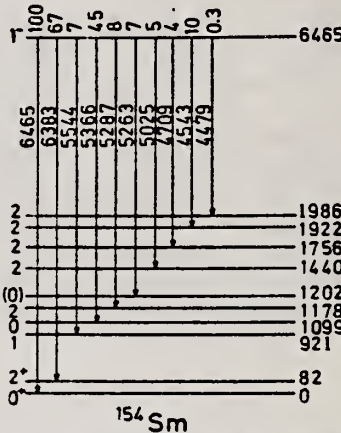


Fig. 2. Decay scheme of the 6465 keV level of ^{154}Sm showing level energies and relative intensities. The level spins are those obtained by combining the results of the present work (table 1) and those reported in refs. ^{2,3)}.

TABLE 4

Values of Γ , Γ_0 , and the energy separation δ (between the incident γ -line and the resonance level)

Scatterer	E_γ (keV)	Γ (meV)	Γ_0 (meV)	δ (eV)
^{146}Nd	7163	125±50	41±13	13.7±0.6
^{154}Sm	6465	105±50	25±13	3.6±2.0

REF G.M. Gurevich, L.E. Lazareva, V.M. Mazur, S.Yu. Merkulov,
 G.V. Solodukhov, V.A. Tyutin
 JETP Lett. 28, 157 (1978)
 Pis'ma Zh. Eksp. Teor. Fiz. 28, 168 (1978)

ELEM. SYM.	A	Z
Sm	154	62

METHOD

REF. NO.

78 Gu 7

hg

REACTION	RESULT	EXCITATION ENERGY	SOURCE		DETECTOR		ANGLE
			TYPE	RANGE	TYPE	RANGE	
G,MU-T	ABX	THR-31	C	UKN	NAI-D		4PI
		-					

The absorption method is used to measure the total photoabsorption cross section curves for deformed ^{154}Sm , ^{156}Gd , ^{168}Er , ^{174}Yb , ^{184}W , and ^{186}W nuclei in the region of the $E1$ giant resonance. The behavior of the resonance widths for nuclei in the interval $A = 153$ to 186 is discussed.

PACS numbers: 24.30.Cz, 25.20.+y, 27.70.+q

TABLE I.

Nucleus	E_1 MeV	σ_1 mb	Γ_1 MeV	E_2 MeV	σ_2 mb	Γ_2 MeV	Γ MeV	Q_0 b	β	$\sigma_a L / 0.06 \frac{ZN}{A}$
^{154}Sm	12.2	188	3.4	15.7	207	5.7	8.1 ± 0.2	6.3 ± 0.3	0.32 ± 0.02	1.28
^{156}Gd	12.3	206	3.2	15.7	220	5.5	7.7 ± 0.2	6.2 ± 0.3	0.31 ± 0.02	1.30
^{168}Er	11.9	222	3.2	15.5	275	4.5	7.4 ± 0.2	7.5 ± 0.7	0.32 ± 0.03	1.26
^{174}Yb	12.3	297	2.9	15.5	320	4.9	7.1 ± 0.2	7.0 ± 0.6	0.30 ± 0.02	1.52
^{184}W	11.9	315	2.9	14.8	321	4.7	6.8 ± 0.2	7.2 ± 0.8	0.27 ± 0.03	1.50
^{186}W	12.0	246	3.3	14.5	332	5.1	6.4 ± 0.2	6.2 ± 0.8	0.23 ± 0.03	1.48
Average error	$\pm 1.3\%$	$\pm 10.5\%$	$\pm 7.5\%$	$\pm 1.3\%$	$\pm 9.4\%$	$\pm 3.8\%$	—	—	—	—

(over)

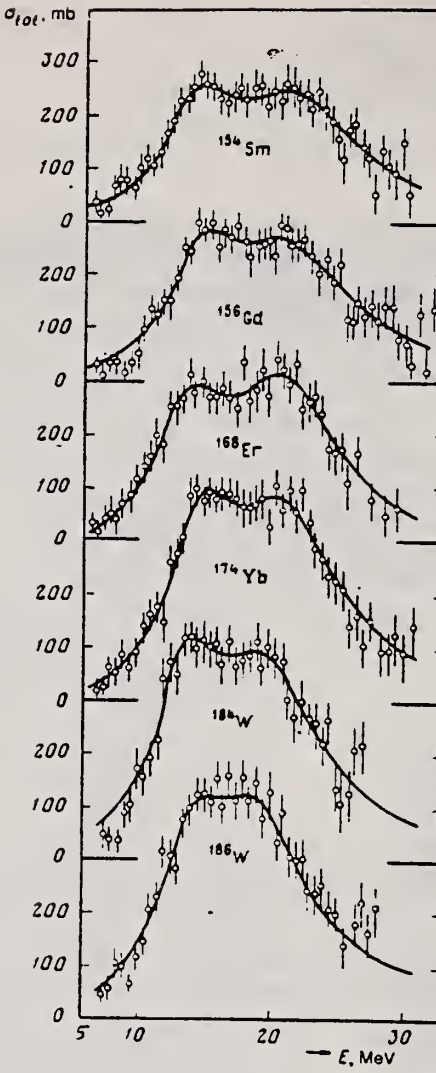


FIG. 2. Total cross sections of the photoabsorption of the nuclei ^{154}Sm , ^{156}Gd , ^{168}Er , ^{174}Yb , ^{186}W , and ^{188}W . The mean squared errors are shown.

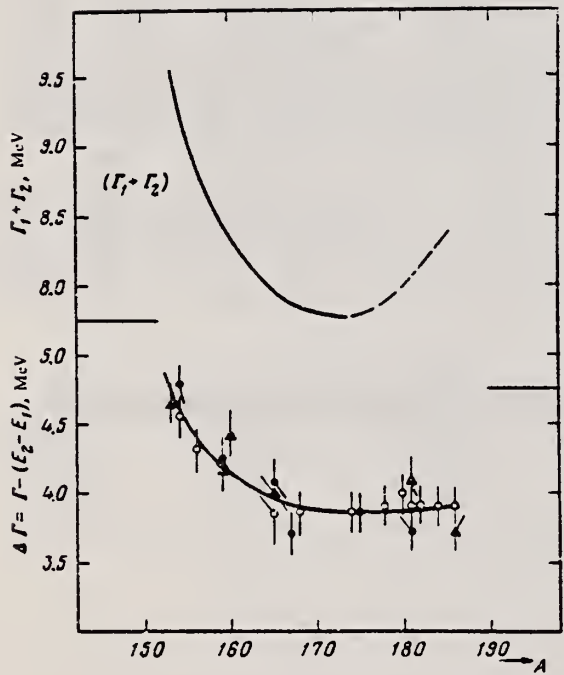


FIG. 3. Experimental values of $\Delta\Gamma = \Gamma - (E_2 - E_1)$ in the region of deformed nuclei with $A = 153-186$: ○—present work and " "; ●—Saclay group; ▲—Livermore group. Owing to a small systematic deviations of the absolute values, the ordinate scales for the Saclay and Livermore data are shifted 0.15 MeV upward and downward, respectively. The $(\Gamma_1 + \Gamma_2)$ curve was obtained from the $\Delta\Gamma$ curve after introduction of corrections in the interval $A = 175-186$.

ELEM. SYM.	A	Z
Sm	154	62
REF. NO.	81 Gu 2	hg

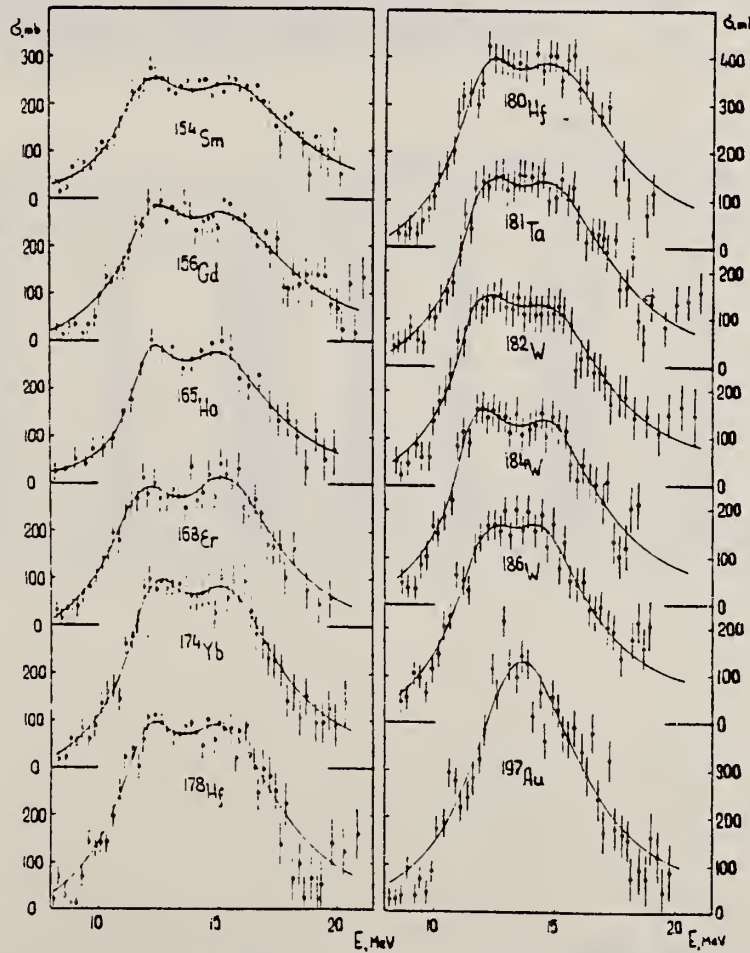
METHOD

REACTION	RESULT	EXCITATION ENERGY	SOURCE	DETECTOR	ANGLE		
			TYPE	RANGE	TYPE	RANGE	
G.MU-T	ABX	THR-20	C	27	NAT-D		4PI

Abstract: The curves of the total gamma-absorption cross sections (σ_{tot}) in the EI giant resonance energy range for the nuclei ^{154}Sm , ^{156}Gd , ^{165}Ho , ^{168}Er , ^{174}Yb , ^{178}Hf , ^{180}Hf , ^{181}Ta , ^{182}W , ^{184}W , ^{186}W and ^{197}Au have been measured using the absorption-method. Parameters of the Lorentz curves fitting the measured cross sections σ_{tot} are given. Quadrupole moments (Q_0) and nuclear deformation parameters (β) were obtained.

For deformed nuclei in the $\sim 155 < A < \sim 180$ region a violation of the correlation between giant resonance widths (Γ) and nuclear deformation parameters was found. Γ_1 and Γ_2 , the widths of the resonances corresponding to vibrations of nucleons along and across the nuclear deformation axis, were observed to decrease with the increase of A which could be accounted for by the presence of an $N = 108$ subshell.

E NUCLEAR REACTIONS ^{154}Sm , ^{156}Gd , ^{165}Ho , ^{168}Er , ^{174}Yb , ^{178}Hf , ^{180}Hf , ^{181}Ta ,
 ^{182}W , ^{184}W , ^{186}W , ^{197}Au (γ, X), $E = 7-20$ MeV; measured total $\sigma(E)$; deduced integrated σ ,
 Lorentz line parameters, ^{154}Sm , ^{156}Gd , ^{165}Ho , ^{168}Er , ^{174}Yb , ^{178}Hf , ^{181}Ta , ^{182}W , ^{184}W ,
 ^{186}W , ^{197}Au deduced β , Q_0 , Γ , giant resonance evolution. Enriched, natural targets.



(OVER)

Fig. 2. Total nuclear γ -absorption cross sections (σ_{tot}) measured by the absorption method for ^{154}Sm , ^{156}Gd , ^{165}Ho , ^{168}Er , ^{174}Yb , ^{178}Hf , ^{180}Hf , ^{181}Ta , ^{182}W , ^{184}W , ^{186}W and ^{197}Au . RMS error bars are shown.

TABLE 2
Parameters of Lorentz curves fitting the experimental data on σ_{tot}

Nucleus	E_1 (MeV)	σ_1 (mb)	Γ_1 (MeV)	E_2 (MeV)	σ_2 (mb)	Γ_2 (MeV)	$\frac{\sigma_2 \Gamma_2}{\sigma_1 \Gamma_1}$	Γ (MeV)
^{154}Sm	12.2	188	3.4	15.7	207	5.7	1.85	8.1
^{156}Gd	12.3	206	3.2	15.7	220	5.5	1.81	7.7
^{165}Ho	12.3	202	2.3	15.2	239	4.8	2.47	7.0
^{168}Er	11.9	222	3.2	15.5	275	4.5	1.73	7.4
^{174}Yb	12.3	297	2.9	15.5	320	4.9	1.80	7.1
^{178}Hf	12.2	291	3.1	15.5	334	4.9	1.80	7.2
^{180}Hf	12.2	286	3.2	15.3	324	5.1	1.81	7.1
^{181}Ta	12.1	272	3.0	15.0	316	5.1	1.97	6.8
^{182}W	11.9	267	3.2	14.8	303	5.6	2.01	6.8
^{184}W	11.9	315	2.9	14.8	321	4.7	1.65	6.8
^{186}W	12.0	246	3.3	14.5	332	5.1	2.07	6.4
^{197}Au	13.7	535	5.2	-	-	-	-	-
Average error	1.4%	11.2%	9.3%	1.5%	9.7%	4.6%	0.22	0.2 MeV

TABLE 3
Ratios of nuclear ellipsoid axes (k), deformation parameters (β) and intrinsic quadrupole moments (Q_0), calculated from E_2, E_1

Nucleus	^{154}Sm	^{156}Gd	^{165}Ho	^{168}Er	^{174}Yb	^{178}Hf	^{180}Hf	^{181}Ta	^{182}W	^{184}W	^{186}W
k	1.320	1.302	1.259	1.327	1.289	1.296	1.281	1.263	1.271	1.268	1.229
β	0.326 ± 0.017	0.309 ± 0.016	0.266 ± 0.036	0.334 ± 0.032	0.296 ± 0.024	0.303 ± 0.032	0.288 ± 0.036	0.270 ± 0.026	0.278 ± 0.030	0.274 ± 0.032	0.235 ± 0.033
Q_0	6.3 ± 0.3	6.2 ± 0.3	5.8 ± 0.8	7.5 ± 0.7	7.0 ± 0.6	7.5 ± 0.8	7.2 ± 0.9	6.9 ± 0.7	7.2 ± 0.8	7.1 ± 0.8	6.2 ± 0.9

TABLE 4
Integral characteristics of E1 giant resonance

Nucleus	σ_{exp} (MeV \cdot mb)	σ_{exp} 0.06.VZ \cdot 4	σ_{0L} (MeV \cdot mb)	σ_{0L} 0.06.VZ \cdot 4	σ_{int} (mb)	σ_{1L} (mb)	$\sigma_{1L}^{-1/4} \cdot 10^3$ (mb)	σ_{2L} (mb \cdot MeV $^{-1}$)	$\sigma_{2L}^{-1/4} \cdot 10^3$ (mb \cdot MeV $^{-1}$)	σ_{2L} (μ b \cdot MeV $^{-1}$)	$\sigma_{2L}^{-1/4} \cdot 10^3$ (μ b \cdot MeV $^{-1}$)
^{154}Sm	1.94 ± 0.06	0.87	2.86	1.29	117 ± 3.5	156	0.189	9.1 ± 0.3	14.3	3.23	
^{156}Gd	2.07 ± 0.07	0.91	2.95	1.30	143 ± 4.6	163	0.194	10.5 ± 0.4	14.9	3.30	
^{165}Ho	1.86 ± 0.06	0.78	2.53	1.06	155 ± 4.4	160	0.177	10.1 ± 0.3	12.6	2.54	
^{168}Er	2.24 ± 0.06	0.92	3.07	1.26	161 ± 4.3	197	0.212	12.0 ± 0.3	16.0	3.13	
^{174}Yb	2.69 ± 0.05	1.07	3.82	1.52	195 ± 3.4	240	0.247	14.5 ± 0.3	19.2	3.54	
^{178}Hf	2.85 ± 0.07	1.11	3.99	1.55	208 ± 4.9	247	0.247	15.3 ± 0.4	20.2	3.59	
^{180}Hf	2.72 ± 0.06	1.05	4.03	1.56	200 ± 4.4	250	0.246	15.1 ± 0.3	20.7	3.61	
^{181}Ta	2.84 ± 0.07	1.09	3.81	1.46	210 ± 5.3	245	0.239	16.0 ± 0.4	20.0	3.45	
^{182}W	2.86 ± 0.07	1.09	4.01	1.52	211 ± 5.3	256	0.248	16.2 ± 0.4	21.6	3.70	
^{184}W	2.78 ± 0.07	1.05	3.80	1.43	207 ± 5.3	251	0.240	15.9 ± 0.4	20.9	3.51	
^{186}W	2.90 ± 0.07	1.08	3.95	1.48	214 ± 5.3	256	0.241	16.2 ± 0.4	21.6	3.56	
^{197}Au	3.12 ± 0.06	1.10	4.37	1.54	229 ± 4.2	276	0.241	18.6 ± 0.4	23.3	3.49	

Eu

EUROPIUM
Z=63

Europium is a metallic element and the least dense, softest, and most volatile of the rare earths. Europium was discovered in 1896 by E. Demarcay and has been used primarily for research purposes.

Eu

METHOD

Neutron capture gamma rays

REF. NO.

67 Hu 1

EGF

REACTION	RESULT	EXCITATION ENERGY	SOURCE		DETECTOR		ANGLE
			TYPE	RANGE	TYPE	RANGE	
G, N	ABX	9-11	D	9-11	BF ₃ -I		4PI

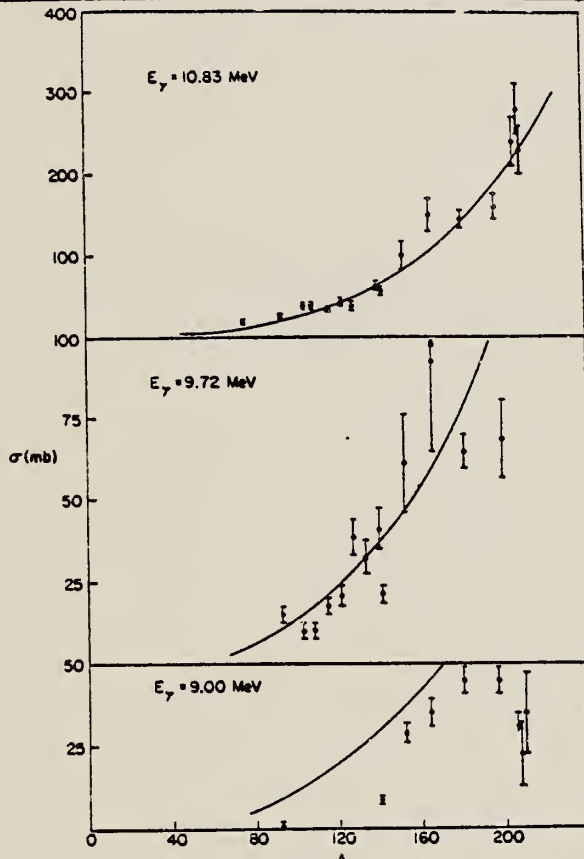


TABLE I
Photoneutron cross sections (mb)

Fig. 1. Cross section (in mb) versus mass number of the target for gamma-ray energies of 9.00, 9.72 and 10.83 MeV. The solid lines are plots of eq. (1) in the text.

Target	7.72 MeV	9.00 MeV	9.72 MeV	10.83 MeV
⁵⁹ Co				9.0 ± 0.8
⁷⁵ As				20.4 ± 1.7
⁹² Nb		0.53 ± 0.10	14.6 ± 2.2	25.8 ± 2.1
¹⁰³ Rh			10.6 ± 1.7	38.8 ± 3.1
¹⁰⁷ Ag			10.0 ± 1.5	37.6 ± 2.9
¹⁰⁹ Ag			17.1 ± 2.6	33.3 ± 2.7
¹¹³ In			20.7 ± 3.1	42.5 ± 3.6
¹¹⁵ Sb			38.7 ± 5.8	38.8 ± 3.1
¹¹⁷ I			31.7 ± 4.8	52.5 ± 3.8
¹³³ Cs		8.61 ± 0.86	40.8 ± 6.5	63.0 ± 5.0
¹³⁹ La			21.5 ± 3.2	58.3 ± 4.1
¹⁴¹ Pt			28.9 ± 3.2	61.3 ± 14.7
¹⁵¹ Eu				102 ± 18
¹⁵³ Eu				
¹⁶⁶ Ho		35.6 ± 4.3	92.2 ± 27.6	150 ± 20
¹⁸¹ Ta	4.14 ± 0.36	45.4 ± 3.7	65.0 ± 5.5	146 ± 12
¹⁹⁷ Au		44.5 ± 3.6	68.4 ± 13.5	160 ± 15
²⁰⁸ Pb		<34.3		238 ± 29
²⁰⁸ Pb		22.6 ± 11.3		280 ± 31
²⁰⁹ Bi		36.1 ± 12.0		226 ± 27

Eu
A=151

Eu
A=151

Eu
A=151

METHOD					REF. NO.		
Betatron; neutron threshold; ion chamber					60 Ge 3	NVB	
REACTION	RESULT	EXCITATION ENERGY	SOURCE		DETECTOR		ANGLE
			TYPE	RANGE	TYPE	RANGE	
G, N	N ₀ X	THR	C	THR	BF ₃ -I		4 PI

THRESHOLD

TABLE I. Summary and comparison of neutron separation energies inferred from present threshold measurements with values predicted from mass data and reaction energies. All energies are expressed in the center-of-mass system in Mev.

Reaction	No. runs	Present results	Other results	Method	Reference
Eu ¹⁵¹ (γ,n)Eu ¹⁵⁰	1	8.04 ± 0.11			

ELEM. SYM.	A	Z
Eu	151	63

METHOD

REF. NO.

70 Se 1

egf

REACTION	RESULT	EXCITATION ENERGY	SOURCE		DETECTOR		ANGLE
			TYPE	RANGE	TYPE	RANGE	
G,XN	ABX	8-24	C	8-24	BF3-I		4PI

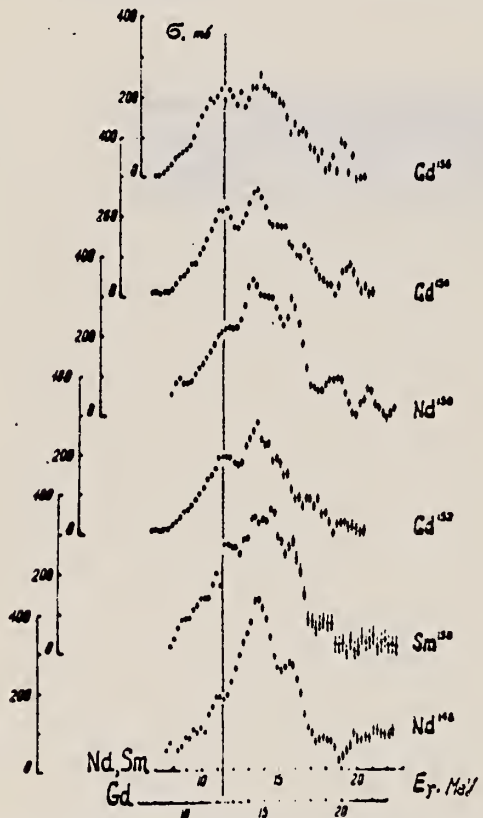


Fig. 1. The variation of the even-even nuclei giant resonance shape with the increase of Z, N in the transitional region $N = 90$. The photoabsorption curves of ^{148}Nd , ^{150}Sm , ^{152}Gd ($N = 88$) ^{150}Nd , ^{154}Gd ($N = 90$) and ^{156}Gd ($N = 92$) are presented (From the bottom). The upper energy scale is for Nd, Sm and the lower is for Gd isotopes. At the energies greater than $(\gamma, 2n)$ threshold the photoabsorption cross section was defined from the photo-neutron cross section by usual correction for neutron multiplicity. Only statistical errors are plotted. The "phase transition" effect in the giant resonance of the nuclei with $N = 88$ is emphasized by the vertical line.

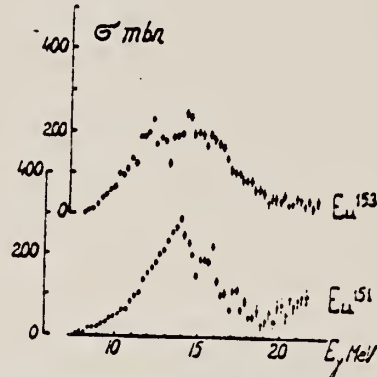


Fig. 2. The photoabsorption cross sections for ^{151}Eu and ^{153}Eu .

REF.

O. V. Vasil'ev and V. A. Semenov
 ZhETF Pis. Red. 11, 520 (1970)
 JETP Letters 11, 356 (1970)

ELEM. SYM.	A	Z
Eu	151	63

METHOD

REF. NO.

70 Va 1

egf

REACTION	RESULT	EXCITATION ENERGY	SOURCE		DETECTOR		ANGLE
			TYPE	RANGE	TYPE	RANGE	
G,XN	ABX	8-22	C	8-22	BF3-I		4PI

488

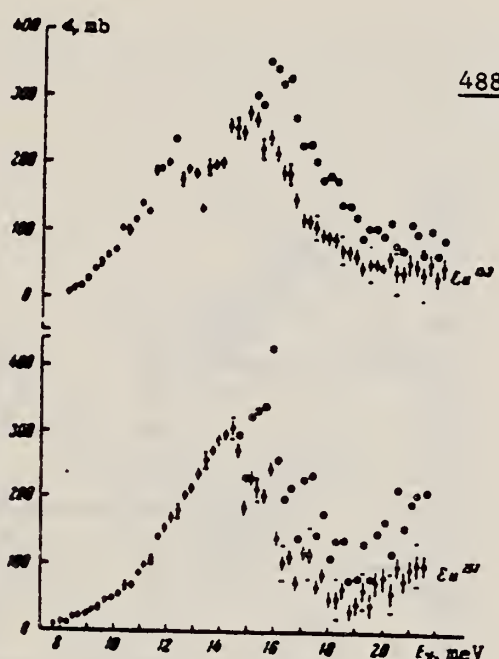


Fig. 2. Photoneutron cross sections and photoabsorption cross sections for Eu^{151} and Eu^{153} . The graphic symbols are the same as in Fig. 1.

METHOD

REF. NO.	71 Va 2	hmg
----------	---------	-----

REACTION	RESULT	EXCITATION ENERGY	SOURCE		DETECTOR		ANGLE
			TYPE	RANGE	TYPE	RANGE	
G,XN	ABX	7-24	C	7-24	BF3-I		4PI
		(7.9-23.25)			(7.9-23.25)		

Table II. Parameters of giant dipole resonance

Isotope	α	β_1	β_1 , MeV	β_1 , MeV	β_{12}	β_{12} , MeV	β_2	β_2 , MeV	β_{122}	β_{122} , MeV	β_{123}	β_{123} , MeV	β_{13}	β_{13} , MeV
Nd ¹⁴⁰	332	13.9	4.1				2.12	1.00						
Sr ⁸⁸	335	14.1	4.0				2.18	0.96						
Gd ¹⁴⁸	147	12.0	3.0	0.683	259	15.0	3.2	1.29	1.09	0.90	1.87	1.25	0.28	
Gd ¹⁵⁰	161	11.9	2.4	0.612	250	15.0	3.5	1.39	2.00	0.89	2.27	1.26	0.29	
Gd ¹⁵²	180	11.9	2.6	0.738	243	15.2	3.6	1.37	2.11	0.94	1.86	1.27	0.31	
Gd ¹⁵⁴	165	11.7	2.6	0.662	249	14.9	3.8	1.49	2.16	0.94	2.25	1.28	0.32	
Eu ¹⁵¹	285	14.0	4.5				2.02	0.92						
Eu ¹⁵³	158	11.9	2.3	0.563	237	15.1	3.6	1.34	1.90	0.86	2.39	1.27	0.31	

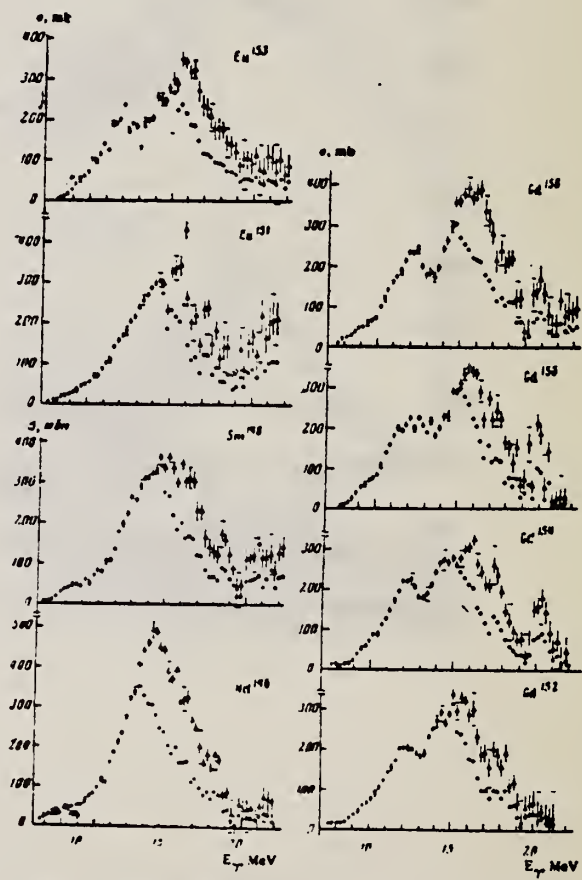


FIG. 1. Photoneutron cross sections and photoabsorption cross sections of Nd¹⁴⁰, Sm¹⁴⁸, Eu¹⁵¹, Eu¹⁵³, Gd¹⁵², Gd¹⁵⁴, Gd¹⁵⁶ and Gd¹⁵⁸. Statistical and rms experimental errors are shown (the latter horizontal bars at 9.42 MeV, 10.42 MeV etc.) At photon energies above the (γ , 2n) threshold the photoabsorption cross section errors are not shown.

Eu
A=153

Eu
A=153

Eu
A=153

ELM. S.I.M.		
Eu	153	63

METHOD					REF. NO.		
Betatron; neutron threshold; ion chamber					60 Ge 3	NVB	
REACTION	RESULT	EXCITATION ENERGY	SOURCE		DETECTOR		ANGLE
			TYPE	RANGE	TYPE	RANGE	
G, N	NOX	THR	C THR		BF3-I		4 PI

THRESHOLD

TABLE I. Summary and comparison of neutron separation energies inferred from present threshold measurements with values predicted from mass data and reaction energies. All energies are expressed in the center-of-mass system in Mev.

Reaction	No. runs	Present results	Other results	Method	Reference
$\text{Eu}^{158}(\gamma, n)\text{Eu}^{157}$	1	8.65 ± 0.13	8.66 ± 0.37	mass data	P W. H. Johnson, Jr., and A. O. Nier, Phys. Rev. 105, 1014 (1957).

METHOD

REF. NO.

Mössbauer effect; Gd_2O_3 source

66 At 1

JDM

REACTION	RESULT	EXCITATION ENERGY	SOURCE		DETECTOR		ANGLE
			TYPE	RANGE	TYPE	RANGE	
G,G	LFT	1	D		SCD		4PI

97-keV level has either $\mu_1 = 3.21 \pm 0.22$ nm
 Or $\mu_1 = (-0.52 \pm 0.22)$ nm

$$T_{1/2} = (2.14 \pm .02) \times 10^{-10} \text{ sec.}$$

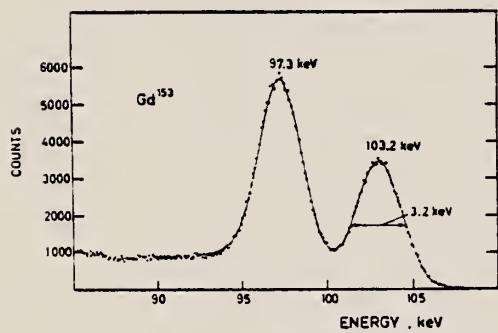


FIG. 1. γ spectrum of a Gd^{153} source taken with a Li-drifted Ge detector.

TABLE I. Summary of experimental results with Eu_2O_3 and EuSO_4 . Γ_m is the measured width of the absorption line at half-maximum and Γ_t is the "true" width.

ABSORBER	η_{97} (%)	Γ_m (mm/sec)	Γ_t (mm/sec)	β_t ($^{\circ}\text{C}$)	Θ_M ($^{\circ}\text{K}$)	$T_{1/2}$ (10^{-10} sec)
Eu_2O_3	3.4 ± 0.3	17.8 ± 0.9	6.54 ± 0.35	5.7 ± 0.4	212 ± 5	2.16 ± 0.20
EuSO_4	2.15 ± 0.2	15.3 ± 1.5	6.59 ± 0.65	0.57 ± 0.07	129 ± 5	2.1 ± 0.2

METHOD

REF. NO.

69 Be 8

hmg

REACTION	RESULT	EXCITATION ENERGY	SOURCE		DETECTOR		ANGLE
			TYPE	RANGE	TYPE	RANGE	
G, N* i_{55}^+	ABX	8-29	D	8-29	BF3-I		4PI
G, 2N** i_{56}^+	ABX	8-29	D	8-29	BF3-I		4PI
G, 3N i_{57}^+	ABX	8-29	D	8-29	BF3-I		4PI

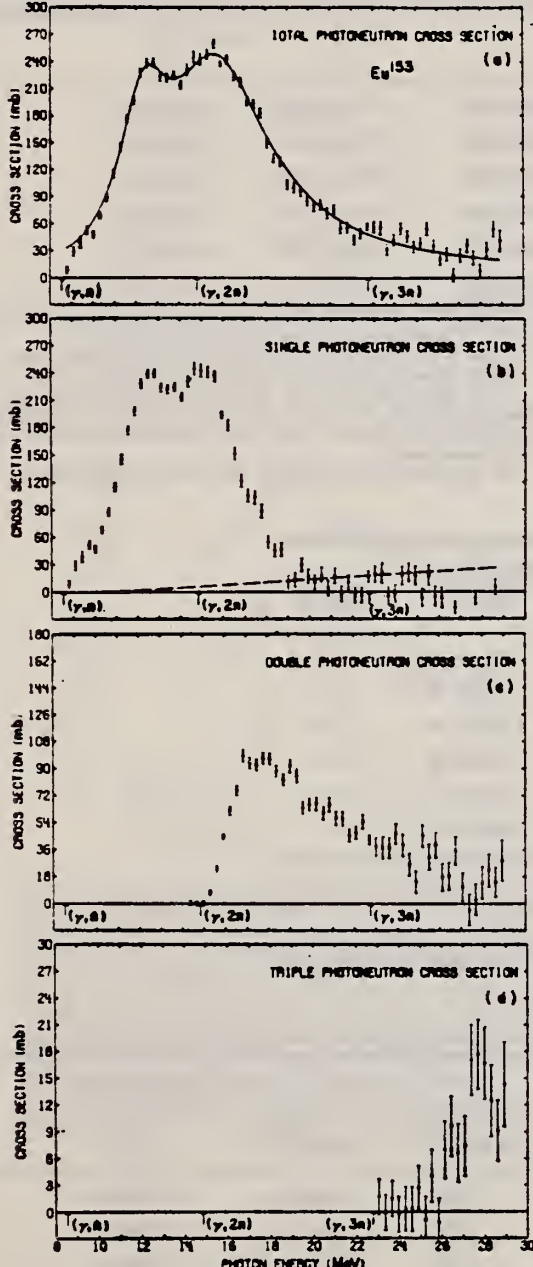


FIG. 5. Photoneutron cross sections for Eu¹⁵³. (a) Total photoneutron cross section $\sigma[(\gamma, n) + (\gamma, pn) + (\gamma, 2n) + (\gamma, p2n) + (\gamma, 3n)]$. The solid line is a two-component Lorentz-curve fit to the giant-resonance data (10.8–18.8 MeV). (b) Single-photoneutron cross section $\sigma[(\gamma, n) + (\gamma, pn)]$. The dashed line represents the maximum systematic error owing to the uncertainty in the normalization of the positron beamstrahlung subtraction. (c) Double-photoneutron cross section $\sigma[(\gamma, 2n) + (\gamma, p2n)]$. (d) Triple photoneutron cross section $\sigma(\gamma, 3n)$.

* INCLUDES NP 154+
 ** INCLUDES 2NP

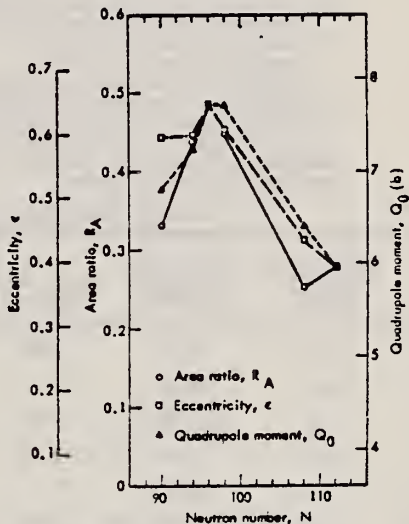


FIG. 9. The area ratio R_A , nuclear eccentricity e , and intrinsic quadrupole moment Q_0 plotted versus neutron number N . The data were scaled between the value for Gd¹⁵⁴ and that for W¹⁵⁴. The absolute scale for Q_0 is based on a mean radius parameter $R_0 = 1.26 \text{ fm}$. The lines merely connect the three sets of data points. The experimental uncertainties have been omitted for clarity but are given in Tables VII and VIII; their average values are 0.065 (17%) for R_A , 0.010 (1.9%) for e , and 0.26b (3.7%) for Q_0 .

[over]

TABLE V. Parameters of Lorentz-curve fits to the giant resonance.

Nucleus	E_{γ} (1) (MeV)	σ_{γ} (1) * (mb)	$\Gamma(1)$ (MeV)	E_{γ} (2) (MeV)	σ_{γ} (2) * (mb)	$\Gamma(2)$ (MeV)
Eu^{152}	12.33 ± 0.06	155 ± 9	2.75 ± 0.26	15.79 ± 0.10	222 ± 6	5.83 ± 0.30
Tb^{150} b	12.22 ± 0.04	181 ± 6	2.64 ± 0.16	15.67 ± 0.06	220 ± 4	4.97 ± 0.19
Gd^{152}	12.23 ± 0.06	215 ± 9	2.77 ± 0.25	15.96 ± 0.09	233 ± 6	5.28 ± 0.30
Ho^{152}	12.28 ± 0.02	214 ± 5	2.57 ± 0.11	15.78 ± 0.04	246 ± 3	5.00 ± 0.17
Ta^{151} c	12.59 ± 0.03	171 ± 8	1.94 ± 0.12	15.13 ± 0.12	265 ± 6	4.98 ± 0.23
W^{186}	12.59 ± 0.03	211 ± 14	2.29 ± 0.14	14.88 ± 0.08	334 ± 8	5.18 ± 0.14

* The uncertainties for σ_{γ} given here are relative. The absolute uncertainty is 7% (10% for Tb^{150} and Ta^{151}).

b The data of Ref. 10 were reanalyzed to obtain the values given in this

and subsequent tables (see text).

c The data of Ref. 11 were reanalyzed to obtain the values given in this and subsequent tables (see text).

- 10 R.L. Bramblett, J. T. Caldwell, R. R. Harvey, S.C. Fultz, Phys. Rev. 133, B869 (1964).
 11 R.L. Bramblett, J.T. Caldwell, G.F. Auchampaugh, S.C. Fultz, Phys. Rev. 129, 2723 (1963)

TABLE VIII. Nuclear radius parameters.

Nucleus	Q_0 * (b)	Ref.	ϵ b	R_0 * (F)	Q_0 d (b)
Eu^{152}	6.99 ± 0.08	c, f	0.595 ± 0.015	1.276 ± 0.018	6.80 ± 0.28
Tb^{150}	7.41 ± 0.11	e	0.598 ± 0.009	1.274 ± 0.013	7.23 ± 0.26
Gd^{152}	7.55 ± 0.17	g	0.645 ± 0.014	1.245 ± 0.020	7.71 ± 0.30
Ho^{152}	7.56 ± 0.11	e	0.604 ± 0.006	1.246 ± 0.011	7.71 ± 0.26
Ta^{151}	6.89 ± 0.21	h, i	0.433 ± 0.010	1.306 ± 0.025	6.43 ± 0.26
W^{186}	5.96 ± 0.05	g, j, k	0.390 ± 0.006	1.259 ± 0.011	5.96 ± 0.21

* Values taken from or computed from the references listed in column 3.

b Values from present data (Table VII).

c Computed from Eq. (2) in the text.

d The "best" values for Q_0 deduced from the present data, computed from

Eq. (2) in the text, taking R_0 to be 1.26 ± 0.02 F.

e M. C. Gleeson and B. Elbek, Nucl. Phys. 15, 134 (1959).

f R. A. Carrigan, Jr., P. D. Gupta, R. B. Sutton, M. N. Suzuki, A. C. Thompson, R. E. Cold, W. V. Prestwich, A. K. Gaigalas, and S. Rabey, Phys. Rev. Letters 20, 874 (1968).

g P. H. Stelson and L. Grodzins, Nucl. Data A1, 21 (1965).

h F. K. McGowan and P. H. Stelson, Phys. Rev. 109, 901 (1958).

i E. M. Bernstein and R. Graetzer, Phys. Rev. 119, 1321 (1960).

j R. C. Barrett, S. Bernow, S. Devons, I. Duerdorff, D. Hitlin, J. W. Kast, W. Y. Lee, E. R. Macagno, J. Rainwater, and C. S. Wu, Columbia University Pergam Nuclear Physics Lab. Report No. NYO-72-191, 1968, p. 74 (unpublished).

k R. G. Steinstad and B. Persson, Phys. Rev. 170, 1072 (1968).

TABLE IX. Integrated cross sections.

Nucleus	$E_{\gamma, \text{max}}$ (MeV)	$\sigma_{\text{int}}[(\gamma, n) + (\gamma, pn)]^*$ (MeV-b)	$\sigma_{\text{int}}[(\gamma, 2n) + (\gamma, p2n)]^*$ (MeV-b)	$\sigma_{\text{int}}(\gamma, 3n) \cdot$ (MeV-b)	$\frac{\sigma_{\text{int}}[(\gamma, 2n) + (\gamma, p2n)]}{\sigma_{\text{int}}(\gamma, \text{total})} \cdot$	$\frac{[\sigma_{\gamma}(1)\Gamma(1) + \sigma_{\gamma}(2)\Gamma(2)]^*}{(\text{MeV-b})} \cdot$	$0.06 NZ/A$ (MeV-b)
Eu^{152}	28.9	1.57	0.67	0.04	0.29 ± 0.04	2.70 ± 0.19	2.22
Tb^{150}	28.0	1.41	0.89	d	0.39 ± 0.08	2.47 ± 0.12	2.31
Gd^{152}	29.5	1.45	1.00	0.08	0.39 ± 0.05	2.87 ± 0.20	2.30
Ho^{152}	28.9	1.73	0.74	0.04	0.29 ± 0.04	2.80 ± 0.09	2.39
Ta^{151}	24.6	1.31	0.88	f	0.40 ± 0.08	2.59 ± 0.15	2.61
W^{186}	28.6	1.66	1.19	0.15	0.40 ± 0.05	3.47 ± 0.17	2.67

* All measured integrated cross-section values are given for an energy region from threshold to $E_{\gamma, \text{max}}$.

b The word "total" in this table refers to the total photoneutron cross section, $\sigma[(\gamma, n) + (\gamma, pn) + (\gamma, 2n) + (\gamma, p2n) + (\gamma, 3n)]$.

c The uncertainties listed here are relative; to get the absolute uncertainty, a systematic uncertainty of 7% (10% for Tb^{150} and Ta^{151}) must be

folded into the values for σ_{γ} .

d Not measured in Ref. 10; $\sigma_{\text{int}}[(\gamma, 2n) + (\gamma, p2n)]$ contains $\frac{1}{2}\sigma_{\text{int}}(\gamma, 3n)$.

e Because $E_{\gamma, \text{max}}$ is so low, these values cannot be compared to the rest.

f Not measured in Ref. 11; the $(\gamma, 3n)$ cross section below 24.6 MeV probably negligible.

TABLE X. Integrated moments* of the measured photoneutron cross section and sum rules.

Nucleus	σ_{-1} (mb)	$\sigma_{-1}/A^{1/2}$ (mb)	σ_{-1} (mb-MeV ⁻¹)	$0.00225 A^{1/2}$	$0.05175 A^{1/2}$	$0.05175 A^{1/2}$
Eu^{152}	148	0.181	10.18	1.03	1.16 ± 0.11	22.2 ± 1.6
Tb^{150}	151	0.175	10.49	1.00	1.14 ± 0.13	23.0 ± 2.3
Gd^{152}	169	0.195	12.09	1.14	1.35 ± 0.13	20.2 ± 1.4
Ho^{152}	166	0.183	11.56	1.04	1.23 ± 0.10	22.2 ± 1.0
Ta^{151} b	(149)	(0.145)	(10.66)	(0.82)	(0.97 ± 0.13)	(28.1 ± 2.8)
W^{186}	203	0.191	14.51	1.06	1.26 ± 0.11	21.6 ± 1.5

* $\sigma_{-1} = \int_{E_{\gamma, \text{min}}}^{E_{\gamma, \text{max}}} \sigma E^{-1} dE$ and $\sigma_{-1} = \int_{E_{\gamma, \text{min}}}^{E_{\gamma, \text{max}}} \sigma E^{-1} dE$. 346

where σ is the total photoneutron cross section.

b Because $E_{\gamma, \text{max}}$ is so low, the values for Ta^{151} cannot be compared to the rest.

METHOD

REF. NO.

70 Se 1

egf

REACTION	RESULT	EXCITATION ENERGY	SOURCE		DETECTOR		ANGLE
			TYPE	RANGE	TYPE	RANGE	
G,XN	ABX	8-24	C	8-24	BF3-I		4PI

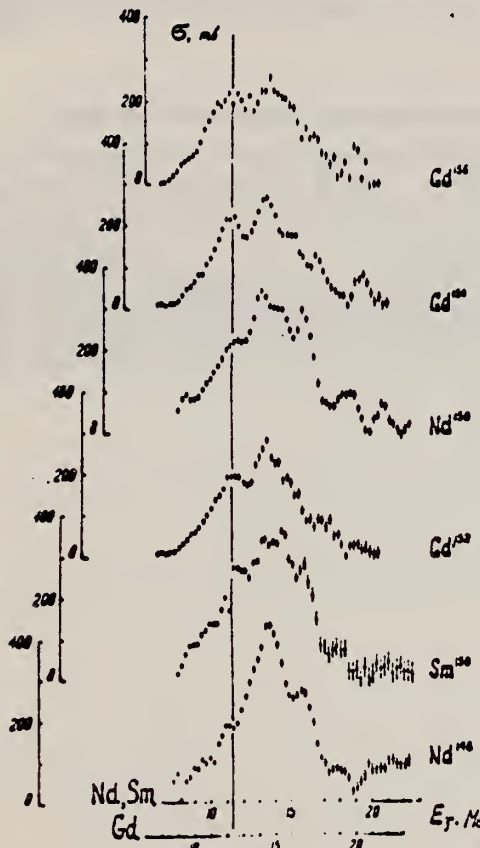


Fig. 1. The variation of the even-even nuclei giant resonance shape with the increase of Z, N in the transitional region $N = 90$. The photoabsorption curves of ^{148}Nd , ^{150}Sm , ^{152}Gd ($N = 88$) ^{150}Nd , ^{154}Gd ($N = 90$) and ^{156}Gd ($N = 92$) are presented (From the bottom). The upper energy scale is for Nd, Sm and the lower is for Gd isotopes. At the energies greater than $(\gamma, 2n)$ threshold the photoabsorption cross section was defined from the photon-neutron cross section by usual correction for neutron multiplicity. Only statistical errors are plotted. The "phase transition" effect in the giant resonance of the nuclei with $N = 88$ is emphasized by the vertical line.

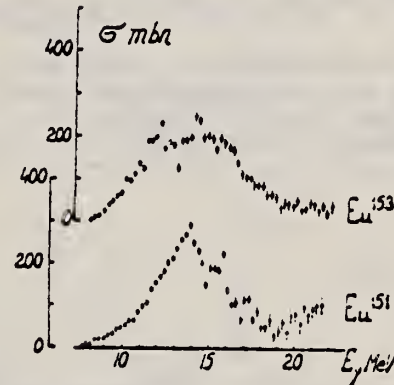


Fig. 2. The photoabsorption cross sections for ^{151}Eu and ^{153}Eu .

O. V. Vasil'ev and V. A. Semenov
 ZhETF Pis. Red. 11, 520 (1970)
 JETP Letters 11, 356 (1970)

ELEM. SYM.	A	Z
Eu	153	63

METHOD

REF. NO.

70 Va 1

egf

REACTION	RESULT	EXCITATION ENERGY	SOURCE		DETECTOR		ANGLE
			TYPE	RANGE	TYPE	RANGE	
G,XN	ABX	8-22	C	8-22	BF3-I		4PI

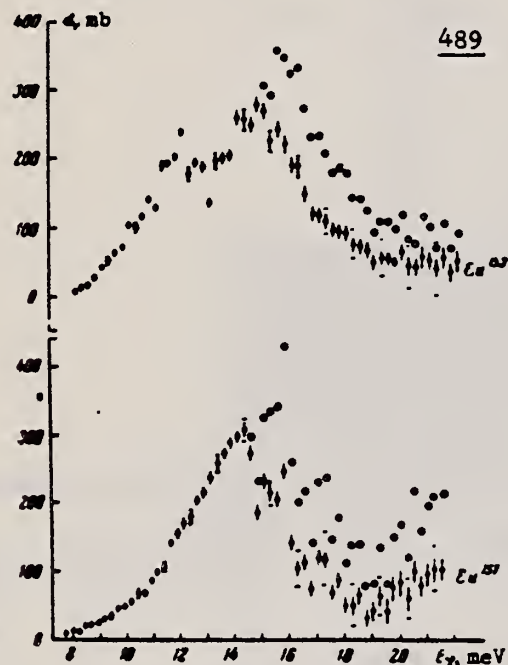
489

Fig. 2. Photoneutron cross sections and photoabsorption cross sections for Eu^{151} and Eu^{153} . The graphic symbols are the same as in Fig. 1.

METHOD

REF. NO.

71 Va 2

hmg

REACTION	RESULT	EXCITATION ENERGY	SOURCE		DETECTOR		ANGLE
			TYPE	RANGE	TYPE	RANGE	
G,XN	ABX	8-24	C	8-24	BF3-I		4PI
		(8.5-23.25)		(8.5-23.25)			

Table II. Parameters of giant dipole resonance

Isotope	σ_{γ} , mb	E_γ , MeV	Γ_γ , MeV	σ_{GDR} , mb	E_γ , MeV	Γ_γ , MeV	σ_{GDR} , mb	σ_{GDR} , mb	σ_{GDR} , mb	σ_{GDR} , mb	β_{eff}
Nd ¹⁴⁴	332	13.8	4.1				2.12	1.00			
Sm ¹⁴⁶	335	14.1	4.0	0.693	259	15.0	3.2	1.29	2.04	0.96	0.38
Gd ¹⁴⁸	147	12.0	3.0				1.99	0.90	1.87	1.25	0.38
Gd ¹⁵⁰	161	11.9	2.6	0.612	250	15.0	3.5	1.39	2.05	0.90	0.27
Gd ¹⁵²	180	11.9	2.6	0.738	243	15.2	3.6	1.37	2.11	0.94	1.86
Gd ¹⁵⁴	165	11.7	2.6	0.682	249	14.9	3.8	1.49	2.16	0.94	2.25
Eu ¹⁵²	285	14.0	4.5				2.02	0.92	2.25	1.28	0.32
Eu ¹⁵⁴	150	11.0	2.3	0.562	237	15.1	3.8	1.34	1.90	0.88	2.30
								1.27	0.31		

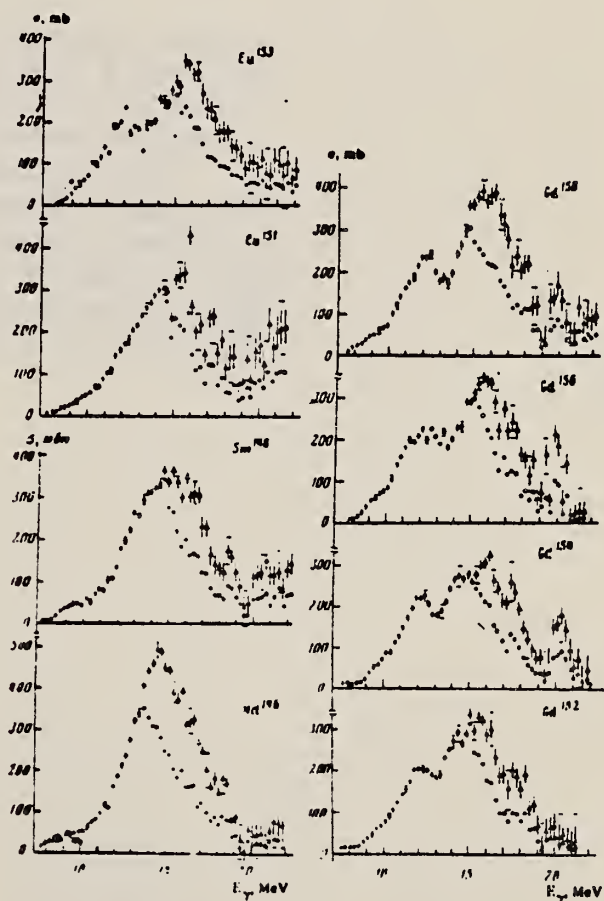


FIG. 1. Photoneutron cross sections and photoabsorption cross sections of Nd¹⁴⁴, Sm¹⁴⁶, Eu¹⁵¹, Eu¹⁵², Gd¹⁵², Gd¹⁵⁴ and Gd¹⁵⁶. Statistical and rms experimental errors are shown (the latter horizontal bars at 9.42 MeV, 10.42 MeV etc.) At photon energies above the (γ , 2n) threshold the photoabsorption cross section errors are not shown.

GADOLINIUM

Z=64

Gadolinium was discovered by J. C. G. de Marignac and P. E. L. de Boisbaudran. In 1880 Marignac isolated a new rare earth from samarskite. In 1885 Boisbaudran isolated the element from Mosander's "didymia" — a mixture of rare earths from which the cerium and lanthanum had been extracted. With Marignac's assent, Boisbaudran named the new element gadolinia in honor of the Finnish chemist J. Gadolin. Elemental gadolinium is a metal resembling steel and is useful in nuclear reactor work because of its high thermal neutron absorption cross section of 46,000 barns.

GD

METHOD				REF. NO.	
REACTION	RESULT	EXCITATION ENERGY	SOURCE	DETECTOR	ANGLE
			TYPE RANGE	TYPE RANGE	
G,F	ABY	THR-900	C 300-900	FRG-I	4PI

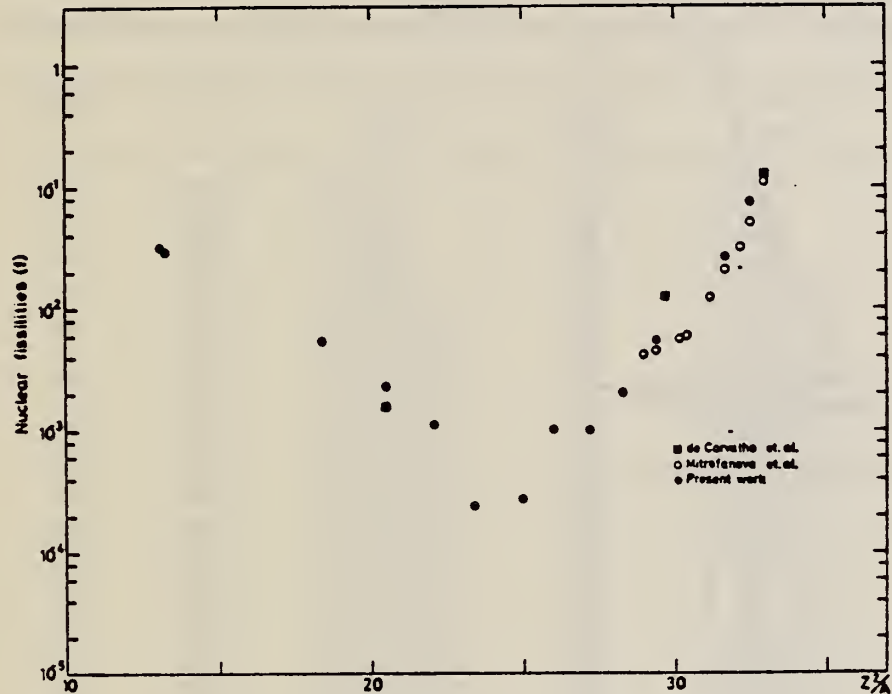
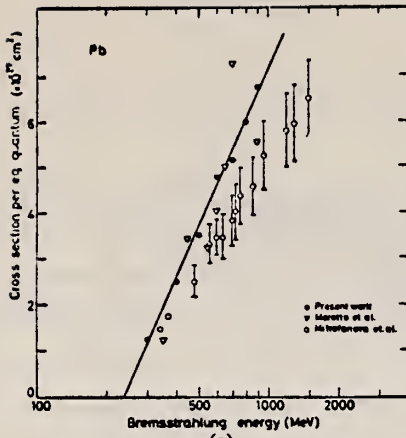


Fig. 2. Nuclear fissionabilities as a function of Z^2/A .

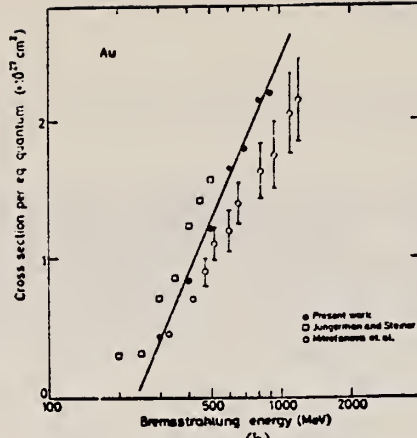
TABLE I
The constant fission cross sections above the threshold

Element	σ_f (cm^2)	Element	σ_f (cm^2)
Pb	$(5.0 \pm 0.2) \times 10^{-27}$	La	$(1.1 \pm 0.1) \times 10^{-29}$
Au	$(1.7 \pm 0.1) \times 10^{-27}$	Sn	$(4.3 \pm 1.1) \times 10^{-29}$
Ta	$(3.3 \pm 0.2) \times 10^{-28}$	Ag	$(8.4 \pm 2.0) \times 10^{-29}$
Yb	$(1.2 \pm 0.2) \times 10^{-28}$	Mo	$(1.7 \pm 0.4) \times 10^{-28}$
Ho	$(5.5 \pm 0.3) \times 10^{-29}$	Cu	$(6.6 \pm 1.2) \times 10^{-28}$
Gd	$(5.3 \pm 0.8) \times 10^{-29}$	Ni	$(5.8 \pm 0.1) \times 10^{-28}$
Nd	$(1.3 \pm 0.2) \times 10^{-29}$		

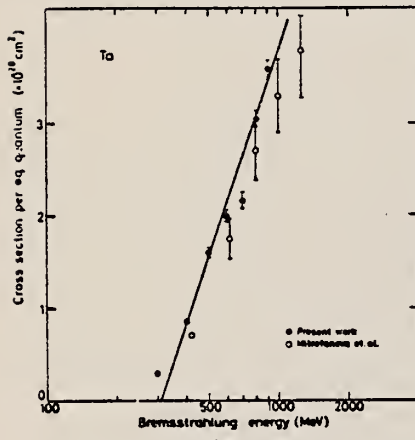
[over]



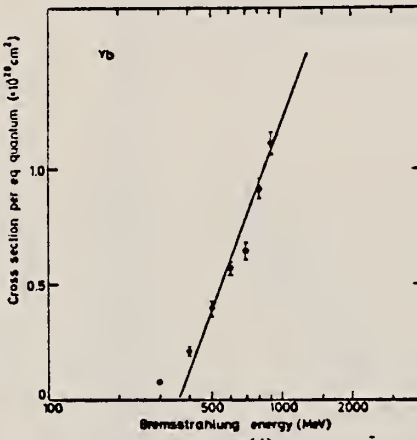
(a)



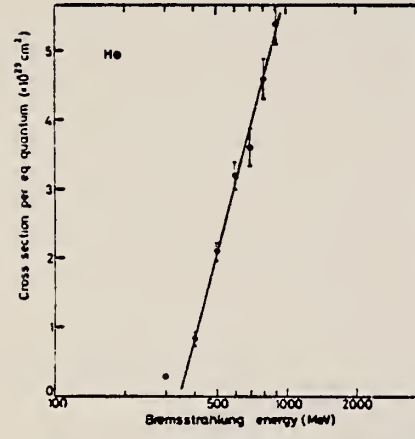
(b)



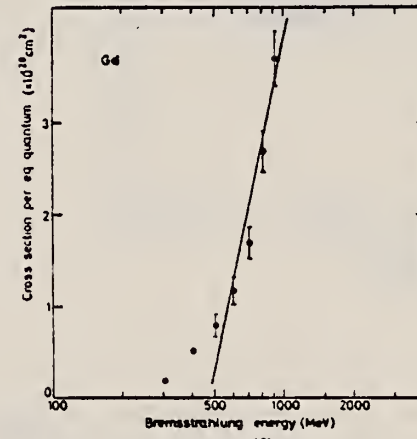
(c)



(d)



(e)



(f)

Fig. 1. Cross sections per equivalent quantum $\sigma_q(E)$ as a function of $\log E$.

ELEM. SYM.	A	Z
Gd		64
76 Em 2	egf	

METHOD

REACTION	RESULT	EXCITATION ENERGY	SOURCE	DECTOR	ANGLE
G,F	ABY	THR-999	C	999	4PI

TABLE I

Measured values of σ_q at $E = 1000$ MeV and deduced values of σ_t assumed constant from E_0 to 1000 MeV999 = 1 GEV

Element	Z^2/A	σ_q (mb)	E_0 (MeV)	σ_t (mb)
Bi	32.96	12.3 ± 0.6	200	7.6 ± 0.6
Pb	32.45	5.4 ± 0.4	220	3.6 ± 0.3
Tl	32.10	4.1 ± 0.3	230	2.8 ± 0.3
Au	31.68	2.0 ± 0.15	240	1.4 ± 0.2
Pt	31.18	1.1 ± 0.08	255	$(8 \pm 0.7) \times 10^{-1}$
Re	30.21	$(3.7 \pm 0.3) \times 10^{-1}$	280	$(2.9 \pm 0.3) \times 10^{-1}$
W	29.78	$(3.5 \pm 0.3) \times 10^{-1}$	290	$(2.8 \pm 0.3) \times 10^{-1}$
Ta	29.45	$(3.3 \pm 0.3) \times 10^{-1}$	300	$(2.7 \pm 0.3) \times 10^{-1}$
Hf	29.04	$(1.7 \pm 0.2) \times 10^{-1}$	310	$(1.4 \pm 0.2) \times 10^{-1}$
Yb	28.31	$(1.3 \pm 0.1) \times 10^{-1}$	330	$(1.2 \pm 0.1) \times 10^{-1}$
Tm	28.18	$(7.5 \pm 0.8) \times 10^{-2}$	335	$(6.8 \pm 0.8) \times 10^{-2}$
Ho	27.21	$(3.6 \pm 0.4) \times 10^{-2}$	355	$(3.5 \pm 0.4) \times 10^{-2}$
Dy	26.80	$(2.6 \pm 0.3) \times 10^{-2}$	360	$(2.5 \pm 0.3) \times 10^{-2}$
Tb	26.58	$(2.5 \pm 0.3) \times 10^{-2}$	370	$(2.5 \pm 0.3) \times 10^{-2}$
Gd	26.04	$(1.6 \pm 0.2) \times 10^{-2}$	380	$(1.7 \pm 0.2) \times 10^{-2}$
Sm	25.56	$(1.3 \pm 0.2) \times 10^{-2}$	390	$(1.4 \pm 0.2) \times 10^{-2}$
Nd	24.96	$(9.2 \pm 0.9) \times 10^{-3}$	405	$(4 \pm 1) \times 10^{-3}$
Ce	24.00	$(8 \pm 0.9) \times 10^{-3}$	420	$(9 \pm 1) \times 10^{-3}$
La	23.39	$(8.4 \pm 0.9) \times 10^{-3}$	430	$(1 \pm 0.1) \times 10^{-3}$
Sb	21.36	$(1.2 \pm 0.2) \times 10^{-2}$	460	$(1.5 \pm 0.3) \times 10^{-2}$
Te	21.19	$(8.8 \pm 1) \times 10^{-3}$	465	$(1.2 \pm 0.2) \times 10^{-2}$
Sn	21.06	$(1.3 \pm 0.2) \times 10^{-2}$	465	$(1.7 \pm 0.3) \times 10^{-2}$
Cd	20.49	$(1.7 \pm 0.3) \times 10^{-2}$	470	$(2.2 \pm 0.4) \times 10^{-2}$
Ag	20.47	$(2 \pm 0.3) \times 10^{-2}$	470	$(2.6 \pm 0.4) \times 10^{-2}$
Zn	13.76	$(2 \pm 0.4) \times 10^{-1}$	515	$(3 \pm 0.6) \times 10^{-1}$
Cu	13.44	$(2.4 \pm 0.5) \times 10^{-1}$	515	$(3.6 \pm 0.8) \times 10^{-1}$
Ni	13.35	$(2.4 \pm 0.5) \times 10^{-1}$	510	$(3.6 \pm 0.8) \times 10^{-1}$
Fe	12.10	$(3 \pm 0.6) \times 10^{-1}$	510	$(4.4 \pm 0.9) \times 10^{-1}$

- ⁴ A.V. Mitrofanova et al., Sov. J. Nucl. Phys. 6, 512 (1968).
⁷ T. Methasiri et al., Nucl. Phys. A167, 97 (1971).
¹² J.R. Nix et al., Nucl. Phys. 81, 61 (1966).
²⁰ N.A. Perifilov et al., JETP (Sov. Phys.) 14, 623 (1962); Proc. Symp. on the physics & chemistry of fission, Salzburg 1965, vol. 2 (IAEA) Vienna, 1965, p. 283.

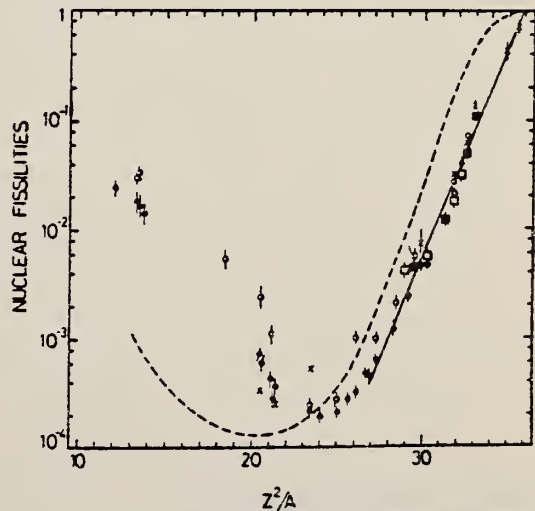


Fig. 2. Nuclear fissilities as a function of Z^2/A . Experimental points: solid circles represent our data; squares, the data from ref. ⁴; open circles, the data from ref. ⁷; and crosses, the data from (p,π) experiments²⁰. The straight line is the best fit calculated from our data for $Z^2/A > 26$. The dashed curve is the curve VI calculated by Nix and Sassi¹².

Gd

A=152

Gd

A=152

Gd

A=152

ELEM. SYM.	A	Z
Gd	152	64

METHOD

REF. NO.

70 Se 1

egf

REACTION	RESULT	EXCITATION ENERGY	SOURCE		DETECTOR		ANGLE
			TYPE	RANGE	TYPE	RANGE	
G, XN	ABX	8-24	C	8-24	BF3-I		4PI

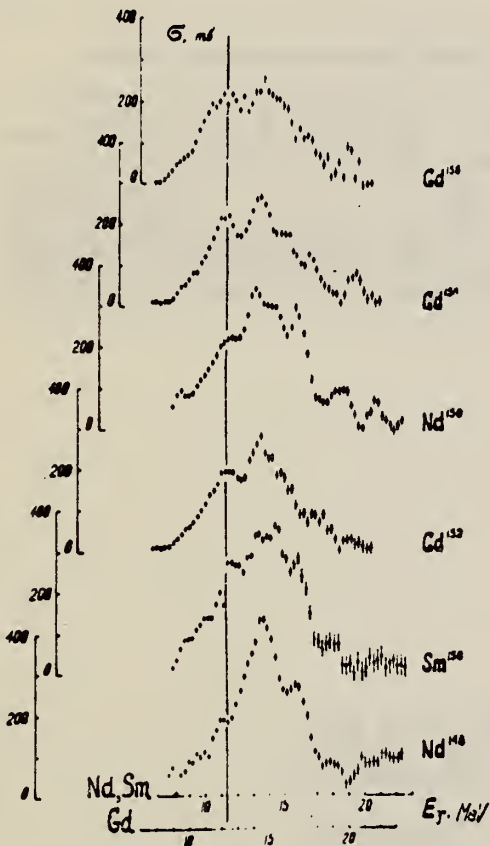


Fig. 1. The variation of the even-even nuclei giant resonance shape with the increase of Z, N in the transitional region $N = 90$. The photoabsorption curves of ^{148}Nd , ^{150}Sm , ^{152}Gd ($N = 88$) ^{150}Nd , ^{154}Gd ($N = 90$) and ^{156}Gd ($N = 92$) are presented (From the bottom). The upper energy scale is for Nd, Sm and the lower is for Gd isotopes. At the energies greater than $(\gamma, 2n)$ threshold the photoabsorption cross section was defined from the photoneutron cross section by usual correction for neutron multiplicity. Only statistical errors are plotted. The "phase transition" effect in the giant resonance of the nuclei with $N = 88$ is emphasized by the vertical line.

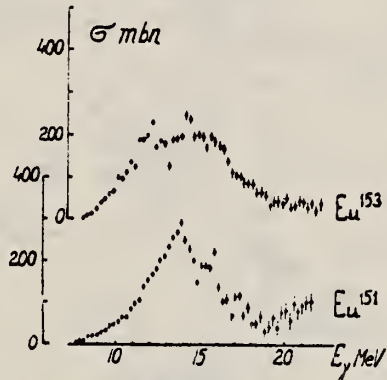


Fig. 2. The photoabsorption cross sections for ^{151}Eu and ^{153}Eu .

METHOD

REF. NO.

70 Va 1

egf

REACTION	RESULT	EXCITATION ENERGY	SOURCE		DETECTOR		ANGLE
			TYPE	RANGE	TYPE	RANGE	
G,XN	ABX	8-22	C	8-22	BF3-I		4PI

490

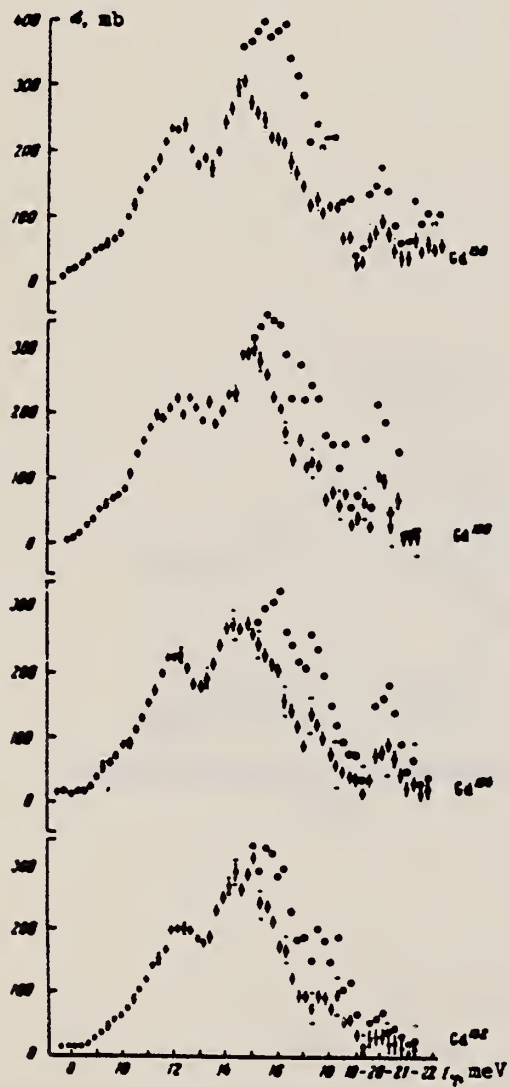
490

Fig. 1. Photoneutron cross sections and cross sections for the photoabsorption by the gadolinium isotopes Gd^{152} , 154 , 156 , 158 (reading upward). The statistical and mean-square errors of the photoabsorption cross sections are given. (The latter are denoted by horizontal strokes at the points 9.42 MeV, 10.42 MeV, etc.) At photon energies above the threshold of the $(\gamma, 2n)$ reaction, the photoneutron cross sections, unlike the absorption cross sections, are denoted by circles.

METHOD	REF. NO.	
	71 Va 2	hmg
REACTION	RESULT	EXCITATION ENERGY
		SOURCE
		TYPE RANGE
G,XN	ABX	8-24
		C 8-24
		(8.0-23.25) (8.0-23.25)
		BF3-I

Table II. Parameters of giant dipole resonance

Isotope	σ_{GDR}	τ_{GDR}	Γ_{GDR}	Δ_{GDR}	Ω_{GDR}	α_{GDR}	β_{GDR}	σ_{photoabs}	$\sigma_{\text{photoneut}}$	σ_{tot}	σ_{inel}	σ_{el}	σ_{RPA}	σ_{RPA}
Nd ¹⁴⁰	332	13.8	4.1						2.12	1.00				
Sm ¹⁴⁴	335	14.1	4.0						2.08	0.98				
Gd ¹⁴⁷	147	12.0	3.0	0.603	259	15.0	3.2	1.29	1.99	0.90	1.87	1.25	0.28	
Gd ¹⁵²	161	11.9	2.4	0.812	250	15.0	3.5	1.39	2.10	0.89	2.27	1.26	0.29	
Gd ¹⁵⁴	180	11.9	2.6	0.739	243	15.2	3.6	1.37	2.11	0.94	1.88	1.27	0.31	
Gd ¹⁵⁶	165	11.7	2.6	0.662	249	14.9	3.8	1.49	2.16	0.94	2.25	1.28	0.32	
Eu ¹⁵⁴	285	14.0	4.5						2.02	0.92				
Eu ¹⁵⁶	150	11.9	2.3	0.562	237	15.1	3.6	1.34	1.90	0.86	2.39	1.27	0.31	

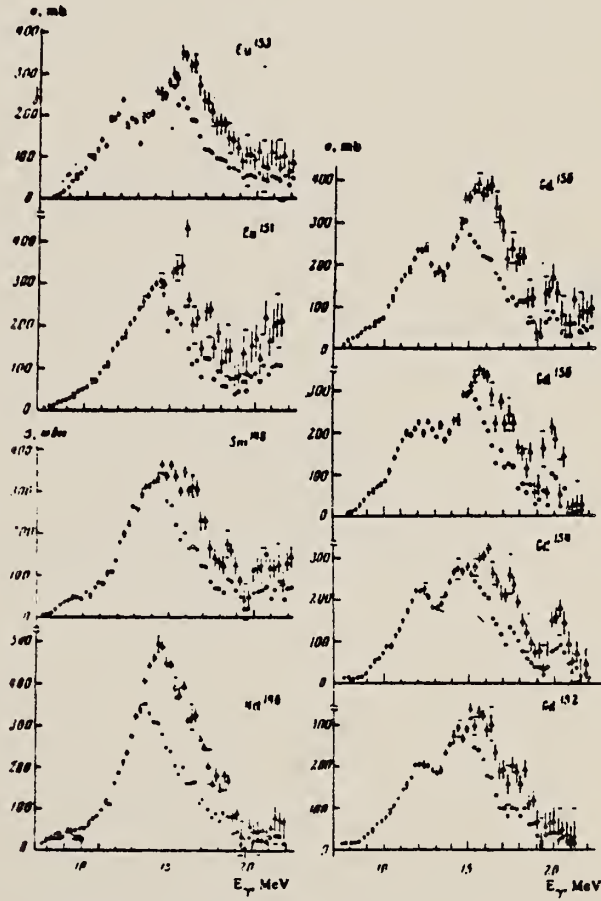


FIG. 1. Photoneutron cross sections and photoabsorption cross sections of Nd¹⁴⁰, Sm¹⁴⁴, Eu¹⁵¹, Eu¹⁵³, Gd¹⁵², Gd¹⁵⁴, Gd¹⁵⁶ and Gd¹⁵⁸. Statistical and rms experimental errors are shown (the latter horizontal bars at 9.42 MeV, 10.42 MeV etc.) At photon energies above the (γ , 2n) threshold the photoabsorption cross section errors are not shown.

G_D
A=154

G_D
A=154

G_D
A=154

METHOD				REF. NO.	
REACTION	RESULT	EXCITATION ENERGY	SOURCE	DETECTOR	ANGLE
			TYPE	RANGE	
G,XN	ABX	8-24	C	8-24	BF3-I
					4PI

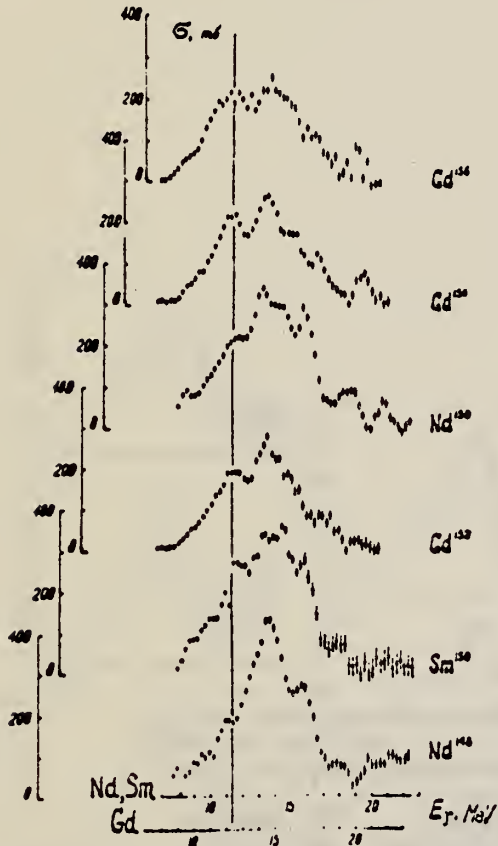


Fig. 1. The variation of the even-even nuclei giant resonance shape with the increase of Z, N in the transitional region $N = 90$. The photoabsorption curves of ^{148}Nd , ^{150}Sm , ^{152}Gd ($N = 88$) ^{150}Nd , ^{154}Gd ($N = 90$) and ^{156}Gd ($N = 92$) are presented (From the bottom). The upper energy scale is for Nd, Sm and the lower is for Gd isotopes. At the energies greater than $(\gamma, 2n)$ threshold the photoabsorption cross section was defined from the photo-neutron cross section by usual correction for neutron multiplicity. Only statistical errors are plotted. The "phase transition" effect in the giant resonance of the nucleus with $N = 88$ is emphasized by the vertical line.

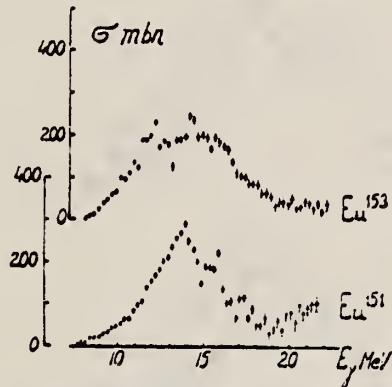


Fig. 2. The photoabsorption cross sections for ^{151}Eu and ^{153}Eu .

METHOD

REF. NO.

70 Va 1

egf

REACTION	RESULT	EXCITATION ENERGY	SOURCE		DETECTOR		ANGLE
			TYPE	RANGE	TYPE	RANGE	
G,XN	ABX	8-22	C	8-22	BF3-I		4PI

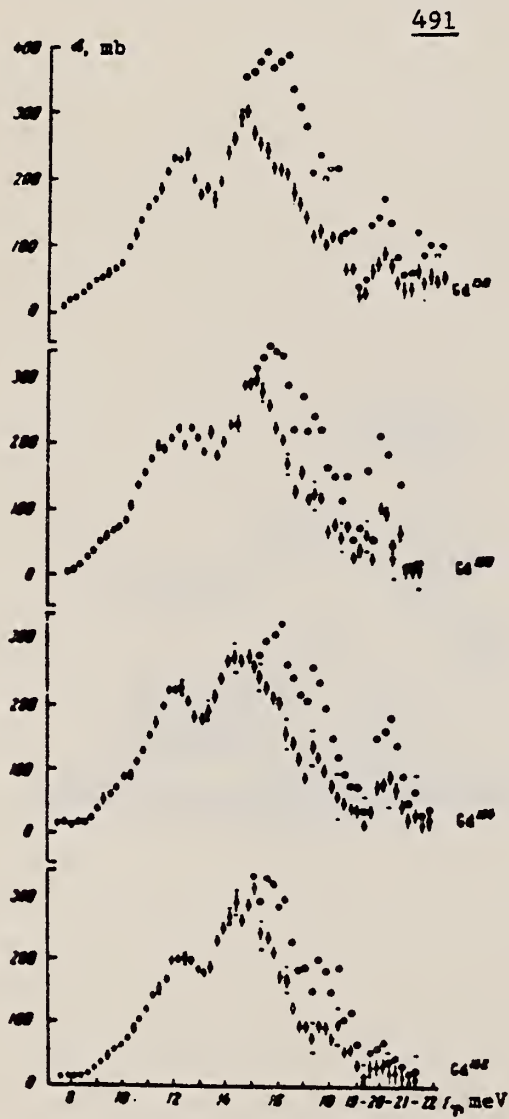
491

Fig. 1. Photoneutron cross sections and cross sections for the photoabsorption by the gadolinium isotopes Gd^{152} , 154 , 156 , 158 (reading upward). The statistical and mean-square errors of the photoabsorption cross sections are given. (The latter are denoted by horizontal strokes at the points 9.42 MeV, 10.42 MeV, etc.) At photon energies above the threshold of the $(\gamma, 2n)$ reaction, the photoneutron cross sections, unlike the absorption cross sections, are denoted by circles.

REACTION	RESULT	EXCITATION ENERGY	SOURCE		DETECTOR		ANGLE
			TYPE	RANGE	TYPE	RANGE	
G, XN	ABX	8-24	C	8-24	BF ₃ -I		4PT
		(8.6-23.25)		(8.6-23.25)			

Table II. Parameters of giant dipole resonance

Isotope	σ_0 , mb	E_1 , MeV	Γ_1 , MeV	$\sigma_{\text{int}1}$, MeV ^b	σ_2 , mb	E_2 , MeV	Γ_2 , MeV	$\sigma_{\text{int}2}$, MeV ^b	α_{int}	δ_{int} N/Z/A	ϵ_{int}	E_{γ}^{int}	β_{int}
Nd ¹⁴⁴	332	13.8	4.1						2.12	1.00			
Sm ¹⁴⁸	335	14.1	4.0						2.08	0.96			
Gd ¹⁴⁸	147	12.0	3.0	0.693	259	15.0	3.2	1.29	1.99	0.90	1.87	1.25	0.23
Gd ¹⁵⁰	161	11.9	2.4	0.612	250	15.0	3.5	1.39	2.00	0.89	2.27	1.26	0.29
Gd ¹⁵²	180	11.9	2.6	0.738	243	15.2	3.6	1.37	2.11	0.94	1.86	1.27	0.31
Gd ¹⁵⁴	165	11.7	2.6	0.662	249	14.9	3.8	1.49	2.16	0.94	2.25	1.28	0.32
Eu ¹⁵¹	285	14.0	4.5						2.02	0.92			
Eu ¹⁵³	150	11.9	2.4	0.582	237	15.1	3.6	1.34	1.90	0.86	2.39	1.27	0.31

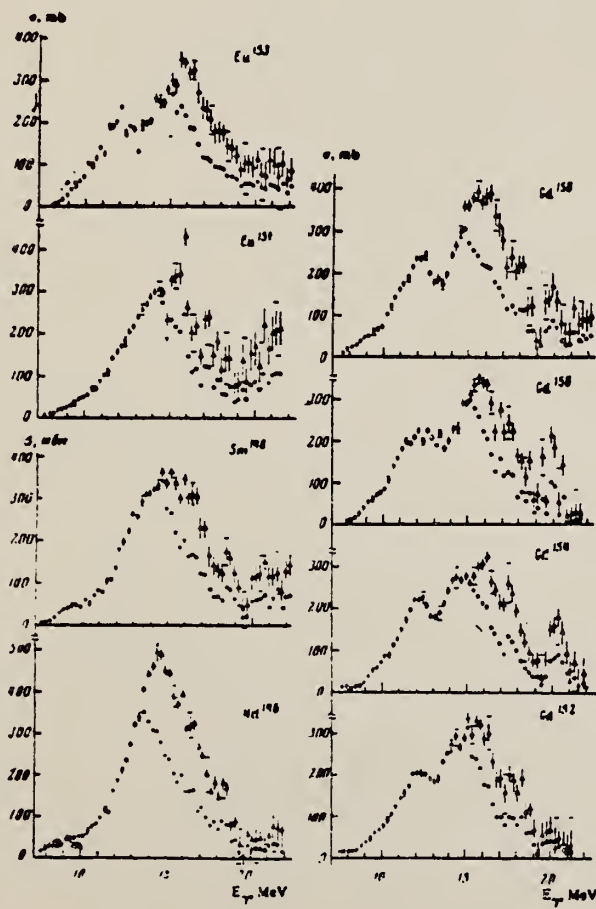


FIG. 1. Photoneutron cross sections and photoabsorption cross sections of Nd¹⁴⁴, Sm¹⁴⁸, Eu¹⁵¹, Eu¹⁵³, Gd¹⁵², Gd¹⁵⁴ and Gd¹⁵⁸. Statistical and rms experimental errors are shown (the latter horizontal bars at 9.42 MeV, 10.42 MeV etc.) At photon energies above the (γ , 2n) threshold the photoabsorption cross section errors are not shown.

GD

A=155

GD

A=155

GD

A=155

Method	Radioactive source; photon scattering; NaI spectrometer					Ref. No.	
						60 De 1	NVB

Reaction	E or ΔE	E_0	Γ	$\int \sigma dE$	$J\pi$	Notes
Gd ¹⁵⁵ (γ, γ)		105 keV	-			<p>Detector at 125°.</p> <p>Lifetime of 105 keV level:</p> $\tau_\gamma = 6.0^{+6}_{-2} \times 10^{-10} \text{ sec.}$ <p>assumes $\Gamma_0/\Gamma = 0.69$ for transition.</p> <p>Source (Eu^{155}) was separated and ~ 99% pure.</p>

Fig. 4. The resonance scattering effect as a function of the velocity of the source. The heavy line represents the theoretical counting rate for $\tau_\gamma = 6 \times 10^{-10} \text{ sec}$ for the geometry used. The dashed curves are the theoretical counting rates for the upper and lower experimental lifetime limits.

The experimental points are shown for comparison purposes.

A.E. Balabanov, N.N. Delyagin, and Hussein el Sayes
 J. Nucl. Phys. (USSR) 2, 209 (1966)
 Sov. J. Nucl. Phys. 2, 150 (1966)

ELEM. SYM.	A	Z
Gd	155	64

METHOD

REF. NO.

66 Ba 3

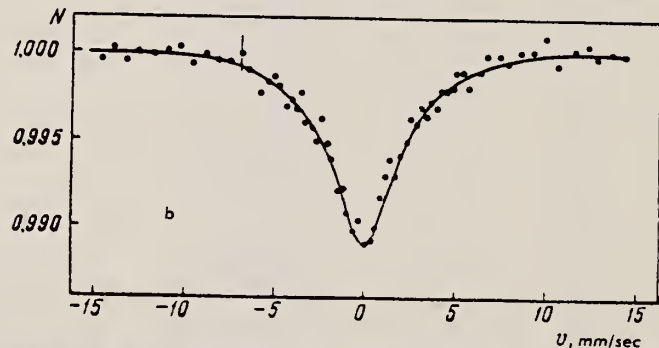
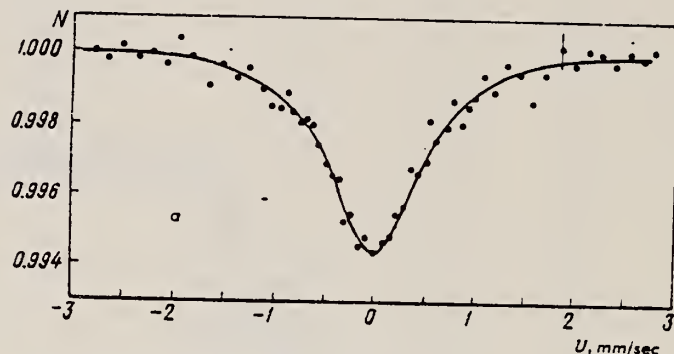
JDM

Mössbauer Effect

REACTION	RESULT	EXCITATION ENERGY	SOURCE		DETECTOR		ANGLE
			TYPE	RANGE	TYPE	RANGE	
G,G	LFT	1	D	1	NAI-D	1	1

Γ for 86.5 keV is 0.37 ± 0.06 mm/sec.

Γ for 60.0 keV is 1.4 ± 0.4 mm/sec $\equiv (2.4 \pm 0.7) \times 10^{-9}$ sec.



Resonance absorption spectra of γ quanta: a—86.5 keV, and b—60.0 keV, from Gd^{155} in gadolinium oxide, measured with a 190 mg/cm^2 absorber at 80°K . The ordinate gives the intensity of γ quanta in relative units; the abscissa is the velocity v of the source relative to the absorber.

METHOD

Mössbauer Effect

REF. NO.
66 St 1

JDM

REACTION	RESULT	EXCITATION ENERGY	SOURCE		DETECTOR		ANGLE
			TYPE	RANGE	TYPE	RANGE	
G, G	LFT	1	D	1	NAI-D	1	

Lower limit for τ of 1st excited state is 0.22 nanoseconds.

G_D
 $A=156$

G_D
 $A=156$

G_D
 $A=156$

METHOD				REF. NO.	
REACTION	RESULT	EXCITATION ENERGY	SOURCE	DETECTOR	ANGLE
			TYPE	RANGE	
G, XN	ABX	8-24	C	8-24	BF ₃ -I
					4PI

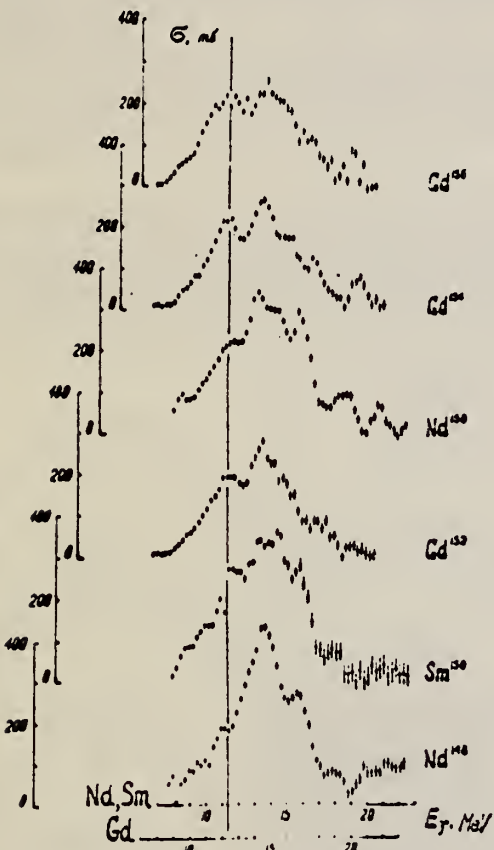


Fig. 1. The variation of the even-even nuclei giant resonance shape with the increase of Z, N in the transitional region $N = 90$. The photoabsorption curves of ^{148}Nd , ^{150}Sm , ^{152}Gd ($N = 88$) ^{150}Nd , ^{154}Gd ($N = 90$) and ^{156}Gd ($N = 92$) are presented (From the bottom). The upper energy scale is for Nd, Sm and the lower is for Gd isotopes. At the energies greater than $(\gamma, 2n)$ threshold the photoabsorption cross section was defined from the photo-neutron cross section by usual correction for neutron multiplicity. Only statistical errors are plotted. The "phase transition" effect in the giant resonance of the nuclei with $N = 88$ is emphasized by the vertical line.

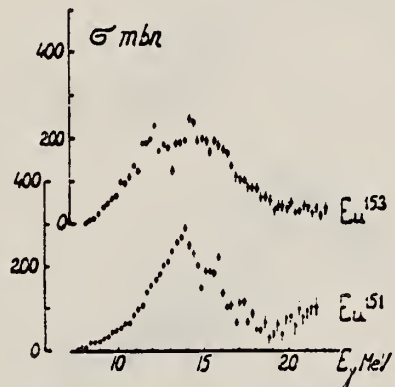


Fig. 2. The photoabsorption cross sections for ^{151}Eu and ^{153}Eu .

ELEM. SYM.	A	Z
Gd	156	64

METHOD

REF. NO.

70 Va 1

egf

REACTION	RESULT	EXCITATION ENERGY	SOURCE		DETECTOR		ANGLE
			TYPE	RANGE	TYPE	RANGE	
G,XN	ABX	8-22	C	8-22	BF3-I		4PI

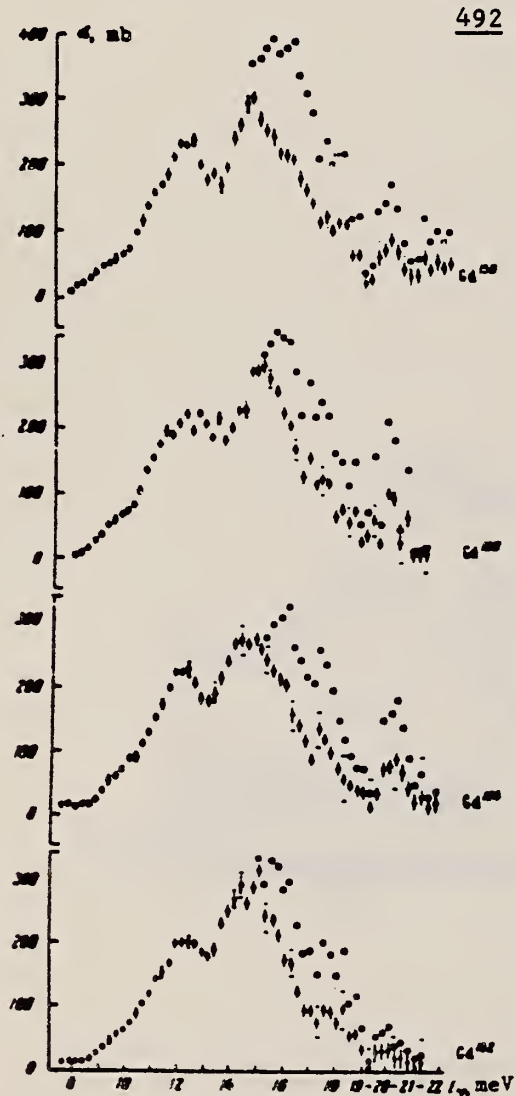


Fig. 1. Photoneutron cross sections and cross sections for the photoabsorption by the gadolinium isotopes Gd¹⁵², ¹⁵⁴, ¹⁵⁶, ¹⁵⁸ (reading upward). The statistical and mean-square errors of the photoabsorption cross sections are given. (The latter are denoted by horizontal strokes at the points 9.42 MeV, 10.42 MeV, etc.) At photon energies above the threshold of the (γ , 2n) reaction, the photoneutron cross sections, unlike the absorption cross sections, are denoted by circles.

METHOD

REF. NO.

81 Gu 2

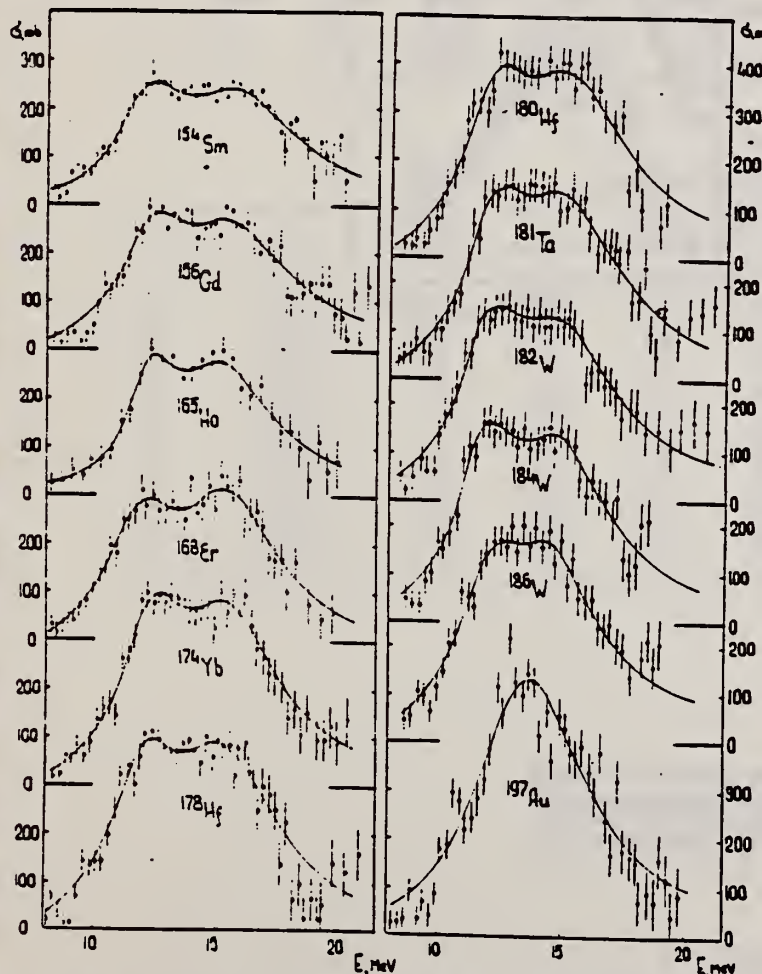
hg

REACTION	RESULT	EXCITATION ENERGY	SOURCE		DETECTOR		ANGLE
			TYPE	RANGE	TYPE	RANGE	
G, MU-T	ABX	THR-20	C	27	NAI-D		4PI

Abstract: The curves of the total gamma-absorption cross sections (σ_{tot}) in the EI giant resonance energy range for the nuclei ^{154}Sm , ^{156}Gd , ^{165}Ho , ^{168}Er , ^{174}Yb , ^{178}Hf , ^{180}Hf , ^{181}Ta , ^{182}W , ^{184}W and ^{197}Au have been measured using the absorption method. Parameters of the Lorentz curves fitting the measured cross sections σ_{tot} are given. Quadrupole moments (Q_0) and nuclear deformation parameters (β) were obtained.

For deformed nuclei in the $\sim 155 < A < \sim 180$ region a violation of the correlation between giant resonance widths (Γ) and nuclear deformation parameters was found. Γ_1 and Γ_2 , the widths of the resonances corresponding to vibrations of nucleons along and across the nuclear deformation axis, were observed to decrease with the increase of A which could be accounted for by the presence of an $N = 108$ subshell.

NUCLEAR REACTIONS ^{154}Sm , ^{156}Gd , ^{165}Ho , ^{168}Er , ^{174}Yb , $^{178,180}\text{Hf}$, ^{181}Ta , $^{182,184,186}\text{W}$, ^{197}Au (γ ; X). $E = 7-20$ MeV: measured total $\sigma(E)$; deduced integrated σ . Lorentz line parameters: ^{154}Sm , ^{156}Gd , ^{165}Ho , ^{168}Er , ^{174}Yb , $^{178,180}\text{Hf}$, ^{181}Ta , $^{182,184,186}\text{W}$, ^{197}Au deduced β , Q_0 , Γ , giant resonance evolution. Enriched, natural targets.



(OVER)

Fig. 2. Total nuclear γ -absorption cross sections (σ_{tot}) measured by the absorption method for ^{154}Sm , ^{156}Gd , ^{165}Ho , ^{168}Er , ^{174}Yb , ^{178}Hf , ^{180}Hf , ^{181}Ta , ^{182}W , ^{184}W , ^{186}W and ^{197}Au . Rms error bars are shown.

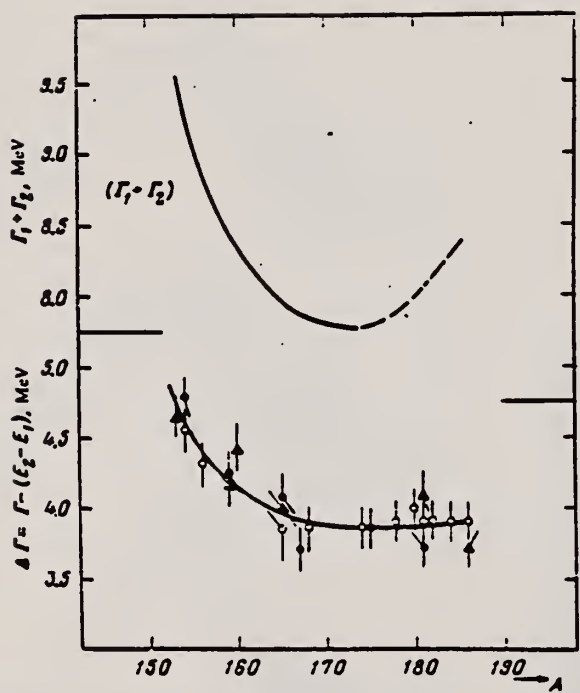


FIG. 3. Experimental values of $\Delta\Gamma = \Gamma - (E_2 - E_1)$ in the region of deformed nuclei with $A = 153-186$: \circ —present work and¹¹; \bullet —Saclay group; \blacktriangle —Livermore group. Owing to a small systematic deviations of the absolute values, the ordinate scales for the Saclay and Livermore data are shifted 0.15 MeV upward and downward, respectively. The $(\Gamma_1 + \Gamma_2)$ curve was obtained from the $\Delta\Gamma$ curve after introduction of corrections in the interval $A = 175-186$.

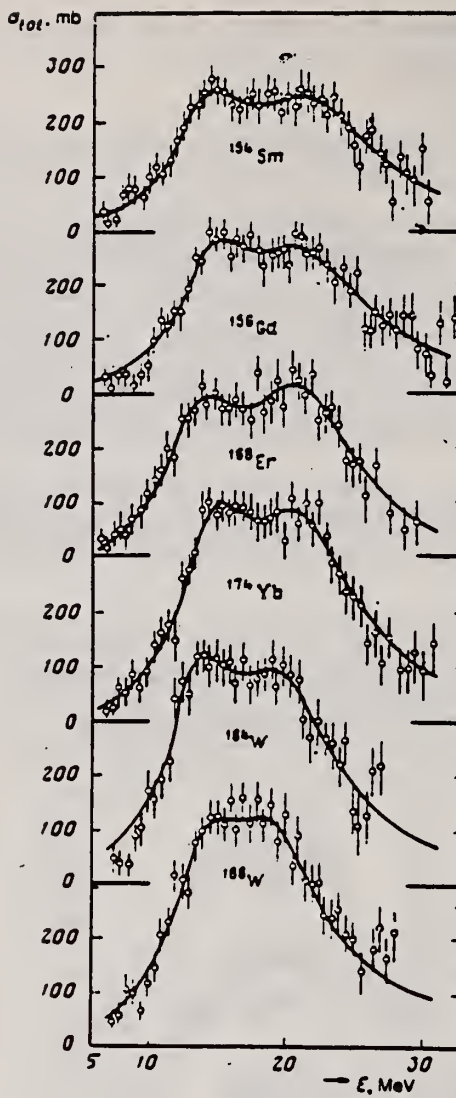


FIG. 2. Total cross sections of the photoabsorption of the nuclei ^{156}Sm , ^{156}Gd , ^{168}Er , ^{176}Yb , ^{186}W , and ^{188}W . The mean squared errors are shown.

TABLE 2
Parameters of Lorentz curves fitting the experimental data on σ_{tot}

Nucleus	E_1 (MeV)	σ_1 (mb)	Γ_1 (MeV)	E_2 (MeV)	σ_2 (mb)	Γ_2 (MeV)	$\frac{\sigma_2 \Gamma_2}{\sigma_1 \Gamma_1}$	Γ (MeV)
^{154}Sm	12.2	188	3.4	15.7	207	5.7	1.85	8.1
^{159}Gd	12.3	206	3.2	15.7	220	5.5	1.81	7.7
^{165}Ho	12.3	202	2.3	15.2	239	4.8	2.47	7.0
^{166}Er	11.9	222	3.2	15.5	275	4.5	1.73	7.4
^{174}Yb	12.3	297	2.9	15.5	320	4.9	1.80	7.1
^{179}Hf	12.2	291	3.1	15.5	334	4.9	1.80	7.2
^{180}Hf	12.2	286	3.2	15.3	324	5.1	1.81	7.1
^{181}Ta	12.1	272	3.0	15.0	316	5.1	1.97	6.8
^{182}W	11.9	267	3.2	14.8	303	5.6	2.01	6.8
^{184}W	11.9	315	2.9	14.8	321	4.7	1.65	6.8
^{186}W	12.0	246	3.3	14.5	332	5.1	2.07	6.4
^{197}Au	13.7	535	5.2					
Average error	1.4 %	11.2 %	9.3 %	1.5 %	9.7 %	4.6 %	0.22	0.2 MeV

TABLE 3
Ratios of nuclear ellipsoid axes (λ), deformation parameters (β) and intrinsic quadrupole moments (Q_0), calculated from E_2, E_1

Nucleus	^{154}Sm	^{159}Gd	^{165}Ho	^{166}Er	^{174}Yb	^{179}Hf	^{180}Hf	^{181}Ta	^{182}W	^{184}W	^{186}W
λ	1.320	1.302	1.259	1.327	1.289	1.296	1.281	1.263	1.271	1.268	1.229
β	0.326 ± 0.017	0.309 ± 0.016	0.266 ± 0.036	0.334 ± 0.032	0.296 ± 0.024	0.303 ± 0.032	0.288 ± 0.036	0.270 ± 0.026	0.278 ± 0.030	0.274 ± 0.032	0.235 ± 0.033
Q_0	6.3 ± 0.3	6.2 ± 0.3	5.8 ± 0.8	7.5 ± 0.7	7.0 ± 0.6	7.5 ± 0.8	7.2 ± 0.9	6.9 ± 0.7	7.2 ± 0.8	7.1 ± 0.8	6.2 ± 0.9

TABLE 4
Integral characteristics of E1 giant resonance

Nucleus	σ_{0LL} (MeV · b)	σ_{0LL} 0.06NZ · A	σ_{0LL} (MeV · b)	σ_{0L} 0.06NZ · A	σ_1 (mb)	σ_{1LL} (mb)	$\sigma_{1LL} A^{-1/3}$ (mb · MeV ⁻¹)	σ_{1L} (mb)	$\sigma_{1L} A^{-1/3}$ (mb · MeV ⁻¹)	σ_{2LL} (mb)	$\sigma_{2LL} A^{-1/3}$ (mb · MeV ⁻¹)
^{154}Sm	1.94 ± 0.06	0.87	2.86	1.29	117 ± 3.5	156	0.189	9.1 ± 0.3	14.3	3.23	
^{159}Gd	2.07 ± 0.07	0.91	2.95	1.30	143 ± 4.6	163	0.194	10.5 ± 0.4	14.9	3.30	
^{165}Ho	1.86 ± 0.06	0.78	2.53	1.06	155 ± 4.4	160	0.177	10.1 ± 0.3	12.6	2.54	
^{166}Er	2.24 ± 0.06	0.92	3.07	1.26	161 ± 4.3	197	0.212	12.0 ± 0.3	16.0	3.13	
^{174}Yb	2.69 ± 0.05	1.07	3.82	1.52	195 ± 3.4	240	0.247	14.5 ± 0.3	19.2	3.54	
^{179}Hf	2.85 ± 0.07	1.11	3.99	1.55	208 ± 4.9	247	0.247	15.3 ± 0.4	20.2	3.59	
^{180}Hf	2.72 ± 0.06	1.05	4.03	1.56	200 ± 4.4	250	0.246	15.1 ± 0.3	20.7	3.61	
^{181}Ta	2.84 ± 0.07	1.09	3.81	1.46	210 ± 5.3	245	0.239	16.0 ± 0.4	20.0	3.45	
^{182}W	2.86 ± 0.07	1.09	4.01	1.52	211 ± 5.3	256	0.248	16.2 ± 0.4	21.6	3.70	
^{184}W	2.78 ± 0.07	1.05	3.80	1.43	207 ± 5.3	251	0.240	15.9 ± 0.4	20.9	3.51	
^{186}W	2.90 ± 0.07	1.08	3.95	1.48	214 ± 5.3	256	0.241	16.2 ± 0.4	21.6	3.56	
^{197}Au	3.12 ± 0.06	1.10	4.37	1.54	229 ± 4.2	276	0.241	18.6 ± 0.4	23.3	3.49	

GD
A=157

GD
A=157

GD
A=157

METHOD

Betatron; neutron threshold; ion chamber

REF. NO.

60 Ge 3

NVB

REACTION	RESULT	EXCITATION ENERGY	SOURCE		DETECTOR		ANGLE
			TYPE	RANGE	TYPE	RANGE	
G, N	NOX	THR	C THR		BF3-I		4 PI

THRESHOLD

TABLE I. Summary and comparison of neutron separation energies inferred from present threshold measurements with values predicted from mass data and reaction energies. All energies are expressed in the center-of-mass system in Mev.

Reaction	No. runs	Present results	Other results	Method	Reference
Gd ¹⁵⁷ (γ,n)Gd ¹⁵⁶	1	6.39 ± 0.11	6.32 ± 0.06	mass data	9

• W. H. Johnson, Jr., and V. B. Bhanot, Phys. Rev. 107, 6 (1957).

GD
A=158

GD
A=158

GD
A=158

O. V. Vasil'ev and V. A. Semenov
 ZhETF Pis. Red. 11, 520 (1970)
 JETP Letters 11, 356 (1970)

REACTION	RESULT	EXCITATION ENERGY	SOURCE		DETECTOR		ANGLE
			TYPE	RANGE	TYPE	RANGE	
G,XN	ABX	8-22	C	8-22	BF3-I		4PI

493

493

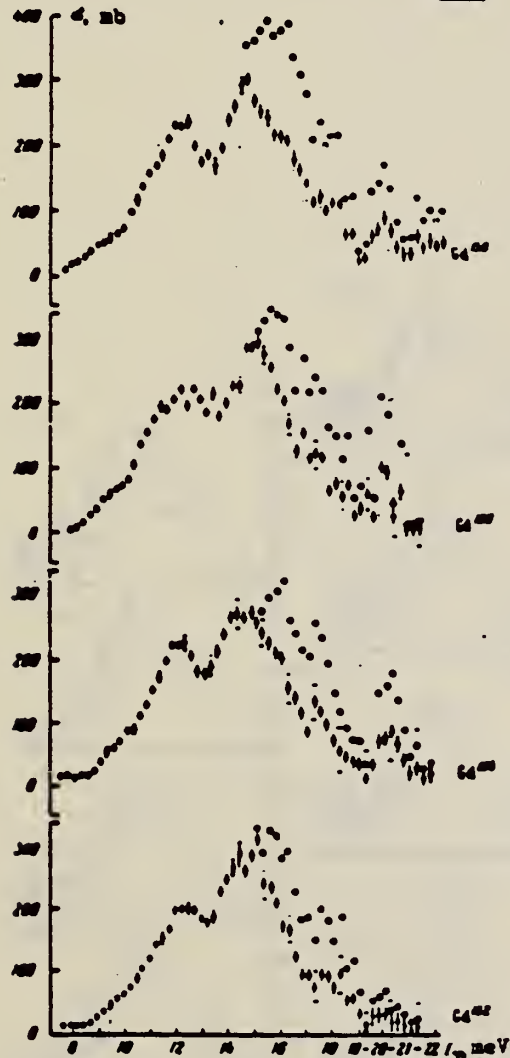


Fig. 1. Photoneutron cross sections and cross sections for the photoabsorption by the gadolinium isotopes Gd^{152} , 153 , 154 , 155 (reading upwarl). The statistical and mean-square errors of the photoabsorption cross sections are given. (The latter are denoted by horizontal strokes at the points 9.42 MeV, 10.42 MeV, etc.) At photon energies above the threshold of the $(\gamma, 2n)$ reaction, the photoneutron cross sections, unlike the absorption cross sections, are denoted by circles.

METHOD

REF. NO.	71 Va 2	hmrg
----------	---------	------

REACTION	RESULT	EXCITATION ENERGY	SOURCE		DETECTOR		ANGLE
			TYPE	RANGE	TYPE	RANGE	
G,XN	ABX	7-24	C	7-24	BF3-I		4PI
		(7.9-23.25)		(7.9-23.25)			

Table II. Parameters of giant dipole resonance

Isotope	$\frac{Z}{A}$	E_{γ} MeV	E_{γ} MeV	$\frac{1}{E_{\gamma}}$ MeV ⁻¹													
Nd ¹⁴⁴	32	13.8	4.1					2.12	1.00								
Sr ⁸⁸	35	14.1	4.0					2.08	0.96								
Gd ¹⁴⁷	32	12.0	3.0	0.693	259	15.0	3.2	1.39	1.79	0.99	1.87	1.25	0.78				
Gd ¹⁵¹	32	11.9	2.6	0.612	250	15.0	3.5	1.39	2.08	0.99	2.27	1.26	0.79				
Gd ¹⁵²	32	11.9	2.6	0.738	243	15.2	3.6	1.37	2.11	0.94	1.86	1.27	0.31				
Gd ¹⁵³	32	11.7	2.6	0.682	240	14.9	3.6	1.69	2.16	0.94	2.25	1.28	0.32				
Eu ¹⁵¹	35	14.0	4.5					2.12	0.92	2.35							
Eu ¹⁵²	35	11.9	2.3	0.562	237	15.1	3.6	1.34	1.90	0.86	2.30	1.27	0.31				

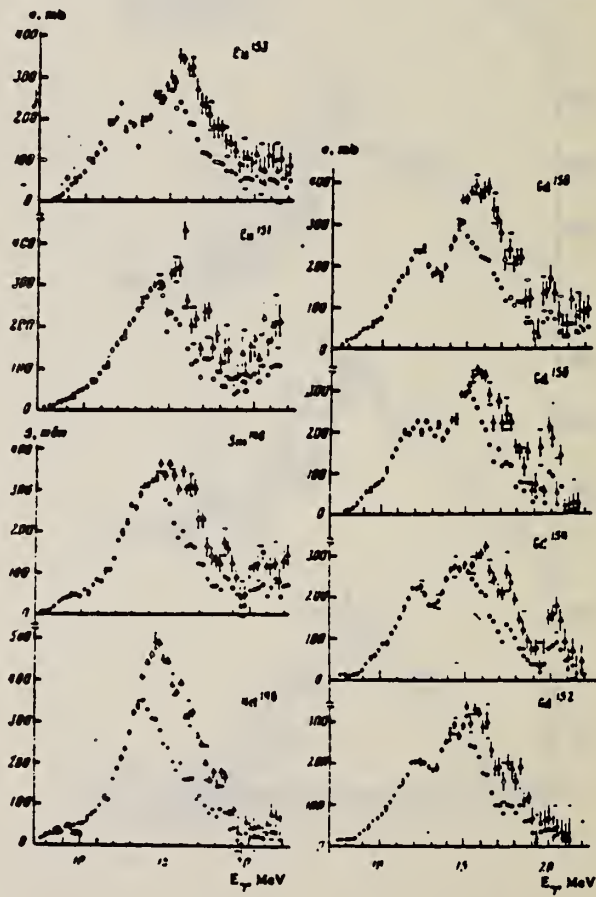


FIG. 1. Photoneutron cross sections and photoabsorption cross sections of Nd¹⁴⁴, Sm¹⁴⁹, Eu¹⁵¹, Eu¹⁵², Gd¹⁵², Gd¹⁵⁴, Gd¹⁵⁶ and Gd¹⁵⁸. Statistical and rms experimental errors are shown (the latter horizontal bars at 9.42 MeV, 10.42 MeV etc.). At photon energies above the (γ , 2n) threshold the photoabsorption cross section errors are not shown.

GD
A=160

GD
A=160

GD
A=160

Elem. Sym.	A	Z
Gd	160	64

Method 33 MeV Synchrotron; radioactivity; NaI spectrometer; ionization chamber

Ref. No.	EH
59 Ca 3	

Reaction	E or ΔE	E_0	Γ	$\int \sigma dE$	$J\pi$	Notes
$Gd^{160}(\gamma, n)$	Bremss. ~ 8-32	13.5	5.3 MeV	2.2 ± 0.4 MeV-b		

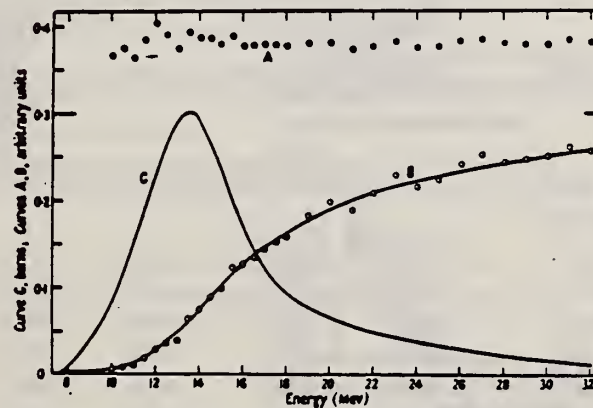


Figure 6. A, the ratio of activation curves $^{160}\text{Gd}(\gamma, n)/^{181}\text{Ta}(\gamma, n)$; B, activation curve for $^{160}\text{Gd}(\gamma, n)$; C, derived cross section: $^{160}\text{Gd}(\gamma, n)$.

METHOD

REF. NO.	69 Be 8	hmg
----------	---------	-----

REACTION	RESULT	EXCITATION ENERGY	SOURCE	DETECTOR		ANGLE
			TYPE	RANGE	TYPE	
G, N^* 159+	ABX	8-29	D	8-29	BF3-I	4PI
$G, 2N^{**}$ 160	ABX	8-29	D	8-29	BF3-I	4PI
$G, 3N$ 161	ABX	8-29	D	8-29	BF3-I	4PI

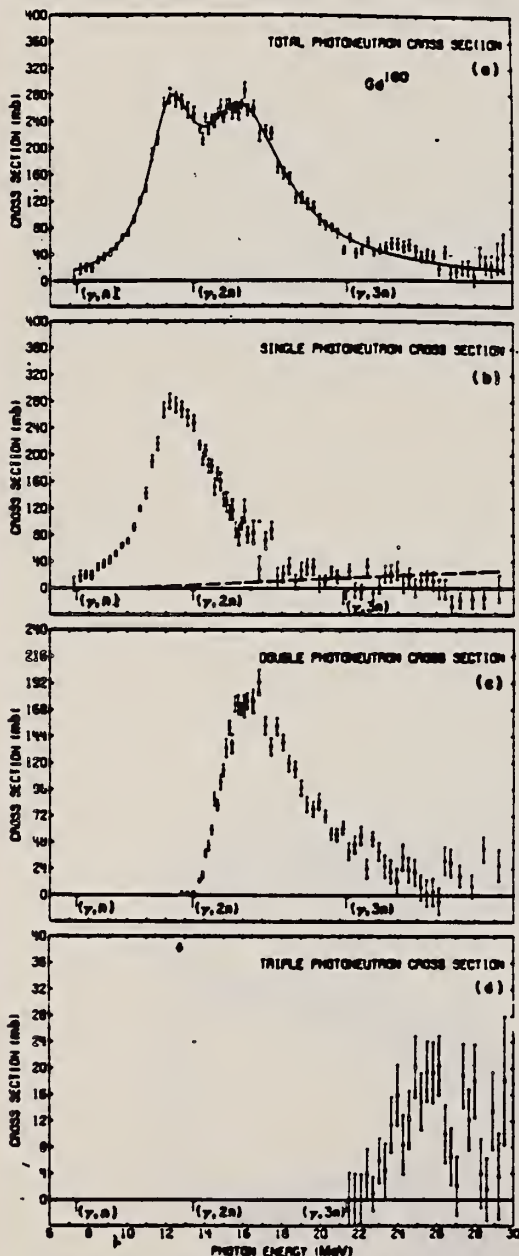


FIG. 6. Photoneutron cross sections for Gd^{160} : (a) $\sigma[\gamma, n] + (\gamma, p\bar{n}) + (\gamma, 2n) + (\gamma, p2n) + (\gamma, 3n)$, (b) $\sigma[(\gamma, n) + (\gamma, p\bar{n})]$, (c) $\sigma[(\gamma, 2n) + (\gamma, p2n)]$ (d) $\sigma(\gamma, 3n)$.

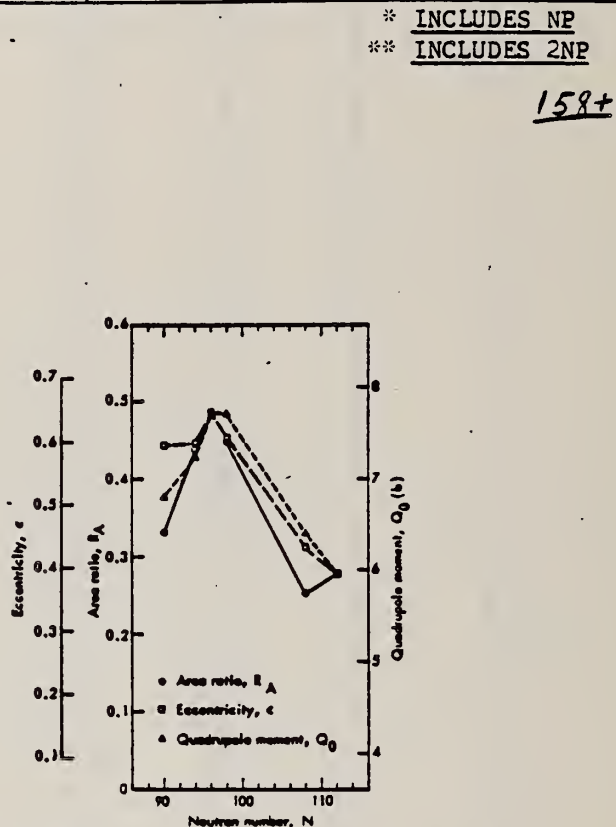


FIG. 9. The area ratio R_A , nuclear eccentricity e , and intrinsic quadrupole moment Q_0 plotted versus neutron number N . The data were scaled between the value for Gd^{160} and that for W^{184} . The absolute scale for Q_0 is based on a mean radius parameter $R_0 = 1.26$ fm. The lines merely connect the three sets of data points. The experimental uncertainties have been omitted for clarity but are given in Tables VII and VIII; their average values are 0.065 (17%) for R_A , 0.010 (1.9%) for e , and 0.26b (3.7%) for Q_0 .

[OVER]

TABLE V. Parameters of Lorentz-curve fits to the giant resonance.

Nucleus	$E_{\gamma}(1)$ (MeV)	$\sigma_{\gamma}(1) \cdot$ (mb)	$\Gamma(1)$ (MeV)	$E_{\gamma}(2)$ (MeV)	$\sigma_{\gamma}(2) \cdot$ (mb)	$\Gamma(2)$ (MeV)
Eu^{152}	12.33 ± 0.06	155 ± 9	2.75 ± 0.26	15.79 ± 0.10	222 ± 6	5.83 ± 0.30
Tb^{152} b	12.22 ± 0.04	181 ± 6	2.64 ± 0.16	15.67 ± 0.06	220 ± 4	4.97 ± 0.19
Gd^{152}	12.23 ± 0.06	215 ± 9	2.77 ± 0.25	15.96 ± 0.09	233 ± 6	5.28 ± 0.30
Ho^{152}	12.28 ± 0.02	214 ± 5	2.57 ± 0.11	15.78 ± 0.04	246 ± 3	5.00 ± 0.17
Ta^{152} c	12.59 ± 0.03	171 ± 8	1.94 ± 0.12	15.13 ± 0.12	265 ± 6	4.98 ± 0.23
W^{152}	12.59 ± 0.03	211 ± 14	2.29 ± 0.14	14.88 ± 0.08	334 ± 8	5.18 ± 0.14

* The uncertainties for σ_{γ} given here are relative. The absolute uncertainty is 7% (10% for Tb^{152} and Ta^{152}).

b The data of Ref. 10 were reanalyzed to obtain the values given in this

and subsequent tables (see text).

c The data of Ref. 11 were reanalyzed to obtain the values given in this and subsequent tables (see text).

- 10 R.L. Bramblett, J. T. Caldwell, R. R. Harvey, S.C. Fultz, Phys. Rev. 133, 8269 (1964).
 11 R.L. Bramblett, J.T. Caldwell, G.F. Auchampach, S.C. Fultz, Phys. Rev. 122, 2723 (1963).

TABLE VIII. Nuclear radius parameters.

Nucleus	$Q_0 \cdot$ (b)	Refs.	ϵ b	$R_0 \cdot$ (F)	$Q_0 \cdot$ (b)
Eu^{152}	6.99 ± 0.08	e, f	0.595 ± 0.015	1.276 ± 0.018	6.80 ± 0.28
Tb^{152}	7.41 ± 0.11	e	0.598 ± 0.009	1.274 ± 0.013	7.23 ± 0.26
Gd^{152}	7.55 ± 0.17	g	0.645 ± 0.014	1.245 ± 0.020	7.71 ± 0.30
Ho^{152}	7.56 ± 0.11	e	0.604 ± 0.006	1.246 ± 0.011	7.71 ± 0.26
Ta^{152}	6.89 ± 0.21	h, i	0.433 ± 0.010	1.306 ± 0.025	6.43 ± 0.26
W^{152}	5.96 ± 0.05	g, j, k	0.390 ± 0.006	1.259 ± 0.011	5.96 ± 0.21

d Values taken from or computed from the references listed in column 3.

e Values from present data (Table VII).

f Computed from Eq. (2) in the text.

g The "best" values for Q_0 deduced from the present data, computed from Eq. (2) in the text, taking R_0 to be 1.26 ± 0.02 F.

h M. C. Cleere and B. Elbek, Nucl. Phys. 15, 134 (1959).

i R. A. Carrigan, Jr., P. D. Gupta, R. B. Sutton, M. N. Suzuki, A. C. Thompson, R. E. Coté, W. V. Prestwich, A. K. Gaigalas, and S. Rabey, Phys. Rev. Letters 20, 874 (1968).

j P. H. Stelson and L. Grodzins, Nucl. Data A1, 21 (1965).

k F. K. McGowan and P. H. Stelson, Phys. Rev. 109, 901 (1958).

l E. M. Bernstein and R. Graetzer, Phys. Rev. 119, 1321 (1960).

m R. C. Barrett, S. Bernow, S. Devona, I. Duerdoh, D. Hidin, J. W. Kart, W. Y. Lee, E. R. Macagno, J. Raiawater, and C. S. Wu, Columbia University Pergam Nuclear Physics Lab. Report No. NYO-72-191, 1964, p. 74 (unpublished).

n R. G. Stokstad and B. Parsons, Phys. Rev. 170, 1072 (1968).

TABLE IX. Integrated cross sections.

Nucleus	$E_{\gamma, \text{max}}$ (MeV)	$\sigma_{\text{int}}[(\gamma, n) + (\gamma, pn)]^a$ (MeV-b)	$\sigma_{\text{int}}[(\gamma, 2n) + (\gamma, p2n)]^a$ (MeV-b)	$\sigma_{\text{int}}[(\gamma, 3n)]^a$ (MeV-b)	$\frac{\sigma_{\text{int}}[(\gamma, 2n) + (\gamma, p2n)]}{\sigma_{\text{int}}(\gamma, \text{total})} b$	$\frac{1}{2}[\sigma_{\text{int}}(\gamma, 1) \Gamma(1) + \sigma_{\text{int}}(\gamma, 2) \Gamma(2)]^c$ (MeV-b)	$0.06 \cdot VZ/4$ (MeV-b)
Eu^{152}	28.9	1.57	0.67	0.04	0.29 ± 0.04	2.70 ± 0.19	2.22
Tb^{152}	28.0	1.41	0.89	d	0.39 ± 0.08	2.47 ± 0.12	2.31
Gd^{152}	29.5	1.45	1.00	0.08	0.39 ± 0.05	2.87 ± 0.20	2.30
Ho^{152}	28.9	1.73	0.74	0.04	0.29 ± 0.04	2.80 ± 0.09	2.39
Ta^{152}	24.6	1.31	0.88	f	0.40 ± 0.08	2.59 ± 0.15	2.61
W^{152}	28.6	1.66	1.19	0.15	0.40 ± 0.05	3.47 ± 0.17	2.67

a All measured integrated cross-section values are given for an energy region from threshold to $E_{\gamma, \text{max}}$.

b The word "total" in this table refers to the total photo-neutron cross section, $\sigma[(\gamma, n) + (\gamma, pn) + (\gamma, 2n) + (\gamma, p2n) + (\gamma, 3n)]$.

c The uncertainties listed here are relative; to get the absolute uncertainty, a systematic uncertainty of 7% (10% for Tb^{152} and Ta^{152}) must be

taken into the values for σ_{γ} .

d Not measured in Ref. 10; $\sigma_{\text{int}}[(\gamma, 2n) + (\gamma, p2n)]$ contains $\sigma_{\text{int}}(\gamma, 3n)$.

e Because $E_{\gamma, \text{max}}$ is so low, these values cannot be compared to the rest.

f Not measured in Ref. 11; the $(\gamma, 3n)$ cross section below 24.6 MeV probably negligible.

TABLE X. Integrated moments^a of the measured photoneutron cross section and sum rules.

Nucleus	σ_{-1} (mb)	$\sigma_{-1/1-1/2}$ (mb)	$\frac{\sigma_{-1}}{(\text{mb-MeV}^{-1})}$	$0.00225 \text{ A}^{4/3}$	$\sigma_{-1} K$	$0.05175 \text{ A}^{2/3}$
Eu^{152}	148	0.181	10.18	1.03	1.16 ± 0.11	22.2 ± 1.6
Tb^{152}	151	0.175	10.49	1.00	1.14 ± 0.13	23.0 ± 2.3
Gd^{152}	169	0.195	12.09	1.14	1.35 ± 0.13	20.2 ± 1.4
Ho^{152}	166	0.183	11.56	1.04	1.23 ± 0.10	22.2 ± 1.6
Ta^{152} b	(149)	(0.145)	(10.66)	(0.82)	(0.97 ± 0.13)	(28.1 ± 2.8)
W^{152}	203	0.191	14.51	1.06	1.26 ± 0.11	21.6 ± 1.5

$$\bullet \quad \sigma_{-1} = \int_{E_{\gamma, \text{min}}}^{E_{\gamma, \text{max}}} \sigma E^{-1} dE \quad \text{and} \quad \sigma_{-1/1-1/2} = \int_{E_{\gamma, \text{min}}}^{E_{\gamma, \text{max}}} \sigma E^{-1/2} dE$$

397

where σ is the total photoneutron cross section.

b Because $E_{\gamma, \text{max}}$ is so low, the values for Ta^{152} cannot be compared to the rest.

ELEM. SYM.	A	Z
Gd	160	64

METHOD

REF. NO.	egf
72 Dr 5	

REACTION	RESULT	EXCITATION ENERGY	SOURCE		DETECTOR		ANGLE
			TYPE	RANGE	TYPE	RANGE	
G, N	ABX	6-33	C	6-33	ACT-I		4PI
G, XP	ABX	15-33	C	14-33	ACT-I		4PI

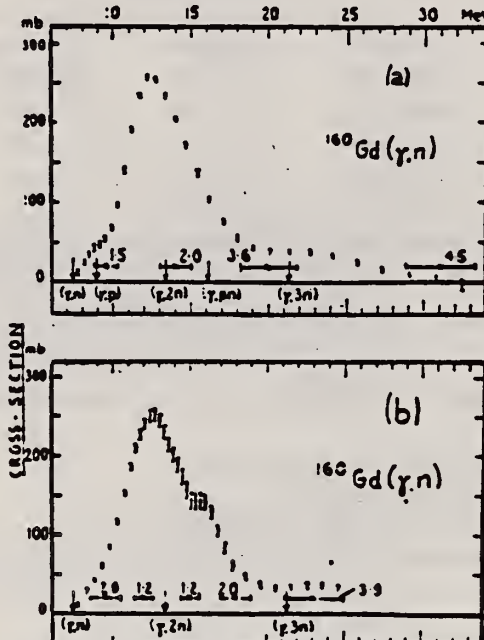
 $\Sigma P = P + NP$ 

Fig. 2. Cross-section error bars represent the correlated statistical counting errors in the cross section, calculated according to the least-structure method of Cook ⁹). The energy resolution, i.e. the half-width of the Cook resolution function, is indicated at representative energies by horizontal errors bars. (a) the $^{160}\text{Gd}(\gamma, n)$ cross section, present experiment (the cross section is strictly that for $[^{160}\text{Gd}(\gamma, n) + ^{160}\text{Gd}(\gamma, p)]$, but the $^{160}\text{Gd}(\gamma, p)$ contribution is small as seen from fig. 3). (b) Same as (a) but here the E1 giant-resonance region is seen with increased resolution, and correspondingly increased statistical error bars.

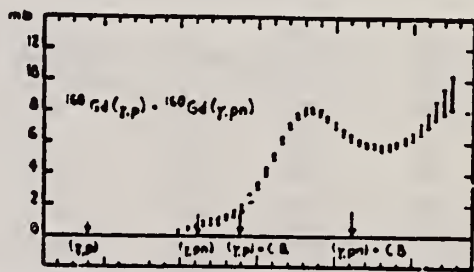


Fig. 3. The $^{160}\text{Gd}(\gamma, p) + ^{160}\text{Gd}(\gamma, pn)$ cross section, present experiment. See also caption of fig. 2.

T_B
A=159

TERBIUM
Z=65

Carol Mosander separated terbium, in 1843, from the oxide then called yttria. He named the substance erbia, but since 1877 it has been known as terbia.

T_B
A=159

T_B
A=159

ELEM. SYM.	A	
Tb	159	65

100 Betatron

REF. NO.
 58 Ch 2 NVB

REACTION	RESULT	EXCITATION ENERGY	SOURCE		DETECTOR		ANGLE
			TYPE	RANGE	TYPE	RANGE	
G, N	RLY	THR	C	THR	BF3-I		4PI

See 58 Ka 1 for cross sections

TABLE I
 MEASURED PHOTONEUTRON THRESHOLDS

THRESHOLD

Reaction	Measured Q value, Mev.	Other Q values, Mev.	Method	Reference
Tb ¹⁵⁹ (γ, n)Tb ¹⁵⁸	8.16±0.05			

ELEM. SYM.	A	Z
Tb	159	65

Betatron; ion chamber

REF. NO.	NVB
58 Fu 1	NVB

REACTION	RESULT	EXCITATION ENERGY	SOURCE		DETECTOR		ANGLE
			TYPE	RANGE	TYPE	RANGE	
G, XN	ABY	7-40	C	7-40	BF ₃ -I		4PI

TABLE I. Target properties and results.

Element	Form used	Weight grams	$\sigma^*(\gamma,n)$ barns	$\frac{S_e E_b}{NZ/4}$ Mev.b	$\frac{\sigma^*(\gamma,n)}{T}$ Mev
Sn	Sn	4.81	0.30	0.064	5.0
I	I	8.55	0.36	0.085	6.0
La	La	10.43	0.34	0.063	5.2
Ce	Ce	4.99	0.45	0.080	4.5
Sm	Sm ₂ O ₃	2.90	0.26	0.073	8.6
Tb	Tb ₂ O ₃	3.04	0.39	0.087	8.7
Ho	Ho ₂ O ₃	1.87	0.41	0.079	7.5
Er	Er ₂ O ₃	5.41	0.50	0.100	8.5
Yb	Yb ₂ O ₃	5.37	0.50	0.090	7.0
Ta	Ta	8.41	0.49	0.077	6.0
Au	Au	3.16	0.68	0.085	4.2
Pb	Pb	8.05	0.75	0.081	3.8

* $\sigma^*(\gamma,n)$ is the maximum value and "T" the full width at $\sigma^*(\gamma,n)/2$ of the neutron production cross section corrected for multiple neutron emission. Data were not fitted with resonance lines to determine these values.
† Integrated neutron production cross sections corrected for multiple neutrons above (γ,n) threshold.

TABLE II. Energies of resonances in deformed nuclei.*

Nucleus	E_a Mev	Ω_a barns	Method	E_a Mev	E_b Mev	$E_{1/2}^*$ Mev	E_{10}^* Mev
¹⁶⁰ Tb	14.7	6.9 ^b	CE	11.9	16.2	10.8	19.5
¹⁶¹ Ho	14.5	7.8 ^b	CE	11.5	16.0	11.0	18.5
¹⁶² Er	14.5	21 ^b	SC	11.5	17.5	11.5	20.0
¹⁶³ Tm	14.5	7.8 ^b	CE	11.6	15.9	11.5	20.0
¹⁶⁴ Ta	14.1	12.6 ^b	SC	10.5	15.9	11.3	17.3
¹⁶⁵ Ta	14.1	6.8 ^b	CE	11.9	15.2	11.3	17.3
¹⁶⁶ Au	13.6	3.75 ^c	SC	12.5	14.1	11.8	16.2

* CE—Coulomb excitation; SC—spectroscopic; $E_{1/2}^*$, E_{10}^* —energies at which giant resonance drops to half its maximum value.

^a Adler, Bohr, Huus, Mottelson, and Winther, Revs. Modern Phys. 28, 432 (1956).

^b M. L. Pool and D. N. Kundu, Chart of Atomic Nuclei (Longs College Book Company, Columbus, 1953).

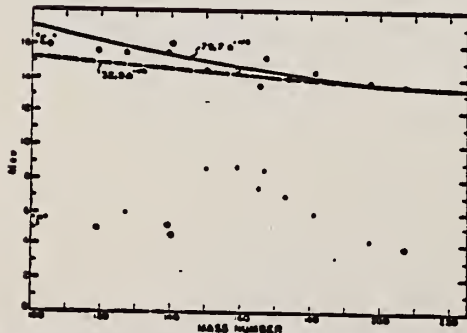


FIG. 6. Mean energy and width of giant resonances. " E_a " and " $E_{1/2}^*$ " are the mean energy for photon absorption and the full width at half maximum of the giant resonance obtained from dashed histograms as in Fig. 5. No attempt was made to fit data with resonance curves to obtain these parameters.

METHOD Betatron; ion chamber

REF. NO.
58 Fu 2 NVB

REACTION	RESULT	EXCITATION ENERGY	SOURCE		DETECTOR		ANGLE
			TYPE	RANGE	TYPE	RANGE	
G, XN	ABX	8-23	C	THR-25	BF3-I		4PI

CF DANOS THEORY

TABLE I. Resonance parameters.

	Tb ¹¹⁰	Ta ¹¹⁰	Au ¹¹⁷
B _{2n} (MeV)	15.2	14.0	14.2
E _n (MeV)	12.5	12.45	13.15
σ _n (Mb)	258	308	255
Γ _n (MeV)	2.4	2.3	2.9
E _g (MeV)	16.3	15.45	13.90
σ _g (Mb)	310	348	365
Γ _g (MeV)	4.0	4.4	4.0

TABLE II. Integral cross sections.

	Tb ¹¹⁰	Ta ¹¹⁰	Au ¹¹⁷
1/2 ∫ σ _n dE / 0.06 NZ	1.27	1.30	1.29
∫ σ _n dE / ∫ σ _g dE	2.00	2.16	1.97
1/2 ∫ σ _n (σ _n + σ _g) dE / 0.06 NZ	1.27	1.35	1.22

TABLE III. Intrinsic quadrupole moments, in barns.

	Tb ¹¹⁰	Ta ¹¹⁰	Au ¹¹⁷
E/E ₀	1.30 ± 0.05	1.25 ± 0.01	1.06 ± 0.03
Q ₀ (R ₀ = 1.09 × 10 ⁻¹³ cm)	5.6 ± 0.6	5.7 ± 0.3	1.6 ± 0.6
Q ₀ (Coulomb excitation)	6.9 ^a	6.8 ^a	2.6 ^b

^a Adler, Bohr, Huus, Mottelson, and Winter, Revs. Modern Phys. 28, 432 (1956).

^b P. H. Stelson and F. K. McGowan, Phys. Rev. 99, 112 (1955).

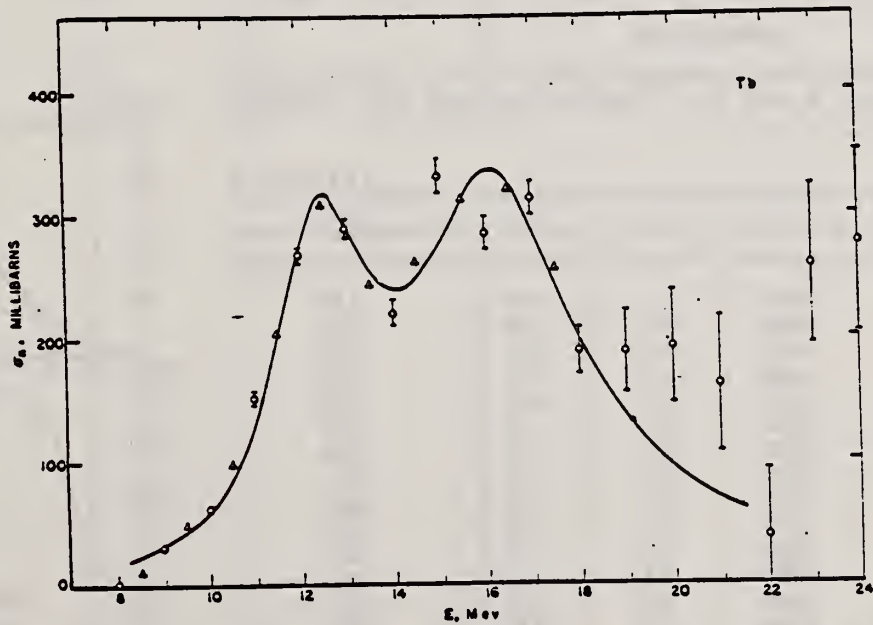


FIG. 5. Neutron cross section for terbium. Circles and triangles represent independent determinations of the cross section from the original data. Errors represent standard deviations based on the statistical uncertainties (\sqrt{n}) in the original activation curve data. The cross section plotted is $\sigma_n = \sigma(\gamma, n) + \sigma(\gamma, 2n) + \sigma(\gamma, pn) + \dots$. The smooth curve is calculated from the parameters given in Table I by using Eq. (5).

L. Katz, G.B. Chidley

Nuclear Reactions at Low and Medium Energies (Academy of Science,
USSR: 1958) 371

ELEM. SYM.	A	Z
Tb	159	65

METHOD Betatron; neutron cross section; BF_3 counters; ion chamber monitor

REF. NO.	NVB
58 Ka 1	

REACTION	RESULT	EXCITATION ENERGY	SOURCE		DETECTOR		ANGLE
			TYPE	RANGE	TYPE	RANGE	
G, XN	ABX	9-22	C	9-22	BF ₃ -I		4PI

Таблица 2

Пороги испускания фотонейтронов

Изотоп	B_{γ} , Мэв	B_m , Мэв	Изотоп	B_{γ} , Мэв	B_m , Мэв
V ₈₁	11.16	20.5	L ₁₃₉	8.81	16.1
Mn ₅₅	10.14	19.2	Pr ₁₄₁	9.46	17.6
Co ₆₀	10.44	18.6	Tb ₁₅₉	8.16	14.8
As ₇₅	10.24	18.1	Ho ₁₆₃	8.10	14.6
Y ₈₉	11.82	20.7	Tm ₁₆₉	8.00	14.7
Nb ₉₃	8.86	17.1	Lu ₁₇₃	7.77	14.2
Rh ₁₀₃	9.46	16.8	Ta ₁₈₁	7.65	13.8
J ₁₂₇	9.14	16.2	Au ₁₉₇	7.96	13.3
Cs ₁₃₃	9.11	16.5	Bi ₂₀₉	7.43	14.5

THRESHOLDS

не приведены, поскольку они превышают 22 Мэв во всех случаях, кроме золота, для которого $B_{\gamma}=21$ Мэв. Свойства сечений $\sigma_C(\gamma)$ сведены в табл. 3.

Таблица 1

Изотоп	E_{\max} , Мэв	$\sigma_n(E_\gamma)$, барн	T , Мэв	$\frac{\sigma}{T}$, Мэв·барн	$Y(22)$, 10^6 нейтрон/100 р.·моль
V ₈₁	18.4	0.062	5.2	0.33	1.62
Mn ₅₅	20.2	0.060	7.0	0.39	2.01
Co ₆₀	18.3	0.068	6.3	0.44	2.30
As ₇₅	16.4	0.090	9.5	0.74	4.25
Y ₈₉	17.1	0.172	5.2	0.93	5.33
Nb ₉₃	18.0	0.156	7.5	1.17	6.80
Rh ₁₀₃	17.5	0.160	9.4	1.40	8.28
J ₁₂₇	15.2	0.273	6.8	1.76	11.9
Cs ₁₃₃	16.5	0.238	7.7	1.59	10.7
La ₁₃₉	15.5	0.325	3.8	1.55	11.2
Pr ₁₄₁	15.0	0.320	4.9	1.93	13.1
Tb ₁₅₉	15.6	0.274	9.8	2.49	18.1
Ho ₁₆₃	13.5	0.305	8.9	2.52	18.7
Tm ₁₆₉	16.4	0.250	8.4	1.91	14.9
Lu ₁₇₃	16.0	0.225	8.4	1.90	23.0
Ta ₁₈₁	14.5	0.380	8.5	3.15	22.0
Au ₁₉₇	13.8	0.475	4.7	3.04	22.6
Bi ₂₀₉	13.2	0.455	5.9	2.89	23.2

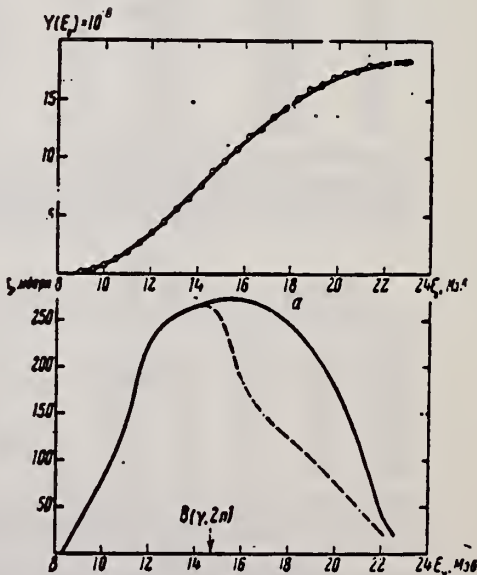


Рис. 12.
а — Выход фотонейтронов для Tb; б — $\sigma_n(E_\gamma)$
и $\sigma_C(\gamma)$ для Tb

Elem. Sym.	A	Z
Tb	159	65

Method radioactive source; photon scattering; NaI spectrometer

Ref. No.
 59 Me 1

5

NVB

Reaction	E or ΔE	E_0	Γ	$\int \sigma dE$	$J\pi$	Notes
Tb(γ, γ)	362 kev	362 keV				<p>Detectors at 125°, 144°.</p> <p>$W(\theta) = 1 + a_2 \cos^2 \theta$, where $a_2 = 0.1 \pm 0.4$</p> <p>Lifetime of γ transition to ground state:</p> $\tau_\gamma = (2.0 \pm 0.3) 10^{-10} \text{ sec.}$ <p>Find transition to be E1 by K-conversion measurements.</p>

ELEM. SYM.	A	Z
Tb	159	65

METHOD

Betatron; neutron threshold; ion chamber

REF. NO.

60 Ge 3

NVB

REACTION	RESULT	EXCITATION ENERGY	SOURCE		DETECTOR		ANGLE
			TYPE	RANGE	- TYPE	RANGE	
G, N	N $\bar{\chi}$ X	THR	C	THR	BF ₃ -I		4 PI

THRESHOLD

TABLE I. Summary and comparison of neutron separation energies inferred from present threshold measurements with values predicted from mass data and reaction energies. All energies are expressed in the center-of-mass system in Mev.

Reaction	No. runs	Present results	Other results	Method	Reference
Tb ¹⁵⁹ (γ , n)Tb ¹⁵⁸	3	8.141 \pm 0.039	8.16 \pm 0.05	threshold	f

Method	18 MeV electron synchrotron; BF_3 counters; ion chamber				Ref. No.
					60 Th 1
Reaction	E or ΔE	E_0	Γ	$\int \sigma dE$	Jπ
$\text{Tb}^{159}(\gamma, xn)$	7-18	12.4 ± 0.2			$\sigma_{\max} = 410 \text{ mb.}$
		16.0 ± 0.2			$\sigma_{\max} = 460 \text{ mb.}$

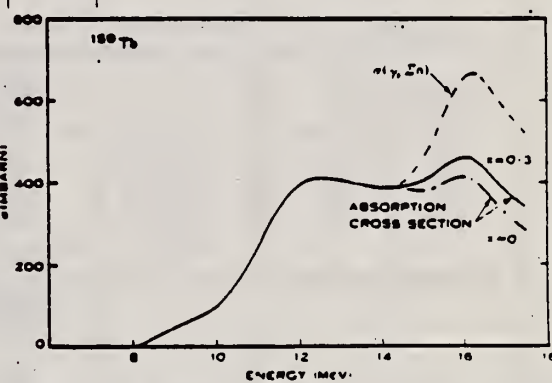


Fig. 8.—Cross section for photon absorption in ^{159}Tb , using statistical theory of nuclear reactions to correct for neutron multiplicity. The factor x is a measure of the probability that a direct photoeffect will occur.

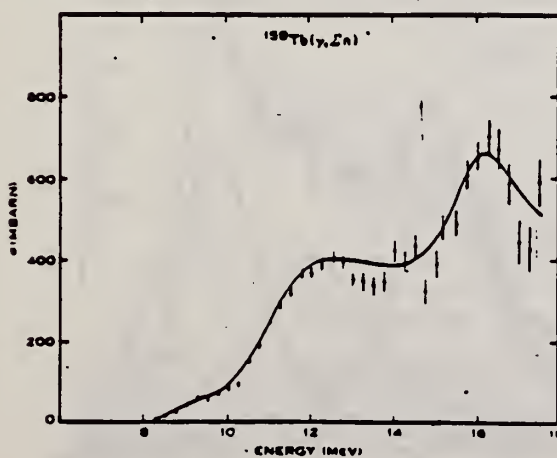


Fig. 6.—Total neutron production cross section for ^{159}Tb .

TABLE 2
 GIANT RESONANCE PARAMETERS IN DEFORMED NUCLEI

Nucleus	^{158}Tb		^{160}Ho	^{161}Tb		
	Reference	Fuller and Weiss (1958)	Present Paper	Present Paper	Fuller and Weiss (1958)	Spicer et al. (1958)
$\Gamma_{\text{G.R.}}$ (MeV)	6.5	6.7 ± 0.5	7 ± 0.5	6.2 ± 0.2	6.1	6.1
E_1 (MeV)	12.5	12.4 ± 0.2	12.1 ± 0.2	12.46	12.46	12.6
$(\sigma_0)_{\max}$ (mbarn)	260	410	420	308	500	
Γ_1 (MeV)	2.4	3.3	2.8	2.3	2.0	
E_2 (MeV)	16.3	16.0 ± 0.2	16.2 ± 0.2	15.46	15.3	
$(\sigma_0)_{\max}$ (mbarn)	310	400	510	348	450	
I_1^* (MeV)	4.0	4.5	4.7	4.4	4.0	
I_2/I_1	2.0	2.0	2.0	2.16	1.8	
E_2/E_1	1.30	1.29 ± 0.03	1.34 ± 0.03	1.25 ± 0.01	1.21 ± 0.03	

Elem. Sym.	A	Z
Tb	159	65

Method

30 MeV Synchrotron - BF₃

Ref. No.

62Bol

BG

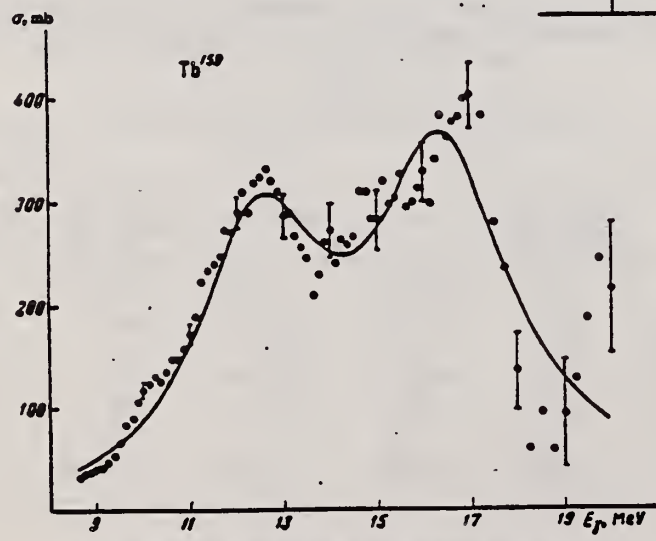
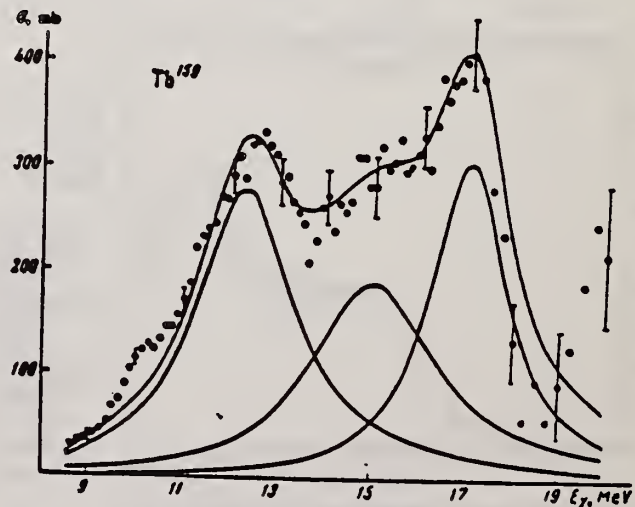
Reaction	E or ΔE	E_0	Γ	$\int \sigma dE$	$J\pi$	Notes
(γ , n) Threshold 21						<p>Best fits of σ_γ by two (Fig.10) and three (Fig.11) Lorentz lines made. 2 Lorentz line approximation less likely. Data for Lorentz line fits given in Table II and Table III.</p>

Table II

Number of line	σ_{max} , mb	E_0 , MeV	Γ , MeV	σ_{Int} , MeV.b	$\frac{\sigma_{Int2}}{\sigma_{Int1}}$	σ_{Int} , MeV.b	$\frac{\sigma_{Int}}{0.05ENZ/A}$	ϵ	Q_{ab} , b
I	—	267	12.5	3.4	1.42	—	—	—	—
II	—	317	16.4	3.4	1.69	1.10	3.11	1.4	0.28

Table III

Number of line	σ_{max} , mb	E_0 , MeV	Γ , MeV	σ_{Int} , MeV.b	$\sigma_{Int1}:\sigma_{Int2}:\sigma_{Int3}$	σ_{Int} , MeV.b	$\frac{\sigma_{Int}}{0.05ENZ/A}$
I	278	12.25	2.5	1.09	—	—	—
II	191	15	3.2	0.96	—	—	—
III	305	17	2.0	0.98	1.09:0.96:0.98	3.01	1.35

FIG. 10. Photon absorption cross section of Tb¹⁵⁹.FIG. 11. Approximation of σ_γ of Tb¹⁵⁹ by three Lorentz lines.

ELEM. SYM.	A	Z
Tb	159	65

METHOD

Positron annihilation; linac; ion chamber

REF. NO.	NVB
64 Br 1	

REACTION	RESULT	EXCITATION ENERGY	SOURCE		DETECTOR		ANGLE
			TYPE	RANGE	TYPE	RANGE	
G,N	361	ABX	D	8 - 28	BF3-I		4PI
G,2N	362	ABX	D	8 - 28	BF3-I		4PI

Level density parameter

$$\alpha = 17 \pm 5 \text{ MeV}^{-1}$$

Quadrupole moment = 7.0 ± 1.1 barns.

28

$$\int_8^{\infty} \sigma(\gamma, n + \gamma, 2n) dE = 2.3 \pm 0.2 \text{ MeV-barns},$$

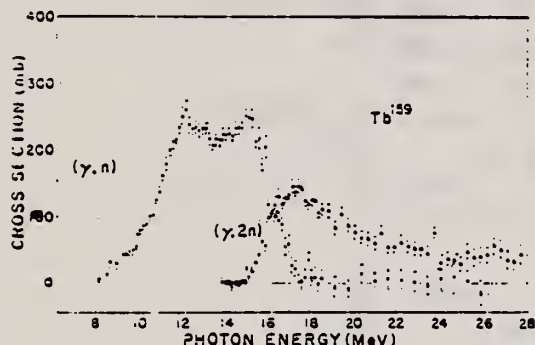


FIG. 4. The (γ, n) and $(\gamma, 2n)$ cross sections of Tb^{159} up to 28 MeV. The (γ, n) cross section decreases rapidly to zero above the $(\gamma, 2n)$ threshold.

TABLE III. Parameters of the Tb^{159} giant resonance.

Parameter	Reference	This experiment	Fuller and Weiss ^a	Thies and Spicer ^b	Bogdankevich <i>et al.</i> ^c
E_0 (MeV)		12.2 ± 0.2	12.5	12.4 ± 0.2	12.5
σ_0 (mb)		183 ± 19	260	410	267
I_0 (MeV)		2.67 ± 0.2	2.4	3.3	3.4
K_0 (MeV)		15.6 ± 0.2	16.1	15.0 ± 0.2	16.4
σ_0 (mb)		133 ± 23	310	460	317
I_0 (MeV)		4.30 ± 0.4	6.0	4.5	3.4
Q_0 (b)		$+7.0 \pm 1.1$	7.7	7.3	7.8
$\int F^2 dE$ (MeV b)		2.3 ± 0.2			

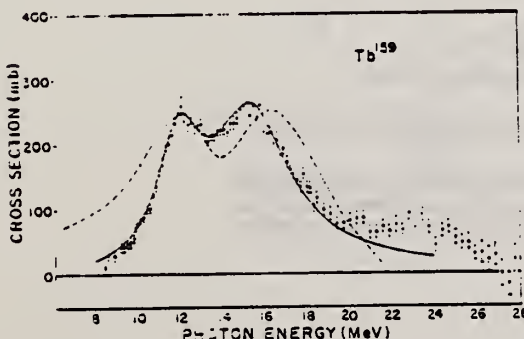
^a See Ref. 31.^b See Ref. 32.^c See Ref. 30.

FIG. 5. The photon absorption cross section of Tb^{159} obtained by adding the (γ, n) and $(\gamma, 2n)$ cross sections of Fig. 4. The electric dipole giant resonance is double peaked due to the quadrupole moment of Tb^{159} . The solid curve is the sum of two Lorentz curves with parameters given in Table III. The dashed curve is from Wilkinson (Ref. 9).

METHOD

Bremsstrahlung scattering

[Page 1 of 2]

REF. NO.

64 La 1

joc

REACTION	RESULT	EXCITATION ENERGY	SOURCE		DETECTOR		ANGLE
			TYPE	RANGE	TYPE	RANGE	
G,G	ABX	10-25	C		NAI-D		DST

TABLEAU I
Le paramètre $a(E)$ de la distribution angulaire

Noyau	11.5-14. MeV			14-17.5 MeV			17.5-20 MeV			20-30 MeV	
	Exp.	Ellipsoidal	Triax.	Exp.	Ellips.	Triax.	Exp.	Ellips.	Triax.	Exp.	Ellips.
Contribution Quadrupolaire %											
Tb	$0.5^{+0.15}_{-0.1}$	0.41	0.39	$0.54^{+0.15}_{-0.1}$	0.70	0.50	25	0.97	0.85	1	
Ho	$0.27^{+0.15}_{-0.1}$	0.44	0.407	$0.43^{+0.10}_{-0.05}$	0.71	0.53	25	0.95	0.9	0.4 ± 0.1	1
Er	$0.27^{+0.15}_{-0.1}$	0.44	0.407	$0.8^{+0.15}_{-0.1}$	0.71	0.53	25	0.95	0.9		1
Ta	$0.6^{+0.15}_{-0.1}$	0.58		$0.68^{+0.15}_{-0.1}$	0.81		20	0.96			
Au				$a_{\text{exp}}(11-20 \text{ MeV}) = 0.9$						0.7 ± 0.1	1
				$a_{\text{th}}(11-20 \text{ MeV}) \approx 1$							

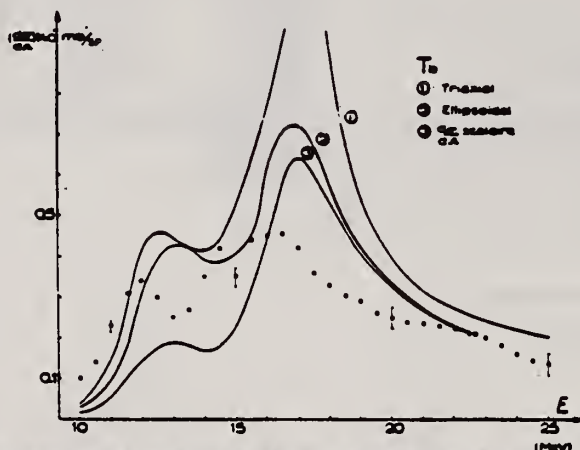


Fig. 3. Sections efficaces différentielles de diffusion obtenues pour le terbium. Les courbes tracées correspondent à l'application des relations de dispersion aux sections efficaces d'absorption de Bogdansovich *et al.*¹⁴) dans le cas d'une diffusion purement scalaire et d'un modèle ellipsoïdal ou triaxial.

METHOD

Bremsstrahlung scattering

[Page 2 of 2]

REF. NO.

64 La 1

JOC

REACTION	RESULT	EXCITATION ENERGY	SOURCE		DETECTOR		ANGLE
			TYPE	RANGE	TYPE	RANGE	

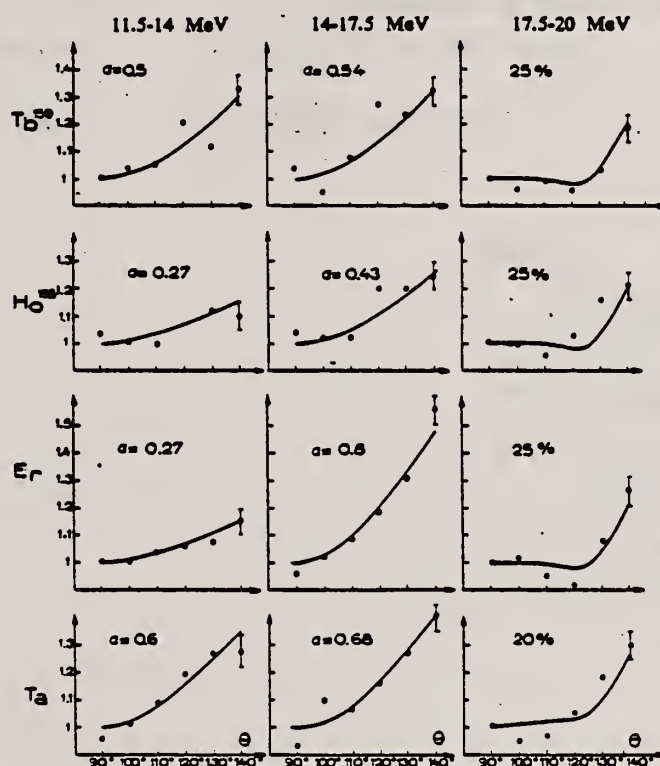


Fig. 8. Répartitions angulaires du rayonnement diffusé obtenues pour le terbium, l'holmium, l'erbium et le tantalum dans les zones d'énergie 11.5-14 MeV, 14-17.5 MeV et 17.5-20 MeV.

U. Atzmony, E. R. Bauminger and S. Ofer
Nuclear Phys. 39, 433 (1966)

ELEM. SYM.	A	Z
Tb	159	65

METHOD

Mössbauer Effect

REF. NO.

66 At 2

JDM

REACTION	RESULT	EXCITATION ENERGY	SOURCE		DETECTOR		ANGLE
			TYPE	RANGE	TYPE	RANGE	
G,G	LFT	1	D		SCD-D		DST

$T_{\frac{1}{2}}$ for 58 keV level $\leq (1.05 \pm 0.15) 10^{-10}$. Magnetic moment of this level = 1.50 ± 0.10 n.m.

(and perhaps 2.10 ± 0.15 n.m. cannot be excluded).

R. S. Raghavan
Phys. Rev. 143, B947 (1966)

ELEM. SYM.	A	Z
Tb	159	65

METHOD

REF. NO.

Centrifuge technique

66 Ra I

JDM

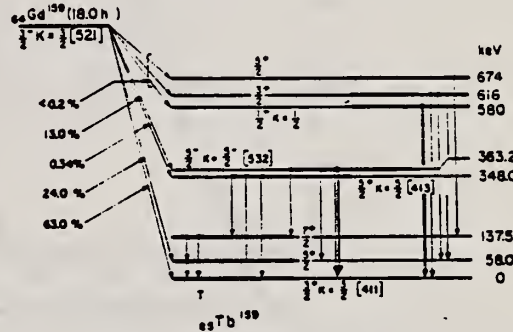
REACTION	RESULT	EXCITATION ENERGY	SOURCE		DETECTOR		ANGLE
			TYPE	RANGE	TYPE	RANGE	
G, G	LFT	1	D	1	NAI - D		DST

$$W = 1 + A_2 P_2 (\cos\theta)$$

For 363 MeV, $A_2 = +(24.3 \pm 3)\%$, $\tau = (2.2 \pm 0.15) \times 10^{-3}$ secs.

For 580 MeV, $A_2 = 0.0 \pm 0.06$, $\tau = (1.1 \pm 0.15) \times 10^{-3}$ secs.

$$\delta_{363} \left(\frac{M2}{E1} \right) = -6 \pm 1\%, \quad \delta_{580} \left(\frac{E2}{M1} \right) = \pm (3 \pm 1.5)\%$$

FIG. 1. Decay scheme of Gd¹⁵⁹-Tb¹⁵⁹.

947

METHOD

REF. NO.

68 Be 5

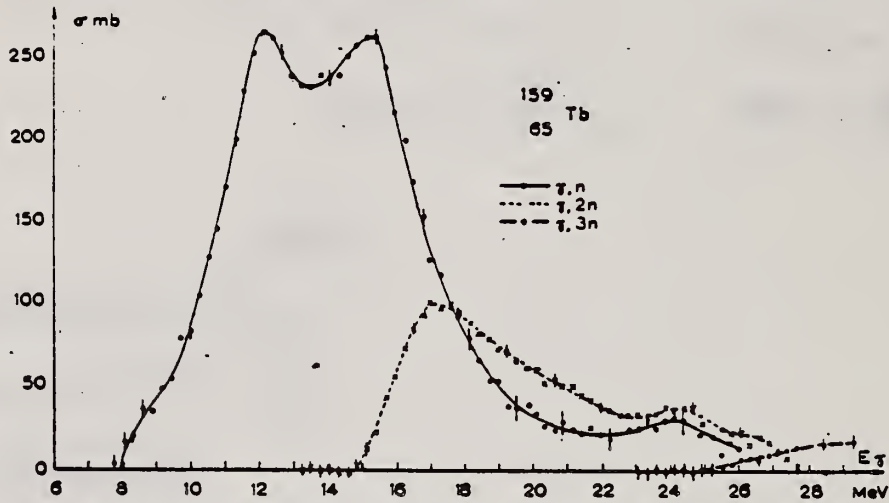
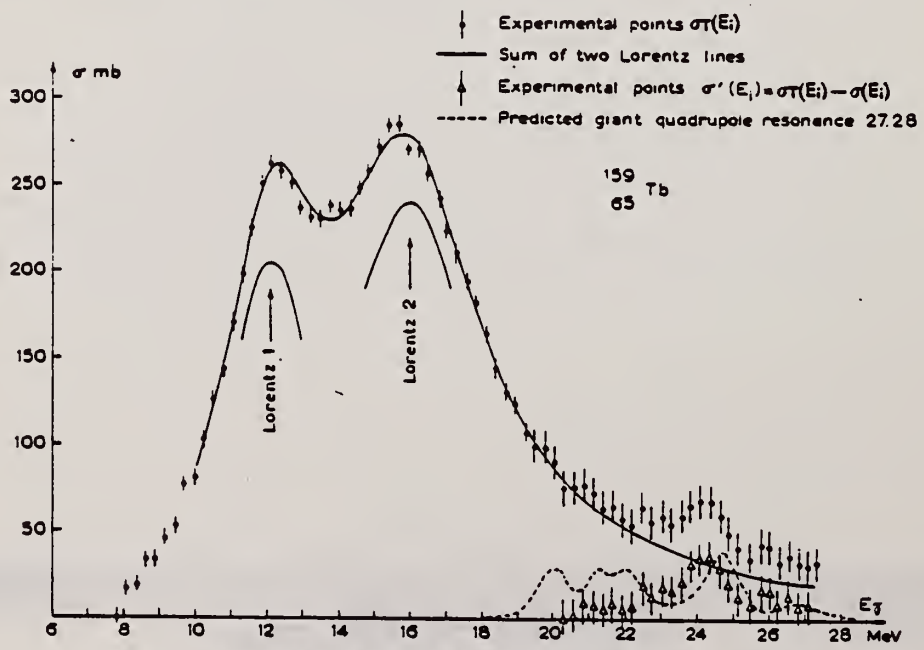
egf

REACTION	RESULT	EXCITATION ENERGY	SOURCE		DETECTOR		ANGLE
			TYPE	RANGE	TYPE	RANGE	
G, N 94	ABX	THR-30	D	7-30	MOD-I		4PI
G, 2N 95							
G, 3N 96+							

TABLE 6
Lorentz line parameters for a two line fit to the total cross section data of $^{159}_{\text{Gd}}\text{Tb}$

$E_1(\text{MeV})$	$\sigma_1(\text{mb})$	$\Gamma_1(\text{MeV})$	E_2	σ_2	Γ_2
12.12	205	3.25	15.97	240	4.87

94+

Fig. 7. Partial photonuclear cross sections $\sigma(y, n)$, $\sigma(y, 2n)$ and $\sigma(y, 3n)$ of $^{159}_{\text{Gd}}\text{Tb}$.Fig. 8. Total cross section data showing a two Lorentz line fit for a $^{159}_{\text{Gd}}\text{Tb}$ target. 414

METHOD					REF. NO.		
REACTION	RESULT	EXCITATION ENERGY	SOURCE		DETECTOR		ANGLE
			TYPE	RANGE	TYPE	RANGE	
G,N	ABY	THR-20	C	20	ACT-I		4PI

ISOMERIC YIELD

TABLE I. THE PARTICULARS OF THE (γ, n) REACTION PRODUCTS AND THE DATA OBTAINED WITH 20 MeV BREMSSTRAHLUNG

Parent (Natural abundance, %)	Nuclide	Half-life of product (sec)	Gamma-ray determined			Limit of detection (μ g)	Yield ($\text{mol}^{-1} \cdot \text{R}^{-1}$)
			Energy (MeV)	Branching ratio (%)	Photopeak activity (cpm/mg) ^a		
²⁴ Mg(78.60)	²³ Mg	9.9	0.511	200	2.04×10^4	0.49	8.1×10^4
⁷⁶ Ge(7.67)	^{75m} Ge	48	0.139	100	6.37×10^4	1.6	1.1×10^4
⁷⁶ Se(23.52)	^{77m} Se	17	0.162	100	1.82×10^4	0.55	1.2×10^4
⁹⁶ Mo(15.86)	^{91m} Mo	65	0.650	57	2.22×10^4	4.5	2.7×10^4
¹⁴⁰ Ce(88.48)	^{139m} Ce	58	0.745	100	1.06×10^4	0.95	1.3×10^4
¹⁴² Nd(27.13)	^{141m} Nd	64	0.760	100	3.19×10^4	3.1	1.4×10^4
¹⁵⁸ Tb(100)	^{159m} Tb	11	0.111	100	2.56×10^4	3.8	2.2×10^4

a) The value corrected at the end of one-minute irradiation with the dose rate of 10^7 R/min; Counting geometry is 20% with a 3"dia. \times 3"NaI(Tl) detector.

L.M. Dautov, Yu.A. Lysikov, U.M. Makhanov, Yu.K. Shubnyi
 Izv. Akad. Nauk SSSR Ser. Fiz. 36, 2544 (1972)
 Bull. Acad. Sci. USSR Phys. Ser. 36, 2210 (1972)

ELEM. SYM.	A	Z
Tb	159	65

METHOD

REF. NO.

72 Da 14

hmg

REACTION	RESULT	EXCITATION ENERGY	SOURCE		DETECTOR		ANGLE
			TYPE	RANGE	TYPE	RANGE	
G,G	ABX	364*	D	364*	SCD-D		92

$$\sigma = (5.5 \pm 0.7) \cdot 10^{-28} \text{ cm}^2 \cdot \text{sr}^{-1}, \quad \Gamma_{0\gamma} = (3.4 \pm 0.4) \cdot 10^{-6} \text{ eV.}$$

* ENERGY IN KEV

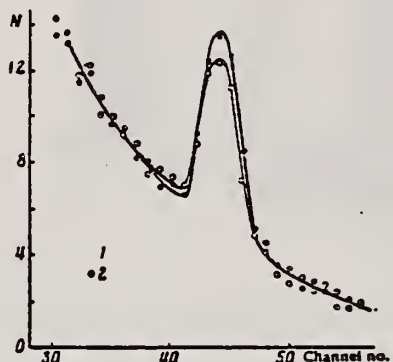


Fig. 3. The spectrum of the scattered radiation in the case ^{159}Gd ^{159}Tb at a source temperature of 1000° C . 1) Terbium scatter; 2) samarium scatter. $N =$ hundreds of pulses in 20 min. In nonresonance conditions ($T = 20^\circ\text{ C}$) the scattering from both scatterers was the same $N_{\text{Tb}}/N_{\text{Sm}} = 1.012 \pm 0.003$.

METHOD			REF. NO.		
REACTION	RESULT	EXCITATION ENERGY	SOURCE	DETECTOR	ANGLE
			TYPE RANGE	TYPE RANGE	
G,N	NOX	THR- 27	C 10- 27	BF3-T	APT

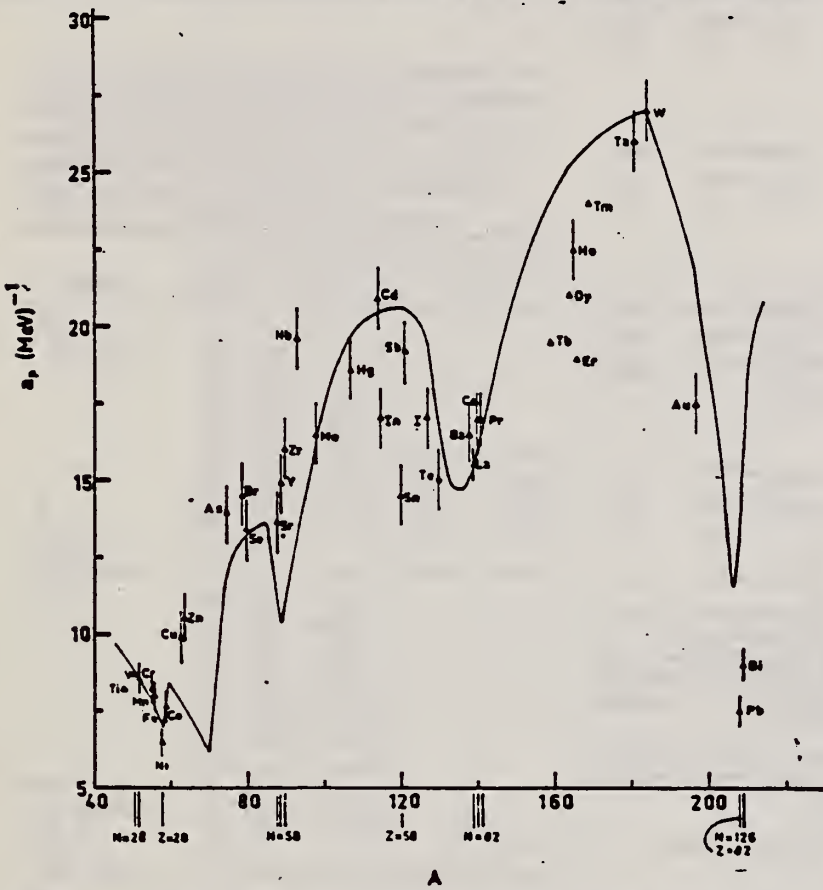


Fig. 12. Experimental values of the level density parameter a_p (Fermi gas formula plus pairing correction) versus atomic number A . The continuous curve is a least-squares fit to the data of a theoretical calculation from Newton ¹⁵.

- 1 H. Baba and S. Baba, Japan Atomic Energy Research Institute report JAERI-1183 (1969).
 2 H. Baba, Nucl. Phys. A159, 625 (1970).
 15 T.D. Newton, Can. J. Phys. 34, 804 (1956).

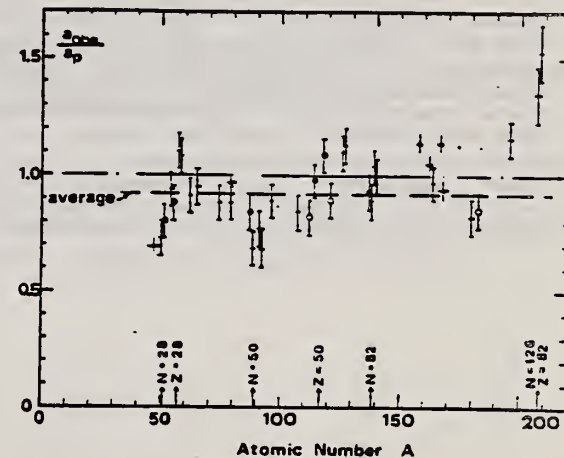


Fig. 15. Ratio a_{res}/a_p versus atomic number A . Here a_{res} is the level density parameter taken from the neutron resonance work of refs. ¹⁻², and a_p is the level density parameter derived from the present (y, n) work. Filled circles represent points where nuclei in the neutron resonance and in the (y, n) experiment were the same. Open circles represent points where the respective nuclei were approximately matched. Triangles represent points which are based on measurement of neutron mean energies at two bremsstrahlung energies only.

(over)

TABLE 3 (continued)

Target	<i>N</i> (residual nucleus) ^{a)}	Goodness of fit ^{b)}		$\bar{E}_n(24)$ (MeV) ^{c)}	T (MeV) ^{d)}	a_p (MeV ⁻¹) ^{e)}	a_{obs} (MeV ⁻¹) ^{f)}	a_{obs}/a_p	
		no p.c.	with p.c.						
Ba	75	1%		F	1.16	$16.5 - ^{136}\text{Ba}$	$15.39 - ^{136}\text{Ba}$	0.93	
	77	2%							
	78	7%							
	79	8%							
	80	11%							
	81	71%							
La	80	100%	F	F	1.25	0.72	$15.5 - ^{138}\text{La}$	$13.76 - ^{139}\text{La}$	0.89
Ce	81	89%	F	G	1.24	0.70	$17.0 - ^{139}\text{Ce}$	$17.8 - ^{141}\text{Ce}$	1.04
	83	11%							
Pr	81	100%	G	G	1.17	0.65	$17.0 - ^{140}\text{Pr}$	$17.05 - ^{142}\text{Pr}$	1.00
Tb ^{g)}	93	100%			1.15		$19.3 - ^{158}\text{Tb}$	$21.85 - ^{160}\text{Tb}$	1.14
Dy ^{g)}	93	2%			1.06		$20.9 - ^{161.5}\text{Dy}$	$21.9 - ^{162}\text{Dy}$	1.05
	94	19%							
	95	25%							
	96	25%							
	97	28%							
Ho	97	100%	P	G	1.06	0.56	$21.4 - ^{166}\text{Ho}$	$20.66 - ^{166}\text{Ho}$	0.97
Er ^{h)}	95	2%			1.11		$19.2 - ^{166}\text{Er}$	$21.9 - ^{166}\text{Er}$	1.14
	97	33%							
	98	23%							
	99	27%							
	191	15%							
Tm ^{h)}	99	100%			1.03		$24.0 - ^{168}\text{Tm}$	$22.58 - ^{170}\text{Tm}$	0.94
Ta	107	100%		G	1.00	0.49	$26.0 - ^{180}\text{Ta}$	$21.2 - ^{181}\text{Ta}$	0.82
W	107	26%	G	F	0.98	0.50	$27.0 - ^{183}\text{W}$	$23.0 - ^{183}\text{W}$	<u>0.85</u>
	108	14%							
	109	31%							
	111	28%							
Au	117	100%		G	1.19		$17.5 - ^{196}\text{Au}$	$20.24 - ^{198}\text{Au}$	1.16
Pb	123	24%		V.P.	1.87	1.20	$7.5 - ^{206}\text{Pb}$	$10.1 - ^{207}\text{Pb}$	1.35
(Z = 82)	124	23%							
	125	52%							
Bi	125	100%	F		1.65	1.03	$9.0 - ^{208}\text{Bi}$	$13.8 - ^{210}\text{Bi}$	1.53

^{a)} Neutron numbers and abundances of respective residual nuclei in (γ , n) experiments.^{b)} These give an assessment of the goodness of fit of a calculated \bar{E}_n versus E_0 curve to the observed data, using the Fermi gas level density formula both without and with pairing corrections.^{c)} Bremsstrahlung photoneutron mean energies \bar{E}_n for peak bremsstrahlung energy $E_0 = 24$ MeV.^{d)} Nuclear temperature from fit with constant-temperature formula.^{e)} Level density parameter a_p derived from the present (γ , n) experiment, using a Fermi gas formula plus pairing correction, and corresponding residual nucleus (the atomic weight shown is the weighted average of atomic weights of the respective isotopes present).^{f)} As column 7, but using data on n-resonance absorption from refs. ^{1,2}.^{g)} Measurements of $\bar{E}_n(E_0)$ for these nuclei were made only for $E_0 = 21, 23$ and 24 MeV.

H.E. Jackson, G.E. Thomas, and K.J. Wetzel
Phys. Rev. C9, 1153 (1974)

ELEM. SYM.	A	Z
Tb	159	65

METHOD

REF. NO.

74 Ja 2

hmg

REACTION	RESULT	EXCITATION ENERGY	SOURCE		DETECTOR		ANGLE
			TYPE	RANGE	TYPE	RANGE	
G,G	ABX	10	D	10	SCD-D		90
		(10.83)		(10.83)			

TABLE I. Differential cross sections measured for elastic and inelastic scattering of 10.83-MeV photons. States or states populated by inelastic scattering are indicated in parentheses below the target. The errors given result from the statistical error in the measurement of the cross section relative to the calibration value, the 90° uranium inelastic cross section.

Nucleus	θ (deg)	$d\sigma/d\omega$ (elastic) (mb/sr)	$d\sigma/d\omega$ (inelastic) (mb/sr)
²³⁵ U			
(2 ⁺ , 45 keV)	20	1.72 ± 0.17	
	30	0.97 ± 0.12	
	50	0.334 ± 0.039	
	60	0.23 ± 0.04	
	70	0.245 ± 0.024	0.136 ± 0.015
	90	0.182 ± 0.017	0.154 ± 0.012
	120	0.189 ± 0.017	0.160 ± 0.013
	150	0.303 ± 0.016	0.160 ± 0.015
²³² Th			
(2 ⁺ , 45 keV)	90	0.129 ± 0.015	0.103 ± 0.007
Pb	20	1.28 ± 0.12	
	30	0.55 ± 0.07	
	50	0.289 ± 0.051	
	60	0.20 ± 0.04	
	70	0.087 ± 0.014	
	90	0.079 ± 0.005	
	120	0.060 ± 0.004	
	150	0.127 ± 0.008	
²⁰⁹ Tl			
($\frac{1}{2}^+$, 910 keV)	90	0.101 ± 0.0062	~0
¹⁸¹ Ta			
($\frac{3}{2}^+$, 136 keV)	90	0.0370 ± 0.0003	0.00656 ± 0.0015
¹⁵⁹ Tb			
($\frac{5}{2}^+$, 58 keV)	90	0.0314 ± 0.0003	0.0110 ± 0.0016
($\frac{7}{2}^+$, 138 keV)			0.00511 ± 0.0011

TABLE III. Comparison of calculated and observed values of the 90° cross sections for elastic scattering and of the ratio at 90° of Raman to elastic scattering by various nuclei for 10.83-MeV photons. The parameters used in the calculations are given in Table II.

Target	$d\sigma_{\text{elas}}(90^\circ)/d\Omega$ (mb/sr)		$d\sigma_{\text{Raman}}^{(90^\circ)}/d\sigma_{\text{elas}}^{(90^\circ)}$	
	Calc	Exp	Calc	Exp
Tb	0.036	0.031 ± 0.003	0.80	0.51 ± 0.06
Ta	0.055	0.037 ± 0.003	0.28	0.18 ± 0.04
Pb	0.076	0.079 ± 0.005	0	
Bi		0.101 ± 0.006	0	~0
Th	0.128	0.129 ± 0.015	0.91	0.80 ± 0.08
U	0.157 ^a	0.182 ± 0.017	1.03	0.85 ± 0.08

^a If the Livermore parameters (Ref. 33) for ²³⁵U are used then this calculated value would be 0.210 mb/sr.

33

C.D. Bowman, G.F. Auchampaugh, and S.C. Fultz, Phys. Rev. 133, B676 (1964).

ELEM. SYM.	A	Z
Tb	159	65

METHOD

REF. NO.
75 Ja 1

hmg

REACTION	RESULT	EXCITATION ENERGY	SOURCE		DETECTOR		ANGLE
			TYPE	RANGE	TYPE	RANGE	
G,G	ABX	11	D	11	SCD-D		DST
		(11.387)		(11.387)			

RATIO RAMAN/ELASTIC

TABLE I. Differential cross sections measured for elastic and inelastic scattering of 11.39-MeV photons. States or states populated by inelastic scattering are indicated in parentheses beside the target. The errors given result from the statistical error in the measurement of the cross section relative to the calibration value, the 90° uranium elastic cross section.

θ (deg)	$d\sigma/d\omega$ (elastic) (mb/sr)	$d\sigma/d\omega$ (inelastic) (mb/sr)
^{238}U (2^+ , 45 keV)		
90	0.169 ± 0.011	0.173 ± 0.016
150	0.355 ± 0.041	0.236 ± 0.24
^{232}Th (2^+ , 45 keV)		
150	0.331 ± 0.035	0.210 ± 0.022
^{181}Ta ($\frac{3}{2}^+$, 136 keV) ($\frac{1}{2}^+$, 301 keV)		
90	0.073 ± 0.008	0.020 ± 0.004 0.009 ± 0.004
150	0.145 ± 0.015	0.017 ± 0.004 0.017 ± 0.004
^{163}Ho ($\frac{3}{2}^+$, 95 keV) ($\frac{1}{2}^+$, 210 keV)		
150	0.141 ± 0.014	0.022 ± 0.004 0.013 ± 0.004
^{158}Tb ($\frac{5}{2}^+$, 58 keV) ($\frac{1}{2}^+$, 138 keV)		
90	0.062 ± 0.006	0.024 ± 0.003 0.013 ± 0.003
150	0.134 ± 0.012	0.042 ± 0.004 0.019 ± 0.004
^{141}Pr		
150	0.030 ± 0.008	...

TABLE III. Comparison of calculated and observed values of the cross sections for elastic scattering and of the ratio of Raman to elastic scattering by various nuclei for 11.387-MeV photons at 90 and 150°. The parameters used in the calculations for column 5 are given in Table II. Column 4 describes results obtained by perturbing those parameter to meet the constraint of Eq. (3) (see text).

Target	Calc.	Exp.	$d\sigma(\theta)d\Omega$ (mb/sr)	$d\sigma_{\text{Raman}}(\theta)/d\sigma_{\text{elastic}}(\theta)$
			$\theta = 150^\circ$	
Pr	0.025	0.030 ± 0.008		0.0 0.0
Tb	0.094	0.134 ± 0.012	0.53 0.57	0.46 ± 0.04
Ho	0.170	0.141 ± 0.014	0.28 0.28	0.25 ± 0.04
Ta	0.160	0.145 ± 0.015	0.23 0.22	0.23 ± 0.04
Th	0.253	0.331 ± 0.035	0.59 0.63	0.64 ± 0.08
U	0.289	0.355 ± 0.041	0.78 0.73	0.67 ± 0.07
$\theta = 90^\circ$				
Tb	0.062	0.062 ± 0.006	0.76 0.82	0.60 ± 0.07
Ta	0.109	0.074 ± 0.008	0.32 0.30	0.33 ± 0.07
U	0.172	0.169 ± 0.008	1.29 1.15	1.03 ± 0.10

METHOD

REF. NO.	76 Em 2	egf
----------	---------	-----

REACTION	RESULT	EXCITATION ENERGY	SOURCE		DETECTOR		ANGLE
			TYPE	RANGE	TYPE	RANGE	
G, F	ABY	THR-999	C	999	TRK-I		4PI

TABLE I

Measured values of σ_q at $E = 1000$ MeV and deduced values of σ_t assumed constant from E_0 to 1000 MeV999 = 1 GEV

Element	Z^2/A	σ_q (mb)	E_0 (MeV)	σ_t (mb)
Bi	32.96	12.3 ± 0.6	200	7.6 ± 0.6
Pb	32.45	5.4 ± 0.4	220	3.6 ± 0.3
Tl	32.10	4.1 ± 0.3	230	2.8 ± 0.3
Au	31.68	2.0 ± 0.15	240	1.4 ± 0.2
Pt	31.18	1.1 ± 0.08	255	$(8 \pm 0.7) \times 10^{-1}$
Re	30.21	$(3.7 \pm 0.3) \times 10^{-1}$	280	$(2.9 \pm 0.3) \times 10^{-1}$
W	29.78	$(3.5 \pm 0.3) \times 10^{-1}$	290	$(2.8 \pm 0.3) \times 10^{-1}$
Ta	29.45	$(3.3 \pm 0.3) \times 10^{-1}$	300	$(2.7 \pm 0.3) \times 10^{-1}$
Hf	29.04	$(1.7 \pm 0.2) \times 10^{-1}$	310	$(1.4 \pm 0.2) \times 10^{-1}$
Yb	28.31	$(1.3 \pm 0.1) \times 10^{-1}$	330	$(1.2 \pm 0.1) \times 10^{-1}$
Tm	28.18	$(7.5 \pm 0.8) \times 10^{-2}$	335	$(6.8 \pm 0.8) \times 10^{-2}$
Ho	27.21	$(3.6 \pm 0.4) \times 10^{-2}$	355	$(3.5 \pm 0.4) \times 10^{-2}$
Dy	26.80	$(2.6 \pm 0.3) \times 10^{-2}$	360	$(2.5 \pm 0.3) \times 10^{-2}$
Tb	26.58	$(2.5 \pm 0.3) \times 10^{-2}$	370	$(2.5 \pm 0.3) \times 10^{-2}$
Gd	26.04	$(1.6 \pm 0.2) \times 10^{-2}$	380	$(1.7 \pm 0.2) \times 10^{-2}$
Sm	25.56	$(1.3 \pm 0.2) \times 10^{-2}$	390	$(1.4 \pm 0.2) \times 10^{-2}$
Nd	24.96	$(9.2 \pm 0.9) \times 10^{-3}$	405	$(1 \pm 0.1) \times 10^{-2}$
Ce	24.00	$(8 \pm 0.9) \times 10^{-3}$	420	$(9 \pm 1) \times 10^{-3}$
La	23.39	$(8.4 \pm 0.9) \times 10^{-3}$	430	$(1 \pm 0.1) \times 10^{-3}$
Sb	21.36	$(1.2 \pm 0.2) \times 10^{-2}$	460	$(1.5 \pm 0.3) \times 10^{-2}$
Te	21.19	$(8.8 \pm 1) \times 10^{-3}$	465	$(1.2 \pm 0.2) \times 10^{-2}$
Sn	21.06	$(1.3 \pm 0.2) \times 10^{-2}$	465	$(1.7 \pm 0.3) \times 10^{-2}$
Cd	20.49	$(1.7 \pm 0.3) \times 10^{-2}$	470	$(2.2 \pm 0.4) \times 10^{-2}$
Ag	20.47	$(2 \pm 0.3) \times 10^{-2}$	470	$(2.6 \pm 0.4) \times 10^{-2}$
Zn	13.76	$(2 \pm 0.4) \times 10^{-1}$	515	$(3 \pm 0.6) \times 10^{-1}$
Cu	13.44	$(2.4 \pm 0.5) \times 10^{-1}$	515	$(3.6 \pm 0.8) \times 10^{-1}$
Ni	13.35	$(2.4 \pm 0.5) \times 10^{-1}$	510	$(3.6 \pm 0.8) \times 10^{-1}$
Fe	12.10	$(3 \pm 0.6) \times 10^{-1}$	510	$(4.4 \pm 0.9) \times 10^{-1}$

- ⁴A.V. Mitrofanova et al., Sov. J. Nucl. Phys. 6, 512 (1968).
⁷T. Methasiri et al., Nucl. Phys. A167, 97 (1971).
¹²J.R. Nix et al., Nucl. Phys. 81, 61 (1966).
²⁰N.A. Perifilov et al., JETP (Sov. Phys.) 14, 623 (1962); Proc. Symp. on the physics & chemistry of fission, Salzburg 1965, vol. 2 (IAEA) Vienna, 1965, p. 283.

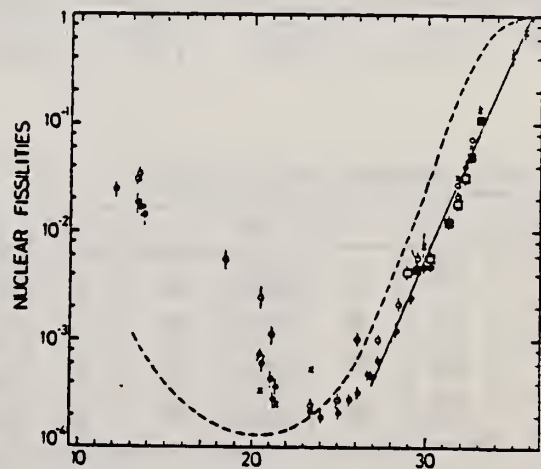


Fig. 2. Nuclear fissilities as a function of Z^2/A . Experimental points: solid circles represent our data; squares, the data from ref. ⁴); open circles, the data from ref. ⁷); and crosses, the data from (p,f) experiments²⁰). The straight line is the best fit calculated from our data for $Z^2/A > 26$. The dashed curve is the curve VI calculated by Nix and Sassi¹²).

B. I. Goryachev, Yu.V. Kuznetsov, V.N. Orlin, N.A. Pzhidaeva,
 V. G. Shevchenko
Yad. Fiz. **23**, 1145 (1976)
Sov. J. Nucl. Phys. **23**, 609 (1976)

ELEM. SYM.	A	Z
Tb	159	65

METHOD

REF. NO.	
76 Go 4	hmg

REACTION	RESULT	EXCITATION ENERGY	SOURCE		DETECTOR		ANGLE
			TYPE	RANGE	TYPE	RANGE	
G, XN	ABX	8-23	C	UKN	BF3-I		4PI
G, 2N	ABX	15-21	C	UKN	SCI-I		4PI

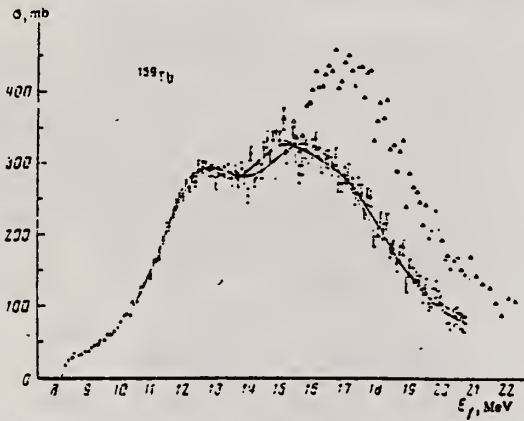


FIG. 3. Photoabsorption cross section σ , in mb, for ^{159}Tb (hollow and solid circles). Above the (γ , 2π) threshold we have shown by the triangles the cross section σ_n . The thin and thick curves show respectively the fits $\sigma_\gamma^{(1)}$ ($\sigma_1 \Gamma_1 : \sigma_2 \Gamma_2 = 1:2$) and $\sigma_\gamma^{(2)}$ ($\sigma_1 \Gamma_1 : \sigma_2 \Gamma_2 : \sigma_3 \Gamma_3 = 1:1:1$).

TABLE 3. Static deformation β and intrinsic quadrupole moment Q_0 .

Nucleus	Present work		Other photoabsorber experiments		Coulomb excitation of nuclei
	β	Q_0 , b	β	Q_0 , b	
^{159}Tb	0.29	6.53 ± 0.6	0.29	$6.57 [15]$ 7.37 [20] 6.6 [21]	$7.07 [16]$
^{164}Ho	0.32	7.73 ± 0.8	0.29	$7.01 [15]$ 7.14 [20] 7.6 [19]	$7.80 [16]$
^{162}Er	0.30	7.39 ± 0.6	0.29	$6.96 [16]$ 7.8 [19]	
^{178}Hf	0.29	6.94 ± 0.6			$6.79 [22]$

TABLE 6. Integrated cross sections.

Nucleus	σ_{int} , MeV-b	$a_0 \cdot 10^{-2} \frac{\text{mb}}{\text{MeV}}$	a_{int} , mb	$a_{int} \cdot 10^4$	σ_{int} , MeV-b	$a_{int} \cdot 10^4$
^{159}Tb	3.79	1.47	210	0.243	15.9	3.41 10^{-3}
^{164}Ho	3.60	1.51	218	0.241	16.1	3.27 10^{-3}
^{162}Er	3.58	1.58	216	0.237	16.1	3.21 10^{-3}
^{178}Hf	3.03	1.20	196	0.198	14.8	2.63 10^{-3}

TABLE 1. Level-density parameters

Nucleus	a , MeV ⁻¹		Nucleus	a , MeV ⁻¹	
	Present work	Other studies		Present work	Other studies
^{159}Tb	—	$7.7 [15]$	^{162}Er	6.1 ± 2.5	$8 [16]$
^{164}Ho	4.2 ± 1.5	$3.1 [15]$	^{178}Hf	17.7 ± 7.3	—

Average	1.41 ± 0.3		0.23 ± 0.04		$3.1 \cdot 10^{-1} \pm 6 \cdot 10^{-4}$
---------	----------------	--	-----------------	--	---

TABLE 2. Parameters of fitted curves $\sigma_\gamma^{(2)}$

Nucleus	E , MeV	σ , mb	Γ , MeV	E , MeV	σ , mb	Γ , MeV	$\sigma \Gamma / \sigma \Gamma_1$	τ	E , MeV	E , MeV
$^{159}\text{ Tb}$	12.29	192	1.91 ± 0.09	13.78	205	3.42 ± 0.13	1.58 ± 0.23	197.3	97	10.4
	12.41	213	1.31 ± 0.03	13.93	282	3.01 ± 0.07	—	216.8	98	10.4
$^{164}\text{ Ho}$	12.31	201	2.74 ± 0.11	16.23	306	3.07 ± 0.17	1.11 ± 0.27	176.0	97	10.4
	12.47	225	1.26 ± 0.06	16.40	293	3.02 ± 0.09	—	200.8	98	10.4
$^{162}\text{ Er}$	12.32	191	2.71 ± 0.14	15.99	344	3.07 ± 0.16	0.38 ± 0.35	193.5	94	10.7
	12.50	214	1.43 ± 0.08	16.21	351	3.09 ± 0.10	—	191.7	95	10.7
$^{178}\text{ Hf}$	12.08	166	2.75 ± 1.0	15.03	281	4.07 ± 0.27	4.00 ± 1.70	172.1	89	10.8
	12.88	216	3.02 ± 0.11	15.48	237	3.87 ± 0.10	—	173.7	90	10.8

Note. The lower values of the parameters in each column were found with the requirement $\sigma_2 \Gamma_1 : \sigma_1 \Gamma_1 = 2:1$.

(over)

- ¹² A.N. Tikhonov, Dokl. Akad. Nauk SSSR 151, 501 (1963),
Eng. transl. in Sov. Mathematics-Doklady.
- ¹⁵ B. L. Berman et al., Phys. Rev. 185, 1576 (1969).
- ¹⁶ R. Bergere et al., Nucl. Phys. A133, 417 (1969).
- ¹⁸ E. G. Fuller et al., Nucl. Phys. 30, 613 (1962).
- ¹⁹ H. Arenhovel et al., Phys. Rev. 157, 1109 (1967).
- ²⁰ R. Bergere et al., Nucl. Phys. A121, 463 (1968).
- ²¹ O.V. Bogdankevich et al., Zh. Eksp. Teor. Fiz. 42,
1502 (1962); Sov. Phys. JETP 15, 1044 (1962).
- ²² B.S. Dzhelepov in *Struktura slozhnykh yader*
(Structure of Complex Nuclei), Atomizdat, 1966, p. 189.

ELEM. SYM.	A	Z
Tb	159	65

METHOD

REF. NO.	76 Su 2	egf
----------	---------	-----

REACTION	RESULT	EXCITATION ENERGY	SOURCE		DETECTOR		ANGLE
			TYPE	RANGE	TYPE	RANGE	
E,p	ABX	11- 18	D	15- 18	MAG-D		125

Proton yields obtained by summing protons with energies above levels given in tables.

TABLE I
Parameters of the present experiment

Target	Atomic number	Purity (%)	Thickness (mg/cm ²)	Lowest proton energy (MeV)	Bin size (keV)	Range of measurement (MeV)
¹⁵⁹ Tb	65	99.9 (natural)	14.87	4.70	100	15.0 -17.5
¹⁶⁵ Ho	67	99.9 (natural)	11.64	4.70	100	15.5 -17.5
¹⁶⁹ Tm	69	99 (natural)	13.40	4.70	100	15.0 -18.0
¹⁷⁵ Lu	71	99.87 (enriched)	5.24	5.34	150	15.05-20.0
¹⁸¹ Ta	73	99.9 (natural)	6.73	6.16	200	16.0 -23.0

TABLE 3
Displacement energies obtained from the present data and the estimates with eqs. (20) and (21)

Target	Resonance	E^* (MeV)	E_d (exp) (MeV)	E_d^* (MeV)	$E_d(\delta = 0.3)^b$ (MeV)
¹⁵⁹ Tb	1st	15.75 ± 0.15	15.58	16.06	15.93
	2nd	16.50 ± 0.15	15.46		
¹⁶⁵ Ho	1st	16.15 ± 0.14	15.64	16.38	16.25
	2nd	16.34 ± 0.14	16.22	16.76	16.63
¹⁶⁹ Tm	1st	15.76 ± 0.13	16.20		
	2nd	16.34 ± 0.14	16.22	16.76	16.63
¹⁷⁵ Lu	1st	16.44 ± 0.13	16.75		
	2nd	17.45 ± 0.15	16.35	17.07	16.93
¹⁸¹ Ta	1st	17.31 ± 0.15	16.40	17.38	17.24

^a) Estimated with eq. (20).

^b) Estimated with eq. (21).

TABLE 4
Deformation parameters of IAS δ_{IAS} derived from the (e, e'p) result

Target	Resonance	IAS	Parent state	$\delta_{IAS} - \delta_p^*$	δ_p (assumed)	δ_{IAS}^*
¹⁵⁹ Tb	1st	$\frac{1}{2}^- [521]$	ground	-0.008	0.31	0.30
	2nd	$\frac{1}{2}^- [512]$	875 keV	-0.016	0.29	
¹⁶⁵ Ho	1st	$\frac{1}{2}^+ [633]$	ground	-0.023	0.30	0.28
	2nd	$\frac{1}{2}^+ [510]$	565 keV	-0.019		0.27
¹⁶⁹ Tm	1st	$\frac{1}{2}^- [521]$	ground	-0.018	0.29	0.27
	2nd	$\frac{1}{2}^- [510]$	565 keV	-0.019		0.27
¹⁷⁵ Lu	1st	$\frac{1}{2}^- [514]$	ground	-0.010	0.28	0.27
	2nd	$\frac{1}{2}^- [503]$	1420 keV	-0.029		0.25
¹⁸¹ Ta	1st	$\frac{1}{2}^- [503]$	670 keV	-0.046	0.26	0.21

The assumed deformation parameters for the parent states δ_p are also shown.

^a) The errors are about ± 0.01 .

ELEM. SYM.	A	Z
Tb	159	65

METHOD

REF. NO.	
77 Ba 7	egf

REACTION	RESULT	EXCITATION ENERGY	SOURCE		DETECTOR		ANGLE
			TYPE	RANGE	TYPE	RANGE	
G,G	ABX	8- 12	D	8- 12	SCD-D		DST

Abstract: Differential cross sections for elastic and inelastic Raman scattering from the deformed heavy nuclei ^{154}Tb , ^{165}Ho and ^{227}Np were measured at five energies between 8.5 and 11.4 MeV. Angular distributions at four angles between 90° and 140° for both elastic and inelastic scattering at 9.0 and 11.4 MeV were also measured. The monoenergetic photons were obtained from thermal neutron capture in Ni and Cr. All the angular distributions and the elastic and Raman scattering at the higher energies are in good overall agreement with theoretical predictions. The theory is based on a modified simple rotator model of the giant dipole resonance in which the effect of Delbrück scattering was included. A trend of both the elastic and Raman scattering at lower energies to be stronger than expected are suggested by the data. However, the ratio between the Raman and elastic scattering seem to be in good agreement with theory throughout the whole energy range. This shows that there is no need to introduce a direct nonresonant component to the imaginary part of the elastic scattering amplitude to explain the experimental data.

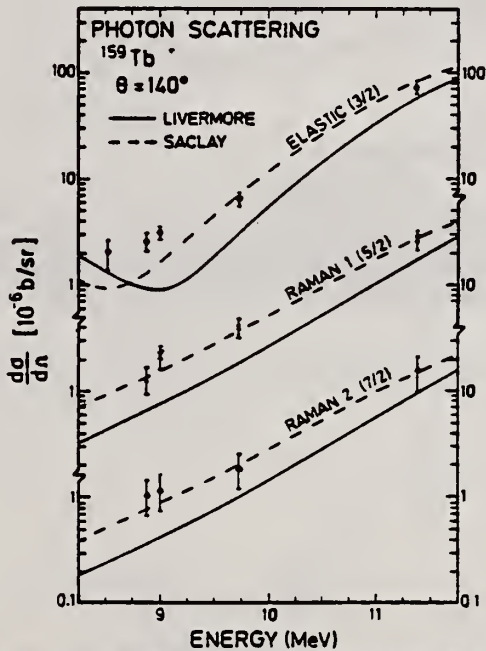


Fig. 5. Elastic and Raman inelastic differential scattering cross sections from ^{159}Tb at 140° . In the solid and dashed lines, the nuclear resonance amplitudes were obtained using parameters extracted from fits made to the Livermore and Saclay measurements respectively. (See text, table 3 and caption to fig. 3.)

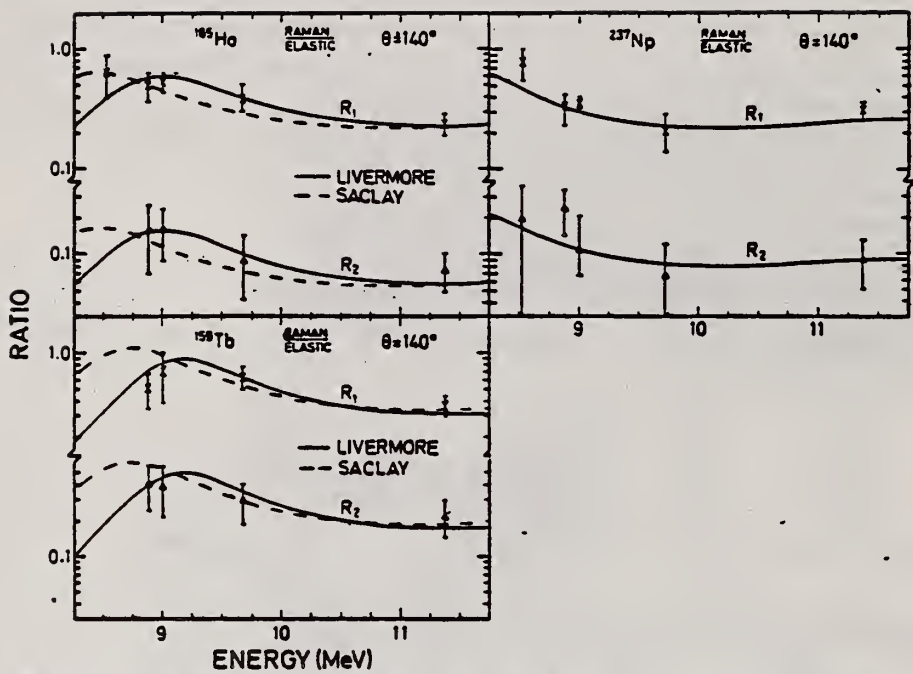


Fig. 6. Ratios of Raman/elastic scattering cross sections at 140° for ^{237}Np , ^{165}Ho and ^{159}Tb targets. Here, R_1 and R_2 refer to the first and second Raman lines. In the solid and dashed lines, the nuclear resonance amplitudes were obtained using parameters extracted from fits made to the Livermore and Saclay measurements respectively. (See text, table 3 and caption to fig. 3.)

ELEM. SYM.	A	Z
Tb	159	65
REF. NO.	77 Mu 3	egf

METHOD

REACTION	RESULT	EXCITATION ENERGY	SOURCE		DETECTOR		ANGLE
			TYPE	RANGE	TYPE	RANGE	
E,A	ABX	12-100	D	100	MAG-D		50

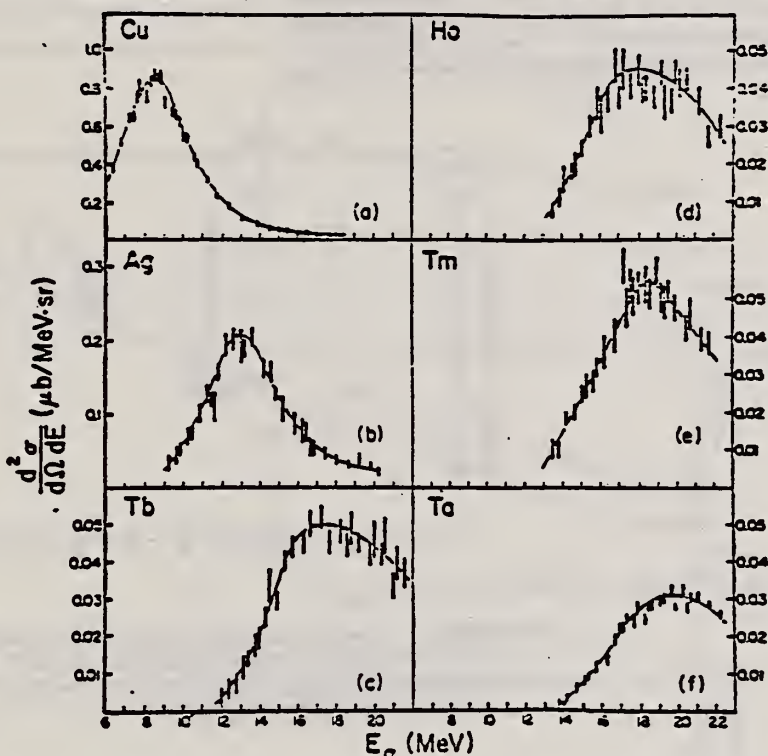
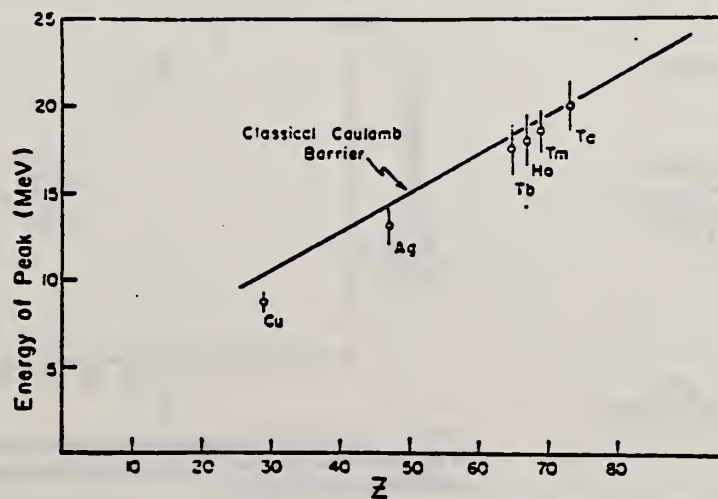


Fig. 1. The α -particle energy spectra at 50° in the lab for the six nuclei studied. Note that as Z increases, the cross section decreases and the energy of the peak increases. Errors are statistical. Curves are to guide the eye.



ELEM. SYM.	A	Z
Tb	159	65

METHOD

REF. NO.

78 Mu 9

hg

REACTION	RESULT	EXCITATION ENERGY	SOURCE	DETECTOR		ANGLE
			TYPE	RANGE	TYPE	
E,A	ABX	5-100	D	100	MAG-D	DST

α particles from the electrodisintegration of seven nuclei with Z between 29 and 79 have been observed. Energy spectra at 50° in the laboratory for six nuclei and angular distributions for five nuclei are reported. The cross sections exhibit a broad peak whose magnitude decreases with increasing Z; the energy of the peak increases as Z increases. Angular distributions at the highest energies measured become increasingly forward peaked suggesting a direct-reaction process.

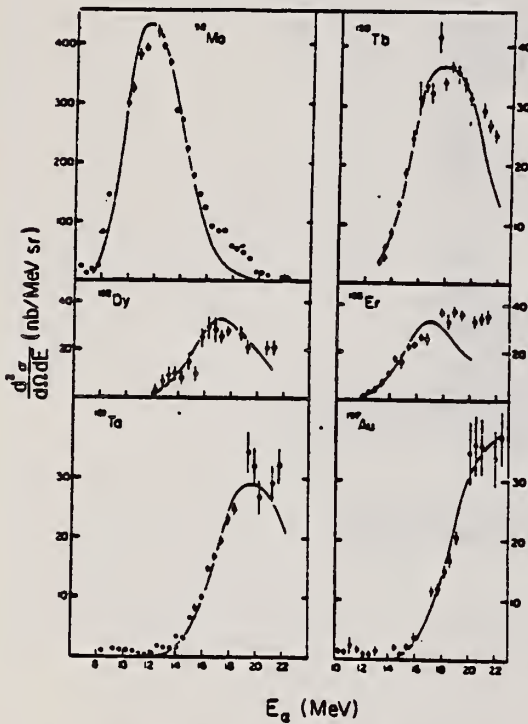


FIG. 2. The α -particle energy spectra at 50° in the laboratory for the four new nuclei studied as well as for two nuclei in which additional data have been obtained. The solid curves are the evaporation model fits described in text.

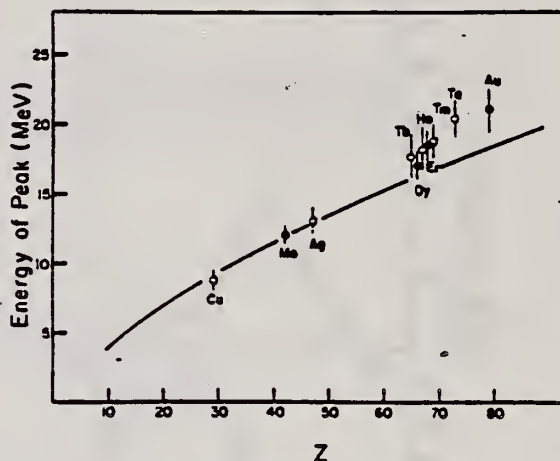


FIG. 3. Energy of the cross section peak as a function of Z. The solid line is the energy of the classical Coulomb barrier. The closed circles are the current work; the open circles are from Ref. 1.

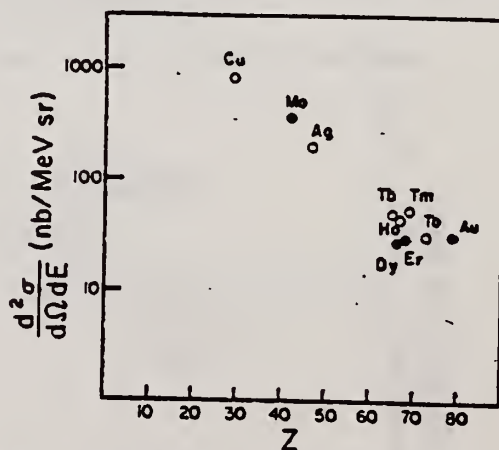


FIG. 4. Magnitude of cross section peak as a function of Z. The closed circles are the current work; the open circles are from Ref. 1.

over

¹J.J. Murphy, II, H.J. Gehrhardt, and D.M. Skopik, Nucl. Phys. A277, 69 (1977).

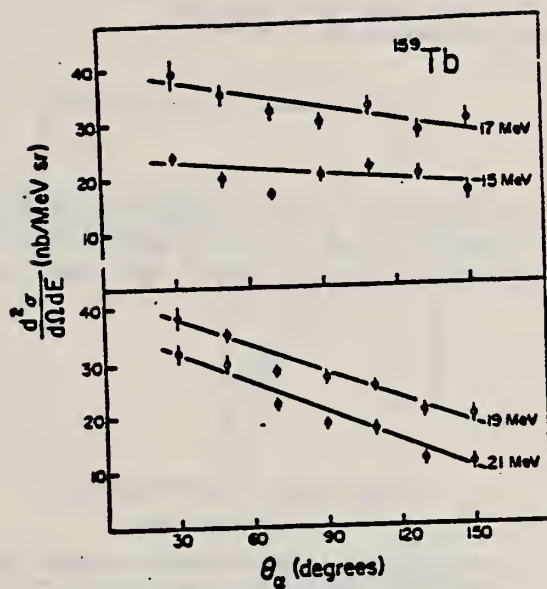


FIG. 6. Angular distributions for terbium. The comments made for Fig. 5 apply here.

ELEM. SYM.	A	Z
Tb	159	65

METHOD

REF. NO.	hg
81 Ja 1	

REACTION	RESULT	EXCITATION ENERGY	SOURCE		DETECTOR		ANGLE
			TYPE	RANGE	TYPE	RANGE	
G.NA24	ABY	THR-800	C	400-800	ACT-I		4PI

Abstract—The cross section for photoproduction of ^{24}Na from ^{159}Tb has been measured in the energy range 400–800 MeV. The present experimental cross section together with earlier measured ones are compared to calculations where ^{24}Na is produced in a binary fission process.

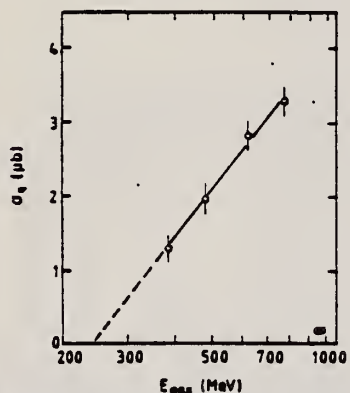


Fig. 1. Measured yields in cross section per equivalent quantum for production of ^{24}Na from ^{159}Tb as a function of maximum bremsstrahlung energy.

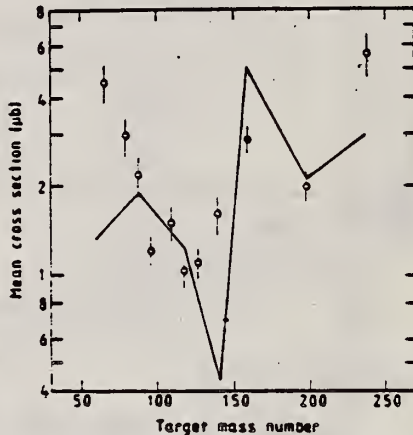


Fig. 2. Experimental mean cross sections as a function of target mass number. Open and filled circles are old and new data respectively. The curve is calculated as described in text.

Dy

DYSPROSIUM

Z=66

Lecoq de Boisbaudran separated what was called holmia into two earths; he called these holmia and dysprosia. The name dysprosium comes from the Greek *dyprositos* meaning "hard to get at".

Dy

METHOD

Betatron; fast neutron yield, angular distribution; Si threshold detector; ion chamber

REF. NO.

61 Ba 2

NJB

REACTION	RESULT	EXCITATION ENERGY	SOURCE		DETECTOR		ANGLE
			TYPE	RANGE	TYPE	RANGE	
G,XN	ABY	THR-22	C	22	THR-I	5+-	DST

In Table 4:

 $\bar{\sigma}$ = average cross section of detector weighted with neutron spectrum δ = neutrons/100 roentgen/mole

$$\bar{\sigma}(\theta) = \bar{\sigma}_0 \sum_{n=1}^{\infty} [1 + A_n P_n (\cos \theta)]$$

TABLE IV

Element	II $\bar{\sigma}_0$	III $\bar{\sigma}_0$	IV $\bar{\sigma}_0$	V $(\bar{\sigma}\Phi) \times 10^{48}$	VI $\Phi_{total} (22 MeV) \times 10^2$	VII $\Phi_{total} / \Phi_{max}$
Hydrogen	245 (1±0.06)	0.01±0.08	-0.00±0.10	1.43	3.21	0.12
Lithium	164 (1±0.03)	0.04±0.04	-0.05±0.05	4.05	0.17	0.10
Magnesium	308 (1±0.02)	0.07±0.03	-0.09±0.04	7.61	0.25	0.12
Iron	200 (1±0.03)	0.05±0.04	-0.17±0.05	4.94	0.18	0.11
Sodium	390 (1±0.02)	0.08±0.03	-0.22±0.04	9.01	0.26	0.15
Chlorine	145 (1±0.03)	0.07±0.07	-0.23±0.09	3.58	0.12	0.12
Argon	347 (1±0.02)	0.05±0.03	-0.29±0.04	8.57	0.30	0.12
Silicon	482 (1±0.03)	0.11±0.04	-0.24±0.05	11.91	0.33	0.15
Turboilium	638 (1±0.03)	0.13±0.06	-0.14±0.08	15.76		
Sulfur	409 (1±0.05)	0.10±0.06	-0.17±0.08	16.10		
Phosphorus	290 (1±0.10)	0.08±0.12	-0.12±0.15	7.16		
Silver	590 (1±0.04)	0.10±0.06	-0.22±0.08	14.57	0.87	0.07
Antimony	905 (1±0.02)	0.02±0.02	-0.26±0.03	22.35		
Chromium	1133 (1±0.03)	0.04±0.04	-0.29±0.05	27.99	1.42	0.08
Vanadium	1048 (1±0.04)	0.10±0.06	-0.38±0.08	25.89		
Gold	1505 (1±0.02)	0.02±0.03	-0.42±0.04	39.40	1.04	0.15
Copper	1316 (1±0.05)	0.05±0.06	-0.39±0.08	32.50		
Boron	1652 (1±0.03)	0.04±0.10	-0.34±0.13	40.80		
Iron	1558 (1±0.02)	0.04±0.03	-0.22±0.04	38.48	2.50	0.06
Aluminum	1365 (1±0.02)	-0.07±0.03	-0.24±0.04	33.71		
Mercury	1345 (1±0.02)	0.04±0.03	-0.31±0.04	33.22		
Lead	2274 (1±0.01)	0.02±0.02	-0.42±0.03	56.17	2.72	0.08
Platinum	2162 (1±0.02)	0.05±0.03	-0.45±0.04	53.40	3.38	0.06
Potassium	3031 (1±0.04)	0.06±0.05	-0.32±0.07	74.87		
Uranium	4630 (1±0.02)	0.05±0.03	-0.17±0.04	114.36		

 $\Phi_{total} = 2.47 \times 10^{-2}$ as millibarn-neutrons. Errors are standard errors due to counting statistics only.200-132-473
200-132-474U.S. DEPARTMENT OF COMMERCE
NATIONAL BUREAU OF STANDARDS

R.F. Barrett, J.R. Birkelund, B.J. Thomas, K.S. Lam, and H.H. Thies
 Nucl. Phys. A210, 355 (1973)

ELEM. SYM.	A	Z
Dy		66

METHOD

REF. NO.	73 Ba 20	egf
----------	----------	-----

REACTION	RESULT	EXCITATION ENERGY	SOURCE	DETECTOR		ANGLE
			TYPE	RANGE	TYPE	
G,N	NOX	THR- 27	C	10- 27	BF3-T	APT

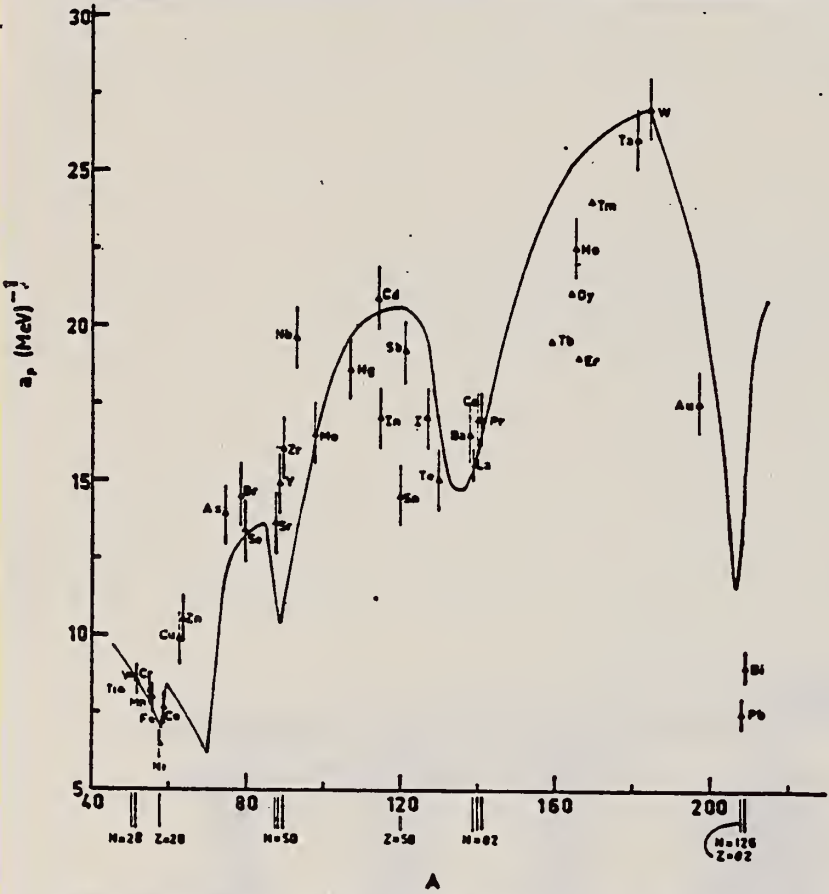


Fig. 12. Experimental values of the level density parameter a_p (Fermi gas formula plus pairing correction) versus atomic number A . The continuous curve is a least-squares fit to the data of a theoretical calculation from Newton¹³.

- 1 H. Baba and S. Baba, Japan Atomic Energy Research Institute report JAERI-1183 (1969).
- 2 H. Baba, Nucl. Phys. A159, 625 (1970)..
- 15 T.D. Newton, Can. J. Phys. 34, 804 (1956).

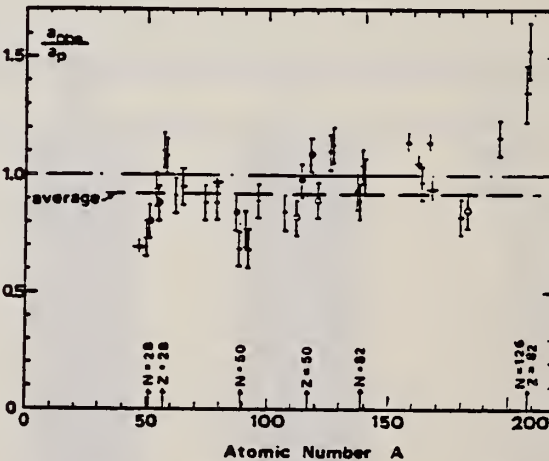


Fig. 15. Ratio a_{ooo}/a_p versus atomic number A . Here a_{ooo} is the level density parameter taken from the neutron resonance work of refs. 1-2), and a_p is the level density parameter derived from the present (γ, n) work. Filled circles represent points where nuclei in the neutron resonance and in the (γ, n) experiment were the same. Open circles represent points where the respective nuclei were approximately matched. Triangles represent points which are based on measurement of neutron mean energies at two bremsstrahlung energies only.

(over)

TABLE 3 (continued)

Target	<i>N</i> (residual nucleus) ^{a)}	Goodness of fit ^{b)}		$\bar{E}_n(24)$ (MeV) ^{c)}	<i>T</i> (MeV) ^{d)}	a_p (MeV ⁻¹) ^{e)}	a_{obs} (MeV ⁻¹) ^{f)}	a_{obs}/a_p	
		no p.c.	with p.c.						
Ba	75	1%	F	1.16	16.5- ¹³⁶ Ba	15.39- ¹³⁶ Ba	0.93		
	77	2%							
	78	7%							
	79	8%							
	80	11%							
	81	71%							
La	80	100%	F	F	1.25	0.72	15.5- ¹³⁸ La	13.76- ¹³⁹ La	0.89
Ce	81	89%	F	G	1.24	0.70	17.0- ¹³⁹ Ce	17.8- ¹⁴¹ Ce	1.04
	83	11%							
Pr	81	100%	G	G	1.17	0.65	17.0- ¹⁴⁰ Pr	17.05- ¹⁴² Pr	1.00
Tb ^{g)}	93	100%			1.15		19.3- ¹⁵⁸ Tb	21.85- ¹⁶⁰ Tb	1.14
Dy ^{g)}	93	2%			1.06		20.9- ^{161.5} Dy	21.9- ¹⁶² Dy	1.05
	94	19%							
	95	25%							
	96	25%							
	97	28%							
Ho	97	100%	P	G	1.06	0.56	21.4- ¹⁶⁴ Ho	20.66- ¹⁶⁴ Ho	0.97
Er ^{g)}	95	2%			1.11		19.2- ¹⁶⁶ Er	21.9- ¹⁶⁶ Er	1.14
	97	33%							
	98	23%							
	99	27%							
	101	15%							
Tm ^{g)}	99	100%			1.03		24.0- ¹⁶⁸ Tm	22.58- ¹⁷⁰ Tm	0.94
Ta	107	100%		G	1.00	0.49	26.0- ¹⁸⁰ Ta	21.2- ¹⁸¹ Ta	0.82
W	107	26%	G	F	0.98	0.50	27.0- ¹⁸³ W	23.0- ¹⁸³ W	0.85
	108	14%							
	109	31%							
	111	28%							
Au	117	100%		G	1.19		17.5- ¹⁹⁶ Au	20.24- ¹⁹⁸ Au	1.16
Pb	123	24%		V.P.	1.87	1.20	7.5- ²⁰⁶ Pb	10.1- ²⁰⁷ Pb	1.35
(Z = 82)	124	23%							
	125	52%							
Bi	125	100%		F	1.65	1.03	9.0- ²⁰⁸ Bi	13.8- ²¹⁰ Bi	1.53

^{a)} Neutron numbers and abundances of respective residual nuclei in (γ , n) experiments.^{b)} These give an assessment of the goodness of fit of a calculated \bar{E}_n versus E_0 curve to the observed data, using the Fermi gas level density formula both without and with pairing corrections.^{c)} Bremsstrahlung photoneutron mean energies \bar{E}_n for peak bremsstrahlung energy $E_0 = 24$ MeV.^{d)} Nuclear temperature from fit with constant-temperature formula.^{e)} Level density parameter a_p , derived from the present (γ , n) experiment, using a Fermi gas formula plus pairing correction, and corresponding residual nucleus (the atomic weight shown is the weighted average of atomic weights of the respective isotopes present).^{f)} As column 7, but using data on n-resonance absorption from refs. ^{1,2}.^{g)} Measurements of $\bar{E}_n(E_0)$ for these nuclei were made only for $E_0 = 21, 23$ and 24 MeV.

ELEM. SYM.	A	Z
Dy		66
METHOD	REF. NO.	
	76 Em 2	egf

REACTION	RESULT	EXCITATION ENERGY	SOURCE		DETECTOR		ANGLE
			TYPE	RANGE	TYPE	RANGE	
G, F	ABY	THR-999	C	999	TRK-I		4PI

999 = 1 GEV

TABLE I

Measured values of σ_n at $E = 1000$ MeV and deduced values of σ_t assumed constant from E_0 to 1000 MeV

Element	Z^2/A	σ_n (mb)	E_0 (MeV)	σ_t (mb)
Bi	32.96	12.3 ± 0.6	200	7.6 ± 0.6
Pb	32.45	5.4 ± 0.4	220	3.6 ± 0.3
Tl	32.10	4.1 ± 0.3	230	2.8 ± 0.3
Au	31.68	2.0 ± 0.15	240	1.4 ± 0.2
Pt	31.18	1.1 ± 0.08	255	$(8 \pm 0.7) \times 10^{-1}$
Re	30.21	$(3.7 \pm 0.3) \times 10^{-1}$	280	$(2.9 \pm 0.3) \times 10^{-1}$
W	29.78	$(3.5 \pm 0.3) \times 10^{-1}$	290	$(2.8 \pm 0.3) \times 10^{-1}$
Ta	29.45	$(3.3 \pm 0.3) \times 10^{-1}$	300	$(2.7 \pm 0.3) \times 10^{-1}$
Hf	29.04	$(1.7 \pm 0.2) \times 10^{-1}$	310	$(1.4 \pm 0.2) \times 10^{-1}$
Yb	28.31	$(1.3 \pm 0.1) \times 10^{-1}$	330	$(1.2 \pm 0.1) \times 10^{-1}$
Tm	28.18	$(7.5 \pm 0.8) \times 10^{-2}$	335	$(6.8 \pm 0.8) \times 10^{-2}$
Ho	27.21	$(3.6 \pm 0.4) \times 10^{-2}$	355	$(3.5 \pm 0.4) \times 10^{-2}$
Dy	26.80	$(2.6 \pm 0.3) \times 10^{-2}$	360	$(2.5 \pm 0.3) \times 10^{-2}$
Tb	26.58	$(2.5 \pm 0.3) \times 10^{-2}$	370	$(2.5 \pm 0.3) \times 10^{-2}$
Gd	26.04	$(1.6 \pm 0.2) \times 10^{-2}$	380	$(1.7 \pm 0.2) \times 10^{-2}$
Sm	25.56	$(1.3 \pm 0.2) \times 10^{-2}$	390	$(1.4 \pm 0.2) \times 10^{-2}$
Nd	24.96	$(9.2 \pm 0.9) \times 10^{-3}$	405	$(1 \pm 0.1) \times 10^{-2}$
Ce	24.00	$(8 \pm 0.9) \times 10^{-3}$	420	$(9 \pm 1) \times 10^{-3}$
La	23.39	$(8.4 \pm 0.9) \times 10^{-3}$	430	$(1 \pm 0.1) \times 10^{-3}$
Sb	21.36	$(1.2 \pm 0.2) \times 10^{-2}$	460	$(1.5 \pm 0.3) \times 10^{-2}$
Te	21.19	$(8.8 \pm 1) \times 10^{-3}$	465	$(1.2 \pm 0.2) \times 10^{-2}$
Sn	21.06	$(1.3 \pm 0.2) \times 10^{-2}$	465	$(1.7 \pm 0.3) \times 10^{-2}$
Cd	20.49	$(1.7 \pm 0.3) \times 10^{-2}$	470	$(2.2 \pm 0.4) \times 10^{-2}$
Ag	20.47	$(2 \pm 0.3) \times 10^{-2}$	470	$(2.6 \pm 0.4) \times 10^{-2}$
Zn	13.76	$(2 \pm 0.4) \times 10^{-1}$	515	$(3 \pm 0.6) \times 10^{-1}$
Cu	13.44	$(2.4 \pm 0.5) \times 10^{-1}$	515	$(3.6 \pm 0.8) \times 10^{-1}$
Ni	13.35	$(2.4 \pm 0.5) \times 10^{-1}$	510	$(3.6 \pm 0.8) \times 10^{-1}$
Fe	12.10	$(3 \pm 0.6) \times 10^{-1}$	510	$(4.4 \pm 0.9) \times 10^{-1}$

- ⁴ A.V. Mitrofanova et al.
 Sov. J. Nucl. Phys. 6,
 512 (1968).
⁷ T. Methasiri et al., Nucl.
 Phys. A167, 97 (1971).
¹² J.R. Nix et al., Nucl. Phys.
81, 61 (1966).
²⁰ N.A. Perifilov et al., JETP
 (Sov. Phys.) 14, 623 (1962);
 Proc. Symp. on the physics &
 chemistry of fission, Salzburg
 1965, vol. 2 (IAEA) Vienna,
 1965, p. 283.

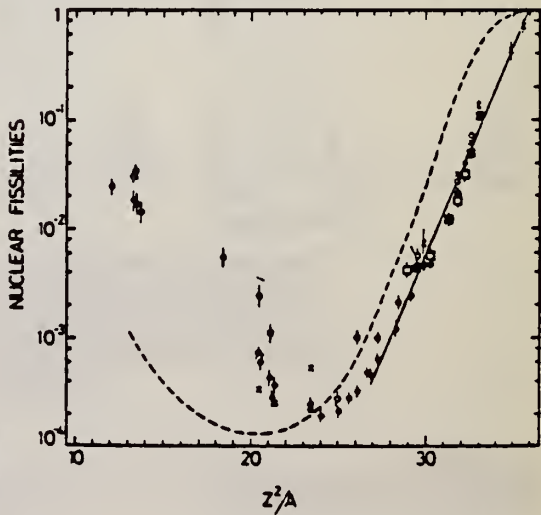


Fig. 2. Nuclear fissilities as a function of Z^2/A . Experimental points: solid circles represent our data; squares, the data from ref. ⁴; open circles, the data from ref. ⁷; and crosses, the data from (p, n) experiments²⁰). The straight line is the best fit calculated from our data for $Z^2/A > 26$. The dashed curve is the curve VI calculated by Nix and Sassi¹².

Dy
A=162

Dy
A=162

Dy
A=162

ELEM. SYM.	A	Z
Dy	162	66

METHOD

REF. NO.
78 Mu 9

REACTION	RESULT	EXCITATION ENERGY	SOURCE		DETECTOR		ANGLE
			TYPE	RANGE	TYPE	RANGE	
E,A	ABX	8-100	D	100	MAG-D		50

α particles from the electrodisintegration of seven nuclei with Z between 29 and 79 have been observed. Energy spectra at 50° in the laboratory for six nuclei and angular distributions for five nuclei are reported. The cross sections exhibit a broad peak whose magnitude decreases with increasing Z; the energy of the peak increases as Z increases. Angular distributions at the highest energies measured become increasingly forward-peaked suggesting a direct-reaction process.

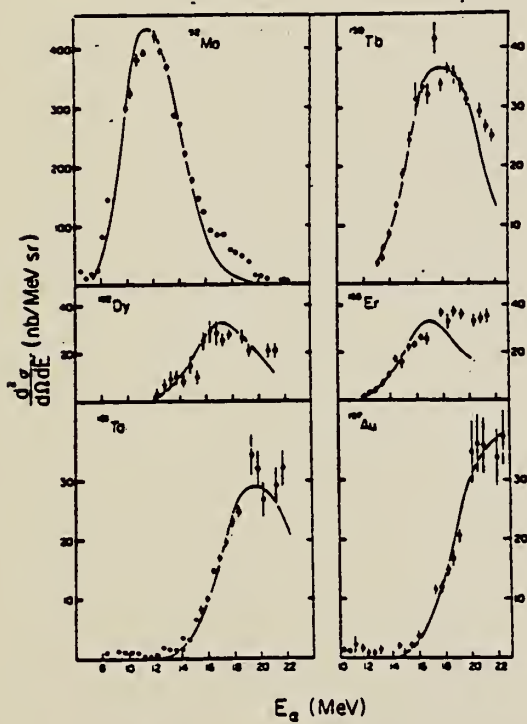


FIG. 2. The α -particle energy spectra at 50° in the laboratory for the four new nuclei studied as well as for two nuclei in which additional data have been obtained. The solid curves are the evaporation model fits described in text.

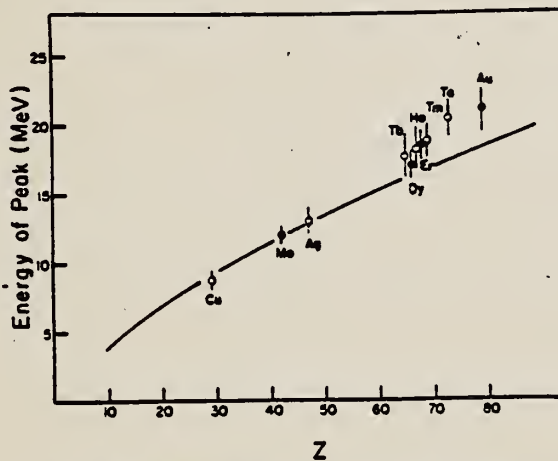


FIG. 3. Energy of the cross section peak as a function of Z. The solid line is the energy of the classical Coulomb barrier. The closed circles are the current work; the open circles are from Ref. 1.

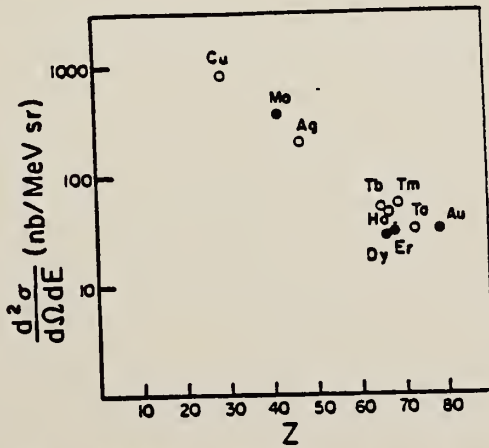


FIG. 4. Magnitude of cross section peak as a function of Z. The closed circles are the current work; the open circles are from Ref. 1.

¹J.J. Murphy, II, H.J. Gehrhardt, and D.M. Skopik, Nucl. Phys. A277, 69 (1977)

DY
A=163

DY
A=163

DY
A=163

CHEM. S. M.	Dy	163	66
REF. NO.	60 Ge 3	NVB	

METHOD

Betatron; neutron threshold; ion chamber

REACTION	RESULT	EXCITATION ENERGY	SOURCE		DETECTOR		ANGLE
			TYPE	RANGE	TYPE	RANGE	
G, N	N ⁰ X	THR	C	THR	BF ₃ -I		4 PI

THRESHOLD

TABLE I. Summary and comparison of neutron separation energies inferred from present threshold measurements with values predicted from mass data and reaction energetics. All energies are expressed in the center-of-mass system in Mev.

Reaction	No. runs	Present results	Other results	Method	Reference
Dy ¹⁶² (γ,n)Dy ¹⁶²	1	6.32 ± 0.11	6.27 ± 0.06	mass data	9

* W. H. Johnson, Jr., and V. B. Bhanot. Phys. Rev. 107, 6 (1957).

Ho
A=165

HOLMIUM
Z=67

Holmium and its compounds are used for research purposes with their limited applications based primarily upon their distinctive electronic and magnetic properties. The element is of great interest to nuclear spectroscopists because there is only one naturally occurring isotope and it has one of the highest nuclear moments of the rare earth series.

Ho
A=165

ELEM. SYM.	A	Z
Hg	165	67

Betatron					REF. NO.	
REACTION	RESULT	EXCITATION ENERGY	SOURCE	DETECTOR	ANGLE	
			TYPE	RANGE	TYPE	RANGE
G, N	RLY	THR	C	THR	BF ₃ -I	4PI

See 58 Ka 1 for cross sections

THRESHOLD

TABLE I
 MEASURED PHOTONEUTRON THRESHOLDS

Reaction	Measured Q value, Mev.	Other Q values, Mev.	Method	Reference
Hg ¹⁶⁴ (γ, n)Hg ¹⁶⁴	8.10 ± 0.05			

REF. NO.

58 Fu 1

NVB

Betatron; ion chamber

REACTION	RESULT	EXCITATION ENERGY	SOURCE		DETECTOR		ANGLE
			TYPE	RANGE	TYPE	RANGE	
G,XN	ABX	7-40	C	7-40	BF ₃ -I		4PI

CF DANOS THEORY

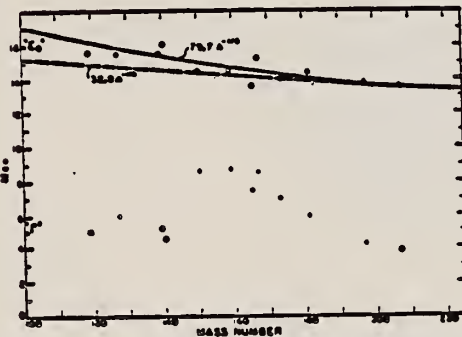


FIG. 6. Mean energy and width of giant resonances. "E_e" and "Γ" are the mean energy for photon absorption and the full width at half maximum of the giant resonance obtained from dashed histograms as in Fig. 5. No attempt was made to fit data with resonance curves to obtain these parameters.

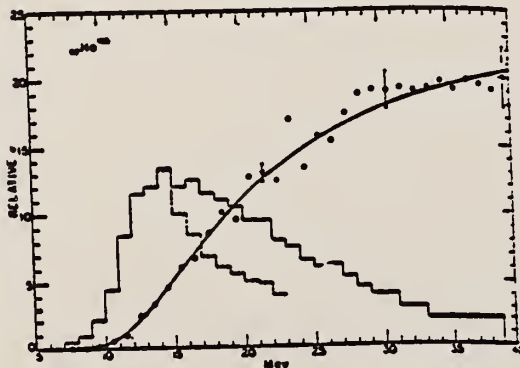


FIG. 5. Relative photoneutron production cross sections for tin, iodine, samarium, holmium, erbium, and lead. The points and smooth curves represent the integral neutron-production cross section defined by $\int_0^\infty \sigma_{Tn}(E) dE$, where $\sigma_{Tn}(E) = \sigma(\gamma,n) + 2\sigma(\gamma,2n) + \sigma(\gamma,3n) + \dots$. The scales are normalized to give approximately the same total neutron yield at 40 Mev. The errors indicated were obtained by propagating the statistical uncertainties, (\sqrt{n}) , in the original activation curve data through the integral cross section matrix. Solid histograms represent first differences of integral cross section curves. Dashed histograms show result of correcting for neutron multiplicity above the $(\gamma,2n)$ threshold.

TABLE I. Target properties and results.

Element	Form used	Weight grams	$\sigma^*(\gamma,n)^*$ barns	$SedE^*$ NZ/A Mev-b	\bar{E}^{**} Mev
Sn	Sn	4.81	0.30	0.064	5.0
I	I	8.55	0.36	0.085	6.0
La	La	10.43	0.34	0.063	5.2
Ce	Ce	4.99	0.45	0.080	4.5
Sm	Sm ₂ O ₃	2.90	0.26	0.073	8.6
Tb	Tb ₂ O ₃	3.04	0.39	0.087	8.7
Ho	Ho ₂ O ₃	1.87	0.41	0.079	7.5
Er	Er ₂ O ₃	5.41	0.50	0.100	8.5
Yb	Yb ₂ O ₃	5.57	0.50	0.090	7.0
Ta	Ta	8.41	0.49	0.077	6.0
Au	Au	3.16	0.68	0.085	4.2
Pb	Pb	8.05	0.75	0.081	3.8

* $\sigma^*(\gamma,n)$ is the maximum value and "Γ" the full width at half maximum of the giant resonance.

** Integrated neutron production cross sections corrected for multiple neutrons above $(\gamma,2n)$ threshold.

TABLE II. Energies of resonances in deformed nuclei.*

Nucleus	E_m Mev	σ barns	Method	E_1 Mev	E_2 Mev	$E_{1/2}^{**}$ Mev	$E_{1/2}^{**}$ Mev
¹⁰⁴ Tb ¹⁶⁰	14.7	6.95	CE	11.9	16.2	10.8	19.3
¹²⁷ I ¹³⁶	14.5	7.85	CE	11.5	16.0	11.0	18.5
¹⁴⁵ Sm ¹⁴⁴	14.5	21 ^b	SC	8.5	17.5	11.5	20.0
¹⁴⁵ Sm ¹⁴⁴	14.5	7.85	CE	11.6	15.9	11.5	20.0
¹⁵¹ Ta ¹⁴⁸	14.1	12.65	SC	10.5	15.9	11.3	17.3
¹⁵¹ Ta ¹⁴⁸	14.1	6.85	CE	11.9	15.2	11.3	17.3
¹⁹⁷ Pt ¹⁹⁶	13.6	3.75 ^c	SC	12.5	14.1	11.8	16.2

* CE—Coulomb excitation; SC—spectroscopic; $E_{1/2}^{**}$ —energies at which giant resonance drops to half its maximum value.

^a Adler, Bohr, Huaas, Motelson, and Winther, Revs. Modern Phys. 28, 432 (1956).

^b M. L. Pool and D. N. Kundu, Chart of Atomic Nuclei (Longs College Book Company, Columbus, 1955).

L. Katz, G.B. Chidley

Nuclear Reactions at Low and Medium Energies (Academy of Science,
USSR: 1958) 371

ELEM. SYM. A

Ho

165

67

METHOD Betatron; neutron cross section; BF_3 counters; ion chamber monitor

REF. NO.

58 Ka 1

NVB

REACTION	RESULT	EXCITATION ENERGY	SOURCE		DETECTOR		ANGLE
			TYPE	RANGE	TYPE	RANGE	
G, XN	ABX	9-22	C	9-22	$\text{BF}_3\text{-I}$		4PI

Таблица 2

Пороги испускания фотонейтринов

Изотоп	$B_{\gamma\gamma}$, Мэв	$B_{\gamma\gamma}$, Мэв	Изотоп	$B_{\gamma\gamma}$, Мэв	$B_{\gamma\gamma}$, Мэв
Vsl	11.16	20.5	Lu ¹⁸⁰	8.81	16.1
Mn ⁵³	10.14	19.2	Pr ¹⁴¹	9.46	17.6
Co ⁵⁹	10.44	18.6	Tb ¹⁵⁹	8.16	14.8
As ⁷⁵	10.24	18.1	Ho ¹⁶³	8.10	14.6
Y ⁸⁸	11.82	20.7	Tm ¹⁶⁹	8.00	14.7
Nb ⁹³	8.86	17.1	Lu ¹⁷³	7.77	14.2
Rb ¹⁰³	9.46	16.8	Ta ¹⁸¹	7.66	13.8
J ¹²⁷	9.14	16.2	Au ¹⁹⁷	7.96	13.3
Cs ¹³³	9.11	16.5	Bi ²⁰⁹	7.43	14.5

THRESHOLDS

не приведены, поскольку они превышают 22 Мэв во всех случаях, кроме золота, для которого $B_{\gamma\gamma}=21$ Мэв. Свойства сечений $\sigma_C(E)$ сведены в табл. 3.

Таблица 1

Изотоп	$E_{\gamma\gamma\text{ макс.}}$, Мэв	$\sigma_n(E_\gamma)$, барн	E_γ , Мэв	$\sigma_C(E_\gamma)$, Мэв·барн	$10^6 \text{ нейтрон}/100 \mu\text{-моль}$
Vsl	18.4	0.062	5.2	0.33	1.62
Mn ⁵³	20.2	0.060	7.0	0.39	2.01
Co ⁵⁹	18.3	0.068	6.3	0.44	2.30
As ⁷⁵	16.4	0.090	9.5	0.74	4.25
Y ⁸⁸	17.1	0.172	5.2	0.93	5.33
Nb ⁹³	18.0	0.150	7.5	1.17	6.80
Rb ¹	17.5	0.160	9.4	1.40	8.28
J ¹²⁷	15.2	0.273	6.8	1.76	11.9
Cs ¹³³	16.5	0.238	7.7	1.59	10.7
La ¹³⁹	15.5	0.325	3.8	1.55	11.2
Pr ¹⁴¹	15.0	0.320	4.9	1.93	13.1
Tb ¹⁵⁹	15.6	0.274	9.8	2.49	18.1
Ho ¹⁶³	13.5	0.305	8.9	2.52	18.7
Tm ¹⁶⁹	16.4	0.250	8.4	1.91	14.9
Lu ¹⁷³	16.0	0.225	8.4	1.90	23.0
Ta ¹⁸¹	14.5	0.380	8.5	3.15	22.0
Au ¹⁹⁷	13.8	0.475	4.7	3.04	22.6
Bi ²⁰⁹	13.2	0.455	5.9	2.89	23.2

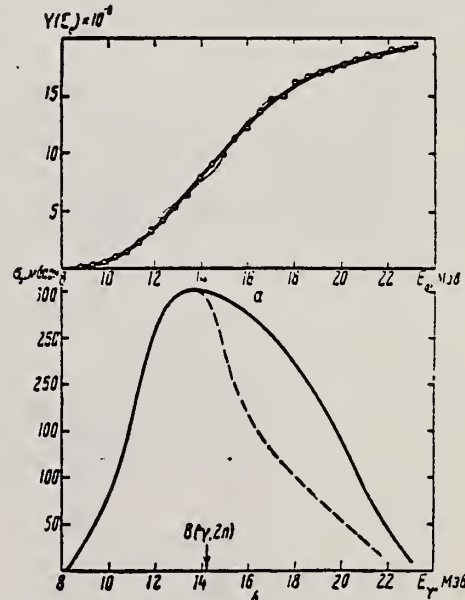


Рис. 13.
а — Выход фотонейтронов для Ho; б — $\sigma_n(E_\gamma)$
и $\sigma_C(E_\gamma)$ для Ho

ELEM. SYM.	A	Z
Hg	165	67

METHOD

Betatron; neutron threshold; ion chamber

REF. NO.

60 Ge 3

NVB

REACTION	RESULT	EXCITATION ENERGY	SOURCE		DETECTOR		ANGLE
			TYPE	RANGE	TYPE	RANGE	
G, N	N ₀ X	THR	C THR		BF ₃ -I		4 PI

THRESHOLD

TABLE I Summary and comparison of neutron separation energies inferred from present threshold measurements with values predicted from mass data and reaction energies. All energies are expressed in the center-of-mass system in Mev.

Reaction	No. runs	Present results	Other results	Method	Reference
Hg ¹⁶² (γ,n)Hg ¹⁶¹	1	8.16 ± 0.08	8.10 ± 0.05	threshold	f

Method 18 MeV electron synchrotron; radioactivity; BF_3 counters; ion chamber

Ref. No.	60 Th 1	EH
----------	---------	----

Reaction	E or ΔE	E_0	Γ	$\int \sigma dE$	$J\pi$	Notes
$\text{Ho}^{165} (\gamma, n)$	8-18	12.1 ± 0.2				$\sigma_{\max} = 420 \text{ mb}$
		16.2 ± 0.2				$\sigma_{\max} = 510 \text{ mb}$

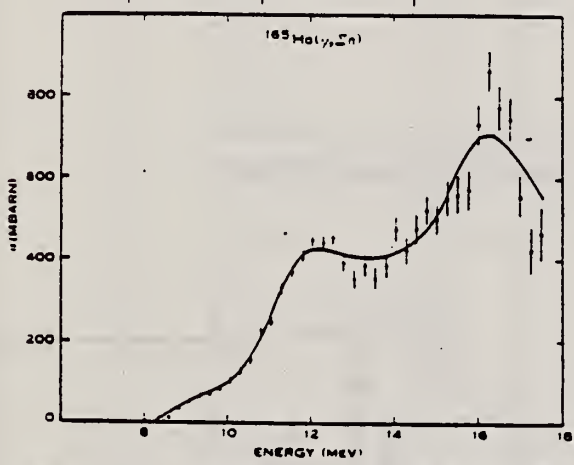


Fig. 7.—Total neutron production cross section for ^{165}Ho .

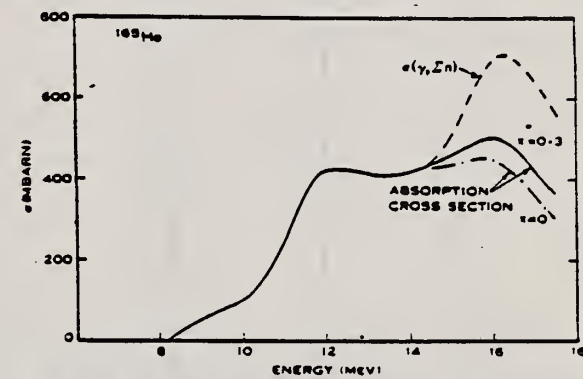


Fig. 9.—Cross section for photon absorption in ^{165}Ho . The correction for neutron multiplicity is applied using statistical theory.

TABLE 2
GIANT RESONANCE PARAMETERS IN DEFORMED NUCLEI

Nucleus	^{158}Tb		^{165}Ho	^{181}Ta		
	Reference	Fuller and Weiss (1958)	Present Paper	Present Paper	Fuller and Weiss (1958)	Spicer et al. (1958)
$\Gamma_{G.R.}$ (MeV)	6.5	6.7 ± 0.5	7	6.2 ± 0.2	6.1	
E_1 (MeV)	12.5	12.4 ± 0.2	12.1	12.45	12.6	
$(\sigma_1)_{\max}$ (mbarn)	260	410	420	308	500	
Γ_1 (MeV)	2.4	3.3	2.8	2.3	2.0	
E_2 (MeV)	16.3	16.0 ± 0.2	16.2	15.45	15.3	
$(\sigma_2)_{\max}$ (mbarn)	310	460	510	348	450	
Γ_2 (MeV)	4.0	4.3	4.7	4.4	4.0	
I_2/I_1	2.0	2.0	2.0	2.16	1.8	
E_2/E_1	1.30	1.29 ± 0.03	1.34 ± 0.03	1.25 ± 0.01	1.21 ± 0.03	

Method

 γ -ray's from thermal α -capture; activation

Ref. No.	61 We 1	JHM
----------	---------	-----

Reaction	E or ΔE^*	E_0	Γ	$\int \sigma dE$	$J\pi$	Notes														
(γ, n)	7.91-10.83					<p>Measurement of 45-kev x-ray from K-capture in Ho¹⁶⁴.</p> <p>Data in Table II (millibarns), Fig. 5.</p> <p>γ thresh. = 7.91 - 8.4 Mev.</p> <table border="1"> <caption>Estimated data points from Figure 5</caption> <thead> <tr> <th>Gamma Ray Energy (MeV)</th> <th>Cross Section (millibarns)</th> </tr> </thead> <tbody> <tr><td>8.0</td><td>100</td></tr> <tr><td>8.4</td><td>100</td></tr> <tr><td>8.8</td><td>120</td></tr> <tr><td>9.2</td><td>150</td></tr> <tr><td>9.6</td><td>200</td></tr> <tr><td>10.0</td><td>300</td></tr> </tbody> </table>	Gamma Ray Energy (MeV)	Cross Section (millibarns)	8.0	100	8.4	100	8.8	120	9.2	150	9.6	200	10.0	300
Gamma Ray Energy (MeV)	Cross Section (millibarns)																			
8.0	100																			
8.4	100																			
8.8	120																			
9.2	150																			
9.6	200																			
10.0	300																			

FIG. 5. Cross section vs energy, Ho¹⁶⁴(γ, n)Ho¹⁶⁵(34 min).

TABLE II. Summary of measured cross sections.

γ -ray source Reaction	Co	Fe	Al	Cu	Cl	Ni	Fe	Cr	Fe	N
Energy (Mev)	7.49	7.64	7.73	7.91	8.36	8.997	9.30	9.72	10.16	10.83
Ta ¹⁸⁰ (γ, n)Ta ¹⁸⁰	0±0.05	0.5±1	4.8±1.6	14±5	32±16	44±15	...	83±33	...	120±48
Au ¹⁹⁷ (γ, n)Au ¹⁹⁸	0±2	34±17	44±11	64±30	50±30
Ho ¹⁶⁴ (γ, n)Ho ¹⁶⁵	0±0.1	29±13	30±13	46±21	36±31	...	260±93
Nb ⁹³ (γ, n)Nb ⁹⁴	0.008±0.005	1.0±0.4	2.4±0.7
Ag ¹⁰⁷ (γ, n)Ag ¹⁰⁸	0±0.1	...	4.4±1.5	22±16	23±7.5

Method	Ref. No.
50 MeV Betatron; BF ₃ , NaI counters	62 Fu 3

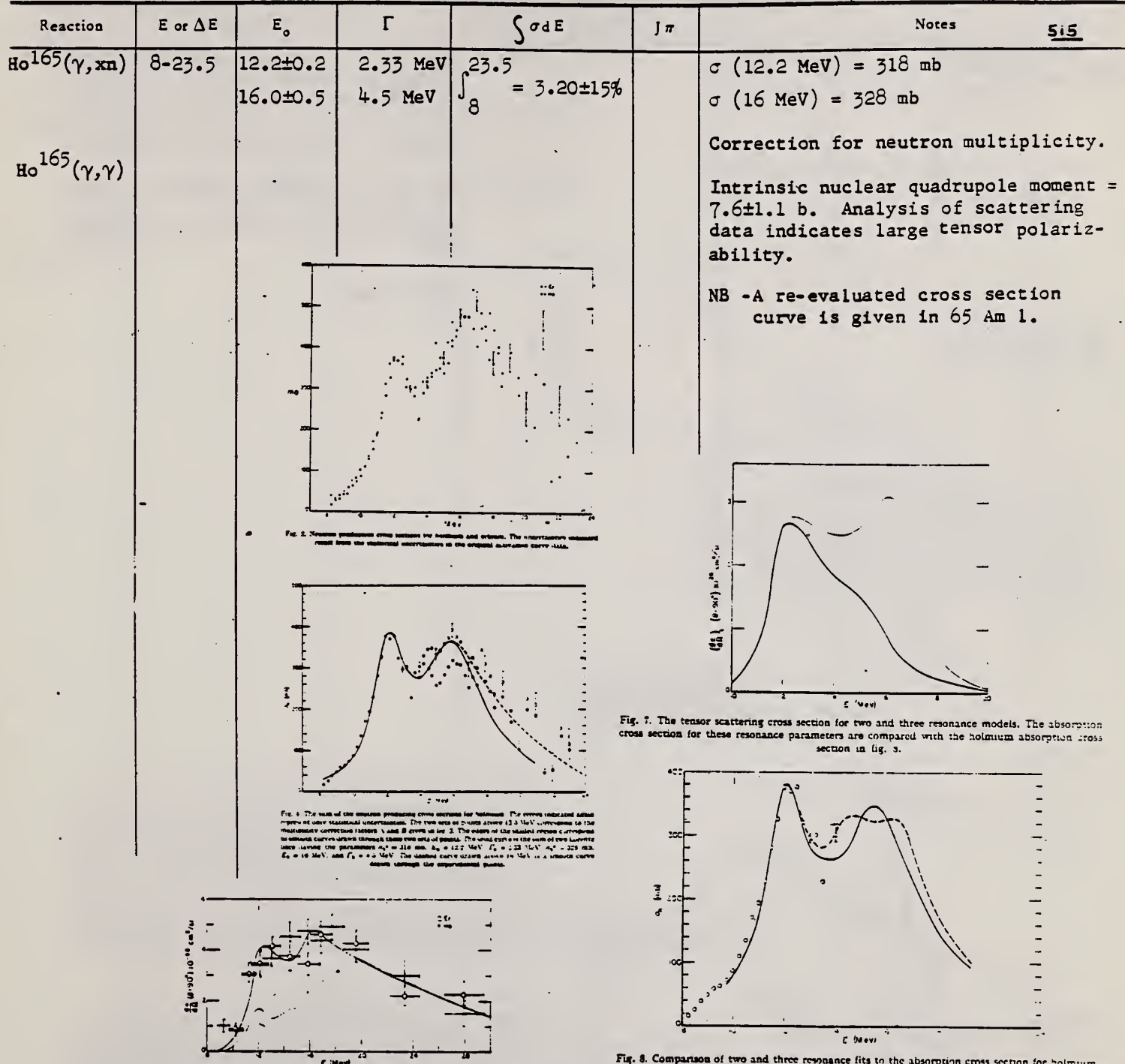


Fig. 6. The differential scattering cross sections for holmium and erbium measured at 90° . The indicated uncertainties are only statistical. The lower smooth curve was calculated using eq. (19) from a curve drawn through the data points of fig. 4. The shaded region corresponds to the limits of the scalar scattering cross section resulting from the limits of the absorption cross section given by the shaded region of fig. 4.

Davydov and Filippov¹⁸ the three resonance energies correspond to a value of γ of about 20° . The values of this parameter normally assigned to nuclei in this part of the periodic table on the basis of their low lying states is only about 10° .

Elem. Sym.	A	Z
Hg	165	67

Method 55 MeV betatron; synchrotron; $\text{Si}^{28}(\text{n},\text{p})\text{Al}^{28}$ activity; $\text{Cu}^{63}(\gamma,\text{n})\text{Cu}^{62}$ monitor.

Ref. No.
62 Re 1
EGF

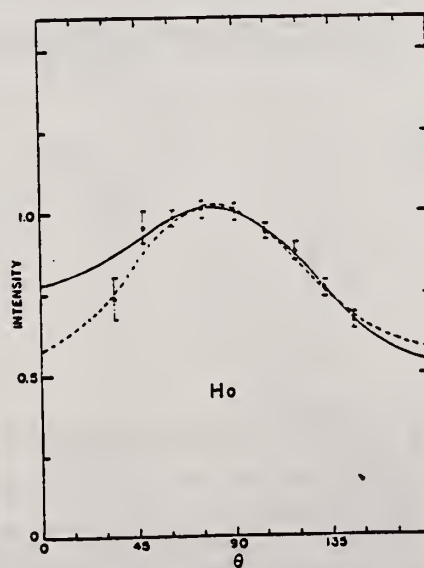
Reaction	E or ΔE	E_0	Γ	$\int \sigma dE$	J/π	Notes
$\text{Ho}^{165}(\gamma,\text{n})$	Bremss. 55					<p>Figure 8: Dotted curve is of form $a_0 + a_1 \cos \theta + a_2 \cos^2 \theta + a_3 \cos^3 \theta$; solid curve is of form $a_0 + a_1 \cos \theta + a_2 \cos^2 \theta$; errors on points are statistical errors in counting only.</p> <p>$E_n \geq 5 \text{ MeV}$</p> 

TABLE 2
Parameters of the fit (1) for the expressions $a_0 + a_1 \cos \theta + a_2 \cos^2 \theta$, $a_0 + a_1 \sin^2 \theta - c \cos \theta$ and $a_0 + a_1 P_1 - a_2 P_2$

	B1(1)	B1(2)	P2	Au	V	Cd	Lu
a_0	1.00 ± 0.02	1.00 ± 0.02	1.00 ± 0.02	1.00 ± 0.03	1.00 ± 0.02	1.00 ± 0.01	
a_1	0.15 ± 0.03	0.18 ± 0.04	0.17 ± 0.04	0.14 ± 0.03	0.17 ± 0.06	0.12 ± 0.03	0.14 ± 0.04
$-a_2$	0.47 ± 0.08	0.49 ± 0.08	0.41 ± 0.09	0.21 ± 0.07	0.15 ± 0.11	0.35 ± 0.09	0.39 ± 0.06
$-A_1^{(1)}$	0.15 ± 0.04	0.21 ± 0.05	0.20 ± 0.05	0.15 ± 0.04	0.19 ± 0.06	0.14 ± 0.04	0.16 ± 0.03
$-A_1^{(2)}$	0.37 ± 0.05	0.31 ± 0.06	0.32 ± 0.07	0.15 ± 0.05	0.11 ± 0.08	0.21 ± 0.05	0.30 ± 0.04
a	0.33 ± 0.06	0.60 ± 0.08	0.59 ± 0.09	0.79 ± 0.07	0.82 ± 0.11	0.66 ± 0.06	0.61 ± 0.06
b	0.47 ± 0.06	0.40 ± 0.05	0.41 ± 0.09	0.21 ± 0.07	0.15 ± 0.11	0.37 ± 0.06	0.39 ± 0.06
c	0.13 ± 0.03	0.18 ± 0.04	0.17 ± 0.04	0.14 ± 0.03	0.17 ± 0.06	0.13 ± 0.03	0.14 ± 0.03

* Renormalized so that $A_0 = 1$

TABLE 4
Parameters of the fit (3) for the expressions $a_0 + a_1 \cos \theta + a_2 \cos^2 \theta - a_3 \cos^3 \theta$, $1 + a_1 P_1 - a_2 P_2 - a_3 P_3$

	B1(1)	B1(2)	P2	Au	V	Cd	Lu
a_0	1.01 ± 0.02	1.00 ± 0.02	1.01 ± 0.03	1.00 ± 0.03	1.00 ± 0.02	1.01 ± 0.02	
a_1	0.12 ± 0.03	0.17 ± 0.07	0.21 ± 0.07	0.07 ± 0.06	0.16 ± 0.06	0.12 ± 0.03	0.17 ± 0.03
$-a_2$	0.58 ± 0.11	0.37 ± 0.15	0.50 ± 0.16	0.05 ± 0.12	0.13 ± 0.23	0.33 ± 0.12	0.47 ± 0.11
$-A_1^{(1)}$	-0.17 ± 0.15	0.05 ± 0.24	-0.17 ± 0.25	0.31 ± 0.19	0.05 ± 0.32	0.02 ± 0.19	-0.17 ± 0.17
$-A_1^{(2)}$	0.11 ± 0.15	0.23 ± 0.18	0.12 ± 0.20	0.27 ± 0.13	0.20 ± 0.22	0.13 ± 0.14	0.09 ± 0.13
a	0.45 ± 0.09	0.25 ± 0.11	0.39 ± 0.12	0.03 ± 0.08	0.09 ± 0.14	0.21 ± 0.09	0.37 ± 0.09
b	-0.08 ± 0.09	0.02 ± 0.11	-0.08 ± 0.12	0.13 ± 0.08	0.02 ± 0.19	0.01 ± 0.08	-0.08 ± 0.08

* Renormalized so that $A_0 = 1$

Ref.

R.L.Bramblett, J.T.Caldwell, G.F.Auchampaugh, S.C.Fultz

Phys. Rev. 129, 2723 (1963)

Elem. Sym.	A	Z
Hg	165	

Method

positron annihilation - 4⁷ parafin moderated neutron detector

Ref. No.	
63Br1	B G

Reaction	E or ΔE	E_0	Γ	$\int \sigma dE$	$J\pi$	Notes
$^{172}\text{Ta} (\gamma, n)$	0 - 28			$1.47 \pm 0.15)_{0}^{28}$		$(\gamma, 2n)$ threshold = 14.8 ± 0.3 MeV Intrinsic quadrupole moment = 7.40 ± 0.90 b
$^{173}\text{Ta} + (\gamma, 2n)$	0 - 28			$0.90 \pm 0.09)_{0}^{28}$		
(γ, n) + $(\gamma, 2n)$	0 - 28	12.1	6.9	$2.37 \pm 0.24)_{0}^{28}$		Level density parameter, $a = 22.0 \text{ MeV}^{-1}$
$^{174}\text{Ta} + (\gamma, np)$		15.2				

722+

Fig. 3. Partial cross-section curves for Ho. Curve A consists of $(17.1n) + 2n$, Curve B consists of $(17.1n) + (17.1n)$, and Curve C consists of $(17.1n) + 2n$.

Element	σ_a (mb)	E_a (MeV)	E_b (MeV)	σ_b (mb)	E_b (MeV)	E_c (MeV)	Q_0 (b)
Ta ¹⁷¹	198	3.00	12.75	224	5.0	15.50	6.71 = 0.74
Ho ¹⁶⁶	200	2.65	12.10	249	4.4	15.75	7.40 ± 0.90 b

Fig. 4. Cross sections for Ho from neutron yield data. Curve A consists of $\sigma(\gamma, n) + 2\sigma(\gamma, 2n) + \sigma(\gamma, np) + \sigma(\gamma, 2n)$ and was obtained from single-neutron counting data. Curve B consists of $2\sigma(\gamma, 2n) + \sigma(\gamma, 2n)$, and was obtained from double-neutron counting data.

Fig. 5. The formation cross section for the compound nucleus Ho-166. The sum curve represents the sum of two Lorentz lines with parameters given in Table III.

TABLE IV. Integrated cross sections, level density parameters, and σ_{-2} values

Element	σ_{tot} (mb/MeV)	0.00225 \pm 0.03 (mb/MeV)	δ (MeV $^{-1}$)	$f_{\pi}^{(2)} \text{ and } K$ (MeV \cdot b)	$f_{\pi}^{(2)} \text{ and } F + W$ (MeV \cdot b)	0.06 \pm 0.1 (MeV \cdot b)
Ta ¹⁸⁰	10.88	13.03	15.7	2.24	1.59	2.01
Hg ¹⁶⁴	10.93	11.17	22.0	2.37	2.68	2.38

METHOD	Betatron; photon scattering	REF. NO.		ANGLE
		63 La 1	NVB	
REACTION	RESULT	EXCITATION ENERGY	SOURCE	DETECTOR
G, G	ABX	9-26	C 9-27	NAI-D
				DST

In figure 4, $W(\theta) = 1 + a(\cos^2 \theta)$

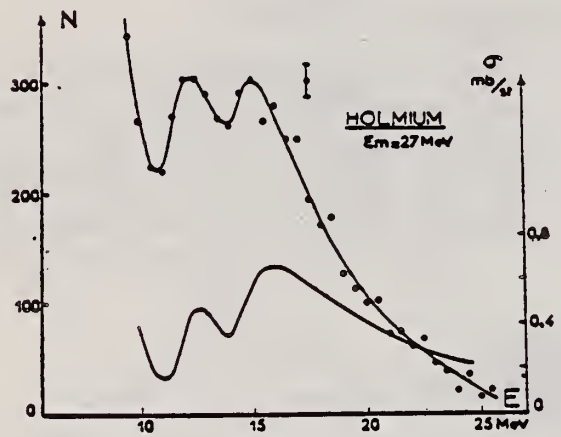


FIG. 2.

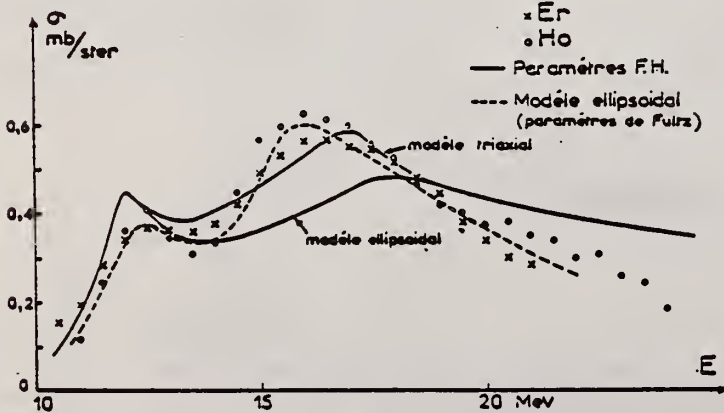


FIG. 3.

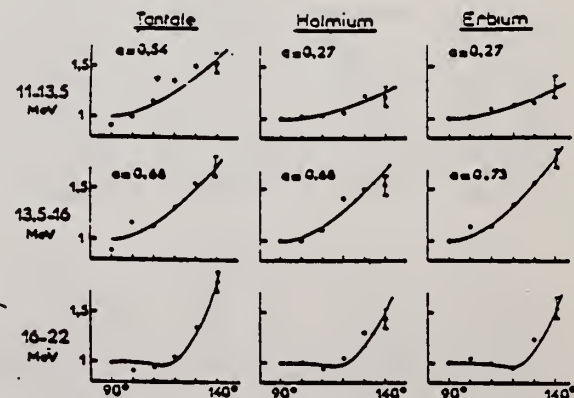


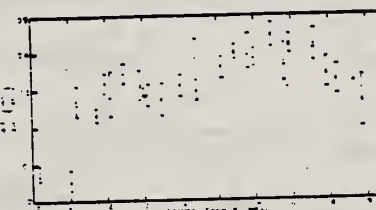
Fig. 4.

Method

25 MeV Betatron - bremsstrahlung monochrometer - NaI

Ref. No.
63Til

B6-

Reaction	E or ΔE	E_0	Γ	$\int \sigma dE$	$J\pi$	Notes
(γ, γ')	10.92 - 19.06	12.49 16.50 see notes				Differential scattering cross section has maxima at 12.49 MeV and 16.50 MeV (135°) Differential scattering cross section (135°) data given in article. Raman scattering considered.
						
						Fig. 8. Differential quasi elastic photon scattering cross section in Ho^{165} . The crosses were obtained at 135° in this experiment and correspond to a resolution of 2° . The circles are from the data of Fuller and Hayward (see reference 2) obtained at 90° with an energy resolution of 10° .

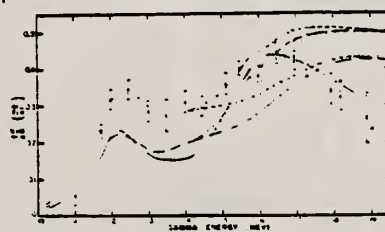


Fig. 9. Predictions for elastic scattering at 135° based on energy dependence of absorption data. All of the curves have been shifted to higher energy by 200 keV and have been reduced by 10% to facilitate comparison with the experimental points obtained in this experiment. The dashed-dot curve is the scalar contribution to the scattering implied directly by the absorption data; the solid curve indicates the scalar prediction based on a two-Lorentz line fit to the absorption data below 17 MeV. The dashed curve includes the elastic part of the tensor scattering implied by the hydrodynamic model.

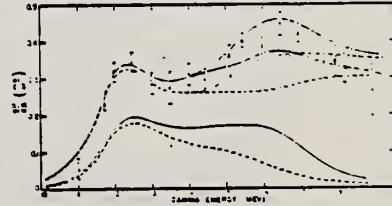


Fig. 10. Predictions for elastic plus Raman scattering at 135° based on absorption data. The upper curves include the scalar contributions obtained from the absorption data by directly applying the dispersion relations; this scalar contribution was assumed to have a dipole angular dependence but no line fitting was used to represent the absorption data. The calculations of the tensor contributions used a two-line fit (dashed curves) or a three-line fit (solid curves). The lower curves give the tensor contributions alone while the upper curves represent the total expected scattering. All of the curves have been shifted up in energy by 100 keV and normalized by a factor of 0.02 to facilitate comparison with the experimental points.

METHOD

Bremsstrahlung scattering

[Page 1 of 2]

REF. NO.	64 La 1	JOC
----------	---------	-----

REACTION	RESULT	EXCITATION ENERGY	SOURCE		DETECTOR		ANGLE
			TYPE	RANGE	TYPE	RANGE	
G,G	ABX	10-25	C	27	NAI-D		DST

TABLEAU 1
Le paramètre $a(E)$ de la distribution angulaire

Noyau	11.5-14. MeV			14-17.5 MeV			17.5-20 MeV			20-30 MeV		
	Exp.	Ellipsoidal	Triax.	Exp.	Ellips.	Triax.	Exp.	Ellips.	Triax.	Exp.	Ellips.	Triax.
Contribution Quadrupolaire %												
Tb	$0.5^{+0.15}_{-0.1}$	0.41	0.39	$0.54^{+0.15}_{-0.1}$	0.70	0.50	25	0.97	0.85	1		
Ho	$0.27^{+0.15}_{-0.1}$	0.44	0.407	$0.43^{+0.10}_{-0.05}$	0.71	0.53	25	0.95	0.9	0.4 ± 0.1	1	
Er	$0.27^{+0.15}_{-0.1}$	0.44	0.407	$0.8^{+0.15}_{-0.1}$	0.71	0.53	25	0.95	0.9	1		
Ta	$0.6^{+0.15}_{-0.1}$	0.58		$0.68^{+0.15}_{-0.1}$	0.81		20	0.96				
Au	$a_{exp}(11-20 \text{ MeV}) = 0.9$											
	$a_{th} (11-20 \text{ MeV}) \approx 1$											

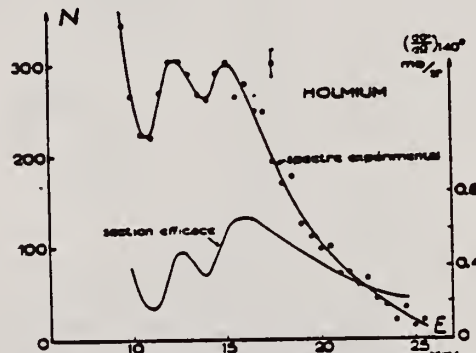


Fig. 1. Résultats expérimentaux et sections efficaces de diffusion déduites pour l'holmium,
 $E_m = 27 \text{ MeV}$.

METHOD

Bremsstrahlung scattering

[Page 2 of 2]

REF. NO.

64 La 1

JOC

REACTION	RESULT	EXCITATION ENERGY	SOURCE		DETECTOR		ANGLE
			TYPE	RANGE	TYPE	RANGE	

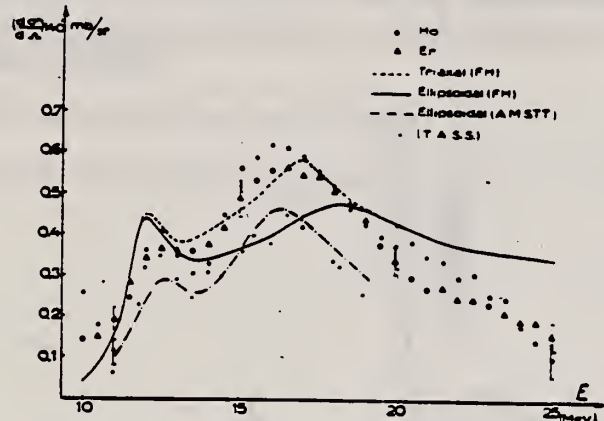


Fig. 3. Sections efficaces expérimentales différentielles de diffusion, obtenues pour l'holmium et l'erbium et comparaison avec les résultats expérimentaux de Tippler *et al.*¹²). (T.A.S.S.). Les courbes tracées correspondent à l'application des relations de dispersion aux sections efficaces d'absorption obtenues par Fuller et Hayward¹³) (F.H.) et Axel, Miller, Schuhl, Tamas et Tzara (A.M.S.T.T.)¹⁴.

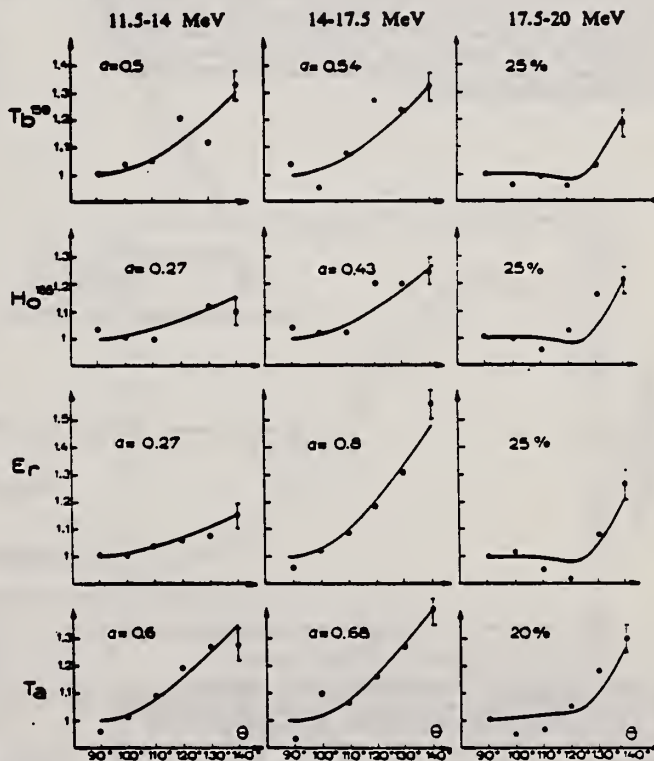


Fig. 8. Répartitions angulaires du rayonnement diffusé obtenues pour le terbium, l'holmium, l'erbium et le tantalum dans les zones d'énergie 11.5-14 MeV, 14-17.5 MeV et 17.5-20 MeV.

ELEM. SYM.	A	Z
Ho	165	67

METHOD

Betatron; ion chamber monitor

REF. NO.	NVB
65 Am 1	

REACTION	RESULT	EXCITATION ENERGY	SOURCE		DETECTOR		ANGLE
			TYPE	RANGE	TYPE	RANGE	
\$G, XN	ABY	10-20	C	10-20	BF ₃ -I		4PI

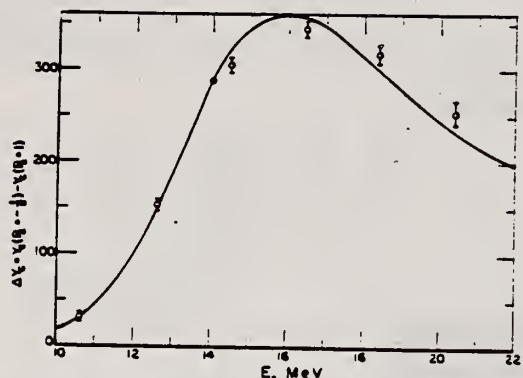
ORIENTED TARGET

Fig. 5. Asymmetry of photoneutron yield measured at 0.29°K. The root mean square errors determined from the estimated uncertainties in the asymmetry measured at 77°K and the rms deviation of the measurements at 0.29°K are indicated in the experimental points. The abscissa represents the peak energy of the bremsstrahlung spectrum.

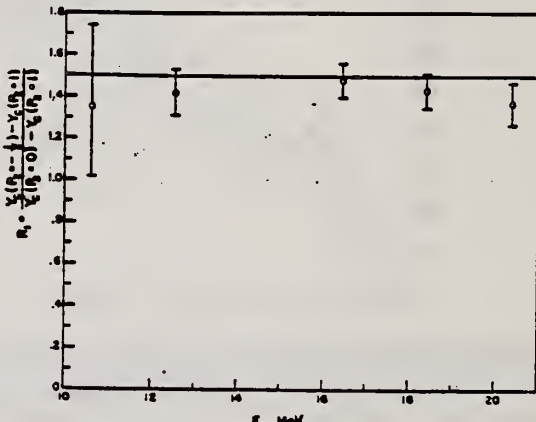


Fig. 6. Dependence of photoneutron yield asymmetry on the angle between the photon-beam direction and the nuclear alignment axis. The uncertainties indicated in the experimental points are defined in the caption for Fig. 5. The line at 1.5 is the value expected for a pure $P_2(\cos\theta)$ dependence of the alignment effect. The ordinate represents the peak energy of the bremsstrahlung spectrum.

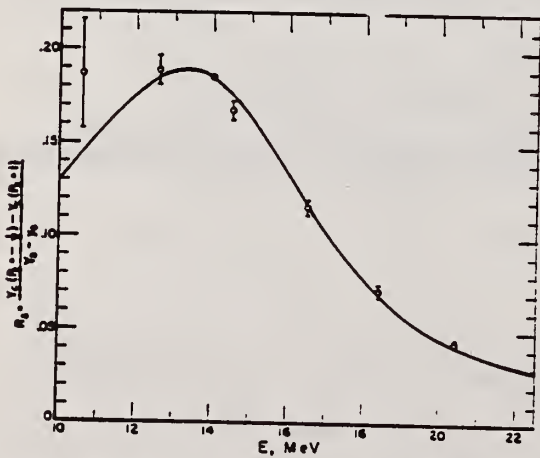


Fig. 7. Asymmetry of photoneutron yield normalized in terms of the orientation-independent yield. The uncertainties indicated in the experimental points are defined in the caption for Fig. 5. The abscissa represents the peak energy of the bremsstrahlung spectrum.

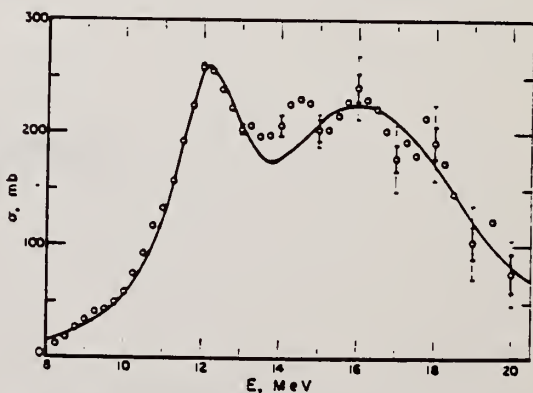


Fig. 8. Photoneutron-producing cross section for Ho¹⁶⁵ as a function of photon energy. The points above 14.25 MeV have been corrected for neutron multiplicity. Horizontal bars represent typical statistical uncertainties in data points. Light extensions on the bars indicate the uncertainties in the multiplicity correction. The smooth curve is calculated from the theory of Danos and Greiner using the parameters given in Table I.

Corrected data from 62 Fu 3.

ELEM. SYM.	A	Z
Ho	165	67

METHOD

[Page 1 of 2]

REF. NO.

Monochromatic gammas from annihilation in flight of positrons.

66 Ax 1

JDM

REACTION	RESULT	EXCITATION ENERGY	SOURCE		DETECTOR		ANGLE
			TYPE	RANGE	TYPE	RANGE	
G,N	719+	ABX	8-20	D	8-20	BF3-I	4PI
G,2N	720	ABX	8-20	D	8-20	BF3-I	4PI
G,G		ABX	13,16	D	13,16	NAI-D	90, 135

$$\sigma_{DE} = 2.54 \text{ MeV-b}$$

$$20 = 7.4 \pm 0.4 \text{ b}$$

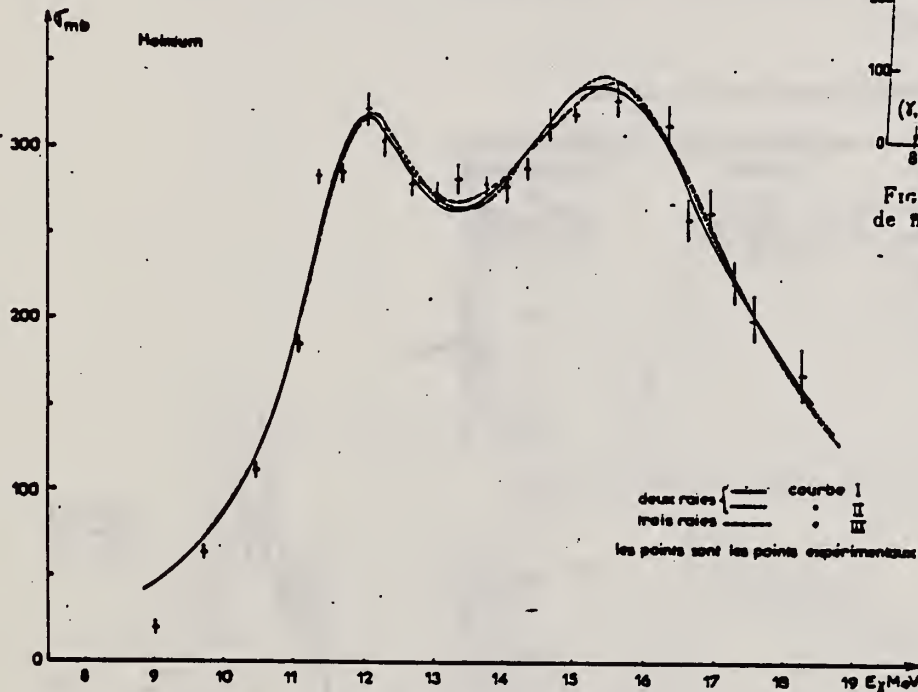


FIG. 5. — Deux ou trois rales de Lorentz.

TABLEAU 1
DÉCOMPOSITION EN DEUX RALES DE LORENTZ

1 ^{re} RÉSONANCE			2 ^{re} RÉSONANCE			E_1/E_2	$\sigma_1 \Gamma_1 / \sigma_2 \Gamma_2$	Γ	$\frac{\Gamma}{2} \sum_i \sigma_i \Gamma_i$	$\int_0^{E_2} \sigma dE$	exp. 0,06 $\frac{NZ}{A} \times 1,4$	σ_0
σ_1 mb	E_1 MeV	Γ MeV	σ_2 mb	E_2 MeV	Γ MeV							b
232 ± 17	12,00 $\pm 0,07$	2,27 $\pm 0,28$	308 ± 16	15,55 $\pm 0,13$	5,0 $\pm 0,6$	1,295 $\pm 0,024$	2,9 $\pm 1,1$	Γ	3,24 $\pm 0,58$	2,54	3,34	7,23 $\pm 0,65$
240 ± 8	12,03 $\pm 0,015$	2,43 $\pm 0,16$	308 ± 6	15,62 $\pm 0,06$	4,69 $\pm 0,20$	1,297 $\pm 0,010$	2,47 $\pm 0,4$	Γ	3,19 $\pm 0,3$			7,39 $\pm 0,4$

ELEM. SYM.	A	Z
Hg	165	67

METHOD

[Page 2 of 2]

REF. NO.

Monochromatic gammas from annihilation in flight of positrons.

66 Ax 1

JDM

TABLEAU 2

DÉCOMPOSITION EN TROIS RAIES DE LORENTZ (courbe n° III de la figure 5)

1 ^{re} RÉSONNANCE			2 ^e RÉSONNANCE			3 ^e RÉSONNANCE			$\sigma_{\text{tot}} = \frac{\pi}{2} \sum_i \sigma_i \Gamma_i$		
σ_1 mb	E_1 MeV	Γ_1	σ_2 mb	E_2 MeV	Γ_2	σ_3 mb	E_3 MeV	Γ_3			
220	12,0	2,34	172	15,0	5,73	151	16,0	3,7	1,75	1,1	3,16

ANGLE
ANGLE
ANGLE
ANGLE
ANGLE

TABLEAU 3

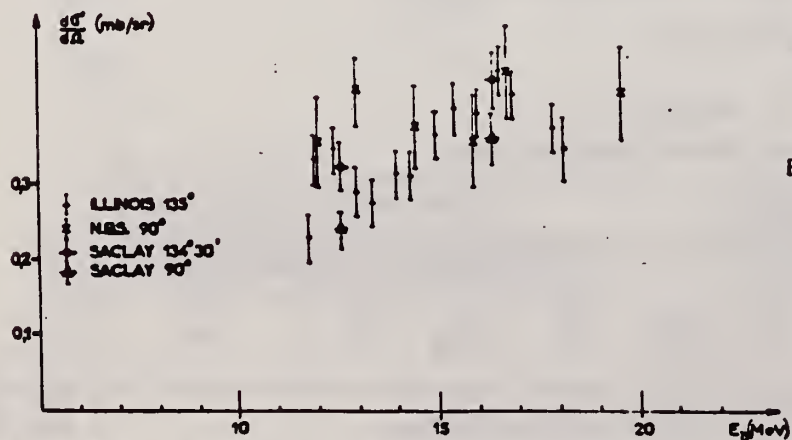
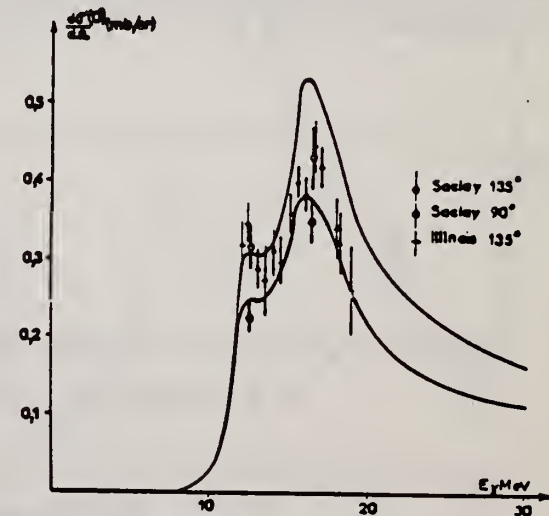
SECTION EFFICACE DIFFÉRENTIELLE DE DIFFUSION ÉLASTIQUE

E MeV	$\theta = 90^\circ$	$\theta = 134^\circ 30'$	$d\sigma (134^\circ 30')/d\Omega (90^\circ)$
12,6	$0,226 \pm 0,020$ mb/sr	$0,314 \pm 0,030$ mb/sr	$1,46 \pm 0,25$
16,4	$0,347 \pm 0,030$ mb/sr	$0,430 \pm 0,040$ mb/sr	$1,24 \pm 0,20$

TABLEAU 4

CALCUL DE $\frac{d\sigma}{d\Omega} (\theta)$ A PARTIR DES COURBES D'ABSORPTION DES PHOTONS

E	$\theta = 90^\circ$	$\theta = 135^\circ$	$d\sigma (135^\circ)/d\sigma (90^\circ)$ calculé	$d\sigma (135^\circ)/d\sigma (90^\circ)$ expérimental
12,6 MeV	0,247 mb/sr	0,307 mb/sr	1,24	1,46 \pm 0,25
16,4 MeV	0,376 mb/sr	0,525 mb/sr	1,40	1,24 \pm 0,20
$d\sigma (16,4)/d\sigma (12,6)$ calculé	1,52	1,71		
$d\sigma (16,4)/d\sigma (12,6)$ expérimental	$1,53 \pm 0,45$	$1,37 \pm 0,27$		

FIG. 6. — Section efficace de diffusion élastique des rayonnements gamma pour le noyau de ^{164}Ho .FIG. 7. — Diffusion élastique (scalaire et tensorielle) des rayonnements gamma par ^{164}Ho .

METHOD

70 MeV Synchrotron

REF. NO.

66 Sc 1

JDM

REACTION	RESULT	EXCITATION ENERGY	SOURCE		DETECTOR		ANGLE
			TYPE	RANGE	TYPE	RANGE	
G, P	SPC	THR-70	C	70	TEL-D	6-14	90, 135
G, D	RLY	THR-70	C	70	TEL-D	6-14	90, 135
G, T	RLY	THR-70	C	70	TEL-D	6-14	90, 135

TABLE I

Numbers of photoparticles from ^{164}Ho with energies in the range 9.0 MeV to 13.5 for a peak photon energy of 70 MeV

Angle (deg)	Protons	Deuterons	Tritons	Deuterons/Protons	Tritons/Deuterons
90	1905	76	19	0.04	0.25
135	1017	35	11	0.03	0.3

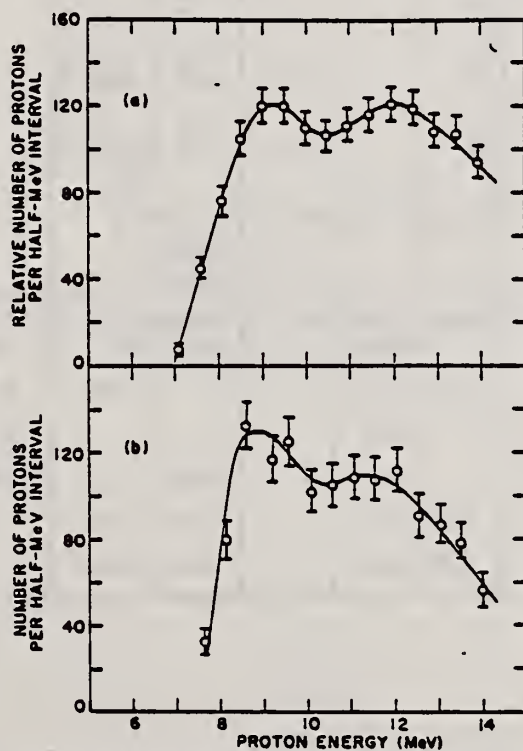


Fig. 5. Upper curve: photoproton spectrum at $90 \pm 6^\circ$ to beam. Lower curve: photoproton spectrum at $135 \pm 6^\circ$ to beam. The upper curve has been normalized to the same beam dose as the lower curve. Both energy scales are corrected for proton energy loss in the target.

METHOD

REF. NO.

67 Ge 2

HMG

REACTION	RESULT	EXCITATION ENERGY	SOURCE		DETECTOR		ANGLE
			TYPE	RANGE	TYPE	RANGE	
G,N	ABY	THR-27	C	22,27	BF3-I		4PI

Table 7. Comparison of neutron yields. Yields are given in units of (neutron cm³/MeV nucleus) × 10⁻²⁴. The estimated uncertainties in Y and Y_c are of the order of 6% and 10%, respectively.

Element	E ₀	Y(E ₀)	UCRL	Saclay	Va.	NBS(Old)	UCRL		Saclay	Va.	NBS(Old)	Ref.
							Exp	Exp				
Pb	27	103	86				0.83					26,30
	22	111	92	116			0.83	1.05				
Au	27	89	97				1.09					24,30,
	22	92	98	88		115	1.07	0.96			1.25	38
Ta	27	81	82	77			1.01	0.95				27,30,
	22	85	79	80		113	0.93	0.94			1.33	38
Ho	27	67	75				1.12					27,31,
	22	69	77	82		103	1.12	1.19			1.49	39
Ag	27	36										
	22	34.8										
Cu	27	14.6	13.2				0.92					28,30
	22	12.6	11.5	12.4			0.91	0.98				
Co	27	12.7	12.1				0.95					29,34
	22	10.6	9.9		13.5		0.94				1.27	
Ca	27	1.69		1.13	1.01				0.67	0.60		32,35
	27	2.35			1.76					0.75		36
Al	27	1.92	1.62		1.38		0.84			0.72		25,37
	27	0.54	0.42	0.48	0.42		0.78	0.89				16,32,
O ¹⁸	27	0.50	0.42	0.33	0.46		0.70	0.66				37
	27	0.50	0.35	0.33	0.46							25,32,
C	27	0.50	0.35	0.33	0.46		0.70	0.66				33

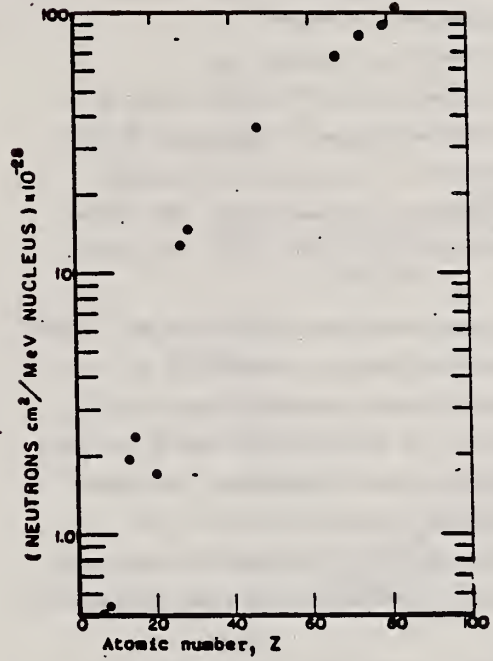


Fig. 31. Absolute neutron yield as a function of atomic number. The neutron yield from calcium ($Z = 20$) is particularly low in comparison with the other elements because its (γ, n) threshold is high compared to the mean energy of the giant resonance.

REF.					ELEM. SYM.	A	Z
J. R. Harrington and B. M. Spicer PICNS-67 Contributions, International Conference on Nuclear Structure, Tokyo, Japan 1967 (Institute for Nuclear Study, University of Tokyo, Tanashi-shi, Tokyo, Japan) 10.16, p. 380					Ho	165	67
METHOD					REF. NO.		
					67 Ha 1		
REACTION	RESULT	EXCITATION ENERGY	SOURCE	DETECTOR			EGF
			TYPE	RANGE	TYPE	RANGE	ANGLE
G,2N	RLX	14-29	C	14-29	ACT-I		4PI

The Electric Quadrupole Giant Resonance of Ho¹⁶⁵*

YIELD TO ISOMERE

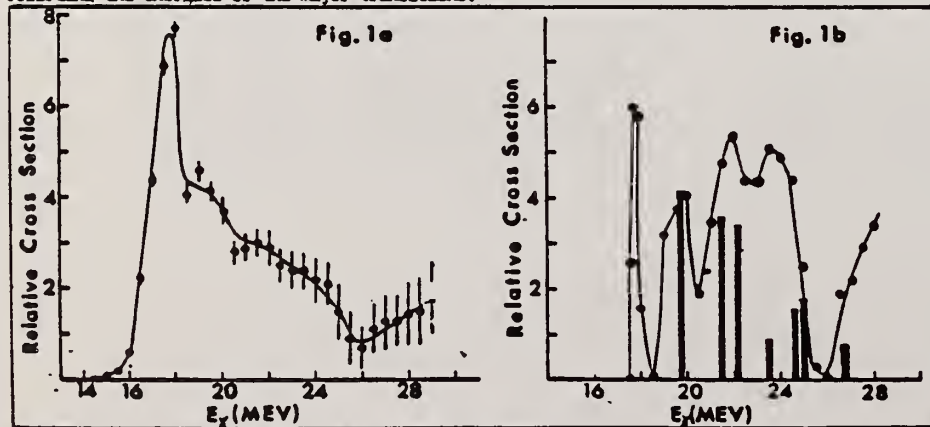
J. R. Harrington and B. M. Spicer

University of Melbourne, Australia

The structure of the electric quadrupole giant resonance of Ho¹⁶⁵ has been sought in the Ho¹⁶⁵(γ ,2n)Ho^{163m} cross section. The yield of Ho^{163m} was measured by counting the 308 keV γ -ray emitted in the decay of the isomeric state of Ho¹⁶³. The half-life of this state (0.8 sec) required that its activity be counted between betatron beam bursts. The yield of Ho^{163m} was measured at 0.5 MeV intervals between threshold and 28 MeV, and the cross section extracted by the method of Penfold and Leiss.

Bramblett et al.¹⁾ showed that the Ho¹⁶⁵(γ ,n) cross section goes to zero at 18 MeV. Therefore, above this energy, the total γ -ray absorption cross section is manifested in the (γ ,2n) and (γ ,3n) cross sections. The statistical theory of nuclear reactions indicates that the (γ ,3n) cross section is not significant below 26 MeV. We confine attention then to the (γ ,2n) cross section, which will consist of contributions from E1 and E2 absorption. The dynamic collective theory of the E1 giant resonance predicts two Lorentz lines for Ho¹⁶⁵, and Bramblett et al.¹⁾ show these at 12.1 and 15.75 MeV, with widths of 2.6 and 4 MeV respectively. Thus the E1 cross section above 20 MeV is smooth, and all structure in the (γ ,2n) cross section should arise from the E2 giant resonance.

The measured cross section is shown in Fig. 1a. An attempt has been made to subtract from this cross section the contribution due to E1 absorption. The result of this subtraction is shown in Fig. 1b together with the prediction of Ligenza, Greiner and Danos²⁾ for the E2 cross section structure. A measure of consistency exists between theory and experiment regarding the energies of the major transitions.



*Supported by a grant from the U.S. Army Research Office.

References: 1) R. L. Bramblett, J. T. Caldwell, G. F. Auchampaugh and S. C. Fultz:

Phys. Rev. 129 (1963) 2723.

2) R. Ligenza, W. Greiner and M. Danos: Phys. Rev. Lett. 16 (1966) 364.

REF.

R. R. Hurst and D. J. Donahue
Nucl. Phys. A91, 365 (1967)

ELEM. SYM.	A	Z
Ho	165	67

METHOD

REF. NO.

67 Hu 1

EGF

Neutron capture gamma rays

REACTION \	RESULT	EXCITATION ENERGY	SOURCE		DETECTOR		ANGLE
			TYPE	RANGE	TYPE	RANGE	
G,N	ABX	9-11	D	9-11	BF ₃ -I		4PI

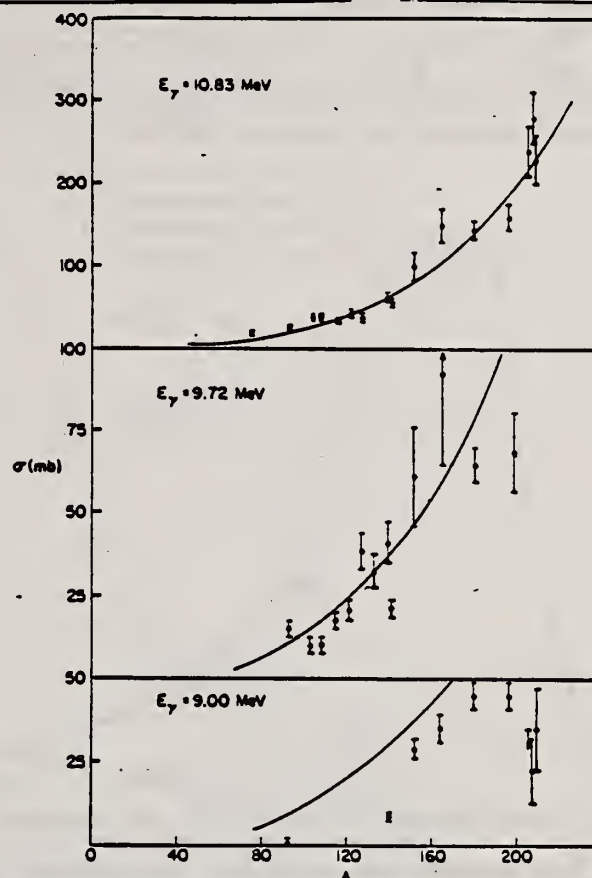


TABLE I
Photoneutron cross sections (mb)

Fig. 1. Cross section (in mb) versus mass number of the target for gamma-ray energies of 9.00, 9.72 and 10.83 MeV. The solid lines are plots of eq. (1) in the text.

Target	7.72 MeV	9.00 MeV	9.72 MeV	10.83 MeV
⁶⁰ Co				9.0 ± 0.8
⁷⁵ As				20.4 ± 1.7
⁹³ Nb		0.53 ± 0.10	14.6 ± 2.2	25.8 ± 2.1
¹⁰³ Rh			10.6 ± 1.7	38.8 ± 3.1
¹⁰⁷ Ag }			10.0 ± 1.5	37.6 ± 2.9
¹⁰⁹ Ag }			17.1 ± 2.6	33.3 ± 2.7
¹¹⁵ In			20.7 ± 3.1	42.5 ± 3.6
¹²¹ Sb }			38.7 ± 5.8	38.8 ± 3.1
¹²³ Sb }			31.7 ± 4.8	52.5 ± 3.8
¹²⁷ I			40.8 ± 6.5	63.0 ± 5.0
¹³³ Cs		8.61 ± 0.86	21.5 ± 3.2	58.3 ± 4.1
¹³⁹ La			28.9 ± 3.2	61.3 ± 14.7
¹⁴¹ Pr				102 ± 18
¹⁵¹ Eu }				150 ± 20
¹⁵³ Eu }				146 ± 12
¹⁶⁴ Ho		35.6 ± 4.3	65.0 ± 5.5	160 ± 15
¹⁶⁸ Ta	4.14 ± 0.36	45.4 ± 3.7	68.4 ± 13.5	238 ± 29
¹⁷⁷ Au		44.5 ± 3.6		280 ± 31
²⁰⁰ Pb		<34.3		226 ± 27
²⁰⁸ Pb		22.6 ± 11.3		
²⁰⁹ Bi		36.1 ± 12.0		

U.S. DEPARTMENT OF COMMERCE
NATIONAL BUREAU OF STANDARDS

ELEM. SYM.	A	Z
Ho	165	67

METHOD

REF. NO.

68 Be 5

egf

[Page 1 of 2]

REACTION	RESULT	EXCITATION ENERGY	SOURCE		DETECTOR		ANGLE
			TYPE	RANGE	TYPE	RANGE	
G, N	90	ABX	THR-30	D	7-30	MOD-I	LPI
G, 2N	91						
G, 3N	92+						

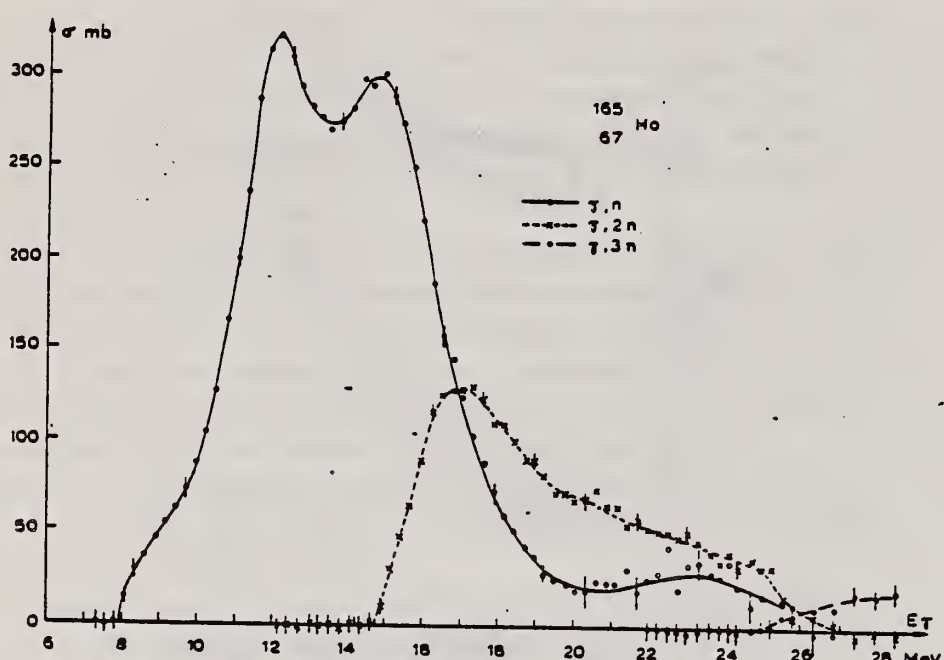


Fig. 4. Partial photonuclear cross sections $\sigma(\gamma, n)$, $\sigma(\gamma, 2n)$ and $\sigma(\gamma, 3n)$ of $^{165}_{\text{Ho}}$.

TABLE 4
 Lorentz line parameters for a two line fit to the total cross section data of $^{165}_{\text{Ho}}$

E_1 (MeV)	σ_1 (mb)	Γ_1 (MeV)	E_2	σ_2	Γ_2
12.07	250	2.7	15.62	285	4.8

METHOD

REF. NO.

[Page 2 of 2]

68 Be 5

egf

REACTION	RESULT	EXCITATION ENERGY	SOURCE		DETECTOR		ANGLE
			TYPE	RANGE	TYPE	RANGE	

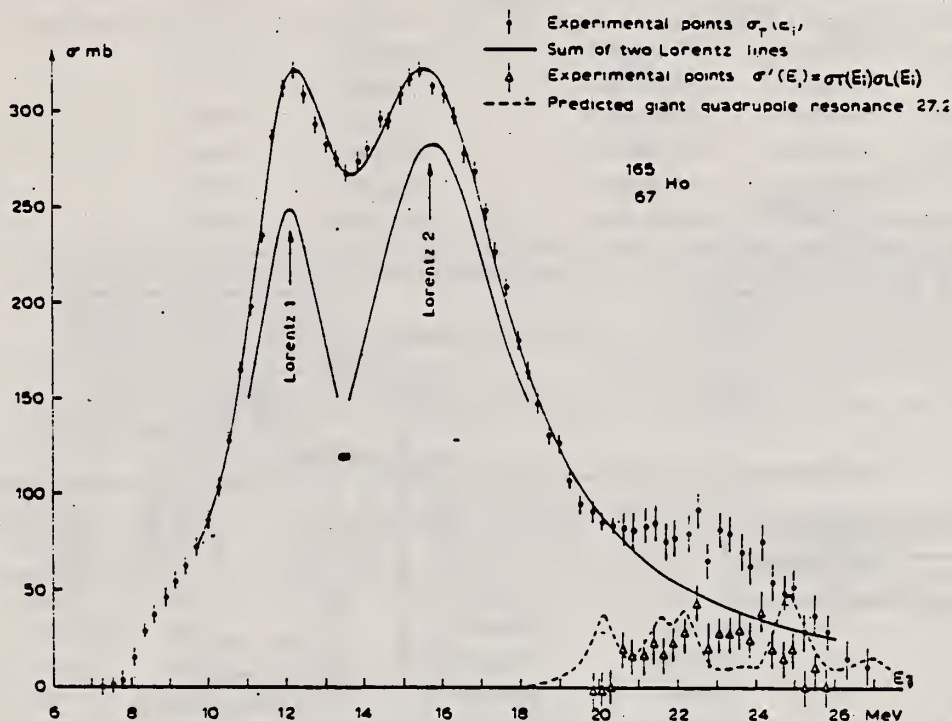


Fig. 5. Total cross section data showing a two Lorentz line fit for a $^{165}_{67}\text{Ho}$ target.

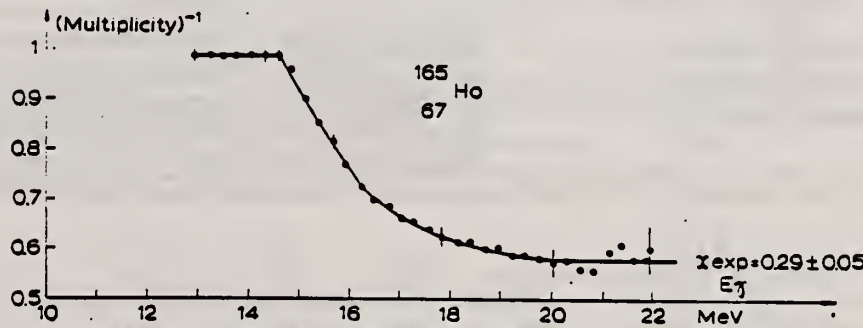


Fig. 6. Reciprocal neutron multiplicity as a function of γ -energy for $^{165}_{67}\text{Ho}$.

ELEM. SYM.	A	Z
Ho	165	67

METHOD

REF. NO.

69 Be 8

hmg

REACTION	RESULT	EXCITATION ENERGY	SOURCE		DETECTOR		ANGLE
			TYPE	RANGE	TYPE	RANGE	
G, N* 163	ABX	8-29	D	8-29	BF3-I		4PI
G, 2N** 164	ABX	8-29	D	8-29	BF3-I		4PI
G, 3N 165+	ABX	8-29	D	8-29	BF3-I		4PI

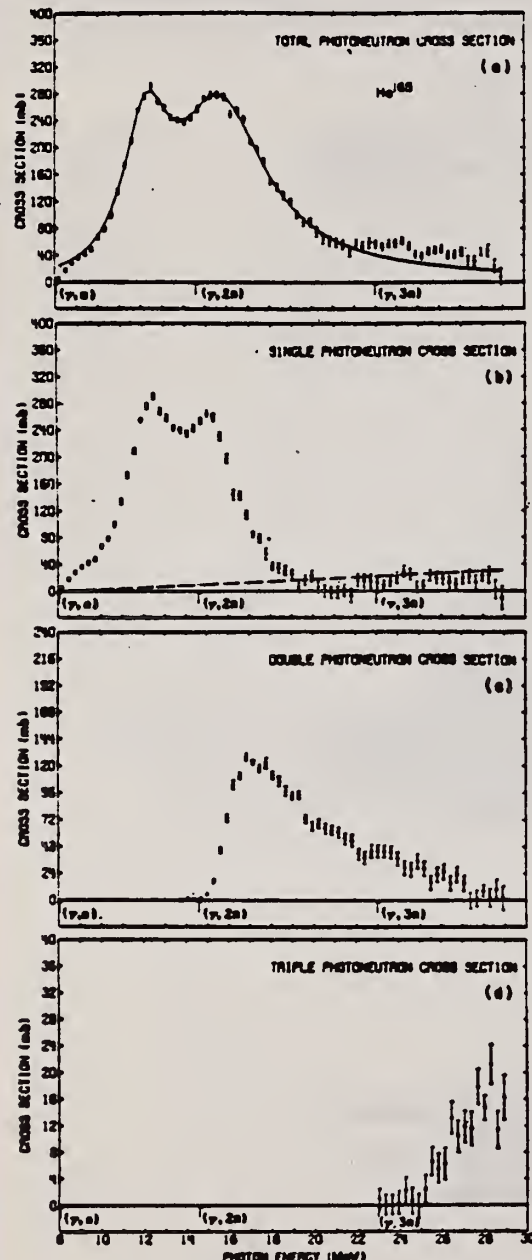


FIG. 7. Photoneutron cross sections for Ho¹⁶⁵: (a) $\sigma[(\gamma, n) + (\gamma, p\gamma) + (\gamma, 2n) + (\gamma, p2n) + (\gamma, 3n)]$, (b) $\sigma[(\gamma, n) + (\gamma, p\gamma)]$, (c) $\sigma[(\gamma, 2n) + (\gamma, p2n)]$, (d) $\sigma(\gamma, 3n)$.

[over]

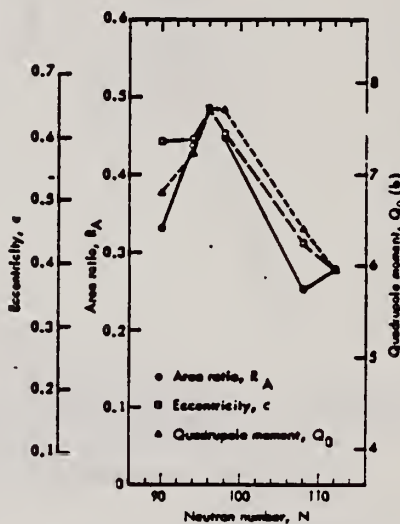


FIG. 9. The area ratio R_A , nuclear eccentricity e , and intrinsic quadrupole moment Q_0 plotted versus neutron number N . The data were scaled between the value for Gd¹⁶⁰ and that for W¹⁸⁰. The absolute scale for Q_0 is based on a mean radius parameter $R_0 = 1.26$ F. The lines merely connect the three sets of data points. The experimental uncertainties have been omitted for clarity but are given in Tables VII and VIII; their average values are 0.005 (17%) for R_A , 0.010 (1.9%) for e , and 0.26b (3.7%) for Q_0 .

TABLE V. Parameters of Lorentz-curve fits to the giant resonance.

Nucleus	E_{γ} (1) (MeV)	$\sigma_{\text{tot}}(1) \cdot (\text{mb})$	$\Gamma(1) (\text{MeV})$	E_{γ} (2) (MeV)	$\sigma_{\text{tot}}(2) \cdot (\text{mb})$	$\Gamma(2) (\text{MeV})$
Eu ¹⁵²	12.33±0.06	153±9	2.75±0.26	15.79±0.10	222±6	5.83±0.30
Tb ¹⁵⁰ b	12.22±0.04	181±6	2.64±0.16	15.67±0.06	220±4	4.97±0.19
Gd ¹⁵²	12.23±0.06	215±9	2.77±0.25	15.96±0.09	233±6	5.28±0.30
Ho ¹⁵²	12.28±0.02	214±5	2.57±0.11	15.78±0.04	246±3	5.00±0.17
Ta ¹⁵¹ c	12.59±0.03	171±8	1.94±0.12	15.13±0.12	265±6	4.98±0.23
W ¹⁸⁶	12.59±0.03	211±14	2.29±0.14	14.88±0.08	334±8	5.18±0.14

^a The uncertainties for σ_{tot} given here are relative. The absolute uncertainty is 7% (10% for Tb¹⁵⁰ and Ta¹⁵¹).

^b The data of Ref. 10 were reanalyzed to obtain the values given in this

and subsequent tables (see text).

^c The data of Ref. 11 were reanalyzed to obtain the values given in this and subsequent tables (see text).

- 10 R. L. Bramblett, J. T. Caldwell, R. R. Harvey, S.C. Fultz, Phys. Rev. 133, B869 (1964).
 11 R. L. Bramblett, J.T. Caldwell, G.F. Auchampaugh, S.C. Fultz, Phys. Rev. 120, 2723 (1963).

TABLE VII. Nuclear radius parameters.

Nucleus	Q_0^{a} (b)	Ref.	ϵ^{b}	R_0^{c} (f)	Q_0^{d} (b)
Eu ¹⁵²	6.99±0.08	e, f	0.595±0.015	1.276±0.018	6.80±0.28
Tb ¹⁵⁰	7.41±0.11	e	0.598±0.009	1.274±0.013	7.23±0.26
Gd ¹⁵²	7.55±0.17	g	0.645±0.014	1.245±0.020	7.71±0.30
Ho ¹⁵²	7.56±0.11	e	0.604±0.006	1.246±0.011	7.71±0.26
Ta ¹⁵¹	6.89±0.21	h, i	0.433±0.010	1.306±0.025	6.43±0.26
W ¹⁸⁶	5.96±0.05	g, j, k	0.390±0.006	1.259±0.011	5.96±0.21

^a Values taken from or computed from the references listed in column 3.

^b Values from present data (Table VII).

^c Computed from Eq. (2) in the text.

^d The "best" values for Q_0 deduced from the present data, computed from Eq. (2) in the text, taking R_0 to be 1.28 ± 0.02 fm.

^e M. C. Gleas and B. Elbek, Nucl. Phys. 13, 134 (1959).

^f R. A. Carrigan, Jr., P. D. Gupta, R. B. Sutton, M. N. Suzuki, A. C. Thompson, R. E. Coté, W. V. Prestwich, A. K. Gagnon, and S. Rabey, Phys. Rev. Letters 20, 874 (1968).

^g P. H. Stelson and L. Grodzins, Nucl. Data A1, 21 (1965).

^h P. K. McGowan and P. H. Stelson, Phys. Rev. 109, 901 (1958).

ⁱ E. M. Bernstein and R. Graetz, Phys. Rev. 119, 1321 (1960).

^j R. C. Barrett, S. Berlow, S. Devone, I. Duerdeth, D. Hidin, J. W. Kast, W. Y. Lee, E. R. Macagno, J. Rajawat, and C. S. Wu, Columbia University Pegram Nuclear Physics Lab. Report No. NYO-72-191, 1962, p. 74 (unpublished).

^k R. G. Stockstad and B. Parsons, Phys. Rev. 170, 1072 (1968).

TABLE IX. Integrated cross sections.

Nucleus	$E_{\gamma, \text{max}}$ (MeV)	$\sigma_{\text{tot}}[(\gamma, n) +$ (γ, p_n)] ^a (MeV \cdot b)	$\sigma_{\text{tot}}[(\gamma, 2n) +$ ($\gamma, p2n$)] ^a (MeV \cdot b)	$\sigma_{\text{tot}}[(\gamma, 3n) +$ (MeV \cdot b)	$\frac{\sigma_{\text{tot}}[(\gamma, 2n) + (\gamma, p2n)]}{\sigma_{\text{tot}}(\gamma, \text{total})}$ ^b	$\frac{[\sigma_{\text{tot}}(1)\Gamma(1) +$ $\sigma_{\text{tot}}(2)\Gamma(2)]}{(\text{MeV}\cdot\text{b})}$	$0.06 NZ/A$ (MeV \cdot b)
Eu ¹⁵²	28.9	1.57	0.67	0.04	0.29±0.04	2.70±0.19	2.22
Tb ¹⁵⁰	28.0	1.41	0.89	d	0.39±0.08	2.47±0.12	2.31
Gd ¹⁵²	29.5	1.45	1.00	0.08	0.39±0.05	2.87±0.20	2.30
Ho ¹⁵²	28.9	1.73	0.74	0.04	0.29±0.04	2.80±0.09	2.39
Ta ¹⁵¹	24.6	1.31	0.88	f	0.40±0.08	2.59±0.15	2.61
W ¹⁸⁶	28.6	1.66	1.19	0.15	0.40±0.05	3.47±0.17	2.67

^a All measured integrated cross-section values are given for an energy region from threshold to $E_{\gamma, \text{max}}$.

^b The word "total" in this table refers to the total photoneutron cross section, $\sigma[(\gamma, n) + (\gamma, p_n) + (\gamma, 2n) + (\gamma, p2n) + (\gamma, 3n)]$.

^c The uncertainties listed here are relative; to get the absolute uncertainty, a systematic uncertainty of 7% (10% for Tb¹⁵⁰ and Ta¹⁵¹) must be

taken into the values for σ_{tot} .

^d Not measured in Ref. 10; $\sigma_{\text{tot}}[(\gamma, 2n) + (\gamma, p2n)]$ contains $\sigma_{\text{tot}}[(\gamma, 3n)]$.

^e Because $E_{\gamma, \text{max}}$ is so low, these values cannot be compared to the rest.

^f Not measured in Ref. 11; the $(\gamma, 3n)$ cross section below 24.6 MeV probably negligible.

TABLE X. Integrated moments^a of the measured photoneutron cross section and sum rules.

Nucleus	σ_{-1} (mb)	$\sigma_{-1}/E^{-1/2}$ (mb)	$\sigma_{-1}/(mb \cdot MeV^{-1})$	σ_{-2} (mb \cdot MeV $^{-1}$)	$0.00225 A^{1/2}$	$0.05175 A^{1/2}$	$0.05175 A^{1/2}$
Eu ¹⁵²	148	0.181	10.18	1.03	1.16±0.11	22.2±1.6	
Tb ¹⁵⁰	151	0.175	10.49	1.00	1.14±0.13	23.0±2.3	
Gd ¹⁵²	169	0.195	12.09	1.14	1.35±0.13	20.2±1.4	
Ho ¹⁵²	166	0.183	11.56	1.04	1.23±0.10	22.2±1.6	
Ta ¹⁵¹ b	(149)	(0.145)	(10.66)	(0.82)	(0.97±0.13)	(28.1±2.8)	
W ¹⁸⁶	203	0.191	14.51	1.06	1.26±0.11	21.6±1.5	

^a $\sigma_{-1} = \int_{E_{\gamma, \text{min}}}^{E_{\gamma, \text{max}}} \sigma E^{-1} dE$ and $\sigma_{-2} = \int_{E_{\gamma, \text{min}}}^{E_{\gamma, \text{max}}} \sigma E^{-2} dE$. 471

where σ is the total photoneutron cross section.

^b Because $E_{\gamma, \text{max}}$ is so low, the values for Ta¹⁵¹ cannot be compared to the rest.

METHOD

REF. NO.

69 Ke 2

hmg

REACTION	RESULT	EXCITATION ENERGY	SOURCE		DETECTOR		ANGLE
			-TYPE	RANGE	TYPE	RANGE	
\$G,XN	ABX	10-21	D	10-21	BF3-I		4PI

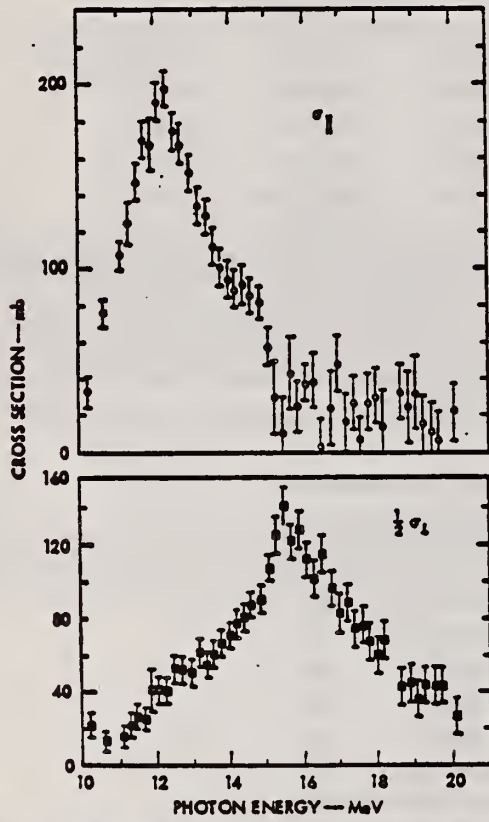


FIG. 14. The intrinsic cross sections for Ho^{165} . The cross section σ_{\parallel} is associated with vibrations along the nuclear symmetry axis. One-half σ_{\perp} is half the cross section associated with vibrations perpendicular to the symmetry axis. The error bars represent statistical errors, and not those due to the uncertainty of f_0 .

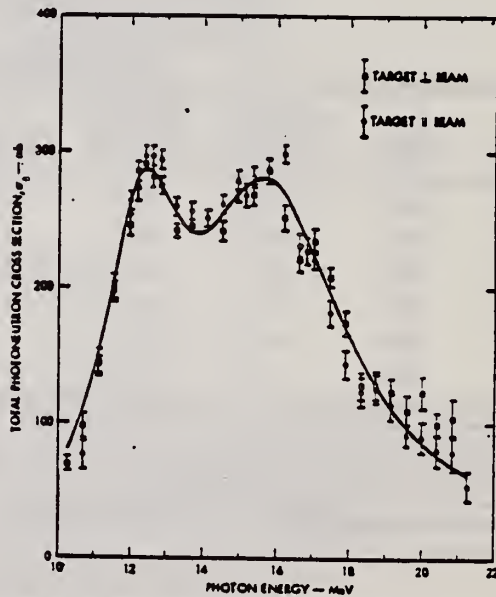


FIG. 10. The two unpolarized cross sections taken with the target oriented parallel to the photon beam and perpendicular to the beam. The target temperature during these measurements was 4.2°K; otherwise, the conditions were identical to those during the polarized runs. The solid line is a two-component Lorentz curve fit to the data, the parameters of which are given in Table III B.

[over]

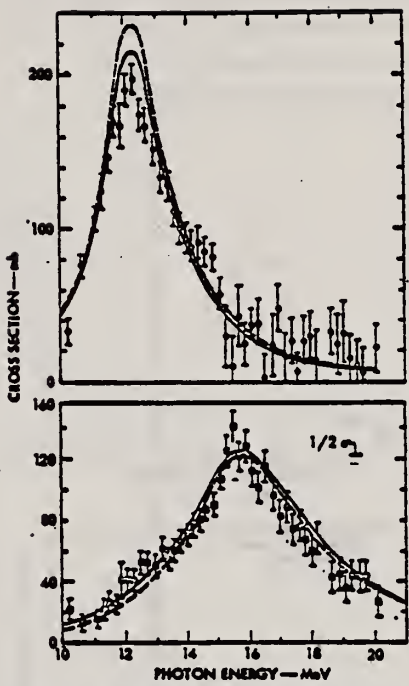


FIG. 16. The intrinsic cross sections for Ho¹⁶⁶. The cross section σ_{11} is associated with vibrations along the 'nuclear symmetry axis; σ_{12} is that associated with vibrations perpendicular to this axis. The error bars represent statistical errors, and not those due to the uncertainty of f_1 . The solid curves are those derived from the elementary collective model; the dashed ones are calculated from the dynamic collective model.

ELEM. SYM.	A	Z
Ho	165	67

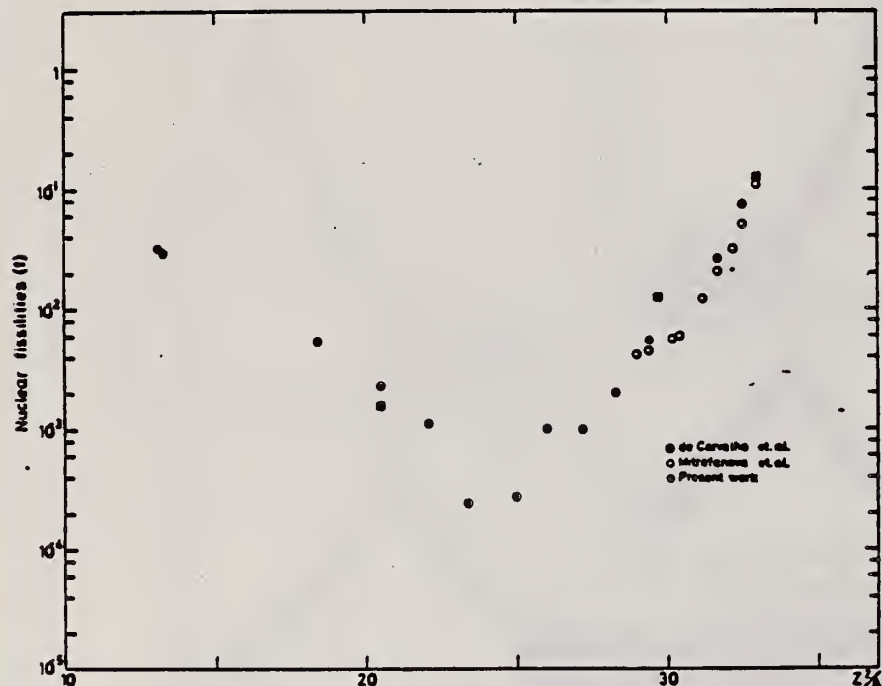
METHOD

REF. NO.

71 Me 1

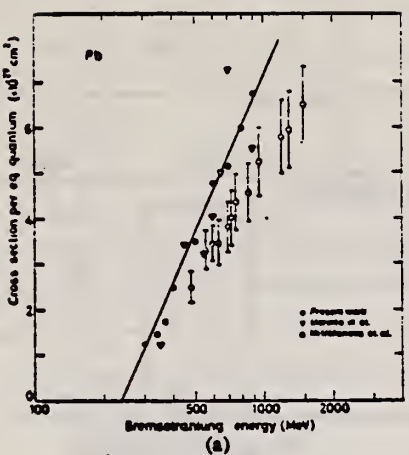
egf

REACTION	RESULT	EXCITATION ENERGY	SOURCE		DETECTOR		ANGLE
			TYPE	RANGE	TYPE	RANGE	
G, F	ABY	THR-900	C	300-900	FRG-I		4PI

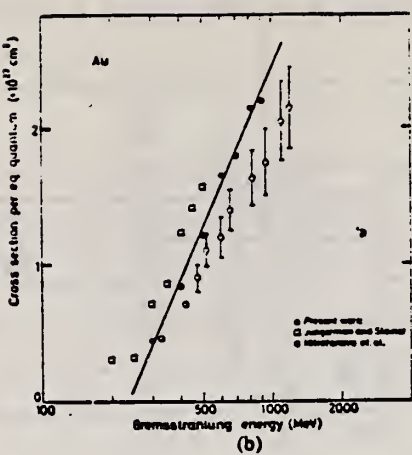
Fig. 2. Nuclear fissilities as a function of Z^2/A .TABLE I
The constant fission cross sections above the threshold

Element	σ_f (cm^2)	Element	σ_f (cm^2)
Pb	$(5.0 \pm 0.2) \times 10^{-27}$	La	$(1.1 \pm 0.1) \times 10^{-29}$
Au	$(1.7 \pm 0.1) \times 10^{-27}$	Sn	$(4.3 \pm 1.1) \times 10^{-29}$
Ta	$(3.3 \pm 0.2) \times 10^{-28}$	Ag	$(8.4 \pm 2.0) \times 10^{-29}$
Yb	$(1.2 \pm 0.2) \times 10^{-28}$	Mo	$(1.7 \pm 0.4) \times 10^{-28}$
Ho	$(5.5 \pm 0.3) \times 10^{-29}$	Cu	$(6.6 \pm 1.2) \times 10^{-29}$
Gd	$(5.3 \pm 0.8) \times 10^{-29}$	Ni	$(5.8 \pm 0.1) \times 10^{-29}$
Nd	$(1.3 \pm 0.2) \times 10^{-29}$		

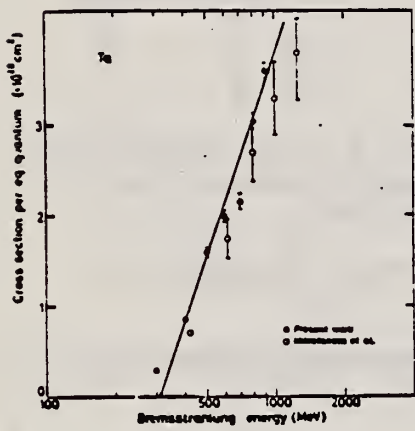
[over]



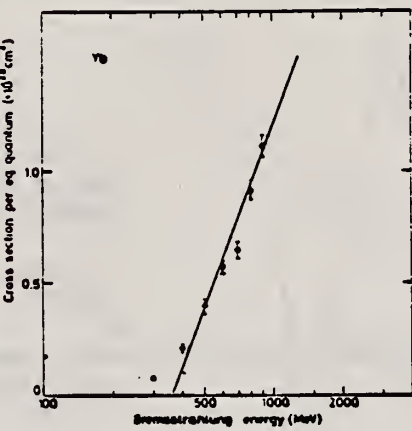
(a)



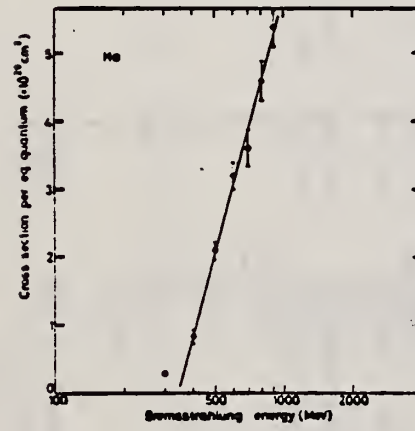
(b)



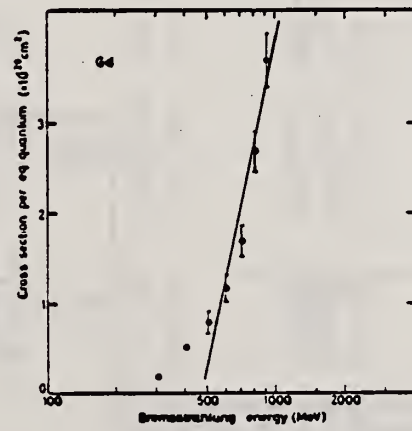
(c)



(d)



(e)



(f)

Fig. 1. Cross sections per equivalent quantum $\sigma_q(E)$ as a function of $\log E$.

R.F. Barrett, J.R. Birkelund, B.J. Thomas, K.S. Lam, and H.H. Thies
 Nucl. Phys. A210, 355 (1973)

ELEM. SYM.	A	Z
Ho	165	67

METHOD

REF. NO.

73 Ba 20

egf

REACTION	RESULT	EXCITATION ENERGY	SOURCE		DETECTOR		ANGLE
			TYPE	γ RANGE	TYPE	RANGE	
G,N	NOX	THR- 27	C	10- 27	BF3-I		4PI

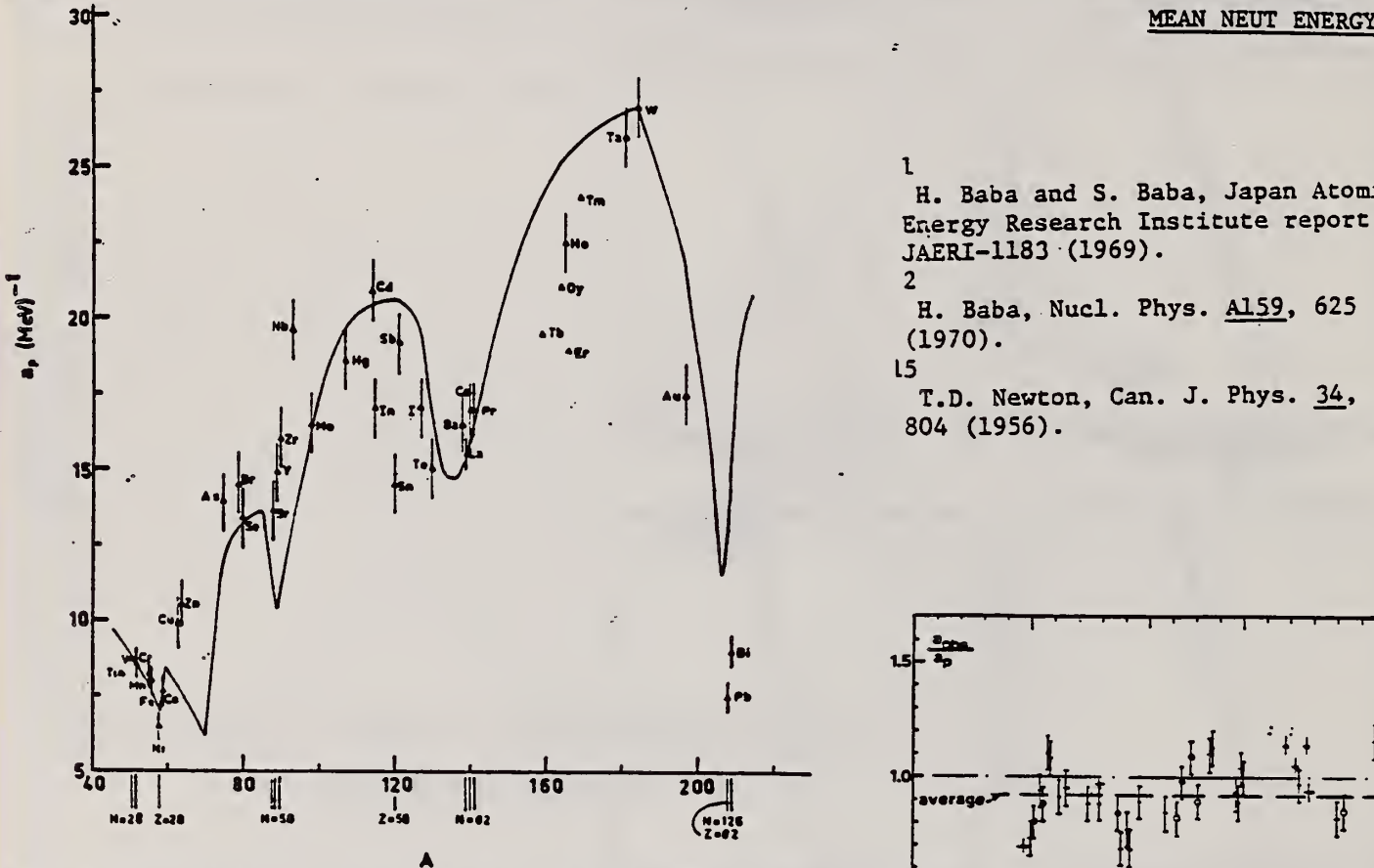


Fig. 12. Experimental values of the level density parameter a_p (Fermi gas formula plus pairing correction) versus atomic number A . The continuous curve is a least-squares fit to the data of a theoretical calculation from Newton ¹⁵.

- 1 H. Baba and S. Baba, Japan Atomic Energy Research Institute report JAERI-1183 (1969).
- 2 H. Baba, Nucl. Phys. A159, 625 (1970).
- 15 T.D. Newton, Can. J. Phys. 34, 804 (1956).

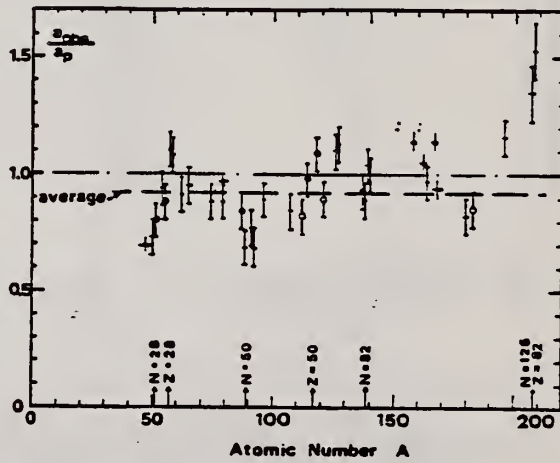


Fig. 15. Ratio a_{res}/a_p versus atomic number A . Here a_{res} is the level density parameter taken from the neutron resonance work of refs. ^{1,2}, and a_p is the level density parameter derived from the present (γ, n) work. Filled circles represent points where nuclei in the neutron resonance and in the (γ, n) experiment were the same. Open circles represent points where the respective nuclei were approximately matched. Triangles represent points which are based on measurement of neutron mean energies at two bremsstrahlung energies only.

(over)

TABLE 3 (continued)

Target	<i>N</i>	Goodness of fit 1) no with p.c.	$E_0(24)$ (MeV) ^{a)}	T	a_p (MeV ⁻¹) ^{b)}	a_{abs} (MeV ⁻¹) ^{c)}	a_{abs}/a_p
Ba	75	1%	F	1.16	16.5- ¹³⁹ Ba	15.39- ¹³⁶ Ba	0.93
	77	2%					
	78	7%					
	79	82%					
	80	11%					
	81	71%	F	1.25	15.5- ¹³⁹ La	13.76- ¹³⁹ La	0.89
	80	100%	F	1.24	17.0- ¹³⁹ Ce	17.8- ¹³⁹ Ce	1.04
	81	89%	F	0.70			
	83	11%	G	1.17	17.0- ¹⁴⁹ Pr	17.05- ¹⁴⁹ Pr	1.00
	81	100%	G	0.65	19.3- ¹⁴⁹ Tb	21.85- ¹⁴⁹ Tb	1.14
	93	100%	G	1.15			
	93	2%	Dy	1.06	20.9- ¹⁶¹ Dy	21.9- ¹⁶¹ Dy	1.05
	94	19%					
	95	25%					
	96	25%					
	97	28%					
	97	100%	P	1.06	21.4- ¹⁴⁴ Ho	20.66- ¹⁴⁴ Ho	0.97
	95	2%	G	1.11	19.2- ¹⁴⁴ Er	21.9- ¹⁴⁴ Er	1.14
	97	33%					
	98	23%					
	99	27%					
	101	15%					
	99	100%					
	107	100%	G	1.00	24.0- ¹⁶⁶ Tm	22.58- ¹⁷⁰ Tm	0.94
	107	26%	G	0.49	26.0- ¹⁶⁶ Ta	21.2- ¹⁶⁷ Ta	0.82
	108	14%	F	0.98	27.0- ¹⁶³ W	23.0- ¹⁶³ W	0.85
	109	31%					
	111	28%					
	117	100%	G	1.19	17.5- ¹⁹⁶ Au	20.24- ¹⁹⁶ Au	1.16
	123	24%	V.P.	1.87	7.5- ²⁰⁹ Pb	10.1- ²⁰⁹ Pb	1.33
(Z = 82)	124	23%					
	125	52%					
	125	100%	F	1.65	9.0- ²⁰⁹ Bi	13.8- ²⁰⁹ Bi	1.53

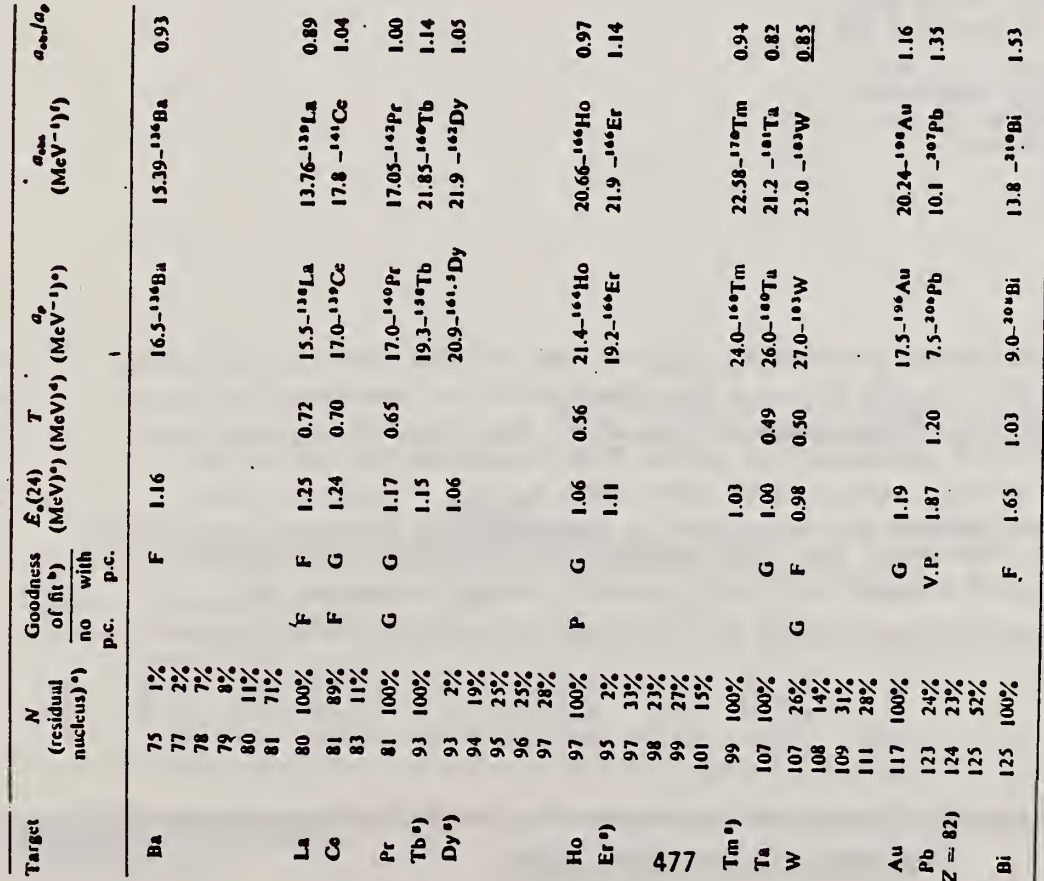


Fig. 10. Same as fig. 5, for praseodymium and holmium.

^{a)} Neutron numbers and abundances of respective residual nuclei in (γ , n) experiments.^{b)} These give an assessment of the goodness of fit of a calculated E_0 versus E_0 curve to the observed data, using the Fermi gas level density formula both without and with pairing corrections.^{c)} Bremsstrahlung photoneutron mean energies E_0 for peak bremsstrahlung energy $E_0 = 24$ MeV.^{d)} Nuclear temperature from fit with constant-temperature formula.^{e)} Level density parameter a_p derived from the present (γ , n) experiment, using a Fermi gas formula plus pairing correction, and corresponding residual nucleus (the atomic weight shown is the weighted average of atomic weights of the respective isotopes present).^{f)} As column 7, but using data on n-resonance absorption from refs. ^{1,2}.^{g)} Measurements of $E_0(E_0)$ for these nuclei were made only for $E_0 = 21, 23$ and 24 MeV.

D.K. Kaipov, Yu.A. Lysikov, and Yu.K. Shubnyi
 Izv. Akad. Nauk SSSR Ser. Fiz. 37, 1095 (1973)
 Bull. Acad. Sci. USSR Phys. Ser. 37, 160 (1973)

ELEM. SYM.	A	Z
Ho	165	67

METHOD

REF. NO.

73 Ka 8

hmg

REACTION	RESULT	EXCITATION ENERGY	SOURCE		DETECTOR		ANGLE
			TYPE	RANGE	TYPE	RANGE	
G,G	ABX	95*	D	95*	SCD-D		UKN

*ENERGY IN KEV

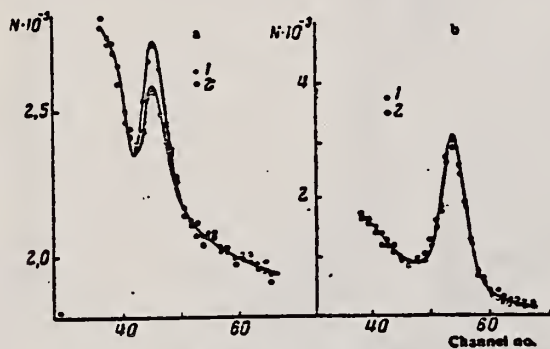


Fig. 2. Scattered radiation spectra: b) with ^{155}Eu source ($E_{\gamma} = 105$ keV). 1) Ho scatterer; 2) (Ta + Cd) scatterer. N is the number of pulses in an interval of 10 min. a) ^{165}Dy source. 1) Ho scatterer; 2) (Ta + Cd) scatterer. N is the number of pulses in an interval of 20 min.

The counting ratio for Ho and Ta + Cd was $N_{\text{Ta}}/N_{\text{Ho}} = 1.065 \pm 0.015$ (this is an average for ten series of measurements). Figure 2a shows the spectrum of the scattered radiation in the region of 100 keV using the ^{165}Dy source. It is clear from this figure that the elastic peak is recorded against a background of strong Compton scattering due to the higher energy ^{165}Dy γ -rays. In this case we have found that $N_{\text{Ta}}/N_{\text{Ho}} = 0.675 \pm 0.118$. The resonance scattering cross section was calculated by comparing the resonance scattering intensities with the Rayleigh intensity, the cross section for which can be calculated exactly. We found that $\sigma = (1.95 \pm 0.35) \cdot 10^{-25} \text{ cm}^2 \cdot \text{sterad}^{-1}$, which corresponds to $\Gamma_{0\gamma} = (4.85 \pm 0.82) \cdot 10^{-6} \text{ ev}$ for the radiation width of the 94.69 keV level of ^{165}Ho , and $\tau_{\gamma} = (1.36 \pm 0.24) \cdot 10^{-10} \text{ sec}$.

METHOD

REF. NO.

74 Ca 7

egf

REACTION	RESULT	EXCITATION ENERGY	SOURCE		DETECTOR		ANGLE
			TYPE	RANGE	TYPE	RANGE	
G, XN	ABX	8- 23	C	8- 23	BF3-I		4PI

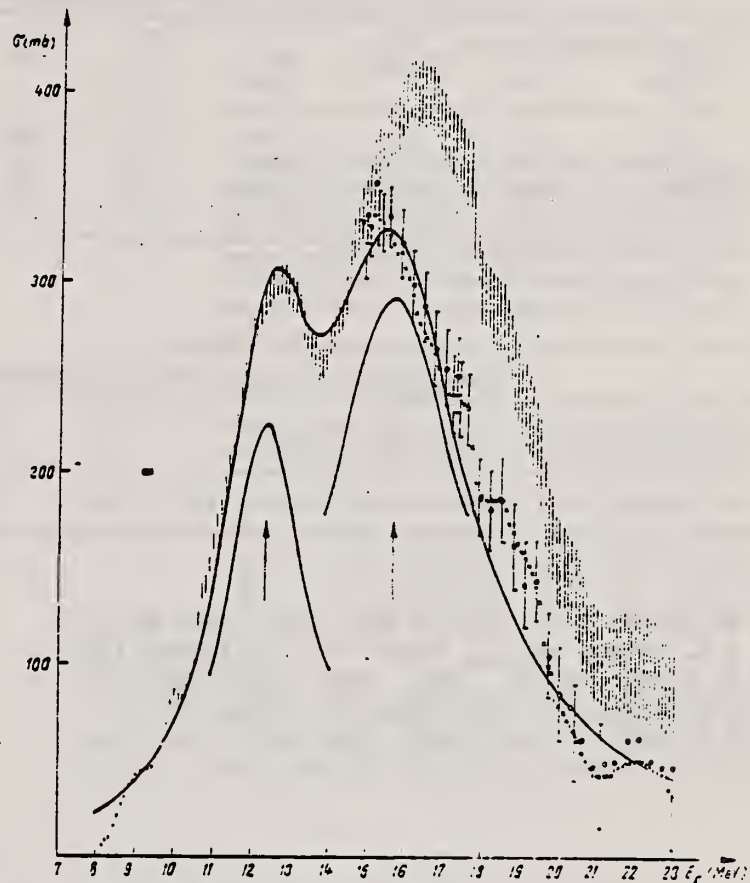


Fig. 1. Total cross section data showing a two Lorentz line fit for ^{165}Ho . The total cross section has been obtained taking into account $\sigma(\gamma, 2n)$ from ref. ³⁾ (○) and from ref. ⁴⁾ (×).

TABLE I
 Comparison between the absolute cross section values for ^{165}Ho

E (MeV)	σ (mb)	E (MeV)	σ (mb)	E_1 (MeV)	σ_1 (mb)	E_2 (MeV)	σ_2 (mb)	Ref.
9	35.6 ± 4	10.83	150 ± 20					¹⁶⁾
9	36 ± 2	10.83	138 ± 6	12.4	290 ± 11	15.3	275 ± 11	³⁾
9	48 ± 5	10.83	165 ± 5	12.2	323 ± 18	15.4	325 ± 18	⁴⁾
9	44 ± 3	10.83	143 ± 8	12.6 ± 0.1	301 ± 10	15.3 ± 0.2	330 ± 18	present

(over)

TABLE 2

Comparison between the Lorentz line parameters for a two line fit of the total cross section data of ^{163}Ho

MET.	E_1	Γ_1	σ_1	E_2	Γ_2	σ_2	$\frac{\int \sigma_2 dE}{\int \sigma_1 dE}$	Ref.
	12.02 ± 0.04	2.35 ± 0.22	236 ± 12	15.59 ± 0.09	4.85 ± 0.4	308 ± 11	2.69	⁵⁾
	12.28 ± 0.025	2.57 ± 0.11	214 ± 15	15.78 ± 0.0044	5.00 ± 0.17	246 ± 18	2.24	³⁾
	12.2	2.33	219	16	5	226	2.60	²⁾
	12.07	2.7	250	15.62	4.8	285	2.07	⁴⁾
	12.30	2.60	225	15.65	4.65	290	2.30	present
	12.15	2.49	204	15.61	4.66	245	2.25	theory

TABLE 3

Integrated cross section, moments of the different measured cross sections and sum rules for ^{163}Ho

σ_{σ} exp. (b · MeV)	σ_{0L} (b · MeV)	$\frac{\sigma_{0L}}{0.06 NZ/A}$	σ_{-1} exp. (mb)	σ_{-1L} (mb)	$\frac{\sigma_{-1L}}{A^{\frac{1}{2}}}$	σ_{-2} exp. (mb · MeV $^{-1}$)	σ_{-2L} (mb · MeV $^{-1}$)	$\frac{\sigma_{-2L}}{A^{\frac{1}{2}}}$	Ref.
2.51	2.81	1.12	166	177	0.20	11.56	13.55	2.73	³⁾
2.79 ± 0.25	3.71	1.34	194 ± 14	208	0.23	14 ± 1	16.07	3.24	⁴⁾
2.60 ± 0.2	3.04	1.27	178 ± 15	171	0.19	12.8 ± 1.5	14.66	2.95	pres
	2.59	1.09		165	0.18		12.35	2.5	

TABLE 4
Parameters used for computation of E1 photoabsorption cross section

ϵ	μ_n $N = 4$	μ_n $N = 5$	μ_n $N = 6$	μ_p $N = 3$	μ_p $N = 4$	μ_p $N = 5$	κ	$\frac{\hbar^2}{2I}$	$\frac{\Delta E (\text{MeV})}{n - p}$	a	$\Gamma (\text{MeV})$
										$\Delta K = 0$	$\Delta K = \pm 1$
0.30	0.45	0.448	0.434	0.35	0.625	0.630	0.05	0.011	0.76	1.05	1.96

- 2) E. Ambler et al., Phys. Rev. 138 (1965) B117
- 3) B.L. Berman et al., Phys. Rev. 125 (1969) 1576
- 4) R. Bergeret et al., Nucl. Phys. A121 (1961) 463
- 5) P. Axel et al., J. de Phys. 27 (1966) 262
- 16) R.R. Hurst et al., Nucl. Phys. A91 (1967) 365

for
in 1
ela:
high
The
inte
exac
= (4
 τ_Y =

METHOD

REF. NO.

75 Ja 1

hmg

REACTION	RESULT	EXCITATION ENERGY	SOURCE		DETECTOR		ANGLE
			TYPE	RANGE	TYPE	RANGE	
G, G	ABX	11	D	11	SCD-D		150
		(11.387)		(11.387)			

TABLE I. Differential cross sections measured for elastic and inelastic scattering of 11.39-MeV photons. States or states populated by inelastic scattering are indicated in parentheses beside the target. The errors given result from the statistical error in the measurement of the cross section relative to the calibration value, the 90° uranium elastic cross section.

θ (deg)	$d\sigma/d\omega$ (elastic) (mb/sr)	$d\sigma/d\omega$ (inelastic) (mb/sr)
^{238}U (2°, 45 keV)		
90	0.169 ± 0.011	0.173 ± 0.016
150	0.355 ± 0.041	0.236 ± 0.24
^{232}Th (2°, 45 keV)		
150	0.331 ± 0.035	0.210 ± 0.022
^{181}Ta ($\frac{1}{2}^+$, 136 keV) ($\frac{1}{2}^+$, 301 keV)		
90	0.073 ± 0.008	0.020 ± 0.004
		0.009 ± 0.004
150	0.145 ± 0.015	0.017 ± 0.004
		0.017 ± 0.004
^{183}Ho ($\frac{3}{2}^+$, 95 keV) ($\frac{3}{2}^+$, 210 keV)		
150	0.141 ± 0.014	0.022 ± 0.004
		0.013 ± 0.004
^{183}Tb ($\frac{3}{2}^+$, 58 keV) ($\frac{1}{2}^+$, 138 keV)		
90	0.062 ± 0.006	0.024 ± 0.003
		0.013 ± 0.003
150	0.134 ± 0.012	0.042 ± 0.004
		0.019 ± 0.004
^{161}Pr		
150	0.030 ± 0.008	...

TABLE III. Comparison of calculated and observed values of the cross sections for elastic scattering and of the ratio of Raman to elastic scattering by various nuclei for 11.387-MeV photons at 90 and 150°. The parameters used in the calculations for column 5 are given in Table II. Column 4 describes results obtained by perturbing those parameter to meet the constraint of Eq. (3) (see text).

Target	Calc.	Exp.	$d\sigma(\theta)/d\Omega$ (mb/sr)	$d\sigma_{\text{Raman}}(\theta)/d\sigma_{\text{elastic}}(\theta)$
			$\theta = 150^\circ$	
Pr	0.025	0.030 ± 0.008		0.0 0.0
Tb	0.094	0.134 ± 0.012	0.53 0.57	0.46 ± 0.04
Ho	0.170	0.141 ± 0.014	0.28 0.28	0.25 ± 0.04
Ta	0.160	0.145 ± 0.015	0.23 0.22	0.23 ± 0.04
Th	0.253	0.331 ± 0.035	0.59 0.63	0.64 ± 0.08
U	0.289	0.355 ± 0.041	0.78 0.73	0.67 ± 0.07
$\theta = 90^\circ$				
Tb	0.062	0.062 ± 0.008	0.76 0.82	0.60 ± 0.07
Ta	0.109	0.074 ± 0.008	0.32 0.30	0.38 ± 0.07
U	0.172	0.169 ± 0.009	1.29 1.15	1.03 ± 0.10

ELEM. SYM.	A	Z
Hg	165	67

METHOD

REF. NO.
76 Em 2

REACTION	RESULT	EXCITATION ENERGY	SOURCE		DETECTOR		ANGLE
			TYPE	RANGE	TYPE	RANGE	
G,F	ABY	THR-999	C	999	TRK-I		4PI

TABLE I

Measured values of σ_q at $E = 1000$ MeV and deduced values of σ_t assumed constant from E_0 to 1000 MeV

Element	Z^2/A	σ_q (mb)	E_0 (MeV)	σ_t (mb)
Bi	32.96	12.3 ± 0.6	200	7.6 ± 0.6
Pb	32.45	5.4 ± 0.4	220	3.6 ± 0.3
Tl	32.10	4.1 ± 0.3	230	2.8 ± 0.3
Au	31.68	2.0 ± 0.15	240	1.4 ± 0.2
Pt	31.18	1.1 ± 0.08	255	$(8 \pm 0.7) \times 10^{-1}$
Re	30.21	$(3.7 \pm 0.3) \times 10^{-1}$	280	$(2.9 \pm 0.3) \times 10^{-1}$
W	29.78	$(3.5 \pm 0.3) \times 10^{-1}$	290	$(2.8 \pm 0.3) \times 10^{-1}$
Ta	29.45	$(3.3 \pm 0.3) \times 10^{-1}$	300	$(2.7 \pm 0.3) \times 10^{-1}$
Hf	29.04	$(1.7 \pm 0.2) \times 10^{-1}$	310	$(1.4 \pm 0.2) \times 10^{-1}$
Yb	28.31	$(1.3 \pm 0.1) \times 10^{-1}$	330	$(1.2 \pm 0.1) \times 10^{-1}$
Tm	28.18	$(7.5 \pm 0.8) \times 10^{-2}$	335	$(6.8 \pm 0.8) \times 10^{-2}$
Ho	27.21	$(3.6 \pm 0.4) \times 10^{-2}$	355	$(3.5 \pm 0.4) \times 10^{-2}$
Dy	26.80	$(2.6 \pm 0.3) \times 10^{-2}$	360	$(2.5 \pm 0.3) \times 10^{-2}$
Tb	26.58	$(2.5 \pm 0.3) \times 10^{-2}$	370	$(2.5 \pm 0.3) \times 10^{-2}$
Gd	26.04	$(1.6 \pm 0.2) \times 10^{-2}$	380	$(1.7 \pm 0.2) \times 10^{-2}$
Sm	25.56	$(1.3 \pm 0.2) \times 10^{-2}$	390	$(1.4 \pm 0.2) \times 10^{-2}$
Nd	24.96	$(9.2 \pm 0.9) \times 10^{-3}$	405	$(1 \pm 0.1) \times 10^{-2}$
Ce	24.00	$(8 \pm 0.9) \times 10^{-3}$	420	$(9 \pm 1) \times 10^{-3}$
La	23.39	$(8.4 \pm 0.9) \times 10^{-3}$	430	$(1 \pm 0.1) \times 10^{-3}$
Sb	21.36	$(1.2 \pm 0.2) \times 10^{-3}$	460	$(1.5 \pm 0.3) \times 10^{-3}$
Te	21.19	$(8.8 \pm 1) \times 10^{-3}$	465	$(1.2 \pm 0.2) \times 10^{-3}$
Sn	21.06	$(1.3 \pm 0.2) \times 10^{-3}$	465	$(1.7 \pm 0.3) \times 10^{-3}$
Cd	20.49	$(1.7 \pm 0.3) \times 10^{-3}$	470	$(2.2 \pm 0.4) \times 10^{-3}$
Ag	20.47	$(2 \pm 0.3) \times 10^{-2}$	470	$(2.6 \pm 0.4) \times 10^{-3}$
Zn	13.76	$(2 \pm 0.4) \times 10^{-1}$	515	$(3 \pm 0.6) \times 10^{-1}$
Cu	13.44	$(2.4 \pm 0.5) \times 10^{-1}$	515	$(3.6 \pm 0.8) \times 10^{-1}$
Ni	13.35	$(2.4 \pm 0.5) \times 10^{-1}$	510	$(3.6 \pm 0.8) \times 10^{-1}$
Fe	12.10	$(3 \pm 0.6) \times 10^{-1}$	510	$(4.4 \pm 0.9) \times 10^{-1}$

- ⁴ A.V. Mitrofanova et al., Sov. J. Nucl. Phys. **6**, 512 (1968).
⁷ T. Methasiri et al., Nucl. Phys. **A167**, 97 (1971).
¹² J.R. Nix et al., Nucl. Phys. **81**, 61 (1966).
²⁰ N.A. Perifilov et al., JETP (Sov. Phys.) **14**, 623 (1962); Proc. Symp. on the physics & chemistry of fission, Salzburg 1965, vol. 2 (IAEA) Vienna, 1965, p. 283.

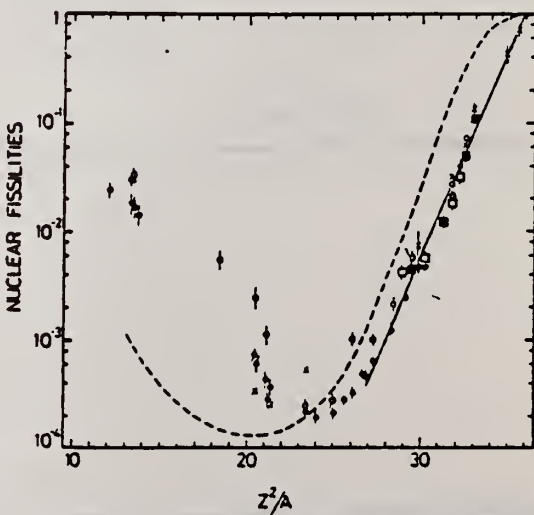


Fig. 2. Nuclear fissilities as a function of Z^2/A . Experimental points: solid circles represent our data; squares, the data from ref.⁴; open circles, the data from ref.⁷; and crosses, the data from (p,n) experiments²⁰. The straight line is the best fit calculated from our data for $Z^2/A > 26$. The dashed curve is the curve VI calculated by Nix and Sassi¹².

METHOD

REF. NO.

76 Go 4

hmg

REACTION	RESULT	EXCITATION ENERGY	SOURCE		DETECTOR		ANGLE
			TYPE	RANGE	TYPE	RANGE	
G, XN	ABX	8- 23	C	UKN	BF3-I		4PI
G, 2N	ABX	14- 21	C	UKN	SCI-I		4PI

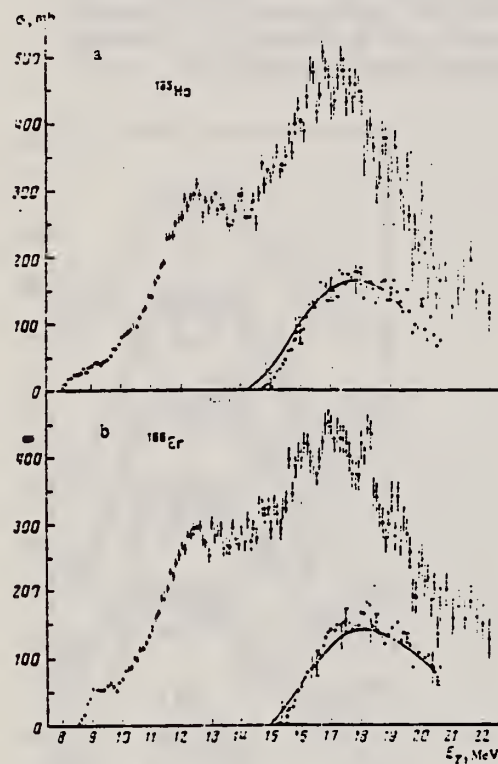


FIG. 1. Photoneutron production cross section σ_n obtained for ^{145}Ho (a) and for ^{146}Er (b). The hollow and solid circles correspond to two independent series of data. The solid curves show the $(\gamma, 2n)$ cross sections calculated from the data of a statistical experiment by the regularization method.^[12] The circles near the curves give the same cross sections calculated from the formula $\sigma_n(1 - f(E, \alpha))$.

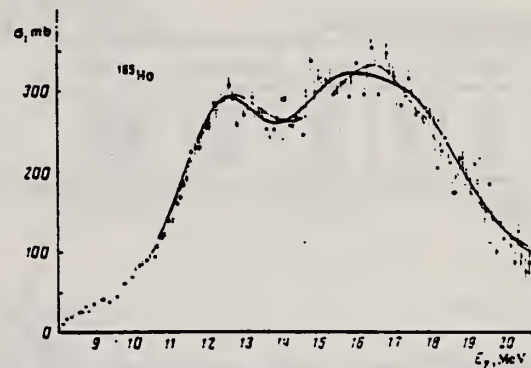


FIG. 5. Cross section σ for ^{145}Ho . The thin and thick curves show respectively the approximations $\sigma_\gamma^{(1)}$ and $\sigma_\gamma^{(3)}$ (see the caption to Fig. 3).

TABLE 3. Static deformation β and intrinsic quadrupole moment Q_0 .

Nucleus	Present work		Other photonuclear experiments		Coulomb excitation of nuclei
	β	Q_0 b	β	Q_0 b	
^{145}Tb	0.29	6.33 ± 0.6	0.29	$6.37 [13]$	
^{145}Ho	0.32	7.73 ± 0.6	0.29	$7.37 [2]$	
^{146}Er	0.30	7.39 ± 0.6	0.28	$7.01 [13]$	
^{178}Hf	0.28	6.94 ± 0.6	0.31	$7.14 [2]$	$7.80 [13]$
				$7.8 [14]$	
				$6.6 [14]$	
				$6.79 [2]$	

TABLE 1. Level-density parameters

Nucleus	a , MeV $^{-1}$		Nucleus	a , MeV $^{-1}$	
	Present work	Other studies		Present work	Other studies
^{158}Tb	—	$7.7 [15]$	^{145}Er	6.1 ± 2.5	$8 [14]$
^{145}Ho	4.2 ± 1.5	$3.1 [15]$	^{178}Hf	17.7 ± 7.3	—

(over)

TABLE 2. Parameters of fitted curves $\bar{\Gamma}_j^{(1)}$,

Nucleus	E_1 , MeV	σ_1 , mb	Γ_1 , MeV	E_2 , MeV	σ_2 , mb	Γ_2 , MeV	$\sigma_2 \Gamma_2 / \sigma_1 \Gamma_1$	τ^*	β	E_{γ} , MeV	E_{ν} , MeV
^{150}Tb	12.28	172	1.91 ± 0.09	13.78	295	3.42 ± 0.13	1.56 ± 0.23	197.3	97	10.4	20.6
	12.41	213	3.31 ± 0.03	13.93	292	3.01 ± 0.07	2.16 ± 0.2	216.8	98	10.4	20.6
^{151}Ho	12.31	204	2.74 ± 0.11	16.23	306	3.67 ± 0.17	3.11 ± 0.27	176.0	97	10.4	20.6
	12.47	223	2.25 ± 0.06	16.46	293	3.02 ± 0.09	2.00 ± 0.2	200.3	98	10.4	20.6
^{152}Er	12.32	191	2.71 ± 0.14	13.99	316	3.67 ± 0.16	2.38 ± 0.35	133.5	94	10.7	20.6
	12.50	214	3.43 ± 0.08	16.25	294	3.08 ± 0.10	2.1 ± 0.2	101.7	93	10.7	20.6
^{153}Dy	12.68	166	2.55 ± 0	15.03	281	6.01 ± 0.27	4.00 ± 1.70	172.4	89	10.6	20.0
	12.88	216	3.22 ± 0.11	15.46	237	3.37 ± 0.20	2.13 ± 0.2	133.7	90	10.6	20.0

Note. The lower values of the parameters in each column were found with the requirement $\sigma_2 \Gamma_2 : \sigma_1 \Gamma_1 = 2:1$.

TABLE 6. Integrated cross sections.

Nucleus	σ_{int} , MeV \cdot b	$\sigma_{int} \frac{Z^2 Y}{A}$	σ_{int} , mb	$\sigma_{int} A\%$	σ_{int} , MeV \cdot b	$\sigma_{int} A\%$
^{150}Tb	2.09	1.47	210	0.243	15.9	$3.41 \cdot 10^{-4}$
^{151}Ho	1.00	1.51	218	0.241	16.1	$3.27 \cdot 10^{-4}$
^{152}Er	1.36	1.48	216	0.237	16.1	$3.21 \cdot 10^{-4}$
^{153}Dy	3.08	1.29	196	0.196	14.8	$2.93 \cdot 10^{-4}$
Average		1.41 ± 0.3		0.23 ± 0.04		$3.1 \cdot 10^{-4} \pm 6 \cdot 10^{-5}$

¹²A.N. Tikhonov, Dokl. Akad. Nauk SSSR 151, 501 (1963),
Eng. transl. in Sov. Mathematics-Doklady.

¹⁵B. L. Berman et al., Phys. Rev. 185, 1576 (1969).

¹⁶R. Bergere et al., Nucl. Phys. A133, 417 (1969).

¹⁸E. G. Fuller et al., Nucl. Phys. 30, 613 (1962).

¹⁹H. Arenhovel et al., Phys. Rev. 157, 1109 (1967).

²⁰R. Bergere et al., Nucl. Phys. A121, 463 (1968).

²¹O.V. Bogdankevich et al., Zh. Eksp. Teor. Fiz. 42,
1502 (1962); Sov. Phys. JETP 15, 1044 (1962).

²²B.S. Dzhelepov in Struktura slozhnykh yader
(Structure of Complex Nuclei), Atomizdat, 1966, p. 189.

ELEM. SYM.	A	Z
REF. NO.	Ho	165
	76 Gu 5	hmg

METHOD

REACTION	RESULT	EXCITATION ENERGY	SOURCE		DETECTOR		ANGLE
			TYPE	RANGE	TYPE	RANGE	
G, MU-T	ABX	8-21	C	35	NAI-D		4PI

We measured the total cross section for the absorption of rays in the region of $E1$ resonance for the nuclei ^{165}Ho , ^{178}Hf , ^{180}Hf , ^{181}Ta , ^{182}W , ^{197}Au , and ^{209}Bi . The singularity in the behavior of the resonance widths, observed in the region $160 < A < 185$, is apparently due to the influence of the neutron subshell $N = 108$.

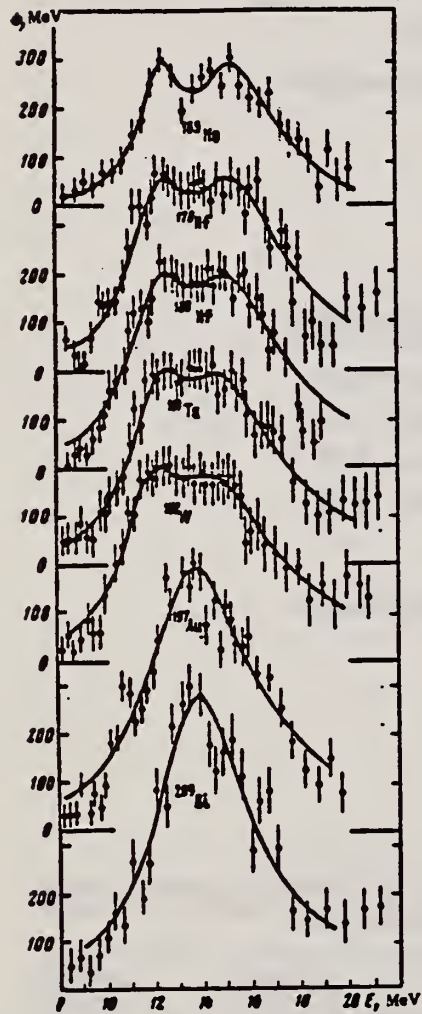


FIG. 1. Total photoabsorption cross sections for the nuclei ^{165}Ho , ^{178}Hf , ^{180}Hf , ^{181}Ta , ^{182}W , ^{197}Au , ^{209}Bi .

USCOMM-NBS-OC

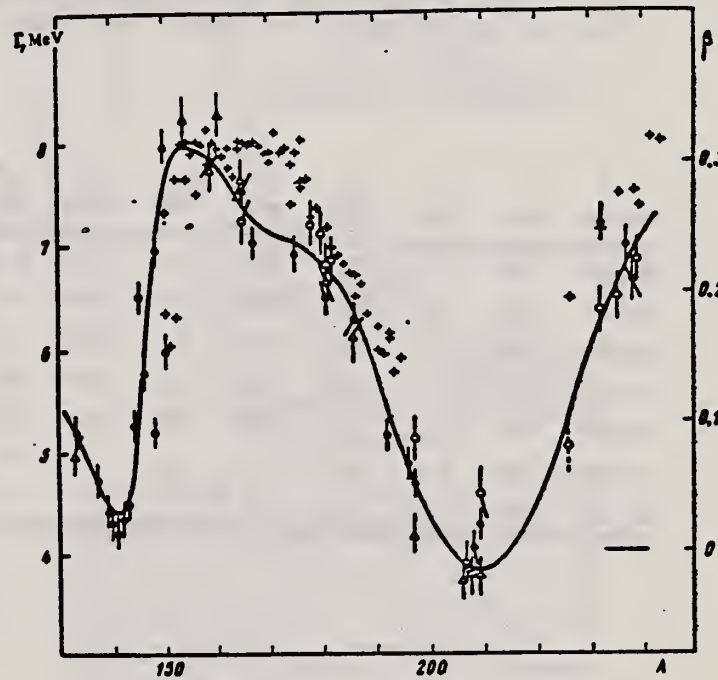


FIG. 2. Widths Γ of $E1$ giant resonance in the region of nuclei with $A > 150$ according to the data of Saclay (●), Livermore (Δ), and the Institute of Nuclear Research of the USSR Academy of Sciences (○). The crosses mark the deformation parameters β .

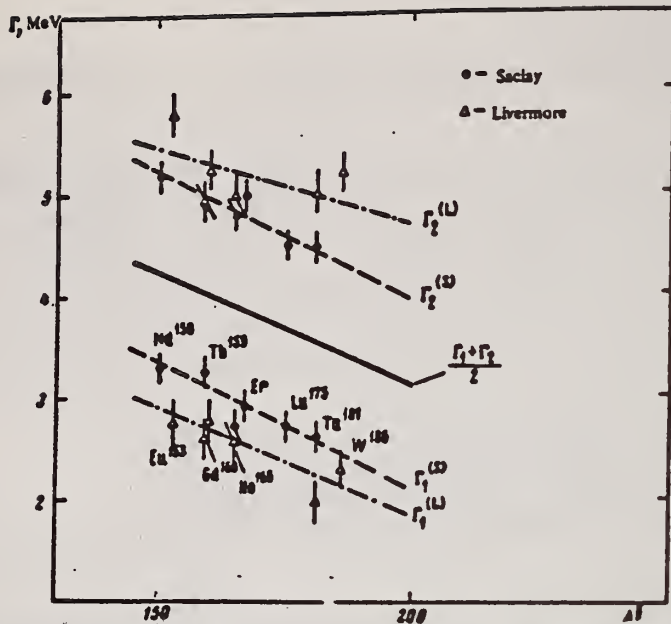


FIG. 3. Width of Lorentz lines approximating the photoabsorption cross sections, for deformed nuclei in the region $150 < A < 185$.

Nucleus	σ_1 mb	Γ_1 MeV	E_1 MeV	σ_2 mb	Γ_2 MeV	E_2 MeV	$\frac{\sigma_2 \Gamma_1}{\sigma_1 \Gamma_2}$	Q_0 b	β
Ho-165	235	2.0	12.2	272	4.0	15.5	2.3	6.8 ± 0.8	0.29
Hf-178	291	3.1	12.2	334	4.9	15.5	1.8	7.5 ± 0.8	0.28
Hf-180	286	3.2	12.2	324	5.1	15.3	1.8	7.2 ± 0.8	0.27
Ta-181	272	3.0	12.1	316	5.1	15.0	2.0	6.8 ± 0.8	0.26
W-182	267	3.2	11.9	303	5.6	14.8	2.0	7.2 ± 0.8	0.26
Au-197	535	5.2	13.7
Bi-209	600	4.6	13.8

METHOD

REF. NO.

76 Mo 11

egf

REACTION	RESULT	EXCITATION ENERGY	SOURCE		DETECTOR		ANGLE
			TYPE	RANGE	TYPE	RANGE	
E,E/	ABX	7- 40	D	75,105	MAG-D		75

Inelastic electron scattering confirms broadening of the isoscalar ($\Delta T=0$) E2 giant resonance in ^{165}Ho as compared to spherical nuclei. Discrepancies in magnitude between results of other experiments are reconciled. The isovector ($\Delta T=1$) E2 giant resonance is, for the first time, observed to be split into at least two parts.

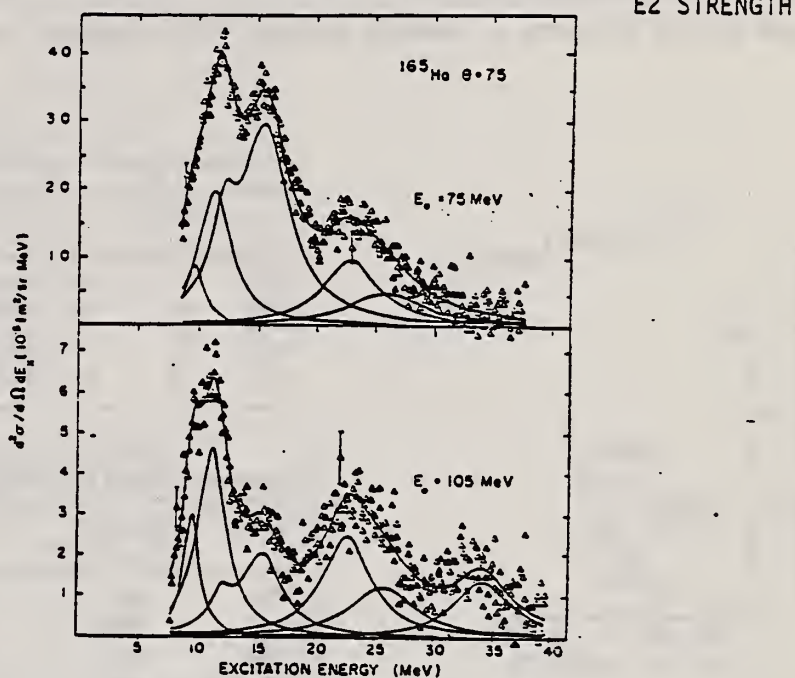


Fig. 1. Spectrum of 75 and 105 MeV electrons, scattered inelastically from ^{165}Ho at a scattering angle of 75° . The resolution is 500 keV. The background which consists of the radiation tail and the machine background has been subtracted. Note that the relative strength of the E1 and E2 resonances more than reverses, if one goes from 75 MeV to 105 MeV. Typical raw spectra; i.e., background not subtracted, may be found in Ref. ⁴. The form of the E1 resonance was taken from (γ, n) measurements (Ref. ⁵); the height was fitted. The energy weighted sum rule exhaustion found for the E1 resonance is 108%, in excellent agreement with the values reported in Ref. ⁶, thus proving the reliability of the background subtraction.

Table 1. Comparison of the natural width of E2 ($\Delta T=0$) resonances in spherical and deformed nuclei. The fifth column shows that the splitting of the giant dipole resonance, i.e., the deformation of the nucleus at about 14 MeV excitation energy, is practically identical in the deformed nuclei considered.

Excitation Method	$\Gamma_{\text{spherical}}$ [MeV]	Γ_{deformed} [MeV]	$\Delta\Gamma$ [MeV]	$\Delta E1$ [MeV] ^a	$E_2 \cdot B(E2)$ [%]
(e,e')	$2.8 \pm 0.2 (^{148}\text{Nd})$ ^b	$5.0 \pm 0.2 (^{150}\text{Nd})$ ^b	2.2	3.74	88
(α,α')	$3.9 \pm 0.2 (^{144}\text{Sm})$ ^c	$4.7 \pm 0.3 (^{151}\text{Sm})$ ^c	0.8	3.57	102
(e,e')	$2.8 \pm 0.2 (^{148}\text{Ce})$ ^d	$4.0 \pm 0.4 (^{165}\text{Ho})$ ^e	1.2	3.53	75
	$2.8 \pm 0.3 (^{208}\text{Pb})$				

^a Ref. ⁸; ^b Ref. ⁷; ^c Ref. ⁸; ^d Ref. ^{1,4}; ^e this work.

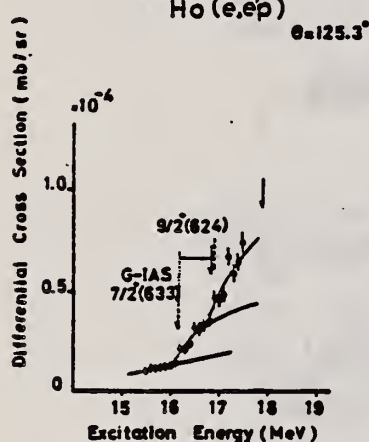
ELEM. SYM.	A	Z
Ho	165	67

METHOD

REF. NO.	76 Su 2	egf
----------	---------	-----

REACTION	RESULT	EXCITATION ENERGY	SOURCE		DETECTOR		ANGLE
			TYPE	RANGE	TYPE	RANGE	
E,p	ABX	11- 18	D	15- 18	MAG-D		125

Proton yields obtained by summing protons with energies above levels given in tables.

Fig. 3. Cross section of the $^{165}\text{Ho}(e, e'p)$ reaction. See also the caption to fig. 2.

Target	Atomic number	Purity (%)	Thickness (mg/cm ²)	Lowest proton energy (MeV)	Bin size (keV)	Range of measurement (MeV)
^{158}Tb	65	99.9 (natural)	14.87	4.70	100	15.0 -17.5
^{165}Ho	67	99.9 (natural)	11.64	4.70	100	15.5 -17.5
^{169}Tm	69	99 (natural)	13.40	4.70	100	15.0 -18.0
^{175}Lu	71	99.87 (enriched)	5.24	5.34	150	15.05-20.0
^{181}Ta	73	99.9 (natural)	6.73	6.16	200	16.0 -23.0

Target	Resonance	Displacement energies obtained from the present data and the estimates with eqs. (20) and (21)			
		E^* (MeV)	E_d (exp) (MeV)	E_d^* (MeV)	$E_d(\delta = 0.3)^a$ (MeV)
^{158}Tb	1st	15.75 ± 0.15	15.58		
	2nd	16.50 ± 0.15	15.46	16.06	15.93
^{165}Ho	1st	16.15 ± 0.14	15.64	16.38	16.25
	2nd	16.34 ± 0.14	16.22	16.76	16.63
^{169}Tm	1st	15.76 ± 0.13	16.20		
	2nd	16.34 ± 0.14	16.22	16.76	16.63
^{175}Lu	1st	16.44 ± 0.13	16.75		
	2nd	17.45 ± 0.15	16.35	17.07	16.93
^{181}Ta	1st	17.31 ± 0.15	16.40	17.38	17.24

^a) Estimated with eq. (20).^b) Estimated with eq. (21).TABLE 4
Deformation parameters of IAS δ_{IAS} derived from the (e, e'p) result

Target	Resonance	IAS	Parent state	$\delta_{\text{IAS}} - \delta_p^*$	δ_p (assumed)	δ_{IAS}^*
^{158}Tb	1st	$\frac{1}{2}^- [521]$	ground	-0.008	0.31	0.30
	2nd	$\frac{1}{2}^- [312]$	875 keV	-0.016		0.29
^{165}Ho	1st	$\frac{1}{2}^+ [633]$	ground	-0.023	0.30	0.28
	2nd	$\frac{1}{2}^- [521]$	ground	-0.018	0.29	0.27
^{169}Tm	1st	$\frac{1}{2}^- [521]$	ground	-0.018	0.29	0.27
	2nd	$\frac{1}{2}^- [510]$	565 keV	-0.019		0.27
^{175}Lu	1st	$\frac{1}{2}^+ [514]$	ground	-0.010	0.28	0.27
	2nd	$\frac{1}{2}^+ [503]$	1420 keV	-0.029		0.25
^{181}Ta	1st	$\frac{1}{2}^+ [503]$	670 keV	-0.046	0.26	0.21

The assumed deformation parameters for the parent states δ_p are also shown.*) The errors are about ± 0.01 .

ELEM. SYM.	A	Z
Ho	165	67
REF. NO.	77 Ba 7	egf

METHOD

REACTION	RESULT	EXCITATION ENERGY	SOURCE		DETECTOR		ANGLE
			TYPE	RANGE	TYPE	RANGE	
G,G	ABX	8- 12	D	8- 12	SCD-D		DST

Abstract: Differential cross sections for elastic and inelastic Raman scattering from the deformed heavy nuclei ^{169}Tb , ^{165}Ho and ^{237}Np were measured at five energies between 8.5 and 11.4 MeV. Angular distributions at four angles between 90° and 140° for both elastic and inelastic scattering at 9.0 and 11.4 MeV were also measured. The monoenergetic photons were obtained from thermal neutron capture in Ni and Cr. All the angular distributions and the elastic and Raman scattering at the higher energies are in good overall agreement with theoretical predictions. The theory is based on a modified simple rotator model of the giant dipole resonance in which the effect of Delbrück scattering was included. A trend of both the elastic and Raman scattering at lower energies to be stronger than expected was suggested by the data. However, the ratio between the Raman and elastic scattering seem to be in good agreement with theory throughout the whole energy range. This shows that there is no need to introduce a direct nonresonant component to the imaginary part of the elastic scattering amplitude to explain the experimental data.

158

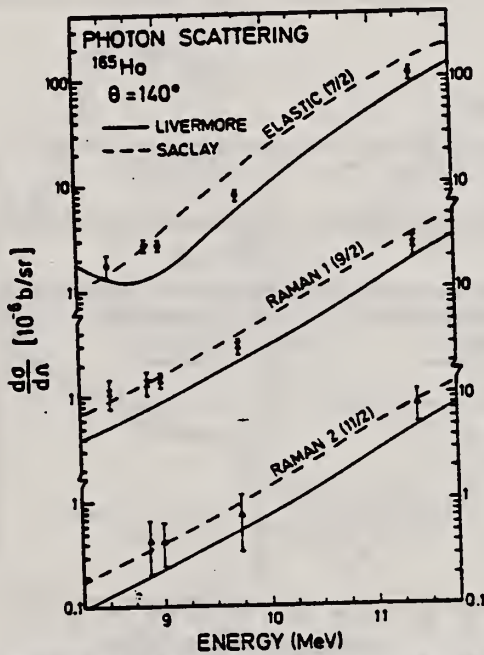


Fig. 4. Elastic and Raman inelastic differential scattering cross sections from ^{165}Ho at 140° . In the solid and dashed lines, the nuclear resonance amplitudes were obtained using parameters extracted from fits made to the Livermore and Saclay measurements respectively. (See text, table 3 and caption to fig. 3.)

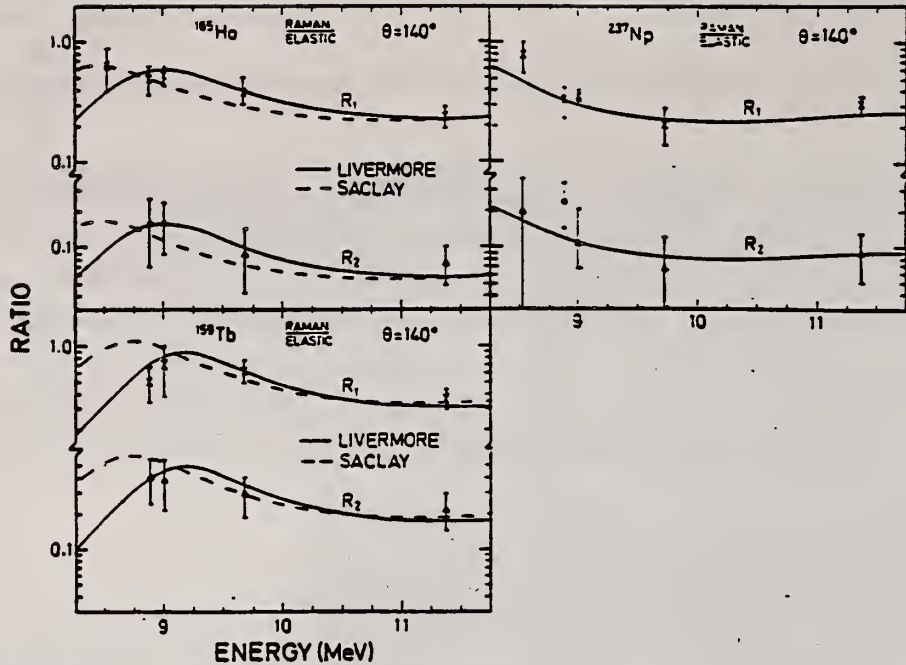


Fig. 6. Ratios of Raman/elastic scattering cross sections at 140° for ^{237}Np , ^{165}Ho and ^{159}Tb targets. Here, R_1 and R_2 refer to the first and second Raman lines. In the solid and dashed lines, the nuclear resonance amplitudes were obtained using parameters extracted from fits made to the Livermore and SACLAY measurements respectively. (See text, table 3 and caption to fig. 3.)

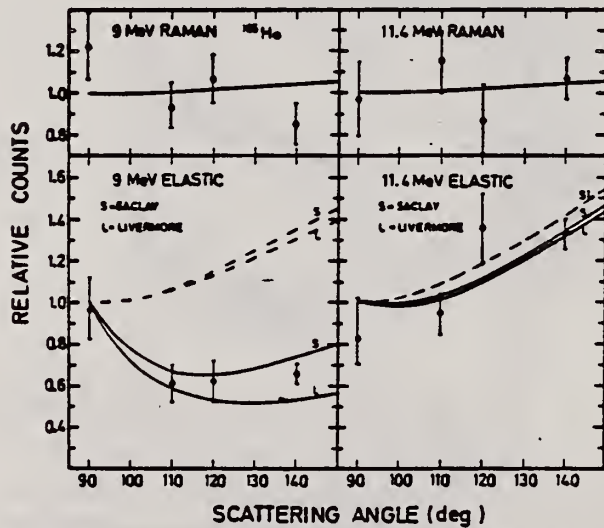


Fig. 8. Angular distributions of elastic and inelastic Raman scattered lines from ^{165}Ho . Here, S and L indicate calculated values where the nuclear resonance amplitudes were extracted from the (γ , n) data of SACLAY and Livermore. See caption to fig. 7.

ELEM. SYM.	A	Z
Ho	165	67

METHOD

REF. NO.	
77 Mu 3	egf

REACTION	RESULT	EXCITATION ENERGY	SOURCE		DETECTOR		ANGLE
			TYPE	RANGE	TYPE	RANGE	
E,A	ABX	14-100	D	100	MAG-D		50

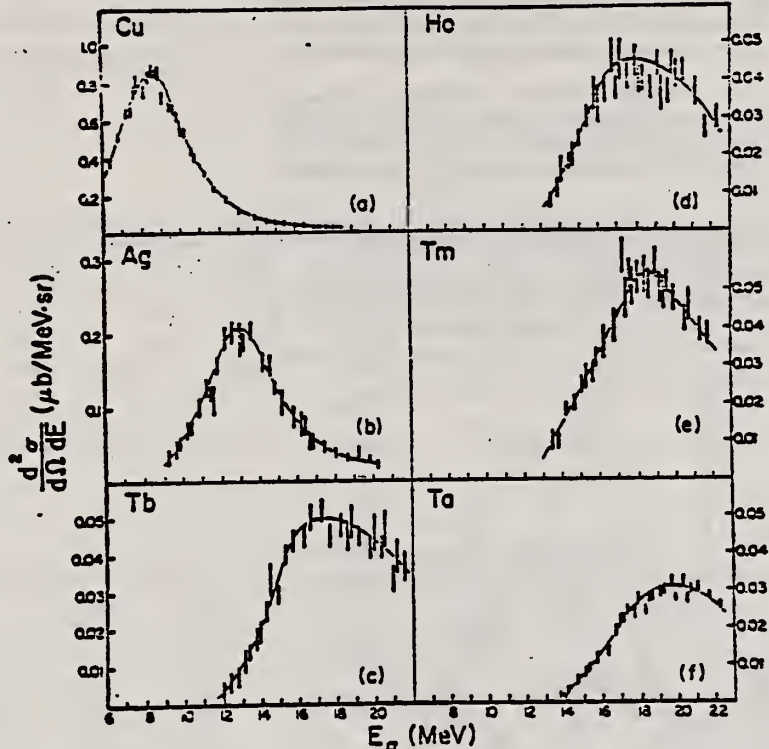


Fig. 1. The α -particle energy spectra at 50° in the lab for the six nuclei studied. Note that as Z increases, the cross section decreases and the energy of the peak increases. Errors are statistical. Curves are to guide the eye.

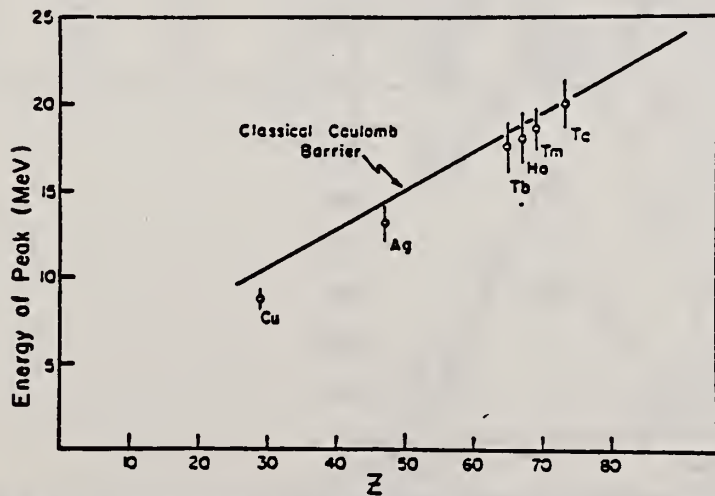


Fig. 2. Energy of the cross section peak as a function of Z . The solid line is the energy of the classical Coulomb barrier.

ELEM. SYM.	A	Z
Ho	165	67

METHOD

REF. NO.

81 Gu 2

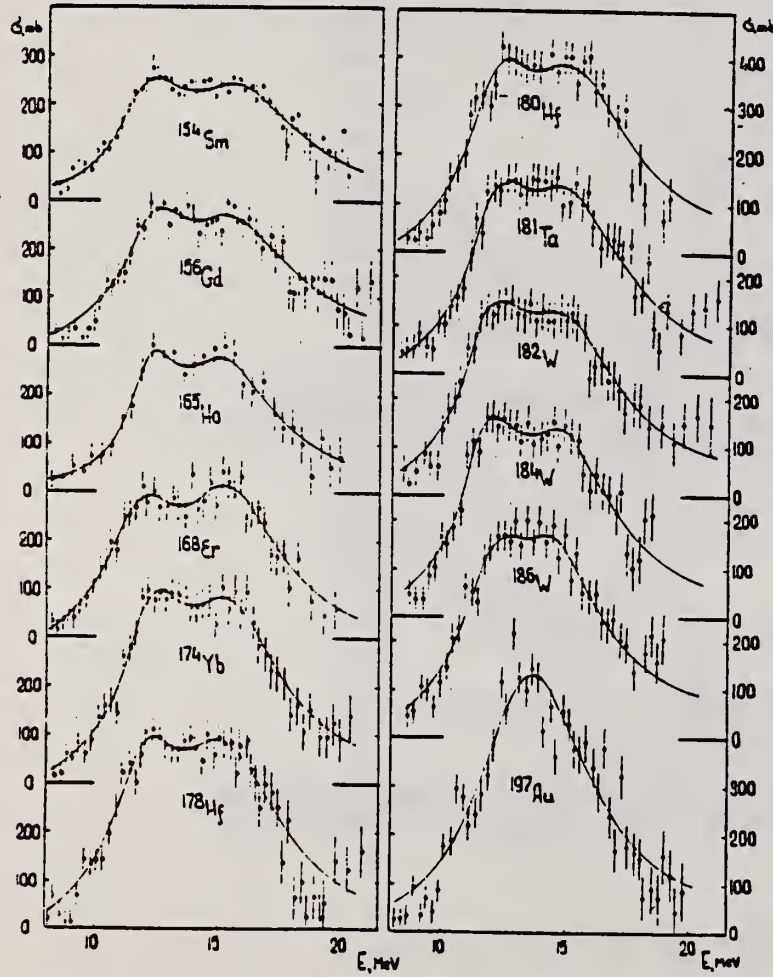
hg

REACTION	RESULT	EXCITATION ENERGY	SOURCE	DETECTOR	ANGLE	
			TYPE	RANGE		
G.MII-T	ARX	THR-20	C	27	NAT-D	4PI

Abstract: The curves of the total gamma-absorption cross sections (σ_{tot}) in the E1 giant resonance energy range for the nuclei ^{154}Sm , ^{156}Gd , ^{165}Ho , ^{168}Er , ^{174}Yb , 178 - ^{180}Hf , ^{181}Ta , ^{182}W , ^{186}W and ^{197}Au have been measured using the absorption method. Parameters of the Lorentz curves fitting the measured cross sections σ_{tot} are given. Quadrupole moments (Q_0) and nuclear deformation parameters (β) were obtained.

For deformed nuclei in the $\sim 155 < A < \sim 180$ region a violation of the correlation between giant resonance widths (Γ) and nuclear deformation parameters was found. Γ_1 and Γ_2 , the widths of the resonances corresponding to vibrations of nucleons along and across the nuclear deformation axis, were observed to decrease with the increase of A which could be accounted for by the presence of an $N = 108$ subshell.

E NUCLEAR REACTIONS ^{154}Sm , ^{156}Gd , ^{165}Ho , ^{168}Er , ^{174}Yb , 178 - ^{180}Hf , ^{181}Ta , 182 - ^{184}W , ^{197}Au (γ , X). $E = 7$ - 20 MeV; measured total $\sigma(E)$; deduced integrated σ . Lorentz line parameters. ^{154}Sm , ^{156}Gd , ^{165}Ho , ^{168}Er , ^{174}Yb , 178 - ^{180}Hf , ^{181}Ta , 182 - ^{184}W , ^{197}Au deduced β , Q_0 , Γ , giant resonance evolution. Enriched, natural targets.



(OVER)

Fig. 2. Total nuclear gamma-absorption cross sections (σ_{tot}) measured by the absorption method for ^{154}Sm , ^{156}Gd , ^{165}Ho , ^{168}Er , ^{174}Yb , 178 - ^{180}Hf , ^{181}Ta , 182 - ^{184}W , ^{186}W and ^{197}Au . Rms error bars are shown.

TABLE 2

Parameters of Lorentz curves fitting the experimental data on σ_{tot}

Nucleus	E_1 (MeV)	σ_1 (mb)	Γ_1 (MeV)	E_2 (MeV)	σ_2 (mb)	Γ_2 (MeV)	$\frac{\sigma_2 \Gamma_2}{\sigma_1 \Gamma_1}$	Γ (MeV)
^{154}Sm	12.2	188	3.4	15.7	207	5.7	1.85	8.1
^{156}Gd	12.3	206	3.2	15.7	220	5.5	1.81	7.7
^{165}Ho	12.3	202	2.3	15.2	239	4.8	2.47	7.0
^{168}Er	11.9	222	3.2	15.5	275	4.5	1.73	7.4
^{174}Yb	12.3	297	2.9	15.5	320	4.9	1.80	7.1
^{178}Hf	12.2	291	3.1	15.5	334	4.9	1.80	7.2
^{180}Hf	12.2	286	3.2	15.3	324	5.1	1.81	7.1
^{181}Ta	12.1	272	3.0	15.0	316	5.1	1.97	6.8
^{182}W	11.9	267	3.2	14.8	303	5.6	2.01	6.8
^{184}W	11.9	315	2.9	14.8	321	4.7	1.65	6.8
^{186}W	12.0	246	3.3	14.5	332	5.1	2.07	6.4
^{197}Au	13.7	535	5.2					
Average error	1.4%	11.2%	9.3%	1.5%	9.7%	4.6%	0.22	0.2 MeV

TABLE 3
Ratios of nuclear ellipsoid axes (k), deformation parameters (β) and intrinsic quadrupole moments (Q_0), calculated from E_1, E_2

Nucleus	^{154}Sm	^{156}Gd	^{165}Ho	^{168}Er	^{174}Yb	^{178}Hf	^{180}Hf	^{181}Ta	^{182}W	^{184}W	^{186}W
k	1.320	1.302	1.259	1.327	1.289	1.296	1.281	1.263	1.271	1.268	1.229
β	0.326	0.309	0.266	0.334	0.296	0.303	0.288	0.270	0.278	0.274	0.235
± 0.017	± 0.016	± 0.036	± 0.032	± 0.024	± 0.032	± 0.036	± 0.026	± 0.030	± 0.032	± 0.031	
Q_0	6.3	6.2	5.8	7.5	7.0	7.5	7.2	6.9	7.2	7.1	6.2
± 0.3	± 0.3	± 0.8	± 0.7	± 0.6	± 0.8	± 0.9	± 0.7	± 0.8	± 0.8	± 0.9	

TABLE 4
Integral characteristics of EI giant resonance

Nucleus	$\sigma_{\text{tot},\text{p}}$ (MeV \cdot mb)	$\sigma_{\text{tot},\text{p}}$ (0.06 VZ/A)	$\sigma_{\text{tot},\text{L}}$ (MeV \cdot mb)	σ_{tot} (0.06 VZ/A)	σ_{tot} (mb)	$\sigma_{\text{tot,L}}$ (mb)	$\sigma_{\text{tot},\text{L}}^{-1/4} \cdot A^{+3}$ (mb)	$\sigma_{\text{tot},\text{L}}$ (mb \cdot MeV $^{-1}$)	$\sigma_{\text{tot},\text{L}}$ (mb \cdot MeV $^{-1}$)	$\sigma_{\text{tot},\text{L}}$ (μ b \cdot MeV $^{-1}$)
^{154}Sm	1.94 ± 0.06	0.87	2.86	1.29	117 ± 3.5	156	0.189	9.1 ± 0.3	14.3	3.23
^{156}Gd	2.07 ± 0.07	0.91	2.95	1.30	143 ± 4.6	163	0.194	10.5 ± 0.4	14.9	3.30
^{165}Ho	1.86 ± 0.06	0.78	2.53	1.06	155 ± 4.4	160	0.177	10.1 ± 0.3	12.6	2.54
^{168}Er	2.24 ± 0.06	0.92	3.07	1.26	161 ± 4.3	197	0.212	12.0 ± 0.3	16.0	3.13
^{174}Yb	2.69 ± 0.05	1.07	3.82	1.52	195 ± 3.4	240	0.247	14.5 ± 0.3	19.2	3.54
^{178}Hf	2.85 ± 0.07	1.11	3.99	1.55	208 ± 4.9	247	0.247	15.3 ± 0.4	20.2	3.59
^{180}Hf	2.72 ± 0.06	1.05	4.03	1.56	200 ± 4.4	250	0.246	15.1 ± 0.3	20.7	3.61
^{181}Ta	2.84 ± 0.07	1.09	3.81	1.46	210 ± 5.3	245	0.239	16.0 ± 0.4	20.0	3.45
^{182}W	2.86 ± 0.07	1.09	4.01	1.52	211 ± 5.3	256	0.248	16.2 ± 0.4	21.6	3.70
^{184}W	2.78 ± 0.07	1.05	3.80	1.43	207 ± 5.3	251	0.240	15.9 ± 0.4	20.9	3.51
^{186}W	2.90 ± 0.07	1.08	3.95	1.48	214 ± 5.3	256	0.241	16.2 ± 0.4	21.6	3.56
^{197}Au	3.12 ± 0.06	1.10	4.37	1.54	229 ± 4.2	276	0.241	18.6 ± 0.4	23.3	3.49

METHOD					REF. NO.	
REACTION	RESULT	EXCITATION ENERGY	SOURCE	DETECTOR	ANGLE	
			TYPE	RANGE		
G,G	ABX	2-7		2-7	SCD-0	90

2.60-6.76 MEV

Elastic scattering by nuclei in the range of mass numbers between 64 and 238 has been studied with monochromatic photons in the energy range between 2 and 8 MeV. These photons were provided either by a $Ti(n,\gamma)$ source installed in the tangential through channel of the Grenoble high flux reactor, or by ^{24}Na and ^{56}Co sources produced by deuteron bombardment of Al or Fe at the Göttingen cyclotron. The photoexcitation of 23 nuclear levels has been observed and the decay properties and groundstate widths of the majority of these levels have been determined. For the lead scattering target the coherent elastic differential cross section has been studied in detail. There is evidence that below the photo-neutron threshold the elastic scattering via virtual photoexcitation of the nucleus can be approximated by extrapolating the real part of the Giant Dipole Resonance amplitude along a Lorentzian curve. Coulomb corrections to Delbrück scattering seem to play a small role at 6.5 MeV.

Table 4. Properties of levels observed by photoexcitation. $(d\sigma/d\Omega)^{exp}$: experimental differential cross section per identified isotope or element for resonance scattering through $\theta=90^\circ$. I^{π} : spin-parity of excited level; $W(\theta)$: angular correlation function: $g=(2I_{ex}+1)/(2I_g+1)$; Γ_0 : radiative groundstate transition width, Γ : total level width. Errors in the last digits are given in parentheses

Isotope	E , (MeV)	$(d\sigma/d\Omega)^{exp}$ ($\mu b/st$)	I^{π}	Γ_0/Γ	$W(\theta)g\Gamma_0/\Gamma$ (meV)	Γ_0^r (meV)	Γ_0^s (meV)
^{238}U	2.754	13 (4)	(1)	0.77	0.145	0.084	-
^{238}U	3.254	421 (5)	1^-	0.24	0.83	1.5	0.52(15) ^a
^{209}Bi	6.555	2.1 (4) · 10 ²	-	-	0.74	0.74 ^b	-
^{209}Bi	7.168	1.7 (3) · 10 ²	$9/2^-$	1.00	710	786	-
^{203}Tl	6.418	8.75(30) · 10 ³	$1/2^+$	0.28	30	102	82 (40) ^a
Tl	6.759	7 (3)	-	-	-	-	-
Hg	6.555	68 (17)	-	-	-	-	-
^{186}W	6.418	5.2 (3) · 10 ²	1^-	0.32	1.75	2.4	-
^{184}W	6.555	9.8 (10) · 10 ²	(1)	0.52	3.44	2.9	-
^{184}W	6.759	46 (10)	(1)	0.58	0.17	0.13	-
^{181}Ta	3.010	174 (17)	-	0.72	0.42	0.59	-
^{181}Ta	6.418	62 (4)	-	0.73	0.2	0.27 ^c	-
^{181}Ta	6.759	4.8 (12)	-	-	0.018	0.018 ^b	-
^{169}Ho	6.418	10.3 (30)	-	-	0.035	0.035 ^b	-
^{169}Ho	6.759	5.6 (14)	-	-	0.021	0.021 ^b	-
Nd	2.754	2.6 (5)	-	-	-	-	-
Nd	3.254	14.0 (10)	-	-	-	-	-
Ce	6.759	13.4 (10)	-	-	-	-	-
^{121}Sb	3.452	2.20 (5) · 10 ³	-	0.60	2.9	4.9 ^b	-
^{100}Mo	6.418	1.53 (4) · 10 ⁴	1^-	0.88	52	26	25 (8) ^a
^{94}Mo	6.555	4.4 (4) · 10 ³	(1)	0.33	15	21	-
Mo	6.759	6.2 (15)	-	-	-	-	-
Mo	7.168	8.2 (26) · 10 ²	-	-	-	-	-

^a [11] ^b $W(\theta)g\Gamma_0/\Gamma = 1$ assumed ^c $W(\theta)g = 1$ assumed

^d [28] (a small correction has been applied to the data of [28])

^e Upper limits in case not all the transitions to lower levels were observed

^f Present work ^g Previous work

(OVER)

Table I. Differential cross sections for elastic scattering ($d\sigma/d\Omega$)^{exp} of photons from ^{59}Co and ^{24}Na sources by different scattering targets, in units of $\mu\text{b}/\text{sr}$. Errors in the last digits are given in parentheses.

θ deg	Scattering targets	2.599 ^a (MeV)	2.754 ^b (MeV)	3.010 ^a (MeV)	3.202 ^a (MeV)	3.254 ^b (MeV)	3.273 ^a (MeV)	3.452 ^a (MeV)
90	^{238}U	52.7(25)	57.5(25) ^c	56(16)	47(4)	456 (10) ^c	34(6)	49(14)
	^{209}Bi	33.1(30)	32 (2)	33(11)	32(4)	25.6(20)	29(6)	33(15)
	^{nat}Pb	31.5(23)	31.0(16)	35 (8)	27(3)	26.6(22)	25(4)	23 (8)
	^{nat}Tl	31.5(33)	-	27(12)	32(5)	24 (3)	22(7)	34(15)
	^{nat}Hg	30.0(27)	-	24(10)	28(5)	25.5(18)	26(8)	20 (8)
	^{nat}W	22.5(11)	-	17 (7)	19(3)	18.4(15)	18(5)	21 (6)
	^{181}Ta	20.0(15)	19.2 (6)	193(20) ^c	20(4)	17.3(21)	18(5)	21 (8)
	^{165}Ho	15.9(13)	-	17(10)	13(6)	15.6(20)	18(8)	-
	^{nat}Nd	11.4 (7)	14.2 (5) ^d	15 (7)	14(3)	24.2(12) ^d	13(3)	9 (6)
	^{nat}Ce	11.1 (9)	11.0 (5)	-	11(3)	9.5(13)	8(4)	-
	^{127}I	8.4(10)	8.6 (5)	-	9(2)	7 (1)	5(3)	-
	^{nat}Sb	8.0(11)	-	-	10(4)	6.8(19)	-	1.270(50) ^c
	^{nat}Sn	6.5 (7)	7.0 (5)	-	5(2)	7.6 (8)	6(3)	-
	^{nat}Cd	6.2 (5)	-	-	6(2)	6.6 (8)	7(3)	-
120	^{238}U	55.1(25)	64 (4) ^c	43(15)	55(5)	574 (10) ^c	48(5)	48(11)
	^{181}Ta	27.5(15)	25.0 (9)	227(20) ^c	22(5)	21 (2)	22(8)	-
	^{nat}Nd	17.9(30)	17.0 (9) ^d	-	-	29.8(47) ^d	-	-

^a ^{59}Co source in Fe lattice ^b ^{24}Na source in Al lattice (part of data have been published elsewhere)

^c Transitions to excited states observed in addition to the ground-state transition

^d Photoexcitation of nuclear level identified from the size of the differential cross section

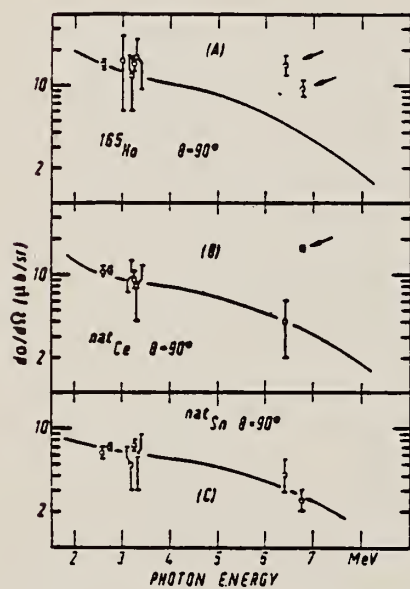


Fig. 11. Same as Fig. 9 but for (A) ^{165}Ho , (B) ^{nat}Ce and (C) ^{nat}Sn

ELEM. SYM.	A	Z
Ho	165	67

METHOD

REF. NO.	
82 Zu 2	egf

REACTION	RESULT	EXCITATION ENERGY	SOURCE	DETECTOR	ANGLE	
			TYPE	RANGE		
G,G	ABX	3-6	D	3-6	SCD-D	DST

SOURCE 141PR(N,G)

A procedure is presented to determine total photoabsorption cross sections σ_t by resonant scattering of γ -rays. It is shown that σ_t follows along the GDR lorentzian line down to 3.5 MeV. Indications for nonstatistical deviations from the lorentzian line are observed.

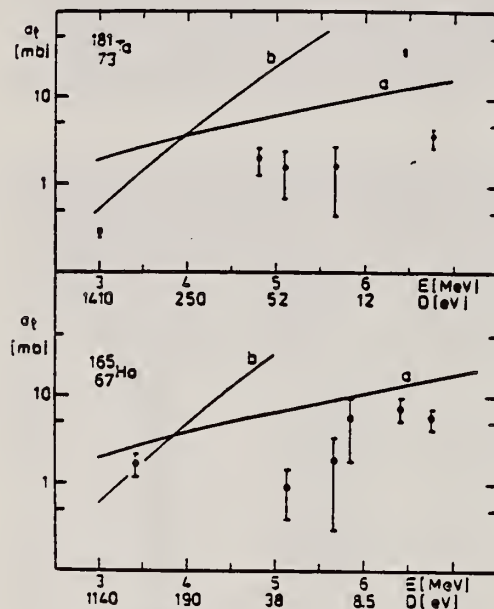


Fig. 2. Total photoabsorption cross section for ¹⁸¹Ta and ¹⁶⁵Ho versus energy. Curve a: extrapolated lorentzian according to ref. [13]. Curve b: total photoabsorption cross section predicted by the Weisskopf model with hindrance factor 3×10^{-5} .

Ho
A=166

Ho
A=166

Ho
A=166

ELEM. SYM.	A	Z
Ho	166	67

METHOD

REF. NO.

73 Mc 6

egf

REACTION	RESULT	EXCITATION ENERGY	SOURCE		DETECTOR		ANGLE
			TYPE	RANGE	TYPE	RANGE	
N,G	RLX	14- 20	D	7- 14	NAI-D		UKN

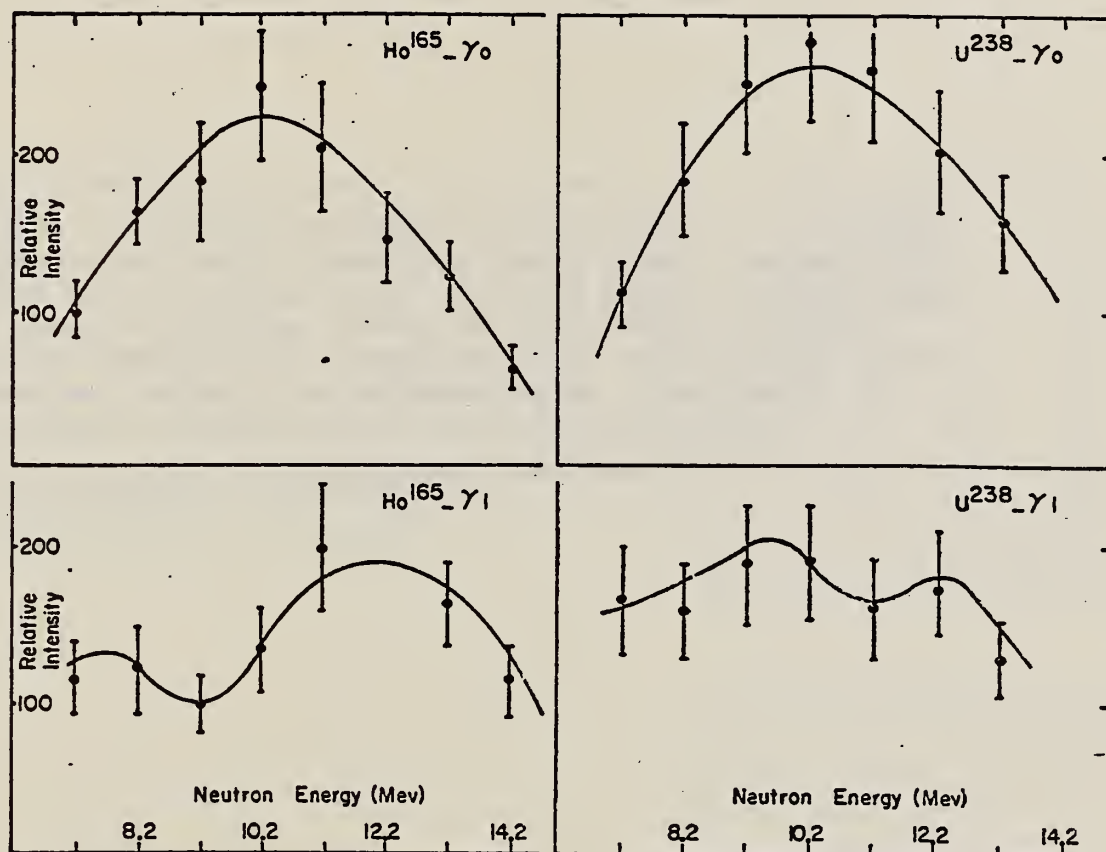


FIG. 1. The total (n,γ) cross section for ^{165}Ho and ^{238}U targets. The upper figs. show the data for transitions to the ground states of the final nucleus. The lower figs. show the data for transitions corresponding to the first peak found in the observed spectra below the one belonging to the ground state transition.

ER

ERBIUM

Z=68

Erbia is one of the three fractions that C. G. Mosander discovered (1842) in Gadolin's yttria oxide. The metallic form was not produced until 1834 when Klemm and Bommer made a chemical reduction. During the late 1940's the Atomic Energy Commission developed separation methods based on the then new synthetic ion exchange resins. The element is available in high purity in up to ton quantities.

ER

Betatron; ion chamber

REF. NO.

58 Fu 1

NVB

REACTION	RESULT	EXCITATION ENERGY	SOURCE		DETECTOR		ANGLE
			TYPE	RANGE	TYPE	RANGE	
G, XN	ABX	7-40	C	7-40	BF ₃ -I		4PI

CF DANOS THEORY

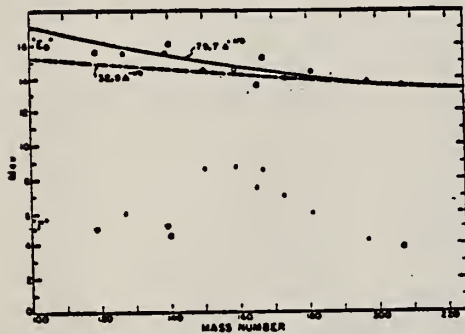


FIG. 6. Mean energy and width of giant resonances. "E_m" and "Γ" are the mean energy for photon absorption and the full width at half maximum of the giant resonance obtained from dashed histograms as in Fig. 5. No attempt was made to fit data with resonance curves to obtain these parameters.

TABLE I. Target properties and results.

Element	Form used	Weight grams	$\sigma^*(\gamma, n)$ ^a barns	$\frac{SedE}{N^2/A}$ Mev ^b	$\frac{\sigma^*(\gamma, n)}{MeV}$
Sn	Sn	4.81	0.30	0.064	5.0
I	I	8.55	0.36	0.085	6.0
La	La	10.43	0.34	0.063	5.2
Ce	Ce	4.99	0.45	0.080	4.5
Sm	Sm ₂ O ₃	2.90	0.26	0.073	8.6
Tb	Tb ₂ O ₃	3.04	0.39	0.087	8.7
Ho	Ho ₂ O ₃	1.87	0.41	0.079	7.5
Er	Er ₂ O ₃	5.41	0.50	0.100	8.5
Yb	Yb ₂ O ₃	5.57	0.50	0.090	7.0
Ta	Ta	8.41	0.49	0.077	6.0
Au	Au	3.16	0.68	0.085	4.2
Pb	Pb	8.05	0.75	0.081	3.8

^a $\sigma^*(\gamma, n)$ is the maximum value and "Γ" the full width at $\sigma^*(\gamma, n)/2$ of the neutron production cross section corrected for multiple neutron emission. Data were not fitted with resonance lines to determine these values.

^b Integrated neutron production cross sections corrected for multiple neutrons above ($\gamma, 2n$) threshold.

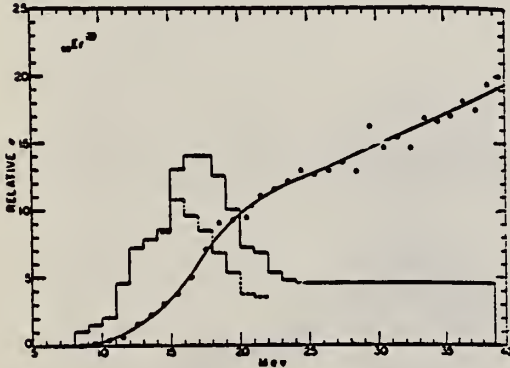


FIG. 5. Relative photoneutron production cross sections for tin, iodine, samarium, holmium, erbium, and lead. The points and smooth curves represent the integral neutron-production cross section defined by $\int_E^\infty \sigma_{Tn}(E)dE$, where $\sigma_{Tn}(E) = \sigma(\gamma, n) + 2\sigma(\gamma, 2n) + \sigma(\gamma, 3n) + \dots$. The scales are normalized to give approximately the same total neutron yield at 40 Mev. The errors indicated were obtained by propagating the statistical uncertainties, (\sqrt{n}) , in the original activation curve data through the integral cross section matrix. Solid histograms represent first differences of integral cross section curves. Dashed histograms show result of correcting for neutron multiplicity above the ($\gamma, 2n$) threshold.

TABLE II. Energies of resonances in deformed nuclei.*

Nucleus	E_m Mev	σ^* barns	Method	E_1 Mev	E_2 Mev	$E_{1/2}^{+}$ Mev	$E_{1/2}^{-}$ Mev
¹⁰⁸ Tb	14.7	6.9 ^b	CE	11.9	16.2	10.8	19.5
¹³¹ I	14.5	7.8 ^b	CE	11.5	16.0	11.0	18.5
¹⁵¹ Ho	14.5	21 ^b	SC	8.3	17.5	11.5	20.0
¹⁵³ Er	14.5	7.8 ^b	CE	11.6	15.9	11.5	20.0
¹⁵⁴ Ta	14.1	12.6 ^b	SC	10.3	15.9	11.3	17.3
¹⁵⁴ Ta	14.1	6.8 ^b	CE	11.9	15.2	11.3	17.3
¹⁹⁷ Au	13.6	3.75 ^c	SC	12.5	14.1	11.8	16.2

* CE—Coulomb excitation; SC—spectroscopic; $E_{1/2}^{+}$, $E_{1/2}^{-}$ —energies at which giant resonance drops to half its maximum value.

^b Adler, Bohr, Huus, Mottelson, and Winther, Revs. Modern Phys. 28, 432 (1956).

^c M. L. Pool and D. N. Kundu, Chart of Atomic Nuclei (Longs College Book Company, Columbus, 1955).

Method 50 MeV betatron; BF_3 , NaI counters

Ref. No.	62 Fu 3	JHH
----------	---------	-----

Reaction	γ E or ΔE	E_0	Γ	$\int \sigma dE$	$J\pi$	Notes
Er(γ , xn)	8-23.5	12.2 ± 0.2 16.0 ± 0.5	2.33 MeV 4.5 MeV	$\int_8^{23.5} = 3.20 \pm 15\%$		$\sigma(12.2 \text{ MeV}) = 318 \text{ mb.}$ $\sigma(16 \text{ MeV}) = 328 \text{ mb.}$ Correction for neutron multiplicity.
Er (γ, γ)						Intrinsic nuclear quadrupole moment = $7.6 \pm 1.1 \text{ b}$. Analysis of scattering data indicates large tensor polarizability.

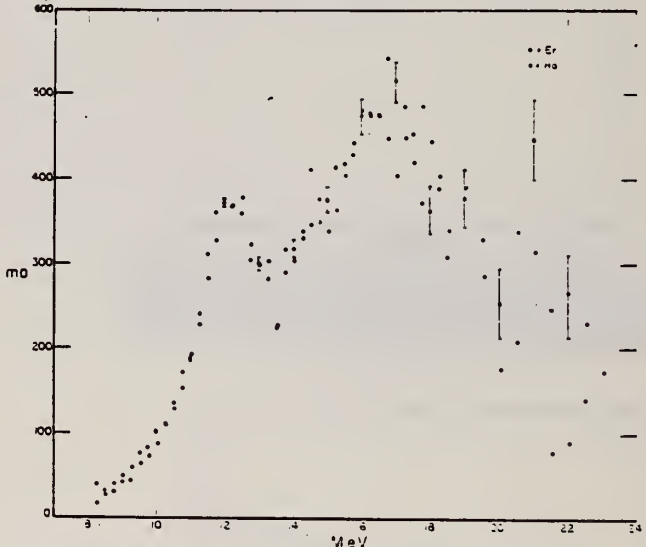


Fig. 2. Neutron production cross sections for holmium and erbium. The uncertainties indicated result from the statistical uncertainties in the original activation curve data.

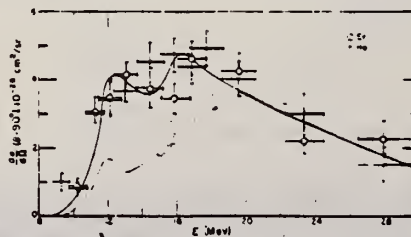


Fig. 3. The differential scattering cross sections for holmium and erbium measured at 90°. The indicated uncertainties are only statistical. The lower smooth curve was calculated using eq. (9) from a curve drawn through the data points of fig. 4. The shaded region corresponds to the limits of the scalar scattering cross section resulting from the limits of the absorption cross section given by the shaded region of fig. 4.

METHOD Linac; isomer yield; activity					REF. NO. 63 Ka 2	NVB
REACTION	RESULT	EXCITATION ENERGY	SOURCE	DETECTOR	ANGLE	
			TYPE	RANGE		
G,G/	RLY	1 (0.21)	C 4	ACT-I	4PI	

Table II. The isomers observed

Isomer	Observed value		Referenced value ⁽¹⁾⁽²⁾	
	Half-life	Energy (MeV)	Half-life	Energy (MeV)
Se-77m	17.5 sec	0.160	17.5 sec	0.161
Br-79m	4.80 sec	0.209	4.8 sec	0.208
Sr-87m	2.3 hr	0.390	2.8 hr	0.388
Y-89m	15.0 sec	0.920	14 sec	0.915
Rh-103m	58 min	*	57 min	0.040
Ag-107m	42 sec	0.95	44 sec	0.094
Ag-109m			40 sec	0.088
Cd-111m	47 min	0.150, 0.255	49 min	0.150, 0.247
In-115m	4.5 hr	0.335	4.5 hr	0.335
Sn-117m	17 day	0.160	14 day	0.159, 0.161
Ba-137m	2.6 min	0.660	2.6 min	0.662
Er-167m	2.10 sec	0.209	2.5 sec	0.208
Hf-179m	18.5 sec	0.157, 0.215	19 sec	0.161, 0.217
W-183m	5.4 sec	0.200, 0.170, 0.115	5.5 sec	0.1025, 0.2915 others
Ir-191m	4.90 sec	0.129, <0.07	4.9 sec	0.042-0.129
Pt-195m	4.5 day	0.065**	4.1 day	0.031-0.130
Au-197m	7.0 sec	0.10, 0.27, 0.40	7.2 sec	0.130, 0.270, 0.407
Hg-199m	43 min	0.160, 0.370	42 min	0.158, 0.368

* This isomer was measured with a G-M flow counter.

** This value corresponds to Pt-K X-ray energy.

Table III. Induced activation rate

Element	Beam energy (MeV)	Counting rate ($\times 10^{10}$ cpm)	Sample form
Se	5	1300	metallic pellet
Br	4	1600	NaBr grain
Sr	6	0.3	SrCO ₃ powder
Y	5	90	metallic grain
Rh	5	0.2**	RhCl ₃ grain
Ag	5	180	metallic plate
Cd	6	0.5	CdCl ₂ grain
In	6	8	metallic plate
Sn	6	0.0005	metallic plate
Ba	5	0.6	BaS powder
Er	4	4900	Er ₂ O ₃ powder
Hf	5	1600	metallic plate
W	5	120	metallic powder
Ir	5	2100	metallic powder
Pt	5	0.3	metallic plate
Au	4	4300	metallic plate
Hg	6	0.09	metallic liquid

* The value measured with a G-M flow counter.

METHOD

Betatron; photon scattering

REF. NO.

63 La 1

NVB

REACTION	RESULT	EXCITATION ENERGY	SOURCE		DETECTOR		ANGLE
			TYPE	RANGE	TYPE	RANGE	
G,G	ABX	9-26	C	9-27	NAI-D		DST

In Figure 4, $W(\theta) = 1 + a \cos^2 \theta$

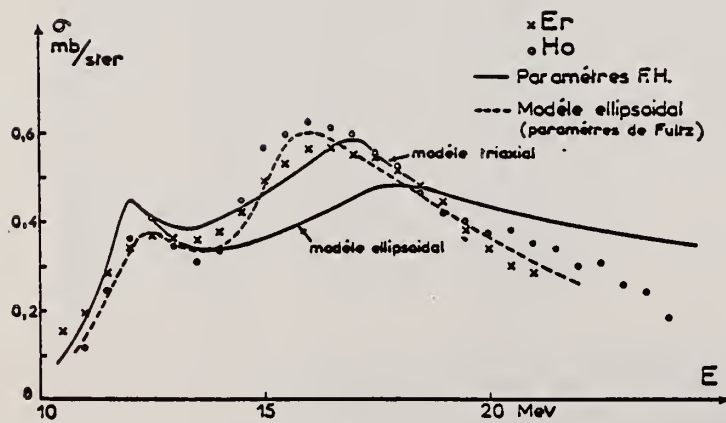


FIG. 3.

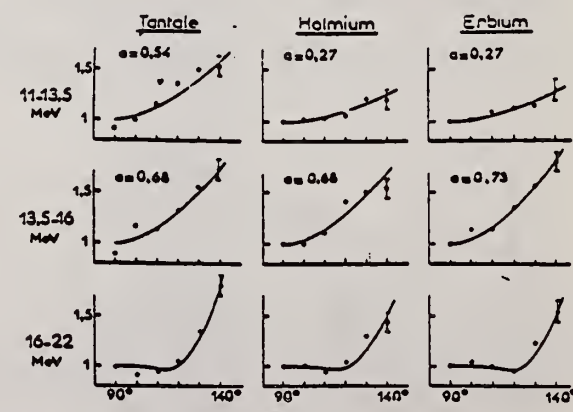


FIG. 4.

METHOD

Bremsstrahlung scattering

[Page 1 of 2]

REF. NO.

64 La 1

JOC

REACTION	RESULT	EXCITATION ENERGY	SOURCE		DETECTOR		ANGLE
			TYPE	RANGE	TYPE	RANGE	
G,G	ABX	10-25	C		NAI-D		DST

TABLEAU I
Le paramètre $a(E)$ de la distribution angulaire

Noyau	11.5-14. MeV			14-17.5 MeV			17.5-20 MeV			20-30 MeV		
	Exp.	Ellipsoidal	Triax.	Exp.	Ellips.	Triax.	Exp.	Ellips.	Triax.	Exp.	Ellips.	
Contribution Quadrupolaire %												
Tb	$0.5^{+0.15}_{-0.1}$	0.41	0.39	$0.54^{+0.15}_{-0.1}$	0.70	0.50	25	0.97	0.85			1
Ho	$0.27^{+0.15}_{-0.1}$	0.44	0.407	$0.43^{+0.10}_{-0.05}$	0.71	0.53	25	0.95	0.9	0.4 ± 0.1		1
Er	$0.27^{+0.15}_{-0.1}$	0.44	0.407	$0.8^{+0.15}_{-0.1}$	0.71	0.53	25	0.95	0.9			1
Ta	$0.6^{+0.15}_{-0.1}$	0.58		$0.68^{+0.15}_{-0.1}$	0.81		20	0.96				
Au				$a_{\text{exp}}(11-20 \text{ MeV}) = 0.9$						0.7 ± 0.1		1
				$a_{\text{th}}(11-20 \text{ MeV}) \approx 1$								

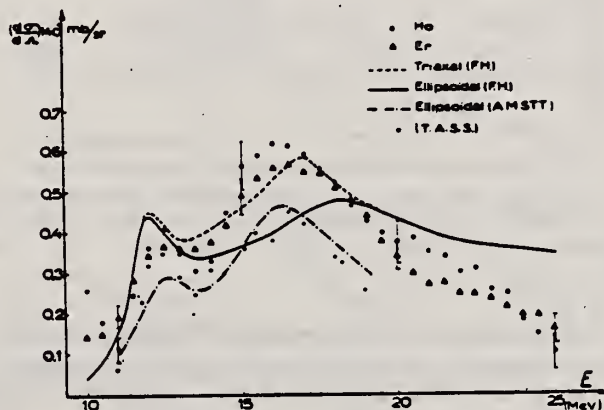


Fig. 3. Sections efficaces expérimentales différentielles de diffusion, obtenues pour l'holmium et l'erbium et comparaison avec les résultats expérimentaux de Tipler *et al.*¹⁰. (T.A.S.S.). Les courbes tracées correspondent à l'application des relations de dispersion aux sections efficaces d'absorption obtenues par Fuller et Hayward¹¹ (F.H.) et Axel, Miller, Schuhl, Tamas et Tzara (A.M.S.T.T.)¹².

METHOD

REF. NO.

Bremsstrahlung scattering

[Page 2 of 2]

64 La 1

JOC

REACTION	RESULT	EXCITATION ENERGY	SOURCE		DETECTOR		ANGLE
			TYPE	RANGE	TYPE	RANGE	

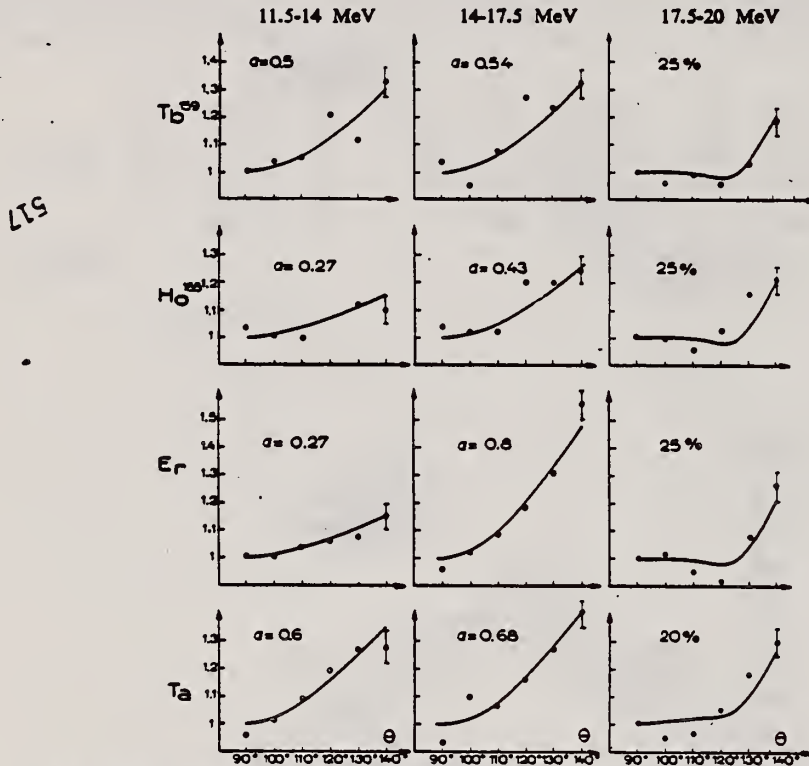


Fig. 8. Répartitions angulaires du rayonnement diffusé obtenues pour le terbium, l'holmium, l'erbium et le tantalum dans les zones d'énergie 11.5-14 MeV, 14-17.5 MeV et 17.5-20 MeV.

METHOD

REF. NO.

69 Be 6

egf

REACTION	RESULT	EXCITATION ENERGY	SOURCE		DETECTOR		ANGLE
			TYPE	RANGE	TYPE	RANGE	
G, N 481	ABX	7-21	D	7-28	MOD-I		4PI
G, 2N 482	ABX	13-27	D	7-28	MOD-I		4PI
G, 3N 483+	ABX	23-28	D	7-28	MOD-I		4PI

x = fraction of total cross section resulting in a direct neutron

n_d = fraction of neutrons emitted by direct effect at an energy where all the evaporation neutrons go to ($\gamma, 2n$) cross section

$$n_d = x/(2-x)$$

481+

TABLEAU 3
 Moments quadrupolaires intrinsèques

Cible	% isotopes	a/b ex	β_2 ex	$\beta_2[B(E_2)]$	Q_0 ex (b)	Q'_0
$^{131}_{\Lambda}$ I	100 % 127 I	0.85	0.172		-2.3 ± 0.4	
$^{148}_{\Lambda}$ Ce	88.5 % 140 Ce 11.1 % 142 Ce			0.104 0.118		
$^{144}_{\Lambda}$ Sm	15 % 147 Sm 11.2 % 148 Sm 13.8 % 149 Sm 7.5 % 150 Sm 26.6 % 152 Sm 22.5 % 154 Sm	1.23	0.219	0.190 0.304 0.351	4.5 ± 0.4	0.158 3.53 5.93 6.58
$^{144}_{\Lambda}$ Er	33.4 % 166 Er 22.9 % 167 Er 27.1 % 168 Er 14.9 % 170 Er	1.314	0.288	0.341 0.339 0.329	6.96 ± 0.4	7.60 7.80 7.60 7.45
$^{171}_{\Lambda}$ Lu	97.4 % 173 Lu	1.282	0.262		6.95 ± 0.3	7.20

TABLEAU 5
 Valeurs de la température nucléaire et du paramètre a de densité des niveaux

x	n_d	Θ (MeV)	$E'_{\gamma} - E_n$ (MeV)	a (MeV $^{-1}$)	a' (MeV $^{-1}$)	a'' (MeV $^{-1}$)
I	0.05 ± 0.005	0.03 ± 0.03	1.30 ± 0.20	10	6 ± 2.5	10 ± 3
$^{140}_{\Lambda}$ Ce	0.21 ± 0.05	0.12 ± 0.03	1.05 ± 0.20	10	9 ± 3.5	7 ± 3
$^{142}_{\Lambda}$ Ce			0.8 ± 0.20	6	9 ± 4	8 ± 3
Sm	0.18 ± 0.04	0.10 ± 0.03				
Er	0.20 ± 0.05	0.11 ± 0.03				(12 ± 4)
Lu	0.26 ± 0.06	0.15 ± 0.03	0.85 ± 0.1	9	12.5 ± 2.5	15 ± 3

[over]

TABLEAU 4
Règles de somme

Noyau cible (éléments naturels)	σ_0 (MeV · b)	σ'_0 (MeV · b)	0.06 $\frac{NZ}{A}$	$\frac{\sigma_0 A}{0.06 NZ}$	$\frac{\sigma'_0 A}{0.06 NZ}$	σ_{-1} (mb)	$\sigma_{-1} A^{-1}$	σ_{-2} (mb · MeV $^{-1}$)	$\sigma_{-2} A^{-1}$
^{133}I	2.02 ± 0.14	2.30 ± 0.12	1.85	1.09 ± 0.07	1.24 ± 0.07	129 ± 0.10	0.20 ± 0.02	8.6 ± 0.6	2.7 ± 0.2
^{139}Cs	2.13 ± 0.15	2.53 ± 0.13	2.04	1.05 ± 0.07	1.24 ± 0.07	140 ± 0.12	0.19 ± 0.02	9.5 ± 0.6	2.5 ± 0.2
^{152}Sm	2.48 ± 0.17	2.92 ± 0.14	2.18	1.14 ± 0.07	1.34 ± 0.07	167 ± 0.14	0.21 ± 0.02	11.8 ± 0.8	2.75 ± 0.2
^{166}Er	2.70 ± 0.19	3.04 ± 0.16	2.42	1.12 ± 0.07	1.26 ± 0.07	186 ± 0.15	0.20 ± 0.02	13.6 ± 1	2.7 ± 0.2
^{175}Lu	2.65 ± 0.18	2.96 ± 0.16	2.53	1.05 ± 0.07	1.17 ± 0.07	182 ± 0.15	0.185 ± 0.02	12.9 ± 1	2.35 ± 0.2
valeur moyenne pour ces 5 corps				1.09 ± 0.07	1.25 ± 0.07		0.20 ± 0.02		2.6 ± 0.2

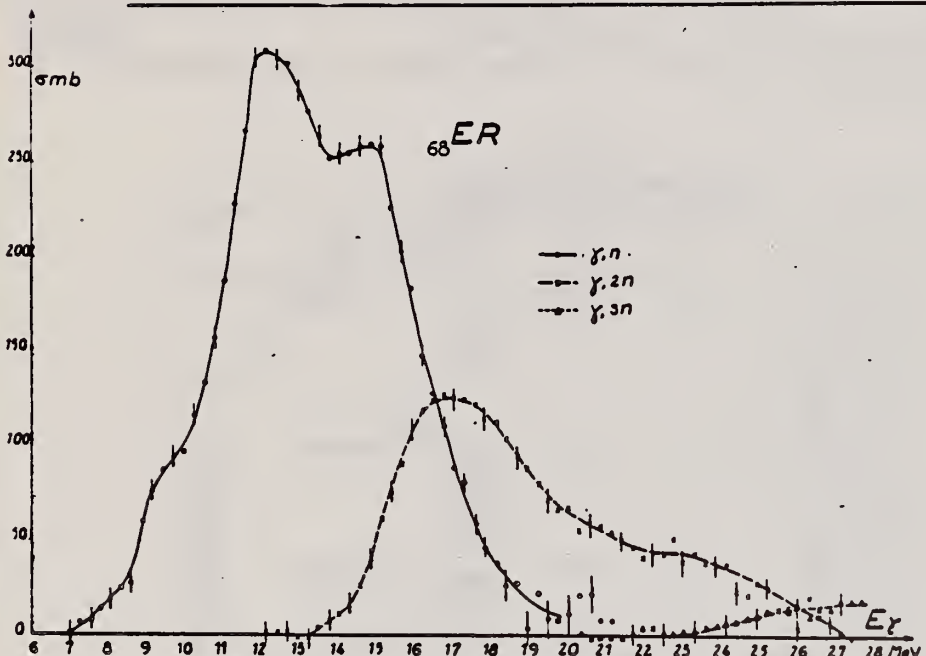


Fig. 7.

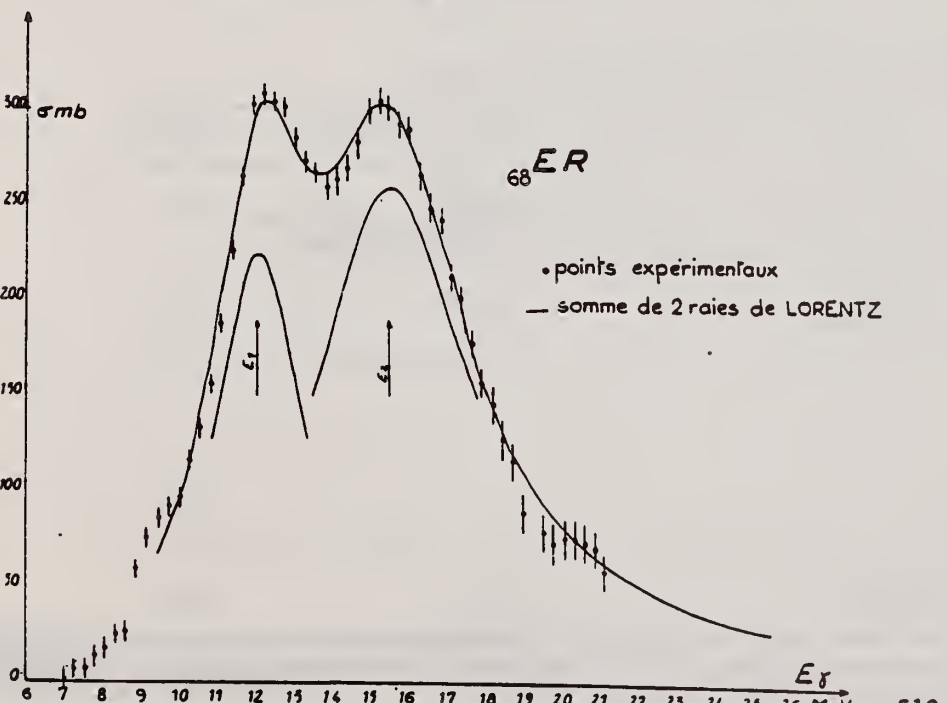


Fig. 8.

METHOD

REF. NO.

73 Ba 20

egf

REACTION	RESULT	EXCITATION ENERGY	SOURCE		DETECTOR		ANGLE
			TYPE	RANGE	TYPE	RANGE	
G,N	NOX	THR- 27	C	10- 27	BF3-I		4PI

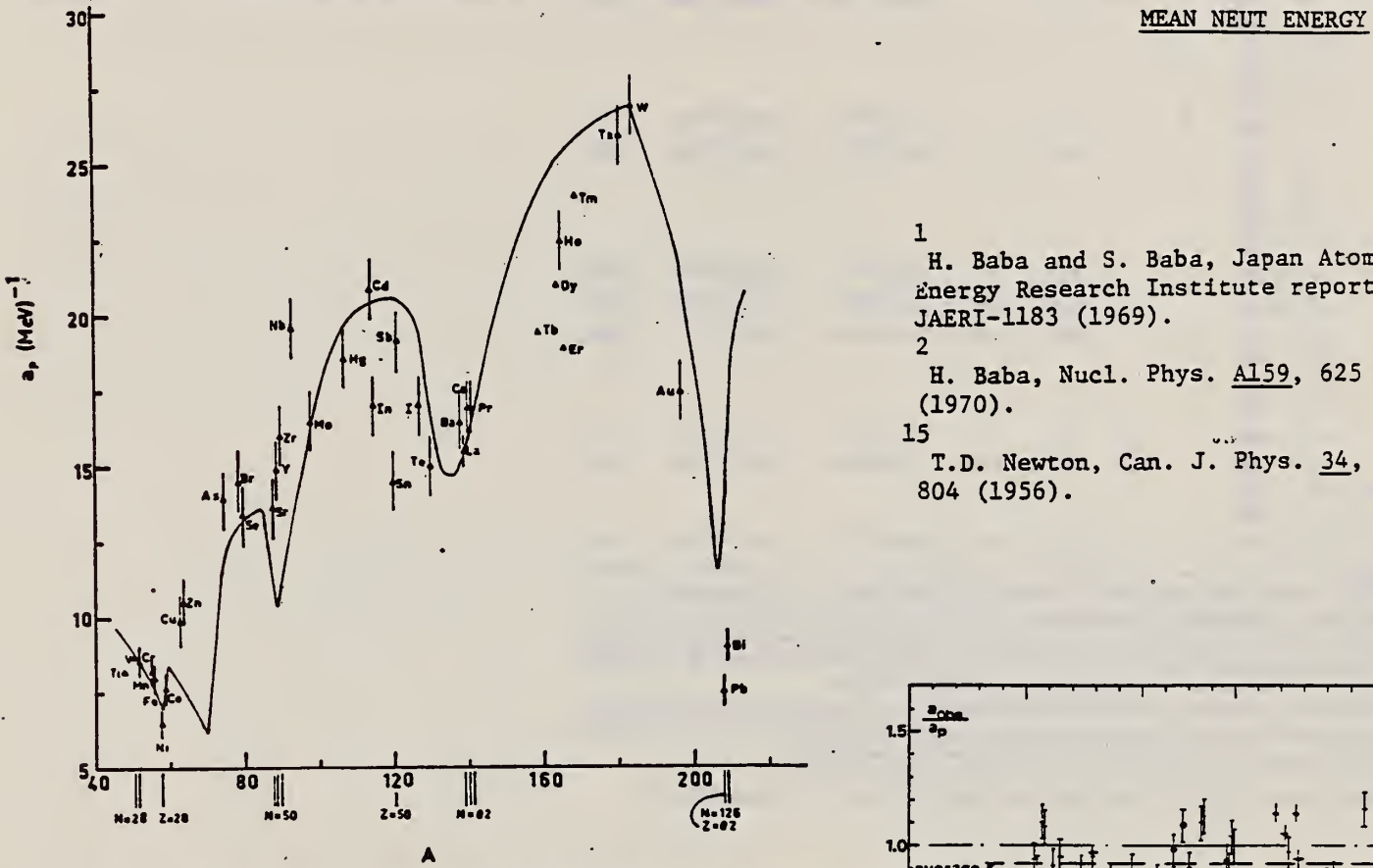


Fig. 12. Experimental values of the level density parameter a_p (Fermi gas formula plus pairing correction) versus atomic number A . The continuous curve is a least-squares fit to the data of a theoretical calculation from Newton ¹⁵.

- 1 H. Baba and S. Baba, Japan Atomic Energy Research Institute report JAERI-1183 (1969).
 2 H. Baba, Nucl. Phys. A159, 625 (1970).
 15 T.D. Newton, Can. J. Phys. 34, 804 (1956).

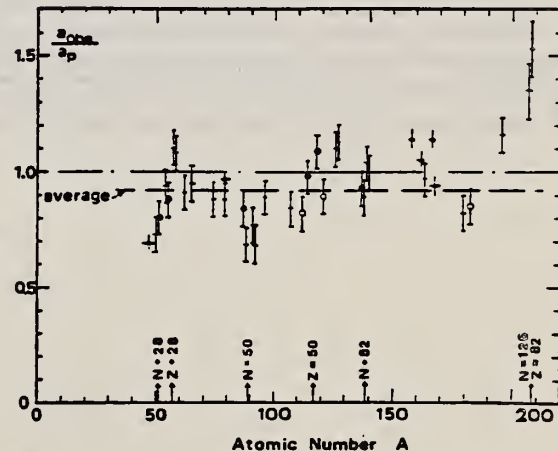


Fig. 15. Ratio a_{obs}/a_p versus atomic number A . Here a_{obs} is the level density parameter taken from the neutron resonance work of refs. ^{1,2}, and a_p is the level density parameter derived from the present (γ, n) work. Filled circles represent points where nuclei in the neutron resonance and in the (γ, n) experiment were the same. Open circles represent points where the respective nuclei were approximately matched. Triangles represent points which are based on measurement of neutron mean energies at two bremsstrahlung energies only.

(over)

TABLE 3 (continued)

Target	<i>N</i> (residual nucleus) ^{a)}	Goodness of fit ^{b)} no with p.c.	$\hat{E}_n(24)$ (MeV) ^{c)}	<i>T</i> (MeV) ^{d)}	a_p (MeV ⁻¹) ^{e)}	a_{obs} (MeV ⁻¹) ^{f)}	a_{obs}/a_p		
Ba	75	1%	F	1.16	16.5- ¹³⁶ Ba	15.39- ¹³⁶ Ba	0.93		
	77	2%							
	78	7%							
	79	8%							
	80	11%							
	81	71%							
La	80	100%	F	F	1.25	0.72	15.5- ¹³⁸ La	13.76- ¹³⁹ La	0.89
Ce	81	89%	F	G	1.24	0.70	17.0- ¹³⁹ Ce	17.8- ¹⁴¹ Ce	1.04
	83	11%							
Pr	81	100%	G	G	1.17	0.65	17.0- ¹⁴⁰ Pr	17.05- ¹⁴² Pr	1.00
Tb ^{g)}	93	100%			1.15		19.3- ¹⁵⁸ Tb	21.85- ¹⁶⁰ Tb	1.14
Dy ^{g)}	93	2%			1.06		20.9- ^{161.5} Dy	21.9- ¹⁶² Dy	1.05
	94	19%							
	95	25%							
	96	25%							
	97	28%							
Ho	97	100%	P	G	1.06	0.56	21.4- ¹⁶⁴ Ho	20.66- ¹⁶⁶ Ho	0.97
Er ^{g)}	95	2%			1.11		19.2- ¹⁶⁶ Er	21.9- ¹⁶⁶ Er	1.14
	97	33%							
	98	23%							
	99	27%							
	101	15%							
Tm ^{g)}	99	100%			1.03		24.0- ¹⁶⁸ Tm	22.58- ¹⁷⁰ Tm	0.94
Ta	107	100%		G	1.00	0.49	26.0- ¹⁸⁰ Ta	21.2- ¹⁸¹ Ta	0.82
W	107	26%	G	F	0.98	0.50	27.0- ¹⁸³ W	23.0- ¹⁸³ W	0.85
	108	14%							
	109	31%							
	111	28%							
Au	117	100%		G	1.19		17.5- ¹⁹⁶ Au	20.24- ¹⁹⁸ Au	1.16
(Z = 82) Pb	123	24%		V.P.	1.87	1.20	7.5- ²⁰⁶ Pb	10.1- ²⁰⁷ Pb	1.35
	124	23%							
	125	52%							
Bi	125	100%	F	1.65	1.03	9.0- ²⁰⁸ Bi	13.8- ²¹⁰ Bi	1.53	

^{a)} Neutron numbers and abundances of respective residual nuclei in (γ , n) experiments.^{b)} These give an assessment of the goodness of fit of a calculated \hat{E}_n versus E_0 curve to the observed data, using the Fermi gas level density formula both without and with pairing corrections.^{c)} Bremsstrahlung photoneutron mean energies \hat{E}_n for peak bremsstrahlung energy $E_0 = 24$ MeV.^{d)} Nuclear temperature from fit with constant-temperature formula.^{e)} Level density parameter a_p derived from the present (γ , n) experiment, using a Fermi gas formula plus pairing correction, and corresponding residual nucleus (the atomic weight shown is the weighted average of atomic weights of the respective isotopes present).^{f)} As column 7, but using data on n-resonance absorption from refs. ^{1, 2}.^{g)} Measurements of $\hat{E}_n(E_0)$ for these nuclei were made only for $E_0 = 21, 23$ and 24 MeV.

ER
A=166

ER
A=166

ER
A=166

ELEM. SYM.	A	Z
Er	166	68

METHOD

REF. NO.
73 Me 4

REACTION	RESULT	EXCITATION ENERGY	SOURCE		DETECTOR		ANGLE
			TYPE	RANGE	TYPE	RANGE	
\$ G,G	LFT	2	C	2	SCD-D		DST

1.66, 1.81 MEV LEVS

In addition to the previously known 1^+ states of ^{166}Er at 1663 and 1830 keV, levels at 1812 ± 1 keV (^{166}Er), 1786 ± 1 keV (^{166}Er), and 1824 ± 1 keV (^{170}Er) have been excited using electron bremsstrahlung. Based on the observed angular distributions of the scattered photons, all three previously unknown levels were found to have spin 1. Linear polarization measurements using a two-slab Ge(Li) polarimeter led to negative parity assignments for the 1786- and 1824-keV levels but were inconclusive with respect to the less strongly excited 1812-keV level. Below 1.9 MeV, the 1663-, 1786-, and 1824-keV levels are the dominant $E1$ excitations in their respective isotopes, the partial widths of their ground-state transitions being $\Gamma_0 = 32 \pm 5$, 46 ± 5 , and 30 ± 3 meV. The $B(E1; 1^- - \text{g.s.})/B(E1; 1^- - 2^+)$ ratios of 0.52 ± 0.02 , 0.51 ± 0.02 , and 0.53 ± 0.02 differ considerably from the ratio 1.31 ± 0.11 for the 1812-keV level and the reported ratio 0.22 for the 1830-keV 1^- state and are very close to the Alaga value of 0.50 for $K=0^-$ levels.

TABLE II. Comparison of the experimental ratios of the counting rates in the 98 and 127° scattering geometries with the ratios expected for different values of the spins of the excited states.

Isotope	E_{level} (keV)	$N(127^\circ)/N(98^\circ)$		
		Experiment	Theory Spin 1	Theory Spin 2
^{166}Er	1663	1.39 ± 0.11		
^{166}Er	1812	1.40 ± 0.17		
^{166}Er	1786	1.38 ± 0.07	1.36	0.49
^{170}Er	1824	1.33 ± 0.09		

TABLE III. Results of the measurements using the two-slab Ge(Li) polarimeter. $N_{||}$ and N_{\perp} represent the counting rates in the full energy peaks with the slabs parallel and perpendicular to the scattering plane, respectively.

Isotope	E_{level} (keV)	Transition $I_1 - I_2$	E_γ (keV)	$(N_{ } - N_{\perp})/(N_{ } + N_{\perp})$ (%)
^{166}Er	1662	$1^- - 0^+$	1662	+7.4 ± 4.9
		$1^- - 2^+$	1582	+3.7 ± 3.4
^{166}Er	1812	$1 - 0^+$	1812	-5.6 ± 10.0
		$1 - 2^+$		
^{166}Er	1786	$1 - 0^+$	1786	+16.7 ± 7.4
		$1 - 2^+$	1706	-1.4 ± 4.3
^{170}Er	1824	$1 - 0^+$	1824	+9.8 ± 4.8
		$1 - 2^+$	1745	0.0 ± 3.1

TABLE IV. Widths and branching ratios of the $^{166}, 166, 170$ Er levels. The direct results of the NRF scattering experiments are listed in column 5.

Isotope	Level (keV)	Γ_0/Γ_1	$B(E1; 1^- - \text{g.s.})/B(E1; 1^- - 2^+)$	Γ_0^2/Γ (meV)	Γ_0/Γ^a	Γ_0 (meV)
^{166}Er	1663	0.60 ± 0.02^b	0.52 ± 0.02	12.0 ± 1.8	0.38 ± 0.01	32 ± 5
	1812	1.50 ± 0.12	1.31 ± 0.11^c	4.8 ± 0.6	0.60 ± 0.02	8 ± 1
	1830	$\approx 0.33^d$	≈ 0.22	...	≈ 0.25	2.4
^{168}Er	1786	0.59 ± 0.02	0.51 ± 0.02	17.0 ± 1.7	0.37 ± 0.01	46 ± 5
^{170}Er	1824	0.61 ± 0.02	0.53 ± 0.02	11.4 ± 1.1	0.38 ± 0.01	30 ± 3

^a Assuming the absence of branching to levels above the 2^+ state.

^b In good agreement with the value of 0.61 adopted in Ref. 18.

^c This might be the ratio of $B(M1)$'s rather than $B(E1)$'s since the polarization experiment was not conclusive.

^d From the decay of ^{166}Ho ; see Ref. 18.

REF. B.I. Goryachev, Yu.V. Kuznetsov, V.N. Orlin, N.A. Pozhidaeva,
and V.G. Shevchenko
ZhETF Pis. Red. 19, 65 (1974)
JETP Lett. 19, 41 (1974)

ELEM. SYM.	A	Z
Er	166	68

METHOD

REF. NO.	
74 Go 4	hmg

REACTION	RESULT	EXCITATION ENERGY	SOURCE		DETECTOR		ANGLE
			TYPE	RANGE	TYPE	RANGE	
G,XN	ABX	8- 21	C	8- 21	BF3-I		4PI

$\sigma(\gamma, 2n)$ measured but not given.

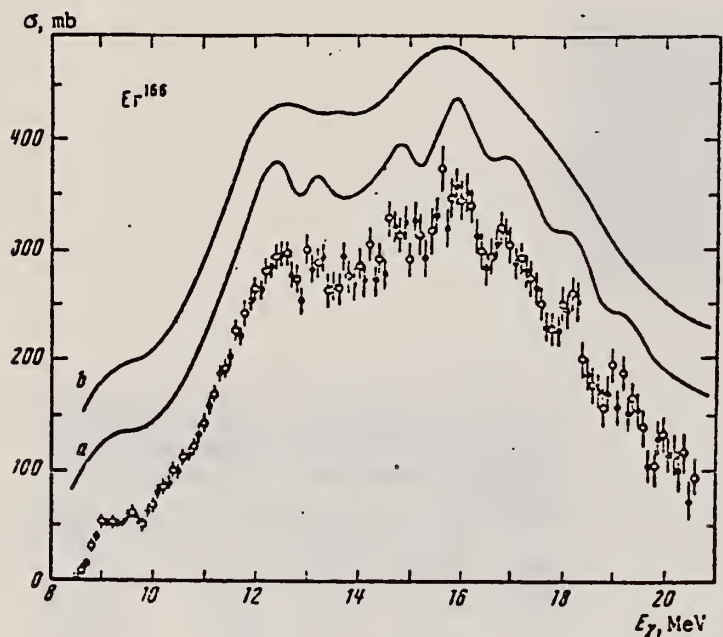


Fig. 1. Cross section σ_y of Er^{166} ; the light and dark circles correspond to two independent series of experimental data. Curves a and b were obtained by the regularization method (see the text) and are shown shifted relative to the ordinate axis.

Note: (γ, sn) cross section determined from $\sigma(\gamma, \text{xn})$ and statistical theory which gives $\sigma(\gamma, 2n)$ consistent with measurements.

See Refs. 6&7 for Regularization Method (Least Structure).

⁶ A.N. Tikhonov, Dokl. Akad. Nauk SSSR 151, 501 (1963).

⁷ B.S. Cook, Nucl. Instr. and Meth. 24, 256 (1963).

Nucleus	σ_{int} , MeV-b	β	Q_0 , b
Er^{166}	3.05 ± 0.3	0.33	7.76
Hf^{178}	3.16 ± 0.3	0.26	6.72

The table lists the values of the integral cross sections σ_{int} calculated from σ_y and the deformation parameters β , as well as the values Q_0 of the intrinsic quadrupole moments of the nuclei, corresponding to the obtained values of β .

REF.

T. Cooper, W. Bertozzi, J. Heisenberg, S. Kowalski
 W. Turchinetz, C. Williamson, L. Cardman, S. Fivozinsky,
 J. Lightbody, Jr., and S. Penner
 Phys. Rev. C13, 1083 (1976)

ELEM. SYM.	A	Z
Er	166	68

METHOD

REF. NO.
76 Co 3

REACTION	RESULT	EXCITATION ENERGY	SOURCE	DETECTOR	ANGLE
			TYPE	RANGE	
E,E/	FMF	1, 1	D	34-111	MAG-D
					DST

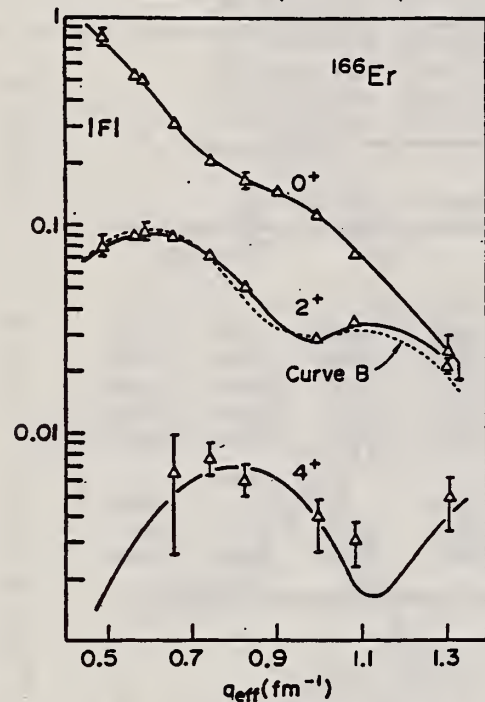


FIG. 5. Measured form factors for the elastic (0^+) and the inelastic 0.081-MeV (2^+) and 0.265-MeV (4^+) states in ^{166}Er . The solid line represents the quoted best fit. Curve B gives the result for the 2^+ state using a deformed Fermi distribution.

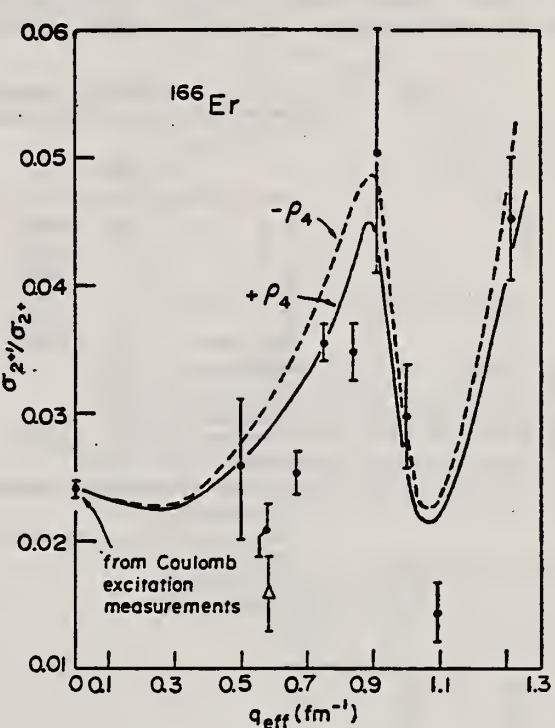


FIG. 9. Ratio of the cross sections observed for exciting the 0.786-MeV ($2''$) γ -vibrational level to that for exciting the 0.081-MeV ($2'$) state. The best fit curves differ only in the sign of the P_4 component of the charge distribution, since the sign is not determined by form factor fits to the ground state rotational band data.

(over)

TABLE IV. Cross sections of ^{168}Er .

Energy (MeV)	Angle (deg)	q_{eff} (fm $^{-1}$)	Elastic			2^+	4^+	$2^+\gamma$ vibrational
			$\frac{d\sigma}{d\Omega_{\text{exp}}}$ (mb)	$\frac{d\sigma}{d\Omega_{\text{bestfit}}}$ (mb)	$\frac{d\sigma}{d\Omega_{\text{exp}}}$ (mb)			
34.65	109.95	0.495	$0.948 \times 10 \pm 4\%$	0.933×10	$0.964 \times 10^{-1} \pm 6\%$...	$0.258 \times 10^{-2} \pm 22\%$	
39.64	127.81	0.588	$0.146 \times 10 \pm 5\%$	0.142×10	$0.433 \times 10^{-1} \pm 4\%$...	$0.681 \times 10^{-3} \pm 18\%$	
44.51	109.95	0.577	$0.241 \times 10 \pm 5\%$	0.237×10	$0.761 \times 10^{-1} \pm 3\%$...	$0.163 \times 10^{-2} \pm 10\%$	
54.88	109.95	0.663	$0.588 \pm 4\%$	0.566	$0.484 \times 10^{-1} \pm 3\%$	$0.231 \times 10^{-3} \pm 49\%$	$0.121 \times 10^{-2} \pm 2\%$	
64.82	110.16	0.746	$0.170 \pm 3\%$	0.177	$0.214 \times 10^{-1} \pm 2\%$	$0.246 \times 10^{-3} \pm 17\%$	$0.735 \times 10^{-3} \pm 3\%$	
75.99	110.13	0.831	$0.886 \times 10^{-1} \pm 7\%$	0.850×10^{-1}	$0.754 \times 10^{-2} \pm 3\%$	$0.106 \times 10^{-3} \pm 15\%$	$0.275 \times 10^{-3} \pm 6\%$	
84.17	110.01	0.906	$0.521 \times 10^{-1} \pm 5\%$	0.512×10^{-1}	$0.240 \times 10^{-2} \pm 7\%$	$0.513 \times 10^{-4} \pm 57\%$	$0.124 \times 10^{-3} \pm 18\%$	
95.23	110.03	0.999	$0.235 \times 10^{-1} \pm 3\%$	0.239×10^{-1}	$0.151 \times 10^{-2} \pm 4\%$	$0.303 \times 10^{-4} \pm 30\%$	$0.444 \times 10^{-4} \pm 13\%$	
95.00	127.81	1.092	$0.497 \times 10^{-2} \pm 3\%$	0.485×10^{-2}	$0.937 \times 10^{-3} \pm 4\%$	$0.859 \times 10^{-5} \pm 39\%$	$0.139 \times 10^{-4} \pm 2\%$	
110.20	147.24	1.315	$0.165 \times 10^{-3} \pm 10\%$	0.172×10^{-3}	$0.977 \times 10^{-4} \pm 15\%$	$0.483 \times 10^{-5} \pm 13\%$	$0.423 \times 10^{-5} \pm 11\%$	

TABLE IX. Transition charge parameters of ^{168}Er and ^{176}Yb .

	Units	^{168}Er			^{176}Yb		
		ρ_0	ρ_2	ρ_4	ρ_0	ρ_2	ρ_4
c	fm	6.1610	5.8632	5.3556	6.3306	6.0151	5.1866
t	fm	0.4872	0.5598	0.7271	0.4868	0.5188	0.9093
β_2		0.3266	0.3503	0.3325	0.3100	0.3346	0.3874
β_4		0.0	0.0	0.0199	-0.054	-0.054	-0.0875
β_6		-0.0180	-0.0180	-0.0180 ^a	-0.006	-0.006	-0.006 ^a
rms radius	fm	5.2380 ^b			5.3150 ^c		
$B(E2)$	$e^2 b^2$		5.670 ^d			5.350 ^e	
$B(E4)$	$e^2 b^4$			0.0919			0.0092
$\chi^2/\text{freedom}$		0.42	2.62	2.68	1.18	1.23	3.14
Transition radius	fm	5.2380	6.9088	8.4777	5.3150	6.8689	6.6962

^a Reference 3.^b Interpolated value from nearest neighbors.^c Reference 23.^d Reference 25.^e Reference 24.

³ D.L. Hendrie, Phys. Lett. 36, 571 (1973); ibid. et al. Phys. Lett. 26B, 127 (1968).

²³ A. Thompson (private commun.) Eidgenoessische TH Zuerich, 1974 (unpublished).

²⁴ R.O. Sayer et al., Phys. Rev. C1, 1525 (1970).

²⁵ P.H. Stelson, Nucl. Data Al, 21 (1965).

REF. B.I. Goryachev, Yu.V. Kuznetsov, V.N. Orlin, N.A. Pzhidaeva,
 V.G. Shevchenko
 Yad. Fiz. 23, 1145 (1976)
 Sov. J. Nucl. Phys. 23, 609 (1976)

ELEM. SYM.	A	z
Er	166	68

METHOD

REF. NO.

76 Go 4

hmg

REACTION	RESULT	EXCITATION ENERGY	SOURCE		DETECTOR		ANGLE
			TYPE	RANGE	TYPE	RANGE	
G, XN	ABX	8- 23	C	UKN	BF3-I		4PI
G, 2N	ABX	15- 21	C	UKN	SCI-I		4PI

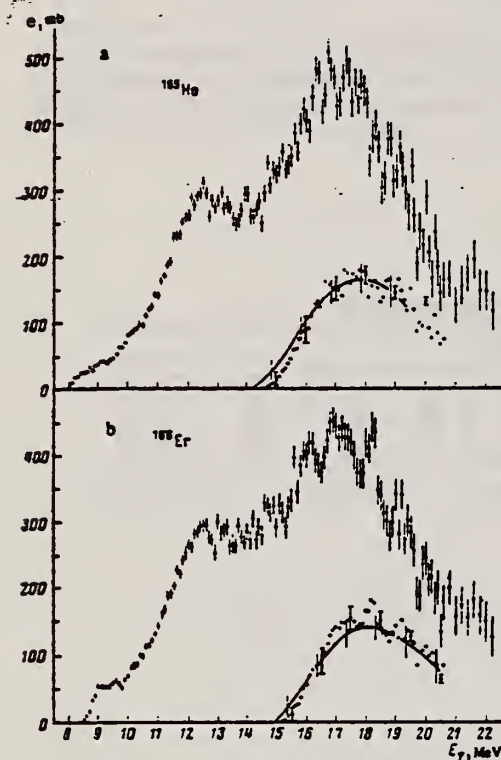


FIG. 1. Photoneutron production cross section σ_n obtained for ^{165}Ho (a) and for ^{166}Er (b). The hollow and solid circles correspond to two independent series of data. The solid curves show the $(\gamma, 2n)$ cross sections calculated from the data of a statistical experiment by the regularization method.^[12] The circles near the curves give the same cross sections calculated from the formula $\sigma_n(1 - f(E, a))$.

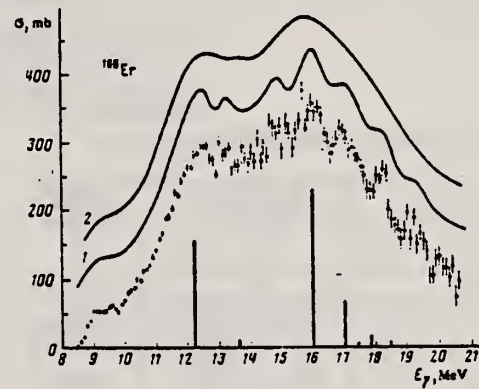


FIG. 6. Cross section σ_γ for ^{166}Er : The hollow and solid circles correspond to two independent series of experimental data. Curves 1 and 2 were obtained by the regularization method and are shown shifted along the ordinate axis. The heavy vertical bars show the dipole transition spectrum calculated by means of a version of the dynamic collective model based on a rotational-vibrational model of surface oscillations.

TABLE 4. Parameters of curve fitted to the cross section σ_γ in ^{166}Er .

Number of resonance	E_γ , MeV	σ_γ , mb	Γ_γ , MeV	$\epsilon_\gamma \Gamma_\gamma = \Gamma_1$
1	12.26	210	2.63	1.00
2	13.44	34	0.94 ± 0.27	0.06 ± 0.02
3	14.77	161	2.25 ± 0.15	0.63 ± 0.05
4	15.93	112	0.93 ± 0.08	0.19 ± 0.01
5	16.99	89	1.08 ± 0.12	0.17 ± 0.01
6	17.7	114	4.67 ± 0.44	0.93 ± 0.01
7	15.2	62	0.53 ± 0.16	0.06 ± 0.02

$\chi^2 = 79.3$, $f = 75$, $E_\gamma = 10.73$ MeV, $E_\gamma = 20.1$ MeV

TABLE 1. Level-density parameters

Nucleus	a , MeV ⁻¹		Nucleus	a , MeV ⁻¹	
	Present work	Other studies		Present work	Other studies
^{158}Tb	—	$7.7^{[15]}$	^{166}Er	6.1 ± 2.5	$8^{[16]}$
^{165}Ho	4.2 ± 1.5	$3.1^{[15]}$	^{179}Hf	17.7 ± 7.3	—

(over)

TABLE 2. Parameters of fitted curves $\sigma_{\gamma}^{(2)}$

Nucleus	E_1 , MeV	σ_{γ} , mb	Γ_1 , MeV	E_2 , MeV	σ_{γ} , mb	Γ_2 , MeV	$\sigma_{\Gamma_1 \times \Gamma_2}$	χ^2	f	E_{γ} , MeV	E_{γ} , MeV
^{160}Yb	12.28	102	2.91 ± 0.09	13.76	295	3.42 ± 0.13	2.58 ± 0.23	197.3	97	10.4	20.6
	12.41	213	3.31 ± 0.03	13.93	292	3.01 ± 0.07	$2 \pm$	218.8	98	10.4	20.6
^{164}Ho	12.31	204	2.74 ± 0.11	16.23	306	3.07 ± 0.17	3.11 ± 0.27	176.0	97	10.4	20.6
	12.47	223	3.21 ± 0.06	16.46	243	3.01 ± 0.09	$2 \pm$	200.8	98	10.4	20.6
^{166}Er	12.32	191	2.71 ± 0.14	13.99	304	3.67 ± 0.16	3.38 ± 0.33	129.5	94	10.7	20.6
	12.50	214	3.43 ± 0.08	16.15	253	3.09 ± 0.10	$2 \pm$	161.7	95	10.7	20.6
^{170}Yb	12.68	106	2.55 ± 0.10	15.03	281	6.01 ± 0.27	4.00 ± 1.78	172.1	89	10.6	20.0
	12.88	216	3.22 ± 0.11	15.46	237	3.87 ± 0.20	$2 \pm$	173.7	90	10.6	20.0

Note. The lower values of the parameters in each column were found with the requirement $\sigma_1 \Gamma_2 : \sigma_2 \Gamma_1 = 2:1$.

TABLE 3. Static deformation β and intrinsic quadrupole moment Q_0 .

Nucleus	Present work		Other photonuclear experiments		Coulomb excitation of nuclei
	β	Q_0 , b	β	Q_0 , b	
^{160}Yb	0.29	6.33 ± 0.6	0.29	$6.37 [18]$	$7.07 [19]$
			0.32	$7.37 [20]$	
			0.29	$6.6 [18]$	
^{164}Ho	0.32	7.73 ± 0.6	0.29	$7.01 [18]$	$7.80 [19]$
			0.30	$7.14 [18]$	
			0.31	$7.6 [18]$	
^{166}Er	0.30	7.39 ± 0.6	0.28	$6.96 [18]$	
			0.31	$7.6 [18]$	
^{170}Yb	0.28	6.94 ± 0.6			$6.79 [21]$

TABLE 6. Integrated cross sections.

Nucleus	σ_{γ} , MeV-b	$\sigma_{\gamma} \cdot 10^4 \frac{\text{Z}^2 Y}{A}$	σ_{γ} , mb	$\sigma_{\gamma} A^{4/3}$	σ_{γ} , MeV-b	$\sigma_{\gamma} A^{4/3}$
^{160}Yb	3.79	1.47	210	0.243	15.9	$2.41 \cdot 10^{-3}$
^{164}Ho	3.60	1.31	218	0.241	16.1	$3.22 \cdot 10^{-4}$
^{166}Er	3.56	1.38	216	0.237	16.1	$3.21 \cdot 10^{-4}$
^{170}Yb	-3.05	1.20	196	0.196	14.8	$2.03 \cdot 10^{-4}$
Average		1.41 \pm 0.3		0.23 \pm 0.04		$3.1 \cdot 10^{-3} \pm 6 \cdot 10^{-4}$

¹² A.N. Tikhonov, Dokl. Akad. Nauk SSSR 151, 501 (1963), Eng. transl. in Sov. Mathematics-Doklady.

¹⁵ B. L. Berman et al., Phys. Rev. 185, 1576 (1969).

¹⁶ R. Bergere et al., Nucl. Phys. A133, 417 (1969).

¹⁸ E. G. Fuller et al., Nucl. Phys. 30, 613 (1962).

¹⁹ H. Arenhovel et al., Phys. Rev. 157, 1109 (1967).

²⁰ R. Bergere et al., Nucl. Phys. A121, 463 (1968).

²¹ O.V. Bogdankevich et al., Zh. Eksp. Teor. Fiz. 42, 1502 (1962); Sov. Phys. JETP 15, 1044 (1962).

²² B.S. Dzhelepov in Struktura slozhnykh yader (Structure of Complex Nuclei), Atomizdat, 1966, p. 189.

ELEM. SYM.	A	Z
Er	166	68

METHOD

REF. NO.
76 Me 4

hmg

REACTION	RESULT	EXCITATION ENERGY	SOURCE		DETECTOR		ANGLE
			TYPE	RANGE	TYPE	RANGE	
G,G	LFT	1- 4	C	2- 4	SCD-D		DST
		(1.66 - 3.19)					

13 STATES, 1.66-3.19

Some 40 states in $^{166,168,170}\text{Er}$, most of them previously unknown, have been excited using bremsstrahlung with ≤ 4.2 MeV endpoint energy. For all but three of these levels, the angular distribution of the resonantly scattered radiation favors the assignment of spin 1. For some of the strongly excited levels, linear polarization measurements have been performed. They indicate that these levels have positive parity. The branching ratios further characterize them as $K = 1$ excitations.

TABLE II. Properties of levels excited in ^{166}Er with photons of ≤ 3.3 MeV energy.

E_{level} (MeV)	I^{π}	Γ_0^2/Γ (meV)	$(\Gamma_c/\Gamma)^2$	Γ_0 (meV)
1.663 ^b	1 ⁻	12.0 ± 0.8	0.39 ± 0.01	32 ± 5
1.812 ^b	1 ⁺ c	4.8 ± 0.6	0.60 ± 0.02	8 ± 1
1.830 ^b	1 ⁻		~ 0.25	2.4
2.201	1 ⁽⁺⁾	5.4 ± 0.9	0.36 ± 0.03	15 ± 3
2.464	(1)	3.9 ± 0.8	0.63 ± 0.08	6 ± 2
2.524	(1)	8.3 ± 1.7	0.71 ± 0.10	12 ± 3
2.601	(1)	15.4 ± 1.6	0.62 ± 0.10	25 ± 5
2.679	(1)	9.1 ± 1.9	0.56 ± 0.08 d	16 ± 5
2.768	(1)	5.8 ± 1.1	0.46 ± 0.09	13 ± 4
2.782	(2)	2.2 ± 0.5	0.7 ± 0.2	3 ± 1
2.811	1	18.6 ± 2.3	0.32 ± 0.04	58 ± 11
3.141	1	35.0 ± 4.0	0.72 ± 0.05	49 ± 7
3.193	1	23.8 ± 2.7	0.71 ± 0.05	33 ± 5

^a This is really $\Gamma_0/(\Gamma_0 + \Gamma_1)$ since, in addition to the ground state transitions, only the cascade γ rays to the first 2⁺ state at 80.6 keV could be observed in the presence of the nonresonant background, which increased rapidly with decreasing γ energy.

^b See Ref. 1.^c See Ref. 9.^d (Combining our value $\Gamma_0/\Gamma = 0.60 \pm 0.15$ with the ratio 0.55 ± 0.09 reported in Ref. 11.)

¹F.R. Metzger et al., Phys. Rev. C8, 1099 (1973).

⁹F. R. Metzger et al., Bull. Am. Phys. Soc. 18, 1386 (1973).

¹¹S. B. Burson et al., Phys. Rev. C158, 1161 (1967).

ELEM. SYM.	A	Z
Er	166	68

METHOD

REF. NO.
 78 Mu 9 hg

REACTION	RESULT	EXCITATION ENERGY	SOURCE		DETECTOR		ANGLE
			TYPE	RANGE	TYPE	RANGE	
E,A	ABX	7-100	D	100	MAG-D		DST

α particles from the electrodisintegration of seven nuclei with Z between 29 and 79 have been observed. Energy spectra at 50° in the laboratory for six nuclei and angular distributions for five nuclei are reported. The cross sections exhibit a broad peak whose magnitude decreases with increasing Z ; the energy of the peak increases as Z increases. Angular distributions at the highest energies measured become increasingly forward peaked suggesting a direct-reaction process.

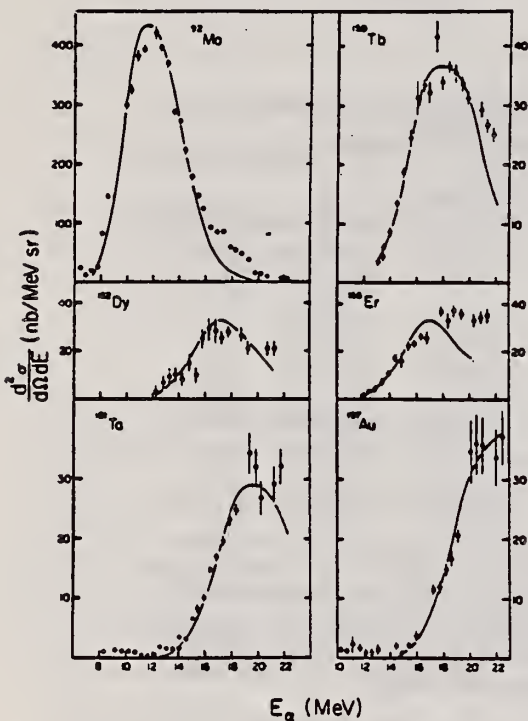


FIG. 2. The α -particle energy spectra at 50° in the laboratory for the four new nuclei studied as well as for two nuclei in which additional data have been obtained. The solid curves are the evaporation model fits described in text.

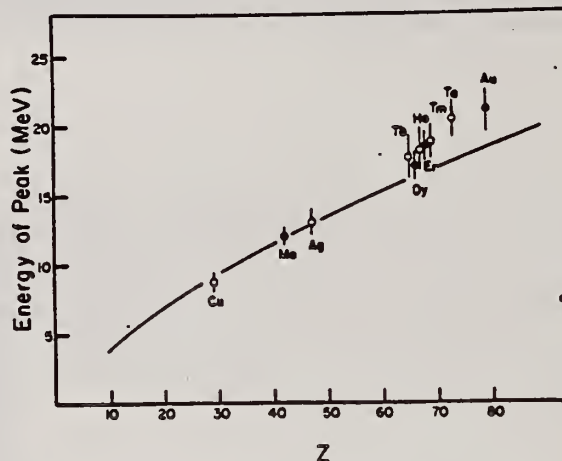


FIG. 3. Energy of the cross section peak as a function of Z . The solid line is the energy of the classical Coulomb barrier. The closed circles are the current work; the open circles are from Ref. 1.

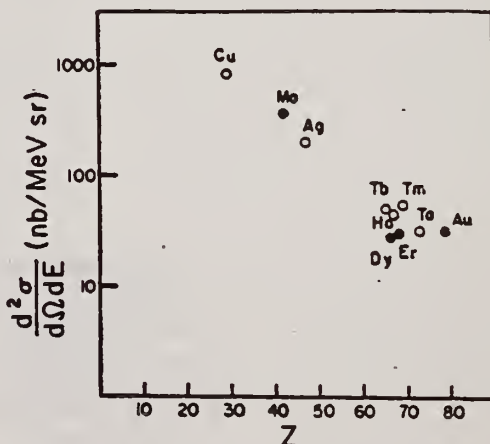


FIG. 4. Magnitude of cross section peak as a function of Z . The closed circles are the current work; the open circles are from Ref. 1.

¹J.J. Murphy, II, H.J. Gehrhardt, and D.M. Skopik, Nucl. Phys. A277, 69 (1977).

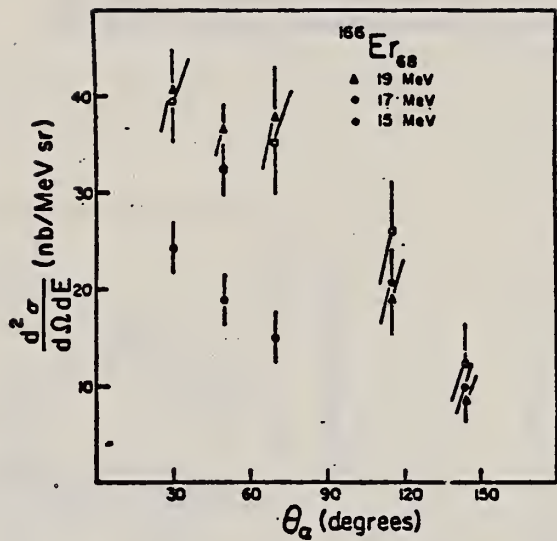


FIG. 7. Angular distributions for erbium. The comments made for Fig. 5 apply here.

ELEM. SYM.	A	Z
ER	166	68
REF. NO.	80 Na 1	hg

METHOD

REACTION	RESULT	EXCITATION ENERGY	SOURCE	DETECTOR	ANGLE
			TYPE RANGE	TYPE RANGE	
G,G/	SPC	16	D 14-17	MAG-D	DST
		(16.4)	(14.4-16.6)		

Quasi-monochromatic photons in the range $E_\gamma = 14.4-16.6$ MeV have been used to study inelastic scattering to the 2^+ , γ -vibrational band head in ^{166}Er . The results for transitions to this branch are drastically smaller (by a factor $\approx 3-5$) than the predictions of the dynamic collective model (DCM).

BRAN RATIO, VIBR ELAS

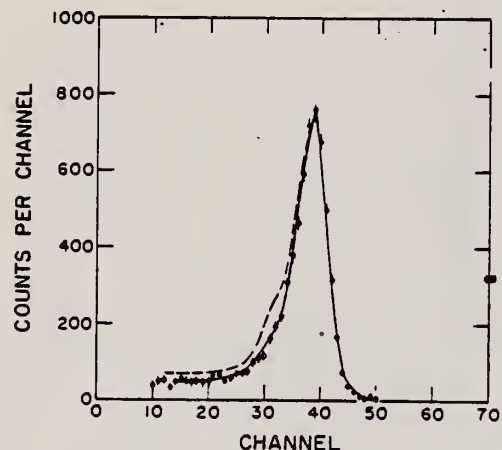


Fig. 1. Spectra at 109° of 16.4 MeV tagged photons scattered from $^{166,168}\text{Er}$ measured with a $24 \times 30 \text{ cm}^2$ NaI detector. This spectrum was obtained by merging separate spectra of energies 16.2, 16.4 and 16.6 MeV. The solid line is the shape of the detector response to elastically scattered photons, which was obtained with a ^{209}Bi target. The dashed line shows the calculated spectrum obtained by adding a 10% inelastic branch (to the 785 keV level) to the pure elastic peak.

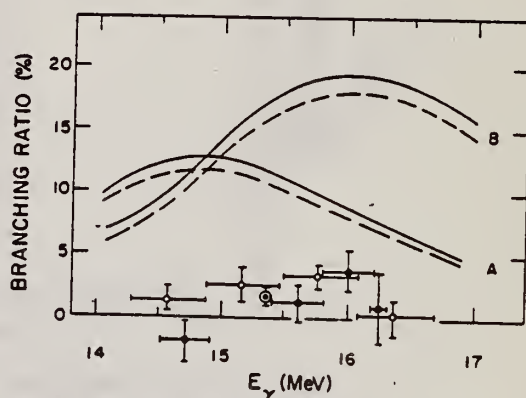


Fig. 2. Measured and calculated branching ratios of the vibrational inelastic to the elastic plus rotational inelastic cross sections. The closed (open) circles are data taken at 90° (109°). The double circle represents the measured average branching ratio over all energies. The solid (dashed) lines, A and B, are the results obtained at 90° (109°) using the parameters given in table 1 and the DCM code of Arenhövel [12].

ER
A=167

ER
A=167

ER
A=167

METHOD

Betatron; neutron threshold; ion chamber

REF. NO.

60 Ge 3

NVB

REACTION	RESULT	EXCITATION ENERGY	SOURCE		DETECTOR		ANGLE
			TYPE	RANGE	TYPE	RANGE	
G, N	N _O X	THR	C THR		BF ₃ -I		4 PI

THRESHOLD

TABLE I. Summary and comparison of neutron separation energies inferred from present threshold measurements with values predicted from mass data and reaction energies. All energies are expressed in the center-of-mass system in Mev.

Reaction	No. runs	Present results	Other results	Method	Reference
Er ¹⁶⁷ (γ , n)Er ¹⁶⁶	1	6.64 ± 0.08 (6.56)	6.45 ± 0.06	mass data	q

* W. H. Johnson, Jr., and V. B. Bhanot, Phys. Rev. 107, 6 (1957).

TABLE II. Comparison of measured threshold energies with neutron binding energies predicted by mass data for transitions with $\Delta I \geq 7/2$. All energies in Mev.

Reaction	ΔI^a	Observed threshold	Mass data Q value	$E_b - Q$	Excited state energy
Cr ⁵⁸ (γ , n)Cr ⁵¹	7/2	12.18 ± 0.14	12.053 ± 0.004 ^b	0.13 ± 0.14	...
Y ⁸⁹ (γ , n)Y ⁸⁸	7/2	11.59 ± 0.08	11.53 ± 0.40 ^c	0.06 ± 0.41	0.387 ^d
In ¹¹³ (γ , n)In ¹¹⁴	7/2	9.22 ± 0.03	9.33 ± 0.43 ^e	-0.13 ± 0.43	0.191 ^e
Ce ¹⁴⁰ (γ , n)Ce ¹⁴¹	(7/2) ^f	7.24 ± 0.07	6.97 ± 0.07 ^f	0.27 ± 0.10	...
Nd ¹⁴⁴ (γ , n)Nd ¹⁴⁴	7/2	6.38 ± 0.16	5.97 ± 0.19 ^f	0.41 ± 0.25	0.690 ^e
Sm ¹⁴⁹ (γ , n)Sm ¹⁴⁸	7/2	6.45 ± 0.16	5.87 ± 0.28 ^f	0.58 ± 0.33	0.562 ^e
Er ¹⁶⁷ (γ , n)Er ¹⁶⁶	7/2	6.65 ± 0.08	6.45 ± 0.06 ^g	0.20 ± 0.10	0.081 ^e
Hf ¹⁷⁷ (γ , n)Hf ¹⁷⁶	7/2	6.69 ± 0.03	6.28 ± 0.06 ^g	0.64 ± 0.07	0.088 ^e
Hf ¹⁷⁹ (γ , n)Hf ¹⁷⁸	9/2	6.31 ± 0.07	6.17 ± 0.06 ^g	0.14 ± 0.09	0.093 ^e
Hf ¹⁸⁰ (γ , n)Hf ¹⁷⁹	9/2	7.85 ± 0.11	7.32 ± 0.06 ^g	0.53 ± 0.13	0.375 ^e

^a D. Strominger, J. M. Hollander, and G. T. Seaborg, Revs. Modern Phys. 30, 585 (1958).

^b C. F. Giess and J. L. Benson, Phys. Rev. 110, 712 (1958).

^c Henry E. Duckworth, *Mass Spectroscopy* (Cambridge University Press, New York, 1958), p. 177.

^d S. Dzlepov and L. K. Peker, Atomic Energy of Canada Limited Report Tr. AECL-457 (unpublished).

^e The discrepancy in the case of Ce¹⁴⁰ predicts a ground-state spin for Ce¹⁴¹ of 0, since the spin of Ce¹⁴¹ is known to be 7/2.

^f W. H. Johnson, Jr., and A. O. Nier, Phys. Rev. 105, 1014 (1957).

^g W. H. Johnson, Jr., and V. B. Bhanot, Phys. Rev. 107, 6 (1957).

ER
A=168

ER
A=168

ER
A=168

ELEM. SYM.	A	Z
Er	168	68

METHOD

REF. NO.

73 Me 4

hmg

REACTION	RESULT	EXCITATION ENERGY	SOURCE		DETECTOR		ANGLE
			TYPE	RANGE	TYPE	RANGE	
\$ G,G	LFT	2	C	2	SCD-D		DST

1.786 MEV LEVEL

In addition to the previously known 1^- states of ^{166}Er at 1663 and 1830 keV, levels at 1812 ± 1 keV (^{166}Er), 1786 ± 1 keV (^{166}Er), and 1824 ± 1 keV (^{170}Er) have been excited using electron bremsstrahlung. Based on the observed angular distributions of the scattered photons, all three previously unknown levels were found to have spin 1. Linear polarization measurements using a two-slab Ge(Li) polarimeter led to negative parity assignments for the 1786- and 1824-keV levels but were inconclusive with respect to the less strongly excited 1812-keV level. Below 1.9 MeV, the 1663-, 1786-, and 1824-keV levels are the dominant $E1$ excitations in their respective isotopes, the partial widths of their ground-state transitions being $\Gamma_0 = 32 \pm 5$, 46 ± 5 , and 30 ± 3 meV. The $B(E1; 1^- \rightarrow \text{g.s.})/B(E1; 1^- \rightarrow 2^+_1)$ ratios of 0.52 ± 0.02 , 0.51 ± 0.02 , and 0.53 ± 0.02 differ considerably from the ratio 1.31 ± 0.11 for the 1812-keV level and the reported ratio 0.22 for the 1830-keV 1^- state and are very close to the Alaga value of 0.50 for $K=0^-$ levels.

TABLE III. Results of the measurements using the two-slab Ge(Li) polarimeter. N_{\parallel} and N_{\perp} represent the counting rates in the full energy peaks with the slabs parallel and perpendicular to the scattering plane, respectively.

Isotope	E_{level} (keV)	Transition $I_1 - I_2$	E_{γ} (keV)	$(N_{\parallel} - N_{\perp})/(N_{\parallel} + N_{\perp})$ (%)
^{166}Er	1662	$1^- - 0^+$	1662	$+7.4 \pm 4.9$
		$1^- - 2^+$	1582	$+3.7 \pm 3.4$
^{181}Er	1812	$1^- - 0^+$	1812	-5.6 ± 10.0
		$1^- - 2^+$		
^{166}Er	1786	$1^- - 0^+$	1786	$+16.7 \pm 7.4$
		$1^- - 2^+$	1706	-1.4 ± 4.3
^{170}Er	1824	$1^- - 0^+$	1824	$+9.8 \pm 4.8$
		$1^- - 2^+$	1745	0.0 ± 3.1

TABLE II. Comparison of the experimental ratios of the counting rates in the 98° and 127° scattering geometries with the ratios expected for different values of the spins of the excited states.

Isotope	E_{level} (keV)	$N(127^\circ)/N(98^\circ)$	
		Theory	Experiment
^{166}Er	1663	1.39 ± 0.11	
^{166}Er	1812	1.40 ± 0.17	
^{166}Er	1786	1.38 ± 0.07	
^{170}Er	1824	1.33 ± 0.09	
		1.36	0.49

TABLE IV. Widths and branching ratios of the $^{166}, 166, 170$ Er levels. The direct results of the NRF scattering experiments are listed in column 5.

Isotope	Level (keV)	Γ_0/Γ_1	$B(E1; 1^- \rightarrow \text{g.s.})/B(E1; 1^- \rightarrow 2^+_1)$	Γ_0^2/Γ (meV)	Γ_0/Γ^*	Γ_0 (meV)
^{166}Er	1663	0.60 ± 0.02^b	0.52 ± 0.02	12.0 ± 1.8	0.38 ± 0.01	32 ± 5
	1812	1.50 ± 0.12	1.31 ± 0.11^c	4.8 ± 0.6	0.60 ± 0.02	8 ± 1
	1830	$\approx 0.33^d$	≈ 0.22	...	≈ 0.25	2.4
^{166}Er	1786	0.59 ± 0.02	0.51 ± 0.02	17.0 ± 1.7	0.37 ± 0.01	46 ± 5
^{170}Er	1824	0.61 ± 0.02	0.53 ± 0.02	11.4 ± 1.1	0.38 ± 0.01	30 ± 3

^a Assuming the absence of branching to levels above the 2^+_1 state.

^b In good agreement with the value of 0.61 adopted in Ref. 18.

^c This might be the ratio of $B(M1)$'s rather than $B(E1)$'s since the polarization experiment was not conclusive.

^d From the decay of ^{166}Ho ; see Ref. 18.

ELEM. SYM.	A	Z
Er	168	68

METHOD					REF. NO.		
REACTION	RESULT	EXCITATION ENERGY	SOURCE		DETECTOR		ANGLE
			TYPE	RANGE	TYPE	RANGE	
G,G	LFT	1- 4 (1.786-3.481)	C	I- 4	SCD-D		DST

20 STATES, 1.79-3.48

Some 40 states in $^{166,168,170}\text{Er}$, most of them previously unknown, have been excited using bremsstrahlung with ≤ 4.2 MeV endpoint energy. For all but three of these levels, the angular distribution of the resonantly scattered radiation favors the assignment of spin 1. For some of the strongly excited levels, linear polarization measurements have been performed. They indicate that these levels have positive parity. The branching ratios further characterize them as $K = 1$ excitations.

TABLE III. Properties of levels excited in ^{168}Er with photons of ≤ 3.5 MeV energy.

E_{level} (MeV)	I^*	Γ_0^2/Γ (meV)	$(\Gamma_0/\Gamma)^a$	Γ_0 (meV)
1.786 ^b	1 ⁻	17.0 ± 1.7	0.37 ± 0.01	46 ± 5
1.935	(1)	1.5 ± 0.4	~ 1	~ 1.5
(2.136)	(1, 2)	2.1 ± 0.6^c	0.62 ± 0.15	3.4 ± 1.3
2.363	(1)	3.1 ± 0.5	0.8 ± 0.1	4 ± 1
2.417	(1)	3.3 ± 0.9	0.36 ± 0.07	9 ± 3
2.495	(1)	6.5 ± 0.8	0.66 ± 0.06	10 ± 2
2.676	(1)	10.4 ± 1.1	0.76 ± 0.05	14 ± 2
2.728	(1)	7.6 ± 1.0	0.50 ± 0.05	15 ± 3
2.792	1	12.0 ± 1.2	0.9 ± 0.1	13 ± 2
2.798	1	13.7 ± 1.4	0.9 ± 0.1	15 ± 3
2.828	(1)	4.3 ± 0.9	0.62 ± 0.10	7 ± 2
2.849	(1)	5.1 ± 1.5	0.70 ± 0.12	7 ± 3
2.856	(1)	3.3 ± 1.1	0.35 ± 0.07	10 ± 4
2.946	(1)	4.6 ± 1.2	0.39 ± 0.05	12 ± 4
3.358	1	30.7 ± 4.0	0.61 ± 0.04	50 ± 8
3.391	1 ⁽⁺⁾	78 ± 7	0.69 ± 0.03	113 ± 12
3.410	(1)	16.6 ± 2.2	0.54 ± 0.05	31 ± 6
3.458	1	37 ± 5	0.63 ± 0.06	59 ± 10
3.469	(1)	23 ± 6	?	
3.481	(1)	17 ± 5	0.42 ± 0.07	41 ± 14

^aThis is really $\Gamma_0/(\Gamma_0 + \Gamma_1)$ since, in addition to the ground state transition, only the cascade transitions to the first 2^+ state at 79.8 keV could be observed.

^bSee Ref. 1.^c(Assuming spin 1.)

¹F. R. Metzger et al., Phys. Rev. C8, 1099 (1973).

REF. G.M. Gurevich, L.E. Lazareva, V.M. Mazur, S.Yu. Merkulov,
 G.V. Solodukhov, V.A. Tyutin
 JETP Lett. 28, 157 (1978)
 Pis'ma Zh. Eksp. Teor. Fiz. 28, 168 (1978)

ELEM. SYM.	A	Z
Er	168	68
REF. NO.		
78 Gu 7		hg

METHOD

REACTION	RESULT	EXCITATION ENERGY	SOURCE		DETECTOR		ANGLE
			TYPE	RANGE	TYPE	RANGE	
G,MU-T	ABX	THR-30	C	UKN	NAI-D		4PI

The absorption method is used to measure the total photoabsorption cross section curves for deformed ^{154}Sm , ^{156}Gd , ^{168}Er , ^{174}Yb , ^{184}W , and ^{186}W nuclei in the region of the E1 giant resonance. The behavior of the resonance widths for nuclei in the interval $A = 153$ to 186 is discussed.

PACS numbers: 24.30.Cz, 25.20.+y, 27.70.+q

TABLE I.

Nucleus	E_1 MeV	σ_1 mb	Γ_1 MeV	E_2 MeV	σ_2 mb	Γ_2 MeV	Γ MeV	Q_o b	β	$\sigma_{oL} / 0.06 \frac{ZN}{A}$
^{154}Sm	12.2	188	3.4	15.7	207	5.7	8.1 ± 0.2	6.3 ± 0.3	0.32 ± 0.02	1.28
^{156}Gd	12.3	206	3.2	15.7	220	5.5	7.7 ± 0.2	6.2 ± 0.3	0.31 ± 0.02	1.30
^{168}Er	11.9	222	3.2	15.5	275	4.5	7.4 ± 0.2	7.5 ± 0.7	0.32 ± 0.03	1.26
^{174}Yb	12.3	297	2.9	15.5	320	4.9	7.1 ± 0.2	7.0 ± 0.6	0.30 ± 0.02	1.52
^{184}W	11.9	315	2.9	14.8	321	4.7	6.8 ± 0.2	7.2 ± 0.8	0.27 ± 0.03	1.50
^{186}W	12.0	246	3.3	14.5	332	5.1	6.4 ± 0.2	6.2 ± 0.8	0.23 ± 0.03	1.48
Average error	$\pm 1.3\%$	$\pm 10.5\%$	$\pm 7.5\%$	$\pm 1.3\%$	$\pm 9.4\%$	$\pm 3.8\%$	—	—	—	—

(over)

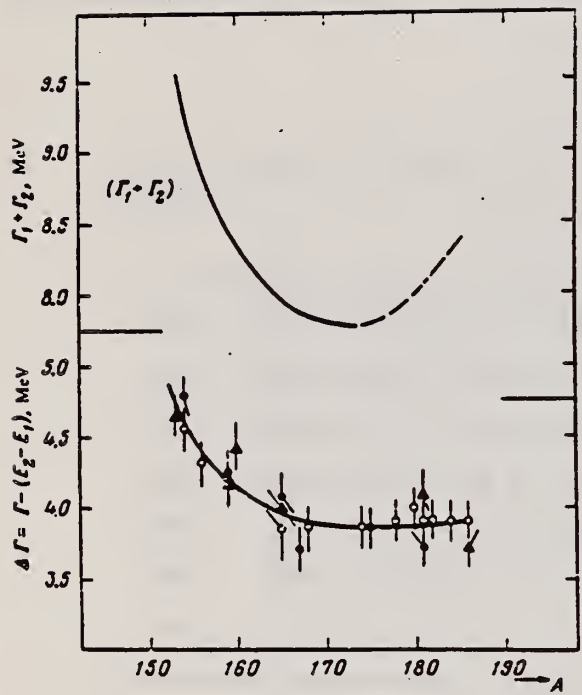


FIG. 3. Experimental values of $\Delta\Gamma = \Gamma - (E_2 - E_1)$ in the region of deformed nuclei with $A = 153-186$: ○—present work and " "; ●—Saclay group; ▲—Livermore group. Owing to a small systematic deviations of the absolute values, the ordinate scales for the Saclay and Livermore data are shifted 0.15 MeV upward and downward, respectively. The $(\Gamma_1 + \Gamma_2)$ curve was obtained from the $\Delta\Gamma$ curve after introduction of corrections in the interval $A = 175-186$.

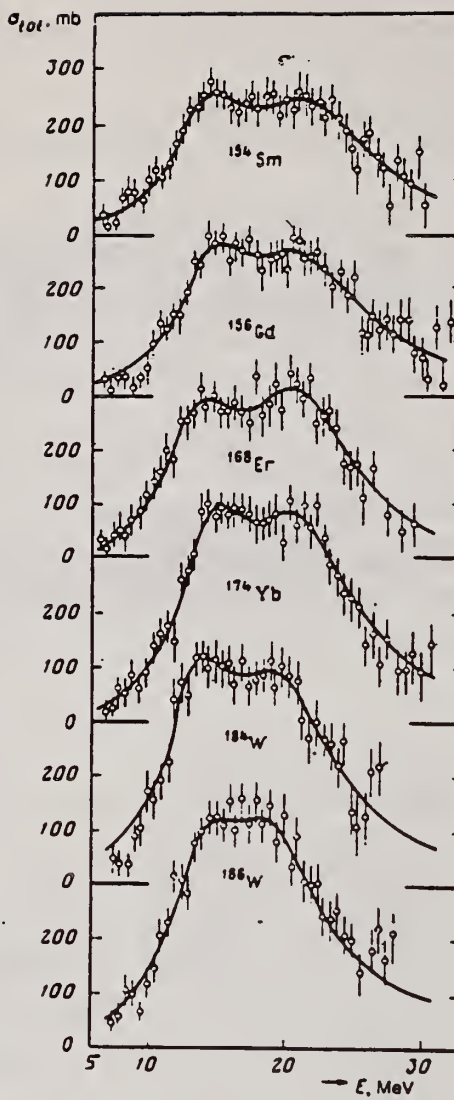


FIG. 2. Total cross sections of the photoabsorption of the nuclei ^{154}Sm , ^{156}Gd , ^{168}Er , ^{174}Yb , ^{184}W , and ^{186}W . The mean squared errors are shown.

ELEM. SYM.	A	Z
Er	168	68

METHOD

REF. NO.	hg
81 Gu. 2	

REACTION	RESULT	EXCITATION ENERGY	SOURCE	DETECTOR	ANGLE	
			TYPE	RANGE		
G, MU-T	ABX	THR-20	C	27	NAI-D	4PI

Abstract: The curves of the total gamma-absorption cross sections (σ_{tot}) in the E1 giant resonance energy range for the nuclei ^{154}Sm , ^{156}Gd , ^{165}Ho , ^{168}Er , ^{174}Yb , 178 , ^{180}Hf , ^{181}Ta , ^{182}W , ^{184}W , ^{186}W and ^{197}Au have been measured using the absorption method. Parameters of the Lorentz curves fitting the measured cross sections σ_{tot} are given. Quadrupole moments (Q_0) and nuclear deformation parameters (β) were obtained.

For deformed nuclei in the $\sim 155 < A < \sim 180$ region a violation of the correlation between giant resonance widths (Γ) and nuclear deformation parameters was found. Γ_1 and Γ_2 , the widths of the resonances corresponding to vibrations of nucleons along and across the nuclear deformation axis, were observed to decrease with the increase of A which could be accounted for by the presence of an $N = 108$ subshell.

NUCLEAR REACTIONS ^{154}Sm , ^{156}Gd , ^{165}Ho , ^{168}Er , ^{174}Yb , 178 , ^{180}Hf , ^{181}Ta , 182 , 184 , ^{186}W , ^{197}Au (γ , X). $E = 7$ -20 MeV; measured total $\sigma(E)$; deduced integrated σ , Lorentz line parameters. ^{154}Sm , ^{156}Gd , ^{165}Ho , ^{168}Er , ^{174}Yb , 178 , ^{180}Hf , ^{181}Ta , 182 , 184 , ^{186}W , ^{197}Au deduced β , Q_0 , Γ , giant resonance evolution. Enriched, natural targets.

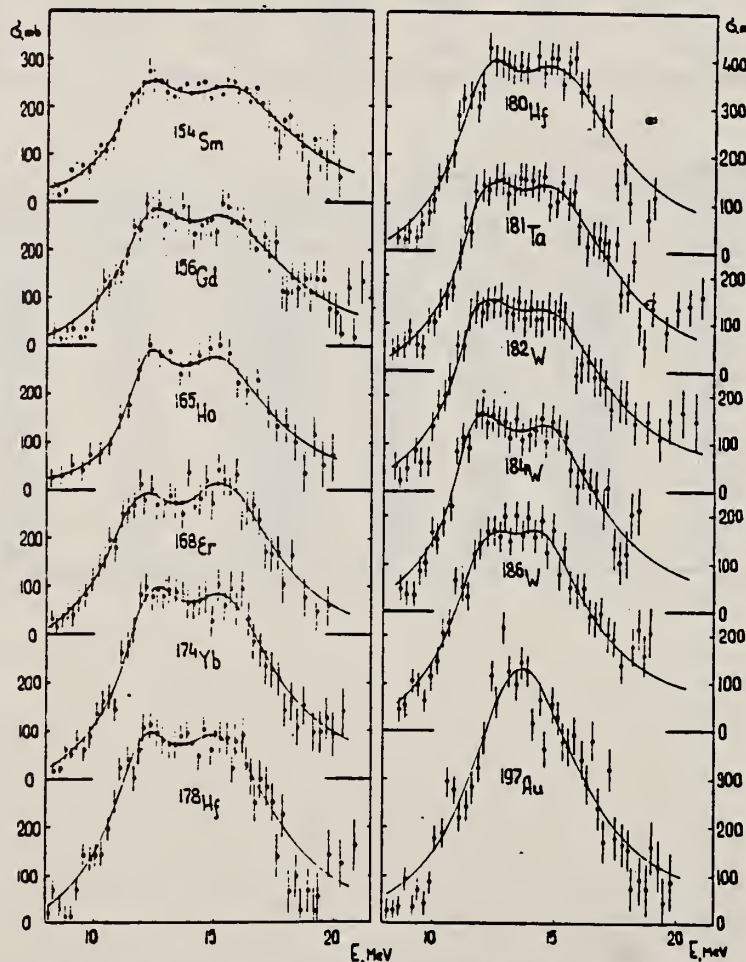


Fig. 2. Total nuclear γ -absorption cross sections (σ_{tot}) measured by the absorption method for ^{154}Sm , ^{156}Gd , ^{165}Ho , ^{168}Er , ^{174}Yb , ^{178}Hf , ^{180}Hf , ^{181}Ta , ^{182}W , ^{184}W , ^{186}W and ^{197}Au . Rms error bars are shown.

TABLE 2
Parameters of Lorentz curves fitting the experimental data on σ_{tot}

Nucleus	E_1 (MeV)	σ_1 (mb)	Γ_1 (MeV)	E_2 (MeV)	σ_2 (mb)	Γ_2 (MeV)	$\frac{\sigma_2 \Gamma_2}{\sigma_1 \Gamma_1}$	Γ (MeV)
^{154}Sm	12.2	188	3.4	15.7	207	5.7	1.85	8.1
^{156}Gd	12.3	206	3.2	15.7	220	5.5	1.81	7.7
^{165}Ho	12.3	202	2.3	15.2	239	4.8	2.47	7.0
^{168}Er	11.9	222	3.2	15.5	275	4.5	1.73	7.4
^{174}Yb	12.3	297	2.9	15.5	320	4.9	1.80	7.1
^{178}Hf	12.2	291	3.1	15.5	334	4.9	1.80	7.2
^{180}Hf	12.2	286	3.2	15.3	324	5.1	1.81	7.1
^{181}Ta	12.1	272	3.0	15.0	316	5.1	1.97	6.8
^{182}W	11.9	267	3.2	14.8	303	5.6	2.01	6.8
^{184}W	11.9	315	2.9	14.8	321	4.7	1.65	6.8
^{186}W	12.0	246	3.3	14.5	332	5.1	2.07	6.4
^{197}Au	13.7	535	5.2					
Average error	1.4 %	11.2 %	9.3 %	1.5 %	9.7 %	4.6 %	0.22	0.2 MeV

TABLE 3
Ratios of nuclear ellipsoid axes (k), deformation parameters (β) and intrinsic quadrupole moments (Q_0), calculated from E_2/E_1

Nucleus	^{154}Sm	^{156}Gd	^{165}Ho	^{168}Er	^{174}Yb	^{178}Hf	^{180}Hf	^{181}Ta	^{182}W	^{184}W	^{186}W
k	1.320	1.302	1.259	1.327	1.289	1.296	1.281	1.263	1.271	1.268	1.229
β	0.326 ± 0.017	0.309 ± 0.016	0.266 ± 0.036	0.334 ± 0.032	0.296 ± 0.024	0.303 ± 0.032	0.288 ± 0.036	0.270 ± 0.026	0.278 ± 0.030	0.274 ± 0.032	0.235 ± 0.033
Q_0	6.3 ± 0.3	6.2 ± 0.3	5.8 ± 0.8	7.5 ± 0.7	7.0 ± 0.6	7.5 ± 0.8	7.2 ± 0.9	6.9 ± 0.7	7.2 ± 0.8	7.1 ± 0.8	6.2 ± 0.9

TABLE 4
Integral characteristics of E1 giant resonance

Nucleus	σ_{0LL} (MeV \cdot mb)	σ_{0RR} (MeV \cdot mb)	σ_{0L} (MeV \cdot mb)	σ_{0L} (MeV \cdot mb)	σ_+ (mb)	σ_{-1L} (mb)	$\sigma_{-1L} \cdot 10^{-4}$ (mb)	σ_{-2L} (mb \cdot MeV $^{-1}$)	σ_{-2L} (mb \cdot MeV $^{-1}$)	σ_{-2L} (μ b \cdot MeV $^{-1}$)
^{154}Sm	1.94 ± 0.06	0.87	2.86	1.29	117 ± 3.5	156	0.189	9.1 ± 0.3	14.3	3.23
^{156}Gd	2.07 ± 0.07	0.91	2.95	1.30	143 ± 4.6	163	0.194	10.5 ± 0.4	14.9	3.30
^{165}Ho	1.86 ± 0.06	0.78	2.53	1.06	155 ± 4.4	160	0.177	10.1 ± 0.3	12.6	2.54
^{168}Er	2.24 ± 0.06	0.92	3.07	1.26	161 ± 4.3	197	0.212	12.0 ± 0.3	16.0	3.13
^{174}Yb	2.69 ± 0.05	1.07	3.82	1.52	195 ± 3.4	240	0.247	14.5 ± 0.3	19.2	3.54
^{178}Hf	2.85 ± 0.07	1.11	3.99	1.55	208 ± 4.9	247	0.247	15.3 ± 0.4	20.2	3.59
^{180}Hf	2.72 ± 0.06	1.05	4.03	1.56	200 ± 4.4	250	0.246	15.1 ± 0.3	20.7	3.61
^{181}Ta	2.84 ± 0.07	1.09	3.81	1.46	210 ± 5.3	245	0.239	16.0 ± 0.4	20.0	3.45
^{182}W	2.86 ± 0.07	1.09	4.01	1.52	211 ± 5.3	256	0.248	16.2 ± 0.4	21.6	3.70
^{184}W	2.78 ± 0.07	1.05	3.80	1.43	207 ± 5.3	251	0.240	15.9 ± 0.4	20.9	3.51
^{186}W	2.90 ± 0.07	1.08	3.95	1.48	214 ± 5.3	256	0.241	16.2 ± 0.4	21.6	3.56
^{197}Au	3.12 ± 0.06	1.10	4.37	1.54	229 ± 4.2	276	0.241	18.6 ± 0.4	23.3	3.49

ER

A=170

ER

A=170

ER

Ref. K. Miyano, T. Kuroyanagi
Nuclear Phys. 49, 315 (1963)

Elem. Sym.	A	Z
Er	170	68

Method						Ref. No.
	Linac; radioactivity					63 Mi 3
Reaction*	E or ΔE	E_0	Γ	$\int \sigma dE$	$J\pi$	Notes
$^{170}\text{Er}(\gamma, p)$	Bremss. 21					Mostly identification of Ho^{169} and study of decay scheme No cross section data.

ELEM. SYM.	A	Z
Er	170	68
REF. NO.	73 Me 4	
REF. NO.	hmg	

METHOD

REACTION	RESULT	EXCITATION ENERGY	SOURCE		DETECTOR		ANGLE
			TYPE	RANGE	TYPE	RANGE	
\$ G,G	LFT	2	C	2	SCD-D		DST

1.824 MEV LEVEL

In addition to the previously known 1^- states of ^{166}Er at 1663 and 1830 keV, levels at 1812 ± 1 keV (^{166}Er), 1786 ± 1 keV (^{166}Er), and 1824 ± 1 keV (^{170}Er) have been excited using electron bremsstrahlung. Based on the observed angular distributions of the scattered photons, all three previously unknown levels were found to have spin 1. Linear polarization measurements using a two-slab Ge(Li) polarimeter led to negative parity assignments for the 1786- and 1824-keV levels but were inconclusive with respect to the less strongly excited 1812-keV level. Below 1.9 MeV, the 1663-, 1786-, and 1824-keV levels are the dominant $E1$ excitations in their respective isotopes, the partial widths of their ground-state transitions being $\Gamma_0 = 32 \pm 5$, 46 ± 5 , and 30 ± 3 meV. The $B(E1; 1^- - \text{g.s.})/B(E1; 1^- - 2^+_1)$ ratios of 0.52 ± 0.02 , 0.51 ± 0.02 , and 0.53 ± 0.02 differ considerably from the ratio 1.31 ± 0.11 for the 1812-keV level and the reported ratio 0.22 for the 1830-keV 1^- state and are very close to the Alaga value of 0.50 for $K=0^-$ levels.

TABLE III. Results of the measurements using the two-slab Ge(Li) polarimeter. N_1 and N_2 represent the counting rates in the full energy peaks with the slabs parallel and perpendicular to the scattering plane, respectively.

Isotope	E_{level} (keV)	Transition $I_1 - I_2$	E_γ (keV)	$(N_1 - N_2)/(N_1 + N_2)$ (%)
^{166}Er	1662	$1^- - 0^+$	1662	$+7.4 \pm 4.9$
		$1^- - 2^+$	1582	$+3.7 \pm 3.4$
	1812	$1^- - 0^+$	1812	-5.6 ± 10.0
^{166}Er	1786	$1^- - 0^+$	1786	$+16.7 \pm 7.4$
		$1^- - 2^+$	1706	-1.4 ± 4.3
^{170}Er	1824	$1^- - 0^+$	1824	$+9.8 \pm 4.8$
		$1^- - 2^+$	1745	0.0 ± 3.1

TABLE II. Comparison of the experimental ratios of the counting rates in the 98 and 127° scattering geometries with the ratios expected for different values of the spins of the excited states.

Isotope	E_{level} (keV)	$N(127^\circ)/N(98^\circ)$		
		Experiment	Theory Spin 1	Spin 2
^{166}Er	1663	1.39 ± 0.11		
^{166}Er	1812	1.40 ± 0.17		
^{166}Er	1786	1.38 ± 0.07	1.36	0.49
^{170}Er	1824	1.33 ± 0.09		

TABLE IV. Widths and branching ratios of the $^{166}, 168, 170\text{Er}$ levels. The direct results of the NRF scattering experiments are listed in column 5.

Isotope	Level (keV)	Γ_0/Γ_1	$B(E1; 1^- - \text{g.s.})/B(E1; 1^- - 2^+_1)$	Γ_0^2/Γ (meV)	Γ_0/Γ^*	Γ_0 (meV)
^{166}Er	1863	0.60 ± 0.02^b	0.52 ± 0.02	12.0 ± 1.8	0.38 ± 0.01	32 ± 5
	1812	1.50 ± 0.12	1.31 ± 0.11^c	4.8 ± 0.8	0.60 ± 0.02	8 ± 1
	1830	$\approx 0.33^d$	≈ 0.22	...	≈ 0.25	2.4
^{166}Er	1786	0.59 ± 0.02	0.51 ± 0.02	17.0 ± 1.7	0.37 ± 0.01	46 ± 5
^{170}Er	1824	0.61 ± 0.02	0.53 ± 0.02	11.4 ± 1.1	0.38 ± 0.01	30 ± 3

^a Assuming the absence of branching to levels above the 2^+_1 state.

^b In good agreement with the value of 0.81 adopted in Ref. 18.

^c This might be the ratio of $B(M1)$'s rather than $B(E1)$'s since the polarization experiment was not conclusive.

^d From the decay of ^{166}Ho ; see Ref. 18.

ELEM. SYM.	A	Z
Er	170	68

METHOD

REF. NO.

76 Me 4

hmg

REACTION	RESULT	EXCITATION ENERGY	SOURCE		DETECTOR		ANGLE
			TYPE	RANGE	TYPE	RANGE	
G,G	LFT	1- 4 (1.824-3.406)	C	1- 4	SCD-D		DST

Some 40 states in $^{164,168,170}\text{Er}$, most of them previously unknown, have been excited using bremsstrahlung with ≤ 4.2 MeV endpoint energy. For all but three of these levels, the angular distribution of the resonantly scattered radiation favors the assignment of spin 1. For some of the strongly excited levels, linear polarization measurements have been performed. They indicate that these levels have positive parity. The branching ratios further characterize them as $K = 1$ excitations.

10 STATES, 1.82-3.41TABLE IV. Properties of levels excited in ^{170}Er with photons of ≤ 4.2 MeV energy.

E_{level} (MeV)	I^π	Γ_0^2/Γ (meV)	$(\Gamma_0/\Gamma)^2$	Γ_0 (meV)
1.824 ^b	1^-	11.4 ± 1.1	0.38 ± 0.01	30 ± 3
2.039	$(1^+, 2^+)^c$	1.2 ± 0.3^d	0.52^c	2.3 ± 0.7^d
2.133	(1)	3.7 ± 0.5	0.72 ± 0.05	5 ± 1
2.701	(1)	11.5 ± 2.2	0.67 ± 0.06	17 ± 4
2.751	(1)	3 ± 1	~ 1	3 ± 1
2.789	1^+	24.4 ± 2.5	0.67 ± 0.02	37 ± 4
2.930	(1)	3.3 ± 1.0	0.50 ± 0.15	7 ± 3
2.938	(1)	5.3 ± 1.2	0.60 ± 0.10	9 ± 3
3.064	(1)	14.1 ± 3.9	0.33 ± 0.09	43 ± 7
3.406	$1^{(+)}$	100 ± 12	0.69 ± 0.02	145 ± 18

^aThis is really $\Gamma_0/(\Gamma_0 + \Gamma_1)$ since, in addition to the ground state transitions, only the cascade γ rays to the first 2^+ state at 79.3 keV could be observed.

^bSee Ref. 1.

^cSee Ref. 5.

^d(Assuming spin 1.)

¹F. R. Metzger et al., Phys. Rev. C8, 1099 (1973).

⁵K. Kawade et al., J. Phys. Soc. Japan 36, 1221 (1974).

THULIUM

Z=69

Thulium is a very rare metallic element belonging to the rare earth group and was discovered in 1879 by P. T. Cleve while examining crude erbium oxide. The name comes from the Latin word *Thule* meaning the remote part of the northernmost inhabitable world. In 1911, C. James obtained a pure compound of the substance by the fractional crystallization of its impure bromate; this separation involved more than 15,000 operations.

TM
A=169

ELEM. SYM.	A	Z
Tm	169	69

Betatron					REF. NO.
REACTION	RESULT	EXCITATION ENERGY	SOURCE	DETECTOR	ANGLE
			TYPE RANGE	TYPE RANGE	
G, N	RLY	THR	C THR	BF ₃ -I	4PI

See 58 Kà 1 for cross sections

THRESHOLD

TABLE I
 MEASURED PHOTONEUTRON THRESHOLDS

Reaction	Measured Q value, Mev.	Other Q values, Mev.	Method	Reference
Tm ¹⁶⁹ (γ, n)Tm ¹⁶⁸	8.00 ± 0.05			

Tm¹⁶⁹(γ, n)Tm¹⁶⁸ 8.00 ± 0.05

METHOD Betatron; neutron cross section; BF_3 counters; ion chamber monitor

REF. NO.	58 Ka 1	NVB
----------	---------	-----

REACTION	RESULT	EXCITATION ENERGY	SOURCE		DETECTOR		ANGLE
			TYPE	RANGE	TYPE	RANGE	
G,XN	ABX	8-22	C	8-22	BF_3 -I		4PI

Таблица 2
 Пороги испускания фотонейтронов

Изотоп	B_{γ} , Мэв	B_m , Мэв	Изотоп	B_{γ} , Мэв	B_m , Мэв
V ⁵¹	11,16	20,5	L ¹³⁰	8,81	16,1
Mn ⁵⁵	10,14	19,2	Pr ¹⁴¹	9,46	17,6
Co ⁵⁹	10,44	18,6	Tb ¹⁵⁰	8,16	14,8
As ⁷⁵	10,24	18,1	Ho ¹⁶³	8,10	14,6
Y ⁸⁹	11,82	20,7	Tm ¹⁶⁹	8,00	14,7
Nb ⁹³	8,86	17,1	Lu ¹⁷⁵	7,11	14,2
Rb ¹⁰³	9,46	16,8	Ta ¹⁸¹	7,66	13,8
J ¹²⁷	9,14	16,2	Au ¹⁹⁷	7,96	13,3
Cs ¹³³	9,11	16,5	Bi ²⁰⁹	7,43	14,5

THRESHOLDS

не приведены, поскольку они превышают 22 Мэв во всех случаях, кроме золота, для которого $B_{3\pi} = 21$ Мэв. Свойства сечений $\sigma_C(\gamma)$ сведены в табл. 3.

Таблица 1

Изотоп	$E_{\text{ макс.}}$, Мэв	$\sigma_n(E_\gamma)$, барн	Γ , Мэв	$\frac{\sigma_n}{M\text{эв}} \cdot \text{барн}$	$Y(22)$, 10 ⁴ нейтрон/100 г-моль
V ⁵¹	18,4	0,062	5,2	0,33	1,62
Mn ⁵⁵	20,2	0,060	7,0	0,39	2,01
Co ⁵⁹	18,3	0,068	6,3	0,44	2,30
As ⁷⁵	16,4	0,090	9,5	0,74	4,25
Y ⁸⁹	17,1	0,172	5,2	0,93	5,33
Nb ⁹³	18,0	0,150	7,5	1,17	6,80
Rb ¹⁰³	17,5	0,160	9,4	1,40	8,28
J ¹²⁷	15,2	0,273	6,8	1,76	11,9
Cs ¹³³	16,5	0,238	7,7	1,59	10,7
La ¹³⁰	15,5	0,325	3,8	1,55	11,2
Pr ¹⁴¹	15,0	0,320	4,9	1,93	13,1
Tb ¹⁵⁰	15,6	0,274	9,8	2,49	18,1
Ho ¹⁶⁵	13,5	0,305	8,9	2,52	18,7
Tm ¹⁶⁹	16,4	0,250	8,4	1,91	14,9
Lu ¹⁷⁵	16,0	0,225	8,4	1,90	23,0
Ta ¹⁸¹	14,5	0,380	8,5	3,15	22,0
Au ¹⁹⁷	13,8	0,475	4,7	3,04	22,6
Bi ²⁰⁹	13,2	0,455	5,9	2,89	23,2

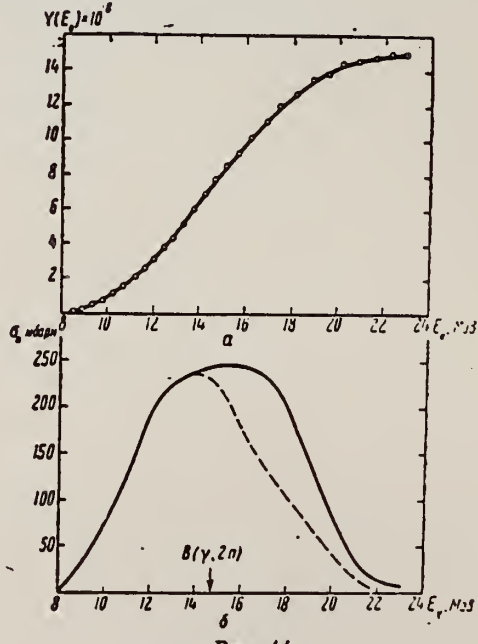


Рис. 14.
 а — Выход фотонейтронов для Tm; б — $\sigma_n(E_\gamma)$ для Tm
 и $\sigma_C(\gamma)$ для Tm

ELEM. SYM.	A	Z
Tm	169	69

METHOD

Betatron; neutron threshold; ion chamber

REF. NO.

60 Ge 3

NVB

REACTION	RESULT	EXCITATION ENERGY	SOURCE		DETECTOR		ANGLE
			TYPE	RANGE	TYPE	RANGE	
G, N	NOX	THR	C	THR	BF3-I		4 PI

THRESHOLD

TABLE I. Summary and comparison of neutron separation energies inferred from present threshold measurements with values predicted from mass data and reaction energies. All energies are expressed in the center-of-mass system in Mev.

Reaction	No. runs	Present results	Other results	Method	Reference
$Tm^{169}(\gamma, n)Tm^{168}$	2	8.11 ± 0.05	8.00 ± 0.05	threshold	f

METHOD

REF. NO.

73 Ba 20

egf

REACTION	RESULT	EXCITATION ENERGY	SOURCE		DETECTOR		ANGLE
			TYPE	RANGE	TYPE	RANGE	
G,N	NOX	THR- 27	C	10- 27	BF3-I		4PI

MEAN NEUT ENERGY

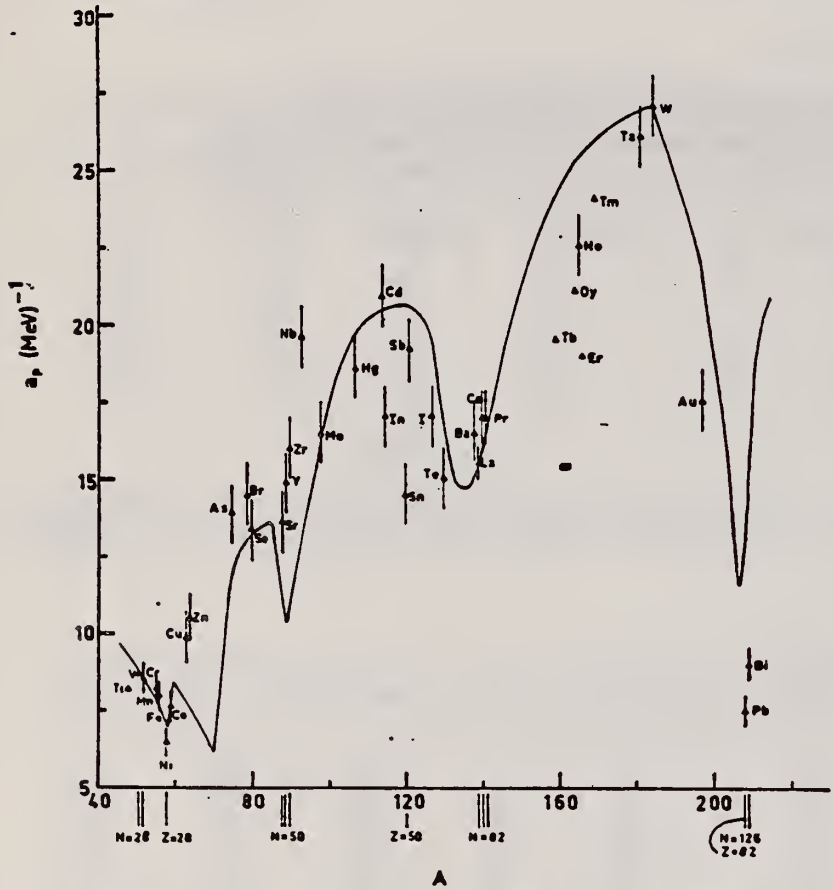


Fig. 12. Experimental values of the level density parameter a_p (Fermi gas formula plus pairing correction) versus atomic number A . The continuous curve is a least-squares fit to the data of a theoretical calculation from Newton ¹⁵.

1 H. Baba and S. Baba, Japan Atomic Energy Research Institute report JAERI-1183 (1969).

2 H. Baba, Nucl. Phys. A159, 625 (1970).

15 T.D. Newton, Can. J. Phys. 34, 804 (1956).

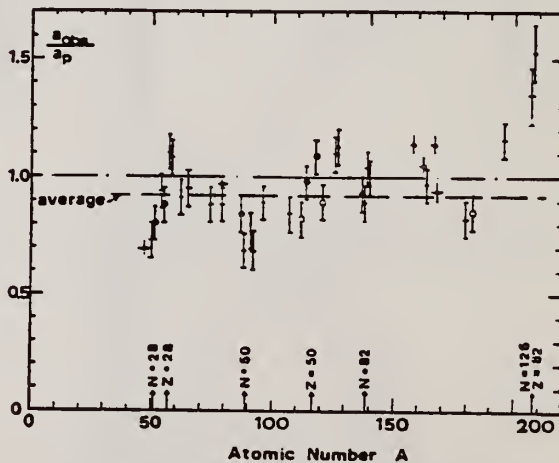


Fig. 15. Ratio a_{res}/a_p versus atomic number A . Here a_{res} is the level density parameter taken from the neutron resonance work of refs. ¹⁻³, and a_p is the level density parameter derived from the present (γ, n) work. Filled circles represent points where nuclei in the neutron resonance and in the (γ, n) experiment were the same. Open circles represent points where the respective nuclei were approximately matched. Triangles represent points which are based on measurement of neutron mean energies at two bremsstrahlung energies only.

(over)

TABLE 3 (continued)

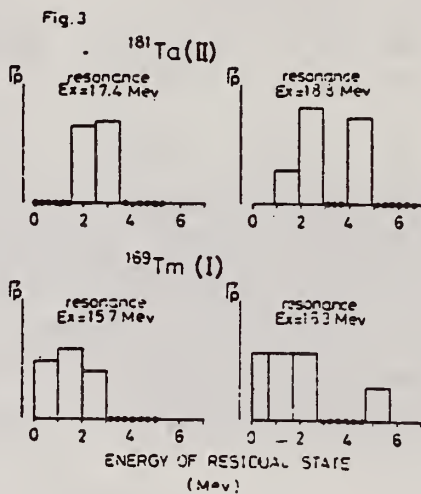
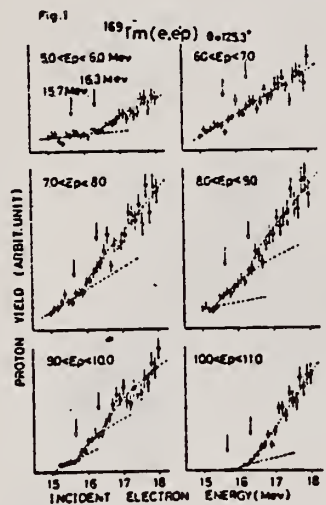
Target	<i>N</i> (residual nucleus) ^{a)}	Goodness of fit ^{b)}		$\hat{E}_n(24)$ (MeV) ^{c)}	<i>T</i> (MeV) ^{d)}	a_p (MeV ⁻¹) ^{e)}	a_{obs} (MeV ⁻¹) ^{f)}	a_{obs}/a_p	
		no p.c.	with p.c.						
Ba	75	1%	F	1.16	16.5- ¹³⁶ Ba	15.39- ¹³⁶ Ba	0.93		
	77	2%							
	78	7%							
	79	8%							
	80	11%							
	81	71%							
La	80	100%	F	F	1.25	0.72	15.5- ¹³⁸ La	13.76- ¹³⁹ La	0.89
Ce	81	89%	F	G	1.24	0.70	17.0- ¹³⁹ Ce	17.8- ¹⁴¹ Ce	1.04
	83	11%							
Pr	81	100%	G	G	1.17	0.65	17.0- ¹⁴⁰ Pr	17.05- ¹⁴² Pr	1.00
Tb ^{g)}	93	100%			1.15		19.3- ¹⁵⁸ Tb	21.85- ¹⁶⁰ Tb	1.14
Dy ^{g)}	93	2%			1.06		20.9- ^{161.5} Dy	21.9- ¹⁶² Dy	1.05
	94	19%							
	95	25%							
	96	25%							
	97	28%							
Ho	97	100%	P	G	1.06	0.56	21.4- ¹⁶⁴ Ho	20.66- ¹⁶⁶ Ho	0.97
Er ^{g)}	95	2%			1.11		19.2- ¹⁶⁶ Er	21.9- ¹⁶⁶ Er	1.14
	97	33%							
	98	23%							
	99	27%							
	101	15%							
Tm ^{g)}	99	100%			1.03		24.0- ¹⁶⁸ Tm	22.58- ¹⁷⁰ Tm	0.94
Ta	107	100%		G	1.00	0.49	26.0- ¹⁸⁰ Ta	21.2- ¹⁸¹ Ta	0.82
W	107	26%	G	F	0.98	0.50	27.0- ¹⁸³ W	23.0- ¹⁸³ W	<u>0.85</u>
	108	14%							
	109	31%							
	111	28%							
Au	117	100%		G	1.19		17.5- ¹⁹⁶ Au	20.24- ¹⁹⁸ Au	1.16
Pb	123	24%		V.P.	1.87	1.20	7.5- ²⁰⁶ Pb	10.1- ²⁰⁷ Pb	1.35
(Z = 82)	124	23%							
	125	52%							
Bi	125	100%		F	1.65	1.03	9.0- ²⁰⁸ Bi	13.8- ²¹⁰ Bi	1.53

^{a)} Neutron numbers and abundances of respective residual nuclei in (γ , n) experiments.^{b)} These give an assessment of the goodness of fit of a calculated \hat{E}_n versus E_0 curve to the observed data, using the Fermi gas level density formula both without and with pairing corrections.^{c)} Bremsstrahlung photoneutron mean energies \hat{E}_n for peak bremsstrahlung energy $E_0 = 24$ MeV.^{d)} Nuclear temperature from fit with constant-temperature formula.^{e)} Level density parameter a_p derived from the present (γ , n) experiment, using a Fermi gas formula plus pairing correction, and corresponding residual nucleus (the atomic weight shown is the weighted average of atomic weights of the respective isotopes present).^{f)} As column 7, but using data on n-resonance absorption from refs. ^{1, 2}.^{g)} Measurements of $\hat{E}_n(E_0)$ for these nuclei were made only for $E_0 = 21, 23$ and 24 MeV.

A. Suzuki, K. Shoda, M. Sugawara, T. Saito, H. Miyase,
 S. Oikawa, and J. Uegaki
 PICNS-73, Vol. I, p. 195 Asilomar

ELEM. SYM.	A	
Tm	169	69

METHOD	REF. NO.				
REACTION	RESULT	EXCITATION ENERGY	SOURCE	DETECTOR	ANGLE
E, P	RLY	5- 20	D	15- 20	MAG-D



ELEM. SYM.	A	Z			
Tm	169	69			
REF. NO.					
76 Em 2		egf			
REACTION	RESULT	EXCITATION ENERGY	SOURCE	DETECTOR	ANGLE
G, F	ABY	THR-999	C 999	TRK-I	4PI

TABLE I

Measured values of σ_q at $E = 1000$ MeV and deduced values of σ_t assumed constant from E_0 to 1000 MeV999 = 1 GEV

Element	Z^2/A	σ_q (mb)	E_0 (MeV)	σ_t (mb)
Bi	32.96	12.3 ± 0.6	200	7.6 ± 0.6
Pb	32.45	5.4 ± 0.4	220	3.6 ± 0.3
Tl	32.10	4.1 ± 0.3	230	2.8 ± 0.3
Au	31.68	2.0 ± 0.15	240	1.4 ± 0.2
Pt	31.18	1.1 ± 0.08	255	$(8 \pm 0.7) \times 10^{-1}$
Re	30.21	$(3.7 \pm 0.3) \times 10^{-1}$	280	$(2.9 \pm 0.3) \times 10^{-1}$
W	29.78	$(3.5 \pm 0.3) \times 10^{-1}$	290	$(2.8 \pm 0.3) \times 10^{-1}$
Ta	29.45	$(3.3 \pm 0.3) \times 10^{-1}$	300	$(2.7 \pm 0.3) \times 10^{-1}$
Hf	29.04	$(1.7 \pm 0.2) \times 10^{-1}$	310	$(1.4 \pm 0.2) \times 10^{-1}$
Yb	28.31	$(1.3 \pm 0.1) \times 10^{-1}$	330	$(1.2 \pm 0.1) \times 10^{-1}$
Tm	28.18	$(7.5 \pm 0.8) \times 10^{-2}$	335	$(6.8 \pm 0.8) \times 10^{-2}$
Ho	27.21	$(3.6 \pm 0.4) \times 10^{-2}$	355	$(3.5 \pm 0.4) \times 10^{-2}$
Dy	26.80	$(2.6 \pm 0.3) \times 10^{-2}$	360	$(2.5 \pm 0.3) \times 10^{-2}$
Tb	26.58	$(2.5 \pm 0.3) \times 10^{-2}$	370	$(2.5 \pm 0.3) \times 10^{-2}$
Gd	26.04	$(1.6 \pm 0.2) \times 10^{-2}$	380	$(1.7 \pm 0.2) \times 10^{-2}$
Sm	25.56	$(1.3 \pm 0.2) \times 10^{-2}$	390	$(1.4 \pm 0.2) \times 10^{-2}$
Nd	24.96	$(9.2 \pm 0.9) \times 10^{-3}$	405	$(1 \pm 0.1) \times 10^{-2}$
Ce	24.00	$(8 \pm 0.9) \times 10^{-3}$	420	$(9 \pm 1) \times 10^{-3}$
La	23.39	$(8.4 \pm 0.9) \times 10^{-3}$	430	$(1 \pm 0.1) \times 10^{-3}$
Sb	21.36	$(1.2 \pm 0.2) \times 10^{-2}$	460	$(1.5 \pm 0.3) \times 10^{-2}$
Te	21.19	$(8.8 \pm 1) \times 10^{-3}$	465	$(1.2 \pm 0.2) \times 10^{-2}$
Sn	21.06	$(1.3 \pm 0.2) \times 10^{-2}$	465	$(1.7 \pm 0.3) \times 10^{-2}$
Cd	20.49	$(1.7 \pm 0.3) \times 10^{-2}$	470	$(2.2 \pm 0.4) \times 10^{-2}$
Ag	20.47	$(2 \pm 0.3) \times 10^{-2}$	470	$(2.6 \pm 0.4) \times 10^{-2}$
Zn	13.76	$(2 \pm 0.4) \times 10^{-1}$	515	$(3 \pm 0.6) \times 10^{-1}$
Cu	13.44	$(2.4 \pm 0.5) \times 10^{-1}$	515	$(3.6 \pm 0.8) \times 10^{-1}$
Ni	13.35	$(2.4 \pm 0.5) \times 10^{-1}$	510	$(3.6 \pm 0.8) \times 10^{-1}$
Fe	12.10	$(3 \pm 0.6) \times 10^{-1}$	510	$(4.4 \pm 0.9) \times 10^{-1}$

- ⁴ A.V. Mitrofanova et al.
Sov. J. Nucl. Phys. 6,
512 (1968).
- ⁷ T. Methasiri et al., Nucl.
Phys. A167, 97 (1971).
- ¹² J.R. Nix et al., Nucl. Phys.
81, 61 (1966).
- ²⁰ N.A. Perfilov et al., JETP
(Sov. Phys.) 14, 623 (1962);
Proc. Symp. on the physics &
chemistry of fission, Salzburg
1965, vol. 2 (IAEA) Vienna,
1965, p. 283.

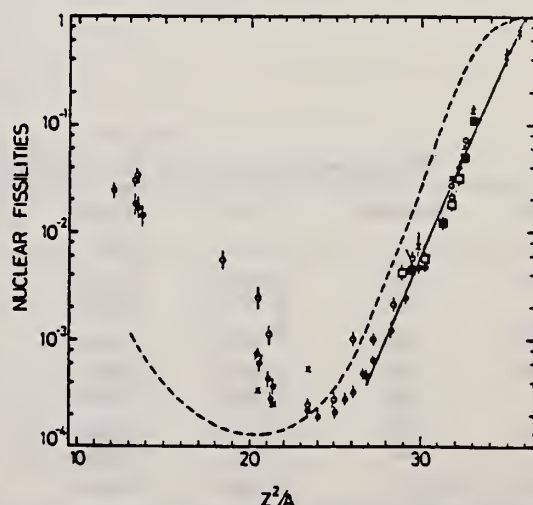


Fig. 2. Nuclear fissilities as a function of Z^2/A . Experimental points: solid circles represent our data; squares, the data from ref. ⁴; open circles, the data from ref. ⁷; and crosses, the data from (p,f) experiments²⁰). The straight line is the best fit calculated from our data for $Z^2/A > 26$. The dashed curve is the curve VI calculated by Nix and Sassi¹².

ELEM. SYM.	A	Z
Tm	169	69

METHOD

REF. NO.
76 Su 2

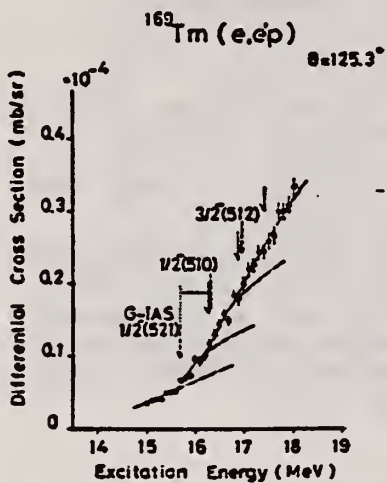
egf

REACTION	RESULT	EXCITATION ENERGY	SOURCE		DETECTOR		ANGLE
			TYPE	RANGE	TYPE	RANGE	
E, p	ABX	10- 18	D	15- 18	MAG-D		125

Proton yields obtained by summing protons with energies above levels given in tables.

TABLE 1
Parameters of the present experiment

Target	Atomic number	Purity (%)	Thickness (mg/cm ²)	Lowest proton energy (MeV)	Bin size (keV)	Range of measurement (MeV)
¹⁵⁹ Tb	65	99.9 (natural)	14.87	4.70	100	15.0 - 17.5
¹⁶⁵ Ho	67	99.9 (natural)	11.64	4.70	100	15.5 - 17.5
¹⁶⁹ Tm	69	99 (natural)	13.40	4.70	100	15.0 - 18.0
¹⁷⁵ Lu	71	99.87 (enriched)	5.24	5.34	150	15.05-20.0
¹⁸¹ Ta	73	99.9 (natural)	6.73	6.16	200	16.0 - 23.0

Fig. 4. Cross section of the ¹⁶⁹Tm(e, e'p) reaction. See also the caption to fig. 2.TABLE 3
Displacement energies obtained from the present data and the estimates with eqs. (20) and (21)

Target	Resonance	E^* (MeV)	E_d (exp) (MeV)	E_d^* (MeV)	$E_d(\delta = 0.3)^a$ (MeV)
¹⁵⁹ Tb	1st	15.75 ± 0.15	15.58	16.06	15.93
	2nd	16.50 ± 0.15	15.46		
¹⁶⁵ Ho	1st	16.15 ± 0.14	15.64	16.38	16.25
	2nd	16.34 ± 0.14	16.22	16.76	16.63
¹⁶⁹ Tm	1st	15.76 ± 0.13	16.20		
	2nd	16.34 ± 0.14	16.22		
¹⁷⁵ Lu	1st	16.44 ± 0.13	16.75		
	2nd	17.45 ± 0.15	16.35	17.07	16.93
¹⁸¹ Ta	1st	17.31 ± 0.15	16.40	17.38	17.24

^a) Estimated with eq. (20).^b) Estimated with eq. (21).

TABLE 4

Deformation parameters of IAS δ_{IAS} derived from the (e, e'p) result

Target	Resonance	IAS	Parent state	$\delta_{IAS} - \delta_p^*$	δ_p (assumed)	δ_{IAS}^*
¹⁵⁹ Tb	1st	$\frac{1}{2}^- [521]$	ground	-0.008	0.31	0.30
	2nd	$\frac{1}{2}^- [512]$	875 keV	-0.016		0.29
¹⁶⁵ Ho	1st	$\frac{3}{2}^+ [633]$	ground	-0.023	0.30	0.28
	2nd	$\frac{1}{2}^- [512]$	ground	-0.019		0.27
¹⁶⁹ Tm	1st	$\frac{1}{2}^- [521]$	ground	-0.018	0.29	0.27
	2nd	$\frac{1}{2}^- [510]$	565 keV	-0.019		0.27
¹⁷⁵ Lu	1st	$\frac{1}{2}^- [514]$	ground	-0.010	0.28	0.27
	2nd	$\frac{1}{2}^- [503]$	1420 keV	-0.029		0.25
¹⁸¹ Ta	1st	$\frac{1}{2}^- [503]$	670 keV	-0.046	0.26	0.21

The assumed deformation parameters for the parent states δ_p are also shown.^a) The errors are about ± 0.01 .U.S. DEPARTMENT OF COMMERCE
NATIONAL BUREAU OF STANDARDS

ELEM. SYM.	A	Z
Tm	169	69
METHOD	REF. NO.	
	77 Mu 3	egf

REACTION	RESULT	EXCITATION ENERGY	SOURCE		DETECTOR		ANGLE
			TYPE	RANGE	TYPE	RANGE	
E,A	ABX	13-100	D	100	MAG-D		DST

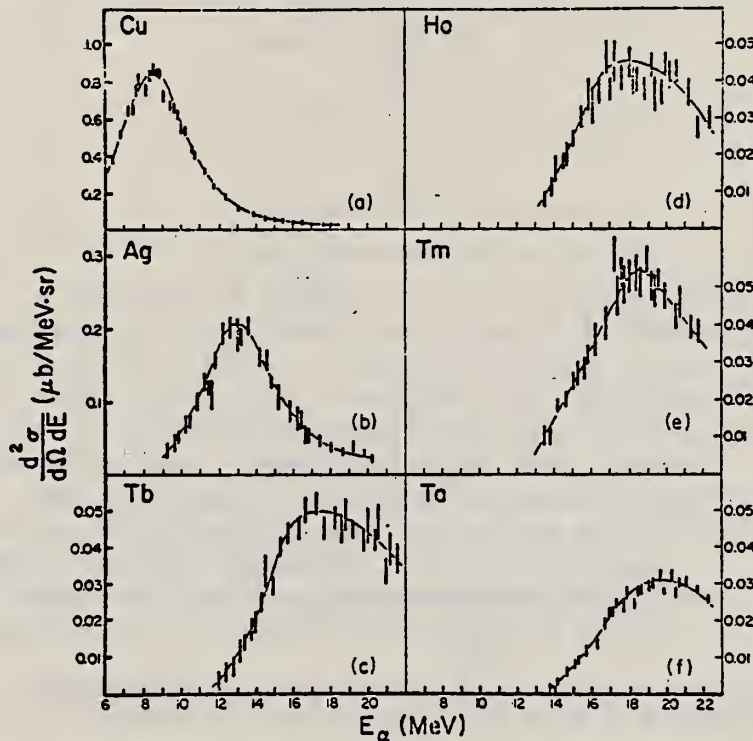
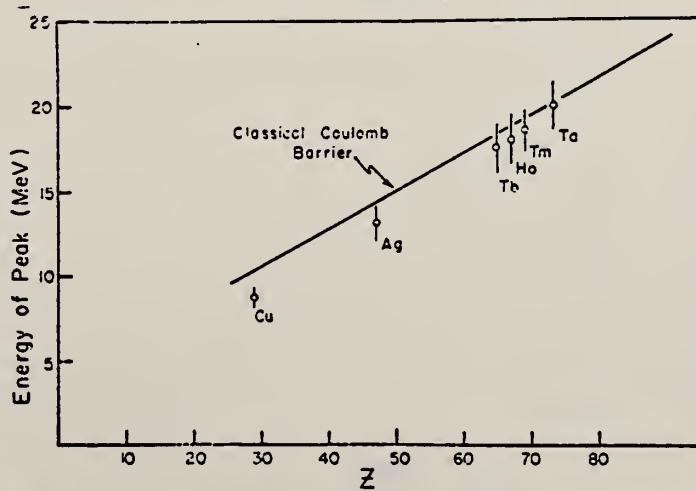


Fig. 1. The α -particle energy spectra at 50° in the lab for the six nuclei studied. Note that as Z increases, the cross section decreases and the energy of the peak increases. Errors are statistical. Curves are to guide the eye.



(over)

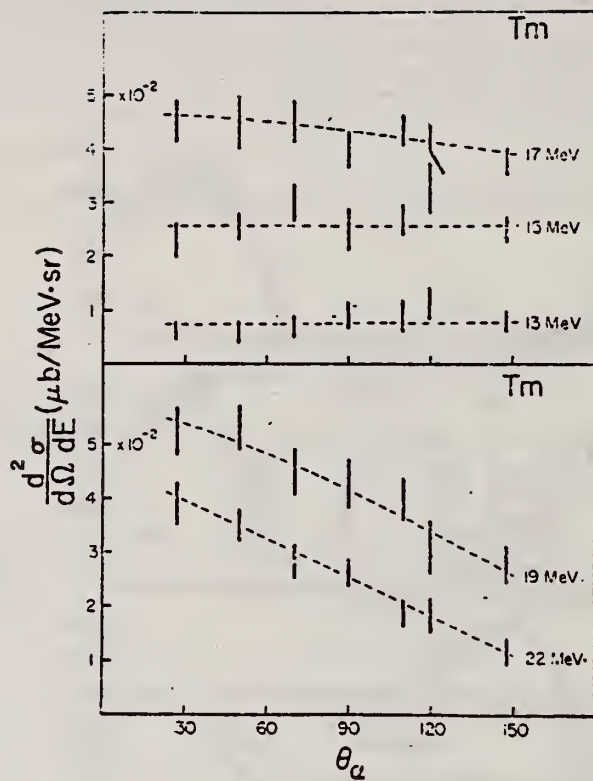


Fig. 5. Angular distributions for thulium ($Z = 69$). The forward peaking at high energies is taken as evidence of α -clusters in this nucleus. Errors are statistical. Curves are to guide the eye.

YTTERBIUM

Z=70

Ytterbium is a fascinating element of the Periodic Table primarily because of its valence variation in different environments. In the divalent state the element has a completed 4f level but in the trivalent state this level is incomplete with thirteen electrons. This dual valence gives rise to interesting and variable chemical and alloying properties. The application of modest pressure (16,0000 atm) changes the electrical conductivity from metallic to semiconducting. Higher pressures increase the semiconducting properties until at a pressure of 40,000 atm, ytterbium reverses to its metallic conducting state.

Betatron; ion chamber

REF. NO.

58 Fu 1

NVB

REACTION	RESULT	EXCITATION ENERGY	SOURCE		DETECTOR		ANGLE
			TYPE	RANGE	TYPE	RANGE	
G, XN	ABY	7-40	C	7-40	BF ₃ -I		4PI

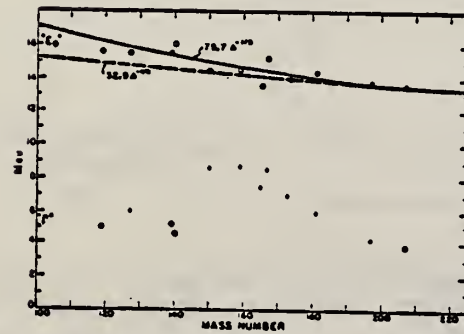


FIG. 6. Mean energy and width of giant resonances. " $E_{\bar{}}^{\circ}$ " and " Γ " are the mean energy for photon absorption and the full width at half maximum of the giant resonance obtained from dashed histograms as in Fig. 5. No attempt was made to fit data with resonance curves to obtain these parameters.

TABLE I. Target properties and results.

Element	Form used	Weight grams	$\sigma^{\text{tot}}(\gamma,n)^a$ barns	$\frac{\sigma^{\text{tot}}(n)}{N/Z/A}$ Mev-b	$\frac{\sigma^{\text{tot}}(n)}{N/Z/A}$ Mev
Sn	Sn	4.81	0.30	0.064	5.0
I	I	8.55	0.36	0.083	6.0
La	La	10.43	0.34	0.063	5.2
Ce	Ce	4.99	0.45	0.080	4.5
Sm	Sm ₂ O ₃	2.90	0.26	0.073	8.6
Tb	Tb ₂ O ₃	3.04	0.39	0.087	8.7
Ho	Ho ₂ O ₃	1.87	0.41	0.079	7.5
Er	Er ₂ O ₃	5.41	0.50	0.100	8.3
Yb	Yb ₂ O ₃	5.57	0.50	0.090	7.0
Ta	Ta	8.41	0.49	0.077	6.0
Au	Au	3.16	0.68	0.085	4.2
Pb	Pb	8.05	0.75	0.081	3.8

^a $\sigma^{\text{tot}}(\gamma,n)$ is the maximum value and " Γ " the full width at $\sigma^{\text{tot}}(\gamma,n)/2$ of the neutron production cross section corrected for multiple neutron emission. Data were not fitted with resonance lines to determine these values.

^b Integrated neutron production cross sections corrected for multiple neutrons above ($\gamma,2n$) threshold.

ELEM. SYM.	A	Z
Yb		70

METHOD

REF. NO.

71 Me 1

egf

REACTION	RESULT	EXCITATION ENERGY	SOURCE		DETECTOR		ANGLE
			TYPE	RANGE	TYPE	RANGE	
G, F	ABY	THR-900	C	300-900	FRG-I		4PI

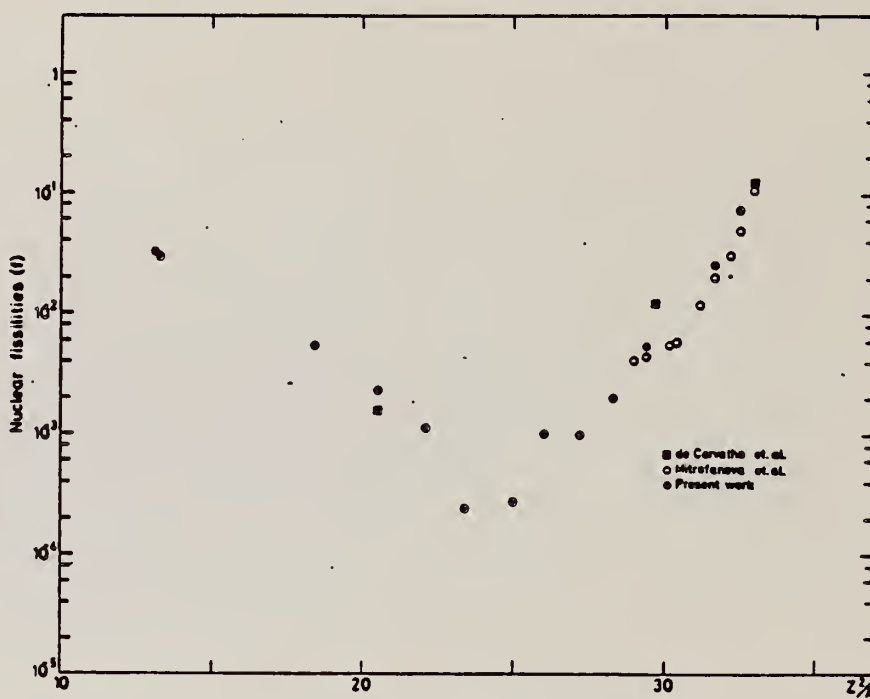
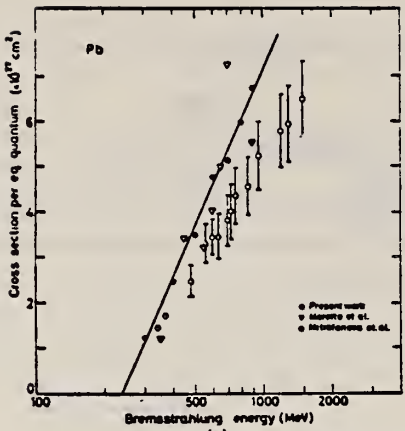
Fig. 2. Nuclear fissilities as a function of Z^2/A .

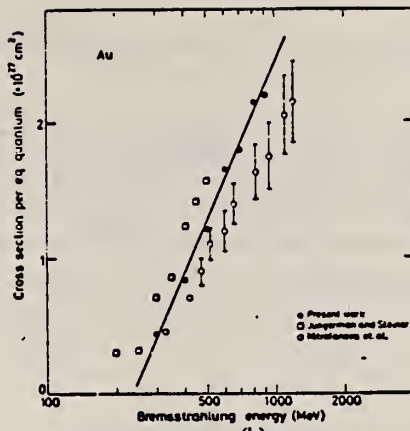
TABLE I
The constant fission cross sections above the threshold

Element	σ_f (cm^2)	Element	σ_f (cm^2)
Pb	$(5.0 \pm 0.2) \times 10^{-27}$	La	$(1.1 \pm 0.1) \times 10^{-29}$
Au	$(1.7 \pm 0.1) \times 10^{-27}$	Sn	$(4.3 \pm 1.1) \times 10^{-29}$
Ta	$(3.3 \pm 0.2) \times 10^{-28}$	Ag	$(8.4 \pm 2.0) \times 10^{-29}$
Yb	$(1.2 \pm 0.2) \times 10^{-28}$	Mo	$(1.7 \pm 0.4) \times 10^{-28}$
Ho	$(5.5 \pm 0.3) \times 10^{-29}$	Cu	$(6.6 \pm 1.2) \times 10^{-28}$
Gd	$(5.3 \pm 0.8) \times 10^{-29}$	Ni	$(5.8 \pm 0.1) \times 10^{-28}$
Nd	$(1.3 \pm 0.2) \times 10^{-29}$		

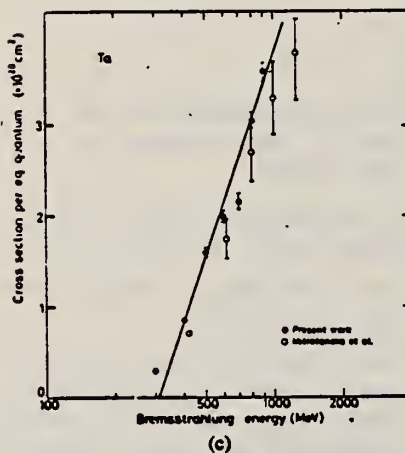
[over]



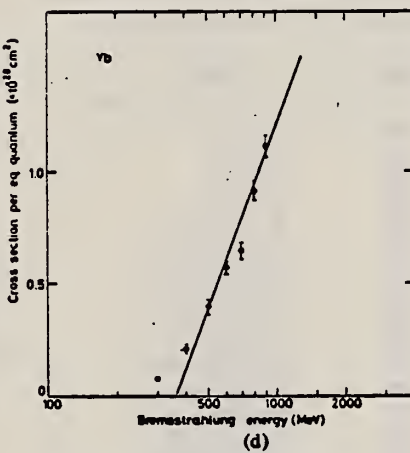
(a)



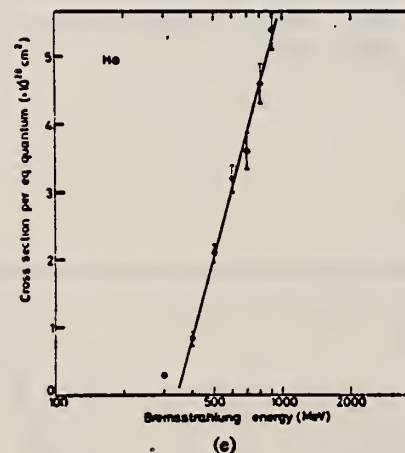
(b)



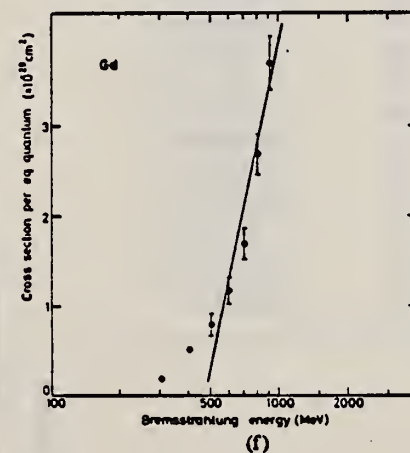
(c)



(d)



(e)



(f)

Fig. 1. Cross sections per equivalent quantum $\sigma_q(E)$ as a function of $\log E$.

ELEM. SYM.	A	Z
Yb		70

METHOD

REF. NO.	76 Em 2	egf
----------	---------	-----

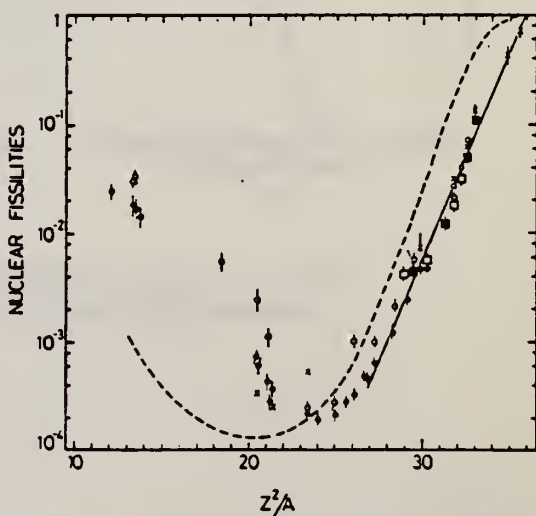
REACTION	RESULT	EXCITATION ENERGY	SOURCE		DETECTOR		ANGLE
			TYPE	RANGE	TYPE	RANGE	
G, F	ABY	THR-999	C	999	TRK-I		4PI

999 = 1 GEV

TABLE I
Measured values of σ_t at $E = 1000$ MeV and deduced values of σ_t assumed constant from E_0 to 1000 MeV

Element	Z^2/A	σ_t (mb)	E_0 (MeV)	σ_t (mb)
Bi	32.96	12.3 ± 0.6	200	7.6 ± 0.6
Pb	32.45	5.4 ± 0.4	220	3.6 ± 0.3
Tl	32.10	4.1 ± 0.3	230	2.8 ± 0.3
Au	31.68	2.0 ± 0.15	240	1.4 ± 0.2
Pt	31.18	1.1 ± 0.08	255	$(8 \pm 0.7) \times 10^{-1}$
Re	30.21	$(3.7 \pm 0.3) \times 10^{-1}$	280	$(2.9 \pm 0.3) \times 10^{-1}$
W	29.78	$(3.5 \pm 0.3) \times 10^{-1}$	290	$(2.8 \pm 0.3) \times 10^{-1}$
Ta	29.45	$(3.3 \pm 0.3) \times 10^{-1}$	300	$(2.7 \pm 0.3) \times 10^{-1}$
Hf	29.04	$(1.7 \pm 0.2) \times 10^{-1}$	310	$(1.4 \pm 0.2) \times 10^{-1}$
Yb	28.31	$(1.3 \pm 0.1) \times 10^{-1}$	330	$(1.2 \pm 0.1) \times 10^{-1}$
Tm	28.18	$(7.5 \pm 0.8) \times 10^{-2}$	335	$(6.8 \pm 0.8) \times 10^{-2}$
Ho	27.21	$(3.6 \pm 0.4) \times 10^{-2}$	355	$(3.5 \pm 0.4) \times 10^{-2}$
Dy	26.80	$(2.6 \pm 0.3) \times 10^{-2}$	360	$(2.5 \pm 0.3) \times 10^{-2}$
Tb	26.58	$(2.5 \pm 0.3) \times 10^{-2}$	370	$(2.5 \pm 0.3) \times 10^{-2}$
Gd	26.04	$(1.6 \pm 0.2) \times 10^{-2}$	380	$(1.7 \pm 0.2) \times 10^{-2}$
Sm	25.56	$(1.3 \pm 0.2) \times 10^{-2}$	390	$(1.4 \pm 0.2) \times 10^{-2}$
Nd	24.96	$(9.2 \pm 0.9) \times 10^{-3}$	405	$(1 \pm 0.1) \times 10^{-2}$
Ce	24.00	$(8 \pm 0.9) \times 10^{-3}$	420	$(9 \pm 1) \times 10^{-3}$
La	23.39	$(8.4 \pm 0.9) \times 10^{-3}$	430	$(1 \pm 0.1) \times 10^{-3}$
Sb	21.36	$(1.2 \pm 0.2) \times 10^{-2}$	460	$(1.5 \pm 0.3) \times 10^{-2}$
Te	21.19	$(8.8 \pm 1) \times 10^{-3}$	465	$(1.2 \pm 0.2) \times 10^{-2}$
Sn	21.06	$(1.3 \pm 0.2) \times 10^{-2}$	465	$(1.7 \pm 0.3) \times 10^{-2}$
Cd	20.49	$(1.7 \pm 0.3) \times 10^{-2}$	470	$(2.2 \pm 0.4) \times 10^{-2}$
Ag	20.47	$(2 \pm 0.3) \times 10^{-2}$	470	$(2.6 \pm 0.4) \times 10^{-2}$
Zn	13.76	$(2 \pm 0.4) \times 10^{-1}$	515	$(3 \pm 0.6) \times 10^{-1}$
Cu	13.44	$(2.4 \pm 0.5) \times 10^{-1}$	515	$(3.6 \pm 0.8) \times 10^{-1}$
Ni	13.35	$(2.4 \pm 0.5) \times 10^{-1}$	510	$(3.6 \pm 0.8) \times 10^{-1}$
Fe	12.10	$(3 \pm 0.6) \times 10^{-1}$	510	$(4.4 \pm 0.9) \times 10^{-1}$

- 4 A.V. Mitrofanova et al.
Sov. J. Nucl. Phys. 6,
512 (1968).
7 T. Methasiri et al., Nucl.
Phys. A167, 97 (1971).
12 J.R. Nix et al., Nucl. Phys.
81, 61 (1966).
20 N.A. Perifilov et al., JETP
(Sov. Phys.) 14, 623 (1962);
Proc. Symp. on the physics &
chemistry of fission, Salzburg
1965, vol. 2 (IAEA) Vienna,
1965, p. 283.

Fig. 2. Nuclear fissilities as a function of Z^2/A . Experimental points: solid circles represent our data; squares, the data from ref. 4; open circles, the data from ref. 7; and crosses, the data from (p,f) experiments²⁰). The straight line is the best fit calculated from our data for $Z^2/A > 26$. The dashed curve is the curve VI calculated by Nix and Sassi¹².

γ_B
A=173

γ_B
A=173

γ_B
A=173

METHOD					REF. NO.		
Betatron; neutron threshold; ion chamber					60 Ge 3		
REACTION	RESULT	EXCITATION ENERGY	SOURCE		DETECTOR		ANGLE
			TYPE	RANGE	TYPE	RANGE	
G, N	N ₀ X	THR	C	THR	BF ₃ -I		4 PI

THRESHOLD

TABLE I. Summary and comparison of neutron separation energies inferred from present threshold measurements with values predicted from mass data and reaction energies. All energies are expressed in the center-of-mass system in Mev.

Reaction	No. runs	Present results	Other results	Method	Reference
Yb ¹⁷² (γ, n)Yb ¹⁷²	1	6.50 ± 0.08	6.35 ± 0.06	mass data	q

» W. H. Johnson, Jr., and A. O. Nier, Phys. Rev. 105, 1014 (1957).

YB
A=174

YB
A=174

YB
A=174

METHOD

REF. NO.

69 Mo 1

hmg

REACTION	RESULT	EXCITATION ENERGY	SOURCE		DETECTOR		ANGLE
			TYPE	RANGE	TYPE	RANGE	
E, F	ABX	THR-999	D	60-999	TRK-I		DST
G, F	ABX	THR-999	C	60-999	TRK-I		DST

Tabular data given; angular distribution isotopes

999= 1 GEV

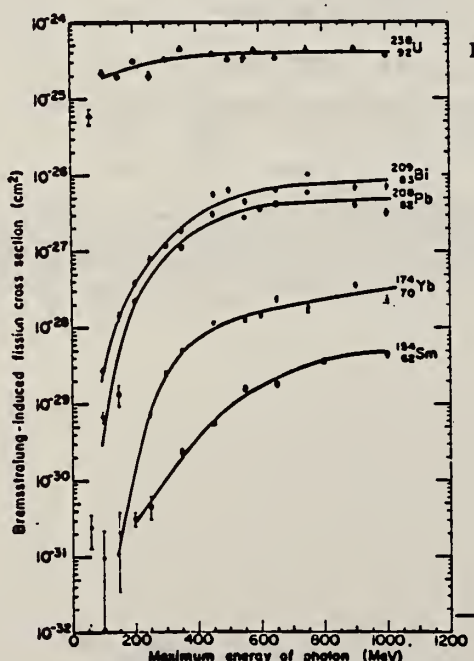


FIG. 4. Bremsstrahlung-induced fission cross section per equivalent quantum. **NUCLEAR DATA SHEET** 567

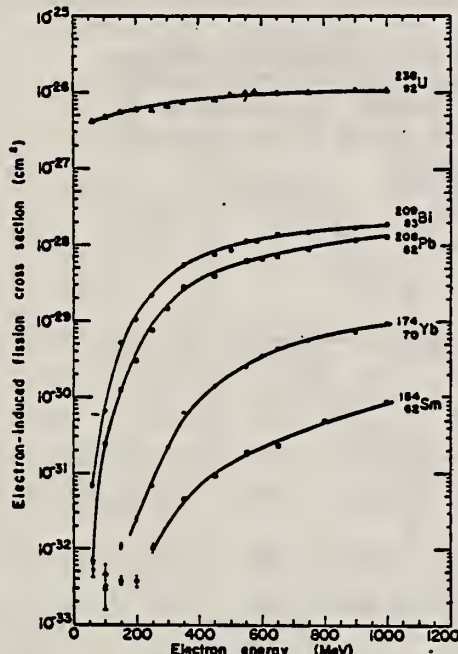


FIG. 2. Electron-induced fission cross-section data. Different symbols for the same isotope refer to different targets.

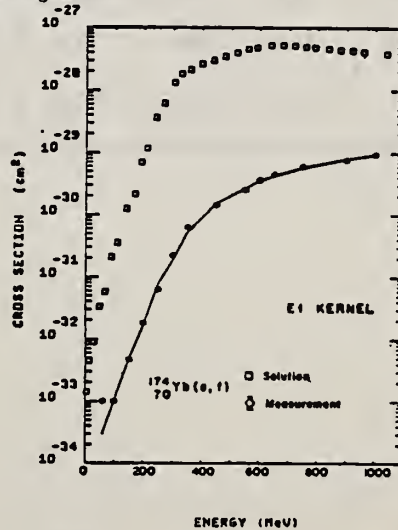


FIG. 9. Photofission cross section as a function of energy for ¹⁷⁴Yb (open squares) as obtained by unfolding the electron-induced fission cross-section data (diamonds) with the E1 kernel. The solid line is the fit to the electron-induced fission cross sections which is obtained by folding back the photofission cross section into the E1 kernel.

REF. G.M. Gurevich, L.E. Lazareva, V.M. Mazur, S.Yu. Merkulov,
 G.V. Solodukhov, V.A. Tyutin
 JETP Lett. 28, 157 (1978)
 Pis'ma Zh. Eksp. Teor. Fiz. 28, 168 (1978)

ELEM. SYM.	A	Z
Yb	174	70

METHOD

REF. NO.
 78 Gu 7
 hg

REACTION	RESULT	EXCITATION ENERGY	SOURCE		DETECTOR		ANGLE
			TYPE	RANGE	TYPE	RANGE	
G, MU-T	ABX	THR-31	C	UKN	NAI-D		4PI

The absorption method is used to measure the total photoabsorption cross section curves for deformed ^{154}Sm , ^{156}Gd , ^{168}Er , ^{174}Yb , ^{184}W , and ^{186}W nuclei in the region of the E1 giant resonance. The behavior of the resonance widths for nuclei in the interval $A = 153$ to 186 is discussed.

PACS numbers: 24.30.Cz, 25.20.+y, 27.70.+q

TABLE I.

Nucleus	E_1 MeV	σ_1 mb	Γ_1 MeV	E_2 MeV	σ_2 mb	Γ_2 MeV	Γ MeV	Q_0 b	β	$\sigma_{\alpha} L / 0.06 \frac{ZN}{A}$
^{154}Sm	12.2	188	3.4	15.7	207	5.7	8.1 ± 0.2	6.3 ± 0.3	0.32 ± 0.02	1.28
^{156}Gd	12.3	206	3.2	15.7	220	5.5	7.7 ± 0.2	6.2 ± 0.3	0.31 ± 0.02	1.30
^{168}Er	11.9	222	3.2	15.5	275	4.5	7.4 ± 0.2	7.5 ± 0.7	0.32 ± 0.03	1.26
^{174}Yb	12.3	297	2.9	15.5	320	4.9	7.1 ± 0.2	7.0 ± 0.6	0.30 ± 0.02	1.52
^{184}W	11.9	315	2.9	14.8	321	4.7	6.8 ± 0.2	7.2 ± 0.8	0.27 ± 0.03	1.50
^{186}W	12.0	246	3.3	14.5	332	5.1	6.4 ± 0.2	6.2 ± 0.8	0.23 ± 0.03	1.48
Average error	$\pm 1.3\%$	$\pm 10.5\%$	$\pm 7.5\%$	$\pm 1.3\%$	$\pm 9.4\%$	$\pm 3.8\%$	—	—	—	—

(over)

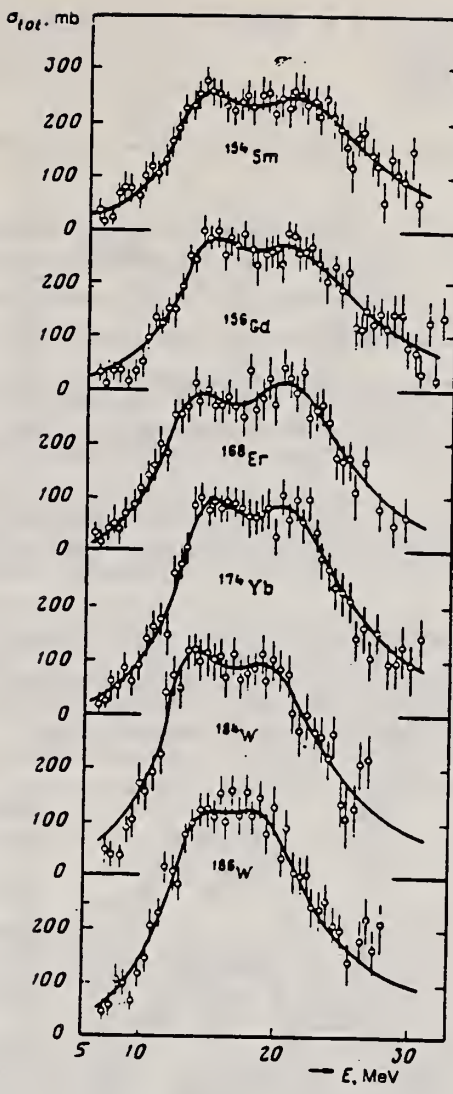


FIG. 2. Total cross sections of the photoabsorption of the nuclei ^{154}Sm , ^{156}Gd , ^{168}Er , ^{176}Yb , ^{186}W , and ^{188}W . The mean squared errors are shown.

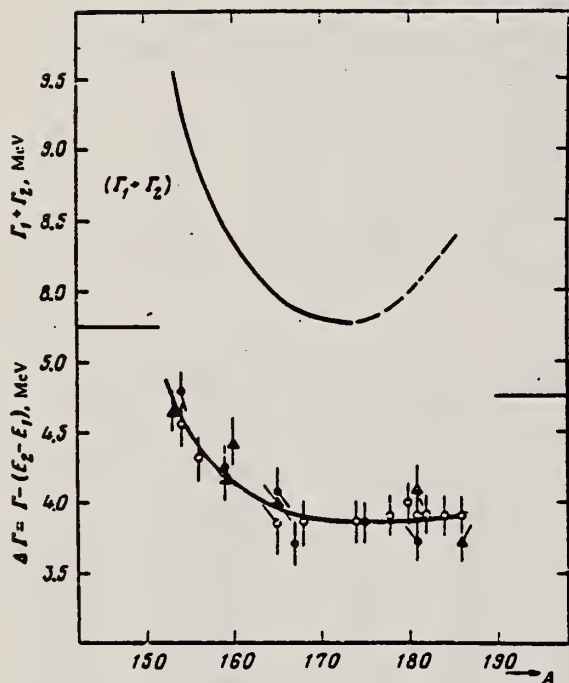


FIG. 3. Experimental values of $\Delta\Gamma = \Gamma - (E_2 - E_1)$ in the region of deformed nuclei with $A = 153-186$: ○—present work and¹¹; ●—Saclay group; ▲—Livermore group. Owing to a small systematic deviations of the absolute values, the ordinate scales for the Saclay and Livermore data are shifted 0.15 MeV upward and downward, respectively. The $(\Gamma_1 + \Gamma_2)$ curve was obtained from the $\Delta\Gamma$ curve after introduction of corrections in the interval $A = 175-186$.

ELEM. SYM.	A	Z
Yb	174	70

METHOD

REF. NO.

81 Gu 2

hg

REACTION	RESULT	EXCITATION ENERGY	SOURCE	DETECTOR	ANGLE
			TYPE	RANGE	
G.MU-T	ABX	THR-20	C	27	NAI-D 4PI

Abstract: The curves of the total gamma-absorption cross sections (σ_{tot}) in the E1 giant resonance energy range for the nuclei ^{154}Sm , ^{156}Gd , ^{164}Ho , ^{168}Er , ^{174}Yb , ^{178}Hf , ^{180}Hf , ^{181}Ta , ^{182}W , ^{184}W and ^{197}Au have been measured using the absorption method. Parameters of the Lorentz curves fitting the measured cross sections σ_{tot} are given. Quadrupole moments (Q_0) and nuclear deformation parameters (β) were obtained.

For deformed nuclei in the $\sim 155 < A < \sim 180$ region a violation of the correlation between giant resonance widths (Γ) and nuclear deformation parameters was found. Γ_1 and Γ_2 , the widths of the resonances corresponding to vibrations of nucleons along and across the nuclear deformation axis, were observed to decrease with the increase of A which could be accounted for by the presence of an $N = 108$ subshell.

E NUCLEAR REACTIONS ^{154}Sm , ^{156}Gd , ^{164}Ho , ^{168}Er , ^{174}Yb , ^{178}Hf , ^{180}Hf , ^{181}Ta , ^{182}W , ^{184}W , ^{186}W , ^{197}Au (γ ; X). $E = 7\text{--}20$ MeV: measured total $\sigma(E)$; deduced integrated σ . Lorentz line parameters. ^{154}Sm , ^{156}Gd , ^{164}Ho , ^{168}Er , ^{174}Yb , ^{178}Hf , ^{181}Ta , 182 , 184 , ^{186}W , ^{197}Au deduced β , Q_0 , Γ , giant resonance evolution. Enriched, natural targets.

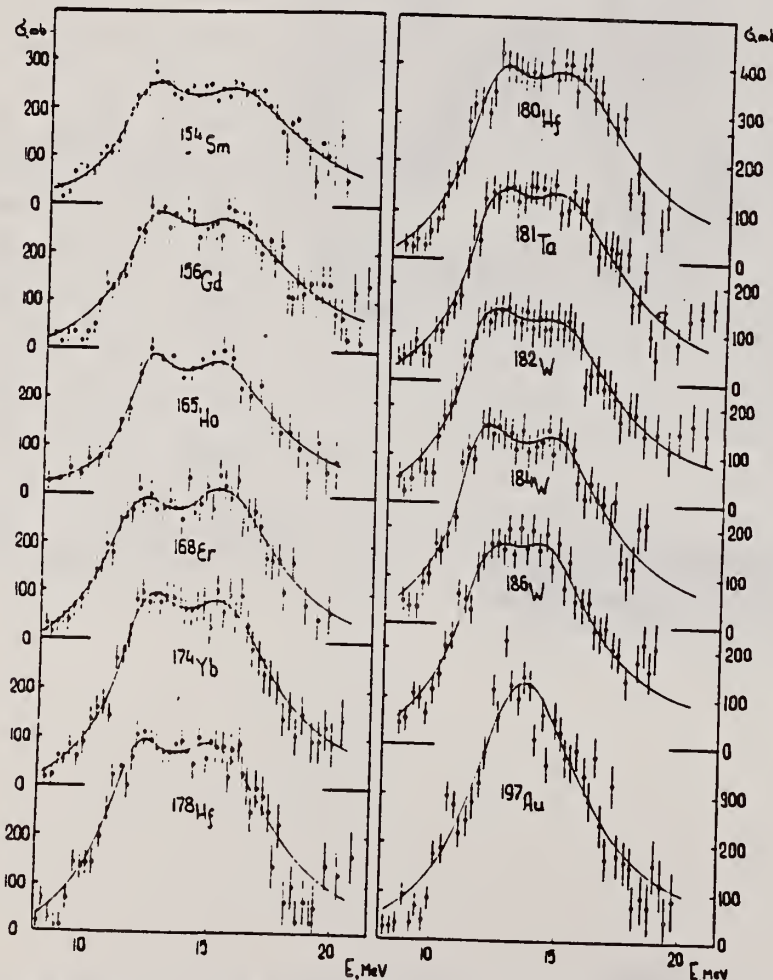


Fig. 2. Total nuclear γ -absorption cross sections (σ_{tot}) measured by the absorption method for ^{154}Sm , ^{156}Gd , ^{164}Ho , ^{168}Er , ^{174}Yb , ^{178}Hf , ^{180}Hf , ^{181}Ta , ^{182}W , ^{184}W , ^{186}W and ^{197}Au . Rms error bars are shown. 570

(OVER)

TABLE 2
Parameters of Lorentz curves fitting the experimental data on σ_{tot}

Nucleus	E_1 (MeV)	σ_1 (mb)	Γ_1 (MeV)	E_2 (MeV)	σ_2 (mb)	Γ_2 (MeV)	$\frac{\sigma_2 \Gamma_2}{\sigma_1 \Gamma_1}$	Γ (MeV)
^{154}Sm	12.2	188	3.4	15.7	207	5.7	1.85	8.1
^{156}Gd	12.3	206	3.2	15.7	220	5.5	1.81	7.7
^{165}Ho	12.3	202	2.3	15.2	239	4.8	2.47	7.0
^{168}Er	11.9	222	3.2	15.5	275	4.5	1.73	7.4
^{174}Yb	12.3	297	2.9	15.5	320	4.9	1.80	7.1
^{178}Hf	12.2	291	3.1	15.5	334	4.9	1.80	7.2
^{180}Hf	12.2	286	3.2	15.3	324	5.1	1.81	7.1
^{181}Ta	12.1	272	3.0	15.0	316	5.1	1.97	6.8
^{182}W	11.9	267	3.2	14.8	303	5.6	2.01	6.8
^{184}W	11.9	315	2.9	14.8	321	4.7	1.65	6.8
^{186}W	12.0	246	3.3	14.5	332	5.1	2.07	6.4
^{197}Au	13.7	535	5.2					
Average error	1.4 °	11.2 °	9.3 °	1.5 °	9.7 °	4.6 °	0.22	0.2 MeV

TABLE 3
Ratios of nuclear ellipsoid axes (k), deformation parameters (β) and intrinsic quadrupole moments (Q_0), calculated from E_2, E_1

Nucleus	^{154}Sm	^{156}Gd	^{165}Ho	^{168}Er	^{174}Yb	^{178}Hf	^{180}Hf	^{181}Ta	^{182}W	^{184}W	^{186}W
k	1.320	1.302	1.259	1.327	1.289	1.296	1.281	1.263	1.271	1.268	1.229
β	0.326 ± 0.017	0.309 ± 0.016	0.266 ± 0.036	0.334 ± 0.032	0.296 ± 0.024	0.303 ± 0.032	0.288 ± 0.036	0.270 ± 0.026	0.278 ± 0.030	0.274 ± 0.032	0.235 ± 0.033
Q_0	6.3 ± 0.3	6.2 ± 0.3	5.8 ± 0.8	7.5 ± 0.7	7.0 ± 0.6	7.5 ± 0.8	7.2 ± 0.9	6.9 ± 0.7	7.2 ± 0.8	7.1 ± 0.8	6.2 ± 0.9

TABLE 4
Integral characteristics of E1 giant resonance

Nucleus	$\sigma_{0,exp}$ (MeV · b)	$\sigma_{0,exp}$ $0.06NZ^{-1}A$	σ_{0L} (MeV · b)	σ_{0I} $0.06NZ^{-1}A$	σ_1 (mb)	σ_{-1L} (mb)	$\sigma_{+1L}^{-1/3}$ (mb)	σ_{-2L} (mb · MeV $^{-1}$)	σ_{+2L} (mb · MeV $^{-1}$)	σ_{-3L} (mb · MeV $^{-1}$)
^{154}Sm	1.94 ± 0.06	0.87	2.86	1.29	117 ± 3.5	156	0.189	9.1 ± 0.3	14.3	3.23
^{156}Gd	2.07 ± 0.07	0.91	2.95	1.30	143 ± 4.6	163	0.194	10.5 ± 0.4	14.9	3.30
^{165}Ho	1.86 ± 0.06	0.78	2.53	1.06	155 ± 4.4	160	0.177	10.1 ± 0.3	12.6	2.54
^{168}Er	2.24 ± 0.06	0.92	3.07	1.26	161 ± 4.3	197	0.212	12.0 ± 0.3	16.0	3.13
^{174}Yb	2.69 ± 0.05	1.07	3.82	1.52	195 ± 3.4	240	0.247	14.5 ± 0.3	19.2	3.54
^{178}Hf	2.85 ± 0.07	1.11	3.99	1.55	208 ± 4.9	247	0.247	15.3 ± 0.4	20.2	3.59
^{180}Hf	2.72 ± 0.06	1.05	4.03	1.56	200 ± 4.4	250	0.246	15.1 ± 0.3	20.7	3.61
^{181}Ta	2.84 ± 0.07	1.09	3.81	1.46	210 ± 5.3	245	0.239	16.0 ± 0.4	20.0	3.45
^{182}W	2.86 ± 0.07	1.09	4.01	1.52	211 ± 5.3	256	0.248	16.2 ± 0.4	21.6	3.70
^{184}W	2.78 ± 0.07	1.05	3.80	1.43	207 ± 5.3	251	0.240	15.9 ± 0.4	20.9	3.54
^{186}W	2.90 ± 0.07	1.08	3.95	1.48	214 ± 5.3	256	0.241	16.2 ± 0.4	21.6	3.56
^{197}Au	3.12 ± 0.06	1.10	4.37	1.54	229 ± 4.2	276	0.241	18.6 ± 0.4	23.3	3.49

YB
A=176

YB
A=176

YB
A=176

REF.	T. Cooper, W. Bertozzi, J. Heisenberg, S. Kowalski, W. Turchinetz, C. Williamson, L. Cardman, S. Fivozinsky, J. Lightbody, Jr., and S. Penner Phys. Rev. Cl3, 1083 (1976)	ELEM. SYM.	A	Z
METHOD	Yb	176	70	

REF. NO.	76 Co 3	hmrg
----------	---------	------

REACTION	RESULT	EXCITATION ENERGY	SOURCE		DETECTOR		ANGLE
			TYPE	RANGE	TYPE	RANGE	
E.E/	FMF	1, 1	D	34-111	MAG-D		DST

LEVELS .082,.267

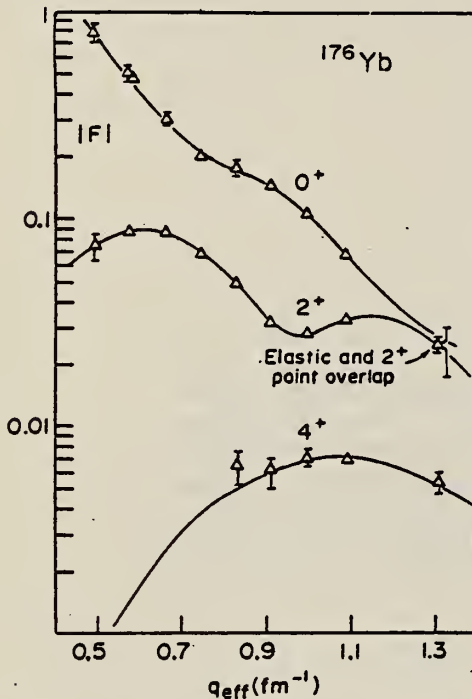


FIG. 6. Measured form factors for the elastic (0^+) and the inelastic 0.081-MeV (2^+) and 0.267-MeV (4^+) states in ^{176}Yb . The fitted curves are based on a best fit deformed Fermi charge distribution.

TABLE IX. Transition charge parameters of ^{166}Er and ^{176}Yb .

	Units	ρ_0	ρ_2	ρ_4	ρ_0	ρ_2	ρ_4
c	fm	6.1610	5.8632	5.8556	6.3306	6.0151	5.1866
t	fm	0.4872	0.5598	0.7271	0.4568	0.5188	0.9093
β_2		0.3266	0.3503	0.3325	0.3100	0.3346	0.3874
β_4		0.0	0.0	0.0199	-0.054	-0.054	-0.0875
β_6		-0.0180	-0.0180	-0.0180 ^a	-0.006	-0.006	-0.006 ^a
rms radius	fm	5.2380 ^b			5.3150 ^c		
$B(E2)$	$e^2 b^2$		5.670 ^d			5.350 ^e	
$B(E4)$	$e^2 b^2$			0.0919			0.0092
$\chi^2/\text{freedom}$		0.42	2.62	2.68	1.18	1.23	3.14
Transition radius	fm	5.2380	6.9088	8.4777	5.3150	6.8689	6.6962

^a Reference 3.

^b Interpolated value from nearest neighbors.

^c Reference 23.

^d Reference 25.

^e Reference 24.

³ D.L. Hendrie, Phys. Lett. 36, 571 (1973); ibid. et al. Phys. Lett. 26B, 127 (1968).

²³ A. Thompson (priv. commun.) Eidgenoessische TH Zuerich, 1974 (unpublished).

²⁴ R.O. Sayer et al., Phys. Rev. Cl, 1525 (1970).

²⁵ P.H. Stelson, Nucl. Data Al, 21 (1965).

TABLE V. Cross sections of ^{176}Yb .

Energy (MeV)	Angle (deg)	q_{eff} (fm $^{-1}$)	Elastic		2^+ $d\sigma$ $d\Omega_{\text{exp}}$ (mb)	4^+ $d\sigma$ $d\Omega_{\text{exp}}$ (mb)
			$d\sigma$ $d\Omega_{\text{exp}}$ (mb)	$d\sigma$ $d\Omega_{\text{beam}}$ (mb)		
34.72	109.95	0.498	0.995×10	$\pm 5\%$	0.964×10	$0.379 \times 10^{-1} \pm 8\%$
39.62	127.81	0.591	0.146×10	$\pm 3\%$	0.145×10	$0.463 \times 10^{-1} \pm 4\%$
44.53	109.95	0.580	0.245×10	$\pm 5\%$	0.239×10	$0.707 \times 10^{-1} \pm 4\%$
54.90	109.95	0.666	0.591	$\pm 5\%$	0.569	$0.456 \times 10^{-1} \pm 3\%$
64.77	110.16	0.749	0.178	$\pm 4\%$	0.191	$0.205 \times 10^{-1} \pm 2\%$
74.97	110.13	0.834	0.108	$\pm 7\%$	0.967×10^{-1}	$0.795 \times 10^{-2} \pm 3\%$
85.09	110.03	0.917	$0.561 \times 10^{-1} \pm 4\%$	0.537×10^{-1}	$0.248 \times 10^{-2} \pm 4\%$	$0.929 \times 10^{-4} \pm 19\%$
95.30	110.03	1.002	$0.244 \times 10^{-1} \pm 4\%$	0.246×10^{-1}	$0.154 \times 10^{-2} \pm 5\%$	$0.103 \times 10^{-3} \pm 10\%$
95.00	127.81	1.098	$0.444 \times 10^{-2} \pm 4\%$	0.453×10^{-2}	$0.100 \times 10^{-2} \pm 3\%$	$0.416 \times 10^{-4} \pm 9\%$
110.21	147.24	1.319	$0.170 \times 10^{-3} \pm 9\%$	0.246×10^{-3}	$0.139 \times 10^{-3} \pm 12\%$	$0.596 \times 10^{-5} \pm 25\%$

L

LUTETIUM
Z=71

Lutetium was discovered independently by C. A. von Welsbach and G. Urbain in 1907-08. Urbain called the new oxide *lutecia* — an old Roman name for his native city, Paris. Of all the rare earth metals, lutetium is the hardest and the most dense.

L

L

METHOD

REF. NO.

69 Be 6

egf

REACTION	RESULT	EXCITATION ENERGY	SOURCE		DETECTOR		ANGLE
			TYPE	RANGE	TYPE	RANGE	
G, N 484	ABX	7-24	D	7-28	MOD-I		4PI
G, 2N 485	ABX	14-28	D	7-28	MOD-I		4PI
G, 3N 486†	ABX	24-28	D	7-28	MOD-I		4PI

 x = fraction of total cross section resulting in a direct neutron

612

 n_d = fraction of neutrons emitted by direct effect at an energy where all the evaporation neutrons go to $(\gamma, 2n)$ cross section $n_d = x/(2-x)$ TABLEAU 3
Moments quadrupolaires intrinsèques

Cible	% isotopes	a/b ex	β_2 ex	$\beta_2[B(E_2)]$	Q_0 ex (b)	Q' ex
^{133}I	100 % ^{127}I	0.85	0.172		-2.3 ± 0.4	
^{148}Ce	88.5 % ^{140}Ce			0.104		
	11.1 % ^{142}Ce			0.118		
^{145}Sm	15 % ^{147}Sm					0.158
	11.2 % ^{148}Sm					
	13.8 % ^{149}Sm					
	7.5 % ^{150}Sm	1.23	0.219	0.190	4.5 \pm 0.4	3.53
	26.6 % ^{152}Sm			0.304		5.93
	22.5 % ^{154}Sm			0.351		6.58
^{149}Er	33.4 % ^{166}Er			0.341		7.60
	22.9 % ^{167}Er					7.80
	27.1 % ^{168}Er	1.314	0.288	0.339	6.96 \pm 0.4	7.60
	14.9 % ^{170}Er			0.329		7.45
^{171}Lu	97.4 % ^{175}Lu	1.282	0.262		6.95 \pm 0.3	7.20

TABLEAU 5
Valeurs de la température nucléaire et du paramètre a de densité des niveaux

x	n_d	Θ (MeV)	$E'_\gamma - E_n$ (MeV)	a (MeV $^{-1}$)	a' (MeV $^{-1}$)	a'' (MeV $^{-1}$)
I	0.05 ± 0.005	0.03 ± 0.03	1.30 ± 0.20	10	6 ± 2.5	10 ± 3
^{140}Ce	0.21 ± 0.05	0.12 ± 0.03	1.05 ± 0.20	10	9 ± 3.5	7 ± 3
^{142}Ce			0.8 ± 0.20	6	9 ± 4	8 ± 3
Sm	0.18 ± 0.04	0.10 ± 0.03				
Er	0.20 ± 0.05	0.11 ± 0.03				(12 ± 4)
Lu	0.26 ± 0.06	0.15 ± 0.03	0.85 ± 0.1	9	12.5 ± 2.5	15 ± 3

TABLEAU 4
Règles de somme

Noyau cible (éléments naturels)	σ_0 (MeV · b)	σ'_0 (MeV · b)	0.06	$\frac{NZ}{A}$	$\frac{\sigma_0 A}{0.06 NZ}$	$\frac{\sigma'_0 A}{0.06 NZ}$	σ_{-1} (mb)	$\sigma_{-1} A^{-1}$	σ_{-2} (mb · MeV $^{-1}$)	$\sigma_{-2} A^{-1}$
^{55}Fe	2.02 ± 0.14	2.30 ± 0.12	1.85	1.09 ± 0.07	1.24 ± 0.07	129 ± 0.10	0.20 ± 0.02	8.6 ± 0.6	2.7 ± 0.2	
^{144}Ce	2.13 ± 0.15	2.53 ± 0.13	2.04	1.05 ± 0.07	1.24 ± 0.07	140 ± 0.12	0.19 ± 0.02	9.5 ± 0.6	2.5 ± 0.2	
^{142}Sm	2.48 ± 0.17	2.92 ± 0.14	2.18	1.14 ± 0.07	1.34 ± 0.07	167 ± 0.14	0.21 ± 0.02	11.8 ± 0.8	2.75 ± 0.2	
^{144}Er	2.70 ± 0.19	3.04 ± 0.16	2.42	1.12 ± 0.07	1.26 ± 0.07	186 ± 0.15	0.20 ± 0.02	13.6 ± 1	2.7 ± 0.2	
^{71}Lu	2.65 ± 0.18	2.96 ± 0.16	2.53	1.05 ± 0.07	1.17 ± 0.07	182 ± 0.15	0.185 ± 0.02	12.9 ± 1	2.35 ± 0.2	
valeur moyenne pour ces 5 corps					1.09 ± 0.07	1.25 ± 0.07		0.20 ± 0.02		2.6 ± 0.2

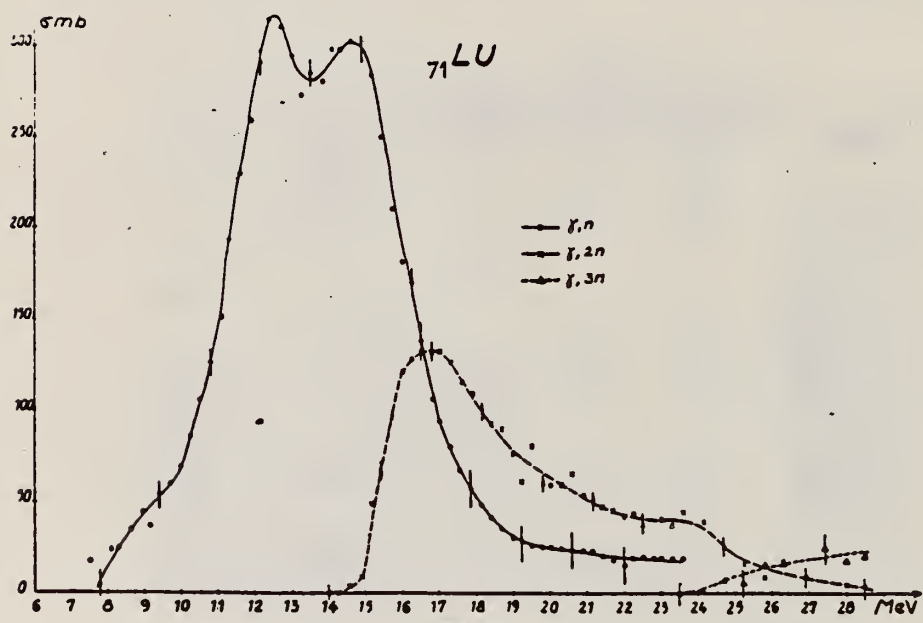


Fig. 9.

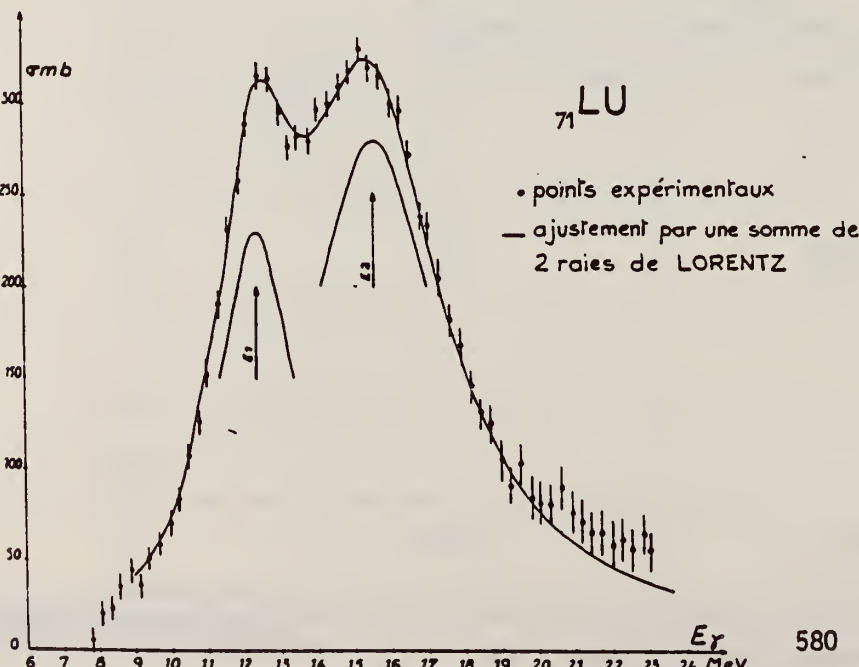


Fig. 10.

Lu

A=175

Lu

A=175

Lu

A=175

L. Katz, G.B. Chidley

Nuclear Reactions at Low and Medium Energies (Academy of Science,
USSR: 1958) 371

ELEM. SYM.

Lu

175

71

METHOD Betatron; neutron cross section; BF₃ counters; ion chamber monitor

REF. NO.

58 Ka 1

NVB

REACTION	RESULT	EXCITATION ENERGY	SOURCE		DETECTOR		ANGLE
			TYPE	RANGE	TYPE	RANGE	
G,XN	ABX	8-22	C	8-22	BF ₃ -I		4PI

Таблица 2

Пороги испускания фотонейтронов

Изотоп	B _{in} , Мэв	B _{in} , Мэв	Изотоп	B _{in} , Мэв	B _{in} , Мэв
V ₅₁	11.16	20.5	L ₁₃₀	8.81	16.1
Mn ₅₅	10.14	19.2	Pr ₁₄₁	9.46	17.6
Co ₅₈	10.44	18.6	Tb ₁₃₉	8.16	14.8
As ₇₅	10.24	18.1	Ho ₁₆₅	8.10	14.6
Y ₈₉	11.82	20.7	Tm ₁₆₉	8.00	14.7
Nb ₉₃	8.86	17.1	Lu ₁₇₅	7.77	14.2
Rh ₁₀₃	9.46	16.8	Ta ₁₈₁	7.66	13.8
J ₁₂₇	9.14	16.2	Au ₁₉₇	7.96	13.3
Cs ₁₃₃	9.11	16.5	Bi ₂₀₉	7.43	14.5

THRESHOLDS

не приведены, поскольку они превышают 2. Мэв во всех случаях, кроме золота, для которого $B_{3n} = 21$ Мэв. Свойства сечений $\sigma_0(\gamma)$ сведены в табл. 3.

Таблица 1

Изотоп	E _{чако} , Мэв	$\sigma_0(E_T)$, барн	Γ , Мэв	$\frac{\sigma_0}{\Gamma}$, Мэв·барн	$\Upsilon(22)$, 10 ⁸ нейтрон/100 р·моль
V ₅₁	18,4	0,062	5,2	0,33	1,62
Mn ₅₅	20,2	0,060	7,0	0,39	2,01
Co ₅₈	18,3	0,068	6,3	0,44	2,30
As ₇₅	16,4	0,090	9,5	0,74	4,25
Y ₈₉	17,1	0,172	5,2	0,93	5,33
Nb ₉₃	18,0	0,156	7,5	1,17	6,80
Rh ₁₀₃	17,5	0,160	9,4	1,40	8,28
J ₁₂₇	15,2	0,273	6,8	1,76	11,9
Cs ₁₃₃	16,5	0,238	7,7	1,59	10,7
La ₁₃₉	15,5	0,325	3,8	1,55	11,2
Pr ₁₄₁	15,0	0,320	4,9	1,93	13,1
Tb ₁₃₉	15,6	0,274	9,8	2,49	18,1
Ho ₁₆₅	13,5	0,305	8,9	2,52	18,7
Tm ₁₆₉	16,4	0,250	8,4	1,91	14,9
Lu ₁₇₅	16,0	0,225	8,4	1,90	23,0
Ta ₁₈₁	14,5	0,380	8,5	3,15	22,0
Au ₁₉₇	13,8	0,475	4,7	3,04	22,6
Bi ₂₀₉	13,2	0,455	5,9	2,89	23,2

Method 24 MeV betatron; neutron yield; BF_3 counters; Victoreen dosimeter

Ref. No.
58 Ki 1

EH

Reaction	E or ΔE	E_0	Γ	$\int \sigma dE$	$J\pi$	Notes
Lu ¹⁷⁵ (γ , n) Bremss. 8-23	16	8.4 MeV	$\int_{23}^{23} = 1.9 \text{ MeV-mb}$			$\sigma = 225 \text{ mb}; E_{th} = 7.77 \pm 0.05 \text{ MeV}$ Neutron yield at 20 MeV is $1.95 \times 10^9 \text{ n/mole/100 r.}$

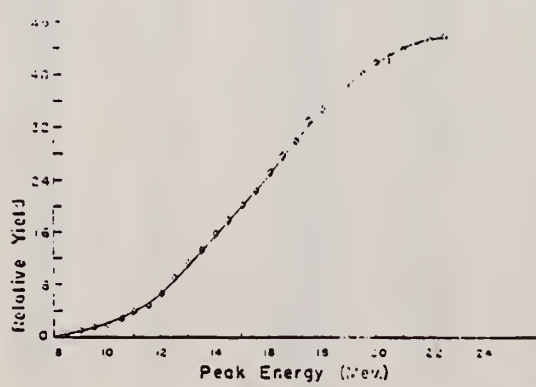
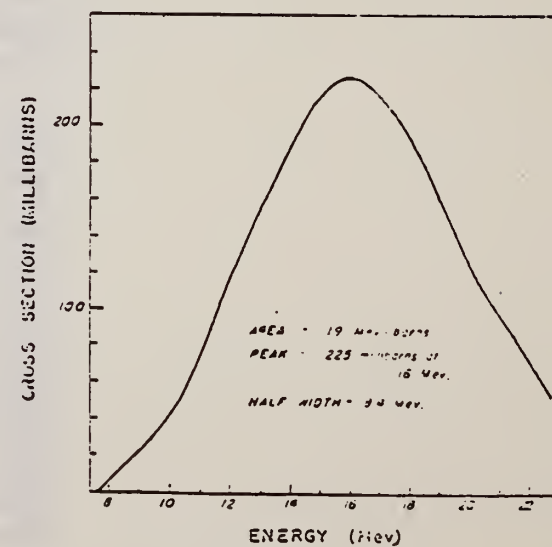


FIG. 2.



REF.

K. N. Geller, J. Halpern, and E. G. Muirhead
 Phys. Rev. 118, 1302-12 (1960)

ELEM. SYM.

Lu

175

71

METHOD

Betatron; neutron threshold; ion chamber

REF. NO.

60 Ge 3

NVB

REACTION	RESULT	EXCITATION ENERGY	SOURCE		DETECTOR		ANGLE
			TYPE	RANGE	TYPE	RANGE	
G, N	N ₀ X	THR	C	THR	BF ₃ -I		4 PI

THRESHOLD

TABLE I. Summary and comparison of neutron separation energies inferred from present threshold measurements with values predicted from mass data and reaction energies. All energies are expressed in the center-of-mass system in Mev.

Reaction	No. runs	Present results	Other results	Method	Reference
Lu ¹⁷⁵ (γ,n)Lu ¹⁷⁴	1	7.88 ± 0.08			

Method Hf ¹⁷⁵ source on centrifuge rotor; nuclear resonance fluorescence; NaI				Ref. No.	
				62 De 2	JHH

Reaction	E or ΔE	E_0	Γ	$\int \sigma dE$	$J\pi$	Notes
Lu ¹⁷⁵ (γ, γ)	345 keV		$\frac{\Gamma_0}{\hbar} =$ 5.16 ± 0.26 $\times 10^{-10}$ sec		$5/2^+$ E 2 M1	Mean lifetime $\tau_\gamma = (4.71 \pm 0.10) 10^{-10}$ sec $w(\theta) = 1 + (-0.20 \pm 0.28) P_2(\cos \theta)$

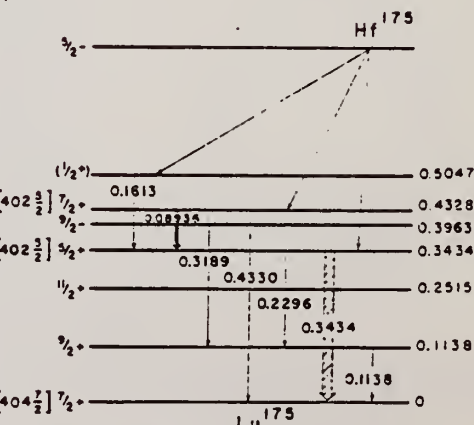


Fig. 1. The decay scheme of Hf¹⁷⁵. Energies are given in MeV

ELEM. SYM.	A	Z
Lu	175	71

METHOD

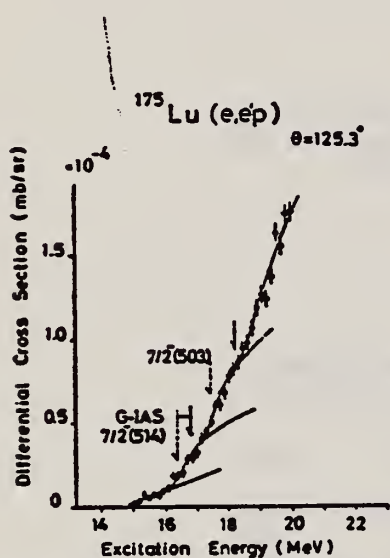
REF. NO.

76 Su 2

egf

REACTION	RESULT	EXCITATION ENERGY	SOURCE		DETECTOR		ANGLE
			TYPE	RANGE	TYPE	RANGE	
E, p	ABX	11- 20	D	15- 20	MAG-D		125

Proton yields obtained by summing protons with energies above levels given in tables.

Fig. 5. Cross section of the $^{175}\text{Lu}(e, e'p)$ reaction. See also the caption to fig. 2.TABLE 1
Parameters of the present experiment

Target	Atomic number	Purity (%)	Thickness (mg/cm ²)	Lowest proton energy (MeV)	Bin size (keV)	Range of measurement (MeV)
^{158}Tb	65	99.9 (natural)	14.87	4.70	100	15.0-17.5
^{165}Ho	67	99.9 (natural)	11.64	4.70	100	15.5-17.5
^{169}Tm	69	99 (natural)	13.40	4.70	100	15.0-18.0
^{175}Lu	71	99.87 (enriched)	5.24	5.34	150	15.05-20.0
^{181}Ta	73	99.9 (natural)	6.73	6.16	200	16.0-23.0

TABLE 3
Displacement energies obtained from the present data and the estimates with eqs. (20) and (21)

Target	Resonance	E^* (MeV)	E_d (exp) (MeV)	$E_d^*(\delta = 0.3)^b$ (MeV)	$E_d(\delta = 0.3)^b$ (MeV)
^{158}Tb	1st	15.75 ± 0.15	15.58	16.06	15.93
	2nd	16.50 ± 0.15	15.46		
^{165}Ho	1st	16.15 ± 0.14	15.64	16.38	16.25
	2nd	16.34 ± 0.14	16.22	16.76	16.63
^{169}Tm	1st	15.76 ± 0.13	16.20		
	2nd	16.34 ± 0.14	16.22	16.76	16.63
^{175}Lu	1st	16.44 ± 0.13	16.75		
	2nd	17.45 ± 0.15	16.35	17.07	16.93
^{181}Ta	1st	17.31 ± 0.15	16.40	17.38	17.24

^{a)} Estimated with eq. (20).^{b)} Estimated with eq. (21).TABLE 4
Deformation parameters of IAS δ_{IAS} derived from the (e, e'p) result

Target	Resonance	IAS	Parent state	$\delta_{IAS} - \delta_p^a)$	δ_p	$\delta_{IAS}^b)$
^{158}Tb	1st	$\frac{1}{2}^- [521]$	ground	-0.008	0.31	0.30
	2nd	$\frac{1}{2}^- [512]$	875 keV	-0.016	0.29	
^{165}Ho	1st	$\frac{3}{2}^+ [633]$	ground	-0.023	0.30	0.28
	2nd	$\frac{1}{2}^- [521]$	ground	-0.018	0.29	0.27
^{169}Tm	1st	$\frac{1}{2}^- [510]$	565 keV	-0.019	0.27	
	2nd	$\frac{1}{2}^- [510]$	565 keV	-0.019	0.27	
^{175}Lu	1st	$\frac{3}{2}^- [514]$	ground	-0.010	0.28	0.27
	2nd	$\frac{3}{2}^- [503]$	1420 keV	-0.029	0.25	
^{181}Ta	1st	$\frac{3}{2}^- [503]$	670 keV	-0.046	0.26	0.21

The assumed deformation parameters for the parent states δ_p are also shown.^{a)} The errors are about ± 0.01 .

ELEM. SYM.	A	Z
LU	175	71
REF. NO.	77 Ba 9	egf

METHOD

REACTION	RESULT	EXCITATION ENERGY	SOURCE		DETECTOR		ANGLE
			TYPE	RANGE	TYPE	RANGE	
G,G	ABX	8- 12	D	8- 12	SCD-D		140

Abstract: Differential cross sections for elastic and inelastic Raman scattering from ^{175}Lu and ^{171}Ta were measured. Five photon energies between 8.5 and 11.4 MeV were used and were obtained from the (n, γ) reaction on Ni and Cr using thermal neutrons. The results are compared with calculations using a modified simple rotator model (SRM) of the giant dipole resonance (GDR) in which the effect of Delbrück scattering was incorporated. In general, fair agreement between theory and experiment is obtained. A new set of GDR parameters is extracted, based on photon scattering data and, as expected, yield better agreement between experimental and predicted cross sections.

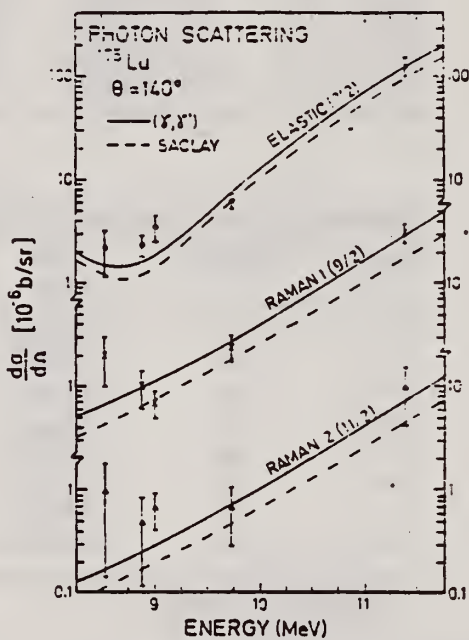


Fig. 4. Elastic and Raman inelastic differential cross sections for ^{175}Lu at 140° . The dashed line is calculated using GDR parameters extracted from the photoneutron data of the Saclay group. The solid line is calculated using GDR parameters extracted from the present photon scattering data (table 2). The elastic curves include contributions from Thomson, Delbrück, and nuclear resonance scattering.

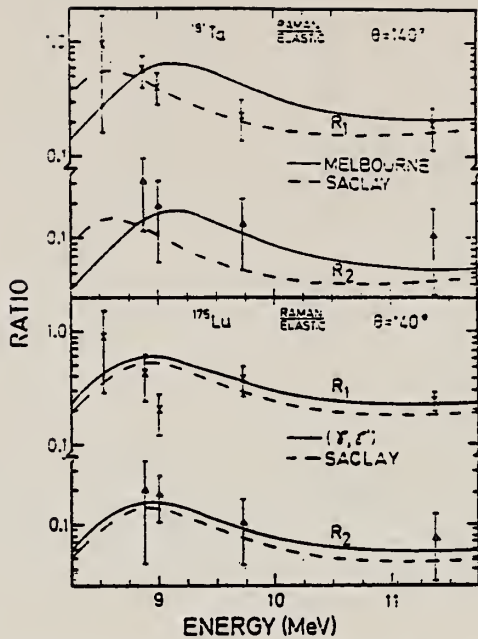


Fig. 5. Ratios of Raman/elastic scattering cross sections at 140° for ^{175}Lu and ^{181}Ta . R_1 and R_2 refer to the first and second Raman lines (fig. 1). The GDR parameters used in calculating the nuclear resonance amplitudes are explained in the captions to figs. 3 and 4.

TABLE I
Differential cross sections (in $\mu\text{b}/\text{sr}$) of elastic and Raman inelastic scattering at $\theta = 140^\circ$

E (MeV)	^{175}Lu			^{181}Ta		
	elastic $I_0 = \frac{3}{2}^+$	Raman 1 $\frac{3}{2}^+, 114$	Raman 2 $\frac{5}{2}^+, 251$	elastic $I_0 = \frac{3}{2}^+$	Raman 1 $\frac{3}{2}^+, 136$	Raman 2 $\frac{5}{2}^+, 301$
8.53	2.2 ± 1.0	2.0 ± 1.0	0.9 ± 0.7	1.8 ± 0.7	1.7 ± 0.7	
8.88	2.3 ± 0.6	1.0 ± 0.5	0.5 ± 0.3	1.8 ± 0.4	1.0 ± 0.3	0.5 ± 0.3
9.00	3.5 ± 1.0	0.7 ± 0.2	0.7 ± 0.2	2.5 ± 0.3	1.0 ± 0.3	0.5 ± 0.3
9.72	6.2 ± 1.1	2.4 ± 0.7	0.7 ± 0.4	7.6 ± 1.0	1.7 ± 0.7	1.0 ± 0.6
11.39	120 ± 20	31 ± 7	10 ± 5	107 ± 15	21 ± 8	11 ± 8
11.39 *)				131 ± 14	17 ± 4	17 ± 4

*) Experimental results of ref. ³) (calculated for 140° from measured values at 150°).

³H.E. Jackson, G.E. Thomas and K.J. Wetzel, Phys. Rev. C11, 1664 (1975)

Lu

A=176

Lu

A=176

Lu

A=176

ELEM. SYM.	A	Z
Lu	176	71

METHOD	REF. NO.	egf			
G,G/	82 Wa 4				
REACTION	RESULT	EXCITATION ENERGY	SOURCE	DETECTOR	ANGLE
			TYPE RANGE	TYPE RANGE	
G,G/	ABY	1	C 1.3*	ACT-I	4PI

A photoexcitation process by gamma rays from a ^{60}Co source has been studied for the nuclei of ^{87}Sr , ^{111}Cd , ^{115}In , and ^{176}Lu . The induced isomeric activity was measured with a Ge(Li) detector. The flux of photons scattered into the target has been estimated with the Monte Carlo method using the single-scattering approximation. From the observed induced activities and the calculated photon flux, the integral cross sections for isomer production by photoexcitation were obtained and compared with other experimental data.

1=1.08 MEV, *CO-60

TABLE II
Integral Cross Sections for the Isomer Production by Photoexcitation ($\times 10^{-25} \text{ cm}^2 \cdot \text{eV}$)

	^{87}Sr	^{111}Cd	^{115}In	^{176}Lu	Photon Source	Reference
Chertok and Booth		0.6 \pm 0.2	0.71 \pm 0.23		Bremsstrahlung	5
Booth and Brownson	$0.85^{+0.4}_{-0.3}$		1.15 \pm 0.4		Bremsstrahlung	6
Boivin et al.		$0.8^{+0.4}_{-0.05}$	3^{+4}_{-2}		Bremsstrahlung	7
Lakosi et al.		1.02 \pm 0.26	1.05 \pm 0.27		^{60}Co	11
Yoshihara	3.0 \pm 0.8 ^a	1.5 \pm 0.3	2.3 \pm 0.4	69 ± 12^a 140 ± 30^a	^{60}Co	3
Veres	0.5 to 0.62	0.8 to 1.5	0.9 to 5		^{60}Co	23
Present work	4.2 \pm 0.6 ^b 5.6 \pm 0.8 ^c	1.1 \pm 0.2	3.5 \pm 0.2	39 ± 27^b 48 ± 34^c	^{60}Co	

^aObtained as the relative value to ^{115}In .

^bProvided that the partial level width $g\Gamma_0 = 1 \times 10^{-3} \text{ eV}$.

^cProvided that the partial level width $g\Gamma_0 = 1 \times 10^{-4} \text{ eV}$.

DEFINITIONS OF ABBREVIATIONS AND SYMBOLS

Note: In this list definitions are given for various photoneutron reactions in which the following symbols are used: γ , NL, nN, SN and XN. Corresponding definitions apply for reactions involving other nuclear particles where the symbol N (neutron) is replaced by, e.g. P, D, T, HE, A etc. Where unknown reactions result in the production of a specific radionuclide, the chemical symbol and mass number is listed as the reaction product, e.g. a G,NA22 reaction in ^{59}Co .

A	alpha particle		response function. Contrast with D = discrete.
ANAL	analysis	CCH	cloud chamber
ABI	absolute integrated cross-section data	CF	compared with
ABX	absolute cross-section data	CHRGD	charged
ABY	absolute yield data. Often means cross-section per equivalent quantum is listed.	CMPT	Compton
ACT	measurement of induced radioactivity of the target	COIN COINC	coincidence, coincide
ASM	asymmetric, asymmetry	COH	coherent
AVG	average	CK	Cerenkov
BBL	bubble chamber	D	deuteron or discrete. When discrete, it is used to describe a photon source or a detector response function. Contrast with C = continuous.
BEL B(EL)	reduced electric radiative transition probability	DLTE	energy loss
BF3	BF ₃ neutron counter with moderator e.g., Halpern detector, long counter	DLTQ	momentum transfer
BML	reduced magnetic radiative transition probability, B(ML)	DST	distribution
BREAKS	levels located by "breaks" in the yield curve	DT BAL	detailed balance
BRKUP	breakup	E	electron
BRMS	bremsstrahlung	E/	inelastically scattered electron
BTW	between	E+	positron
C	continuous. Used to describe a photon source or a detector	EDST	energy distribution or spectrum
		E/N	used only to indicate a coincidence experiment as in (E,E/N).

N	N stands for any outgoing particle measured in coincidence with an inelastically scattered electron. Distinguish from e.g., (E,N) which is used to represent an electron induced reaction when only the outgoing particle N is detected.	KE	kinetic energy
EMU	emulsions (photographic plates)	L	may be an integer or zero that always follows a reaction product symbol. This is used to indicate transitions to specific states in the residual nuclide. When the letter is used as in (G,NL) the cross section given is that for the sum of transitions to two or more specific final states.
EXCIT	excited		
F	fission	LFT	excited state lifetime
FMF	form factor	LIM	limit
FM-1	inverse femtometers	LY,LVS	level, levels
FRAG	fragment	LQD	liquid
G	photon	MAG	magnetic spectrometer
G/	inelastically scattered photon	MEAS	measurement(s)
G-WIDTH	gamma-ray transition width	MGC	magnetic Compton spectrometer
HAD	hadrons, hadron production	MGP	magnetic pair spectrometer
HE He3	^3He particle	MOD	moderated neutron detector <u>not</u> employing a BF_3 counter, e.g. rhodium foil, Szilard-Chalmers reaction, ^3He , ^6Li reactions, GD loaded liquid scintillator, etc.
INT	interaction, integral, intensity		
INC	includes	MSP	mass spectrometer
ION	ionization chamber	MULT	multiple, multipole, multiplicity
ISOB	isobaric	MU-T	used only in combination with G to indicate a total photon absorption cross section measurement, i.e. (G,MU-T)
ISM	isomer		
J	multiplicity of particle defined by following symbol e.g. (G,PJN) with remark $J = 2,3,5,7$	N	neutron (see also XN and SN). The notation (G,N) is used to indicate a reaction in which only a single neutron is emitted, i.e. the reaction that can, in many cases, be measured by observing the radioactive decay of the residual nuclide.
JPI J-PI	spin and parity of a nuclear state		
K	second multiplicity index, e.g. (G,JPKN) with both J & K positive integers greater than 1		

nN	where n is any integer. (G,nN) indicates the sum over all reaction cross sections in which n neutrons are emitted.	SN	sum of neutron producing reactions, $\sigma(\gamma, SN) = \sigma(\gamma, N) + \sigma(\gamma, NP) + \sigma(\gamma, 2N) + \sigma(\gamma, 3N) + \text{etc.}$
NAI	NaI(Tl) spectrometer	SPC	photon or particle energy spectrum
NEUT	neutron(s)	SPK	spark chamber
NOX	no cross-section data	SPL	spallation
P	proton (see also XP)	STAT	statistical
PART	particle(s)	SYM	symmetric, symmetry
PHOT	photon(s)	T	triton
PI	pion, usually written as PI+, PI-, PI0 to indicate charge	TEL	counter telescope
POL	polarized or polarization	THR	threshold for reaction or threshold detector, e.g., $^{29}\text{Si}(n, p)^{29}\text{Al}$.
Q-SQUAR	momentum transfer squared (q^2)	TOF	time-of-flight detector
RCL	recoil	TRK	tracks of particles or fragments observed in solid materials (glass, mylar, etc.)
REL	relative	TRNS	transition
RLI	relative integrated cross-section data	UKN	unknown
RLX	relative cross-section data	UNK	
RSP	reaction spectrometer	VIB	vibrational
RLY	relative yield data	VIR PHOT	virtual photon(s)
SCTD	scattered	XN	all neutrons, total neutron yield, $\sigma(\gamma, XN) = \sigma(\gamma, N) + 2\sigma(\gamma, 2N) + 3\sigma(\gamma, 3N) + \sigma(\gamma, NP) + \text{etc.}$
SCD	semiconductor (solid state) detector	XP	all protons, total proton yield $\sigma(\gamma, XP) = \sigma(\gamma, P) + \sigma(\gamma, NP) + 2\sigma(\gamma, 2P) + \text{etc.}$
SCI	scintillator detector other than NaI, e.g., CsI, KI, organic (liquid or solid), stilbene, He	XX	reaction products defined in REMARKS
SEP	separation	XXX	
SEP ISOTP	separated isotope used	YLD	yield
SIG	SIGMA (cross section)		

4PI

a 4π geometry was used or a method like radioactivity or a total absorption measurement

products was determined.
The polarized particle is indicated in REMARKS.

999

energy defined in REMARKS

* or @

indicates the measurement involved beams or targets that were either polarized or aligned, or that the polarization of the reaction

symbols used to indicate that the units associated with the numerals on one or both sides of the symbol in a specific column are not MeV. The units are defined in REMARKS.

U.S. DEPT. OF COMM. BIBLIOGRAPHIC DATA SHEET (See instructions)				1. PUBLICATION OR REPORT NO.	2. Performing Organ. Report No.	3. Publication Date
4. TITLE AND SUBTITLE						
Photonuclear Data-Abstract Sheets 1955-1982						
5. AUTHOR(S)						
E.G. Fuller and Henry Gerstenberg						
6. PERFORMING ORGANIZATION (If joint or other than NBS, see instructions)				7. Contract/Grant No. NATIONAL BUREAU OF STANDARDS DEPARTMENT OF COMMERCE WASHINGTON, D.C. 20234		
				8. Type of Report & Period Covered		
9. SPONSORING ORGANIZATION NAME AND COMPLETE ADDRESS (Street, City, State, ZIP)						
10. SUPPLEMENTARY NOTES						
<input checked="" type="checkbox"/> Document describes a computer program; SF-185, FIPS Software Summary, is attached.						
11. ABSTRACT (A 200-word or less factual summary of most significant information. If document includes a significant bibliography or literature survey, mention it here)						
These abstract sheets cover most classes of experimental photonuclear data leading to information of the electromagnetic matrix element between the ground and excited states of a given nucleus. This fifteen volume work contains nearly 7200 abstract sheets and covers 89 chemical elements from hydrogen through americium. It represents a twenty-seven year history of the study of electromagnetic interactions. The sheets are ordered by target element, target isotope, and by an assigned bibliographic reference code. Information is given on the type of measurement, excitation energies studied, source type and energies, detector type, and angular ranges covered in the measurement. For a given reference, the relevant figures and tables are mounted on a separate sheet for each nuclide studied.						
12. KEY WORDS (Six to twelve entries; alphabetical order; capitalize only proper names; and separate key words by semicolons)						
data-abstract sheets, elements, experimental, isotopes, nuclear physics, photonuclear reactions						
13. AVAILABILITY						
<input type="checkbox"/> Unlimited <input checked="" type="checkbox"/> For Official Distribution. Do Not Release to NTIS <input type="checkbox"/> Order From Superintendent of Documents, U.S. Government Printing Office, Washington, D.C. 20402. <input type="checkbox"/> Order From National Technical Information Service (NTIS), Springfield, VA. 22161				14. NO. OF PRINTED PAGES 15. Price		

